Molecular Self-Assembly of Peptide Bolaamphiphiles and Their Applications in Nanocatalysis and Biology

Ph.D. Thesis

by

Indrajit Maity

DISCIPLINE OF CHEMISTRY

INDIAN INSTITUTE OF TECHNOLOGY INDORE

NOVEMBER, 2014

Molecular Self-Assembly of Peptide Bolaamphiphiles and Their Applications in Nanocatalysis and Biology

A THESIS

Submitted in partial fulfillment of the
requirements for the award of the degree
of
DOCTOR OF PHILOSOPHY

by

Indrajit Maity

DISCIPLINE OF CHEMISTRY
INDIAN INSTITUTE OF TECHNOLOGY INDORE
NOVEMBER, 2014

INDIAN INSTITUTE OF TECHNOLOGY INDORE

CANDIDATE'S DECLARATION

I hereby certify that the work which is being presented in the thesis entitled **MOLECULAR SELF-ASSEMBLY OF PEPTIDE BOLAAMPHIPHILES AND THEIR APPLICATIONS IN NANOCATALYSIS AND BIOLOGY** in the partial fulfillment of the requirements for the award of the degree of **DOCTOR OF PHILOSOPHY** and submitted in the **DISCIPLINE OF CHEMISTRY, INDIAN INSTITUTE OF TECHNOLOGY INDORE**, is an authentic record of my own work carried out during the time period from May 2010 to November 2014 under the supervision Dr. APURBA K. DAS, Assistant professor, Discipline of Chemistry.

The matter presented in this thesis has not been submitted by me for the award of any other degree of this or any other institute.

(INDRAJIT MAITY)

This is to certify that the above statement made by the candidate is correct to the best of my knowledge.

(NAME OF THESIS SUPERVISOR)

INDRAJIT MAITY has successfully given his Ph.D. Oral Examination held on **…….**

Signature(s) of Thesis Supervisor(s)
Date:

Convener, DPGC
Date:

Signature of PSPC Member
Date:

Signature of PSPC Member
Date:

Signature of External Examiner
Date:

ACKNOWLEDGEMENTS

I would like to express my profound gratitude and indebtedness to my supervisor Dr. Apurba K. Das for giving me such a great opportunity to work on a stimulating research field. His excellent guidance, consistent support and advice motivated me to encounter with challenges in my research career. His enormous knowledge, scientific views and admirable supervision in each step throughout my whole research career made the completion of this thesis possible.

I am also grateful to Dr. Sampak Samanta and Dr. Shaibal Mukherjee for their precious suggestions and guidance.

I wish to express my gratitude to prof. Pradeep Mathur (Director, Indian Institute of Technology Indore) for his valuable support and providing all the facilities at Indian Institute of Technology Indore.

With great pleasure, I am grateful to Dr. Tushar Mukherjee for collaborative research work on photophysical study and his consistent support and motivation. I am very thankful to our collaborator, Dr. Hamendra S. Parmar (Department of Biotechnology, Devi Ahilya Vishwavidyalaya, Indore, India) for cell culture experiments.

I am deeply thankful to Dr. Chelvam Venkatesh (Head, Discipline of Chemistry, Indian Institute of Technology Indore) for his help and support in various aspects. I am also respectful to Dr. Suman Mukhopadhyay, Dr. Rajneesh Misra, Dr. Tridib K. Sarma, Dr. Biswarup Pathak, Dr. Sanjay Singh, Dr. Satya S. Bulusu, Dr. Shaik M. Mobin and Dr. Anjan Chakraborty for their valuable guidance and suggestion during my research career.

I feel pleasure to thank my group members, Dr. Dnyaneshwar B. Rasale, Mr. Maruthi Konda, Mr. Manoj K. Manna, Mr. Sagar Biswas, Mr. Soumitra Bhowmik, Mr. Ankan Biswas ans Mr. Sahidul Mondal for their bighearted co-operation and help to make my research work smooth and successful.

It has been an amazing experience to work with many friends and colleagues in research laboratory. It is good moment to record my thanks to Mr. Shivendra Singh, Mr. Mriganka Das, Mr. Surajit Chatterjee, Mr. Arpan Bhattacharya, Mr. Anupam Das, Mr. Biju Majumdar, Mrs. Veenu Mishra, Ms. Anvita Srivastav, Ms. Sonam Mandani, Mr. Bhausaheb Dhokale, Mr. Rajendar Nasani, Mr. Prabhat Gautam, Mr. Bhagwati Sharma, Mr. Debashis Majee, Ms. Anuradha Dagar, Dr. Pradeep Jaiswal, Dr. Deepa Dey and all other fellow friends of this Department (Chemistry) for their co-operation and help in various ways.

I am very thankful to Dr. Pallab Pahari and Mr. Totan Ghosh for their continuous help and support.

I also wish to thank to Ms. Sarita Batra, Mr. Kinny Pandey, Mr. Ghanshyam Bhavsar and Mr. Manish Kushwaha for their technical help and support.

I am grateful to Dr. C. Upendra and Ms. Shanu Shukla for their memorable help.

Finally, I wish to express my deep, heartfelt gratitude to my parents Mr. Rathikanta Maity and Smt. Jhuma Maity for their sacrifice, support, encouragement and patience during this tenure. I would like to show my respect and thanks to my elder brothers Mr. Manojit Maity and Mr. Avijit Maity for their care, affection and support.

Indrajit Maity

Dedicated to My Beloved

Parents

ABSTRACT

Bolaamphiphiles are an interesting class of amphiphilic molecules, which can self-assemble to form well-defined nanostructures in aqueous solutions. Generally, two hydrophilic end groups are covalently attached with a hydrophobic spacer in a bolaamphiphile molecule. Low molecular weight self-assembled soft nanostructured materials draw great attraction for wide range of applications in the fields of nanoscience, bioscience and supramolecular electronics. Despite this potential, stimuli responsive self-assembled peptide bolaamphiphilic materials have yet to be fully established for tissue regeneration strategies associated with their cytotoxicity and stem cell proliferation and the ethical considerations surrounding their usage. Furthermore, there is wide interest to develop novel self-assembled nanostructural architectures for the fabrication of metal nanoparticles and their applications in chemical reactions.

The main objectives of present study are:

(a) Incorporation of a flexible alkane chain in order to achieve different structures due to conformational heterogeneity in bolaamphiphiles.

(b) To control molecular self-assembly of peptide bolaamphiphiles with the help of external stimuli.

(c) To study nanostructural transition of a peptide bolaamphiphile driven by molecular self-assembly.

(d) Utilization of nanostructural soft materials in the field of nanocatalysis.

(e) Exploration of lipase catalysed inclusion of gastrodigenin p-hydroxybenzyl alcohol with peptide bolaamphiphiles to mimic with a natural dissipative system.

(f) To investigate dose dependent cytotoxicity and cell proliferation behaviour of self-assembled peptide bolaamphiphiles based hydrogel scaffold.

1. Exploiting Self-Assembly Driven Dynamic Peptide-Based Nanostructured Library

The present study has described a development of dynamic peptide based library in gel phase medium. The reaction between tyrosine rich peptide bolaamphiphile **1** (HO-Tyr-Phe-Suc-Phe-Tyr-OH) and dimethyl sulphate (DMS) facilitates the formation of a

predominant nanostructured product in gel phase medium. The dynamic peptide bolaamphiphile based library is driven by self-assembly of molecules, which lead to appreciable product distribution in gel phase medium.

2. Sonication Induced Peptide-Appended Bolaamphiphile Hydrogels for *In Situ* Generation and Catalytic Activity of Pt Nanoparticles

Peptide bolaamphiphiles HO-Tyr-Leu-Suc-Phe-Tyr-OH **15,** HO-Phe-Phe-Suc-Leu-Phe-OH **16** and HO-Phe-Leu-Suc-Val-Phe-OH **17** are synthesized. Phenylalanine rich peptide bolaamphiphile **16** self-assembles into well-defined twisted nanoribbons whereas tyrosine rich functional material **15** self-assembles into nanofibrillar structure which is used as a template for in situ generation of platinum nanoparticles. Furthermore, hydrogenation reactions are catalyzed by in situ synthesized Pt nanoparticles such as *p*-phenylenediamine, which is prepared by the reaction of *p*-nitroaniline with Pt nanoparticles.

3. Peptide Nanofibers Decorated with Pd Nanoparticles to Enhance the Catalytic Activity for C-C Coupling Reactions in Aerobic Conditions

We demonstrate the self-assembly of a peptide bolaamphiphile **25** (HO-F-Y-Suc-Y-F-OH) for the fabrication of Pd nanoparticles on peptide bolaamphiphile nanofibers to enhance the catalytic ability for C-C coupling reactions under mild and aerobic conditions. The peptide nanofibers are anticipated to anchor the aromatic reactants and metal nanoparticles, which would result in an enhanced catalytic activity for C-C coupling reactions. Various spectroscopic techniques are used to investigate the self-assembly process. This indicates that self-assembled peptide bolaamphiphiles could be used to switch and control the activity of a material's functionality.

4. Peptide-Nanofiber-Supported Palladium Nanoparticles as an Efficient Catalyst for the Removal of N-Terminus Protecting Groups

We report sonication-induced formation of a tyrosine-and tryptophan-based peptide bolaamphiphile (HO-Tyr-Trp-Suc-Trp-Tyr-OH **30**) hydrogel. The peptide nanofibers are used as a template to synthesize Pd nanoparticles. The Pd nanoparticles are decorated on the surface of peptide bolaamphiphile nanofibers, which provide extra stability to the Pd

nanoparticles. We also report a general method in which peptide-nanofiber-supported Pd nanoparticles can efficiently deprotect various types of N-protecting groups from the N-terminus of amino acids and peptides in the presence of $NaBH_4$ in aqueous medium at room temperature.

5. Self-Programmed Nanovesicle to Nanofiber Transformation of a Dipeptide Appended Bolaamphiphile and Its Dose Dependent Cytotoxic Behavior

We describe a sonication-induced phenylalanine and tryptophan-rich peptide bolaamphiphile (HO-Trp-Tyr-Suc-Trp-Tyr-OH **35**) self-assembly through the synergistic effects of H-bonding and π-π stacking interactions. The self-assembling peptide bolaamphiphiles form a self-supporting nanostructured fluorescent hydrogel where self-programmed nanostructural transition from nanovesicles to the nanofibers occurs through the structural continuity of stable β-sheets. The molecular conformations and arrangements for both the cases were investigated thoroughly by various spectroscopic techniques including FT-IR, fluorescence and circular dichroism (CD). The spectroscopic studies suggest loose β-sheet arrangements of peptide bolaamphiphiles inside the vesicles. Moreover, peptide bolaamphiphiles are self-assembled into more ordered and compact β-sheet arrangements inside the nanofibers. Furthermore, the peptide bolaamphiphile shows dose-dependent cytotoxic and cell-proliferation behaviour.

6. Lipase Catalyzed Dissipative Self-Assembly of a Thixotropic Peptide Bolaamphiphile Hydrogel for Human Umbilical Cord Stem Cells Proliferation

We report lipase catalysed inclusion of gastrodigenin to peptide bolaamphiphiles. The lipase catalysed reactions of peptide bolaamphiphiles with gastrodigenin (p-hydroxy benzylalcohol) generates dynamic combinatorial libraries (DCL) in aqueous medium. The peptide bolaamphiphile **37** reacts with p-hydroxy benzylalcohol in presence of lipase and self-assembles to produce nanofibrillar thixotropic hydrogel. The subsequent hydrolysis results in dissipation of energy to form non-assembling bolaamphiphile **37** with collapsed nanofibers. Furthermore, 3D cell culture experiments with the thixotropic DCL hydrogel matrix at different time periods, significantly supports the cells survival and proliferation of human umbilical cord mesenchymal stem cells.

LIST OF PUBLICATIONS IN JOURNALS

1. **Maity I.**, Parmar H. B., Rasale D. B., Das A. K. (2014), Self-programmed nanovesicle to nanofiber transformation of a dipeptide appended bolaamphiphile and its dose dependent cytotoxic behavior, *J. Mater. Chem. B*, 2, 5272-5279 (DOI: 10.1039/c4tb00365a).

2. **Maity I.**, Manna M. K., Rasale D. B., Das A. K. (2014), Peptide-nanofiber-supported palladium nanoparticles as an efficient catalyst for the removal of N-terminus protecting groups, *ChemPlusChem*, 79, 413-420 (DOI: 10.1002/cplu.201300348).

3. **Maity I.**, Rasale D. B., Das A. K. (2014), Peptide nanofibers decorated with Pd nanoparticles to enhance the catalytic activity for C-C coupling reactions in aerobic conditions, *RSC Adv*., 4, 2984-2988 (DOI: 10.1039/c3ra44787a).

4. **Maity I.**, Mukherjee T. K., Das A. K. (2014), Photophysical study of a π-stacked β-sheet nanofibril forming peptide bolaamphiphile hydrogel, *New J. Chem*., 38, 376-385 (DOI: 10.1039/c3nj00814b).

5. **Maity I.**, Rasale D. B., Das A. K. (2013), Exploiting a self-assembly driven dynamic nanostructured library, *RSC Adv*., 3, 6395-6400 (DOI: 10.1039/c3ra22401e).

6. **Maity I.**, Rasale D. B., Das A. K. **(**2012), Sonication induced peptide-appended bolaamphiphile hydrogels for in situ generation and catalytic activity of Pt nanoparticles, *Soft Matter*, 8, 5301-5308 (DOI: 10.1039/c2sm25126d).

7. Das A. K., **Maity I.**, Parmar H. B., McDonald T. O., Konda M. (2015), Lipase catalyzed dissipative self-assembly of a thixotropic peptide bolaamphiphile hydrogel for human umbilical cord stem cells proliferation, *Biomacromolecules*, (DOI: 10.1021/bm501835v).

8. Rasale D. B, **Maity I.**, Das A. K. (2014), In situ generation of redox active peptides driven by selenoester mediated native chemical ligation, *Chem. Commun*., 50, 11397-11400 (DOI: 10.1039/c4cc03835e).

9. Rasale D. B., **Maity I.**, Das A. K. (2014), Lipase catalyzed inclusion of gastrodigenin for the evolution of blue light emitting peptide nanofibers, *Chem. Commun*., 50, 8685-8688 (DOI: 10.1039/c4cc02484b).

10. Konda M., **Maity I.**, Rasale D. B., Das A. K. (2014), A new class of phase selective synthetic β-amino acid based peptide gelator: From mechanistic aspects to oil spill recovery, *ChemPlusChem*, **79**, 1482-1488. (DOI: 10.1002/cplu.201402120).

11. Rasale D. B., **Maity I.**, Konda M., Das A. K. (2013), Peptide self-assembly driven by oxo-ester mediated native chemical ligation, *Chem. Commun*., 49, 4815-4817 (DOI: 10.1039/c3cc41475b).

12. Rasale D. B., **Maity I.**, Das A. K. (2013), Colorimetric enzyme sensing assays via in situ synthesis of gold nanoparticles, *J Clust Sci*., 24, 1163-1170 (DOI 10.1007/s10876-013-0606-z).

13. Rasale D. B., **Maity I.**, Das A. K. (2012), Emerging π-stacked dynamic nanostructured library, *RSC Adv*., 2, 9791-9794 (DOI: 10.1039/c2ra21334f).

14. Manna M. K., Pandey S. K., **Maity I.**, Mukherjee S., Das A. K., Aromatic capped peptide self-assembly directed evolution of lamellar photoconductor hybrids, (**manuscript submitted 2014**).

CONFERENCE PRESENTATIONS

1. **Maity I.**, Rasale D. B., Das A. K., Sonication induced functional peptide hydrogel: A template for in situ generation of metal nanoparticles, International symposium on recent trends of research in chemistry, Midnapore College, West Bengal, India (31st October-1st November, 2012) **Poster Presentation.**

2. 2012 Winter workshop on engineering at nanoscale: From materials to bio-sensors (December 10 - 12, 2012), **Oral Presentation**.

TABLE OF CONTENTS

LIST OF FIGURES

Chapter 1: General Introduction

(the red zones represent the hydrophobic pillar[5] arene skeletons and the blue parts denote glycol chains) in chloroform from **1**, and the reversible disassembly and re-assembly of the giant vesicles under external stimuli. (Ref: 78).

Figure 1.13. (a) Molecular structure of an aspartic acid appended perylene derivative. (b) Typical FE-SEM image of a DAPI dried gel. AFM topology of (c) DAPI gel and (d) LAPI gel prepared on a freshly cleaved mica surface. (Ref: 96)

Figure 1.14. The TEM image of **1** positively stained with uranyl acetate (a) shows the preferential staining of fiber peripheries, with line profile inset, and the TEM image of **2** positively stained with uranyl acetate (b) shows staining at both cores and peripheries, with line profile and high magnification insets. The molecular graphics rendition of the cross section of the nanofibers of **1** (c) illustrates hydrophilic domains A and C separated by the hydrophobic section B. (Ref: 104)

Figure 1. 15. Structures of various types of peptide appended bolaamphiphiles (top). TEM images of peptide nanostructures composed of DFAG (a), DFGG (b), DGAG (c), DFAV (d), DFVG (e), and DVAG (f) (bottom).(Ref: 107)

Figure 1.16. (a) Structures of lysine-based bolaamphiphiles A ($R=O^-$) and B (R = OMe) and the assembly of A into rings, which stack to give tubes. (b) TEM image of bolaamphiphile A in water (250 mm; carbon-coated copper grid); 2% (w/w) uranyl acetate as negative stain. Blue insets: Two nanotubes and one nanoring. (c) Tapping-mode AFM image of bolaamphiphile A in water (250 mm) on freshly cleaved mica. Red inset: Section analysis showing uniform height of the assemblies. Height indicated by red arrows: ca. 9 nm. (Ref: 117)

Figure 1.17. Molecular structure of the bolaamphiphile (HDGA) and melamine; and model of formation of supramolecular nanotubes from a two component assembly with different molar ratios and mechanisms. (Ref : 122)

Figure 1.18. A schematic illustration for the molecular packing of the organic nanotube with 7-9 nm inner diameters, which self-assembled from the asymmetric bolaamphiphile 1(Top). TEM image of the organic nanotubes negatively stained with phosphotungstate. The hollow cylinder nanospace of the organic nanotubes can be visualized as it is relatively darker compared to its surrounding (Bottom). (Ref: 127)

Chapter 3: Exploiting a Self-Assembly Driven Dynamic Nanostructured Library

Chapter 4: Sonication Induced Peptide-Appended Bolaamphiphile Hydrogels for In Situ Generation and Catalytic Activity of Pt Nanoparticles

Figure 4.24. ESI-MS spectrum of HO-Phe-Val-Suc-Leu-Phe-OH **17.**

Figure 4.25. (a) photographs of peptide bolaamphiphile hydrogel **15** and Pt nanoparticles embedded in gel nanonetworks of peptide bolaamphiphile **15** upon sonication. (b) Proposed mechanism of peptide bolaamphiphile **15** self-assembly.

Figure 4.26. (a) Concentration dependence gelation temperature (T_{gel} / $^{\circ}C$) of (a) the hydrogel of peptide bolaamphiphile **15,** (b) the hydrogel of peptide bolaamphiphiles **16** and (c) concentration-temperature phase diagram ln (φ) vs temp (K) of hydrogels **15** and **16**, where φ is the mole fraction and K is the temperature in Kelvin.

Figure 4.27. Dynamic rheology (frequency sweep) of (a) peptide bolaamphiphile **15** (c = 20 mmol L^{-1}) and (b) peptide bolaamphiphile **16** (c = 25 mmol L^{-1}). In each case storage modulus G´ is higher than loss modulus G´´. For both cases G´ > 10^5 Pa at low frequency and storage modulus is higher than loss modulus by a factor of 7-14 indicates excellent solid like property of gel materials.

Figure 4.28. (a) FT-IR spectra of (i) solid powder and (ii) hydrogel of peptide bolaamphiphile **15** indicating antiparallel β sheet structure in gel phase. FT-IR spectra of (i) solid powder and (ii) hydrogel of peptide bolaamphiphile **16.**

Figure 4.29. (a) Fluorescence emission spectra of (i) solution (c = 5 mmol L^{-1}, λ_{ex} = 276 nm, λ_{em} = 306 nm) and (ii) the hydrogel of peptide bolaamphiphile **15** (c = 20 mmol L^{-1}, λ_{ex} = 276 nm, λ_{em} = 306 nm). (b) Fluorescence emission spectra of peptide bolaamphiphile **16** (i) after 30 min of sonication and (ii) after 2 days of sonication. Emission maxima at 300 nm and a broad pronounced peak at 370-450 nm correspond to π-π stacking interactions and higher order aggregation in the gel phase.

Figure 4.30. SEM micrographs of (a) suspension of peptide bolaamphiphile **15** prior to sonication, (b) hydrogel of peptide bolaamphiphile **15** made by sonication shows entangled helical fibers and (c) hydrogel of peptide bolaamphiphile **16** indicates the fibrous aggregates.

Figure 4.31. TEM micrographs of (a) the hydrogel of peptide bolaamphiphile **15** shows entangled nanofibers with diameters ranging from 30-39 nm, (b) the hydrogel of peptide bolaamphiphile **16** assembled into nanoribbon and nanofibriller structures and (c) twisted nanoribbon like morphology with diameter 64-70 nm adopted by peptide bolaamphiphile **16** in the gel phase.

Chapter 5: Peptide Nanofibers Decorated with Pd Nanoparticles to Enhance the Catalytic Activity for C–C Coupling Reactions in Aerobic Conditions

Figure 6.6. ESI-MS spectrum of HO-W-Suc-W-OH **33.**

Figure 6.7. ^{1}H NMR spectrum (400 MHz, $CDCl_3$) of MeO-Y-W-Suc-W-Y-OMe **34**.

Figure 6.8. ESI-MS spectrum of MeO-Y-W-Suc-W-Y-OMe **34**.

Figure 6.9. ^{1}H NMR spectrum (400 MHz, DMSO-d_6) of HO-Y-W-Suc-W-Y-OH **30.**

Figure 6.10. ^{13}C NMR spectrum (100 MHz, DMSO-d_6) of HO-Y-W-Suc-W-Y-OH **30.**

Figure 6.11. ESI-MS spectrum of HO-Y-W-Suc-W-Y-OH **30.**

Figure 6.12. ^{1}H NMR spectrum (400 MHz, DMSO-d_6) of Boc-Tyr-C_{hex}-OH D**3.**

Figure 6.13. ESI-MS spectrum (400 MHz, DMSO-d_6) of Boc-Tyr-C_{hex}-OH D**3.**

Figure 6.14. ^{1}H NMR spectrum (400 MHz, DMSO-d_6) of Boc-Tyr-C_{hex}-Aib-OH D**4.**

Figure 6.15. ESI-MS spectrum of Boc-Tyr-C_{hex}-Aib-OH D**4.**

Figure 6.16. ^{1}H NMR spectrum (400 MHz, DMSO-d_6) of Nmoc-Phe(1)-Phe(2)-OH D**8.**

Figure 6.17. ESI-MS spectrum of Nmoc-Phe(1)-Phe(2)-OH D**8.**

Figure 6.18. Frequency sweep of peptide bolaamphiphile hydrogel **30** (c = 10 mmol L^{-1}). Storage modulus G' is higher than the loss modulus G". G'>10^4 Pa at low frequency, and the storage modulus is higher than the loss modulus by a factor of 5-10, which indicates excellent solid-like behavior of the gel materials.

Figure 6.19. (a) FTIR spectrum of peptide bolaamphiphile hydrogel **30** (c = 10 mmol L^{-1}), which indicates the formation of a supramolecular β-sheet structure in the gel phase and (b) the CD spectrum of hydrogel **30** (c = 100 μm) reveals the formation of a β-sheet structure through extensive hydrogen-bonding interactions.

Figure 6.20. The fluorescence spectra of the peptide bolaamphiphile hydrogel **30** (c = 10 mmol L^{-1}), the results of which suggest extensive π–π stacking interactions between the aromatic residues of peptide bolaamphiphile **30** during the self-assembly process.

Figure 6.21. (a) A SEM image showing the entangled nanofibrous aggregates and (b) an AFM image showing the nanofiber morphology of hydrogel **30**. (c) AFM image of peptide bolaamphiphile hydrogel **30** and it′s (d) three dimensional image.

Figure 6.22. Wide-angle powder XRD pattern of (i) peptide bolaamphiphile **30** powder and (ii) its dried hydrogel **30**. The powder X-ray diffraction pattern exhibits the characteristic pattern of a β-sheet structure of peptide bolaamphiphile **30**, which is adopted through π–π stacking interactions between the aromatic moieties through the self-assembly process.

Chapter 7: Self-Programmed Nanovesicle to Nanofiber Transformation of a Dipeptide Appended Bolaamphiphile and Its Dose Dependent Cytotoxic Behaviour

height of nanovesicles is 30 nm which is twice of the wall thickness estimated from TEM images.

Figure 7.11. AFM images show the (a) association of two vesicles towards formation of a nanocapsule and (b) the matured nanocapsules.

Figure 7.12. Fluorescence microscopic images showing the encapsulation of a physiological dye, Congo red, by nanovesicles.

Figure 7.13. Optical microscopic image clearly shows the formation of vesicles where distribution of nano to micro vesicles are observed.

Figure 7.14. FT-IR spectra for both the nanostructures of nanovesicles and nanofibers. The FT-IR spectra show the more ordered β-sheet arrangement inside the nanofibers rather than nanovesicles.

Figure 7.15. CD spectra for both the nanostructures of nanovesicles and nanofibers. The spectroscopic studies confirm a more compact β-sheet arrangement inside the nanofibers rather than nanovesicles through the synergistic effect of hydrogen bonding and π-π stacking interactions.

Figure 7.16. Fluorescence spectra (concentration: 10 mmol L^{-1}, λ_{ex} = 280 nm) for both the nanostructures of nanovesicles and nanofibers.

Figure 7.17. PXRD for both the nanovesicles and nanofibers confirm the loose molecular arrangement inside the nanovesicles and a more compact molecular arrangement inside the nanofibers.

Figure 7.18. ^{1}H NMR (400 MHz) spectrum of dried hydrogel at 1 day (nanovesicle state) in DMSO-d_6.

Figure 7.19. ^{1}H NMR (400 MHz) spectrum of dried hydrogel at 5 day (nanofiber state) in DMSO-d_6.

Figure 7.20. ^{1}H-^{1}H COSY spectrum of dried hydrogel at 1 day (nanovesicle state) in DMSO-d_6.

Figure 7.21. ^{1}H-^{1}H COSY spectrum of dried hydrogel at 5 day (nanofiber state) in DMSO-d_6.

Figure 7.22. ROESY spectrum of dried hydrogel at 1 day (nanovesicle state) in DMSO-d_6.

Chapter 8: Lipase Catalyzed Dissipative Self-Assembly of a Thixotropic Peptide Bolaamphiphile Hydrogel for Human Umbilical Cord Stem Cells Proliferation.

enzymatic energy dissipation (Pd) (ester hydrolysis) is lower than the consumption of the energy (Pc) (esterification) to allow the formation of self-assembled architecture.

Figure 8.22. (a) The lipase catalyzed esterification reaction initially leads to form the mixture of monoester and di-ester. After the lag phase, the self-assembly process solely drives to form the di-ester. (b) The DCL **37** forms the nanofibrillar hydrogel whereas (c) the solution of DCL **38** forms nanotape structures in supramolecular level.

Figure 8.23. HPLC chromatograms (a) peptide bolaamphiphile **25** (HO-Phe(4)-Tyr(3)-Suc-Tyr(1)-Phe(2)-OH) and DCL, (b) peptide bolaamphiphile **39** (HO-Ala(4)-Tyr(3)-Suc-Tyr(1)-Ala(2)-OH) and DCL, (c) peptide bolaamphiphile **40** (HO-Val(4)-Tyr(3)-Suc-Tyr(1)-Val(2)-OH) and DCL and (d) peptide bolaamphiphile **3**(HO-Leu(4)-Leu(3)-Suc-Leu(1)-Leu(2)-OH) and DCL.

Figure 8.24. The product distribution of a dynamic system from the lipase catalyzed reaction of (a) peptide bolaamphiphile **37**, (b) it's 3D presentation and (c) peptide bolaamphiphile **38**, (d) it's 3D presentation with a chemical energy in the form of *p*-hydroxy benzylalcohol as determined by HPLC over time at 37 °C.

Figure 8.25. (a) Real time HPLC and mass analysis for the generation of DCL **37** via the enzymatic reaction of peptide bolaamphiphile **37** with *p*-hydroxy benzylalcohol (M_{37me} and M_{37de} are the mass of monoester and di-ester of bolaamphiphile **37**). (b) The ^{1}H NMR spectrum of di-ester **37** in DMSO-d_6 confirms the involvement of aliphatic hydroxyl group of *p*-hydroxy benzylalcohol in esterification reaction.

Figure 8.26. (a) Real time HPLC and mass analysis for the generation of DCL **38** via the enzymatic reaction of peptide bolaamphiphile **38** with *p*-hydroxy benzylalcohol (M_{38me} and M_{38de} are the mass of monoester and di-ester of bolaamphiphile **38**). (b) The ^{1}H NMR spectrum of di-ester **38** in DMSO-d_6 confirms the involvement of aliphatic hydroxyl group of *p*-hydroxy benzylalcohol in esterification reaction.

Figure 8.27. Real time FT-IR spectra of dynamic reactions of (a) peptide bolaamphiphile **37** and (b) peptide bolaamphiphile **38**, show the formation of β-sheet structures with progression of the enzymatic reactions.

Figure 8.28. Real time CD spectra of dynamic reactions of (a) peptide bolaamphiphile **37** and (b) peptide bolaamphiphile **38**, show the formation of ordered β-sheet structures with progression of the enzymatic reactions.

Figure 8.29. Real time UV-Vis spectra of (a) DCL **37** and (b) DCL **38**.

Figure 8.30. Real time fluorescence spectra of dynamic reactions of (a) peptide bolaamphiphile **37** and (b) peptide bolaamphiphile **38**, show significant red shift with progression of both the reactions from 0 minute (Mixture of peptide bolaamphiphile and *p*-hydroxybenzyl alcohol before enzyme addition) to 15 days. This revealed that π-π stacking interactions facilitate the product formation in enzymatic dynamic reactions.

Figure 8.31. Excitation (gray line) and emission spectra (black line) of DCL **37** at (a) 0 day (prior to enzyme addition, λ_{ex}= 341 nm), (b) at 6 day (λ_{ex}= 416 nm), (c) at 10 day (λ_{ex}= 420 nm) and (d) at 15 day (λ_{ex}= 420 nm).

Figure 8.32. Excitation (gray line) and emission spectra (black line) of DCL **38** at (a) 0 day (prior to enzyme addition, λ_{ex}= 365 nm), (b) at 6 day (λ_{ex}= 418 nm), (c) at 10 day (λ_{ex}= 418 nm) and (d) at 15 day (λ_{ex}= 420 nm).

Figure 8.33. PXRD spectra for both the DCL **37** and DCL **38** confirm that self-assembling molecules arranged into β-sheet structures in their respective nanoarchitectures.

Figure 8.34. (a) Scanning electron microscopy and (b) Transmission electron microscopy images of DCL **37** hydrogel at 10^{th} day of dynamic reaction reveal entangled nanofibrillar morphology. (c) Scanning electron microscopy and (d) Transmission electron microscopy images of DCL **38** at 10^{th} day of dynamic reaction show nanotapes morphology.

Figure 8.35. Scanning electron microscopic images of (a) DCL **25** (HO-Phe(4)-Tyr(3)-Suc-Tyr(1)-Phe(2)-OH based DCL) shows nanodisk like structure and (b) DCL **39** (HO-Ala(4)-Tyr(3)-Suc-Tyr(1)-Ala(2)-OH based DCL) reveals spherical morphology after 10 days of enzymatic reaction. (c) DCL **40** (HO-Val(4)-Tyr(3)-Suc-Tyr(1)-Val(2)-OH based DCL) shows nanosheets like structures whereas (d) DCL **3** (HO-Leu(4)-Leu(3)-Suc-Leu(1)-Leu(2)-OH based DCL) demonstrates crystalline nanofibers after 10 days of enzymatic reaction.

Figure 8.36. (a) Frequency sweep of DCL **37** hydrogel (c = 20 mmol L^{-1}). Storage modulus G' is higher than the loss modulus G". G' >10^3 Pa at low frequency, and the storage modulus is higher than the loss modulus by a factor of 5-10, which indicates

excellent solid-like behavior of the gel materials. (b)The step strain experiment shows the thixotropic nature of DCL **37** hydrogel. Concentration was maintained at 20 mM.

Figure 8.37. Stem cell viability based on (a) MTT , (b) XTT and (c) DNA leaching assay within the peptide hydrogels. Data are means ± S.E.M. (n=3); ^{m}, P<0.001; ^{n}, P<0.01 and ^{o}, P<0.05 as compared to the respective media control values. (S.E.M represents *standard error* of *measurement*).

Annexure 1:

Annexure 2:

LIST OF TABLE

LIST OF COMPOUNDS

1. HO-Tyr(4)-Phe(3)-Suc-Phe(1)-Tyr(2)-OH **1**

2. HO-Tyr(4)-Leu(3)-Suc-Leu(1)-Tyr(2)-OH **2**

3. HO-Leu(4)-Leu(3)-Suc-Leu(1)-Leu(2)-OH **3**

4. HO-Gly(4)-Leu(3)-Suc-Leu(1)-Gly(2)-OH **4**

5. HO-Suc-Phe(1)-OMe **5**

6. MeO-Phe(2)-Suc-Phe(1)-OMe **6**

7. HO-Phe(2)-Suc-Phe(1)-OH **7**

8. MeO-Tyr(4)-Phe(3)-Suc-Phe(1)-Tyr(2)-OMe **8**

9. HO-Suc-Leu(1)-OMe **9**

10. MeO-Leu(2)-Suc-Leu(1)-OMe **10**

11. HO-Leu(2)-Suc-Leu(1)-OH **11**

12. MeO-Tyr(4)-Leu(3)-Suc-Leu(1)-Tyr(2)-OMe **12**

13. MeO-Leu(4)-Leu(3)-Suc-Leu(1)-Leu(2)-OMe **13**

14. $PhCH_2O$-Gly(4)-Leu(3)-Suc-Leu(1)-Gly(2)-OCH_2Ph **14**

15. HO-Tyr(4)-Leu(3)-Suc-Phe(1)-Tyr(2)-OH **15**

16. HO-Phe(4)-Leu(3)-Suc-Phe(1)-Phe(2)-OH **16**

17. HO-Phe(4)-Leu(3)-Suc-Val(1)-Phe(2)-OH **17**

18. MeO-Leu(2)-Suc-Phe(1)-OMe **18**

19. HO-Leu(2)-Suc-Phe(1)-OH **19**

20. MeO-Tyr(4)-Leu(3)-Suc-Phe(1)-Tyr(2)-OMe **20**

21. MeO-Phe(4)-Leu(3)-Suc-Phe(1)-Phe(2)-OMe **21**

22. MeO-Val(2)-Suc-Leu(1)-OMe **22**

23. HO-Val(2)-Suc-Leu(1)-OH **23**

24. MeO-Phe(4)-Val(3)-Suc-Leu(1)-Phe(2)-OMe **24**

25. HO-Phe(4)-Tyr(3)-Suc-Tyr(1)-Phe(2)-OH **25**

26. HO-Tyr(1)-Suc-OMe **26**

27. MeO-Tyr(2)-Suc-Tyr(1)-OMe **27**

28. HO-Tyr-(2)-Suc-Tyr(1)-OH **28**

29. MeO-Phe(4)-Tyr(3)-Suc-Tyr(1)-Phe(2)-OMe **29**

30. HO-Tyr(4)-Trp(3)-Suc-Trp(1)-Tyr(2)-OH **30**

31. HO-Suc-Trp(1)-OMe **31**

32. MeO-Trp(2)-Suc-Trp(1)-OMe **32**

33. HO-Trp(2)-Suc-Trp(1)-OH **33**

34. MeO-Tyr(4)-Trp(3)-Suc-Trp(1)-Tyr(2)-OMe **34**

35. HO-Trp(4)-Phe(3)-Suc-Leu(1)-Trp(2)-OH **35**

36. MeO-Trp(4)-Phe(3)-Suc-Leu(1)-Trp(2)-OMe **36**

37. HO-Trp(4)-Tyr(3)-Suc-Tyr(1)-Trp(2)-OH **37**

38. HO-Trp(4)-Leu(3)-Suc-Leu(1)-Trp(2)-OH **38**

39. HO-Ala(4)-Tyr(3)-Suc-Tyr(1)-Ala(2)-OH **39**

40. HO-Val(4)-Tyr(3)-Suc-Tyr(1)-Val(2)-OH **40**

41. MeO-Trp(4)-Tyr(3)-Suc-Tyr(1)-Trp(2)-OMe **41**

42. MeO-Trp(4)-Leu(3)-Suc-Leu(1)-Trp(2)-OMe **42**

43. MeO-Ala(4)-Tyr(3)-Suc-Tyr(1)-Ala(2)-OMe **43**

44. MeO-Val(4)-Tyr(3)-Suc-Tyr(1)-Val(2)-OMe **44**

45. Boc-Tyr-C_{hex}-OH **D3**

46. Boc-Tyr-C_{hex}-Aib-OH **D4**

47. Nmoc-Phe(1)-Phe(2)-OH **D8**

ABBREVIATION

Abbreviations used for amino acids, peptide bolaamphiphiles, derivatives, substituents, reagents etc. are in accordance with the recommendations of the IUPAC-IUB commission on Biochemical Nomenclature, 1974, *Pure and Applied Chemistry*, 40, 315-331. Other symbols, nomenclature etc. are based on the list in *J. Biol.Chem*., 1989, 669-671. All amino acids are in L- configuration. Standard three letter coding is useful for all amino acids. Additional abbreviations used in this thesis are listed below.

Ala (A)	Alanine
AFM	Atomic Force Microscope
AcOH	Acetic Acid
Boc	*tert*-butyloxycarbonyl
CD	Circular Dichroism
$CDCl_3$	Chloroform-d
DCL	Dynamic Combinatorial Library
DCC	Dicyclohexylcarbodiimide
DCU	Dicyclohexyl Urea
DIPC	Diisopropylcarbodiimide
DIU	Diisopropyl Urea
DMSO	Dimethyl Sulfoxide
DMS	Dimethyl Sulphate
DMF	Dimethyl Formamide
ddH_2O	Double Distilled Water
ESI-MS	Electrospray Ionization Mass Spectrometry
FTIR	Fourier Transform Infrared Spectroscopy
Phe (F)	Phenylalanine
Fmoc	Fluorenylmethyloxycarbonyl
HOBt	1-Hydroxybenzotriazole
HPLC	High Performance Liquid Chromatography
HCl	Hydrochloric Acid
Leu (L)	Leucine

MeOH	Methanol
Me	Methyl
MeI	Methyl Iodide
M	Molar
$NaBH_4$	Sodium Borohydrate
Nmoc	Naphthalene-2-methoxycarbonyl
NaCl	Sodium Chloride
NaOH	Sodium Hydroxide
$NaHCO_3$	Sodium Bicarbonate
NMR	Nuclear Magnetic Resonance
NPs	Nanoparticles
OCH_3	Methyl Ester
Pd	Palladium
Ph	Phenyl
pH	Negative Logarithm of Hydrogen Ion Activity ($-\log_{10} [H_3O^+]$)
Pt	Platinum
PXRD	Powder X-ray Diffraction
SEM	Scanning Electron Microscope
S.E.M.	Standard Error of Measurement
TEM	Transmission Electron Microscope
TFA	Trifluoroacetic Acid
T_{gel}	Gel Melting Temperature
TLC	Thin Layer Chromatography
TCSPC	Time Correlated Single Photon Counting
Tyr (Y)	Tyrosine
Trp (W)	Tryptophan
UV-Vis	UV-Visible Spectroscopy
Val (V)	Valine
WBC	White Blood Corpuscle
WAXS	Wide Angle X-ray Scattering

NOMENCLATURE

θ (Theta)	Angle
λ (Lambda)	Wavelength
$[\alpha]_D^{20}$	Specific Rotation
Å	Angstrom
s	Singlet
d	Doublet
t	Triplet
st	Strong
nm	Nanometer
ω	Angular Frequency
τ	Life Time
δ	Chemical Shift
μM	Micrometer (Length)
μL	Microliter (Volume)
γ	Gamma
G'	Storage Modulus
G"	Loss Modulus

Chapter 1

General Introduction

'**S**elf-assembly' is a process in which a dis-ordered system of pre-existing components forms an organized structure or patterns by some non-covalent interactions.[1] When the constitutive components are molecules, the process called molecular self-assembly. The evolution of life emerged through chemical reactions that are directed *via* self-assembly of biomolecules with different scales of complexity. Natural processes including the formation of the cytoskeleton and the phospholipid membrane, are examples of protein self-assembly which are dynamic in nature.[2,3] Evolution in nature occurred through a range of self-assembling nanoscale systems based on lipids, nucleic acids and amino acids. In this process, the molecular building blocks spontaneously arrange themselves to form highly ordered structures with well defined properties. Therefore, self-assembly process is a fundamental construction principle for biological materials, which is engaged in various systems, ranging from double-stranded DNA to complex structures such as tobacco mosaic virus.[4,5] The observation of self-assembled structures inside the cellular system (*e.g.* lipid assemblies, folded proteins, protein complexes, or structured nucleic acids) or the organization of fiber-like polymers and membrane ion channels acts as the machinery of life.[6,7] The self-assembled bioactive small molecules competent of degradation over time into predictable metabolites are perfect building blocks as scaffolds to regenerate tissues and organs. The biological building blocks such as sugars, amino acids and nucleic acids offer the widest variety of functionality and cell signaling capacity with rapid and facile synthesis of complex molecules.[8] Now-a-days, enormous effort for development of new technologies based on self-assembly of small bioactive and biocompatible molecules generates a great opportunity for molecular design which can be tailored for a broad range of applications. Thus, this approach aims to mimic nature's remarkable ability to self-assemble functional complex shapes or patterns with nanoscale precision. Supramolecular chemistry, biology and materials engineering are smartly connected to create self-assembling materials that mimic biological microstructures, achieve mechanical action, or generate molecular electronic or sensor devices.[9] Conventionally, objects and devices have been designed through a ''top-down'' approach where an item is carved or moulded out of a larger bulk material. A ''bottom-up'' approach provides an alternative route to the development of nanoscale objects and devices (Figure 1.1).

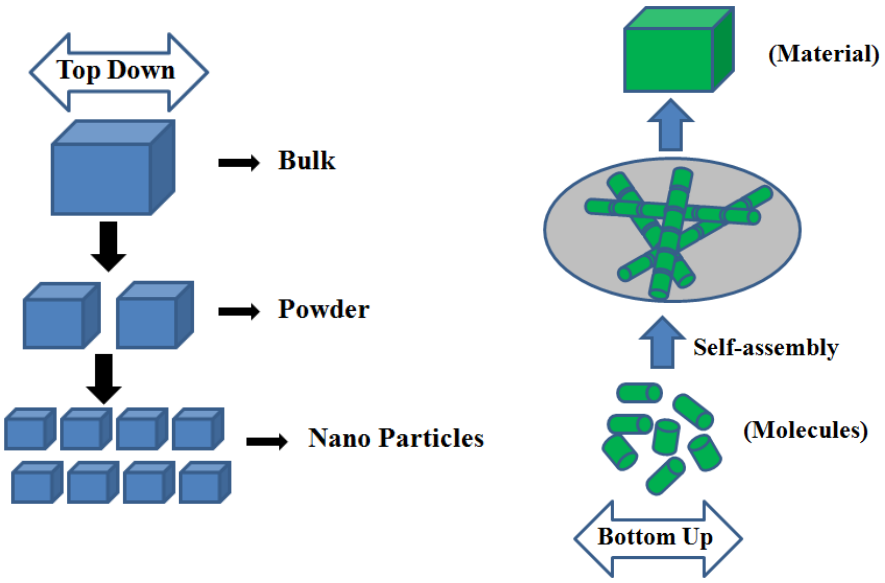

Figure 1.1. *Schematic representation of "top-down" and "bottom-up" fabrication approaches.*

1.1 Bottom-Up Approach

In 1959, Richard Feynman presented a lecture entitled ''There's plenty of room at the bottom'', proposing the plan of a ''bottom-up'' approach for the fabrication of higher ordered structures *via* self-assembly process using individual atoms and molecules as building blocks.[10] One of the main challenges in supramolecular chemistry is to construct the architectures with homogeneous and structurally well-defined design with tunable properties to cover a wide range of potential applications. Therefore, a correct design and good understanding of the rules governing the molecular self-assembly of specific building blocks are key factors for designing the smart supramolecular architectures with predictable properties and functions.[4] Generally, bottom-up fabrication indicates the arrangement of smaller components into a more complex assembly. An example is the use of small individual ''Lego'' pieces to build structures from the bottom-up (Figure 1.2(a)). Molecular self-assembly process is based on bottom-up strategies for developing the higher ordered functional materials. In this process, nature creates the macromolecules and bio-architectures using amino acids, nucleic acids, sugars or lipids as building blocks with optimize function. Self-assembly process is solely a bottom-up process.

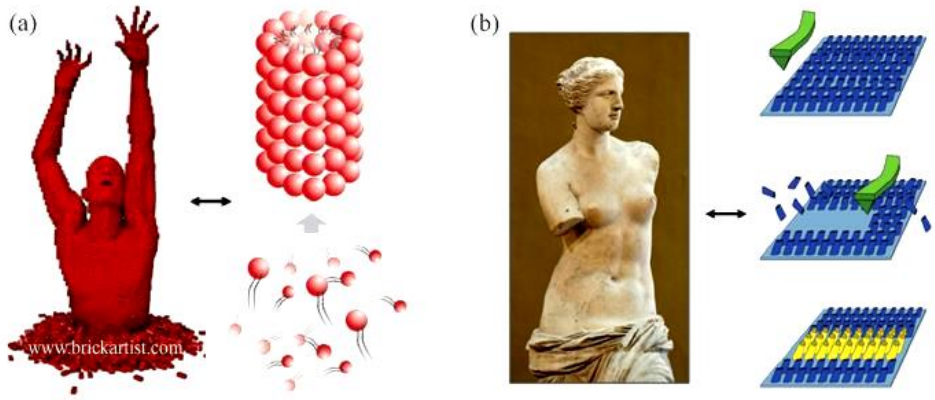

Figure 1.2. *The bottom-up and top-down fabrication: (a) self-assembly of a micellar structure and the building of a sculpture using Lego pieces and (b) a nanografting patterned substrate and the carting of a stone sculpture (Ref: 17).*

In the last two decades, the understanding of nanoscience and the field of self-assembly has grown tremendously. Now, we have the ability to design the self-assembled supramolecular structures of peptides, proteins and other amphiphiles including tapes,[11] belts,[12] fibers,[13] tubes,[14] and vesicles,[15] by using the bottom-up technique. In general, self-assembling systems are based on five key parts: the subunits, a driving force, a repulsive force, a binding force and an environment (Figure 1.3).[16] The subunits, such as peptides or proteins in this case, are the building-blocks of the assembled material where the driving force allows them to interact by the random movement of the sub-units. The repulsive forces such as electrostatic or hydrophobic/hydrophilic repulsions are very essential for the reversibility of the system.

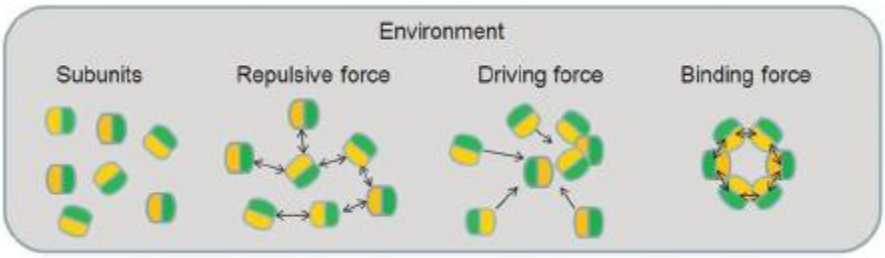

Figure 1.3. *Schematic representation of five key parts of a self-assembling system: the subunits, the repulsive, driving and binding forces, and the environment. (Ref: 16)*

The binding forces are non-covalent interactions including hydrogen bonding, van der Waals, ionic, dipole-dipole and hydrophobic interactions which give the stability to the assembled structures. Reversibility of the system is achieved due to comparable magnitudes of binding and repulsive forces. Finally, the environment is the medium in which the subunits, forces and assembled structures interact.

1.2 Top-Down Approach

Top-down fabrication is defined as the creation of a prearranged structure either by etching down a bulk material or by manipulating components into specific locations. The crafting of a sculpture using a variety of tools, a well-defined structure is generated (Figure 1.2 (b)).[17] The top-down technique was invented in 1798 when Alois Asnefeler proposed the process of lithography. Now, the use of top-down strategy is useful to design well-defined reproducible structures which are closely parallel the size scales of cells in a controlled and systematic manner. This unique technique started the beginning of a new era in materials and biological science.[18] This method covers a wide range of length scales, materials, processing conditions, operating mechanisms and costs. Now, use of self-assembly process demonstrates a number of top-down techniques to allow the fabrication of some impressive, functional materials based on peptides and proteins. The amphiphilic behaviour of peptides and proteins is closely linked to their ultimate functionality. There are a variety of bolaamphiphilic molecules that have been explored in combination with top-down techniques. Bolaamphiphiles are attractive building-block for the development of materials. Matsui and co-workers have developed a bolaamphiphile system which self-assembles in aqueous medium into well-defined nanotubes upon pH reduction. These nanotubes are patterned into the gold surfaces coated with 1-octadecanethiol SAMs using a nanoshaving strategy.[19] With the modification of the peptide nanotubes with mercaptoethylamine, it was possible to produce their assembly on the exposed gold areas. To improve pattern complexity, this technique was utilized by functionalizing the nanotubes with antibodies that recognize specific antigens on the surface rather than the thiol-containing molecule.[20] These types of ordered materials governed from the self-assembly process with this top-down

approach can have promising opportunities for micro/ nanofabricated devices and bioelectronics.

The "bottom up" self-assembly processes are occuring in nature from the prebiotic condition. The self-assembled nanostructures of biological molecules are very significant in biological world. The amino acids and theirs complex biopolymer polypeptides play a significant role in prebiotic condition for "origine of life". The simple functionality and structural flexibility of peptide made it as an attractive architecture in the development of self-assembled nanostructures. The self-assembly of single and more polypeptide chain leads to formation of complex structure which are known as proteins. Chemically, proteins are formed of amino acids, bound by peptide bonds. Proteins are very important bioarchitectures which serve a wide range of functions in living organisms. They are the basic structural elements in cell, tissue and organism, fulfilling a series of functions. The high variety of the properties of these macromolecules is due to the immense possibilities of arrangement of monomeric units.

1.3 Conformational Analysis of Peptides and Proteins

1.3.1 Primary Structure

There are 20 natural amino acids which are involved in the synthesis of peptides and proteins in biological cells. Except glycine (G), all are chiral and exist in the L-form in nature. In all natural α-amino acids, same carbon atom contains both the $-NH_2$ and -COOH functionalities. Peptides adopt specific configurations depending on the amino acid sequence in its backbone.

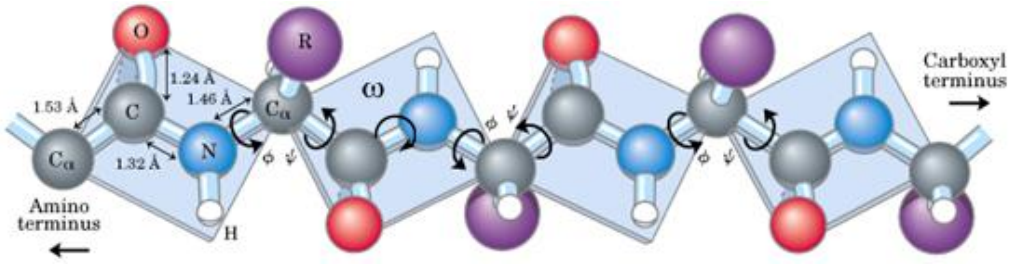

Figure 1.4. *Peptide backbone with dihedral angles φ (phi), ψ (psi) and ω (omega).*

The backbone dihedral angles φ (phi), ψ (psi) and ω (omega) of polypeptides are involved with the backbone atoms C-N-C^{α}-C, N-C^{α}-C-N and C^{α}-C-N-C^{α} (Figure 1.4). The value of ω is ranging from 180^{o} to 0^{o} depending upon the *trans* and *cis* conformations of peptide bond. The other two dihedral angles φ and ψ play a vital role for the backbone conformation of polypeptide chain. The Ramachandran plot based on sterically allowed values of φ and ψ is very important for understanding the secondary structures in polypeptides and proteins backbone.[21]

1.3.2 Ramachandran Plot

In 1963, G. N. Ramachandran developed an easy method to understand the polypeptides and proteins structure based on backbone dihedral angles φ and ψ in a steric contour diagram, known as Ramachandran plot. Assuming the hard sphere model of atoms with dimensions to their van der Waals radii, each conformation and structure was examined for close contacts between atoms. Therefore, φ and ψ angles have important significance to determine the sterically allowed or disallowed regions in Ramachandran plot. There are only three sterically allowed regions in this plot in which the values of φ and ψ angles produces the right-handed α-helix (common), left-handed α-helix (very rare) and β-sheets.[22] In the Figure 1.5, the white areas represented the sterically disallowed regions for all amino acids except glycine where atoms in the polypeptide are closer than the sum of their van der Waals radii.[23]

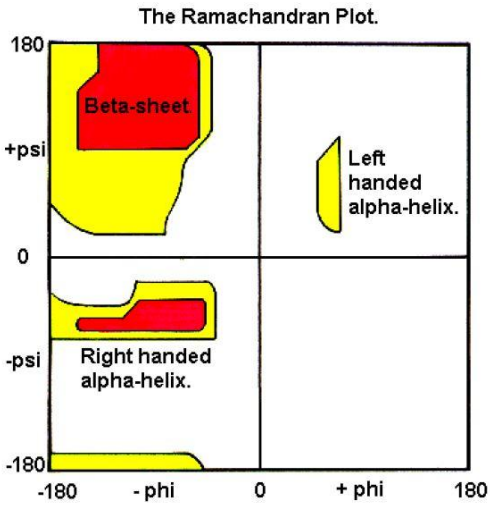

Figure 1.5. *The sterically allowed regions of regular conformations of the polypeptides and proteins on a Ramachandran plot.*

The red regions in this plot are corresponding to the allowed regions for right-handed α-helix and β-sheets. The yellow areas indicate the allowed regions if slightly shorter van der Waals radi are used in the calculation.This reveals an additional

region corresponding to the left-handed α-helix. 3_{10}-helix occurs close to the upper right of the α-helical region and is on the edge of allowed region indicating lower stability. Therefore, the diversity of secondary structures is generated with the various sets of dihedral angles.

1.3.3 Secondary Structures

The regular folding patterns depending on the dihedral angles φ (phi), ψ (psi) and ω (omega) of polypeptide chain in a protein is known as secondary structure. It is a regular and repetitive organization, stabilized by hydrogen bonding interactions between the components of the polypeptide chain. In 1951, Linus Pauling *et al.* proposed the two main types of secondary structure of protein as helices and β-sheets.[24] Beside them, reverse turns are also exist in protein structures.

(a) Helices

Helices are the well-studied secondary structures which are frequently found in polypeptides and proteins. Helices are stabilized through the hydrogen bonding interactions. Various types of helices are reported.[25] These are given below.

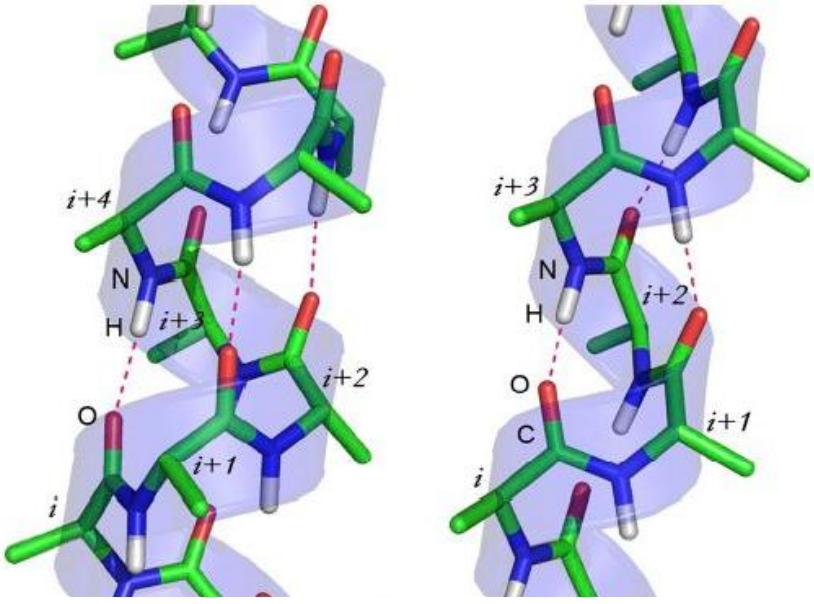

Figure 1.6. *Side views of α-helical conformation (left) and 3_{10}-helical conformation (right). Dotted lines indicate hydrogen bonds between atoms in the backbone of polypeptide.*

(I) α-helix

The α-helix is a common rigid arrangement of polypeptide chain (Figure 1.6). There are two types of α-helixes which are known as right-handed α-helix (φ, -57; ψ, -47) and left-handed α-helix (φ, 57; ψ, 47) depending upon the screw direction of the polypeptide backbone.[26] The left-handed α-helix is sterically not allowed for L-amino acids due to the close proximity of the side chains and the C=O group.[27] The α-helix arrangement is stabilized by the hydrogen bonding interaction between the carbonyl group of residue *i* and the nitrogen of the amide group in residue (*i*+4).[28] The α-helix has a periodicity of 3.6 residues per turn so that the consecutive residues make an angle of 100° around the helical axis with a helical rise per residue of 1.5 Å and a helical pitch of 5.4 Å.

(II) 3_{10} helix

3_{10} helix is less abundant compare to α-helix in protein structure.[29] The hydrogen bonding in 3_{10} helix occurs between the carbonyl group in residue *i* and the nitrogen of the amide group in residue (*i*+3), where 10 atoms are associated in the ring formed by making the hydrogen bond. 3_{10} helix has three residues per turn with an angle of 120° between consecutive residues.[30] The helical rise per residue of 1.93-2.0 Å, and a helical pitch of 5.8-6 Å are reported for 3_{10} helix (Figure 1.6). Generally, a 3_{10} helix is more tightly bound, longer, and thinner than a α-helix with the same number of residues. The 3_{10}-helix typically adopts dihedral angles (φ, ψ) near (-49°, -26°).[31] 3_{10}-helix most often occurs as a single turn transition between the end of an α-helix and the next portion of the polypeptide chain.

(III) π-helix

π-helix is extremely rare within protein crystal structures. The π-helix is more loosely arranged than the α-helix via the *i* to (*i* + 5) hydrogen-bonding pattern between carbonyl oxygen and nitrogen backbone atoms.[32] A amino acids in a standard π-helix are arranged in a right-handed helical structure. Each amino acid corresponds to an 87° turn in the helix and a translation of 1.15 Å along the helical axis. A single turn of π-helix contains 16 atoms, and thus the π-helix is defined as a 4.4_{16}-helix.[33]

(b) β-Sheets

The β-sheet is the second form of regular secondary structure in proteins. β-sheet is almost extended rather than being tightly coiled as in the α helix. In β-sheet, the dihedral angles (φ, ψ) are close to -120°, 140° which fall in the sterically allowed region in upper left quadrant of the Ramachandran plot.[34] Most of the β strands are arranged adjacent to the other strands and form an extensive hydrogen bonding network in which the N-H groups in the backbone of one strand create hydrogen bonds with the C=O groups in the backbone of the adjacent strands. The distance between adjacent amino acids along a β-strand is approximately 3.5 Å. The side chains of adjacent amino acids point in opposite directions. There are two types of β-sheets which are known as parallel β-sheets and antiparallel β-sheets (Figure 1.7). In parallel β-sheets arrangement, the two adjacent strands are running in the same direction held together by hydrogen bonds between the strands but the successive strands are running through in opposite direction in antiparallel β-sheets arrangement.[35,36]

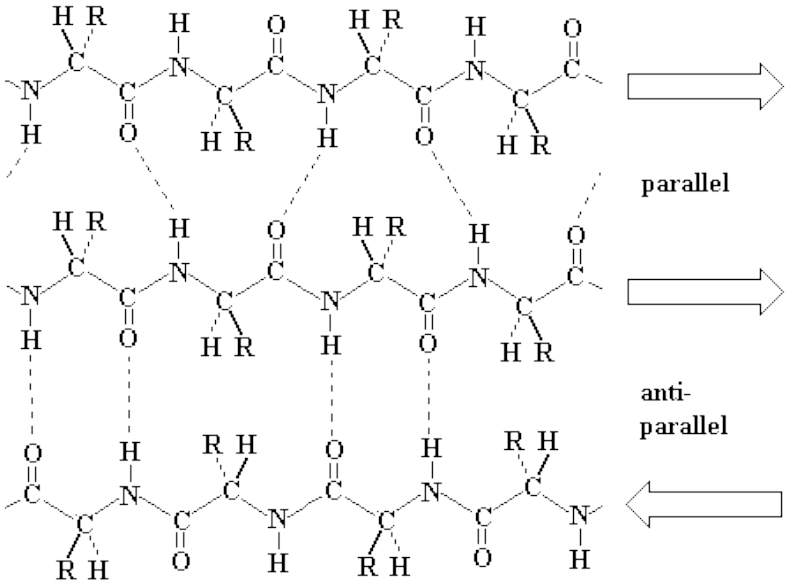

Figure 1.7. *The hydrogen bonding patterns in parallel and antiparallel β-sheet arrangement. The direction of peptide strands are marked with arrows and hydrogen bonds are shown with dash lines.*

The antiparallel β-sheet arrangement is more stable than parallel β-sheet arrangement because it allows the inter-strand hydrogen bonds between carbonyls and amines to be

planar, which is their preferred orientation. The peptide backbone dihedral angles (φ, ψ) are about (-140°, 135°) in antiparallel sheets. The parallel β-sheets orientation is slightly less stable because it introduces non-planarity in the inter-strand hydrogen bonding pattern. The dihedral angles (φ, ψ) are about (-120°, 115°) in parallel sheets. The β-sheet model is found both in fibrous and globular proteins. The higher ordered association of β-sheets is implicated in the formation of the protein aggregates and fibrils observed in many human diseases, such as Alzheimer's disease and Parkinson's disease.[37]

(c) Reverse turns

Turns are the third 'classical' secondary structures in proteins. In 1968, Venkatachalam found the presence of turn structures in the peptides and proteins.[38] Turns are classified into α-turn, β-turn and γ-turn according to the separation between the two end residues.[39]

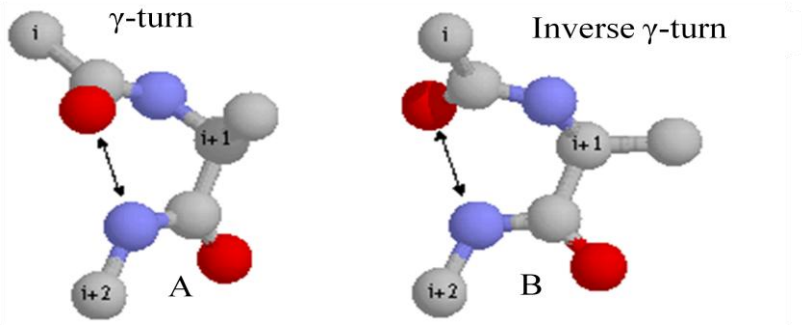

Figure 1.8. *γ-turn and reverse γ-turn.*

In β-turn, hydrogen bonding occurs between the carbonyl oxygen of residue *i* and the amide nitrogen of (*i+3*) where as in γ-turn, it is between the carbonyl oxygen of residue *i* and the amide nitrogen of (*i+2*) (Figure 1.8). A turn can be transformed into its inverse turn (*mirror image turn*) by changing the sign on all of its dihedral angles. As an example, the γ-turn has two forms, a classical form with (φ, ψ) dihedral angles of roughly (75°, -65°) and an inverse form with dihedral angles (-75°, 65°). Three types of important β-turns (Figure 1.9) and its mirror image conformations are designated as I, II, III and I',

II', III'.[40,41] Several examples of reverse turn structures in peptides and proteins have been reported in literature.[42]

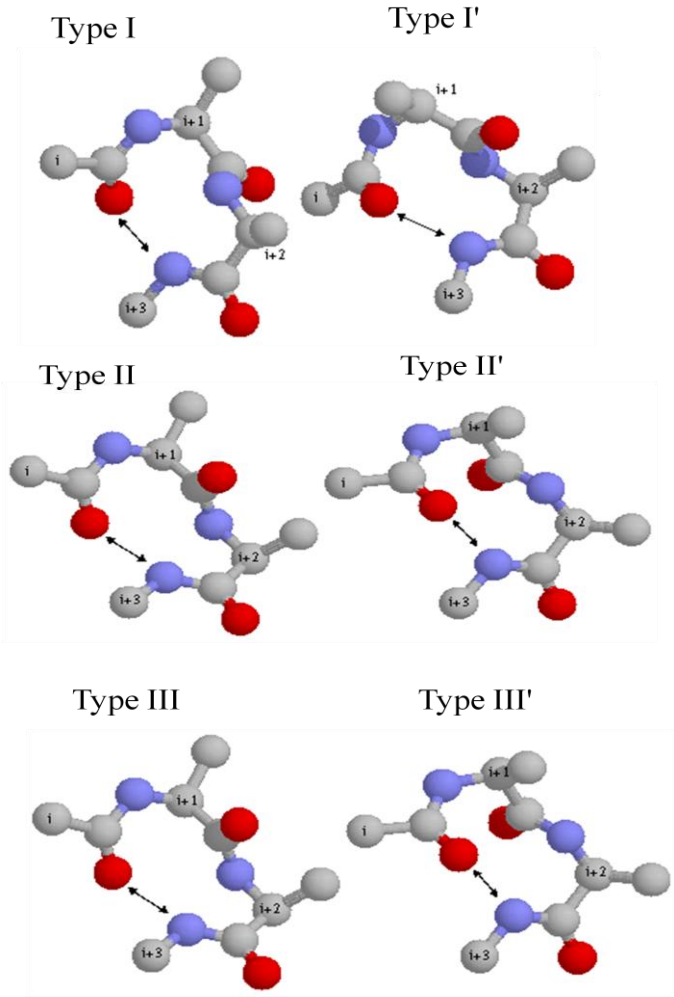

Figure 1.9. *Various types of β-turns (types I and I', types II and II', types III and III').*

The peptide and peptide derivatives are very attractive due to their structural diversity, folding and their function. The several hydrogen bonding site on the backbone and optimum hydrophobic/hydrophilic balance make them an ideal self-assembling architectures among all the biomolecules. The peptide and peptide based molecules self-assemble into well-defined secondary structures, which on further assembly to form supramolecular hierarchical nanostructures. The formation of higher ordered hierarchical structures may lead the formation of a gel. Various stimuli such as sonication,[43,44]

light,[45] temperature,[46] pH,[47] metal ions[48] and enzyme [49] can tune the self-assembly and gelation process. The supramolecular gel is explaned below.

1.4 Supramolecular Gel

Gels are unique soft solid materials used in our daily life in the form of commercial products such as soap, shampoo, toothpaste, hair gel and other cosmetics, as well as contact lenses and gel pens *etc*. They have a wide range of applications in the fields as diverse as food, medicine, materials science, cosmetics, pharmacology, sanitation *etc*.[50] In 1974, Flory gave a definition of gel as ‘‘a gel has a continuous structure that is permanent on the analytical time scale and is solid-like in its rheological behavior.’’[51] In general, gels are viscoelastic semi solid-like materials with an elastic cross-linked network formed from the entrapment of solvent which is the major component. The solid-like appearance of a gel is a result of the entrapment and adhesion of the liquid in the large surface area solid 3D matrix. The formation of the solid matrix is a result of cross-linking of the polymeric strands of (macro) molecules by physical or chemical forces. As gel is a semi-solid material, it has own shape and free-standing ability which is easily tested by the simple test tube inversion method. It is made of about 99% of a liquid and of 1% of a solid gelator component. Gelatin is the first studied gelator which is a mixture of peptides and proteins. It can entrap water and forms a semi-solid colloid gel. The biodegradable and biocompatible gelatin is frequently used in the fields of pharmaceutical and medical applications.[52] Several kinds of gels have potential applications in biomedical science, due to their high water content and mechanical similarity to natural tissues. Gels can be classified into chemical gels and physical gels (Figure. 1.10). Chemical gels[53] are actually made *via* the formation of covalent chemical bonds, while physical gels are characterized by dynamic cross-links that are constantly created and broken, changing their state between solid and liquid under influence of environmental factors. Now a day, ‘low molecular weight gelators’ (LMWGs) attract tremendous attention in the field of research. The gelation mechanism of such class of molecules depends on a hierarchical self-assembly process which occurs through various types of non-covalent interactions such as hydrogen bonding, π-π stacking, van der Waals interactions to form supramolecular assembly referred to as fibrils. The fibrils often then

assemble into higher ordered supramolecular structures referred to as fibres which can entrap the solvent molecules and interact with one another to form a self-supporting semi solid gel material.

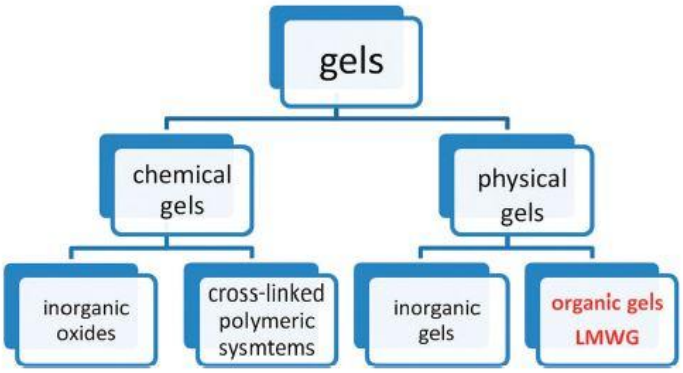

Figure 1.10. *General classification of gels.*

Some useful definitions are given below.[54]

Hydrogel: a gel made of a LMWG and water.

Organogel: a gel made of a LMWG and any kind of organic solvent.

Xerogel: a solid formed after evaporation of the solvent in a hydrogel or an organogel by drying with unhindered shrinkage. Xerogels usually retain high porosity (15–50%) and enormous surface area, along with very small pore size (1-10 nm).

Aerogel: a solid material formed when solvent removal occurs under supercritical conditions. The network does not shrink and a highly porous, low-density material is produced. Aerogels have some exceptional properties including very low density, high specific surface areas, and excellent thermal insulation properties.

Recently, peptide and peptide based gelators draw a great interest due to their biodegradable, biocompatible and non-toxic nature. Bing Xu *et al.* (2007) reported an enzymatic hydrogelation inside E. coli, and the subsequent intracellular hydrogelation inhibited the growth of the bacteria.[55] Ulijn group (2006) demonstrated the spontaneous self-assembly of Fmoc-dipeptides into fibrous hydrogels under physiological conditions.

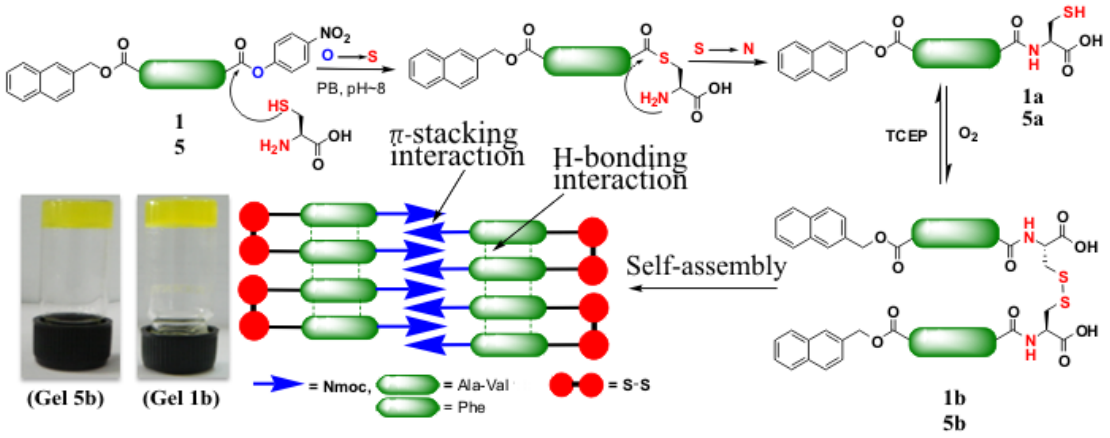

Figure 1.11. *Native chemical ligation at Nmoc-protected-p-NP esters. The cysteine amino acid induces O-S exchange with Nmoc-protected-p-NP* ***1*** *or* ***5*** *(step I) to form a thioester intermediate. Subsequent S - N acyl transfer furnishes the peptide bond* ***1a*** *or* ***5a*** *(step II). Air oxidation provides the formation of ligated disulfide* ***1b*** *or* ***5b*** *(step III) resulting in supramolecular peptide gels. (Ref: 57)*

The fibrous hydrogels were used as biomaterial for supporting cell culture of chondrocytes in two and three dimensions.[56] Our group recently (2013) described the oxo-ester mediated native chemical ligation (NCL) reaction as a promising route of peptide self-assembly to design supramolecular nanofibrious self-supporting gels.[57] Cysteine is efficiently coupled with Nmoc-protected peptide oxo-esters to form amide bond via NCL reaction. The supramolecular gels are formed via oxidation of the Nmoc-protected peptides synthesized via the NCL reaction (Figure 1.11). Apart from N-capped peptide, the peptide bolaamphiphiles are also promising building block to design supramolecular nanostructures.

1.5 Bolaamphiphiles

Besides the peptides and other amphiphilic molecules,[58,59] a special class of self-assembling building block is known as bolaamphiphile (two-headed amphiphile).[60,61] They are named after the ‘bola’ because of the structural similarity of a South American weapon ‘bola’ which is made of two balls connected by a string. In a bolaamphiphile molecule, there are two hydrophilic head groups connected by a hydrophobic spacer.[62] As with conventional amphiphiles, the chemical functionality of the head groups and

spacer can be varied to tune the self-assembling behavior of bolaamphiphiles. Archaebacterial plasma membranes, existing in harsh environment, contain preferentially bolaamphiphilic compounds as constituents. As they have two hydrophilic head groups separated by one or two hydrophobic spacers, they exhibit no polymorphism as compared to simple amphiphiles. They form relatively thinner monolayers than bilayer membranes. They can also create spherical vesicles by incorporating the unsymmetrical hydrophilic headgroups.[63]

Chart 1. *Various types reported of bolaamphiphiles.*

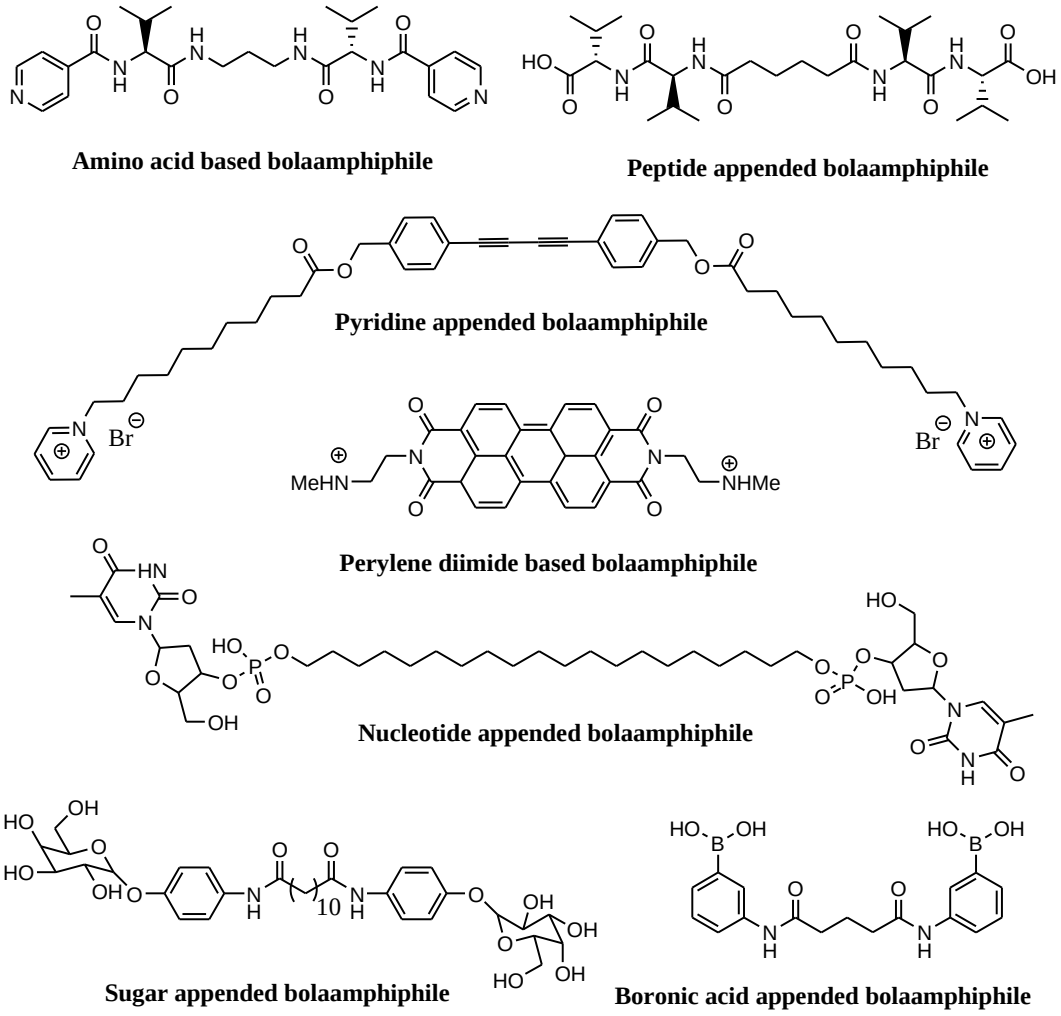

These structural advantages of bolaamphiphiles amplify the stability of the self-assembled membranes as compared to mono-head amphiphiles. By increasing the hydrogen bond energy and the number of hydrogen bonding site in a bolaamphiphile, we can tune the self-assemble process to form supramolecular high-axial ratio nanostructures[64] including linear ribbons, helical ribbons, and tubular structures, depending on the molecular chirality. Several groups have designed several types of bolaamphiphiles[65,66] carrying sugar, peptide, and nucleobase moieties with potential multiple hydrogen bond functionalities as a hydrophilic group at both ends, which are connected by various types of hydrophobic spacer (chart 1). Several groups have also reported the convenient route to design hydrogel, organogel and liquid crystal with the bolaamphiphile skeletons.[67-71]

1.6 Vesicle Forming Bolaamphiphiles

Bolaamphiphiles are interesting building blocks which can self-assemble to produce various types of nanostructures such as nanovesicle, nanofibers, nanotubes and others. Among them, 0D vesicle is one of the important nanostructures which have potential applications in biosciences and nanosciences. Vesicles are colloidal aggregates that are mostly spherical in shape which can entrap solvent molecules. An unsymmetric bolaamphiphile with a large headgroup of succinic acid at one end and a smaller headgroup of sulfonate at another end formed small vesicles where the two carboxylate groups of succinic moiety were all on the outer surface and the smaller sulfonate groups exclusively at the inner surface.[72] A unique unsymmetrical bola was reported containing two unsymmetrical hydrophilic head groups called carboxylic acid and a sulfonate group.[73] This bolaamphiphile self-assembled into large vesicles with diameters between 200 and 500 nm which were observed in TEMs. Another fullerene containing bolaamphiphile was investigated and was found to produce vesicles with a diameter of about 30-50 nm upon sonication.[74] A phenyl (bis salicylideneimine) unit based bolaamphiphile with two cationic head groups also formed vesicles.[75] Sugawara *et al. (2008)* developed a self-reproducing system of giant multi-lamellar vesicles (GMVs). The hydrolysis of a bolaamphiphile, *N*-[10-[4-[[4-[2 (trimethylammonio) ethoxy] phenyl] imino] phenoxy]-decyl]-*N*-dimethyl-*N*-dodecylammonium dibromide directed to form a

membrane molecule with two hydrophobic chains *N*,*N*-dimethyl-*N*-[10-(4-formylphenoxy)-decyl]-*N*-dodecylammonium bromide which self-assembled into giant multilamellar vesicles.[76] Huang and coworkers *(2003)* observed the formation of nanovesicles with a diameter of about 20-60 nm from the mixture of simple structured bolaamphiphiles, sodium eicosanedioate ($NaOOC(CH_2)_{18}COONa$, or SEDA), and conventional cationic surfactant dodecyltriethylammonium bromide (DEAB). This is an example of first synthetic mixed vesicles which are stable at high temperature over 80 °C.[77] Again, a novel bolaamphiphilic pillar[5] arene was reported which can spontaneously form responsive reverse multilamellar giant vesicles in chloroform and a gel in water-tetrahydrofuran (5 : 1, v/v). These vesicles were not only stable for weeks, but also showed reversible thermal and dynamic properties under external physical stimuli. KPF_6 and benzo-18-crown-6 were used as switches to turn-off and re-turn-on the assembly of vesicles. Moreover, the aggregation behaviour of this bolaamphiphilic pillar[5] arene was tuned by simply introducing host-guest chemistry. The gel showed reversible gel-sol phase transitions by heating and cooling, or adding and removing potassium cations (Figure 1.12).[78] Chen *et al. (2011)* demonstrated an orotic acid derived bolaamphiphile 1,12-diaminododecane diorotate (DDO) with molecular recognition functional moieties where both the self-aggregation behavior and molecular recognition with melamine were extensively studied. This bolaamphiphile self-assembled into vesicles in aqueous solutions at 25 ^oC. Hydrogen-bonding interactions played a vital role for the DDO monomer binding with melamine. The dissociation of the aggregates took place and were guided to form an entropically driven molecular recognition process at the higher concentration above its critical aggregation concentration. As complicated binding sites can be constructed through self-assembly at the vesicle interface rather than simple molecular modules, this bolaamphiphile with the molecular recognition functional group made it possible to generate well-defined recognition sites to mimic biomolecular receptors.[79] Bhattacharya *et al.* reported the modulation of vesicular properties by variation of shapes of bolaform counter ions in hybrid-ion paired surfactants.[80] A highly hydrophilic fused aggregates (microsponges) from a C12 spermine bolaamphiphile was also reported.[81] The aggregation of the bolaamphiphile 1,12-[*N*,N-bis(3-aminopropyl)-1,4-butane diamine] dodecane (12G1) molecule was found to take place in water at a

concentration of 1.75 mM as determined using various fluorescent and colorimetric probes and surface tension measurements. Electron microscopy images showed that 12G1 formed monolayer vesicles of 20 nm in size at a concentration of 2.6 mM and even larger fused aggregates when the concentration was increased to 35 mM.

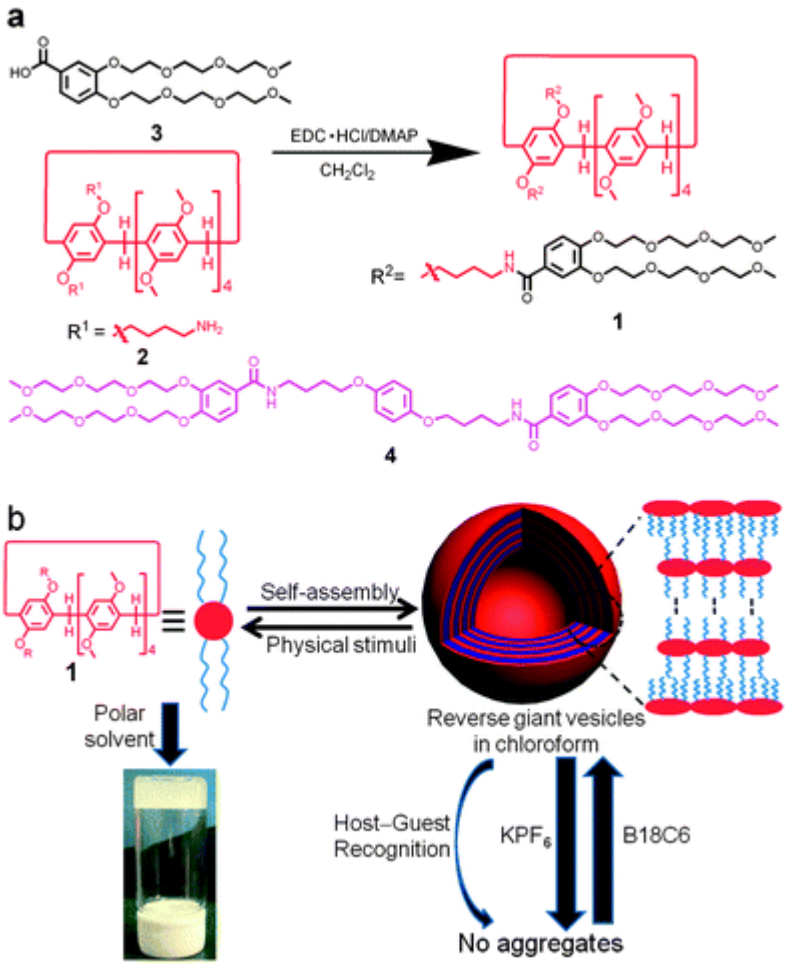

Figure 1.12. *(a) Synthesis of bolaamphiphilic pillar[5] arene **1** and chemical structure of model compound **4**, (b) pictorial representation of the formation of a gel in water-tetrahydrofuran (5/1, v/v) from **1**, the formation of reverse multilamellar giant vesicles (the red zones represent the hydrophobic pillar[5] arene skeletons and the blue parts denote glycol chains) in chloroform from **1**, and the reversible disassembly and re-assembly of the giant vesicles under external stimuli. (Ref: 78).*

1.7 Nanofiber Forming Bolaamphiphiles

The bolaamphiphiles can self-assemble into nanofibrillar morphology at higher order supramolecular level. The self-assembly of bipolar phosphocholine bolaamphiphiles were well-studied which were found to form nanofibers.[82.84] The temperature-dependent self-assembly of the single-chain bolaamphiphile dotriacontan-1,1′-diyl-bis[2-(trimethylammonio) ethyl phosphate] (PC-C32-PC) was investigated by Blume *et al*.[85] At room temperature the bolaamphiphile, in which two phosphocholine hydrophilic headgroups were connected by a C32 alkyl chain, found to form hydrogel by forming a dense network of nanofibers. Interestingly, the self-assembly process was not driven by hydrogen bonding interactions but solely by hydrophobic interactions of the long alkyl chains. With a thickness of roughly the molecular length, nanofibers showed a helical superstructure. The aggregation behavior of another bolaamphiphile dotriacontane-1,32-diyl-bis[2 (dimethylammonio)ethylphosphate] (Me_2PE-C32-Me_2PE) was investigated depending on the pH value. This bolaamphiphile self-assembled into helical fibers of approximately 5 nm thickness with an all-trans conformation of the alkyl chains. The nanofibers network entrapped water molecules to form hydrogel very effectively. It was found that the protonation of headgroups depends on the pH value of the solution which directly influenced the ability of the molecules to aggregate into fibers.[86] Shimizu *et al.(2001)* investigated the self-assembly behavior of complementary 1,ω-thymine, 1,ω-adenine, and 1,ω-(thymine, adenine) based bolaamphiphiles, [N,N'-bis[3-(2,4-dihydroxy-5-methylpyrimidine-1-yl)propionyl]1,n diaminoalkane [T-n-T (n) 10, 11, 12)], N, N'-bis[3-(6-aminopurine-9-yl)propionyl]1,n-diaminoalkane [A-n-A (n) 10, 11, 12)], and N-[3-(2,4-dihydroxy-5-methylpyrimidine-1-yl)propionyl], N'-[3-(6-aminopurine-9-yl)propionyl]1,n-diaminoalkane [T-n-A (n) 10, 11, 12)]. The spontaneous homo- and hetero-assembly of these nucleobase based bolaamphiphiles were well-studied. The supramolecular nanofibers with the width of 15-30 nm were observed from an equimolar mixture of T-10-T and A-10-A in 10% ethanolic/aqueous solutions. The heteroditopic T-12-A bolaamphiphile also self-assembled to form supramolecular fibers.[87]

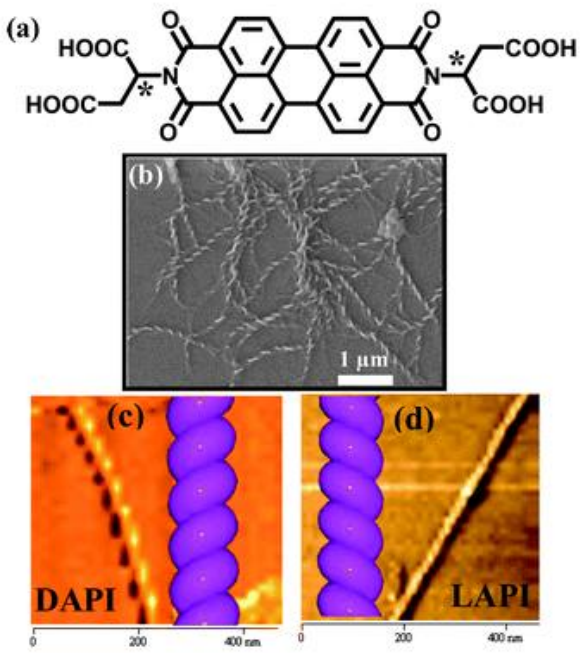

Figure 1.13. *(a) Molecular structure of an aspartic acid appended perylene derivative. (b) Typical FE-SEM image of a DAPI dried gel. AFM topology of (c) DAPI gel and (d) LAPI gel prepared on a freshly cleaved mica surface. (Ref: 96)*

Another bolaamphiphile (DMAPPC-C32-POH) was found to self-assemble in aqueous medium to form nanofibrous hydrogel at low pH value whereas at pH 10, only short fiber segments were formed without any gelation.[88] Reinhoudt *et al (2002)* reported an azobenzene based bolaamphiphile bearing sugar groups (*β*-D-glucopyranoside) as heads which self-assembed to form a nanofibrous hydrogel.[89]A new class of cyclohexane bis-urea based bolaamphiphile hydrogelators were also developed by Feringa *et al*. Gelation was obtained with organic solvents, water and strongly basic aqueous solutions like 25% ammonia. The hydrogels contain the network of fibers, in which all urea groups are involved in intermolecular hydrogen bonding interactions.[90] Amino acid based bolaamphiphiles are also excellent self-assembling precursor to form nanofiber. Novel bolaamphiphilic gelators on the basis of L-glutamic acid, with different lengths of alkyl chains as spacers, were developed by Liu and coworkers. Depending on the structure, bolaamphiphiles were able to form gel with a variety of solvents, from hexane to water/methanol mixture where nanofiber structures were obtained in nearly all the organogels.[91] Recently *(2012)*, a bolaamphiphile (5,5-B2NBr8) containing a functional

bipyridine moiety as the mesogenic core was reported which was found to self-assemble into uniform fibrous structure in aqueous solution, when the concentration was higher than critical micelle concentration.[92] The conformational and thermal behavior of a pH-sensitive bolaform hydrogelator has also been investigated which can assembled into nanofibrillar aggregates in higher ordered supramolecular level.[93] Recently *(2012)*, the binary self-assembly of a cytidylic acid appended bolaamphiphile (C18C) with small di- and tri-carboxylic acids, and the formation of supramolecular helical nanofibers of the C18C in lemon juice were reported. The citric acid containing lemon juice acts as a building block to form helical nanofibers via molecular recognition with the cytosine moiety. Only the binary self-assembly of C18C and malonic (MA), succinic (SA), glutaric (GA), and citric (CA) acids formed hydrogels and nanofibers at pH 4.7.[94] A series of bolaamphiphiles with 4-hydroxycinnamoyl head groups and different length of the alkyl spacers (n = 6-12) were designed. It was observed that both the length and odd-even number of the spacers can finely alter the molecular packing. The assemblies were changed from J aggregate to H aggregate when the spacer length was changed from 6 to 12 methylene units. For the assembly of bolaamphiphiles with odd-numbered spacers, diverse morphologies such as nanospirals and nanofibers were observed depending on the chain length and surface pressures. The spacer effect in the assembly can be understood from the cooperation between H bond of the phenolic hydroxyl and the amide groups, π-π stacking as well as the hydrophobic interactions of the alkyl spacer.[95] Recently, Malik *et al.(2013)* designed a pair of perylene based bolaamphiphiles (L-aspartic acid (S), LAPI, and D-aspartic acid (R), DAPI) with amino acid at each end which self-assembled to form hydrogel. Diluted solution of hydrogel of DAPI, showed the formation of right-handed helical fibers of 20 nm diameter with an average pitch length of 20 nm whereas LAPI hydrogel produced an entangled network of left-handed helical fibers of more or less the same diameter and pitch length (Figure 1.13). The non-covalent forces drove the formation of self-assembled nanofibers with a preferred helicity determined by the stereogenic centers. The hydrophobic core of the aggregated species forces them to coil until formation of the thick filaments that keep the original helical sense of the subunit. These fibers are stabilized by π-stacking of the aromatic perylene core and the hydrogen bonding interactions of the carboxyl groups.[96]

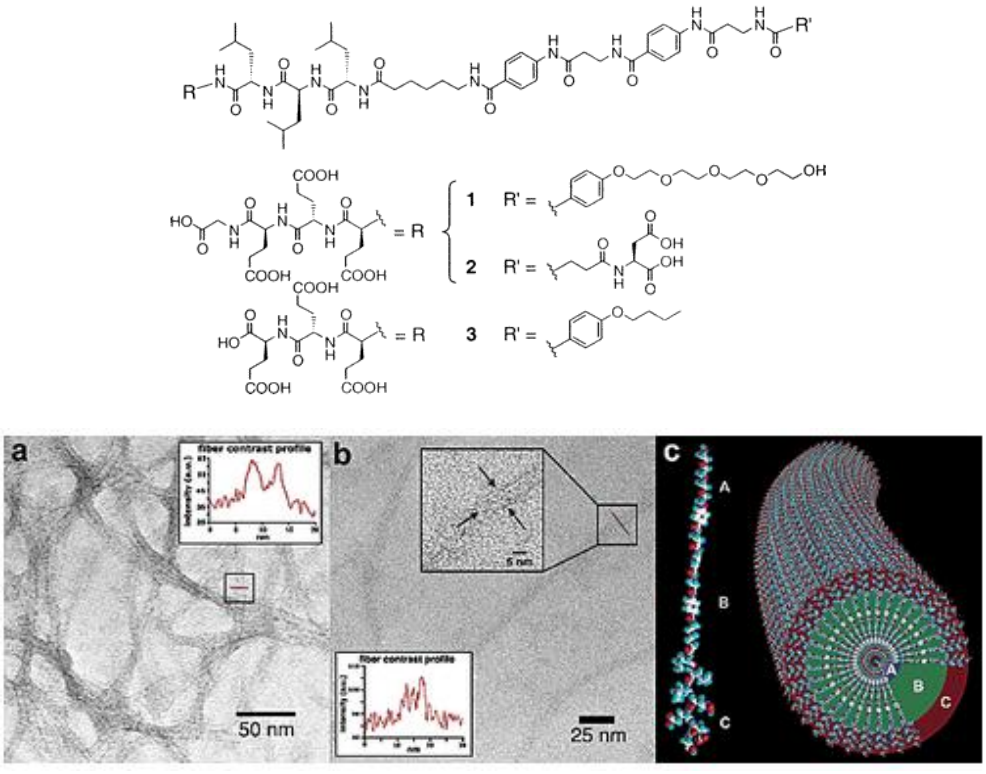

Figure 1.14. *The TEM image of **1** positively stained with uranyl acetate (a) shows the preferential staining of fiber peripheries, with line profile inset, and the TEM image of **2** positively stained with uranyl acetate (b) shows staining at both cores and peripheries, with line profile and high magnification insets. The molecular graphics rendition of the cross section of the nanofibers of **1** (c) illustrates hydrophilic domains A and C separated by the hydrophobic section B. (Ref: 104)*

Another report on a simple pH triggered gelation approach to fabricate well-defined nanofibers from a perylene based bolaamphiphile in aqueous media was demonstrated by Zang *et al*. The nanofibers as prepared exhibited strong fluorescence polarization and one-dimensional enhanced charge transport, both of which resulted from the anisotropic and enhanced electronic coupling between the intermolecular π-π stacking along the nanofiber.[97] Recently, Meijer group *(2013)* exploited an ureidopyrimidinone-poly-(ethylene glycol)s (UPy-PEG) based bolaamphiphile fiber.[98] Shimizu *et al*. envisaged the binary self-assembly of nucleotide appended fiber forming bolaamphiphiles.[99,100] The Quaternary self-assembly of a thymidylic acid-appended bolaamphiphile, with

heteropolymeric DNA as a template, produced supramolecular helical nanofibers in the presence of specific target DNA.[101]

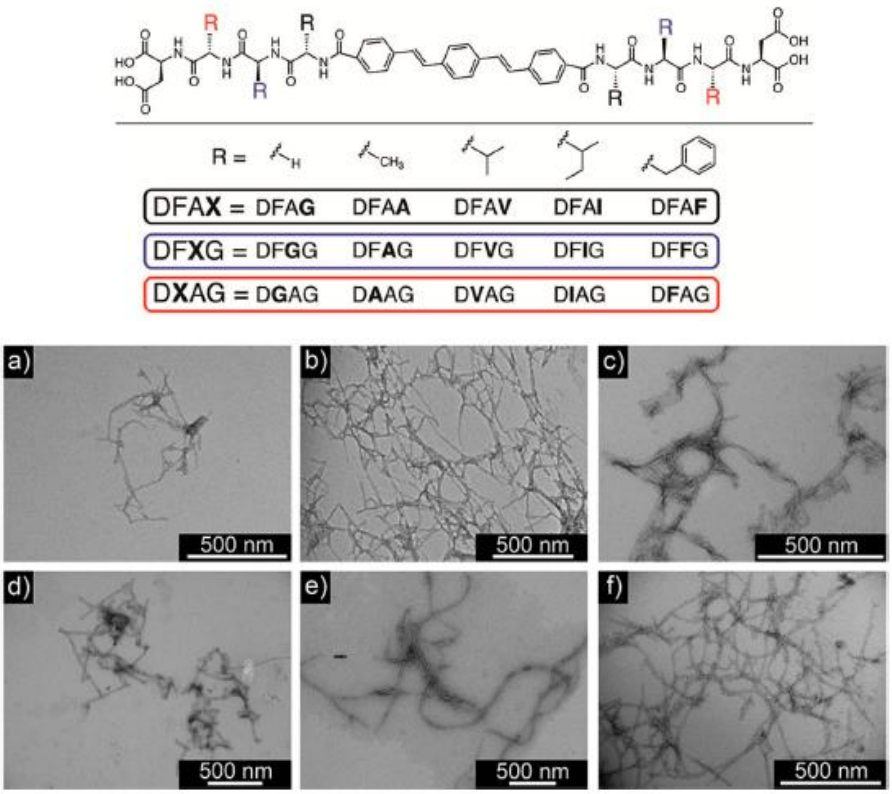

Figure 1.15. *Structures of various types of peptide appended bolaamphiphiles (top). TEM images of peptide nanostructures composed of DFAG (a), DFGG (b), DGAG (c), DFAV (d), DFVG (e), and DVAG (f) (bottom).(Ref: 107)*

Previously, Shimizu *et al. (1998)* investigated the self-assembly of dicarboxylic L-valyl-L-valine bolaamphiphiles in aqueous medium. The bolaamphiphiles formed nanoscale fibers with widths of 10-30 nm, *via* proton-triggered self-assembly in water, which were dominated by both intralayer, lateral hydrogen-bond networks between end carboxylic acid groups and parallel β-sheet networks between amide groups.[102] It has been reported that perylene bolaamphiphiles self-assembled with melamine to form hydrogel. The luminescent gel network was formed by H-type aggregation of the perylene core, supramolecularly cross-linked by melamine units. As a result of controlled aggregation, the extended fluorescent nanofibers were observed.[103] Previously, Stupp *et al.(2003)*

designed peptide based bolaamphiphiles. These peptide-based bolaamphiphiles self-assemble in water to form nanofibers with hydrophilic cores as well as hydrophilic surfaces (Figure 1.14). These nanofibers could be used as both bioactive structures as well as ion channels in biomedical applications.[104] They also demonstrated the self-assembly of novel peptidic quinquethiophene bolaamphiphiles that formed self supporting hydrogels at low concentrations. The bolaamphiphiles self-assembled into 1D nanofibers consisting of a π-π stacked thiophene core with amino acids on the periphery.[105] Tovar *et al. (2011)* found that the aligned nanofibers from peptide based bolaamphiphile hydrogel displayed unique photophysical and anisotropic electrical responses as evidenced by the alignment of representative π-conjugated peptide nanostructures.[106] Recently, the same group *(2014)* systematically presented peptide based bolaamphiphiles which self-assembled into nanofibrillar structures via π-π stacking interaction. The incorporation of various amino acids at specific residue locations along the molecular peptide backbone led to pronounced changes in the observed photophysical behavior of the fibrillar structures (Figure 1.15).[107]

1.8 Nanotubular Bolaamphiphiles

Many amphiphiles and bolaamphiphiles can self-assemble to generate various morphologies, including micelles, rods, and vesicular aggregates.[108] Nanotube formation is, however, limited in example.[109,110] The reason for this limitation is that nanotube formation generally requires highly ordered molecular packing and anisotropic intermolecular interactions. Inspite of this limitation, some interesting examples of bolaamphiphiles based nanotubes are reported in literature. Fuhrhop *et al.(1993)* have reported the unsymmetrical bolaamphiphiles having one amino acid (D- and L-lysine or D and L-ornithine) head group and one ammonium chloride head group which self-assembled into rod micelles and nanotubes.[111] Unsymmetrical bolaamphiphiles containing D-glucose and carboxylic acid head groups were designed to produce nanotubular structures exclusively.[112] Previously, Matsui *et al.(2001)* reported peptide bolaamphiphile of bis(*N*-α-amido-glycylglycine)-1,7-heptane dicarboxylate, which assembled into tubular structure with the diameters of 20 nm to 3 μm in an acidic

solution (pH 6). This tubular structure is assembled through the intermolecular hydrogen bonding interactions between the amide and carboxylic acid groups.[113] It was found that, the bolaamphiphile peptide reassembled into well-organized macroscopic bundles of the peptide nanotubes in presence of Ni^{2+} ions, whereas, the addition of EDTA to a suspension of peptide nanotube bundles resulted in dis-assembly of the bundles into peptide nanotubes with diameters between 40 and 140 nm. A majority of the free amide sites of the peptide nanotubes were involved in the intercalation of nickel ions, which act as bridges to bundle adjacent peptide nanotubes.[114] A vitamin C based bolaamphiphile 1,12-diascorbyl dodecanedioate (BOLA12) was also observed to form well defined hollow nanotube in aqueous medium.[115] The self-assembly and molecular packing of an unsymmetrical bolaamphiphile, sodium 4-(6-hydroxyhexyloxy) cinnamate (SHHC) was studied which was able to form tube-like structures in aqueous solution at pH 9.2. With increasing pH from 9.2 to 12.0, the low-curvatured tubes transformed into spherical vesicles, which was in line with the increased outer leaflet head group area.[116] Parquette *et al. (2010)* have demonstrated the hierarchical self-assembly of a n-type nanotube. L-lysine appended naphthalene based bolaamphiphile which formed a transparent gel in water at concentrations as low as 1% (w/w). Transmission electron microscopy (TEM) revealed that the bolaamphiphile self-assembled to form micrometer-long nanotubes with uniform diameters of (12±1) nm. The nanotube assembles *via* a monolayer nanoring that further stacks into the nanotube structure (Figure 1.16).[117] Amino acid based bolaamphiphiles are found to self-assemble into hollow nanotubes.[118,119] Liu *et al.(2005)* reported the L-glutamic acid based bolaamphiphile N, N-eicosanedioyl-di-L-glutamic acid (EDGA) which can self-assemble into helical spherical-nanotubes in mixed solvent as methanol/water or ethanol/water.[120] The helical spherical-nanotubes were different from common nanotubes which are generally flat at the inner and outer surfaces of the tubes and the helical pitches are usually difficult to distinguish. In comparison with common nanotubes, this L-glutamic acid based bolaamphiphile spherical-nanotube was formed from a bent ribbon, while the conventional nanotubes were mediated from a flat sheet or ribbon. The glutamic acid based bolaamphiphiles nanotubes were used as the template to generate silica nanotubes.[121]

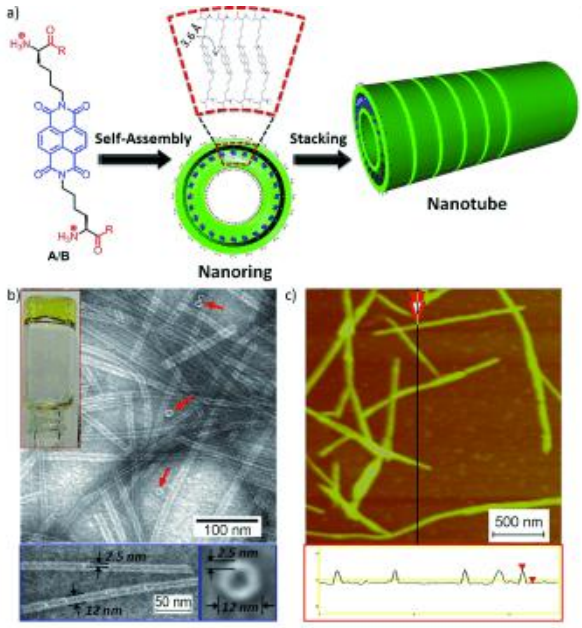

Figure 1.16. *(a) Structures of lysine-based bolaamphiphiles A (R=O⁻) and B (R = OMe) and the assembly of A into rings, which stack to give tubes. (b) TEM image of bolaamphiphile A in water (250 mm; carbon-coated copper grid); 2% (w/w) uranyl acetate as negative stain. Blue insets: Two nanotubes and one nanoring. (c) Tapping-mode AFM image of bolaamphiphile A in water (250 mm) on freshly cleaved mica. Red inset: Section analysis showing uniform height of the assemblies. Height indicated by red arrows: ca. 9 nm. (Ref: 117)*

Recently, Liu *et al. (2014)* established the fine tuning of the length, diameter and wall thickness of supramolecular nanotubes by using the co-assembly of two-component small organic molecules (Figure 1.17).[122] The hierarchical co-assembly of an L-glutamic acid based bolaamphiphile (HDGA) and melamine in water with different molar ratios could tune the dimension of nanotube. When HDGA and melamine are co-assembled with a molar ratio equal to 1:2, no nanotubes were found but the microspheres with diameters of 10-30 μm were detected. With increasing the molar ratio of HDGA/melamine to 1/4, well-defined supramolecular nanotubes were observed with the length, diameter and wall thickness of about 1 μm, 100 nm and 30 nm, respectively. The co-assembly with the molar ratio of 1/12 (HDGA/melamine) led the formation of larger supramolecular nanotube with length of 10 μm. The diameters were measured as greater than 1 μm and wall thicknesses of about 100 nm. Interestingly, when the amount of melamine was further increased (HDGA/melamine = 1/24), much shorter but perfect supramolecular

nanotubes were observed. The length of the nanotubes was about several micrometers, with the diameter reaching 500 nm and the wall thickness of about 50 nm. Interfacial assembly of cinnamoyl-terminated bolaamphiphiles into nanotube structure was also reported.[123] The sugar based bolaamphiphiles are the interesting precursor which can produce the well-defined nanotubular structure.[124]

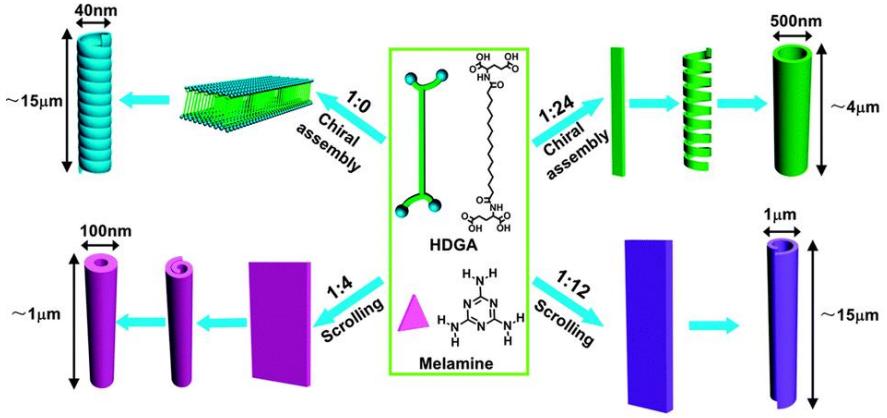

Figure 1.17. *Molecular structure of the bolaamphiphile (HDGA) and melamine; and model of formation of supramolecular nanotubes from a two component assembly with different molar ratios and mechanisms. (Ref : 122)*

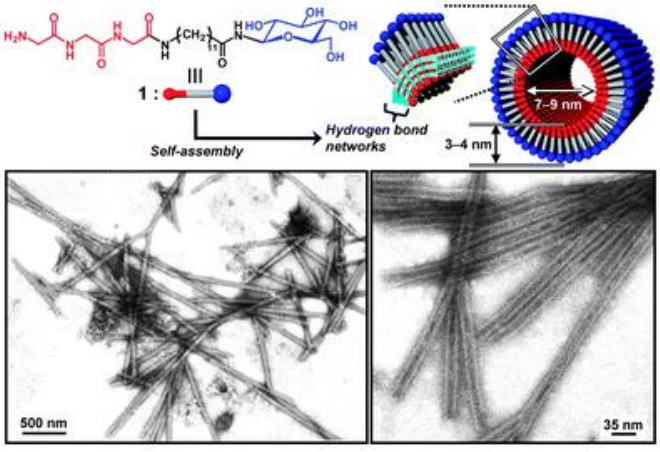

Figure 1.18. *A schematic illustration for the molecular packing of the organic nanotube with 7-9 nm inner diameters, which self-assembled from the asymmetric bolaamphiphile **1** (Top). TEM image of the organic nanotubes negatively stained with phosphotungstate. The hollow cylinder nanospace of the organic nanotubes can be visualized as it is relatively darker compared to its surrounding (Bottom). (Ref: 127)*

It was reported that unsymmetrical bolaamphiphiles, *ω*-[*N*-*β*-D glucopyranosylcarbamoyl] alkanoic acids, with even-numbered oligomethylene chains (12, 14, 16, 18, and 20 carbons) self-assembled in water to form nanotubular structure.[125] Shimizu *et al.(2009)* have demonstrated for the first time the self-assembly of supramolecular nanotube hydrogel consisting of a novel sugar and peptide appended bolaamphiphile by pH control under room temperature. It was found that the nanotube contained unique property of protein stabilization by encapsulation and slow release of a fixed protein without deformation of the nanotube hydrogel. Therefore, the nanotube hydrogel can be widely used as a novel soft material in biological and medical nanotechnologies.[126] Another similar bolaamphiphile, N-{11-[(β-D-glucopyranosyl)carbamoyl]undecanyl}-glycylglycylglycine amide was observed to self-assemble into an organic nanotube with 7-9 nm inner diameters, 3-4 nm thickness and several tens of micrometers in length which can encapsulate and release the guest molecules such as fluorescent dyes, oligo DNAs and spherical proteins efficiently (Figure 1.18).[127] A new family of oligopeptide-based bolaamphiphiles, with carboxylic acid head group at each end, has been accounted by Shimizu and his coworkers. Only sodium or potassium salts (acid soap) of the bolaamphiphiles produced well-defined tubular structure in aqueous medium. All the tubes were found to encapsulate a number of vesicular assemblies inside the aqueous compartment. The tube formation strongly depends on the connecting alkylene chain length, the alkylene even-odd carbon numbers, and constituent amino acid residues. Vectorial formation of acid-anion dimers and loose interpeptide hydrogen-bond networks are responsible for the tubular self-assembly.[128-131] Recently, sugar-bile acid-based bolaamphiphiles nanotubes were reported where the average tube diameter decreases with time.[132] The real time analysis showed that at early stage tubular scrolls were formed via the rolling of layers. At long time scales, a further evolution occurred where the tubules both elongated and became narrower. It demonstrated that scrolls were formed as intermediate structures in the self-assembly process of monodisperse single-walled tubules.

1.9 Ribbon, Sheet and Other Nanostructures Forming Bolaamphiphiles

There are many reports of bolaamphiphiles based vesicles, nanofibers and nanotubes but in addition of these nanostructures, bolaamphiphiles can adopt ribbon, sheet, rod and wire type structures at nanoscale. Zhang *et al. (2005)* reported the diaryldiketopyrrolopyrrole (DPP) dye based bolaamphiphiles having cationic head groups.[133] A series of bolaamphiphiles with different spacer lengths were synthesized, namely, 2,5-bis(n-(1-pyridinium)alkyl)-3,6-bis-(2-thienyl)-1,4-dioxopyrrolo[3,4-c]pyrrole ditosylate salts, abbreviated as DPP-n, where n (n = 7, 11, 15) corresponds to the number of methylene units in the alkyl chain spacer. Among them, the DPP-11 formed disk like structures with diameters ranging from several hundreds of nanometers to one micrometer in aqueous medium. It was found that disk like structures stack together to form double layers, triple layers, or even multilayers. The average thickness of the disk was about 3.7 nm. This value was good in agreement with the length of a single DPP-11 molecule, suggesting the disks form a monolayer structure with the thickness of a single molecule. The self-assembly of the bolaamphiphiles is mainly driven by the synergistic effect of hydrophobic and π-π stacking interactions. The same group have established the self-assembly of bolaamphiphiles containing electron-rich naphthalene (BNAPH and IBNAPH) and electron-deficient naphthalene diimide (BNDI) groups. [134] They proposed that when BNDI was complexed with BNAPH, an X-shape super-amphiphile would be formed, and the self-assembly of this superamphiphile would lead to one-dimensional nanostructures. The complexation of BNDI and IBNAPH would form an H-shape superamphiphile for the 2, 6-substitution of the two alkyl chains on the naphthalene, which favors the formation of two dimensional membranes (Figure 1.19). The self-assembly of the X-shape superamphiphiles of BNDI-BNAPH led to the formation of nanorod with a width of 3.7 nm which may arise from the face-centered packing of naphthalene and naphthalene diimide aromatic surfaces. The H shaped superamphiphiles of BNDI-IBNAPH formed two dimensional nanosheets with the average thickness of about 3.3 nm. Recently *(2014)*, the role of hydrotropic counter anions on the self-assembled structures of cationic bolaamphiphiles was investigated by Zhang *et al*.[135]

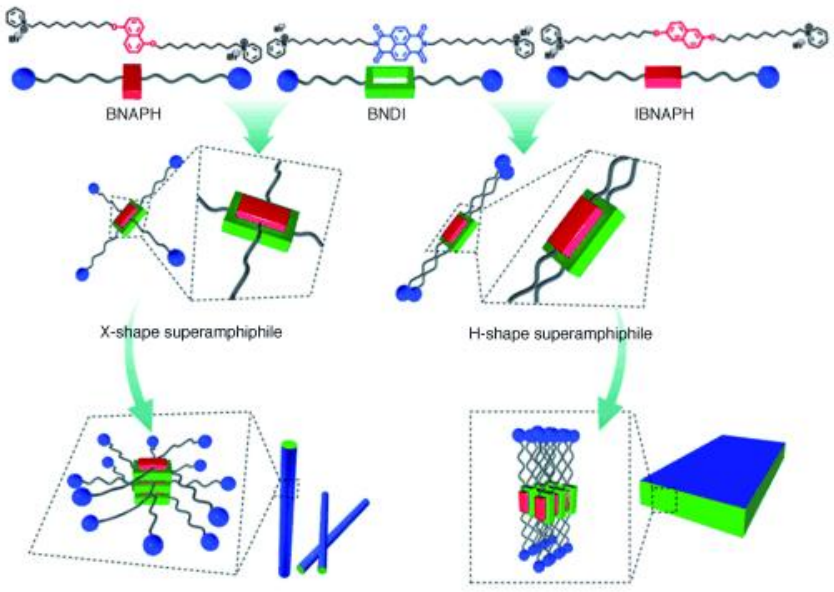

Figure 1.19. *Schematic representation of the X- and H-shape superamphiphiles and their assembly into one dimensional and two-dimensional nanostructures, respectively. (Ref: 134)*

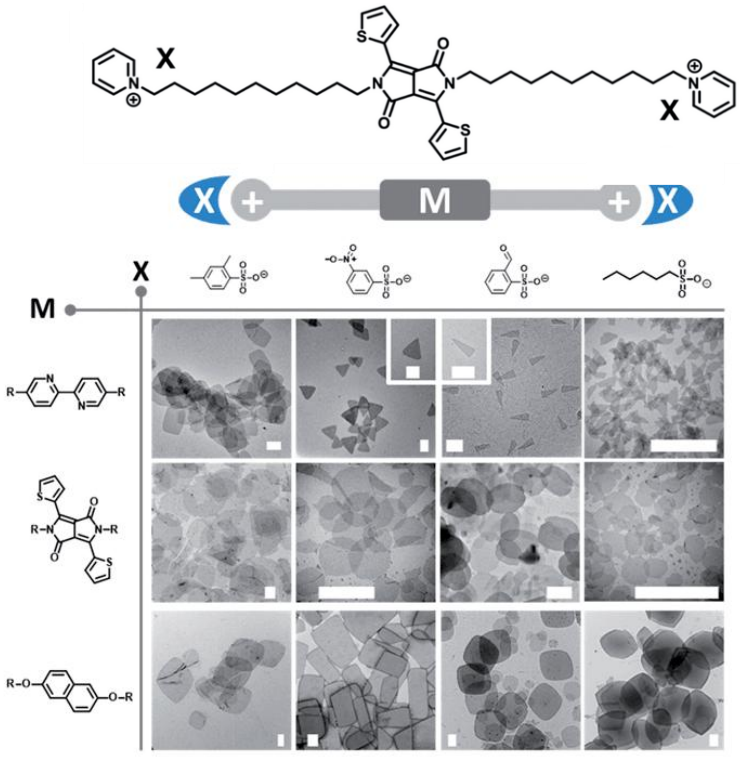

Figure 1.20. *The molecular structures of the effective counter anion and the embedded conjugated moiety both decide the shape of the obtained 2D planar structures. The scale bar is 2 μm. (Ref: 135)*

The hydrotropic counter anion can induce the formation of two-dimensional (2D) planar aggregates depending on its polar head, and the size and substitution pattern of its organic portion. 2D planar aggregates with triangular, quadrangular, and hexagonal shapes were observed by varying the counter anions which is one of the interesting organic self-assembled structures with controlled features (Figure1.20). It was reported that L-lysine appended tetrachloroperylene bisimide (Lys-4ClPBI-Lys) bolaamphiphiles spontaneously self-assembled into a uniform monolayer film in water at pH ranging from 9 to 1, due to synergistic interaction of directional π-π interactions and intermolecular hydrogen bonding.[136] The naphthalene diimide (NDI) bolaamphiphilic molecules were also found to self assemble in water to form organic nanoparticles.[137] Sijbesma *et al.(2010)* reported rod-like nanostructures from bis-urea based bolaamphiphiles.[138] Recently, Wang *et al.(2014)* nicely demonstrated that platinum (II) acetylide based bolaamphiphile equipped with two solvophilic B18C6 moieties on the periphery, exhibits a strong tendency to form spherical aggregates in a polar methanol/chloroform (3/1,v/v) solution. High-affinity host-guest molecular recognition directs to the cooperative complexation behaviors between L-alanine ester salt and the homoditopic platinum (II) acetylide bolaamphiphile. Interestingly, the disappearance of nanospheres derived from bolaamphiphile was visualized accompanied by the formation of disordered coagulated assemblies upon addition of L-alanine ester.[139] Formation of conducting wires from polythiophene based bolaamphiphiles were previously reported.[140] A filament-shaped, discrete artificial viruses, with β-sheet peptide-based supramolecular bolaamphiphile (Glu-KW) was also designed by Lee and his colleague.[141] The combination of hydrophobic and electrostatic interactions produced by the alternating placement of hydrophobic and charged amino acids in β-sheet peptides, promoted β-sheet interaction and subsequent self-assembly into bilayered filamentous β ribbon nanostructures. The β ribbon maintained its discrete and short nanoribbon morphology even after siRNA complexation. It is anticipated that this type of artificial virus will ultimately lead to the generation of safe and efficient artificial viruses for gene and drug delivery. It was observed that the mixed system of zinc ions, a bolaamphiphile, and triblock peptide copolymers led to the formation of nanoribbon hydrogels.[142] The self-assembly behavior of a new bolaamphiphile with a bistriazole-pyrene unit as the core and with two

pyridinium salt terminated alkyl groups, was investigated. Interestingly, this bolaamphiphile formed monomolecule-layer nano-ribbons through self-assembly in an aqueous solution. The strong π-π stacking interaction generated by the bistriazole-pyrene unit was responsible for the formation of 2D nanostructures.[143] Recently, one of the interesting example of self-assembly of self-complementary 2-guanidiniocarbonyl pyrrole 5-carboxylate zwitterionic bolaamphiphiles have been demonstrated by Schmuck *et al*. Aggregation of dimers of these zwitterionic bolaamphiphiles to higher supramolecular structures was achieved by introduction of *sec*-amide substituents at the 3-position. The 3-position substituted butyl amide led to self-assemble into one-dimensional nanorod-like stacks. Hydrogen bonding and π-π stacking interactions were supposed to promote this aggregation mode, which was further affected by the nature of the amide substituent (*e.g.*, steric demand), enabling the formation of bundles of strands or even two-dimensional sheets. Several typical nanostructures like vesicles, tubes, and flat sheets were formed reversibly under acidic conditions, which reassembled into the original rod-like aggregates upon readjustment to neutral pH.[144]

1.10 Nanostructural Transition

Precise control of supramolecular architecture is an important challenge in the field of self-assembly.[145] Self-assembly of biomolecules including peptides, proteins, lipids and nuclic acid based molecules has been an attractive research area by which it is possible to make vesicles,[146] nanotubes,[147,148] nanoribbons,[149,150] and helices.[151] The various shapes of these nanostructures are resulted from an interplay of several factors, including hydrophobic interactions, hydrogen bonding, electrostatic interactions, steric effects, and *π-π* stacking,[152,153] along with the possible involvement of growth kinetics.[154] The complex balance of these forces makes the self-assembly behaviour interesting and a further understanding of how these forces interact to evolve different morphologies, including metastable structures, is an important focus of current research. Several examples of peptide based nanostructural transition from one nanostructure to another nanostructure were reported.[155,158] Bolaamphiphile, an interesting class of amphiphile molecule also has drawn a great attention because of its ability to lead the morphological transformation from one nanostructure to another nanostructure in supramolecular level.

Liu *et al. (2010)* observed the morphological transformation with L-glutamic acid based bolaamphiphiles by varying the pH of aqueous solution.[159] Two bolaamphiphiles 1,4-butyloxy-bis(4-benzoyl-L-glutamic acid) (BECA4) and 1,12-dodecyloxy-bis(4-benzoyl-L-glutamic acid) (BECA12) were subjected to investigate the effect of pH on bola's morphology. At a low pH of 3, bolaamphiphile (BECA4) with short spacers formed hydrogel with nanofibrous morphology, whereas, bolaamphiphile (BECA12) with long spacer self-assembled into hydrogel with nanoribbon-nanotubular morphology. At high pH of 12, the nanofibers of BECA4 turned to vesicles but nanoparticles for BECA12 were observed at pH 12. The change in environmental pH can induce different interaction modes between the head groups of bolaamphiphiles which causes the morphological transformation from one nanostructure to another nanostructure. An L-histidine terminated bolaamphiphile (BolaHis) was recently *(2013)* reported to form hydrogels and self-assembled into single-wall nanotubes and single molecular thick fibers triggered by proton and copper ions, respectively. When BolaHis/Cu^{2+} hydrogels were transferred into BolaHis/H^{+} hydrogels, nanofiber was changed into single-wall nanotubes. The coordination of Cu^{2+} with the imidazole moiety caused the formation of micelles whose aggregation formed a long nanofiber with one-molecular thickness. On the other hand, the protonation of the imidazole may introduce a more stable MLM (monolayer lipid membranes) molecular packing through the hydrogen bond between the neighboring molecules. Due to the chirality of the head-groups, the MLM rolled into the nanotubes.[160] A new type of bolaamphiphile bearing bipyrimidine (bpym-8) was designed and synthesized. The bipyrimidine moiety allowed metal-ligand coordination, thereby influencing the self-assembly of the bolaamphiphile. It was found that bpym-8 self-assembled in water to form spherical aggregates. Interestingly, in presence of the Cu(II) ions the metal coordination with bpym-8 induced the assembly process to change the morphology from spheres to clustered aggregates. It was noted that the assembly of bpym-8 reversibly converted back by removing the Cu(II) ion from the coordination.[161] The rational design of two bola-amphiphiles containing naphthalene (BNAPHV) and naphthalene diimide (BNDIV) and programmable evolution of well-defined 1D and 2D nanostructures have been demonstrated by Zhang and his coworkers.[162]

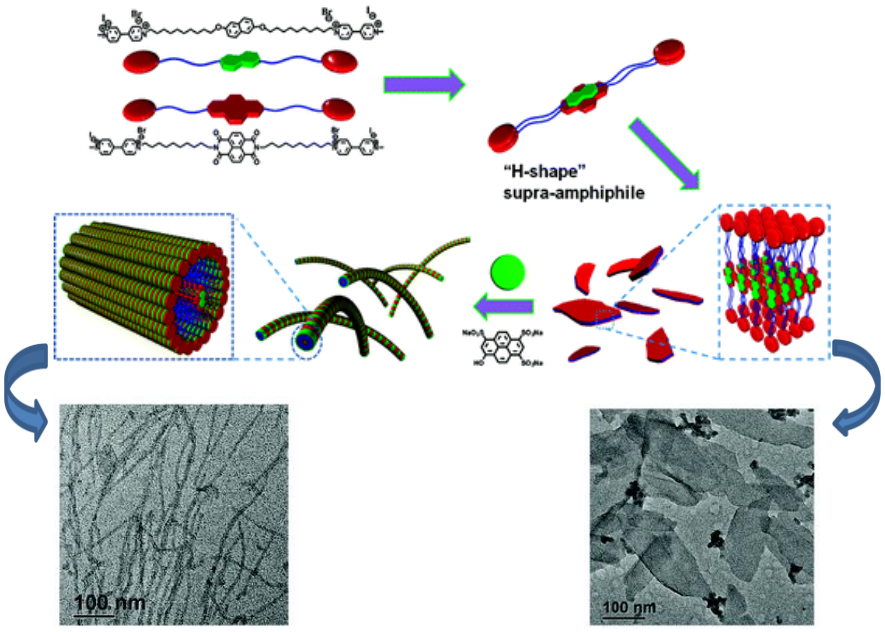

Figure 1.21. *Schematic representation of the morphological transformation from nanosheet to nanofiber by supramolecular bola-amphiphiles. (Ref: 162)*

First, H-shaped supra-amphiphiles were obtained on the basis of directional charge-transfer interactions of naphthalene diimide and naphthalene, leading to the rational fabrication of 2D nanosheets. Second, by complexation of the H-shaped supra-amphiphiles with 8-hydroxypyrene-1, 3, 6-trisulfonic acid trisodium salt (PYR), the nanosheets transform into ultralong nanofibers (Figure 1.21). The charge-transfer complexation of azulene-based bolamphiphile and pyrene in water was recently *(2013)* reported where the self-assembled nanostructures were found to interchange reversibly between cylindrical micelles and disk-like nanosheets in response to interaction with guest molecules.[163] For the last decade, Zhang and his coworkers has established that the self-assembly of cationic bolaamphiphiles usually self-assembled to form one dimensional (1D) or zero dimensional (0D) nanostructures, rather than two dimensional (2D) nanostructures. Recently *(2013)*, they have found a facile counter-ion directed structure switch for such bolamphiphilic moieties. 0D/1D structures formed by self-assembly of cationic bolaamphiphiles can be converted into 2D planar structures by a simple counter-ion change from bromide to tosylate. The cationic bolaamphiphiles (5,5-

B2NBr8) bearing mesogenic cores (CBMs) with counter ion as bromide self-assembled to form 1D fibers in aqueous solution. The same cationic bolaamphiphile aggregated to form 2D structures when the counter-ion was changed from bromide to tosylate. Thus, the counter-ion plays a crucial role in governing the self-assembled structure of CBMs. The strong binding between tosylate counter-ions and cationic head groups drives the formation of 2D planar structures.[164] The structral transition from vesicles to tubular structures has been studied in mixed systems of cationic bolaamphiphile BPHTAB[biphenyl-4,4′-bis(oxyhexamethylenetrimethylammonium bromide)] and its oppositely charged conventional surfactants SDS. This transition attributed that tube like structures are more stable aggregates than vesicles because of the special molecular packing in the aggregates of the mixed systems.[165] Fu *et al.(2007)* observed micelle-vesicle-tube transformation by changing the pH and the addition of NaBr or octanol. In the mixed systems of oppositely charged bola/surfactants, the molecular packing parameter's role was related to the mixing ratio.[166] The heptane bolaamphiphile, bis (*N*-R-amido-glycylglycine)-1,7-heptane dicarboxylate showed nanostructural transition depending upon pH of solution.[167] At pH 4, the heptane bolaamphiphile self-assembled into tubular structure but a helical ribbon structure was formed at pH 8. Nanostructural transition from helical ribbons to nanotube occurred within one day, while the reverse conversion, from the tubules to the helical ribbons, was ten times slower. The structural transition from microsphere to nanotube was also reported with the benzoic diacid diamide based bolaamphiphile by tuning pH from 8 to 7.[168] Shimizu *et al.(2013)* precisely controlled the self-assembled morphologies of asymmetric bolaamphiphiles, N-(2-aminoethyl)-N′-(β-D-glucopyranosyl) alkanediamide [1(n), n = 12, 14, 16, 17, 18, and 20], by association/dissociation with poly (thiopheneboronic acid) (PTB). The association of 0.5 equiv of the boronic acid moiety of PTB with the bolaamphiphiles led to produce nanotapes with parallel molecular packing, whereas, that molecular complex selectively formed nanotubes with antiparallel packing through a dissociation reaction of PTB based on the hydrolysis of the boronate esters in water. Changes in the length of the oligomethylene spacer of 1(n) never affected the molecular packing or self-assembled morphologies. However, it was found that the inner diameters of the nanotubes increased

irregularly in the range of 67.9-79.6 nm as the length of the oligomethylene spacer of 1(n) increased from n = 12 to n = 18.[169]

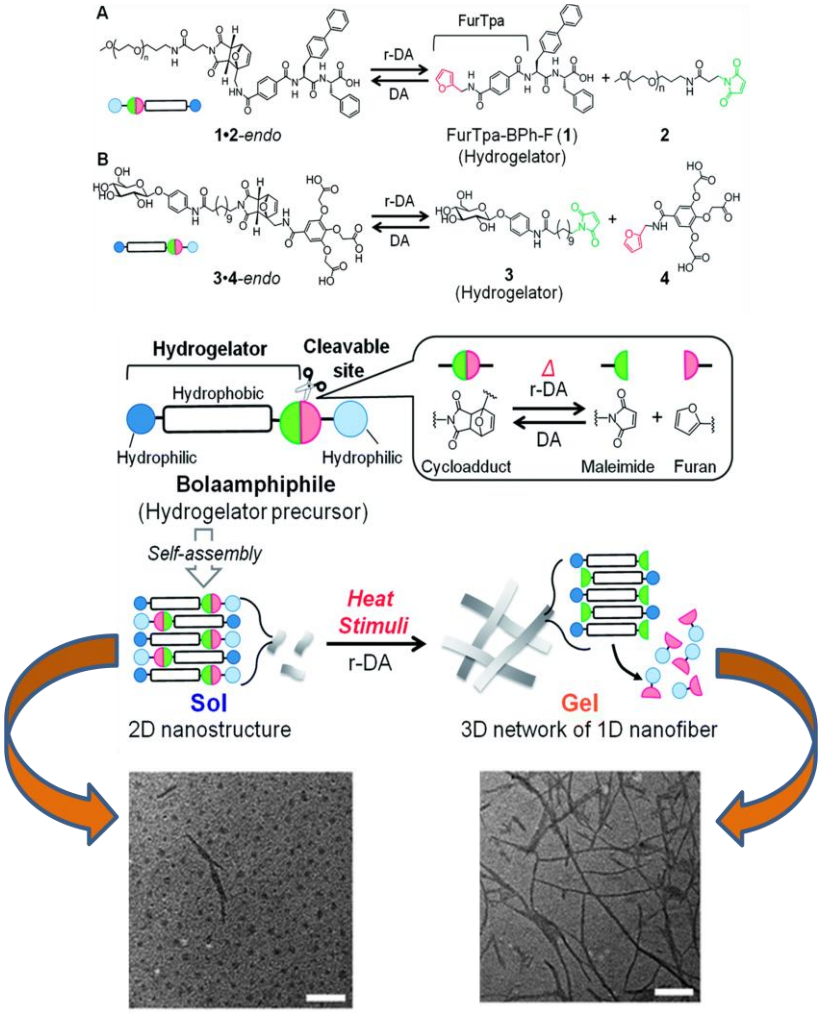

Figure 1.22. *Molecular structure of (A) bolaamphiphile **1·2**-endo constructed from a peptide based hydrogelator **1** bearing a furan and a water-soluble PEG-maleimide **2** through Diels-Alder reaction, and (B) bolaamphiphile **3·4**-endo **3** constructed from a glycolipid-based hydrogelator bearing a maleimide **3** and a water-soluble furan **4**. Schematic representation showing the morphological transformation from spherical aggregate to nanofibers via retro-Diels–Alder (r-DA) reaction (scale bar = 200 nm). (Ref: 175)*

Previously, Viguerie *et al.(2000)* reported the nanostructural transition by tuning the pH of the solution with E-urocanic acid based bolaamphiphiles.[170] Sol-gel phase transition associated with the nanostructural transition from vesicle to nanofiber in sugar-based bolaamphiphiles was explored earlier by Shinkai and his coworkers.[171] The pH-induced

nanostructural transformation of diacetylene based bolaamphiphiles from blue helical ribbons to red nanofibers was reported by Stevens *et al*.[172] Yao and his coworkers systematically investgated the leverage effect of the relative strength of molecular solvophobicity *vs.* solvophilicity on fine-tuning nanomorphologies of perylene diimide bolaamphiphiles.[173] Danino *et al. (2011)* reported the real time evolution of nanostructures from thin ribbon to nanotube with a lysine based bola type molecule N-α-lauryl-lysyl-aminolauryl-lysyl-amide.[174] Hamachi and his coworkers *(2014)* recently developed a unique heat-set supramolecular hydrogel, which was triggered by rationally designed molecular conversion of a glycolipid-based bolaamphiphile into a hydrogelator via retro-Diels-Alder reaction. The gel-sol transition is associated with morphological transformation of supramolecular nanostructures from short nanofibers and spheroidal aggregates (Figure 1. 22).[175]

1.11 Bolaamphiphiles Based Dynamic Combinatorial Library

Dynamic Combinatorial Chemistry (DCC)[176-179] is a promising tool to construct and study chemical complexity as it allocates easy access to molecular networks. For this requirement, dynamic combinatorial chemistry is a powerful approach to tune the self-assembly process with various conditions. The reversible covalent or non-covalent interactions of components result the compound libraries with dynamic composition which is sensitive to various reaction conditions. This process allocates spontaneous generation of all possible combinations of the components and finally it allows to one or two component(s) as major product(s) among the dynamic library members under thermodynamic control. It is expected that it should be possible to use dynamic combinatorial libraries to design molecules which are capable of their own formation through self-assembly in supramolecular level.[180,181] The equilibrium will shift toward the formation of favorable product(s) at the expense of the other library members when two or more molecules of a particular component of library members can stabilize one another through non-covalent interactions as hydrogen bonding and π-π stacking interactions in the formation of supramolecular structure.[182] The imine bond is one kind of dynamic covalent bond which is extensively studied. The first example of self-

assembly of dynamic covalent surfactants was shown by the group of van Esch.[183] This study demonstrated a new approach for pH and temperature-triggered on/off self-assembly of micellar aggregates by reversible displacement of the equilibrium between nonamphiphilic building blocks and their amphiphilic counterparts. The unfavorable equilibrium of imine formation in water was shifted by the stabilization of the product inside micelles. Upon acidification, stabilization of imines provided by the assembly was no longer sufficient, triggering disassembly of the micelles, making the system responsive to pH. Zhang and coworkers investigated the dynamic nature of imine bond formation with several bolaamphiphiles which is tuned by pH switches.[184,185] They reported the formation of dynamic imine bond which is used to bind two bolaamphiphiles together yielding H-shaped supra-amphiphiles. The self-assembly of the H-shaped supraamphiphiles produced the micellar aggregates (Figure 1.23). The benzoic imine bond can be hydrolyzed, leading to the dissociation of H-shaped supra-amphiphiles by changing the pH from basic to slightly acidic condition.

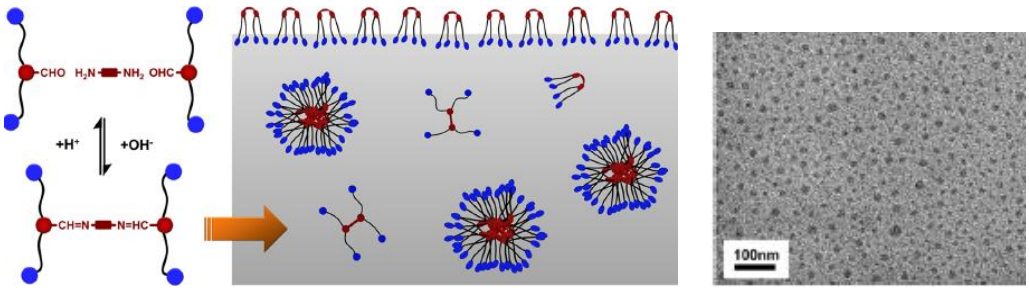

Figure 1.23. *Schematic illustration of the H-shaped supra-amphiphile and its behavior in water at the water-air interface and the formation of self-assembled micellar aggregate from the H-shaped supra-amphiphile. (Ref: 186)*

The H-shaped supra-amphiphiles showed a lower critical micelle concentration than their building blocks, which is very helpful by enhancing the stability of the benzoic imine bond being hydrolyzed by acid.[186] Sanders is one of the pioneer scientist in the field of interlocked molecules. His research mainly focused on the design of catenanes and knots type unusual interlocked molecules via DCC (dynamic combinatorial chemistry)

approach. Sanders *et al.* reported naphthalene diimide (NDI) and naphthalene based bolaamphiphiles as acceptor and donor building blocks to construct [2]-catenanes.[187]

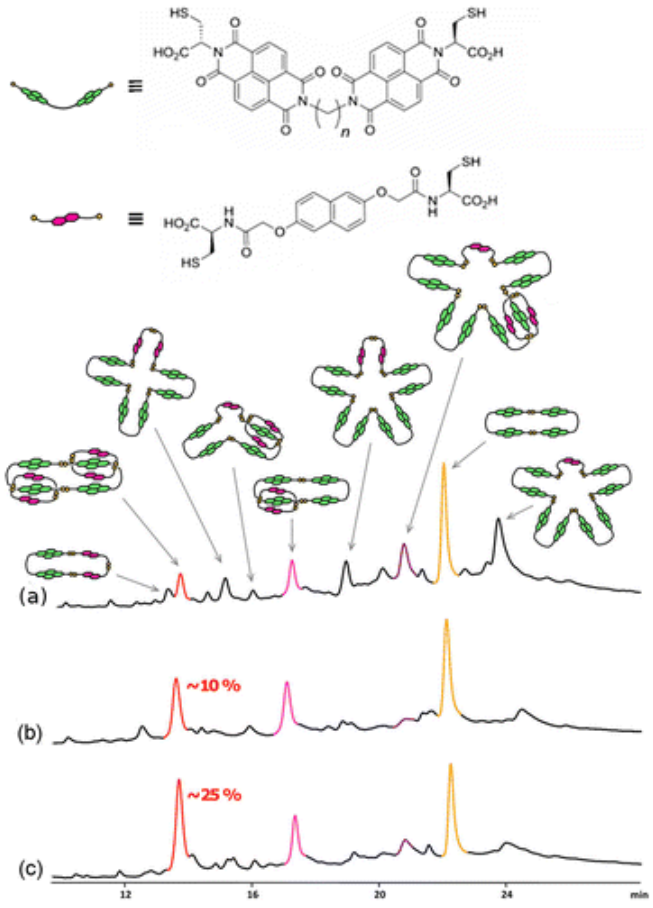

Figure 1.24. *HPLC traces of DCLs formed by donor (red) and acceptor(green) building blocks mixed in ratios: (a) 1:1; (b) 2:1, and (c) 2:1 after stepwise addition of the donor.(Ref:188)*

They investigated various effects stabilizing interlocked structures and fine-tuning of the parameters of the building blocks (linker length, flexibility, chirality) which played a role in the development of uncommon giant macrocycles via DCLs (Figure 1.24).[188] Currently, researchers have been utilizing this DCC strategy to create some remarkable structures with complex topologies like Borromean rings, Solomon links and pentafoil knots.[189] Recently, Sanders and co-workers *(2012)* reported a system containing a trefoil knot with the naphthalene diimide (NDI) based bolaamphiphile molecules. At first, the

kinetically controlled dimeric macrocycles were formed in the reversible reaction but the hydrophobic effect forced the library toward the formation of a thermodynamically controlled trefoil knot later on.[190]

1.12 Applications of Nanostructured Bolaamphiphiles

Molecular self-assembly leads to ordered nanostructures upon equilibration between aggregated and non-aggregated states and provides a number of interesting properties such as self-healing, and high sensitivity to external stimuli. These self-assembled nanostructured materials are now well understood and can be controlled in order to introduce and tune its functional properties for a wide range of applications. The bottom-up construction of nanostructures based on supramolecular self-assembly has been a subject of utmost fundamental interest for the past forty years and chemists have acquired a high control of objects at that scale by encoding their molecular constituents. This field is sufficiently mature to apply its construction rules towards functional nanomaterials with novel properties related to their sizes, defined structures, and dynamics. The self-assembled soft nanostructured materials draw great attraction for wide range of applications in the fields of nanoscience, bioscience and nanotechnology.[191-197]

1.12.1. Applications in Nanosciences

Self-assembled nanostructures provide a key direction for the controlled fabrication of novel nanoscopic materials and devices. There was much interest lately in ordered two and three dimensional device fabrications by using nanowires as building blocks.[198-200] The nanowires with various electronic properties can be synthesized in controlled manner with a variety of chemical methods. Nanocrystals are the materials that can tune their electronic structures via their size and morphology.[201] The electronic structures of nanocrystals were also controlled by their shapes.[202,203] Small organic molecules based nanostructures can control mineralizations and nanocrystal synthesis of various metals in the exact shapes and sizes with high reproducibility and accuracy.[204,205] Therefore, the nanofibers and other nanostructures are used as a template to synthesis metal nanoparticles and nanocrystals in controlled size and shapes.[206-210] Nanotubular

structures are particularly important structural elements because they may serve as a template for the synthesis of nanowires or nanoscaffolds.[211-214] Nanoparticles and nanoclusters are widely used as efficient catalysts for reduction and C-C coupling reactions.[215-218] The peptide based bolaamphiphile bis(*N*-α-amido-glycylglycine)-1,7-heptane dicarboxylate is well known to self-assemble into well-defined nanotube.[219] Matsui *et al.* reported that Cu, Au and Ni nanocrystals can be mineralized in different sizes via the conformation changes of histidine based peptides on the glycylglycine based bolaamphiphile nanotubes, controlled by pH values (Figure 1.25).[220-222] The bolaamphiphile smart nanotubes can tune their electronic properties by simple environmental controls and can be applied as smart building blocks for microelectronic, sensor, and catalytic applications. The same group has demonstrated that histidine-rich peptide molecules were assembled on glycylglycine based bolaamphiphile nanotubes, where the histidine sequenced peptide selectively trapped Au ions for the nucleation of Au nanocrystals. After reduction, highly monodisperse Au nanocrystals were grown on nanotubes. The conformations and the charge distributions of the histidine-rich peptide, and Au ion concentration in the growth solution, are the main factors to control the size and the packing density of Au nanocrystals.[223] The peptide bolaamphiphile based nano-doughnuts, have been used as nano-reactors to synthesis monodisperse Au nanocrystals, where the size of the Au nanocrystal was controlled by the cavity dimension (Figure 1.26).[224] The Au nanocrystals inside the nano-doughnuts were extracted by destroying the nano-doughnuts via long UV irradiation (>10 h). These features may allow the peptide nano-doughnuts to be applied in the fields of nanomaterial syntheses, controlled release systems, and drug delivery. The same bolaamphiphile nanotube was also used as template to grow the ZnS nanocrystals very effficiently.[225] The bolaamphiphile self-assembly is a promising organic support with biochemical activity for the facile creation of metallic catalysts. Recently, Lee *et al. (2014)* reported that the self-assembled nanospherical structure of tyrosine based bolaamphiphile (Tyr- C7) was used as a reactive biomimetic support for the production of Pd catalysts.[226] Alanine appended bolaamphiphile surfactants were also reported as efficient stabilizers for Au NPs in water.[227] Bipolar phospholipids, an exciting class of bolaamphiphile molecules self-assembled into distinct structures of nanoscopic dimensions in water.

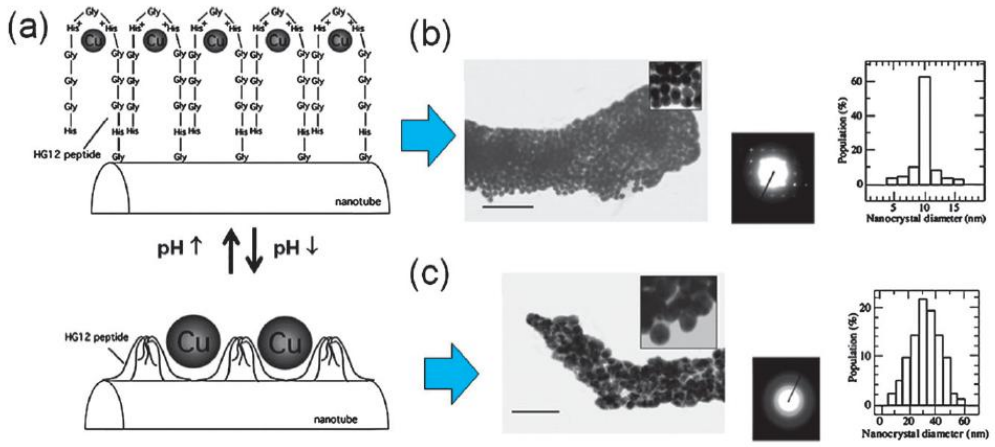

Figure 1.25. *(a) A proposed structure of the Cu nanocrystal–HG12 peptide complex on the template nanotube. The conformation change of peptides influences the nucleation and the growth rate to control the Cu nanoparticle domains on bionanotubes. (b) and (c) Cu nanocrystals grown on the bionanotube at pH 6 and pH 8. (Ref: 220).*

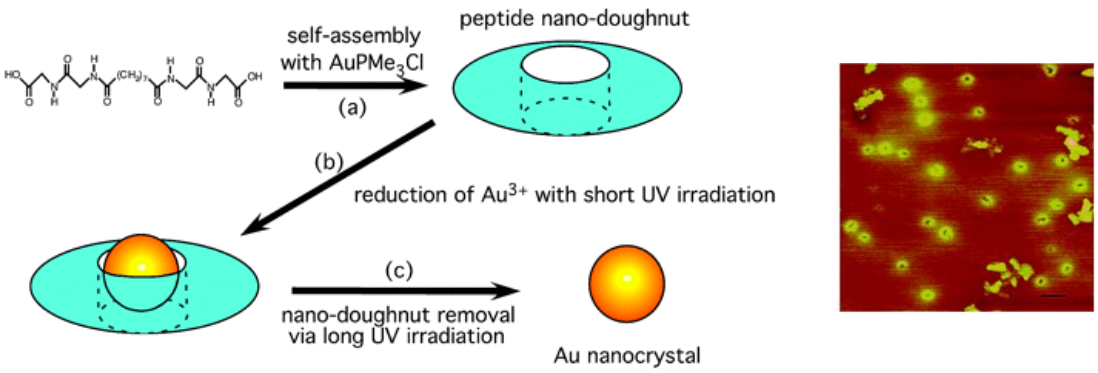

Figure 1.26. *Scheme for the peptide nano-doughnut self-assembly and its application as a nanoreactor: (a) After the peptide monomers are self-assembled to the nano-doughnut in the presence of the organic Au salts, (b) Au ions in the cavity are reduced by short UV irradiation (<20 min). (c) Longer UV irradiation (>10 h) destroys the nano-doughnut to release the Au nanocrystal. (Ref: 224)*

The bolaamphiphile 1, ω-bis(phosphocholines) (PC-Cn-PC), with a methylene chain of 22-32 carbon atoms were found to self-assemble into dense nanofibrous hydrogel. These helical nanofibers were used as template for the fixation of gold nanoparticles (AuNPs) without prior functionalization.[228] Drescher and his coworker *(2012)* reported the novel

silicified bolalipid nanofibers which were used as templates for the fixation of 5 and 2 nm AuNPs, resulting in one of the rare examples of one-dimensional AuNP arrangements in aqueous suspension.[229]

1.12.2 Applications in Biosciences

Self-assembled nanostructured biomaterials are able to interact with biological systems at the nanoscale. The field of nanotechnology has already made a tremendous impact in medicine and biology.[230,231] Nanobiotechnology, as a field is currently leading to promising applications in diagnostics and therapeutics. The biomedical applications of various types of nanomaterials obtained by self-assembly of biomolecules are now well-understood.[232] The self-assembled nanomaterials have been widely used in the field of gene and drug delivery,[233,234] therapeutic applications,[235] antimicrobial activities and cell culture scaffold for tissue engineering *etc*.[236-240] Banerjee *et al.* reported amino-acids appended bolaamphiphile which was able to form metallo-hydrogel with nanofibrilar morphology. The metallo-hydrogel entrapped vitamin B_{12} molecules and the vitamin can be released by changing the pH of the medium, suggesting a possible use of this gel as a carrier of biologically important compounds.[241] Liu *et al.* demonstrated the shrinkage of a bola type peptide dendron hydrogel which could be further used to control the release of vitamin B_1.[242] Stabilization of telomeric DNA in G-quadruplex conformation by various organic compounds has been an important goal for the medicinal chemists seeking to develop new anticancer agents. Bhattacharya *et al.* showed that 1,3-phenylene-bis (piperazinyl benzimidazole) based bolaamphiphiles are able to abet the conversion of the intramolecular quadruplex into parallel stranded intermolecular G-quadruplex DNA. Particularly, these compounds are also capable of inducing and stabilizing the parallel stranded quadruplex from randomly structured DNA in the absence of any stabilizing cation.[243] The same group investigated the anticancer drug delivery mediated by a pH-sensitive self-assembly of a bola type tripeptide.[244] Matsui *et al.* observed that peptide nanotubes can be applied as supports for enzymes. A model enzyme, *Candida rugosa* lipase, was encapsulated in peptide nanotubes, and enhanced the catalytic activity of ester hydrolysis by 33% as compared to free-standing lipases at room temperature.

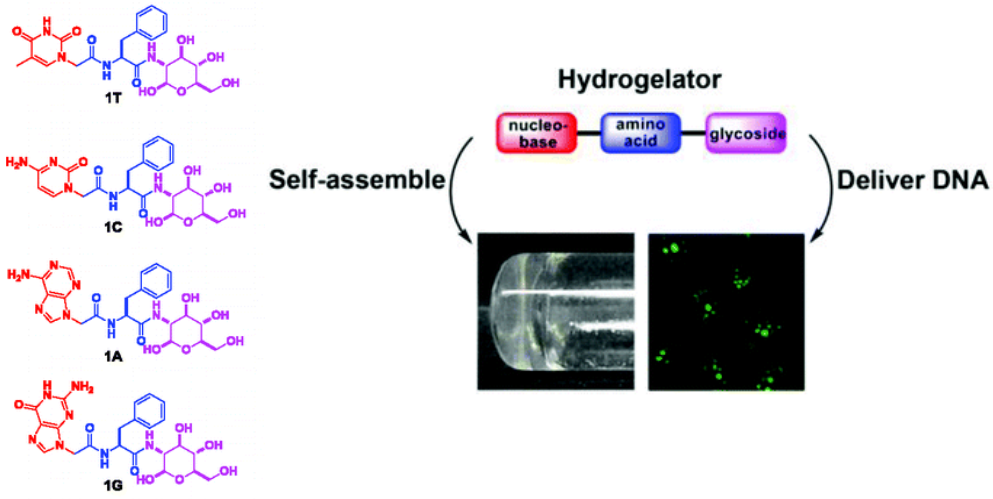

Figure 1.27. *Structures of the hydrogelators (except 1C) consist of nucleobase, amino acid, and glycoside. The hydrogelators deliver DNA into cytosol and nuclei of cells. (Ref: 253)*

At an elevated temperature, 65 °C, the activity of lipases inside the nanotubes was 70% higher than free-standing lipases. The activity enhancement of lipases in the peptide nanotubes is likely induced by the conformation change of lipases to the open form (the enzymatically active structure) as lipases are adsorbed on the inner surfaces of peptide nanotubes.[245] Bolaamphiphiles can serve as a carrier of some important biological molecules. Pucci *et al*. designed dissymmetric hemifluorocarbon bolaamphiphiles for gene delivery. The bolaamphiphile, end-capped with a lysine and a lactobionamide residue, induces a remarkably low cytotoxicity on COS-7 cells and, when self-assembled with DNA plasmid, generates a significant *in vitro* transfection efficiency without the addition of any fusogenic lipid.[246] Kim and his coworker reported the riboflavin (vitamin B2) bolaamphiphile based nanofibrous hydrogel which was used to deliver VEGF-siRNA efficiently into human cells by the endocytosis pathway.[247] Polyamine-containing bolaamphiphiles were reported to bind and compact DNA to form well-defined assemblies which resist nuclease attack and efficiently transfect Chinese hamster ovary cells. Nonspecific uptake is reduced by the incorporation of a low percentage of polyethylene glycol bolaamphiphile and the targeted transfection of a human T cell line has been demonstrated using an internalizing anti-CD3-antibody/bolaamphiphile conjugate incorporated at 0.004% into the supramolecular array. [248] Recently, perylene

bisimide based bolaamphiphile was efficiently used to sense the DNA methyltransferase activity through the monomer-excimer transition.[249] A new class of carbohydrate appended bolaamphiphiles were found to bind with receptors on pathogenic bacteria and it was shown that the nano-assemblies were effective in immobilizing particular bacterial strains.[250] The bolaamphiphile containing peptides and sugar as head groups self-assembled into stable nanoribbons which led to stronger activity in bacterial motility inhibition and agglutination. The mannose and peptide appended bolaamphiphiles nanoribbons showed the specific activity towards a particular strain of pathogenic bacteria. The encapsulation of a fluorescent probe (nile red) in the nanoribbon led to enhance the detection sensitivity by the formation of bacterial clusters.[251] Carbon nanotube and biocompatible bola-amphiphile supramolecular biohybrid materials were found to have potential application in bacterial cell agglutination.[252] Xu *et al.* illustrated a simple way to generate an unprecedented molecular architecture from the basic biological building blocks for the development of sophisticated soft nanomaterials, including supramolecular hydrogels. The designed nucleobase, amino acid, and glycoside based bolaamphiphiles self-assembled into nanofibrous hydrogel. These hydrogelators can hardly inhibit the growth of mammalian cells and the inclusion of glycoside in the hydrogelators significantly enhances their resistance to proteases. The hydrogels do not only exhibit biocompatibility and biostability but also facilitate the entry of nucleic acids into cytosol and nuclei of cells (Figure 1. 27).[253] Thus, bolaamphiphiles have been potentially used as self-assembled nanomaterials for wide range of biological applications.[254]

1.12.3 Supramolecular Electronics

Nanotechnology is revolutionizing a variety of technological applications with excellent physicochemical properties of nanometric building blocks as compared to bulk materials. A simple methodology is necessary to develop smart material building blocks, for nano-devices. Biological-inorganic assemblies were not precisely suitable for the fabrication of electronic devices, a growing number of examples indicate that biomolecules can be used as practical building blocks for electrical circuits. For this purpose, peptide bolaamphiphiles based nanostructures have been widely used to construct the nano-

devices.[255] The biological molecular binding between the multiple-antibody nanotubes and the complementary antigen were very specific due to the antibody-antigen recognition.[256] In this biomimetic approach, multiple nanowires including various antibodies were selectively immobilized on different sites on electric substrates where areas were labeled by complementary proteins (Figure 1. 28). Complex electric device geometries could be fabricated with high yields with the optimum concentrations of proteins on the substrate.[257,258] Matsui *et al.* demonstrated that peptide bolaamphiphile based nanotube was used as templates to fabricate azobenzene and ferrocene nanotubes. These azobenzene and ferrocene nanotubes could recognize the CD SAMs via the host-guest molecular recognition, and the attachment/detachment of nanotubes was controlled by applying UV irradiation and electric fields. This smart building block may be applied to build photoactive and redox active nanometer-scale mechanical switches in electronics.[259,260]

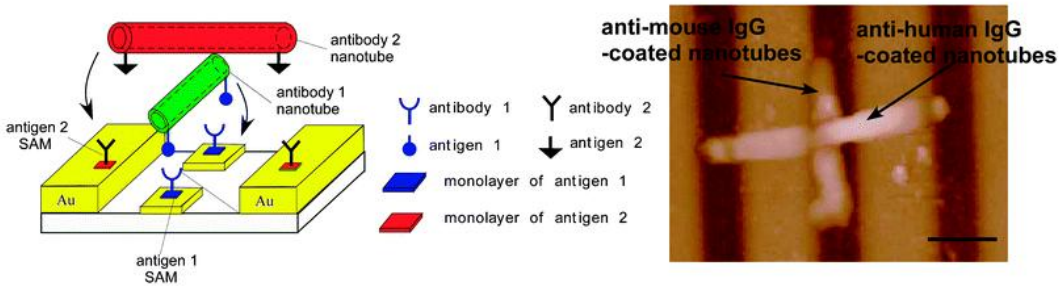

Figure 1.28. *Scheme to assemble two different antibody nanotubes, anti-mouse IgG-coated nanotube and anti-human IgG-coated nanotube, into the cross-bar geometry by biomolecular recognition (left). AFM image of the two antibody nanotubes assembled in the cross-bar geometry (right). Scale bar = 200 nm. (Ref: 257)*

The peptide bolaamphiphile nanotube sensor platform, which contains a pair of electrodes bridged by antibody coated peptide nanotubes, was developed by Matsui and his coworker.[261] The peptide bolaamphiphile nanotube platform could be used to detect HSV-2 at a concentration of 10^2 pfu mL^{-1} within 1 h by a capacitance change between the electrodes. The detection limit can be increased by increasing the number of nanotubes and electrodes on the chip. The specificity of virus detection by this technique is derived from antibody recognition. Thus peptide bolaamphiphile based nanotube biochip is

adequate for the early detection of multiple pathogens which is a key factor to avoid infection (Figure 1. 29).[262]

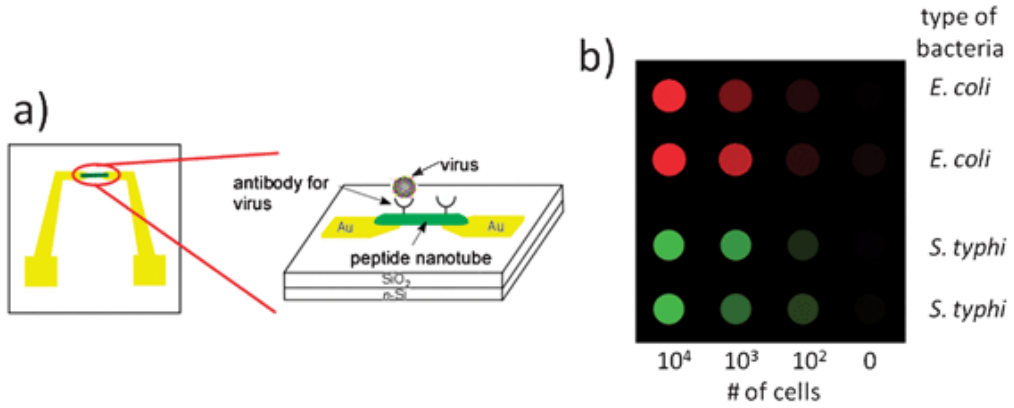

Figure 1.29. *Impedimetric pathogen biosensors assembled from peptide nanotubes, (a) antibody modified nanotubes concentrate virus at the gap between two electrodes and the impedance at high frequency increases, (b) peptide nanotube biochips for the multiplexed detection of bacterial cells via agglutination on an array of impedimetric transducers.(Ref: 262)*

1.13 References

1. Lehn J.-M. (2002), Toward complex matter: Supramolecular chemistry and self-organization, *Proc. Natl. Acad. Sci. U.S.A*, 99, 4763-4768 (DOI: 10.1073/pnas.072065599).

2. Alberts B., Bray D., Lewis J., Raff M., Roberts K., Watson J. D. (1994), Molecular biology of the cell, 3rd ed., Garland Publishing, New York (DOI: 10.1002/mrd.1080380418).

3. Fletcher D. A., Mullins R. D. (2010), Review article cell mechanics and the cytoskeleton, *Nature*, 463, 485-492 (DOI:10.1038/nature08908).

4. Whitesides G. M., Grzybowski B. (2002), Self-assembly at all scales, *Science*, 295, 2418-2421 (DOI: 10.1126/science.1070821).

5. Butler P. J. G. (1999), Self-assembly of tobacco mosaic virus: The role of an intermediate aggregate in generating both specificity and speed, *Phil. Trans. R. Soc. Lond. B*, 354, 537-550 (DOI: 10.1098/rstb.1999.0405).

6. Hamley I. W. (2003), Nanotechnology with soft materials, *Angew. Chem. Int. Ed.*, 42, 1692-1712 (DOI: 10.1002/ange.200200546).

7. Binder W. H., Barragan V., Menger F. M. (2003), Domains and rafts in lipid membranes, *Angew. Chem., Int. Ed.*, 115, 5802-5827 (DOI: 10.1002/anie.200300586).

8. Matson J. B., Stupp S. I. (2012), Self-assembling peptide scaffolds for regenerative medicine, *Chem. Commun*., 48, 26-33 (DOI: 10.1039/C1CC15551B).

9. Hirst A. R., Escuder B., Miravet J. F., Smith D. K. (2008), High-tech applications of self-assembling supramolecular nanostructured gel-phase materials: From regenerative medicine to electronic devices, *Angew. Chem. Int. Ed.*, 47, 8002-8018 (DOI: 10.1002/anie.200800022).

10. Feynman R. P. (1960), There's plenty of room at the bottom, Engineering and Science, 23 (5), pp. 22-36 (ISSN 0013-7812).

11. Anilkumar P., Jayakannan M. (2009), Self-assembled cylindrical and vesicular molecular templates for polyaniline nanofibers and nanotapes, *J. Phys. Chem. B*, 113, 11614-11624 (DOI: 10.1021/jp9043418).

12. Cui H., Muraoka T., Cheetham A. G., Stupp S. I. (2009), Self-assembly of giant peptide nanobelts, *Nano Lett.,* 9, 945-951 (DOI: 10.1021/nl802813f).

13. Komatsu H., Matsumoto S., Tamaru S.-i., Kaneko K., Ikeda M., Hamachi I. (2009), Supramolecular hydrogel exhibiting four basic logic gate functions to fine-tune substance release, *J. Am. Chem. Soc*., 131, 5580-5585 (DOI: 10.1021/ja8098239).

14. Childers W. S., Mehta A. K., Ni R., Taylor J. V., Lynn D. G. (2010), Peptides organized as bilayer membranes, *Angew. Chem. Int. Ed.*, 49, 4104-4107 (DOI: 10.1002/anie.201000212).

15. Das A., Ghosh S. (2014), Stimuli-responsive self-assembly of a naphthalene diimide by orthogonal hydrogen bonding and its co-assembly with a pyrene derivative by a pseudo-intramolecular charge-transfer interaction, *Angew. Chem. Int. Ed.*, 53, 1092-1097 (DOI: 10.1002/anie.201308396).

16. Whitesides G. M., Boncheva M. (2002), Beyond molecules: Self-assembly of mesoscopic and macroscopic components, *Proc. Natl. Acad. Sci. U.S.A*, 99, 4769-4774 (DOI: 10.1073/pnas.082065899).

17. Smith K. H., Tejeda-Montes E., Poch M., Mata A. (2011), Integrating top-down and self-assembly in the fabrication of peptide and protein-based biomedical materials, *Chem. Soc. Rev*., 40, 4563-4577 (DOI: 10.1039/c1cs15064b).

18. Groves J. T., Boxer S. G. (2002), Micropattern formation in supported lipid membranes, *Acc. Chem. Res*., 35, 149-157 (DOI: 10.1021/ar950039m).

19. Banerjee I. A., Yu L. T., MacCuspie R. I., Matsui H. (2004), Thiolated peptide nanotube assembly as arrays on patterned Au substrates, *Nano Lett*., 4, 2437-2440 (DOI: 10.1021/nl0484503).

20. Nuraje N., Banerjee I. A., MacCuspie R. I., Yu L. T, Matsui H. (2004), Biological bottom-up assembly of antibody nanotubes on patterned antigen arrays, *J. Am. Chem. Soc*., 126, 8088-8089 (DOI: 10.1021/ja048617u).

21. Ramachandran G. N., Ramakrishnan C., Sasisekharan V. (1963), Stereochemistry of polypeptide chain configurations, *J. Mol. Biol.*, 7, 95-99 (DOI: 10.1016/S0022-2836(63)80023-6).

22. Hollingsworth S. A., Karplus P. A. (2010), A fresh look at the Ramachandran plot and the occurrence of standard structures in proteins, *Biomol. Concepts*, 1, 271-283 (DOI: 10.1515/bmc.2010.022).

23. Pal D., Chakrabarti P. (2002), On residue in the disallowed region of the Ramachandran map, *Biopolymer*, 63, 195-206 (DOI: 10.1002/bip.10051).

24. Pauling L., Corey R. B. (1951), Configuration of polypeptide chains with favoured orientations around single bonds: Two new pleated sheets, *Proc. Natl. Acad. Sci. U.S.A.*, 37, 729-740 (PMCID: PMC1063460).

25. Barlow D. J., Thronton J. M. (1988), Helix geometry in proteins, *J. Mol. Biol*., 201, 601-619 (DOI: 10.1016/0022-2836(88)90641-9).

26. Pauling L., Corey R. B., Branson H. R. (1951), The structure of proteins: Two hydrogen-bonded helical configurations of the polypeptide chain, *Proc. Natl. Acad. Sci. U.S.A.*, 37, 205-211 (DOI: 10.1073/pnas.37.4.205).

27. Dunitz J. D. (2001), Pauling's left-handed α-helix, *Angew. Chem. Int. Ed*., 40, 4167-4173 (DOI: 10.1002/1521-3773(20011119)40:22<4167::AID ANIE4167>3.0.CO;2-Q)

28. Cooley R. B., Arp D. J., Karplus P. A. (2010), Evolutionary origin of a secondary structure: π-helices as cryptic but widespread insertional variations of α-helices

enhancing protein functionality, *J. Mol. Biol.*, 404, 232-246 (DOI: 10.1016/j.jmb.2010.09.034).

29. Toniolo C., Benedetti E. (1991), The polypeptide 3/10-helix, *Trends Biochem. Sci.*, 16, 350-353 (DOI: 10.1016/0968-0004(91)90142-I).

30. Vieira-Pires R. S., Morais-Cabral J. H. (2010), 3_{10} helices in channels and other membrane proteins, *J. Gen. Physiol*., 136, 585-592 (DOI: 10.1085/jgp.201010508).

31. Ananda K., Vasudev P. G., Sengupta A., Raja K. M. P., Shamala N., Balaram P. (2005), Polypeptide helices in hybrid peptide sequences, *J. Am. Chem. Soc.*, 127, 16668-16674 (DOI: 10.1021/ja055799z).

32. Fodje M. N., Al-Karadaghi S. (2002), Occurrence, conformational features and amino acid propensities for the pi helix, *Protein. Eng*., 15, 353-358. (DOI: 10.1093/protein/15.5.353).

33. Weaver T. M. (2000), The pi-helix translates structure into function, *Protein Sci*., 9, 201-206 (DOI: 10.1110/ps.9.1.201).

34. Gellman S. H. (1998), Minimal model systems for β-sheet secondary structure in proteins, *Curr. Opin. Chem. Biol.*, 2, 717-725 (DOI: 10.1016/S1367-5931(98)80109-9).

35. Hutchinson E. G., Thornton J. M. (1996), PROMOTIF-A program to identify and analyze structural motifs in proteins, *Protein Sci.*, 5, 212-220 (DOI: 10.1002/pro.5560050204).

36. Nesloney C. L., Kelly J. W. (1996), Progress towards understanding β-sheet structure, *Bioorg. Med. Chem*., 4, 739-766 (DOI: 10.1016/0968-0896(96)00051-X).

37. Irvine G. B., El-Agnaf O. M., Shankar G. M., Walsh D. M. (2008), Protein aggregation in the brain: The molecular basis for alzheimer's and parkinson's diseases, *Mol. Med*., 14, 451-464 (DOI: 10.2119/2007-00100.Irvine).

38. Venkatachalam C. M. (1968), Sterochemical criteria for polypeptides and proteins. V. conformations of a system of three linked peptide units, *Biopolymers*, 6, 1425-1436 (DOI: 10.1002/bip.1968.360061006).

39. Némethy G., Printz M. P. (1972), The γ-turn, a possible folded conformation of the polypeptide chain. comparison with the β-turn, *Macromolecules*, 5, 755- (DOI: 10.1021/ma60030a017).

40. Wilmot C. M., Thornton J. M. (1988), Analysis and prediction of the different types of beta-turn in proteins, *J. Mol. Biol*, 203, 221-32 (DOI: 10.1016/0022-2836(88)90103-9).

41. Hutchinson E. G., Thornton J. M. (1994), A revised set of potentials for β-turn formation in proteins, *Protein Sci.*, 3, 2207-2216 (DOI:10.1002/pro.5560031206).

42. Rose G. D., Gierasch L. M., Smith J. A. (1985), Turns in peptides and proteins, *Adv. Protein. Chem.*, 37, 1-109 (DOI: 10.1016/S0065-3233(08)60063-7).

43. Adhikari B., Kraatz H. B. (2014), Redox-triggered changes in the self-assembly of a ferrocene-peptide conjugate, *Chem. Commun*., 50, 5551-5553 (DOI: 10.1039/c3cc49268k).

44. van Herpt J. T., Stuart M. C. A., Browne W. R., Feringa B. L. (2013), Mechanically induced gel formation, *Langmuir*, 29, 8763-8767 (DOI: 10.1021/la401286a).

45. Huang Y., Qiu Z., Xu Y., Shi J., Lina H., Zhang Y. (2011), Supramolecular hydrogels based on short peptides linked with conformational switch, *Org. Biomol. Chem*., 9, 2149-2155, (DOI: 10.1039/c0ob01057j).

46. Edwards W., Smith D. K. (2014), Enantioselective component selection in multicomponent supramolecular gels, *J. Am. Chem. Soc*., 136, 1116-1124 (DOI: 10.1021/ja411724r).

47. Nanda J., Biswas A., Banerjee A. (2013), Single amino acid based thixotropic hydrogel formation and pH-dependent morphological change of gel nanofibers, *Soft Matter*, 9, 4198-4208 (DOI: 10.1039/c3sm27050e).

48. Micklitsch C. M., Knerr P. J., Branco M. C., Nagarkar R., Pochan D. J., Schneider J. P. (2011), Zinc-triggered hydrogelation of a self-assembling β-hairpin peptide, *Angew. Chem. Int. Ed.*, 50, 1577-1579 (DOI: 10.1002/anie.201006652).

49. Li J., Kuang Y., Gao Y., Du X., Shi J., Xu B. (2013), D-amino acids boost the selectivity and confer supramolecular hydrogels of a nonsteroidal anti-inflammatory drug (NSAID), *J. Am. Chem. Soc*., 135, 542-545 (DOI: 10.1021/ja310019x).

50. Sangeetha N. M., Maitra U. (2005), Supramolecular gels: Functions and uses, *Chem. Soc. Rev*., 34, 821-836 (DOI: 10.1039/b417081b).

51. Flory P. J. (1974), Introductory lecture, *Faraday Discuss., Chem. Soc*., 57, 7-18 (DOI: 10.1039/DC9745700007).

52. Sakai S., Hirose K., Taguchi K., Ogushi Y., Kawakami K. (2009), An injectable, *in situ* enzymatically gellable, gelatin derivative for drug delivery and tissue engineering, *Biomaterials*, 30, 3371-3377 (DOI: 10.1016/j.biomaterials.2009.03.030).

53. Van Vlierberghe S., Dubruel P., Schach E. (2011), Biopolymer-based hydrogels as scaffolds for tissue engineering applications: A review, *Biomacromolecules*, 12, 1387-1408 (DOI: 10.1021/bm200083n).

54. Tomasini C., Castellucci N. (2013), Peptides and peptidomimetics that behave as low molecular weight gelators, *Chem. Soc. Rev*., 42, 156-172 (DOI: 10.1039/c2cs35284b).

55. Yang Z., Liang G., Guo Z., Guo Z., Xu B. (2007), Intracellular hydrogelation of small molecules inhibits bacterial growth, *Angew. Chem. Int. Ed.,* 46, 8216-8219 (DOI: 10.1002/anie.200701697).

56. Jayawarna V., Ali M., Jowitt T. A., Miller A. F., Saiani A., Gough J. E., Ulijn R. V. (2006), Nanostructured hydrogels for three-dimensional cell culture through self-assembly of fluorenylmethoxycarbonyl-dipeptides, *Adv. Mater.*, 18, 611-614 (DOI: 10.1002/adma.200501522).

57. Rasale D. B., Maity I., Konda M., Das A. K. (2013), Peptide self-assembly driven by oxo-ester mediated native chemical ligation, *Chem. Commun.,* 49, 4815-4817 (DOI: 10.1039/c3cc41475b).

58. Adamcik J., Castelletto V., Bolisetty S., Hamley I. W., Mezzenga R. (2011), Direct observation of time-resolved polymorphic states in the self-assembly of end-capped heptapeptides, *Angew. Chem. Int. Ed.*, 50, 5495-5498 (DOI: 10.1002/anie.201100807).

59. Fry H. C., Garcia J. M., Medina M. J., Ricoy U. M., Gosztola D. J., Nikiforov M. P., Palmer L. C., Stupp S. I. (2012), Self-assembly of highly ordered peptide amphiphile metalloporphyrin arrays, *J. Am. Chem. Soc.*, 134 , 14646-14649 (DOI: 10.1021/ja304674d)

60. Fuhrhop A. H., Wang T. Y. (2004), Bolaamphiphiles, *Chem. Rev*., 104, 2901-2937 (DOI: 10.1021/cr030602b).

61. Wang C., Wang Z., Zhang X. (2012), Amphiphilic building blocks for self-assembly: From amphiphiles to supra-amphiphiles, *Acc. Chem. Res*., 45, 608-618 (DOI: 10.1021/ar200226d).

62. Shimizu T. (2002), Bottom-up synthesis and structural properties of self-assembled high-axial-ratio nanostructures, *Macromol. Rapid Commun*., 23, 311-331(DOI: 10.1002/1521-3927(20020401)23:5/6<311::AID-MARC311>3.0.CO;2-U).

63. Fuhrhop J.-H., David H.-H., Mathieu J., Liman U., Winter H.-J., Boekema E. (1986), Bolaamphiphiles and monolayer lipid membranes made from 1,6,19,24-tetraoxa-3,21-cyclohexatriacontadiene-2,5,20,23-tetrone, *J. Am. Chem. Soc*., 108, 1785-1791 (DOI: 10.1021/ja00268a013).

64. Shimizu T. (2003), Bottom-up synthesis and morphological control of high-axial-ratio nanostructures through molecular self-assembly, *Polym. J.*, 35, 1-22 (DOI: 10.1295/polymj.35.1).

65. Nakazawa I., Suda S., Masuda M., Asaib M., Shimizu T. (2000), pH dependent reversible polymers formed from cyclic sugar- and aromatic boronic acid-based bolaamphiphiles, *Chem. Commun*., 881-882 (DOI: 10.1039/b001013h).

66. Nakashima N., Asakuma S., Kunitake T. (1985), Optical microscopic study of helical superstructures of chiral bilayer membranes, *J. Am. Chem. Soc*., 107, 509-510 (DOI: 10.1021/ja00288a043).

67. Meister A., Bastrop M., Koschoreck S., Garamus V. M., Sinemus T., Hempel G., Drescher S., Dobner B., Richtering W., Huber K., Blume A. (2007), Structure-property relationship in stimulus-responsive bolaamphiphile hydrogels, *Langmuir*, 23, 7715-7723 (DOI: 10.1021/la7003479).

68. Nebot V. J., Armengol J., Smets J., Prieto S. F., Escuder B., Miravet J. F. (2012), Molecular hydrogels from bolaform amino Acid derivatives: A structure-properties study based on the thermodynamics of gel solubilization, *Chem. Eur. J*., 18, 4063-4072 (DOI: 10.1002/chem.201103193).

69. Bu W., Gao H., Tan X., Dong X., Cheng X., Prehm M., Tschierske C. (2013), A bolaamphiphilic sexithiophene with liquid crystalline triangular honeycomb phase, *Chem. Commun.*, 49, 1756-1758 (DOI: 10.1039/c3cc38859j).

70. Cheng X., Dong X., Wei G., Prehm M., Tschierske C. (2009), Liquid-crystalline triangle honeycomb formed by a dithiophene-based X-shaped bolaamphiphile, *Angew. Chem. Int. Ed*., 48, 8014-8017 (DOI: 10.1002/anie.200903247).

71. Chen B., Zeng X. B., Baumeister U., Diele S., Ungar G., Tschierske C. (2004), Liquid crystals with complex superstructures, *Angew. Chem. Int. Ed*., 43, 4621-4625 (DOI: 10.1002/anie.200460762).

72. Fuhrhop J.-H., Mathieu J. (1983), An unsymmetric monolayer vesicle membrane, *J. Chem. Soc., Chem. Commun*. 144-145 (DOI: 10.1039/C39830000144).

73. Liang K., Hui Y. (1992), Vesicle of hybrid bolaamphiphile: Flip-flop behavior of spin labels, *J. Am. Chem. Soc.*, 114, 6588-6590 (DOI: 10.1021/ja00042a066).

74. Sano M., Oishi K., Ishi-i. T., Shinkai S. (2000), Vesicle formation and its fractal distribution by bola-amphiphilic [60]fullerene, *Langmuir*, 16, 3773-3776 (DOI: 10.1021/la991550h).

75. Wang X., Shen Y., Pan Y., Liang Y. (2001), Bolaamphiphilic single-chain bis-schiff base derivatives: aggregation and thermal behavior in aqueous solution, *Langmuir*,17, 3162-3167 (DOI: 10.1021/la001084s).

76. Toyota T., Takakura K., Kageyama Y., Kurihara K., Maru N., Ohnuma K., Kaneko K., Sugawara T. (2008), Population study of sizes and components of self-reproducing giant multilamellar vesicles**,** *Langmuir***,** 24, 3037-3044 (DOI: 10.1021/la703017s).

77. Yan Y., Huang J., Li Z., Ma J., Fu H., Ye J. (2003), Vesicles with superior stability at high temperature, *J. Phys. Chem. B,* 107, 1479-1482 (DOI: 10.1021/jp026778j).

78. Gao L., Zheng B., Yao Y., Huang F. (2013), Responsive reverse giant vesicles and gel from self-organization of a bolaamphiphilic pillar[5]arene, *Soft Matter*, 9, 7314-7319 (DOI: 10.1039/c3sm51047f).

79. Chen Z.-X., Su X.-X., Deng S.-P. (2011), Molecular recognition of melamine by vesicles spontaneously formed from orotic acid derived bolaamphiphiles, *J. Phys. Chem. B*, 115, 1798-1806 (DOI: 10.1021/jp106385x).

80. Bhattacharya S., De S. (1996), Modulation of vesicular properties by variation of shapes of bolaform counter ions in hybrid-ion paired surfactants, *Chem. Commun*., 1283-1284 (DOI: 10.1039/CC9960001283).

81. Kan P. L., Papahadjopoulos-Sternberg B., Wong D., Waigh R. D., Watson D. G., Gray A. I., McCarthy D., McAllister M., Schatzlein A. G., Uchegbu I. F. (2004), Highly hydrophilic fused aggregates (microsponges) from a C12 spermine bolaamphiphile, *J. Phys. Chem. B,* 108, 8129-8135 (DOI: 10.1021/jp0372237).

82. Meister A., Kohler K., Drescher S., Dobner B., Karlsson G., Edwards K., Hause G., Blume A. (2007), Mixing behaviour of a symmetrical single-chain bolaamphiphile with phospholipids, *Soft Matter*, 3, 1025-1031 (DOI: 10.1039/b703152a).

83. Meister A., Drescher S., Garamus V. M., Karlsson G., Graf G., Dobner B., Blume A. (2008), Temperature-dependent self-assembly and mixing behavior of symmetrical single-chain bolaamphiphiles, *Langmuir*, 24, 6238-6246 (DOI: 10.1021/la800166h).

84. Kohler K., Forster G., Hauser A., Dobner B., Heiser U. F., Ziethe F., Richter W., Steiniger F., Drechsler M., Stettin H., Blume A. (2004), Self-assembly in a bipolar phosphocholine-water system: The formation of nanofibers and hydrogels, *Angew. Chem. Int. Ed*., 43, 245-247 (DOI: 10.1002/anie.200351731).

85. Kohler K., Forster G., Hauser A., Dobner B., Heiser U. F., Ziethe F., Richter W., Steiniger F., Drechsler M., Stettin H., Blume A. (2004), Temperature-dependent behavior of a symmetric long-chain bolaamphiphile with phosphocholine headgroups in water: From hydrogel to nanoparticles, *J. Am. Chem. Soc*., 126, 16804-16813 (DOI: 10.1021/ja046537k).

86. Graf G., Drescher S., Meister A., Dobner B., Blume A. (2011), Self-assembled bolaamphiphile fibers have intermediate properties between crystalline nanofibers and wormlike micelles: Formation of viscoelastic hydrogels switchable by changes in pH and salinity, *J. Phys. Chem. B,* 115, 10478-10487 (DOI: 10.1021/jp205414n).

87. Shimizu T., Iwaura R., Masuda M., Hanada T., Yase K. (2001), Internucleobase-interaction-directed self-assembly of nanofibers from homo- and heteroditopic 1,*ω*-nucleobase bolaamphiphiles, *J. Am. Chem. Soc.*, 123, 5947-5955 (DOI: 10.1021/ja010201i).

88. Graf G., Drescher S., Meister A., Garamus V. M., Dobnere B., Blume A. (2013), Tuning the aggregation behaviour of single-chain bolaamphiphiles in aqueous suspension by changes in headgroup asymmetry, *Soft Matter*, 9, 9562-9571 (DOI: 10.1039/c3sm51778k).

89. Kobayashi H., Friggeri A., Koumoto K., Amaike M., Shinkai S., Reinhoudt D. N. (2002), Molecular design of "super" hydrogelators: Understanding the gelation arocess of Azobenzene-based sugar derivatives in water, *Org. Lett.*, 4, 1423-1426 (DOI: 10.1021/ol025519+).

90. de Loos M., Friggeri A., van Esch J., Kellogg R. M., Feringa B. L. (2005) Cyclohexane bis-urea compounds for the gelation of water and aqueous solutions, *Org. Biomol. Chem.*, 3, 1631-1639 (DOI: 10.1039/B500837A).

91. Wang T., Li Y., Liu M. (2009), Gelation and self-assembly of glutamate bolaamphiphiles with hybrid linkers: Effect of the aromatic ring and alkyl spacers, *Soft Matter*, 5, 1066-1073 (DOI: 10.1039/b813932f).

92. Wu G., Verwilst P., Xu J., Xu H., Wang R., Smet M., Dehaen W., Faul C. F. J., Wang Z., Zhang X. (2012), Bolaamphiphiles bearing bipyridine as mesogenic core: Rational exploitation of molecular architectures for controlled self-assembly, *Langmuir*, 28, 5023-5030 (DOI: 12.1021/la300369w).

93. Kohler K., Meister A., Forster G., Dobner B., Drescher S., Ziethe F., Richter W., Steiniger F., Drechsler M., Hausee G., Blume A. (2006), Conformational and thermal behavior of a pH-sensitive bolaform hydrogelator, *Soft Matter*, 2, 77-86 (DOI: 10.1039/b514163j).

94. Iwaura R., Ohnishi-Kameyama M. (2012), Construction of supramolecular helical nanofibers using renewable biomaterials: Self-assembly of a cytidylic acid-appended bolaamphiphile in lemon juice, *Chem. Commun.*, 48, 6633-6635 (DOI: 10.1039/c2cc17787k).

95. Liu X., Wang T., Liu M. (2012), Interfacial assembly of a series of cinnamoyl-containing bolaamphiphiles: Spacer-controlled packing, photochemistry, and odd-even effect, *Langmuir*, 28, 3474-3482 (DOI: 10.1021/la204653b).

96. Sukul P. K., Singh P. K., Maji S. K., Malik S. (2013), Aggregation induced chirality in a self assembled perylene based hydrogel: Application of the intracellular pH measurement, *J. Mater. Chem. B*, 1, 153-156 (DOI: 10.1039/c2tb00007e).

97. Datar A., Balakrishnana K., Zang L. (2013), One-dimensional self-assembly of a water soluble perylene diimide molecule by pH triggered hydrogelation, *Chem. Commun*., 49, 6894-6896 (DOI: 10.1039/C3CC43359E).

98. Kieltyka R. E., Pape A. C. H., Albertazzi L., Nakano Y., Bastings M. M. C., Voets I. K., Dankers P. Y. W., Meijer E. W. (2013), Mesoscale modulation of supramolecular ureidopyrimidinone-based poly(ethylene glycol) transient networks in water, *J. Am. Chem. Soc*., 135, 11159-11164 (DOI: 10.1021/ja403745w).

99. Iwaura R., Yoshida K., Masuda M., Ohnishi-Kameyama M., Yoshida M., Shimizu T. (2003), Oligonucleotide-templated self-assembly of nucleotide bolaamphiphiles: DNA-like nanofibers edged by a double-helical arrangement of A–T base pairs, *Angew. Chem. Int. Ed.*, 42, 1009-1012 (DOI: 10.1002/anie.200390257).

100. Iwaura R., Kikkawa Y., Ohnishi-Kameyama M., Shimizu T. (2007), Effects of oligo DNA template length and sequence on binary self-assembly of a nucleotide bolaamphiphile, *Org. Biomol. Chem.*, 5, 3450-3455 (DOI: 10.1039/b711687j).

101. Iwaura R., Ohnishi-Kameyama M., Shimizu T. (2008), Nanofiber formation from sequence-selective DNA-templated self-assembly of a thymidylic acid-appended bolaamphiphile, *Chem. Commun.*, 5770-5772 (DOI: 10.1039/B813592D).

102. Kogiso M., Hanada T., Yase K., Shimizu T. (1998), Intralayer hydrogen-bond-directed self-assembly of nano-fibers from dicarboxylic valylvaline bolaamphiphiles, *Chem. Commun*., 1791-1792 (DOI: 10.1039/A803606C).

103. Sukul P. K., Asthana D., Mukhopadhyay P., Summa D., Muccioli L., Zannoni C., Beljonne D., Rowan A. E., Malik S. (2011), Assemblies of perylene diimide derivatives with melamine into luminescent hydrogels, *Chem. Commun*., 47, 11858-11860 (DOI: 10.1039/c1cc14189a).

104. Claussen R. C, Rabatic B. M., Stupp S. I. (2003), Aqueous self-assembly of unsymmetric peptide bolaamphiphiles into nanofibers with hydrophilic cores and surfaces, *J. Am. Chem. Soc*., 125, 12680-12681 (DOI: 10.1021/ja035882r).

105. Stone D. A., Hsua L., Stupp S. I. (2009), Self-assembling quinquethiophene-oligopeptide hydrogelators, *Soft Matter*, 5, 1990-1993 (DOI: 10.1039/b904326h).

106. Wall B. D., Diegelmann S. R., Zhang S., Dawidczyk T. J., Wilson W. L., Katz H. E., Mao H.-Q., Tovar J. D. (2011), Aligned macroscopic domains of optoelectronic nanostructures prepared via shear-flow assemblyof peptide hydrogels, *Adv. Mater.*, 23, 5009-5014 (DOI: 10.1002/adma.201102963).

107. Wall B. D., Zacca A. E., Sanders A. M., Wilson W. L., Ferguson A. L., Tovar J. D. (2014), Supramolecular polymorphism: Tunable electronic interactions within π-conjugated peptide nanostructures dictated by primary amino acid sequence, *Langmuir*, 30, 5946-5956 (DOI:10.1021/la500222y).

108. Lazzari, M.; Lopez-Quintela, M. (2003), Block copolymers as a tool for nanomaterial fabrication, *Adv. Mater.*, 15, 1583-1594 (DOI: 10.1002/adma.200300382).

109. Bose P. P., Das A. K., Hegde R. P., Shamala N., Banerjee A. (2007), pH-sensitive nanostructural transformation of a synthetic self-assembling water-soluble tripeptide: Nanotube to nanovesicle, *Chem. Mater.*, 19, 6150-6157, (DOI: 10.1021/cm0716147).

110. Shao H., Parquette J. R. (2009), Controllable peptide-dendron self-assembly: Interconversion ofnanotubes and fibrillar nanostructures, *Angew. Chem. Int. Ed.*, 48, 2525-2528 (DOI: 10.1002/anie.200805010).

111. Fuhrhop J. H., Spiroski D., Boettcher C. (1993), Molecular monolayer rods and tubules made of alpha-(L-lysine), omega-(amino) bolaamphiphiles, *J. Am. Chem. Soc.*, 115, 1600-1601 (DOI: 10.1021/ja00057a069).

112. Kameta N., Minamikawa H., Masuda M. (2011), Supramolecular organic nanotubes: How to utilize the inner nanospace and the outer space, *Soft Matter*, 7, 4539-4561 (DOI: 10.1039/c0sm01559h).

113. Matsui H., Pan S., Douberly Jr. G. E. (2001), Fabrication of nanocrystal tube using peptide tubule as template and its application as signal-enhancing cuvette, *J. Phys. Chem. B*, 105, 1683-1686 (DOI: 10.1021/jp003166v).

114. Matsui H., Douberly Jr. G. E. (2001), Organization of peptide nanotubes into macroscopic bundles, *Langmuir*, 17, 7918-7922 (DOI: 10.1021/la010910+).

115. Ambrosi M., Fratini E., Alfredsson V., Ninham B. W., Giorgi R., Nostro P. L., Baglioni P. (2006), Nanotubes from a vitamin C-based bolaamphiphile, *J. Am. Chem. Soc.*,128, 7209-7214 (DOI: 10.1021/ja057730x).

116. Zhao Y., Zhao J., Yan Y., Li Z., Huang J. (2010), Unprecedented parallel packing of unsymmetrical bolaamphiphiles driven by π-π stacking of cinnamoyl groups, *Soft Matter*, 6, 3282-3288 (DOI: 10.1039/c002541k).

117. Shao H., Seifert J., Romano N. C., Gao M., Helmus J. J., Jaroniec C. P., Modarelli D. A., Parquette J. R. (2010), Amphiphilic self-assembly of an n-type nanotube, *Angew. Chem. Int. Ed.*, 49, 7688-7691 (DOI: 10.1002/anie.201003415).

118. Gao P., Liu M. (2006), Compression induced helical nanotubes in a spreading film of a bolaamphiphile at the air/water interface, *Langmuir*, 22, 6727-6729 (DOI: 10.1021/la0604836).

119. Cao H., Jiang J., Zhu X., Duan P., Liu M. (2011), Hierarchical co-assembly of chiral lipid nanotubes with an azobenzene derivative: Optical and chiroptical switching, *Soft Matter*, 7, 4654-4660 (DOI: 10.1039/c1sm05219e).

120. Zhan C., Gao P., Liu M. (2005), Self-assembled helical spherical-nanotubes from an L-glutamic acid based bolaamphiphilic low molecular mass organogelator, *Chem. Commun*., 462-464 (DOI: 10.1039/b413259a).

121. Jiang J., Wang T., Liu M. (2010), Creating chirality in the inner walls of silica nanotubes through a hydrogel template: Chiral transcription and chiroptical switch, *Chem. Commun.*, 46, 7178-7180 (DOI: 10.1039/c0cc00891e).

122. Shen Z., Wang T., Liu M. (2014), H-bond and π-π stacking directed self-assembly of two-component supramolecular nanotubes: Tuning length, diameter and wall thickness, *Chem. Commun.*, 50, 2096-2099 (DOI: 10.1039/c3cc48350a).

123. Liu X., Wang T., Liu M. (2011), Interfacial assembly of cinnamoyl-terminated bolaamphiphiles through the air/water interface: Head group-dependent assembly, supramolecular nanotube and photochemical sewing, *Phys. Chem. Chem. Phys.*, 13, 16520-16529 (DOI: 10.1039/c1cp21561b).

124. Kameta N., Masuda M., Minamikawa H., Mishima Y., Yamashita I., Shimizu T. (2007), Functionalizable organic nanochannels based on lipid nanotubes: Encapsulation and nanofluidic behavior of biomacromolecules, *Chem. Mater.*, 19, 3553-3560 (DOI: 10.1021/cm070626p).

125. Masuda M., Shimizu T. (2004), Lipid nanotubes and microtubes: Experimental evidence for unsymmetrical monolayer membrane formation from unsymmetrical bolaamphiphiles, *Langmuir*, 20, 5969-5977 (DOI: 10.1021/la049085y).

126. Kameta N., Yoshida K., Masuda M., Shimizu T. (2009), Supramolecular nanotube hydrogels: Remarkable resistance effect of confined proteins to denaturants, *Chem. Mater*., 21, 5892-5898 (DOI: 10.1021/cm903108h).

127. Kameta N., Minamikawa H., Masuda M., Mizunoc G., Shimizu T. (2008), Controllable biomolecule release from self-assembled organic nanotubes with asymmetric surfaces: pH and temperature dependence, *Soft Matter*, 4, 1681-1687 (DOI: 10.1039/b803742f).

128. Shimizu T., Ohnishi S., Kogiso M. (1998), Cross-section molecular imaging of supramolecular microtubes with contact atomic force microscopy, *Angew. Chem. Int. Ed.*, 37, 3260-3262 (DOI: 10.1002/(SICI)1521-3773(19981217)37:23<3260::AID-ANIE3260>3.0.CO;2-4).

129. Kogiso M., Ohnishi S., Yase K., Masuda M., Shimizu T. (1998), Dicarboxylic oligopeptide bolaamphiphiles: Proton-triggered self-assembly of microtubes with loose solid surfaces, *Langmuir*, 14, 4978-4986 (DOI: 10.1021/la9802419).

130. Shimizu T., Kogiso M., Masuda M. (1997), Noncovalent formation of polyglycine II-type structure by hexagonal self-assembly of linear polymolecular chains, *J. Am. Chem. Soc.*, 119, 6209-6210 (DOI: 10.1021/ja970844r).

131. Henricus M. M., Johnson K. T., Banerjee I. A. (2008), Investigation of insulin loaded self-assembled microtubules for drug release, *Bioconjugate Chem.*, 19, 2394-2400 (DOI: 10.1021/bc800254n).

132. Gubitosi M., Travaglini L., Annibale A. D., Pavel N. V., Tato J. V., Obiols-Rabasa M., Sennato S., Olsson U., Schillén K., Galantini L. (2014), Sugar-bile acid-based bolaamphiphiles: From Scrolls to monodisperse single-walled tubules, *Langmuir*, 30, 6358-6366 (DOI:10.1021/la500908r).

133. Song B., Wang Z., Chen S., Zhang X., Fu Y., Smet M., Dehaen W. (2005), The introduction of π-π stacking moieties for fabricating stable micellar structure: Formation and dynamics of disklike micelles, *Angew. Chem. Int. Ed*., 44, 4731-4735 (DOI: 10.1002/anie.200500980).

134. Liu K., Wang C., Li Z., Zhang X. (2011), Superamphiphiles based on directional charge-transfer interactions: From supramolecular engineering to well-defined nanostructures, *Angew. Chem. Int. Ed.*, 50, 4952-4956 (DOI: 10.1002/anie.201007167).

135. Wu G., Thomas J., Smet M., Wang Z., Zhang X. (2014), Controlling the self-assembly of cationic bolaamphiphiles: Hydrotropic counteranions determine aggregated structures, *Chem. Sci.*, 5, 3267-3274 (DOI: 10.1039/c4sc00860j).

136. Sun Y., Li Z., Wang Z. (2012), Self-assembled monolayer and multilayer films based on L-lysine functionalized perylene bisimide, *J. Mater. Chem.*, 22, 4312-4318 (DOI: 10.1039/c1jm14521e).

137. Kumar M., George S. J. (2011), Green fluorescent organic nanoparticles by self-assembly induced enhanced emission of a naphthalene diimide bolaamphiphile, *Nanoscale*, 3, 2130-2133 (DOI: 10.1039/c1nr10151j).

138. Pal A., Karthikeyan S., Sijbesma R. P. (2010), Coexisting hydrophobic compartments through self-sorting in rod-like micelles of bisurea bolaamphiphiles, *J. Am. Chem. Soc.*, 132, 7842-7843 (DOI: 10.1021/ja101872x).

139. Tian Y.-J., Shi E.-T., Tian Y.-K., Yao R.-S., Wang F. (2014), Cooperative complexation of amino acid derivatives to platinum acetylide-based bolaamphiphile, *Org. Lett.*, 16, 3180-3183 (DOI: 10.1021/ol500752b).

140. Li G., Bhosale S., Wang T., Zhang Y., Zhu H., Fuhrhop J.-H. (2003), Gram-scale synthesis of submicrometer-long polythiophene wires in mesoporous silica matrices, *Angew. Chem. Int. Ed.*, 42, 3818-3821(DOI: 10.1002/anie.200351158).

141. Lim Y.-b., Lee E., Yoon Y.-R., Lee M. S., Lee M. (2008), Filamentous artificial virus from a self-assembled discrete nanoribbon, *Angew. Chem. Int. Ed.*, 47, 4525-4528 (DOI: 10.1002/anie.200800266).

142. Yan Y., de Keizer A., Martens A. A., Oliveira C. L. P., Pedersen J. S., de Wolf F. A., Drechsler M., Stuart M. A. C., Besseling N. A. M. (2009), Polypeptide nanoribbon hydrogels assembled through multiple supramolecular interactions, *Langmuir*, 25, 12899-12908 (DOI: 10.1021/la901834v).

143. Huang J., Wang S., Wu G., Yan L., Dong L., Lai X., Yin S., Song B. (2014), Mono-molecule-layer nano-ribbons formed by self-assembly of bolaamphiphiles, *Soft Matter*, 10, 1018-1023 (DOI: 10.1039/c3sm52365a).

144. Fenske M. T., Meyer-Zaika W., Korth H.-G., Vieker H., Turchanin A., Schmuck C. (2013) Cooperative self-assembly of discoid dimers: Hierarchical formation of nanostructures with a pH switch, *J. Am. Chem. Soc.*, 135, 8342-8349 (DOI: 10.1021/ja4025148).

145. Maiti D. K., Banerjee A. (2013), A synthetic amino acid residue containing a new oligopeptide-based photosensitive fluorescent organogel, *Chem. Asian J.*, 8, 113-120 (DOI: 10.1002/asia.201200617).

146. Koley P., Pramanik A. (2012), Multilayer vesicles, tubes, various porous structures and organo gels through the solvent-assisted self-assembly of two modified tripeptides and their different applications, *Soft Matter*, 8, 5364-5374 (DOI: 10.1039/c2sm25205h).

147. Amdursky N., Molotskii M., Gazit E., Rosenman G. (2010), Elementary building blocks of self-assembled peptide nanotubes, *J. Am. Chem. Soc*., 132, 15632-15636 (DOI: 10.1021/ja104373e).

148. Mason T. O., Chirgadze D. Y., Levin A., Adler-Abramovich L., Gazit E., Knowles T. P. J., Buell A. K. (2014), Expanding the solvent chemical space for self-assembly of dipeptide nanostructures, *ACS Nano*, 8 , 1243-1253 (DOI: 10.1021/nn404237f).

149. Cui H., Muraoka T., Cheetham A. G., Stupp S. I. (2009), Self-assembly of giant peptide nanobelts, *Nano Lett.*, 9, 945-951 (DOI: 10.1021/nl802813f).

150. Choi I., Park I.-S., Ryu J.-H., Lee M. (2012), Control of peptide assembly through directional interactions, *Chem. Commun*., 48, 8481-8483 (DOI: 10.1039/c2cc31872e).

151. Castelletto V., Hamley I. W., Hule R. A., Pochan D. (2009), Helical-ribbon formation by a β-amino acid modified amyloid β-peptide fragment, *Angew. Chem., Int. Ed*., 48, 2317-2320 (DOI: 10.1002/anie.200805500).

152. Shimizu T., Masuda M., Minamikawa H. (2005), Supramolecular nanotube architectures based on amphiphilic molecules, *Chem. Rev.*, 105, 1401-1443 (DOI: 10.1021/cr030072j).

153. Yamamoto Y., Fukushima T., Suna Y., Ishii N., Saeki A., Seki S., Tagawa S., Taniguchi M., Kawai T., Aida T. (2006), Photoconductive coaxial nanotubes of molecularly connected electron donor and acceptor layers, *Science*, 314, 1761-1764 (DOI: 10.1126/science.1134441).

154. Cui H. G., Chen Z. Y., Zhong S., Wooley K. L., Pochan D. J. (2007), Block copolymer assembly via kinetic control, *Science*, 317, 647-650 (DOI: 10.1126/science.1141768).

155. Pashuck E. T., Stupp S. I. (2010), Direct observation of morphological tranformation from twisted ribbons into helical ribbons, *J. Am. Chem. Soc.*, 132, 8819-8821 (DOI: 10.1021/ja100613w).

156. Yan X., He Q., Wang K., Duan L., Cui Y., Li J. (2007), Transition of cationic dipeptide nanotubes into vesicles and oligonucleotide delivery, *Angew. Chem. Int. Ed*., 46, 243 -2434 (DOI: 10.1002/anie.200603387).

157. Q. Meng, Y. Kou, X. Ma,Y. Liang, L. Guo, C. Ni, K. Liu (2012), Tunable self-assembled peptide amphiphile nanostructures, *Langmuir*, 28, 5017-5022 (DOI: 10.1021/la3003355).

158. Maity S., Jana P., Maity S. K., Haldar D. (2011), Fabrication of hollow self-assembled peptide microvesicles and transition from sphere-to-rod structure, *Langmuir*, 27, 3835-384 (DOI: 10.1021/la104461m).

159. Wang T., Jiang J., Liu Y., Li Z., Liu M. (2010), Hierarchical self-assembly of bolaamphiphiles with a hybrid spacer and L-glutamic acid headgroup: pH- and surface-triggered hydrogels, vesicles, nanofibers, and nanotubes, *Langmuir*, 26, 18694-18700 (DOI:10.1021/la103435t).

160. Liu Y., Wang T., Li Z., Liu M. (2013), Copper(II) ion selective and strong acid-tolerable hydrogels formed by an L-histidine ester terminated bolaamphiphile: from single molecular thick nanofibers to single-wall nanotubes, *Chem. Commun.*, 49, 4767-4769 (DOI: 10.1039/c3cc41786g).

161. Song B., Wu G., Wang Z., Zhang X., Smet M., Dehaen W. (2009), Metal-ligand coordination-induced self-assembly of bolaamphiphiles bearing bipyrimidine, *Langmuir*, 25, 13306-13310 (DOI: 10.1021/la903321b).

162. Liu K., Yao Y., Liu Y., Wang C., Li Z., Zhang X. (2012), Self-assembly of supra-amphiphiles based on dual charge-transfer interactions: From nanosheets to nanofibers, *Langmuir*, 28, 10697-10702 (DOI: 10.1021/la3018437).

163. Li F., Song Q., Yang L., Wu G., Zhang X. (2013), Supra-amphiphiles formed by complexation of azulene-based amphiphiles and pyrene in aqueous solution: From cylindrical micelles to disklike nanosheets, *Chem. Commun.*, 49, 1808-1810 (DOI: 10.1039/c3cc00059a).

164. Wu G., Verwilst P., Liu K., Smet M., Faul C. F. J., Zhang X. (2013), Controlling the self-assembly of cationic bolaamphiphiles: Counterion-directed transitions from 0D/1D to exclusively 2D planar structures, *Chem. Sci*., 4, 4486-4493 (DOI: 10.1039/c3sc52342j).

165. Lu T., Han F., Li Z., Huang J., Fu H. (2006), Transitions of organized assemblies in mixed systems of cationic bolaamphiphile and anionic conventional surfactants, *Langmuir*, 22, 2045-2049 (DOI: 10.1021/la0528100).

166. Yan Y., Xiong W., Li X., Lu T., Huang J., Li Z., Fu H. (2007), Molecular packing parameter in bolaamphiphile solutions: Adjustment of aggregate morphology by modifying the solution conditions, *J. Phys. Chem. B*, 111, 2225-2230 (DOI: 10.1021/jp065235x).

167. Matsui H., Gologan B. (2000), Crystalline glycylglycine bolaamphiphile tubules and their pH-sensitive structural transformation, *J. Phys. Chem. B*, 104, 3383-3386 (DOI: 10.1021/jp994117p).

168. Matsui H., Holtman C. (2002), Organic nanotube bridge fabrication by controlling molecular self-assembly processes between spherical and tubular formations, *Nano Lett.*, 2, 887-889 (DOI: 10.1021/nl025606v).

169. Kameta N., Ishikawa K., Masuda M., Shimizu T. (2013), Control of self-assembled morphology and molecular packing of asymmetric glycolipids by association/dissociation with poly(thiopheneboronic acid), *Langmuir*, 29, 13291-13298 (DOI: 10.1021/la4028018).

170. Sirieix J., de Viguerie N. L., Riviere M., Lattes A. (2000), From unsymmetrical bolaamphiphiles to supermolecules, *New J. Chem.*, 24, 1043-1048 (DOI: 10.1039/b005487i).

171. Kobayashi H., Koumoto K., Jung J. H., Shinkai S. (2002), Sol-gel phase transition induced by fiber-vesicle structural changes in sugar-based bolaamphiphiles, *J. Chem. Soc., Perkin Trans.*, 2, 1930-1936 (DOI: 10.1039/b204631h).

172. Song J., Cheng Q., Kopta S., Stevens R. C. (2001), Modulating artificial membrane morphology: pH-Induced chromatic transition and nanostructural transformation of a bolaamphiphilic conjugated polymer from blue helical ribbons to red nanofibers, *J. Am. Chem. Soc.*, 123, 3205-3213 (DOI: 10.1021/ja0035046).

173. Zhang Z., Zhang X., Zhan C., Lu Z., Ding X., He S., Yao J. (2013), The leverage effect of the relative strength of molecular solvophobicity vs. solvophilicity on fine-tuning nanomorphologies of perylene diimide bolaamphiphiles, *Soft Matter*, 9, 3089-3097 (DOI: 10.1039/c2sm27674g).

174. Ziserman L., Lee H.-Y., Raghavan S. R., Mor A., Danino D. (2011), Unraveling the mechanism of nanotube formation by chiral self-assembly of amphiphiles, *J. Am. Chem. Soc*., 133, 2511-2517 (DOI: 10.1021/ja107069f).

175. Ochi R., Nishida T., Ikeda M., Hamachi I. (2014), Design of peptide-based bolaamphiphiles exhibiting heat-set hydrogelation via retro-Diels-Alder reaction, *J. Mater. Chem. B*, 2, 1464-1469 (DOI: 10.1039/c3tb21680b).

176. Ludlow R. F., Otto S. (2008), Systems chemistry, *Chem. Soc. Rev*., 37, 101-108 (DOI: 10.1039/B611921M).

177. Otto S. (2012), Dynamic molecular networks: From synthetic receptors to self-replicators, *Acc. Chem. Res*., 45, 2200-2210 (DOI: 10.1021/ar200246j).

178**.** Corbett P. T., Leclaire J., Vial L., West K. R., Wietor J.-L., Sanders J. K. M., Otto S. (2006), Dynamic combinatorial chemistry, *Chem. Rev*., 106, 3652-3711 (DOI: 10.1021/cr020452p).

179. Lehn J.-M. (2007), From supramolecular chemistry towards constitutional dynamic chemistry and adaptive chemistry, *Chem. Soc. Rev*., 36, 151-160 (DOI: 10.1039/B616752G).

180. Pieters R. J., Huc I., Rebek J. (1994), Reciprocal template effects in a replication cycle, *Angew. Chem., Int. Ed.*, 33, 1579-1581 (DOI: 10.1002/anie.199415791).

181. Lee D. H., Severin K., Yokobayashi Y., Ghadiri M. R. (1997), Emergence of symbiosis in peptide self-replication through a hyper cyclic network, *Nature*, 390, 591-593 (DOI:10.1038/37569).

182. Carnall J. M. A., Waudby C. A., Belenguer A. M., Stuart M. C. A., Peyralans J. J.-P., Otto S. (2010), Mechanosensitive self-replication driven by self-organization, *Science*, 327, 1502-1506 (DOI:10.1126/science.1182767).

183. Minkenberg C. B., Florusse L., Eelkema R., Koper G. J. M., van Esch J. H. (2009), Triggered self-assembly of simple dynamic covalent surfactants, *J. Am. Chem. Soc*., 131, 11274-11275 (DOI: 10.1021/ja902808q).

184. Wang G., Wu G., Wang Z., Zhang X. (2014), Asymmetric and symmetric bolaform supra-amphiphiles: Formation of imine bond influenced by aggregation, *Langmuir*, 30, 1531-1535 (DOI:10.1021/la405000a).

185. Wang G., Wang C., Wang Z., Zhang X. (2011), Bolaform superamphiphile based on a dynamic covalent bond and its self-assembly in water, *Langmuir*, 27, 12375-12380 (DOI:10.1021/la203040e).

186. Wang G., Wang C., Wang Z., Zhang X. (2012), H-shaped supra-amphiphiles based on a dynamic covalent bond, *Langmuir*, 28, 14567-14572 (DOI: 10.1021/la303272b).

187. Au-Yeung, H. Y., Pantos G. D., Sanders J. K. M. (2009), Dynamic combinatorial synthesis of a catenane based on donor–acceptor interactions in water, *Proc. Natl. Acad. Sci. U.S.A*, 106, 10466-10470 (DOI:10.1073/pnas.0809934106).

188. Cougnon F. B. L., Ponnuswamy N., Jenkins N. A., Pantoş G. D., Sanders J. K. M. (2012), Structural parameters governing the dynamic combinatorial synthesis of catenanes in water, *J. Am. Chem. Soc.*, 134, 19129-19135 (DOI: 10.1021/ja3075727).

189. Li J., Nowak P., Otto S. (2013), Dynamic combinatorial libraries: From exploring molecular recognition to systems chemistry, *J. Am. Chem. Soc.*, 135, 9222-9239 (DOI: 10.1021/ja402586c).

190. Ponnuswamy N., Cougnon F. B. L., Clough, J. M., Pantos G. D., Sanders J. K. M. (2012), Discovery of an organic trefoil knot, *Science*, 338, 783-785 (DOI: 10.1126/science.1227032).

191. Vauthey S., Santoso S., Gong H., Watson N., Zhang S. (2002), Molecular self-assembly of surfactant-like peptides to form nanotubes and nanovesicles, *Proc. Natl. Acad. Sci. USA*, 99 5355-5360 (DOI: 10.1073/pnas.072089599).

192. Ellis-Behnke R. G., Liang Y.-X., You S.-W., Tay D. K. C., Zhang S., So K.-F., Schneider G. E. (2006), Nano neuro knitting: Peptide nanofiber scaffold for brain repair and axon regeneration with functional return of vision, *Proc. Natl. Acad. Sci. USA*, 103, 5054-5059 (DOI: 10.1073/pnas.0600559103).

193. Ostrov N., Gazit E. (2010), Genetic engineering of biomolecular scaffolds for the fabrication of organic and metallic nanowires, *Angew. Chem. Int. Ed.*, 49, 3018-3021 (DOI: 10.1002/anie.200906831).

194. Yemini M., Reches M., Gazit E., Rishpon J. (2005), Peptide nanotube-modified electrodes for enzyme-biosensor applications, *Anal. Chem.*, 77, 5155-5159 (DOI: 10.1021/ac050414g).

195. Love J. C., Estroff L. A., Kriebel J. K., Nuzzo R. G., Whitesides G. M. (2005), Self-assembled monolayers of thiolates on metals as a form of nanotechnology, *Chem. Rev*., 105, 1103-1169 (DOI: 10.1021/cr0300789).

196. Ostrov N., Gazit E. (2010), Genetic engineering of biomolecular scaffolds for the fabrication of organic and metallic nanowires, *Angew. Chem., Int. Ed*., 49, 3018-3021 (DOI: 10.1002/anie.200906831).

197. Metallo S. J., Kane R. S., Holmlin R. E., Whitesides G. M. (2003), Using bifunctional polymers presenting vancomycin and fluorescein groups to direct anti-fluorescein antibodies to self-assembled monolayers presenting D-alanine-D-alanine groups, *J. Am. Chem. Soc.*, 125, 4534-4540 (DOI: 10.1021/ja030045a).

198. Collins P. G., Arnold M. S., Avouris P. (2001), Engineering carbon nanotubes and nanotube circuits using electrical breakdown, *Science*, 292, 706-709 (DOI: 10.1126/science.1058782).

199. Cui Y., Wei Q. Q., Park H. K., Lieber C. M. (2001), Nanowire nanosensors for highly sensitive and selective detection of biological and chemical species, *Science*, 293, 1289- 1292 (DOI: 10.1126/science.1062711).

200. Huang Y., Duan X., Cui Y., Lauhon L. J., Kim K. H., Lieber C. M. (2001), Logic gates and computation from assembled nanowire building blocks, *Science*, 294, 1313-1317 (DOI: 10.1126/science.1066192).

201. Alivisatos A. P. (1996), Semiconductor clusters, nanocrystals, and quantum dots, *Science*, 271, 933-937 (DOI: 10.1126/science.271.5251.933).

202. Peng X. G., Manna L., Yang W. D., Wickham J., Scher E., Kadavanich A., Alivisatos A. P. (2000), Shape control of CdSe nanocrystals, *Nature*, 404, 59-61 (DOI: 10.1038/35003535).

203. Murphy C. J., Jana N. R. (2002), Controlling the aspect ratio of inorganic nanorods and nanowires, *Adv. Mater.*, 14, 80-82 (DOI: 10.1002/1521-4095(20020104)14:1<80::AID-ADMA80>3.0.CO;2-#).

204. Dujardin E., Mann S. (2002), Bio-inspired materials chemistry, *Adv. Mater*., 14, 775-788 (DOI: 10.1002/1521-4095(20020605)14:11<775::AID-ADMA775>3.0.CO;2-0).

205. Niemeyer C. M. (2001), Nanoparticles, proteins, and nucleic acids: Biotechnology meets materials science, *Angew. Chem., Int. Ed.*, 40, 4128-4158 (DOI: 10.1002/1521-3773(20011119)40:22<4128::AID-ANIE4128>3.0.CO;2-S).

206. Ray S., Das A. K., Banerjee A. (2006), Smart oligopeptide gels: *In situ* formation and stabilization of gold and silver nanoparticles within supramolecular organogel networks, *Chem. Commun.*, 2816-2818 (DOI: 10.1039/b605498f).

207. Roy S., Banerjee A. (2011), Amino acid based smart hydrogel: Formation, characterization and fluorescence properties of silver nanoclusters within the hydrogel matrix, *Soft Matter*, 7, 5300-5308 (DOI: 10.1039/c1sm05034f).

208. Roy S., Baral A., Banerjee A. (2014), Tuning of silver cluster emission from blue to red using a bio-active peptide in water, *ACS Appl. Mater. Interfaces*, 6, 4050-4056 (DOI: 10.1021/am4055645).

209. Adhikari B., Biswas A., Banerjee A. (2012), Graphene oxide-based supramolecular hydrogels for making nanohybrid systems with Au nanoparticles, *Langmuir*, 28, 1460-1469 (DOI: 10.1021/la203498j).

210. Adhikari B., Biswas A., Banerjee A. (2012), Graphene oxide-based hydrogels to make metal nanoparticle-containing reduced graphene oxide-based functional hybrid hydrogels, *ACS Appl. Mater. Interfaces*, 4, 5472-5482 (DOI: 10.1021/am301373n).

211. Reches M., Gazit E. (2003), Casting metal nanowires within discrete self-assembled peptide nanotubes, *Science*, 300, 625-627 (DOI: 10.1126/science.1082387).

212. Guha S., Banerjee A. (2009), Self-assembled robust dipeptide nanotubes and fabrication of dipeptide-capped gold nanoparticles on the surface of these nanotubes, *Adv. Funct. Mater.*, 19, 1949-1961 (DOI: 10.1002/adfm.200800955).

213. Koley P., Pramanik A. (2011), Nanostructures from single amino acid-based molecules: Stability, fibrillation, encapsulation, and fabrication of silver nanoparticles, *Adv. Funct. Mater.*, 21, 4126-4136 (DOI: 10.1002/adfm.201101465).

214. Ramasamy P., Guha S., Shibu E. S., Sreeprasad T. S., Bag S., Banerjee A., Pradeep T. (2009), Size tuning of Au nanoparticles formed by electron beam irradiation of Au_{25} quantum clusters anchored within and outside of dipeptide nanotubes, *J. Mater. Chem.*, 19, 8456-8462 (DOI: 10.1039/b913405k).

215. Nanda J., Biswas A., Adhikari B., Banerjee A. (2013), A Gel-based trihybrid system containing nanofibers, nanosheets, and nanoparticles: Modulation of the rheological property and catalysis, *Angew. Chem., Int. Ed.*, 52, 5041-5045 (DOI: 10.1002/anie.201301128).

216. Khalily M. A., Ustahuseyin O., Garifullin R., Genc R., Guler M. O. (2012), Supramolecular peptide nanofiber templated Pd nanocatalyst for efficient suzuki coupling reactions in aqueous conditions, *Chem. Commun.*, 48, 11358-11360 (DOI: 10.1039/C2CC36228G).

217. Bhattacharya S., Sengupta S. (2004), Palladium catalyzed alkynylation of aryl halides (Sonogashira reaction) in water, *Tetrahedron Lett.*, 45 8733–8736 (DOI: 10.1016/j.tetlet.2004.09.131).

218. Bhattacharya S., Srivastava A., Sengupta S. (2005), Remarkably facile Heck and Suzuki reactions in water using a simple cationic surfactant and ligand-free palladium catalysts, *Tetrahedron Lett*., 46, 3557-3560 (DOI: 10.1016/j.tetlet.2005.03.118).

219. Shimizu T., Kogiso M., Masuda M. (1996) Vesicle assembly in microtubes, *Nature,* 383, 487-488. (DOI: 10.1038/383487b0).

220. Banerjee I. A., Yu L., Matsui H. (2003), Cu nanocrystal growth on peptide nanotubes by biomineralization: Size control of Cu nanocrystals by tuning peptide conformation, *Proc. Natl. Acad. Sci. USA,* 100, 14678-14682 (DOI: 10.1073/pnas.2433456100).

221. Djalali R., Chen Y.-f., Matsui H. (2002), Au nanowire fabrication from sequenced histidine-rich peptide, *J. Am. Chem. Soc*., 124, 13660- 13661 (DOI: 10.1021/ja028261r).

222. Yu L., Banerjee I. A., Shima M., Rajan K., Matsui H. (2004), Size-controlled Ni nanocrystal growth on peptide nanotubes and their magnetic properties, *Adv. Mater*., 16, 709-712 (DOI: 10.1002/adma.200306373).

223. Djalali R., Chen Y.-f., Matsui H. (2003), Au nanocrystal growth on nanotubes controlled by conformations and charges of sequenced peptide templates, *J. Am. Chem. Soc*., 125, 5873-5879 (DOI:10.1021/ja0299598).

224. Djalali R., Samson J., Matsui H. (2004), Doughnut-shaped peptide nano-assemblies and their applications as nanoreactors, *J. Am. Chem. Soc*., 126, 7935-7939 (DOI:10.1021/ja0319691).

225. Banerjee I. A., Yu L., Matsui H. (2005), Room-temperature wurtzite ZnS nanocrystal growth on Zn finger-like peptide nanotubes by controlling their unfolding peptide structures, *J. Am. Chem. Soc*., 127, 16002-16003 (DOI: 10.1021/ja054907e).

226. Kwak J., Lee S.-Y. (2014), Use of tyrosyl bolaamphiphile self-assembly as a biochemically reactive support for the creation of palladium catalysts, *ACS Appl. Mater. Interfaces*, 6, 6461-6468 (DOI: 10.1021/am406010a).

227. Sistach S., Rahme K., Pérignon N., Marty J.-D., de Viguerie N. L., Gauffre F., Mingotaud C. (2008), Bolaamphiphile surfactants as nanoparticle stabilizers: Application to reversible aggregation of gold nanoparticles, *Chem. Mater.*, 20, 1221-1223 (DOI: 10.1021/cm703091y).

228. Meister A., Drescher S., Mey I., Wahab M., Graf G., Garamus V. M., Hause G., Mo1gel H.-J., Janshoff A., Dobner B., Blume A. (2008), Helical nanofibers of self-assembled bipolar phospholipids as template for gold nanoparticles, *J. Phys. Chem. B*, 112, 4506-4511 (DOI: 10.1021/jp710119j).

229. Drescher S., Hempel G., Binder W. H., Dobner B., Blume A., Meister A. (2012), Functionalization of bolalipid nanofibers by silicification and subsequent one-dimensional fixation of gold nanoparticles, *Langmuir*, 28, 11615-11624 (DOI: 10.1021/la302348t).

230. Saracino G. A. A., Cigognini D., Silva D., Caprini A., Gelain F. (2013), Nanomaterials design and tests for neural tissue engineering, *Chem. Soc. Rev.*, 42, 225-262, (DOI:10.1039/c2cs35065c).

231. Zhao X., Pan F., Xu H., Yaseen M., Shan H., Hauser C. A. E., Zhang S., Lu J. R. (2010), Molecular self-assembly and applications of designer peptide amphiphiles, *Chem. Soc. Rev*., 39, 3480-3498 (DOI: 10.1039/b915923c).

232. Busseron E., Ruff Y., Moulin E., Giuseppone N. (2013), Supramolecular self-assemblies as functional nanomaterials, *Nanoscale*, 2013, 5, 7098-7140 (DOI: 10.1039/c3nr02176a).

233. Deshayes S., Morris M., Heitz F., Divita G. (2008), Delivery of proteins and nucleic acids using a non-covalent peptide-based strategy, *Adv. Drug Delivery Rev*., 60, 537-547 (DOI: 10.1016/j.addr.2007.09.005).

234. Aoyama Y. (2004), Macrocyclic glycoclusters: From amphiphiles through nanoparticles to glycoviruses, *Chem. Eur. J.*, 10, 588-593 (DOI: 10.1002/chem.200305288).

235. Li J., Gao Y., Kuang Y., Shi J., Du X., Zhou J., Wang H., Yang Z., Xu B. (2013), Dephosphorylation of D-peptide derivatives to form biofunctional, supramolecular nanofibers/hydrogels and their potential applications for intracellular imaging and intratumoral chemotherapy, *J. Am. Chem. Soc*., 135, 9907-9914 (DOI: 10.1021/ja404215g).

236. Webber M. J., Tongers J., Renault M.-A., Roncalli J. G., Losordo D. W., Stupp S. I. (2010), Development of bioactive peptide amphiphiles for therapeutic cell delivery, *Acta Biomater*., 6, 3-11 (DOI: 10.1016/j.actbio.2009.07.031).

237. Zhou M., Smith A. M., Das A. K., Hodson N. W., Collins R. F., Ulijn R. V., Gough J. E. (2009), Self-assembled peptide-based hydrogels as scaffolds for anchorage-dependent cells, *Biomaterials*, 30, 2523-2530 (DOI: 10.1016/j.biomaterials.2009.01.010).

238. Naskar J., Roy S., Joardar A., Das S., Banerjee A. (2011), Self-assembling dipeptide-based nontoxic vesicles as carriers for drugs and other biologically important molecules, *Org. Biomol. Chem.*, 9, 6610-6615 (DOI: 10.1039/c1ob05757j).

239. Sargeant T. D., Aparicio C., Goldberger J. E., Cui H., Stupp S. I. (2012), Mineralization of peptide amphiphile nanofibers and its effect on the differentiation of human mesenchymal stem cells, *Acta Biomater*., 8, 2456-2465 (DOI: 10.1016/j.actbio.2012.03.026).

240. Baral A., Roy S., Dehsorkhi A., Hamley I. W., Mohapatra S., Ghosh S., Banerjee A. (2014), Assembly of an injectable noncytotoxic peptide-based hydrogelator for sustained release of drugs, *Langmuir*, 30, 929-936 (DOI: 10.1021/la4043638).

241. Ray S., Das A. K., Banerjee A. (2007), pH-Responsive, bolaamphiphile-based smart metallo-hydrogels as potential dye-adsorbing agents, water purifier, and vitamin B_{12} carrier, *Chem. Mater.*, 19, 1633-1639 (DOI: 10.1021/cm062672f).

242. Qin L., Duan P., Xie F., Zhang L., Liu M. (2013), A metal ion triggered shrinkable supramolecular hydrogel and controlled release by an amphiphilic peptide dendron, *Chem. Commun*., 49, 10823-10825 (DOI: 10.1039/c3cc47004k).

243. Jain A. K., Reddy V. V., Paul A., Muniyappa K., Bhattacharya S. (2009), Synthesis and evaluation of a novel class of G-quadruplex-stabilizing small molecules based on the 1,3-phenylene-bis(piperazinyl benzimidazole) system, *Biochemistry*, 48, 10693-10704 (DOI: 10.1021/bi9003815).

244. Moitra P., Kumar K., Kondaiah P., Bhattacharya S. (2014), Efficacious anticancer drug delivery mediated by a pH-sensitive self-assembly of a conserved tripeptide derived from tyrosine kinase NGF receptor, *Angew. Chem. Int. Ed.*, 53, 1113-1117 (DOI: 10.1002/anie.201307247).

245. Yu L., Banerjee I. A., Gao X., Nuraje N., Matsui H. (2005), Fabrication and application of enzyme-incorporated peptide nanotubes, *Bioconjugate Chem*., 16, 1484-1487 (DOI: 10.1021/bc050199a).

246. Denoyelle S., Polidori A., Brunelle M., Vuillaume P. Y., Laurent S., ElAzhary Y., Pucci B. (2006), Synthesis and preliminary biological studies of hemifluorinated bifunctional bolaamphiphiles designed for gene delivery, *New J. Chem*., 30, 629-646 (DOI: 10.1039/b513944a).

247. Patil S. P., Jeong H. S., Kim B. H. (2012), A low-molecular-weight supramolecular hydrogel of riboflavin bolaamphiphile for VEGF-siRNA deliverywzy, *Chem. Commun*., 48, 8901-8903 (DOI: 10.1039/c2cc34466a).

248. Eaton M. A. W., Baker T. S., Catterall C. F., Crook K., Macaulay G. S., Mason B., Norman T. J., Parker D., Perry J. J. B., Taylor R. J., Turner A., Weir A. N. (2000), A new self-assembling system for targeted gene delivery, *Angew. Chem., Int. Ed*., 39, 4063-4067 (DOI: 10.1002/1521-3773(20001117)39:22<4063::AID-ANIE4063>3.0.CO;2-X).

249. Wang Y., Chen J., Chen Y., Li W., Yu C. (2014), Polymer-induced perylene probe excimer formation and selective sensing of DNA methyltransferase activity through the monomer-excimer transition, *Anal. Chem*., 86, 4371-4378 (DOI: 10.1021/ac500195u).

250. Lim Y.-b., Park S., Lee E., Jeong H., Ryu J.-H., Lee M. S., Lee M. (2007), Glycoconjugate nanoribbons from the self-assembly of carbohydrate-peptide block molecules for controllable bacterial cell cluster formation, *Biomacromolecules*, 8, 1404-1408 (DOI: 10.1021/bm0700901).

251. Lim Y.-b., Park S., Lee E., JRyu.-H., Yoon Y.-R., Kim T.-H., Lee M. (2007), Tunable bacterial agglutination and motility inhibition by self-assembled glyco-nanoribbons, *Chem. Asian J.*, 2, 1363-1369 (DOI: 10.1002/asia.200700163).

252. Yu G., Li J., Yu W., Han C., Mao Z., Gao C., Huang F. (2013), Carbon nanotube/biocompatible bola-amphiphile supramolecular biohybrid materials: Preparation and their application in bacterial cell agglutination, *Adv. Mater*., 25, 6373-6379 (DOI: 10.1002/adma.201302942).

253. Li X., Kuang Y., Shi J., Gao Y., Lin H.-C., Xu B. (2011), Multifunctional, biocompatible supramolecular hydrogelators consist only of nucleobase, amino acid, and glycoside, *J. Am. Chem. Soc.*, 133, 17513-17518 (DOI: 10.1021/ja208456k).

254. Mishra A., Purkayastha B. P. D., Roy J. K., Aswal V. K., Maiti P. (2012), Nanoparticle controlled self-assembly in varying chain extended polyurethanes as potential nanobiomaterials, *J. Phys. Chem. C*, 116, 2260-2270 (DOI: 10.1021/jp210560s).

255. de la Rica R., Matsui H. (2010), Applications of peptide and protein-based materials in bionanotechnology, *Chem. Soc. Rev.*, 39, 3499-3509(DOI: 10.1039/b917574c).

256. Zhao Z., Banerjee I. A., Matsui H. (2005), Simultaneous targeted immobilization of anti-human IgG-coated nanotubes and anti-mouse IgG-coated nanotubes on the complementary antigen-patterned surfaces via biological molecular recognition, *J. Am. Chem. Soc.*, 127, 8930-8931, (DOI: 10.1021/ja051053p).

257. Zhao Z., Matsui H. (2007), Accurate immobilization of antibody-functionalized peptide nanotubes on protein-patterned arrays by optimizing their ligand–receptor interactions, *Small*, 3, 1390-1393 (DOI: 10.1002/smll.200700006).

258. Yang L., Nuraje N., Bai H., Matsui H. (2008), Crossbar assembly of antibody-functionalized peptide nanotubes via biomimetic molecular recognition, *J. Pept. Sci*., 14, 203-209 (DOI: 10.1002/psc).

259. Banerjee I. A., Yu L., Matsui H. (2003), Application of host-guest chemistry in nanotube-based device fabrication: Photochemically controlled immobilization of azobenzene nanotubes on patterned α-CD monolayer/Au substrates via molecular recognition, *J. Am. Chem. Soc*., 125, 9542-9543 (DOI:10.1021/ja0344011).

260. Chen Y.-f., Banerjee I. A., Yu L., Djalali R., Matsui H. (2004), Attachment of ferrocene nanotubes on β-cyclodextrin self-assembled monolayers with molecular recognitions, *Langmuir*, 20, 8409-8413 (DOI: 10.1021/la049560s).

261. de la Rica R., Mendoza E., Lechuga L. M., Matsui H. (2008), Label-free pathogen detection with sensor chips assembled from peptide nanotubes, *Angew. Chem., Int. Ed*., 47, 9752 -9755 (DOI: 10.1002/anie.200804299).

262. de la Rica R., Pejoux C., Fernandez-Sanchez C., Baldi A., Matsui H. (2010), Peptide-nanotube biochips for label-free detection of multiple pathogens, *small*, 6, 1092-1095 (DOI: 10.1002/smll.201000151).

Chapter 2

Materials and Methods

2.1 Introduction

This chapter describes the synthesis of peptide bolaamphiphiles and peptide derivatives by solution phase methodology. This chapter provides detailed characterization techniques such as spectroscopic measurements, and many microscopic studies used in this work.

2.2 Experimental Procedures

2.2.1 Source of Chemicals

All the amino acids, *tert*-butylpyrocarbonate, dicyclohexylcarbodiimide (DCC), N,N'-Diisopropylcarbodiimide (DIPC), 1-hydroxybenzotriazole (HOBt) and benzyl alcohol were purchased from Sigma-Aldrich, U.S.A.; E-Merck, Germany and SRL, India. Deuterated solvents $CDCl_3$, DMSO-d_6 and D_2O for NMR characterization were obtained from Sigma-Aldrich, U.S.A. Slica gel (100-200 mesh) for column chromatography was obtained from SRL and TLC pre-coated silica gel plates (Kieselgel 60F254, Merck) were taken from Merck, India. The succinic anhydride, K_2PtCl_4 and $PdCl_2$ were obtained from SD Fine Chemicals Pvt. Ltd. All the aryl boronic acids and aryl halides were also purchased from SD Fine Chemicals Pvt. Ltd., India. The N-methyl morpholine was taken from SRL, India. All other local chemicals were purchased from local manufactures like SD Fine Chemicals Pvt. Ltd., SRL India, and E-Merck India *etc*. The enzyme Lipase from *candida rugosa* was obtained from Sigma Chemical Company, St. Louis Missouri, U.S.A. The MTT and XTT assay kits for cell culture experiments were purchased from Hi-Media Pvt. Ltd., Mumbai, India.

2.2.2 Purification of Solvents and Reagents

The solvents used during the course of synthesis were distilled accordingly.[1] Chloroform and ethyl acetate were dried with P_2O_5 and distilled. Dioxane was passed through basic alumina before use. Methanol was fractionally distilled with CaO and used.[2] Thionyl chloride was distilled from boiled linseed oil (20 mL/50 g $SOCl_2$). Dimethylformamide (DMF) was fractionally distilled using CaH_2 under reduced pressure.

2.2.3 Amino Acid Derivatives

All amino acid methyl ester hydrochlorides used in the study were prepared by thionyl chloride-absolute methanol procedure[3] and Boc- amino acids used in this work were synthesized using Schnabel's method.[4] The amino acid benzyl ester was synthesized using a simple method involving heating of amino acid with benzyl alcohol in presence of *p*-toluene sulphonic acid in dean stark apparatus.

2.2.4 Solution Phase Peptide Bolaamphiphile Synthesis

The solution phase peptide synthesis[5] is a classical and more powerful approach in peptide chemistry. All the peptide bolaamphiphiles mentioned in this thesis were dipeptide appended bolaamphiphiles with a centrally located flexible succinic acid moiety. All the peptide bolaamphiphiles and peptide derivatives used in this study were synthesized by conventional solution phase methodology. At first step, methyl ester or benzyl ester protected amino acids were reacted with succnic anhydride to form N-terminus succinic acid appended amino acids at room temperature by solution phase methodology. Then, the coupling reactions were successively performed by using conventional coupling agent (DCC / HOBt) or (DIPC / HOBt) by solution phase peptide synthesis. All the coupling reactions were done at room temperature (25 °C). To prevent the racemization problem during the coupling reactions, HOBt was used in the coupling reactions. This reacts with acyl urea and form less reactive ester which is less labile toward racemization. The possibility of formation of diastereomers due to racemization effect was checked by NMR and HPLC. Generally, no diastereomers or very little 1-5% diastereomers were found. For synthesis of peptide derivatives, *tert*-butyloxycarbonyl (Boc-) group was used for N-terminus protection of amino acids. The C-terminus deprotections were performed by saponification for ester groups in alkaline methanolic solutions at room temperature (25 °C).

2.3 Characterization and Purification of Compounds

All the reactions were routinely monitored by thin layer chromatography (TLC) on pre-coated silica gel plates (Kieselgel 60F254, Merck) using $CHCl_3$:MeOH (9:1) or $CHCl_3$:CH_3OH:CH_3COOH (10:2:0.1) as eluents before work up. The crude products

were purified by column chromatography using silica gel (100-200 mesh size) as stationary phase and $CHCl_3$-MeOH as eluents. Detailed characterization was performed at every stage by the analysis of 300 MHz and 400 MHz ^1H NMR and mass spectrometry.

2.3.1 NMR Spectroscopy

All NMR studies were carried out on a Bruker AV 300 MHz spectrometer at 300 K and a Bruker AV 400 MHz NMR. TMS was used as internal reference and the deuterated solvents ($CDCl_3$, DMSO-d_6 and D_2O) were used. The compound concentrations were generally used in the range of 1-10 mmol L^{-1}.

2.3.2 Mass Spectrometry

Mass spectra of some compounds were recorded on a Waters HPLCMS system (Column Symmetry C18, 7mm) by negative mode electrospray ionization. The other compounds were recorded on a Bruker micrOTOF-Q II instrument in positive- and negative-mode electrospray ionizations using methanol/water, acetonitrile/water and chloroform as liquid carrier.

2.3.3 Polarimeter Study

Specific rotations of the synthesized compounds were measured on an Autopol®V automatic polarimeter (Rudolph research analytical). The cell (length = 100 mm, capacity = 2 mL) was used for this study at 20 °C. The compounds were dissolved in highly purified methanol and chloroform.

2.3.4 HPLC Analysis

HPLC grade acetonitrile and water were used for HPLC analysis. The dynamic reaction mixture was characterized by reverse phase symmetry C18 column (250 x 4.6 cm, 5 μm particle size). UV-Vis absorbance was monitored at 280 nm. Separations were achieved by running the column with acetonitrile-water as eluent at a flow rate of 1 mL min^{-1} at 25 °C. The sample preparation involved mixing 100 μL of gel with acetonitrile-water (900 μL, 50:50 mixture). The samples were then filtered through a 0.45 μm syringe filter (Whatman, 150 units, 13 mm diameter, 2.7 mm pore size) prior to injection. A 20 μL of

sample was injected into a Dionex Acclaim ® 120 C 18 column of 250 mm length with an internal diameter of 4.6 mm and 5 μm fused silica particles at a flow rate of 1 mL $min.^{-1}$

Solvent gradiant is given below.

Time/min.	**% of H_2O (0.1% TFA)**	**% of Acetonitrile (0.1% TFA)**
0	80	20
4	80	20
35	20	80
40	20	80
42	80	20

2.3.5 FT-IR Spectroscopy

FT-IR spectra were taken using a Bruker (Tensor 27) FT-IR spectrophotometer. The solid-state measurements were performed using the KBr pellet technique with a scan range between 400 to 4000 cm^{-1} over 64 scans at a resolution of 4 cm^{-1} and at an interval of 1 cm^{-1}. The gel sample was prepared in D_2O, placed between crystal Zn-Se windows and scanned between 900 to 4000 cm^{-1} over 64 scans at a resolution of 4 cm^{-1} and at an interval of 1 cm^{-1}. For DMS (Dimethyl sulphate) and Lipase catalyzed dynamic library, the secondary structures were studied during the course of the reactions. For other peptide bolaamphiphiles, the gels were prepared in D_2O. In FTIR measurement, the reference spectra were recorded with D_2O. One drop of D_2O was placed between two ZnSe windows and the reference spectrum was recorded. Later, the gel sample was placed between two ZnSe windows and the spectrum was taken. After D_2O subtraction, the secondary structures were concluded.

2.3.6 Circular Dichroism (CD) Spectroscopy

Secondary structures of peptide bolaamphiphiles were analyzed with Jasco J-815 circular dischroism spectrometer. For all the case, peptide hydrogel and the Pd nanoparticles embedded in hydrogel, were diluted to final concentration of 10 μM to 500 μM in ddH_2O and measured from 300 nm to 190 nm with 0.1 data pitch, 20 nm/min scanning speed, 1 nm band width and 4 s D.I.T.

2.3.7 Rheology Analysis

Oscillating rheology was used to quantify the final mechanical properties of the peptide bolaamphiphile hydrogels. For each case 2 mL of peptide bolaamphiphile hydrogel (8-25 mmol L^{-1}) was prepared. The experiment was done on a Paar Physica Modular Compact Rheometer (MCR 301, Austria). 50 and 25 mm cone plate with a 1° angle configuration were used and the temperature was set constant at 25 °C. Storage (G') and loss (G") moduli were measured at a strain range of 0.05-0.1% with true gap ranging from 0.05 to 0.097 mm.

2.3.8 UV-Vis Spectroscopy

UV-Vis absorption spectra of the hydrogels and metal nanoparticles in hydrogel were recorded using a Varian Cary100 Bio UV-Vis spectrophotometer.

2.3.9 Fluorescence Spectroscopy

Fluorescence emission spectra of the peptide bolaamphiphiles solutions and hydrogels were recorded on a Horiba Scientific Fluoromax-4 spectrophotometer with a 1 cm path length quartz cell at room temperature. The slit width for the emission was set at 2-5 nm and a 1 nm data pitch. The excitation spectra of these samples were also done in same instrument and same conditions.

2.3.10 Time Correlated Single Photon Counting (TCSPC)

A 2 mL of gel sample was prepared in a quartz cuvette (1 cm × 1 cm) and time correlated single photon counting (TCSPC) experiment was performed on Horiba Yovin (Model: Fluorocube-01-NL) instrument. Sample was excited at 376 nm using a picosecond diode laser (Model: Pico Brite-375L). The signals were collected at magic angle (54.70) polarization using a photomultiplier tube (TBX-07C) as detector, which has a dark counts less than 20 cps. The instrument response function (IRF, FWHM~140 ps) was recorded using a very dilute scattering solution. The data analysis was performed using IBH DAS (version 6, HORIBA Scientific, Edison, NJ) decay analysis software.

The amplitude-weighted lifetime was estimated by

$\langle\tau\rangle = \sum_{i=1}^{n} a_i \tau_i$

where τ_i is the fluorescence lifetime of various fluorescent species and a_i are the normalized pre-exponential factors. The goodness of the fit was judged by reduced chi-squere (χ^2) value.

2.3.11 Field Emission Gun-Scanning Electron Microscopy (FEG-SEM) Study

For SEM study, some hydrogels were dried on a glass slide and coated with gold. Then the micrographs were recorded in a SEM apparatus (Jeol Scanning Microscope-JSM-7600F). The other hydrogel samples were dried on a glass slide and coated with platinum. Then the micrographs were recorded on a SEM apparatus (Jeol Scanning Microscope-JSM-6700F).

2.3.12 Transmission Electron Microscopy (TEM) Study

High resolution transmission electron microscopic images were taken using PHILIPS electron microscope (model: CM 200), JEM 2010 electron microscope and JEM-2100 HRTEM, operated at an accelerating voltage of 200 kV. Dilute solutions of the hydrogel and the metal nanoparticles embedded in hydrogel were dried on carbon-coated copper grids (300 mesh) by slow evaporation in air, then allowed to dry separately in a vacuum at room temperature. The average size of the nanoparticles was determined from the TEM images.

2.3.13 Atomic Force Microscopy (AFM) Study

The morphologies of the hydrogel were also investigated by AFM. The gel samples were diluted in Milli Q water to a final concentration of 0.5 to 2 mmol L^{-1} and placed on a microscopic glass coverslip or mica coverslip. Then, it was dried by slow evaporation. Images were taken using an AIST-NT instrument, model no. smartSPM 1000 in soft tapping-mode.

2.3.14 Fluorescence Microscopy Study

Fluorescence microscopy experiments were performed on a home-built epifluorescence microscopy set-up. An air-cooled argon ion laser (Melles Griot, model 400-A03) with an excitation wavelength of 500 nm was used to excite the vesicle sample placed on an inverted microscope (Nikon, model Eclipse Ti-U). The laser beam was expanded and subsequently focused on the back-focal plane of an oil immersion objective (100 x 1.49 NA Nikon) to illuminate a 60 x 60 μm^2 area of the sample. The PL from the sample was recorded by a B2A filter cube (Nikon) with a 505 nm dichroic mirror and a 520 nm long-pass filter and finally imaged with a back-illuminated EMCCD camera (Andor, model iXon X3 897) at an exposure time of 300 ms. The images were analyzed with an ImageJ (Version 1.46r) NIH.

2.3.15 Optical Microscopy Study

Optical microscopy images were taken with a Zeiss AxioCam ERc5s microscope using 40 × magnification. The samples were diluted in double distilled water and prepared by depositing a few drops on a cover slip.

2.3.16 Wide-Angle X-Ray Diffraction Study

Some data were collected for the powder of peptide bolaamphiphiles and its dried hydrogels on a Rigaku Smart Lab X-ray diffractometer at a wavelength of 1.5406 Å. X-rays were produced using a sealed tube and were detected using a linear counting detector based on silicon strip technology (Scintillator NaI photomultiplier detector). The XRD measurements of rest of the samples were carried out using a Bruker D8 Advance X-ray diffractometer. The X-rays were produced using a sealed tube and the wavelength of the X-ray was 0.154 nm (Cu K-alpha). The X-rays were detected using a fast counting detector based on Silicon strip technology (Bruker LynxEye detector).

2.3 References

1. Vogel, A. I. Text book of practical organic chemistry, 4th edition, ELBS, Longmans, 1978.

2. Marcus Y., Glikberg S. (1985), Recommended method for the purification of solvent and tests for impurities: Methanol and ethanol, *Pure & Appl. Chem.*, 57, 855-864 (DOI: 10.1351/pac 198557060855).

3. Brenner M., Hubber W. (1953), Herstellung von α-mminosaureestern durch alkoholyse der methylester, *Helve. Chem. Acta*, 36, 1109-1115 (DOI: 10.1002/hlca.19530360522).

4. Schnabel E. (1967), *Ann. Chem*., 702, 188-196.

5. Bodanszky M., Bodanszky A. (1984), *The practice of peptide synthesis*, Springer-Verlag, Berlin, Heidelberg, New York, Tokyo, PP.1-282.

Chapter 3

Exploiting a Self-Assembly Driven Dynamic Nanostructured Library

3.1 Introduction

The self-assembly of small peptide based biomolecules provides a unique route in constructing functional complex biomaterials which have potential applications in tissue engineering,[1] drug delivery,[2] biosensing[3] and regenerative medicine.[4] Supramolecular hydrogels formed from the self-assembly of small peptide based molecules have received attention due to their unique merits such as their synthetic economy, biocompatibility, low toxicity and inherent biodegradability.[5] Several stimuli including pH, solvent polarity, ionic strength, sonication and the application of heat and light, have been used to tune the peptide self-assembly process.[6] Recently, it has been reported that the hydrolysis of glucono-δ-lactone (GDL) can lower the pH of a peptide system in a controlled manner, which allows the subsequent formation of a self-supporting hydrogel.[7] Pochan and Schneider have successfully established a route to design a β-hairpin hydrogel by the application of heat and light.[8] Some natural processes, including the formation of the cytoskeleton and the phospholipid membrane, are examples of protein self-assembly which are dynamic in nature.[9] The evolution of life emerged through chemical reactions, such as the directed self-assembly of biomolecules with different scales of complexity, and a bottom up approach has been envisaged to develop new materials.[10]Reversible chemical reactions have been used to introduce covalent bonds and functions that help to self-assemble the molecules *via* non-covalent interactions. Lehn *et al.* described constitutional dynamic libraries based on the G-quartet formation and reversible connections which involve self-organization and component selection to generate a dynamic hydrogel of the highest cohesive strength.[11] Recently, Otto *et al.* reported self-replicating peptide-derived macrocycles that have emerged from a small dynamic combinatorial library. Although all the steps are reversible, kinetically controlled mechano-sensitive self-replicating products were obtained from the self-assembly process.[12] Very recently, we have developed an enzyme catalysed dynamic peptide library which facilitates the formation of a very simple nanostructured predominant product.[13] Enzymatic ester hydrolysis which leads to hydrogel formation has been reported previously.[14] Dynamic reactions in a gel phase medium attract great interest because of their controlled product distribution. There are

various alkylating reagents for the esterification and alkylation reactions of the carboxylic acid and alcoholic functional groups. But in aqueous medium, acid catalyzed esterification and alkylation reactions are reversible which leads to a much lower amount of product conversion. Recently, methyl iodide (MeI) was used as a chemical fuel in the esterification reactions of carboxylic acid groups in a gel medium leading to the formation of monoesters and diesters as products.[15] Our objective is to exploit reversible acid catalysed esterification and alkylation reactions that lead to a single predominant product formation among the library members. Thus, dimethyl sulphate (DMS) was used as a chemical fuel in conjunction with esterification and methylation reactions which allowed the rapid generation of a dynamic combinatorial library. The library members formed a self-supporting hydrogel and showed the formation of a single predominant product. In this chapter, we present a dynamic system of esterification-ester hydrolysis and etherification-ether hydrolysis using a chemical fuel through a reversible chemical reaction in a gel phase medium with an appreciable product distribution, which may lead to a change in the morphology of the self-assembled hydrogelator molecules and the mechanical properties of the supramolecular hydrogel with time.

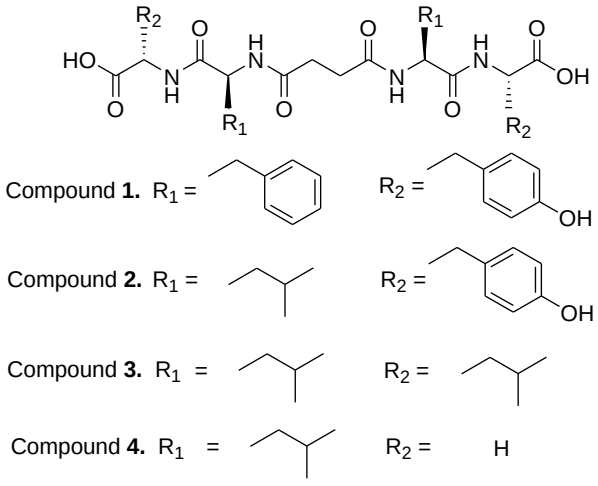

Figure 3.1. *(a) Structures of the peptide bolaamphiphiles used in the dynamic study.*

3.2 Experimental

3.2.(1) Synthesis of Bolaamphiphiles

Peptide bolaamphiphiles **1, 2, 3** and **4** employed in this chapter were synthesized by conventional solution phase methodology. The C-terminus of amino acid was protected as methyl ester. Couplings were mediated by dicyclohexylcarbodiimide-1-hydroxybenzotriazole (DCC-HOBt).The final compounds were purified and fully characterized by FT-IR, ^{1}H NMR, ^{13}C NMR and mass spectral studies.

3.2.1 Synthesis of Bolaamphiphile (HO-Tyr(4)-Phe(3)-Suc-Phe(1)-Tyr(2)-OH) 1:

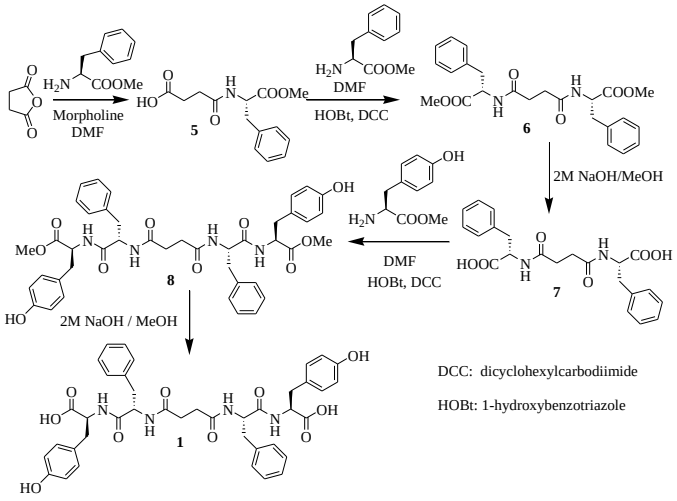

Scheme 3.1. *Synthetic scheme of peptide bolaamphiphile **1**.*

*(a) Synthesis of HO-Suc-Phe(1)-OMe **5**:* 0.5 g (5 mmol) succinic anhydride in 3 mL of DMF was cooled in an ice bath and H-Phe- OMe was isolated from 1.07 g (5 mmol) of the corresponding methyl ester hydrochloride by neutralization and subsequent extraction by ethyl acetate and the ethyl acetate extract was concentrated to 8 mL. It was then added to the reaction mixture, followed immediately by 0.5 g (5 mmol, 550 µL) N-methyl morpholine. The reaction mixture was stirred for overnight. 50 mL of ethyl acetate was added to the reaction mixture and the organic layer was washed with 1M HCl (3 × 50 mL). The ethyl acetate part was dried over anhydrous Na_2SO_4 and filtered. It was evaporated under vacuum to yield **5** as sticky compound. Purification was done by silica gel column (100-200 mesh) using chloroform-methanol (9:1) as eluent.

Yield: 1.12 g (4.01 mmol, 80.2%); FT-IR (KBr): ῡ = 3307 (st), 3085 (m), 1731 (ms), 1652 (st), 1540 (st) cm^{-1}; ^1H NMR (300 MHz, DMSO-d_6, δ_{ppm}): 8.32 (d, *J* = 7.5 Hz, 1H, NH of Phe(1)), 7.15-7.26 (m, 5Hs, aromatic ring protons of Phe(1)), 4.43-4.36 (m, 1H, $C^{\alpha}H$ of Phe(1)), 3.62 (s, 3H, $COOCH_3$), 2.99 (d, *J* = 5.7 Hz, 2H, $C^{\beta}Hs$ of Phe(1)), 2.36-2.29 (m, 4H, -CH_2- of Suc); $[\alpha]_D^{20}$ = +11.47 (*c* = 1 in CH_3OH); MS (ESI) *m/z*: 278.0 [*M*-H]$^-$, $M_{calcd.}$ = 279.

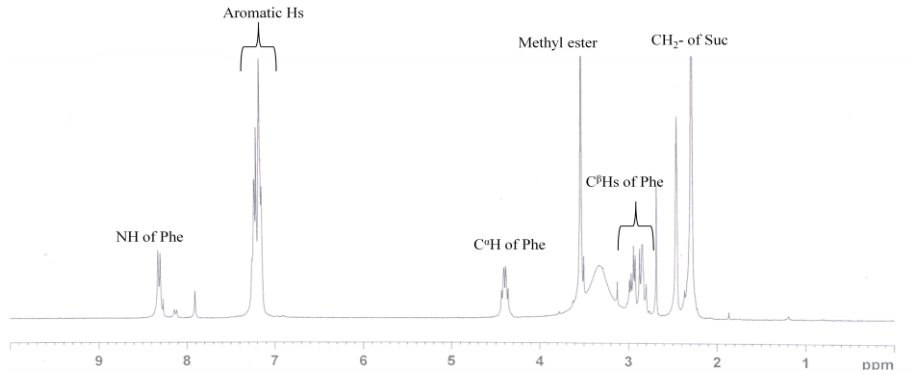

Figure 3.2. *^1H NMR spectrum (300 MHz, DMSO-d_6) of HO-Suc-F-OMe **5**.*

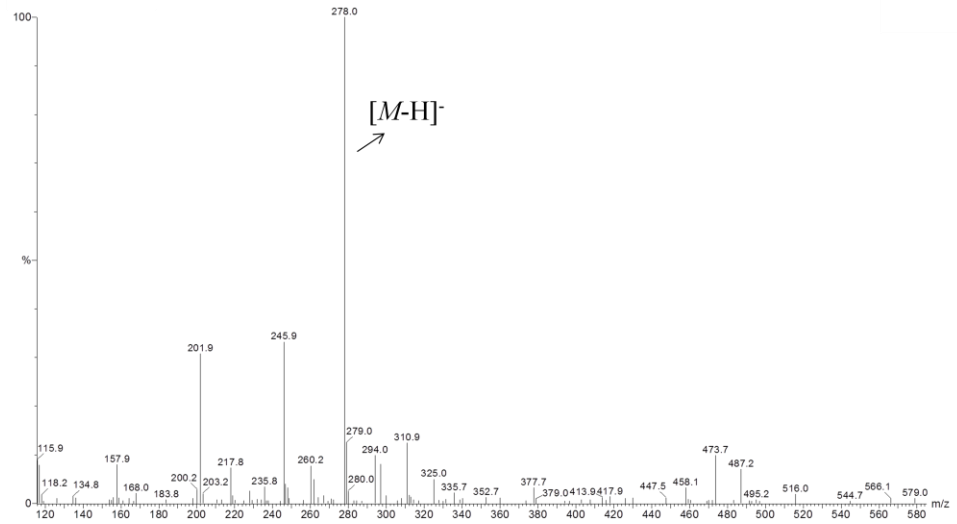

Figure 3.3. *ESI-MS spectrum of HO-Suc-F-OMe **5**.*

(b) Synthesis of MeO-Phe(2)-Suc-Phe(1)-OMe ***6****:* 0.97 g (3.5 mmol) of HO-Suc-Phe(1)-OMe **5** in 3 mL of DMF was cooled in an ice bath and H-Phe-OMe was isolated from 1.5 g (7 mmol) of the corresponding methyl ester hydrochloride by neutralization and subsequent extraction with ethyl acetate and the ethyl acetate extract was concentrated to 8 mL. It was then added to the reaction mixture, followed immediately by 0.68 g (3.85 mmol) DCC and 0.520 g (3.85 mmol) of HOBt. The reaction mixture was stirred for overnight. The residue was taken up in ethyl acetate (50 mL) and the DCU was filtered off. The organic layer was washed with 1M HCl (3 × 50 mL), brine (2 × 50 mL), 1M sodium carbonate (3 × 50 mL), brine (2 × 50 mL) and dried over anhydrous sodium sulfate and evaporated under vacuum to yield **6** as a white solid. Purification was done by silica gel column (100-200 mesh) using chloroform-methanol (9:1) as eluent.

Yield: 1.32 g (3 mmol, 85.7%); FT-IR (KBr): ῡ = 3304 (m), 1733 (ms), 1680 (st), 1642 (st), 1546 (st), 1496 (st) cm^{-1}; ^1H NMR (400 MHz, $CDCl_3$, δ_{ppm}): 7.33-7.24 (m, 10H, ring protons of Phe(1) and Phe(2)), 6.3 (d, J = 7.6 Hz, 2H, NHs of Phe(1) and Phe(2)), 4.88-4.83 (m, 2H, $C^{\alpha}Hs$ of Phe(1) and Phe(2)), 3.73 (s, 6H, $-COOCH_3$), 3.13 and 3.10 (d, J = 6 Hz, 4H, $C^{\beta}Hs$ of Phe(1) and Phe(2)), 2.46 (m, 4H, $-CH_2-$ of Suc); $[\alpha]_D^{20}$ = + 88.58 (c = 0.5 in $CHCl_3$); MS (ESI) m/z: $(M+Na)^+$ Calcd. for $C_{24}H_{28}N_2O_6Na$: 463.1845; found 463.1863.

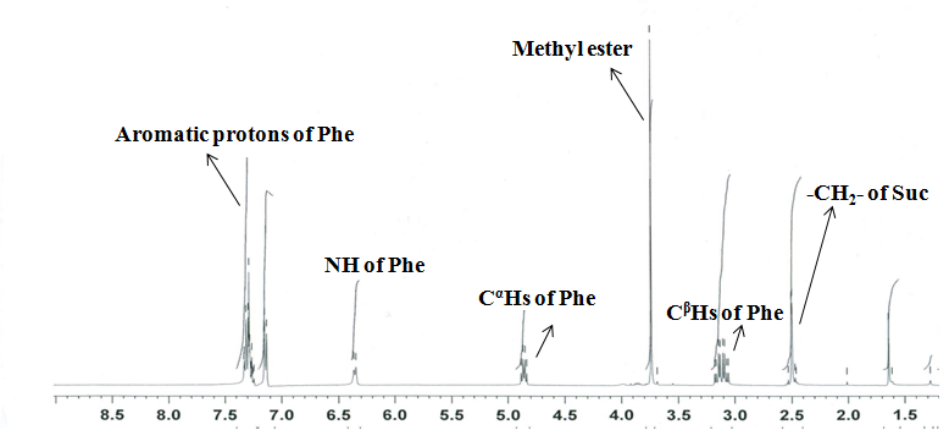

Figure 3.4. *^1H NMR spectrum (400 MHz, $CDCl_3$) of MeO-F-Suc-F-OMe* ***6****.*

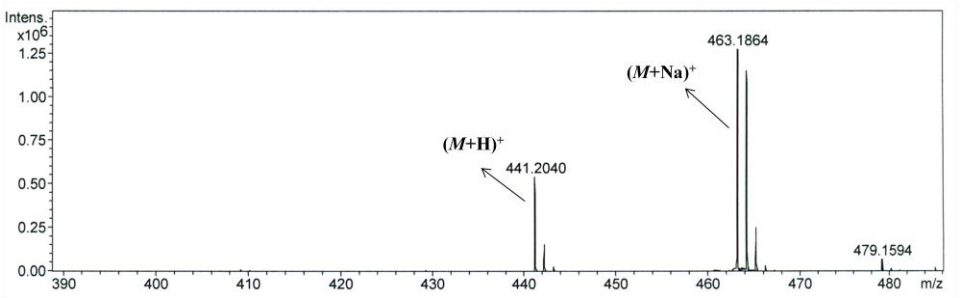

Figure 3.5. *ESI-MS spectrum of MeO-F-Suc-F-OMe* ***6****.*

(c) Synthesis of HO-Phe(2)-Suc-Phe(1)-OH ***7****:* 1.2 g (2.72 mmol) of MeO-Phe(2)-Suc-Phe(1)-OMe **6** in 6 mL MeOH was taken in a round bottom flask and 5 mL of 2M NaOH was added dropwise. The reaction was monitored by thin layer chromatography (TLC). The reaction mixture was stirred for 4 hours. 15 mL of distilled water was added to the reaction mixture and MeOH was removed under vacuum. The aqueous part was washed with diethyl ether (2 × 30 mL). Then it was cooled under ice bath for 10 minutes and then pH was adjusted to 1 by drop wise addition of 1M HCl. It was extracted with ethyl acetate (3 × 50 mL) and then, the ethyl acetate part was dried over anhydrous Na_2SO_4 and evaporated under vacuum to yield **7** as a white solid.

Yield: 1.1 g (2.67 mmol, 98%); FT-IR (KBr): $\tilde{\upsilon}$ = 3375 (st), 3354 (m), 1712 (st), 1616 (st), 1535 (st), 1496 (st) cm^{-1}. ^1H NMR (400 MHz, DMSO-d_6, δ_{ppm}): 8.19 (d, *J* = 8 Hz, 2H, NHs of Phe(1) and Phe(2)), 7.26-7.19 (m, 10H, ring protons of Phe(1) and Phe(2)), 4.37 (m, 2H, C^{α}Hs of Phe(1) and Phe(2)), 3.03 and 2.84 (d, *J* = 8.8 Hz, 4H, C^{β}Hs of Phe(1) and Phe(2)), 2.19 (m, 4H, -CH_2- of Suc); $[\alpha]_D^{20}$ = +23.60 (*c* = 0.5 in CH_3OH); MS (ESI) *m/z*: $(M+Na)^+$ Calcd. for $C_{22}H_{24}N_2O_6Na$: 435.1532; found 435.1528.

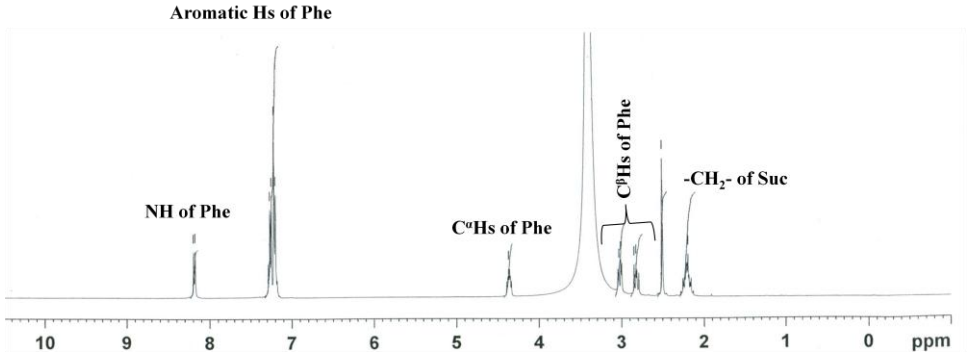

Figure 3.6. *^1H NMR spectrum (400 MHz, DMSO-d_6) of HO-F-Suc-F-OH* ***7****.*

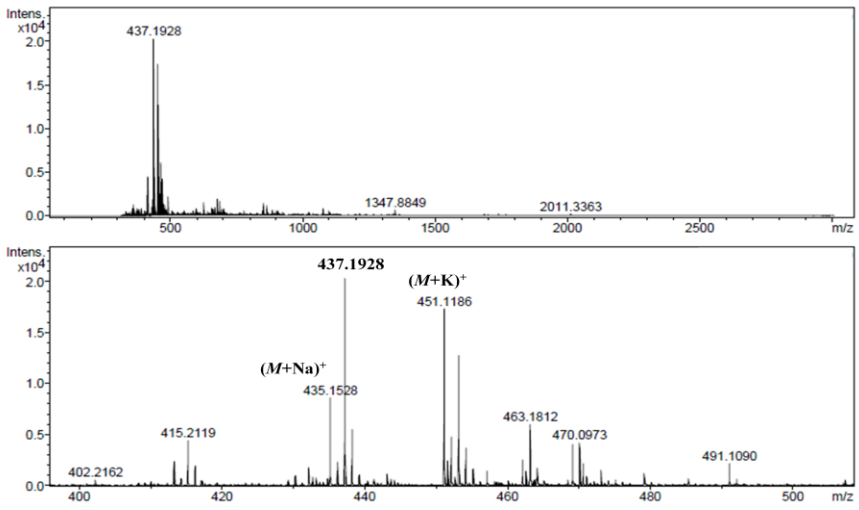

Figure 3.7. *ESI-MS spectra of HO-F-Suc-F-OH **7**.*

*(d) Synthesis of MeO-Tyr(4)-Phe(3)-Suc-Phe(1)-Tyr(2)-OMe **8**:* 1 g (2.42 mmol) of HO-Phe(2)-Suc-Phe(1)-OH **7** in 3 mL of DMF was cooled in an ice bath and H-Tyr-OMe was isolated from 2.24 g (9.7 mmol) of the corresponding methyl ester hydrochloride by neutralization and subsequent extraction with ethyl acetate and the ethyl acetate extract was concentrated to 8 mL. It was then added to the reaction mixture, followed immediately by 1.09 g (5.32 mmol) DCC and 0.718 g (5.32 mmol) of HOBt. The reaction mixture was stirred for overnight. The residue was taken up in ethyl acetate (50 mL) and the DCU was filtered off. The organic layer was washed with 1M HCl (3 × 50 mL), brine (2 × 50 mL), 1M sodium carbonate (3 × 50 mL), brine (2 × 50 mL) and dried over anhydrous sodium sulfate and evaporated under vacuum to yield **8** as a white solid. Purification was done by silica gel column (100-200 mesh) using chloroform-methanol (9:1) as eluent.

Yield: 1.55 g (2.03 mmol, 84%); FT-IR (KBr): ῡ = 3337 (st), 3292 (ms), 1737 (ms), 1616 (st), 1558 (st), 1516 (st) cm^{-1}; ^{1}H NMR (300 MHz, DMSO-d_6, δ_{ppm}): 8.31 (d, *J* = 7.5 Hz, 2H, NHs of Phe(1) and Phe(3)), 7.99 (d, *J* = 8.4 Hz, 2H, NHs of Tyr(2) and Tyr(4)), 7.19-7.12 (m, 10H, ring protons of Phe(1) and Phe(3)), 6.95 (d, *J* = 8.4, Hz, 4H, ring protons of Tyr(2) and Tyr(4)), 6.63 (d, *J* = 8.4, Hz, 4H of Tyr(2) and Tyr(4)), 4.46 (m, 2H, $C^{\alpha}Hs$ of Phe(1) and Phe(3)), 4.34 (m, 2H, $C^{\alpha}Hs$ of Tyr(2) and Tyr(4)), 3.56 (s, 6H, -$COOCH_3$), 2.93 (d, *J* = 8.4 Hz, 4H, $C^{\beta}Hs$ of Phe(1) and Phe(3)), 2.79 (d, *J* = 8.5 Hz, 4H, $C^{\beta}Hs$ of

Tyr(2) and Tyr(4)), 2.12 (m, 4H, -CH_2- of Suc); $[\alpha]_D^{20}$ = -22.22 (*c* = 0.3 in CH_3OH); MS (ESI) *m/z*: $(M+Na)^+$ Calcd. for $C_{42}H_{46}N_4O_{10}Na$: 789.3112; found 789.3188.

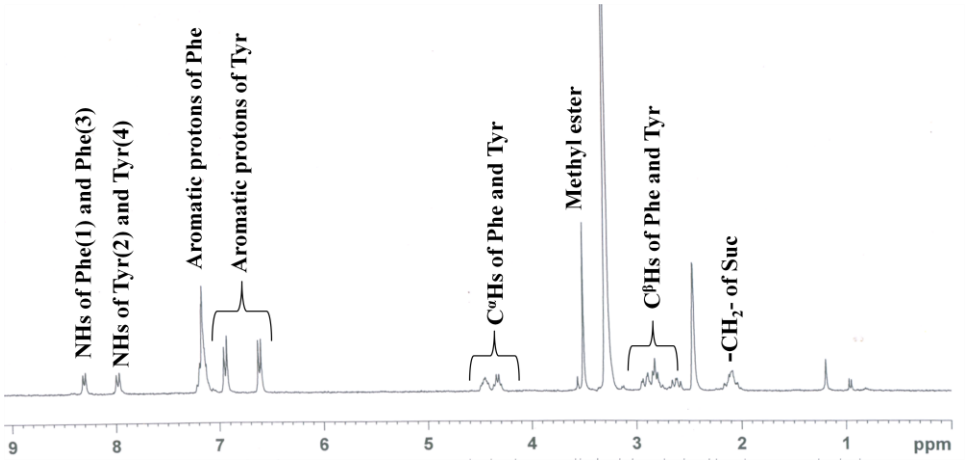

Figure 3.8. *^{1}H NMR spectrum (300 MHz, DMSO-d_6) of MeO-Y-F-Suc-F-Y-OMe* ***8***.

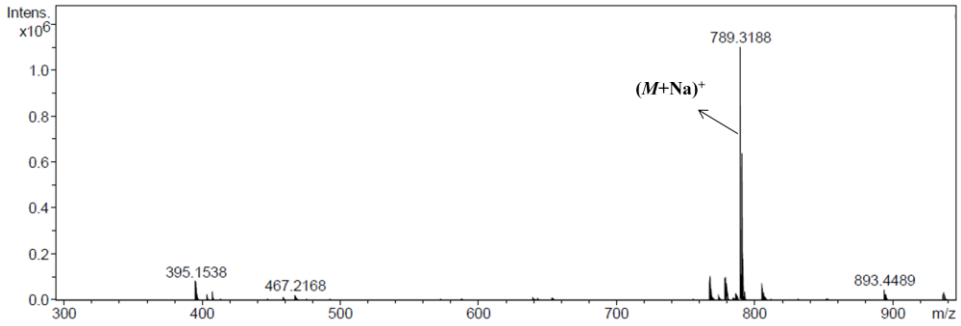

Figure 3.9. *ESI-MS spectrum of MeO-Y-F-Suc-F-Y-OMe* ***8***.

(e) Synthesis of HO-Tyr(4)-Phe(3)-Suc-Phe(1)-Tyr(2)-OH ***1****:* 1.45 g (1.89 mmol) of MeO-Tyr(4)-Phe(3)-Suc-Phe(2)-Tyr(1)-OMe **8** in 10 mL MeOH was taken in a round bottom flask and 6 mL of 2M NaOH was added to it dropwise. The reaction was monitored by thin layer chromatography (TLC). The reaction mixture was stirred for overnight. 15 mL of distilled water was added to the reaction mixture and MeOH was removed under vacuum. The aqueous part was washed with diethyl ether (2 × 30 mL). Then it was cooled under ice water bath for 10 minutes and then pH was adjusted to 1 by

drop wise addition of 1M HCl. It was extracted by ethyl acetate (3 × 50 mL) and then, the ethyl acetate part was dried over anhydrous Na_2SO_4 and evaporated under vacuum to yield **1** as a white solid. Racemization was found around 5% in this hydrolysis reaction. Yield: 1.34 g (1.81 mmol, 96%); FT-IR (KBr): ῡ = 3294 (st), 3278 (ms), 1705 (m), 1640 (st), 1536 (st), 1515 (ms) cm^{-1}; ^1H NMR (400 MHz, DMSO-d_6, δ_{ppm}): 8.19 (d, *J* = 7.6 Hz, 2H, NHs of Phe(1) and Phe(3)), 8.02 (d, *J* = 8.8 Hz, 2H, NHs of Tyr(2) and Tyr(4)), 7.22-7.12 (m, 10H, ring protons of Phe(1) and Phe(3)), 7.02 (d, *J* = 8.4, Hz, 4H, ring protons of Tyr(2) and Tyr(4)), 6.64 (d, *J* = 8.8, Hz, 4H of Tyr(2) and Tyr(4)), 4.49 (m, 2H, $C^{\alpha}Hs$ of Phe(1) and Phe(3)), 4.34 (m, 2H, $C^{\alpha}Hs$ of Tyr(2) and Tyr(4)), 3.20 (d, *J* = 8.4 Hz, 4H, $C^{\beta}Hs$ of Phe(1) and Phe(3)), 2.89 (d, *J* = 10.8 Hz, 4H, $C^{\beta}Hs$ of Tyr(2) and Tyr(4)), 2.51-2.50 (m, 4H, -CH_2- of Suc); ^{13}C NMR (100 MHz, DMSO-d_6, δ_{ppm}): 173.41 and 173.26 (-COOH), 171.57 and 171.43 (-CONH-), 156.40 (Tyr ring), 138.38, 138.30, 130.62, 130.53, 129.62, 128.41, 127.93, 127.88, 126.64, 115.49, 115.42 (aromatic ring) 54.34, 54.13 (C^{α} of Phe and Tyr), 37.87, 36.41 (C^{β} of Phe and Tyr), 31.25 (-CH_2- of Suc); $[\alpha]_D^{20}$ = -13.95 (*c* = 0.5 in CH_3OH); MS (ESI) *m/z*: $(M+Na)^+$ Calcd. for $C_{40}H_{42}N_4O_{10}Na$: 761.2799; found 761.2812.

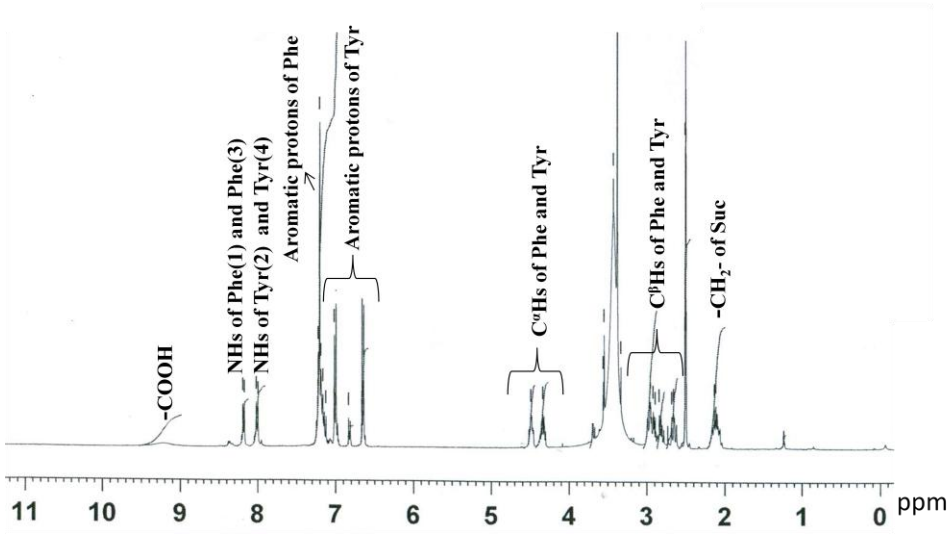

Figure 3.10. *^1H NMR spectrum (400 MHz, DMSO-d_6) of HO-Y-F-Suc-F-Y-OH **1**.*

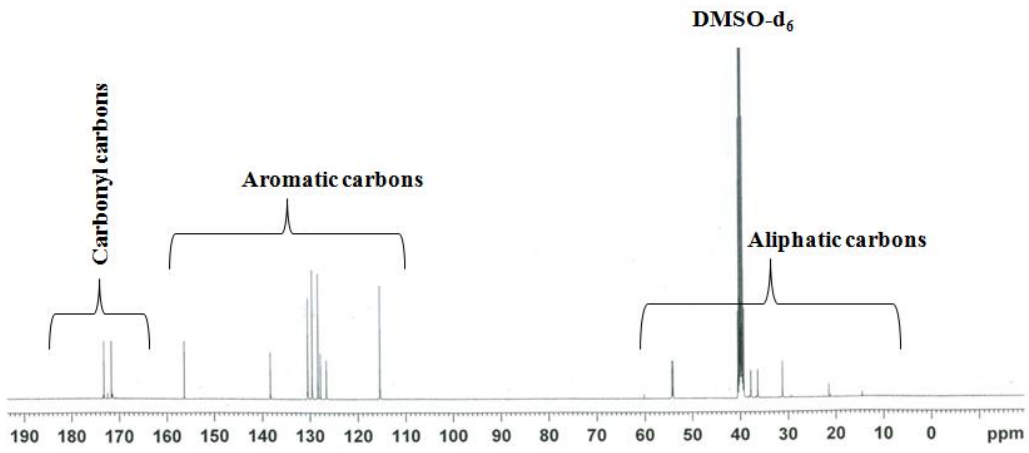

Figure 3.11. *^{13}C NMR spectrum (100 MHz, DMSO-d_6) of HO-Y-F-Suc-F-Y-OH **1**.*

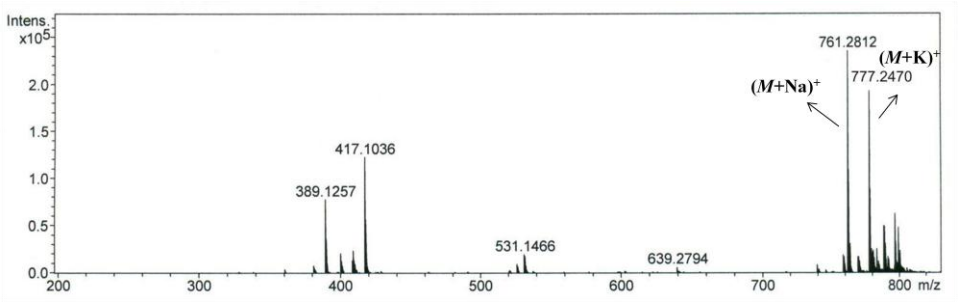

Figure 3.12. *ESI-MS spectrum of HO-Y-F-Suc-F-Y-OH **1**.*

3.2.2 Synthesis of Bolaamphiphile (HO-Tyr(4)-Leu(3)-Suc-Leu(1)-Tyr(2)-OH) 2:

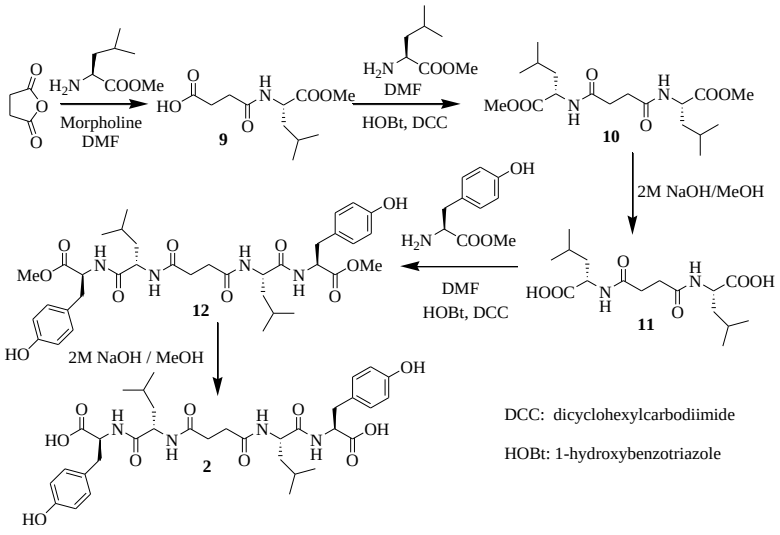

Scheme 3.2. *Synthetic scheme of peptide bolaamphiphile **2**.*

*(a) Synthesis of HO-Suc-Leu(1)-OMe **9**:* 3.021 g (30 mmol) succinic anhydride in 6 mL of DMF was cooled in an ice bath and H-Leu-OMe was isolated from 5.43 g (30 mmol) of the corresponding methyl ester hydrochloride by neutralization and subsequent extraction by ethyl acetate and the ethyl acetate extract was concentrated to 8 mL. It was then added to the reaction mixture, followed immediately by 3.033 g (30 mmol, 3 mL 300 μL) N-methyl morpholine. The reaction mixture was stirred for overnight. 50 mL of ethyl acetate was added to the reaction mixture and the organic layer was washed with 1M HCl (3 × 50 mL.). The ethyl acetate part was dried over anhydrous Na_2SO_4 and filtered. It was evaporated in vacuum to yield **9** as sticky compound. Purification was done by silica gel column (100-200 mesh) using chloroform-methanol (9:1) as eluent.

Yield: 6.24 g (25.46 mmol, ~85%); FT-IR (KBr): ῡ = 3232 (st), 3059 (m), 1731 (ms), 1648 (st), 1558 (st), 1524 (st) cm^{-1}; ^1H NMR (400 MHz, DMSO-d_6, δ_{ppm}): 12.15 (s, 2H, -COOH), 8.32 (d, J = 7.6 Hz, 1H of NH of Leu(1)), 4.33 (m, 1H, $C^{\alpha}H$ of Leu(1)), 3.67 (s, 3H, $COOCH_3$), 2.46-2.42 (m, 4H, $-CH_2-$ of Suc), 1.69 and 1.56 (m, 3H, $C^{\beta}Hs$ and $C^{\gamma}H$ of Leu(1)), 0.96 and 0.90 (d, J = 6.0 Hz, 6H, $C^{\delta}Hs$ of Leu(1)); $[\alpha]_D^{20}$ = - 6.08 (c = 1 in CH_3OH); MS (ESI) m/z: 244.0 $[M\text{-}H]^-$, $M_{calcd.}$ = 245.

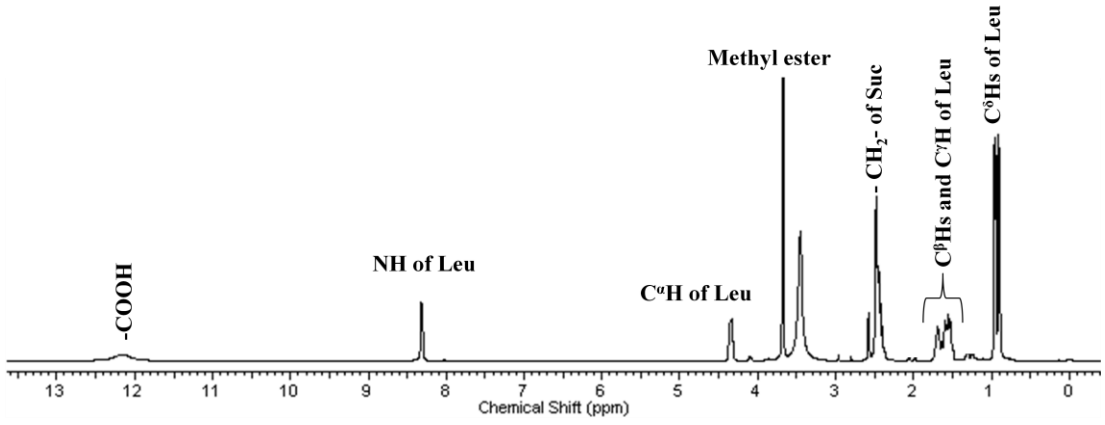

Figure 3.13. *^1H NMR spectrum (400 MHz, DMSO-d_6) of HO-Suc-L-OMe **9**.*

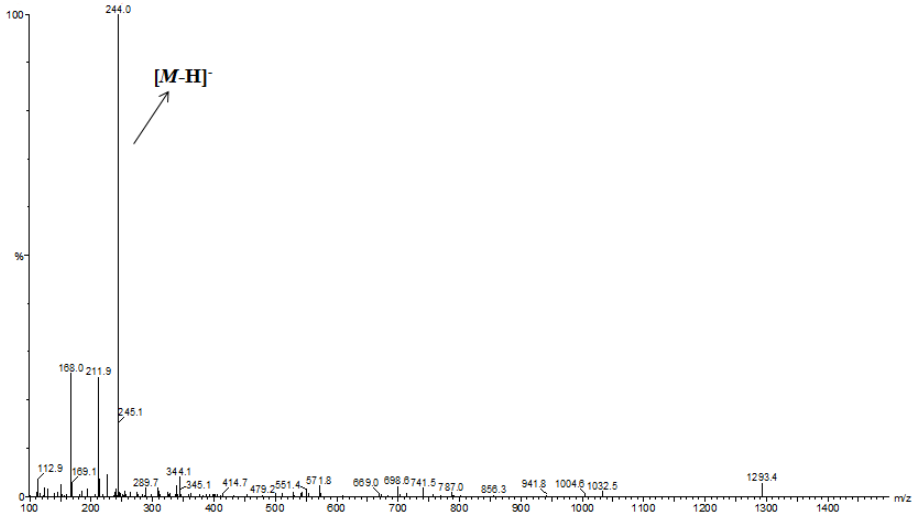

Figure 3.14. *ESI-MS spectrum of HO-Suc-L-OMe* ***9****.*

(b) Synthesis of MeO-Leu(2)-Suc-Leu(1)-OMe ***10****:* 5.49 g (22.5 mmol) of HO-Suc-Leu(1)-OMe **9** in 5 mL of DMF was cooled in an ice bath and H-Leu-OMe was isolated from 8.16 g (45 mmol) of the corresponding methyl ester hydrochloride by neutralization and subsequent extraction with ethyl acetate and the ethyl acetate extract was concentrated to 10 mL. It was then added to the reaction mixture, followed immediately by 5.10 g (24.75 mmol) DCC and 3.33 g (24.75 mmol) of HOBt. The reaction mixture was stirred for overnight. The residue was taken up in ethyl acetate (50 mL) and the DCU was filtered off. The organic layer was washed with 1M HCl (3 × 50 mL), brine (2 × 50 mL), 1M sodium carbonate (3 × 50 mL), brine (2 × 50 mL) and dried over anhydrous sodium sulfate and evaporated under vacuum to yield **10** as a white solid. Purification was done by silica gel column (100-200 mesh) using chloroform-methanol (9:1) as eluent.

Yield: 7.53 g (20.24 mmol, 90%); FT-IR (KBr): ῡ = 3252, 3076 (st), 1745 (ms), 1644 (ms), 1548 (st) cm^{-1}; ^{1}H NMR (400 MHz, $CDCl_3$, δ_{ppm}): 6.60 (d, *J* = 8.0 Hz, 2H, NHs of Leu(1) and Leu(2)), 4.61-4.56 (m, 2H, $C^{\alpha}Hs$ of Leu(1) and Leu(2)), 3.74 (s, 6H, $COOCH_3$), 2.62-2.52 (m, 4H, $-CH_2-$ of Suc), 1.69-1.64 and 1.62-1.58 (m, 6H, $C^{\beta}Hs$ and $C^{\gamma}Hs$ of Leu(1) and Leu(2)), 0.94 (d, *J* = 6.4 Hz, 12H, $C^{\delta}Hs$ of Leu(1) and Leu(2)); $[\alpha]_D^{20}$

= -35.1 (*c* = 1 in CH_3OH); MS (ESI) *m/z*: $(M+Na)^+$ Calcd. for $C_{18}H_{32}N_2O_6Na$: 395.2158; found 395.2180.

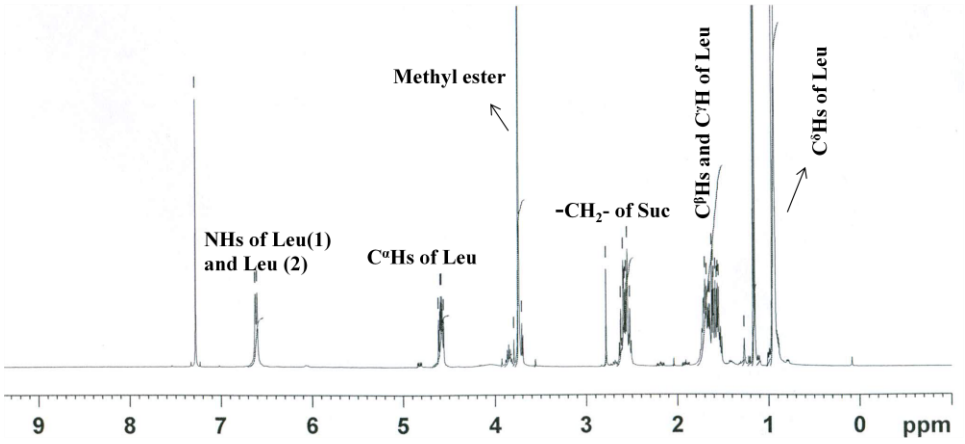

Figure 3.15. *^{1}H NMR spectrum (400 MHz, DMSO-d_6) of MeO-L-Suc-L-OMe **10**.*

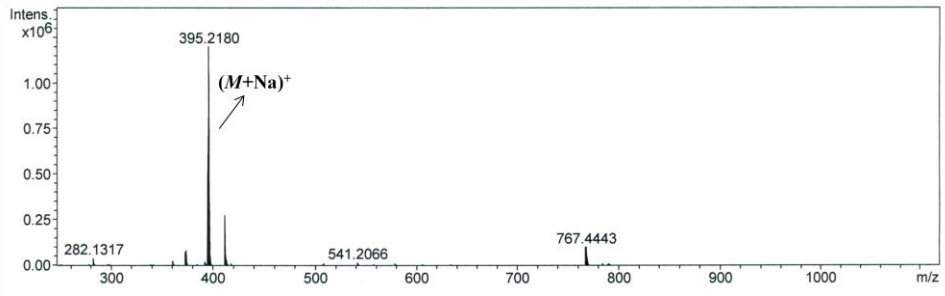

Figure 3.16. *ESI-MS spectrum of MeO-L-Suc-L-OMe **10**.*

*(c) Synthesis of HO-Leu(2)-Suc-Leu(1)-OH **11**:* 6.69 g (18 mmol) of MeO-Leu(2)-Suc-Leu(1)-OMe **10** in 10 mL MeOH was taken in a round bottom flask and 20 mL of 2M NaOH was added to it dropwise. The reaction was monitored by thin layer chromatography (TLC). The reaction mixture was stirred for 5 hours. 15 mL of distilled water was added to the reaction mixture and MeOH was removed under vacuum. The aqueous part was washed with diethyl ether (2 × 30 mL). Then it was cooled under ice bath for 10 minutes and then pH was adjusted to 1 by drop wise addition of 1M HCl. It was extracted with ethyl acetate (3 × 50 mL) and then the ethyl acetate part was dried over anhydrous Na_2SO_4 and evaporated under vacuum to yield **11** as a white solid.

Yield: 5.88 g (17.1 mmol, 95%); FT-IR (KBr): ῡ = 3338 (st), 1706 (ms), 16173 (st), 1568 (st), 1530 (w) cm^{-1}; ^{1}H NMR (400 MHz, DMSO-d_6, δ_{ppm}): 12.46 (s, 2H, -COOH), 8.10 (d, *J* = 7.6 Hz, 2H, NHs of Leu(1) and Leu(2)), 4.22-4.17 (m, 2H, $C^{\alpha}Hs$ of Leu(1) and Leu(2)), 2.40-2.30 (m, 4H, $-CH_2-$ of Suc), 1.62-1.60 and 1.50-1.49 (m, 6H, $C^{\beta}Hs$ and $C^{\gamma}Hs$ of Leu(1) and Leu(2)), 0.89 and 0.84 (d, *J* = 6.4 Hz, 12H, $C^{\delta}Hs$ of Leu(1) and Leu(2)); $[\alpha]_D^{20}$ = - 27.8 (*c* = 0.5 in CH_3OH); MS (ESI) *m/z*: $(M+Na)^+$ Calcd. for $C_{16}H_{28}N_2O_6Na$: 367.1845; found 367.1835.

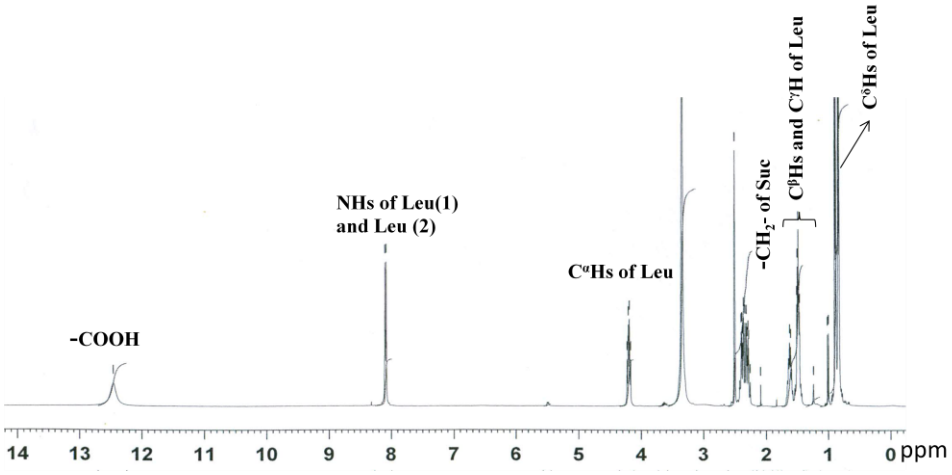

Figure 3.17. *^{1}H NMR spectrum (400 MHz, DMSO-d_6) of HO-L-Suc-L-OH **11**.*

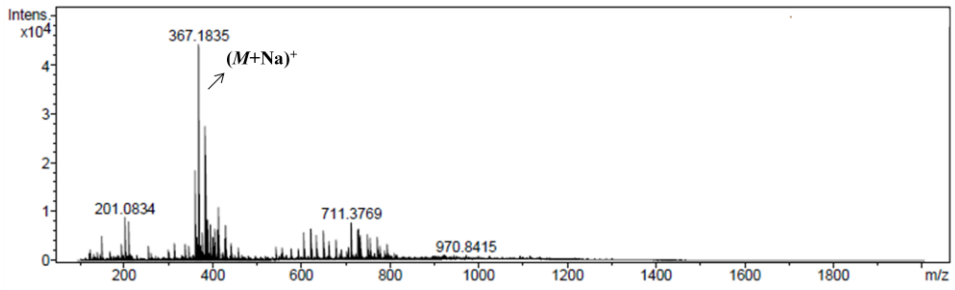

Figure 3.18. *ESI-MS spectrum of HO-L-Suc-L-OH **11**.*

*(d) Synthesis of MeO-Tyr(4)-Leu(3)-Suc-Leu(1)-Tyr(2)-OMe **12**:* 1.72 g (5 mmol) of HO-Leu(2)-Suc-Leu(1)-OH **11** in 3 mL of DMF was cooled in an ice bath and H-Tyr-OMe was isolated from 4.63 g (20 mmol) of the corresponding methyl ester hydrochloride by neutralization and subsequent extraction with ethyl acetate and the ethyl acetate extract

was concentrated to 10 mL. It was then added to the reaction mixture, followed immediately by 2.26 g (11 mmol) DCC and 1.48 g (11 mmol) of HOBt. The reaction mixture was stirred for overnight. The residue was taken up in ethyl acetate (50 mL) and the DCU was filtered off. The organic layer was washed with 1M HCl (3 × 50 mL), brine (2 × 50 mL), 1M sodium carbonate (3 × 50 mL), brine (2 × 50 mL) and dried over anhydrous sodium sulfate and evaporated under vacuum to yield **12** as a white solid. Purification was done by silica gel column (100-200 mesh) using chloroform-methanol (9:2) as eluent to get white solid as product.

Yield: 2.96 g (4.25 mmol, 85%); FT-IR (KBr): $\tilde{\upsilon}$ = 3309 (st), 1745 (ms), 1656 (st), 1547 (st), 1517 (w) cm^{-1}; ^1H NMR (400 MHz, $CDCl_3$, δ_{ppm}): 7.00 (d, *J* = 8 Hz, 4H, ring protons of Tyr(2) and Tyr(4)), 6.94 (d, *J* = 8.4 Hz, 2H, NHs of Leu(1) and Leu(3)), 6.73 (d, *J* = 8.8 Hz, 4H, ring protons of Tyr(2) and Tyr(4)), 6.65 (d, *J* = 8.4 Hz, 2H, NHs of Tyr(2) and Tyr(4)), 4.87 (m, 2H, $C^{\alpha}Hs$ of Tyr(2) and Tyr(4)), 4.47 (m, 2H, $C^{\alpha}Hs$ of Leu(1) and Leu(3)), 3.78 (s, 6H, $-COOCH_3$), 2.99 (d, *J* = 8.4 Hz, 4H, $C^{\beta}Hs$ of Tyr(2) and Tyr(4)), 2.43-2.42 (m, 4H, $-CH_2-$ of Suc), 1.62-1.61 and 1.51 -1.47 (m, 6H, $C^{\beta}Hs$ of Leu(1) and Leu(3), and $C^{\gamma}Hs$ of Leu(1) and Leu(3)); 0.96 and 0.91 (d, *J* = 6 Hz, 12H, $C^{\delta}Hs$ of Leu(1) and Leu(3)); $[\alpha]_D^{20}$ = -26.3 (*c* = 1 in CH_3OH); MS (ESI) *m/z*: $(M+H)^+$ Calcd. for $C_{36}H_{51}N_4O_{10}$: 699.3605; found 699.3648.

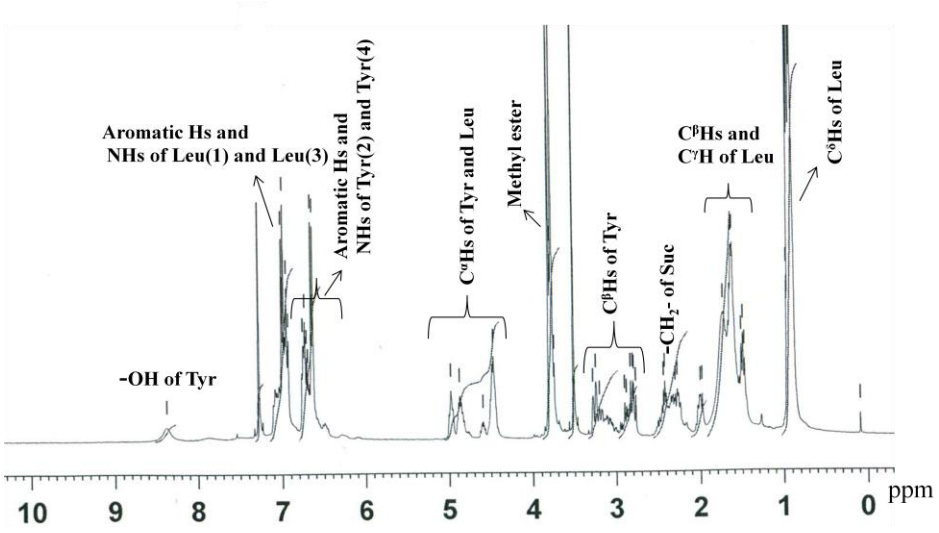

Figure 3.19. *^1H NMR spectrum (400 MHz, $CDCl_3$) of MeO-Y-L-Suc-L-Y-OMe **12**.*

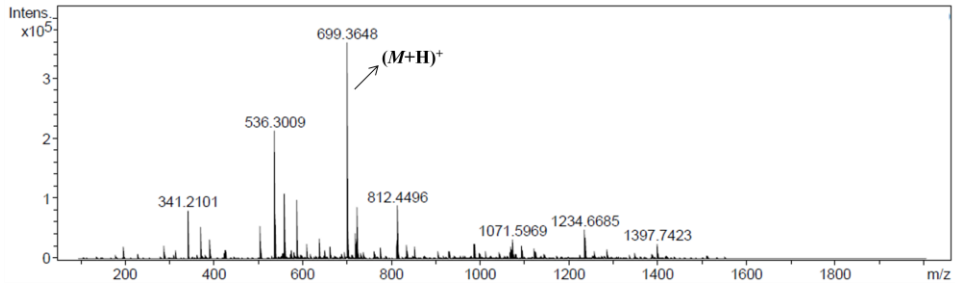

Figure 3.20. *ESI-MS spectrum of MeO-Y-L-Suc-L-Y-OMe* ***12****.*

(e) Synthesis of HO-Tyr(4)-Leu(3)-Suc-Leu(1)-Tyr(2)-OH ***2****:* 2.79 g (4 mmol) of MeO-Tyr(4)-Leu(3)-Suc-Leu(2)-Tyr(1)-OMe **12** in 150 mL MeOH was taken in a round bottom flask and 6 mL of 2M NaOH was added to it dropwise. The reaction was monitored by thin layer chromatography (TLC). The reaction mixture was stirred for overnight. 15 mL of distilled water was added to the reaction mixture and MeOH was removed under vacuum. The aqueous part was washed with diethyl ether (2 × 30 mL). Then it was cooled under ice bath for 15 minutes and then pH was adjusted to 1 by drop wise addition of 1M HCl. It was extracted with ethyl acetate (3 × 50 mL) and then the ethyl acetate part was dried over anhydrous Na_2SO_4 and evaporated under vacuum to yield **2** as a white solid. Racemization was found around 2% in this hydrolysis reaction.
Yield: 2.41 g (3.6 mmol, 90%); FT-IR (KBr): $\tilde{\upsilon}$ = 3293 (bw), 1720 (ms), 1644 (st), 1514 (st) cm^{-1}; ^1H NMR (400 MHz, DMSO-d_6, δ_{ppm}): 8.01 (d, *J* = 8.4 Hz, 2H, NHs of Leu(1) and Leu(3)), 7.94 (d, *J* = 8.4 Hz, 2H, NHs of Tyr(2) and Tyr(4)), 6.98 (d, *J* = 8.4 Hz, 4H, ring protons of Tyr(2) and Tyr(4)), 6.64 (d, *J* = 8.4 Hz, 4H, ring protons of Tyr(2) and Tyr(4)), 4.27 (m, 2H, C^{α}Hs of Tyr(2) and Tyr(4)), 4.24 (m, 2H, C^{α}Hs of Leu(1) and Leu(3)), 2.92 (d, *J* = 8.4 Hz, 2H, C^{β}Hs of Tyr(2)) 2.82 (d, *J* = 8 Hz, 2H, C^{β}Hs of Tyr(4)), 2.32 (m, 4H, -CH_2- of Suc), 1.55 and 1.40 (m, 6H, C^{β}Hs and C^{γ}Hs of Leu(1) and Leu(3)), 0.86 and 0.81 (d, *J* = 6.8 Hz, 12H, C^{δ}Hs of Leu(1) and Leu(3)); ^{13}C NMR (100 MHz, DMSO-d_6, δ_{ppm}): 173.42 (C=O), 171.92 (C=O), 171.68 (C=O), 156.36, 130.56, 128.02, 115.35, 54.52, 51.31, 36.34, 31.30, 24.75, 23.32, 22.04; $[\alpha]_D^{20}$ = - 26.4 (*c* = 0.5 in CH_3OH); MS (ESI) *m/z*: $(M+Na)^+$ Calcd. for $C_{34}H_{46}N_4O_{10}Na$: 693.3112; found 693.3112.

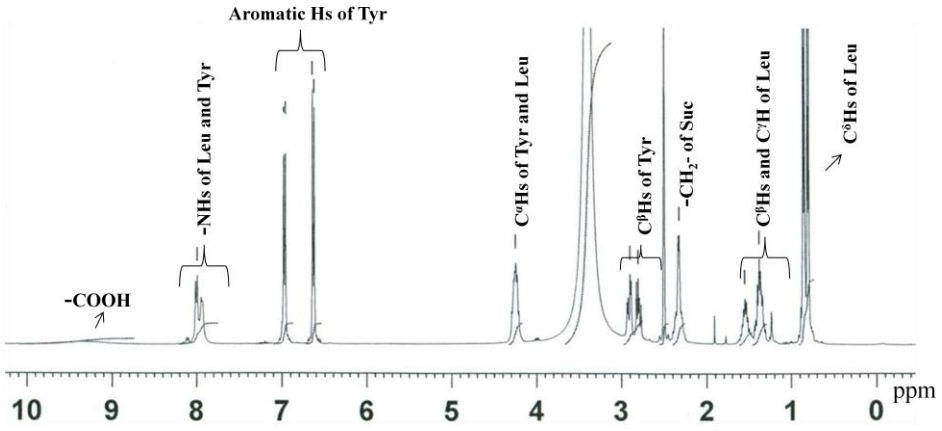

Figure 3.21. *^{1}H NMR spectrum (400 MHz, DMSO-d_6) of HO-Y-L-Suc-L-Y-OH **2**.*

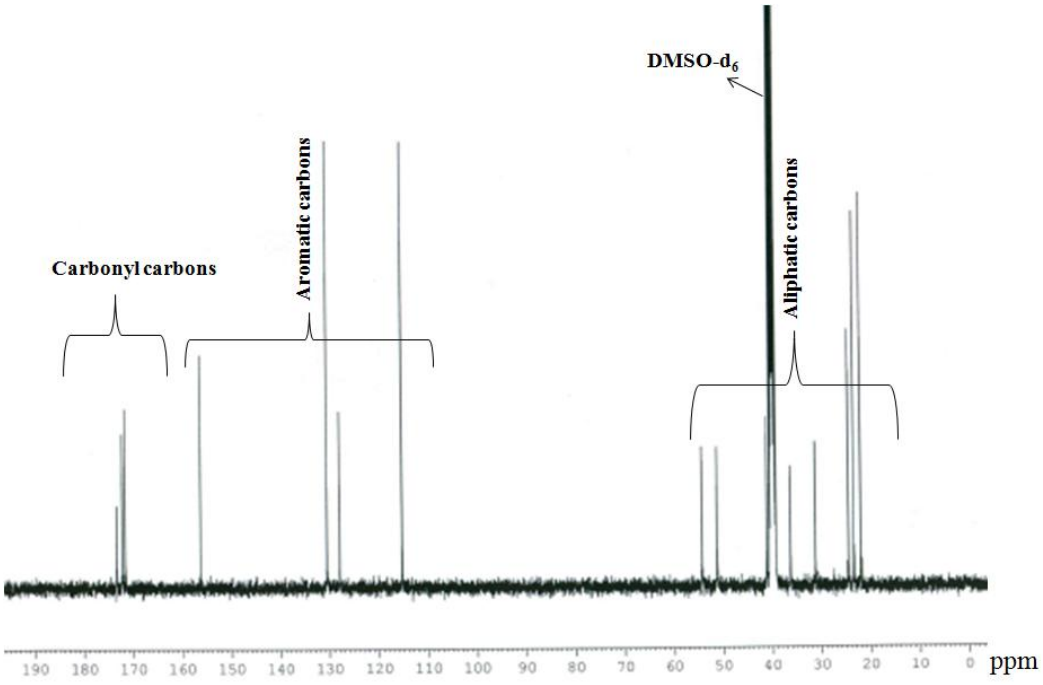

Figure 3.22. *^{13}C NMR spectrum (100 MHz, DMSO-d_6) of HO-Y-L-Suc-L-Y-OH **2**.*

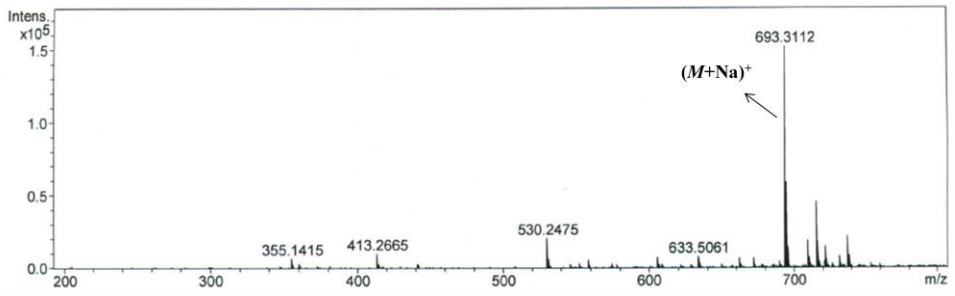

Figure 3.23. *ESI-MS spectrum of HO-Y-L-Suc-L-Y-OH **2**.*

3.2.3 Synthesis of Bolaamphiphile (HO-Leu(4)-Leu(3)-Suc-Leu(1)-Leu(2)-OH) 3:

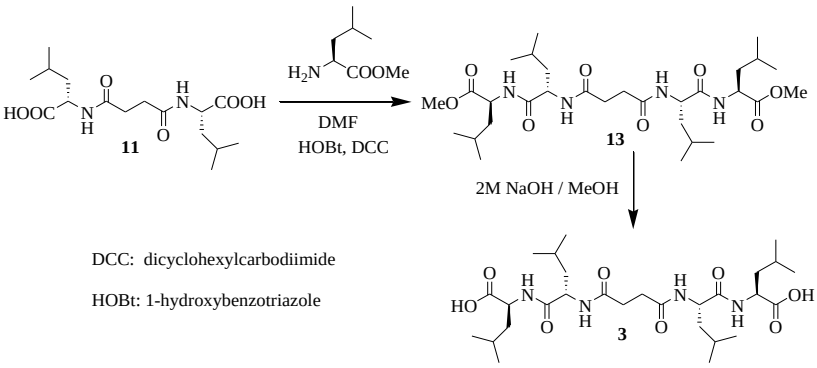

Scheme 3.3. *Synthetic scheme of peptide bolaamphiphile **3**.*

*(a) Synthesis of MeO-Leu(4)-Leu(3)-Suc-Leu(1)-Leu(2)-OMe **13**:* 1.72 g (5 mmol) of HO-Leu(2)-Suc-Leu(1)-OH **11** in 4 mL of DMF was cooled in an ice bath and H-Leu-OMe was isolated from 3.63 g (20 mmol) of the corresponding methyl ester hydrochloride by neutralization and subsequent extraction with ethyl acetate and the ethyl acetate extract was concentrated to 8 mL. It was then added to the reaction mixture, followed immediately by 2.26 g (11 mmol) DCC and 1.48 g (11 mmol) of HOBt. The reaction mixture was stirred for overnight. The residue was taken up in ethyl acetate (50 mL) and the DCU was filtered off. The organic layer was washed with 1M HCl (3 × 50 mL), brine (2 × 50 mL), 1M sodium carbonate (3 × 50 mL), brine (2 × 50 mL) and dried over anhydrous sodium sulfate and evaporated under vacuum to yield **13** as a white solid.

Purification was done by silica gel column (100-200 mesh) using chloroform-methanol (9:1) as eluent to get white solid as product.

Yield: 2.45 g (4.1 mmol, 82%); FT-IR (KBr): ῡ = 3292 (st), 1751 (st), 1640 (st), 1542 (st), 1465 (m) cm^{-1}; ^1H NMR (400 MHz, $CDCl_3$, δ_{ppm}): 6.87 (d, *J* = 8 Hz, 2H, NHs of Leu(1) and Leu(3)), 6.49 (d, *J* = 8 Hz, 2H, NHs of Leu(2) and Leu(4)), 4.54 (m, 2H, $C^{\alpha}Hs$ of Leu(1) and Leu(3)), 4.42 (m, 2H, $C^{\alpha}Hs$ of Leu(2) and Leu(4)), 3.64 (s, 6H, $-COOCH_3$), 2.48 (m, 4H, $-CH_2-$ of Suc), 1.64-1.56 and 1.50-1.46 (m, 12H, $C^{\beta}Hs$ and $C^{\gamma}Hs$ of Leu(1), Leu(2), Leu(3) and Leu(4)), 0.85 (broad, 24H, $C^{\delta}Hs$ of Leu(1), Leu(2), Leu(3) and Leu(4)); $[\alpha]_D^{20}$ = -62.2 (*c* = 0.52 in CH_3OH); MS (ESI) *m/z*: $(M+Na)^+$ Calcd. for $C_{30}H_{54}N_4O_8Na$: 621.3839; found 621.4281.

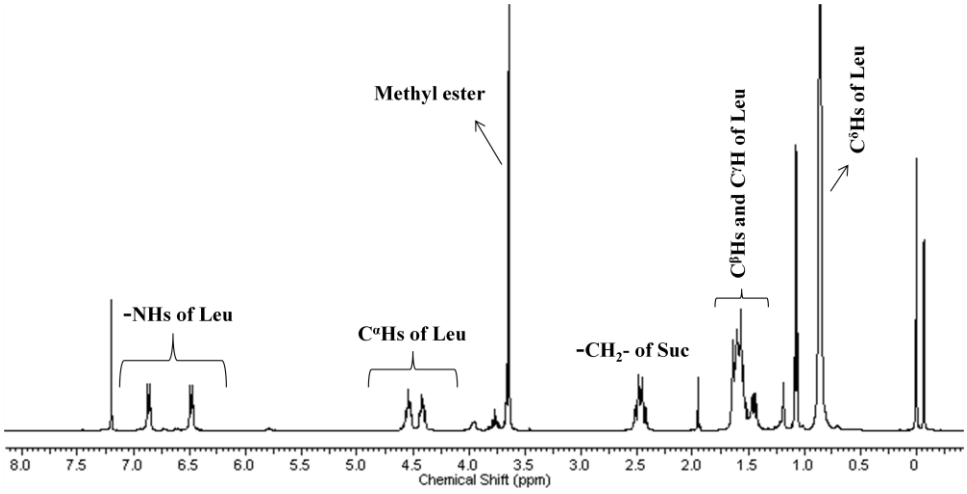

Figure 3.24. *^1H NMR spectrum (400 MHz, $CDCl_3$) of MeO-L-L-Suc-L-L-OMe **13**.*

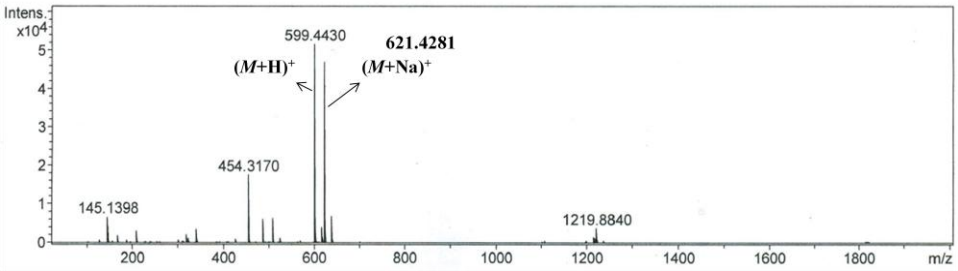

Figure 3.25. *ESI-MS spectrum of MeO-L-L-Suc-L-L-OMe **13**.*

*(b) Synthesis of HO-Leu(4)-Leu(3)-Suc-Leu(1)-Leu(2)-OH **3**:* 2.39 g (4 mmol) of MeO-Leu(4)-Leu(3)-Suc-Leu(2)-Leu(1)-OMe **13** in 10 mL MeOH was taken in a round bottom flask and 7 mL of 2M NaOH was added to it dropwise. The reaction was monitored by thin layer chromatography (TLC). The reaction mixture was stirred for 7 hours. 15 mL of distilled water was added to the reaction mixture and MeOH was removed under vacuum. The aqueous part was washed with diethyl ether (2 × 30 mL). Then it was cooled under ice bath for 10 minutes and then pH was adjusted to 1 by drop wise addition of 1M HCl. It was extracted with ethyl acetate (3 × 50 mL) and then the ethyl acetate part was dried over anhydrous Na_2SO_4 and evaporated under vacuum to yield **3** as a white solid.

Yield: 2.05 g (3.6 mmol, 90%); FT-IR (KBr): ϑ = 3303 (ms), 1724 (st), 1646 (st), 1548 (st) cm^{-1}; ^1H NMR (400 MHz, DMSO-d_6, δ_{ppm}): 12.45 (s, 2H, -COOH), 8.11 (d, *J* = 7.6 Hz, 2H, NHs of Leu(1) and Leu(3)), 8.00 (d, *J* = 8.4 Hz, 2H, NHs of Leu(2) and Leu(4)), 4.39 (m, 2H, C^{α}Hs of Leu(1) and Leu(3)), 4.24 (m, 2H, C^{α}Hs of Leu(2) and Leu(4)), 2.41 (m, 4H, -CH_2- of Suc), 1.64-1.60 and 1.50-1.47 (m, 12H, C^{β}Hs and C^{γ}Hs of Leu(1), Leu(2), Leu(3) and Leu(4)), 0.96, 0.94, 0.90 and 0.88 (d, *J* = 6 Hz, 24H, C^{δ}Hs of Leu(1), Leu(2), Leu(3) and Leu(4)); ^{13}C NMR (100 MHz, DMSO-d_6, δ_{ppm}): 173.88 (C=O), 172.17 (C=O), 171.19 (C=O), 50.57, 50.13, 30.79, 25.18, 23.07, 22.83, 21.61; $[\alpha]_D^{20}$ = -46.45 (*c* = 0.5 in CH_3OH); MS (ESI) *m/z*: $(M+Na)^+$ Calcd. for $C_{28}H_{50}N_4O_8Na$: 593.3526; found 593.3660.

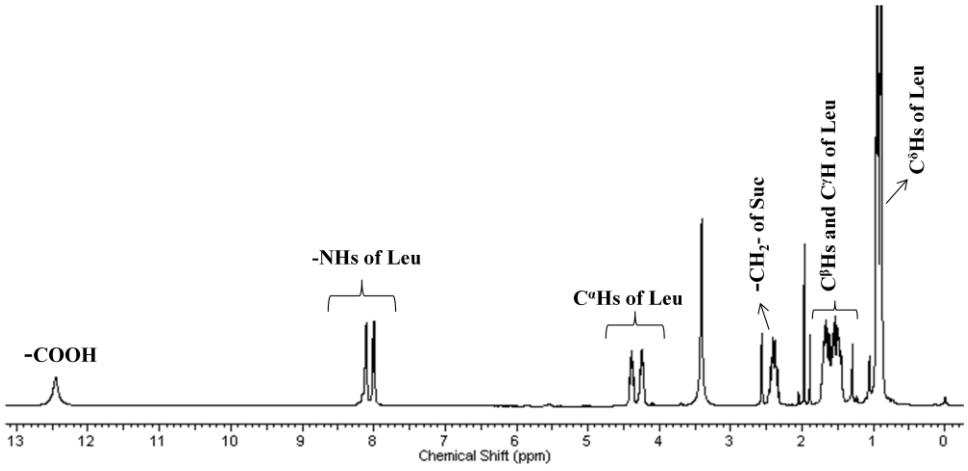

Figure 3.26. *^1H NMR spectrum (400 MHz, DMSO-d_6) of HO-L-L-Suc-L-L-OH **3**.*

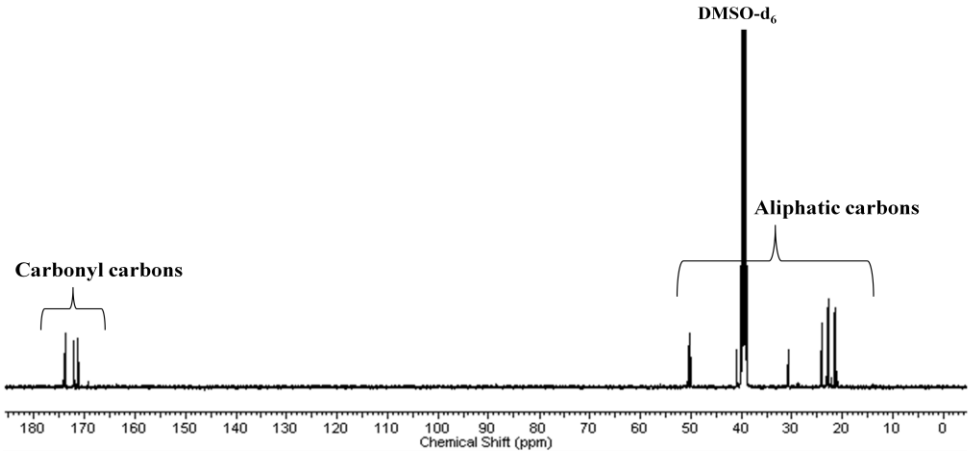

Figure 3.27. *^{13}C NMR spectrum (100 MHz, DMSO-d_6) of HO-L-L-Suc-L-L-OH **3**.*

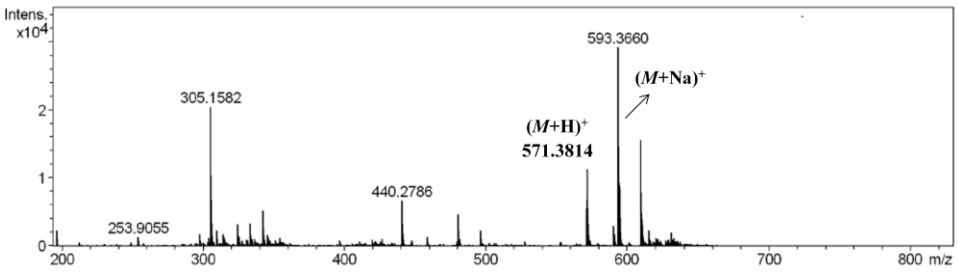

Figure 3.28. *ESI-MS spectrum of HO-L-L-Suc-L-L-OH **3**.*

*3.2.4 Synthesis of Bolaamphiphile (***HO-Gly(4)-Leu(3)-Suc-Leu(1)-Gly(2)-OH***) 4:**

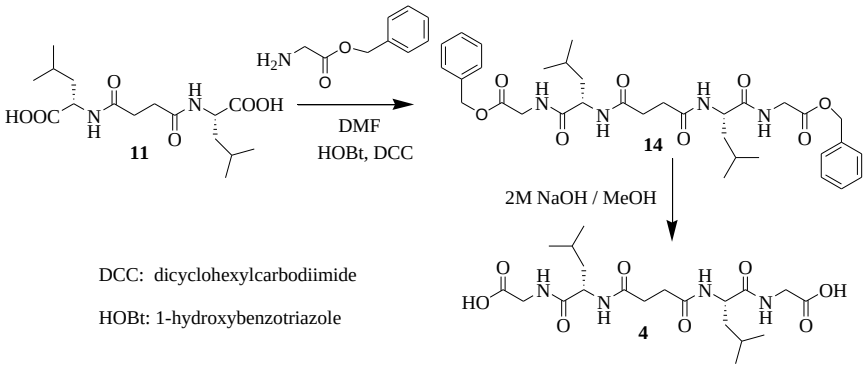

Scheme 3.4. *Synthetic scheme of peptide bolaamphiphile **4**.*

(a) Synthesis of PhCH$_2$O-Gly(4)-Leu(3)-Suc-Leu(1)-Gly(2)-OCH$_2$Ph ***14****:* 1.72 g (5 mmol) of HO-Leu(2)-Suc-Leu(1)-OH **11** in 5 mL of DMF was cooled in an ice bath and H-Gly-OCH$_2$Ph was isolated from 6.74 g (20 mmol) of the corresponding benzyl ester-*p* toluene sulfonic acid salt by neutralization and subsequent extraction with ethyl acetate and the ethyl acetate extract was concentrated to 12 mL. It was then added to the reaction mixture, followed immediately by 2.26 g (11 mmol) DCC and 1.48 g (11 mmol) of HOBt. The reaction mixture was stirred for overnight. The residue was taken up in ethyl acetate (50 mL) and the DCU was filtered off. The organic layer was washed with 1M HCl (3 × 50 mL), brine (2 × 50 mL), 1M sodium carbonate (3 × 50 mL), brine (2 × 50 mL) and dried over anhydrous sodium sulfate and evaporated under vacuum to yield **14** as a white solid. Purification was done by silica gel column (100-200 mesh) using chloroform-methanol (9:1) as eluent to get white solid as product.

Yield: 2.71 g (4.25 mmol, 85%); FT-IR (KBr): $\tilde{\upsilon}$ = 3292 (st), 1734 (ms), 1636 (st), 1546 (st), 1457 (w) cm^{-1}; ^{1}H NMR (400 MHz, $CDCl_3$, δ_{ppm}): 7.37-7.32 (m, 10H, aromatic protons), 7.15 (t, *J* = 5.2 Hz, 2H, NHs of Gly(2) and Gly(4)), 6.74 (d, *J* = 8 Hz, 2H, NHs of Leu(1) and Leu(3)), 5.13 (s, 4H, -COOCH$_2$-Ph), 4.49 (m, 2H, C$^{\alpha}$Hs of Leu(1) and Leu(3)), 4.01 (d, *J* = 5.6 Hz, 4H, C$^{\alpha}$Hs of Gly(2) and Gly(4)), 2.56 (m, 4H, -CH$_2$- of Suc), 1.69-1.63 (m, 6H, C$^{\beta}$Hs and C$^{\gamma}$Hs of Leu(1) and Leu(3)), 0.92 and 0.89 (d, *J* = 6.4 Hz, *J* = 6 Hz, 12H, C$^{\delta}$Hs of Leu(1) and Leu(3)); $[\alpha]_D^{20}$ = -46.45 (*c* = 0.31 in CH_3OH); MS (ESI) *m/z*: $(M+Na)^+$ Calcd. for $C_{34}H_{46}N_4O_8Na$: 661.3213; found 661.3697.

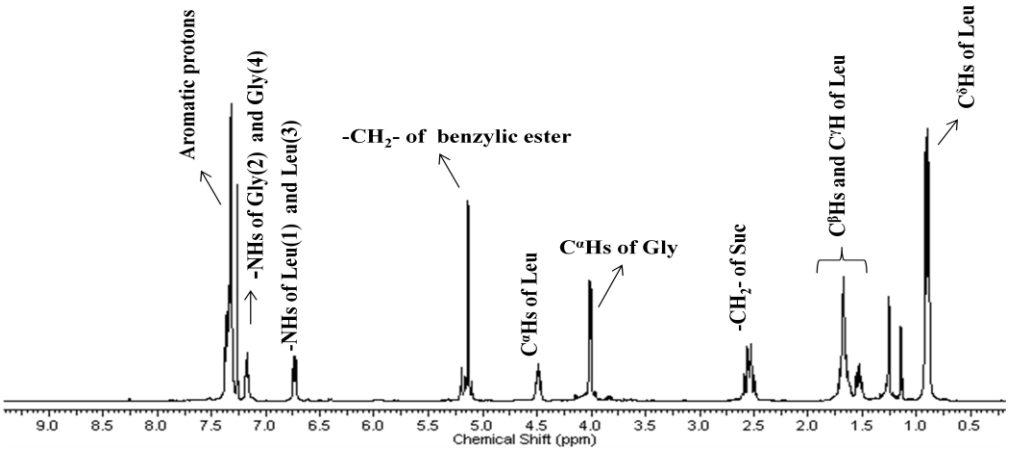

Figure 3.29. *^{1}H NMR spectrum (400 MHz, $CDCl_3$) of PhCH$_2$O-Gly(4)-Leu(3)-Suc-Leu(1)-Gly(2)-OCH$_2$Ph* ***14****.*

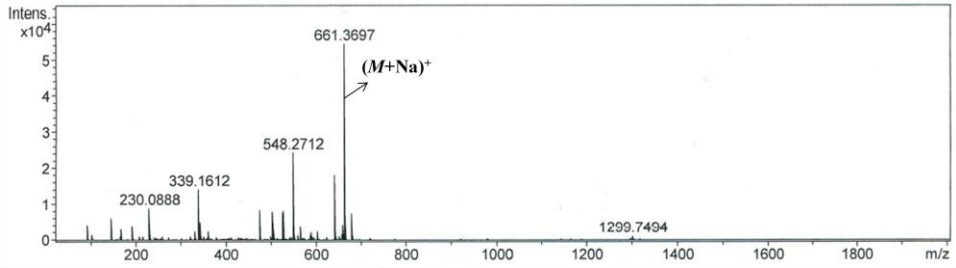

Figure 3.30. *ESI-MS spectrum of $PhCH_2O$-Gly(4)-Leu(3)-Suc-Leu(1)-Gly(2)-OCH_2Ph* ***14****.*

(b) Synthesis of HO-Gly(4)-Leu(3)-Suc-Leu(1)-Gly(2)-OH ***4****:* 2.23 g (3.5 mmol) of $PhCH_2O$-Gly(4)-Leu(3)-Suc-Leu(1)-Gly(2)-OCH_2Ph **14** in 10 mL MeOH was taken in a round bottom flask and 7 mL of 2M NaOH was added to it dropwise. The reaction was monitored by thin layer chromatography (TLC). The reaction mixture was stirred for 7 hours. 15 mL of distilled water was added to the reaction mixture and MeOH was removed under vacuum. The aqueous part was washed with diethyl ether (2 × 30 mL). Then it was cooled under ice bath for 10 minutes and then pH was adjusted to 1 by dropwise addition of 1M HCl. It was extracted with ethyl acetate (3 × 50 mL) and then the ethyl acetate part was dried over anhydrous Na_2SO_4 and evaporated under vacuum to yield **4** as a white solid.

Yield: 1.44 g (3.15 mmol, 90%); FT-IR (KBr): ῡ = 3288 (bw), 1733 (ms), 1641 (st), 1546 (st) cm^{-1}; ^1H NMR (400 MHz, DMSO-d_6, δ_{ppm}): 12.41 (s, 2H, -COOH), 8.13 (t, *J* = 5.6 Hz, 2H, NHs of Gly(2) and Gly(4)), 7.99 (d, *J* = 8 Hz, 2H, NHs of Leu(1) and Leu(3)), 4.22 (m, 2H, C^{α}Hs of Leu(1) and Leu(3)), 3.62 (d, *J* = 5.6 Hz, 4H, C^{α}Hs of Gly(2) and Gly(4)), 2.43 (m, 4H, -CH_2- of Suc), 1.53 and 1.39 (m, 6H, C^{β}Hs and C^{γ}Hs of Leu(1) and Leu(3)); 0.81 and 0.76 (d, *J* = 6.4 Hz, 12H, C^{δ}Hs of Leu(1) and Leu(3)); ^{13}C NMR (100 MHz, DMSO-d_6, δ_{ppm}): 172.51 (C=O), 171.55 (C=O), 171.06 (C=O), 50.68, 30.60, 24.07, 23.05, 21.41; $[\alpha]_D^{20}$ = - 36.0 (*c* = 0.5 in CH_3OH); MS (ESI) *m/z*: $(M+Na)^+$ Calcd. for $C_{20}H_{34}N_4O_8Na$: 481.2274; found 481.2203.

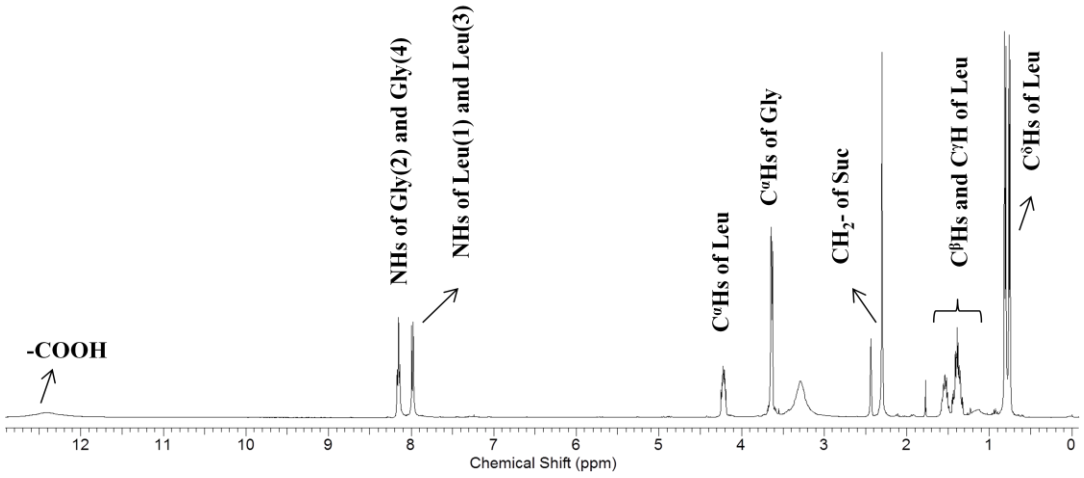

Figure 3.31. *^{1}H NMR spectrum (400 MHz, DMSO-d_6) of HO-Gly(4)-Leu(3)-Suc-Leu(1)-Gly(2)-OH* ***4****.*

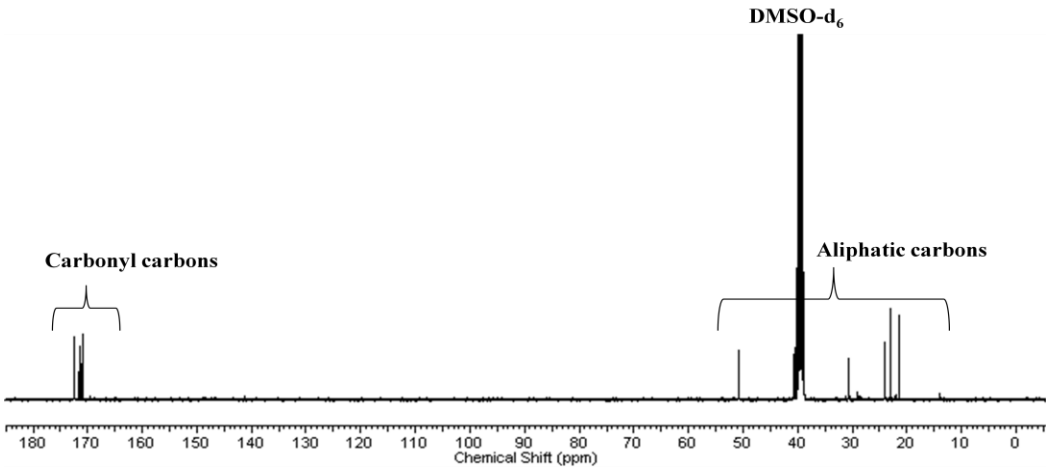

Figure 3.32. *^{13}C NMR spectrum (100 MHz, DMSO-d_6) of HO-Gly(4)-Leu(3)-Suc-Leu(1)-Gly(2)-OH* ***4****.*

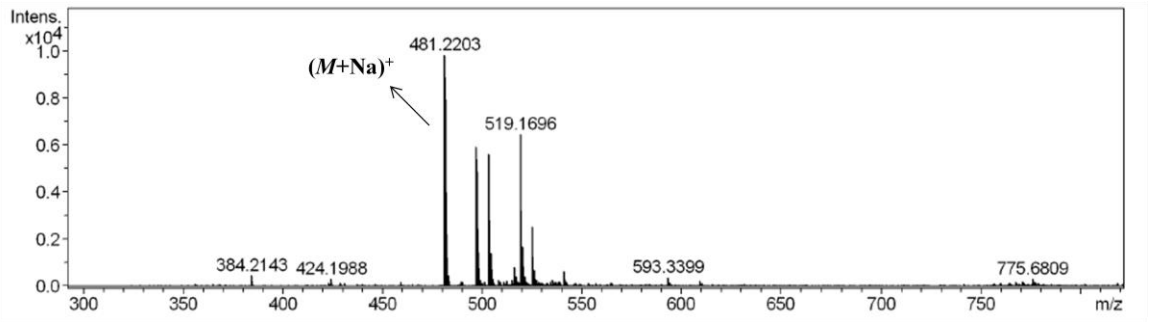

Figure 3.33. *ESI-MS spectrum of HO-Gly(4)-Leu(3)-Suc-Leu(1)-Gly(2)-OH* ***4****.*

3.3 Preparation of Hydrogel and Characterization Techniques

3.3.1 The Preparation of a Dynamic Library in a Gel Medium

30.1 mg (20 mmol L^{-1}) of peptide bolaamphiphile **1** (HO-Y-F-Suc-F-Y-OH) was dispersed in 2 mL K_2CO_3 solution (pH 8, 10 mmol L^{-1}). 100 μL 1M NaOH was added to it and sonicated to dissolve the gelator molecules. After the addition of 19.10 μL (5 equiv.) dimethyl sulphate (DMS), the pH gradually decreased and within 30 minutes an opaque gel formed. The bolaamphiphile **1** turned to a gel at pH 4 upon the addition of 5 equiv. of DMS. The pH reached 6 upon addition of 4 equiv. of DMS. The product conversion was much less at pH 6 and bolaamphiphile **1** did not turn into a hydrogel. The pH reached 2 within 5 min upon the addition of 6 equiv. of DMS and bolaamphiphile **1** tended to precipitate out.

3.3.2 HPLC Analysis

HPLC grade acetonitrile and water were used for HPLC analysis. The dynamic reaction mixture was characterized by reverse phase symmetry C18 column (250 × 4.6 cm, 5 μm particle size). UV-Vis absorbance was monitored at 280 nm. Separations were achieved by running the column with acetonitrile-water as eluent at a flow rate of 1 mL min^{-1} at 25 °C. The sample preparation involved mixing 100 μL of gel with acetonitrile-water (900 μL, 50:50 mixture). The samples were then filtered through a 0.45 μm syringe filter (Whatman, 150 units, 13 mm diameter, 2.7 mm pore size) prior to injection. A 20 μL of sample was injected into a Dionex Acclaim ® 120 C18 column of 250 mm length with an internal diameter of 4.6 mm and 5 μm fused silica particles at a flow rate of 1 mL $min.^{-1}$ Solvent gradiant is given below.

Time/min.	**% of H_2O (0.1% TFA)**	**% of Acetonitrile (0.1% TFA)**
0	80	20
4	80	20
35	20	80
40	20	80
42	80	20

3.3.3 Rheology Analysis

Oscillating rheology was used to quantify the final mechanical properties of the peptide bolaamphiphile hydrogels. The experiment was done using a Paar Physica Modular Compact Rheometer (MCR 301, Austria). A 25 mm cone plate with 1° angle configuration was used and the temperature was set constant at 25 °C. Storage (G') and loss (G") moduli were measured at 0.1% strain with true gap of 0.05 mm.

3.3.4 Fluorescence Spectroscopy Study

The fluorescence emission spectra of the gel (20 mmol L^{-1}) were recorded on a Horiba Scientific Fluoromax-4 spectrophotometer with a quartz cell of path length 1 cm at room temperature. The slit width for the excitation and emission was set at 5 nm and at a 1 nm data pitch. The excitation of the gel sample **1** was performed at 270 nm and the data range was between 280 and 530 nm.

3.3.5 Microscopic Study

For the SEM study, the hydrogel was dried on a glass slide and coated with platinum. Then, the micrographs were recorded using SEM apparatus (Jeol Scanning Microscope-JSM-7600F). A high resolution transmission electron microscopy image was taken using a PHILIPS electron microscope (model: CM 200) operating at an accelerating voltage of 200 kV. A dilute solution of the hydrogel was dried on carbon-coated copper grids (300 mesh) by slow evaporation in air, then allowed to dry separately in a vacuum at room temperature. The morphologies of the hydrogel were also investigated by AFM. The gel sample was diluted in Milli Q water to a final concentration of 0.5 mmol L^{-1} and placed on a microscopic coverslip. Then, it was dried by slow evaporation. Images were taken using an AIST-NT instrument, model no. smartSPM 1000 in soft tapping-mode.

3.4 Results and Discussion

3.4.1 Genaration of Dynamic Library in Hydrogel

Peptide based bolaamphiphiles HO-Tyr-Phe-Suc-Phe-Tyr-OH **1**, HO-Tyr-Leu-Suc-Leu-Tyr-OH **2**, HO-Leu-Leu-Suc-Leu-Leu-OH **3** and HO-Gly-Leu-Suc-Leu-Gly-OH **4**, which feature a dipeptide sequence attached to a centrally located succinic acid moiety, were synthesized and characterized (Figure 3.1). Sequential pH changes trigger the hydrogelation phenomena in peptide bolaamphiphile **1**. DMS (dimethyl sulphate) has previously been used as an alkylating agent.[16] DMS hydrolyses in water to give methanol and sulphuric acid, resulting in a lower pH. In this system, DMS is used as a reagent in the methylation of phenols and the esterification of acids via an S_N2 reaction. The subsequent formation of sulphuric acid lowers the pH to 4, which aids the formation of a self-supporting hydrogel. Alkylation and esterification reactions are reversible and are affected by a change in the pH. A dynamic peptide based library of esters and ethers of peptide bolaamphiphile **1** is formed in a gel phase medium (Figure 3. 34 and Figure 3.35). In the product distribution, 5 equiv. DMS were added homogeneously to a basic solution of peptide bolaamphiphile **1** (20 mmol L^{-1}) and the reaction mixture was kept at room temperature without stirring. Here, DMS was not used only as an alkylating agent but interestingly it can also lower the pH to an optimum level that allows our system to turn to gel. The pH dropped from 10 to 4 over 30 min and it reached 2 after 1 day (Figure 3.36(a)). After 15 min, the gelation process has started and the system turned to gel after 30 min, which was stable for 1 month. The pH of the system slowly decreased and equilibrated 24 h after DMS addition. At the primary stage, the rate of monoester conversion was very fast before gelation. After the primary stage, the rate of monoester conversion slows down, leading to the monoester as the major product. Fibrous aggregates or gels are formed when a monoester of peptide bolaamphiphile **1** is formed in a sufficient amount (19%). The fibers were obtained from the dynamic hydrogel after 6 centrifugation processes and washings with water. ESI-MS showed that the fibers consisted of both the di-acid of the peptide bolaamphiphile and its monoester. This indicates that the monoester may aggregate or self-assemble with the parent bolaamphiphile molecules to form a hydrogel.

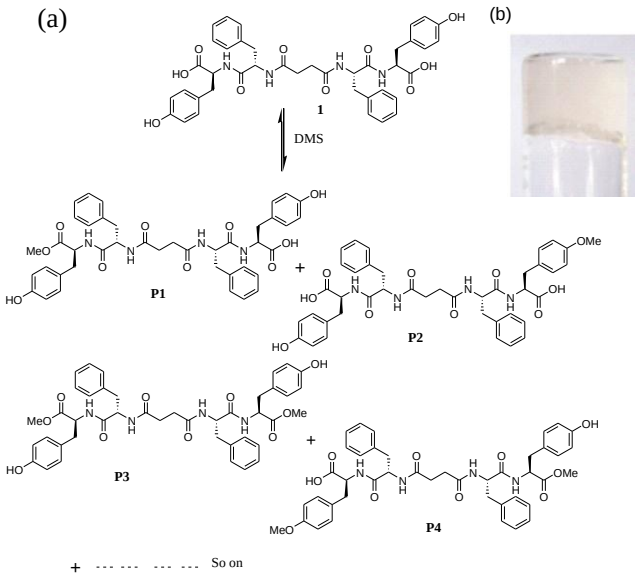

Figure 3.34. *(a) Formation of dynamic library from bolaamphiphile **1**. (**P1**, **P2**, **P3** and **P4** refer the products in dynamic reaction) (b) A photograph of the dynamic hydrogel formed from peptide bolaamphiphile **1**.*

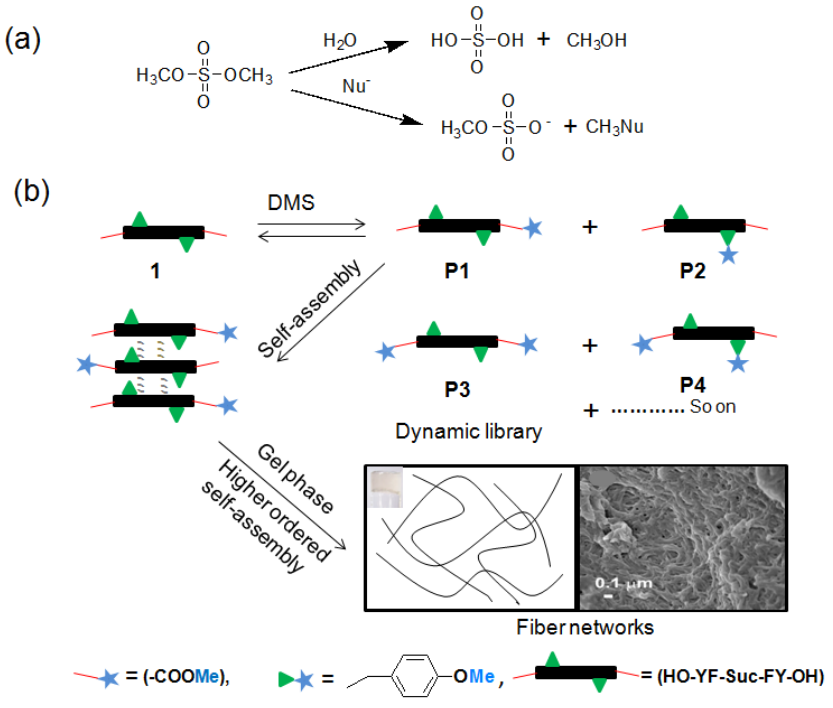

Figure 3.35. *(a) The scheme of DMS hydrolysis and the S_N2 type reaction of the peptide bolaamphiphile. (b) A schematic representation of the highly ordered peptide based bolaamphiphile self-assembly through a dynamic chemical reaction.*

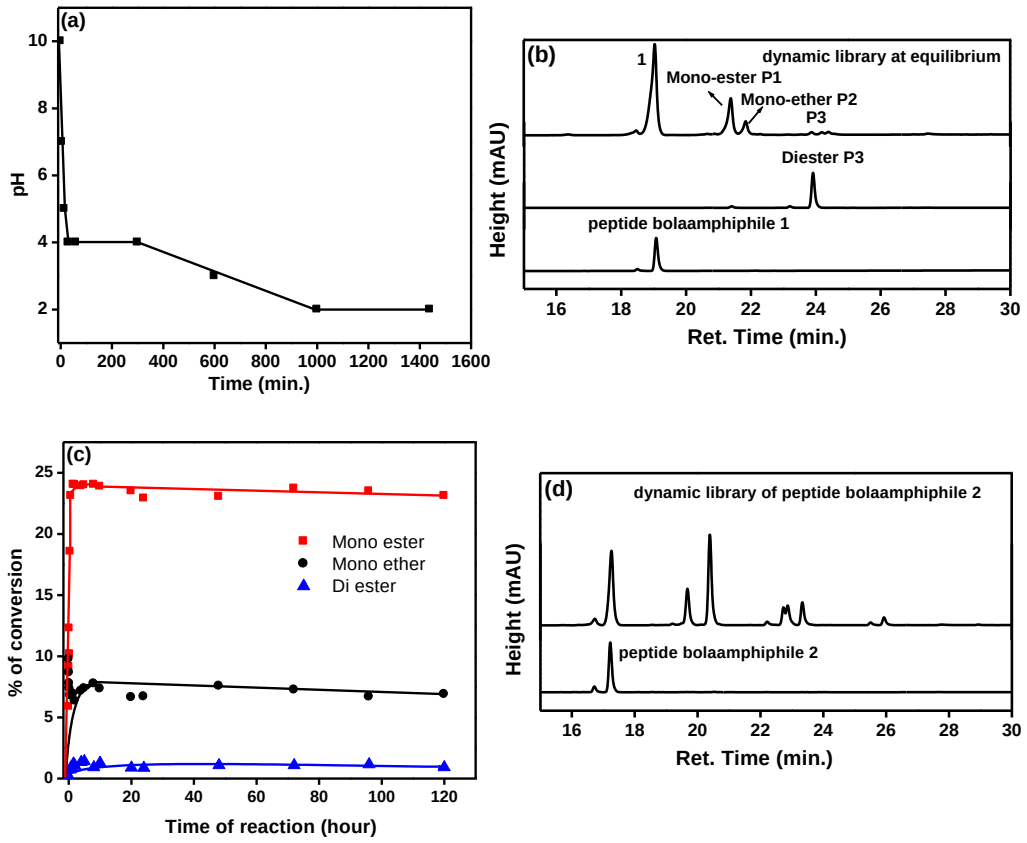

Figure 3.36. *(a) The plot of decrease in pH with time of the reaction. (b) HPLC chromatogram of peptide bolaamphiphile **1** and the dynamic library of peptide bolaamphiphile **1** with DMS reaction at equilibrium. (c) The product distribution of a dynamic system from the reaction of peptide bolaamphiphile **1** with the chemical fuel dimethyl sulphate (DMS) as determined by HPLC over time at 25 °C. (d) HPLC chromatogram of a library of peptide bolaamphiphile **2** (HO-Y-L-Suc-L-Y-OH) which gives a mixture of non-selective products.*

Ten library members were expected to form from the corresponding two carboxylic acids and the two tyrosinyl -OH groups of peptide bolaamphiphile **1** but the HPLC chromatogram only shows six products. ESI-MS, FT-IR and the relative hydrophobicity (log *P*) of the library members indicated that a monoester was synthesized as the major component along with additional products of monoether, diester, monoether with monoester (2 diastereomers) and diether which all have a negligible yield (Figure 3.36(b)). After 5 days of reaction, all the components are at equilibrium. The equilibrium contains 23% of the monoester as the major component (Figure 3.36(c)). Under similar

reaction conditions, another bolaamphiphile, HO-Y-L-Suc-L-Y-OH **2**, does not form a hydrogel and gives a mixture of non-selective products (Figure 3.36(d)). The other two bolaamphiphiles HO-Leu-Leu-Suc-Leu-Leu-OH **3** and HO-Gly-Leu-Suc-Leu-Gly-OH **4** that do not contain phenylalanine residues give a monoester as the predominant product along with a diester of negligible yield (Figure 3.37). Bolaamphiphiles **3** and **4** are not capable of forming hydrogels under similar reaction conditions. The phenylalanine residues in bolaamphiphile **1** help to form a hydrogel by providing π-π stacking interactions.

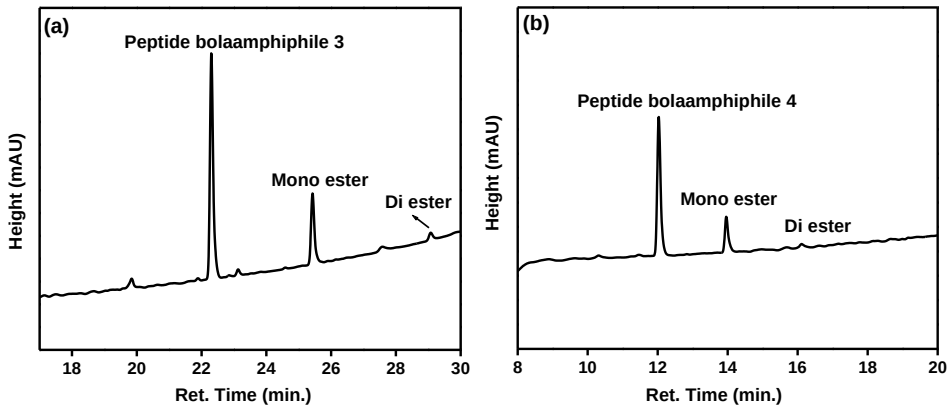

Figure 3.37. *HPLC chromatograms of library of (a) peptide bolaamphiphile **3** (HO-L-L-Suc-L-L-OH) and (b) peptide bolaamphiphile **4** (HO-G-L-Suc-L-G-OH).*

3.4.2 Rheological Study

With the help of rheology,[17] the gelling point of the dynamic hydrogel system was analyzed. Rheological experiments show that the hydrogelation process started 20 min after the addition of DMS, as evidenced by the storage modulus (G') dominating the loss modulus (G") (Figure 3.38). The frequency sweeps of the hydrogel were measured at different time points during the dynamic reaction to investigate the relative change in the mechanical strength of the hydrogel (Figure 3.39 (a)). The frequency sweeps show that the gel is a solid like material (G' > G"). Figure 3.40 shows the comparison between the storage modulus (G') and the loss modulus (G") at a particular point of angular frequency (10.6 s^{-1}) over the course of the reaction at a constant strain of 0.1%. The figure shows that the mechanical properties of the system increased sharply as the reaction time

increased from 20 min to 1 h and G' reached over 10^5 Pa. The values of the storage modulus G' exceeds those of G" by a factor of 7-8 at this stage, which indicates the formation of a strong and rigid hydrogel.

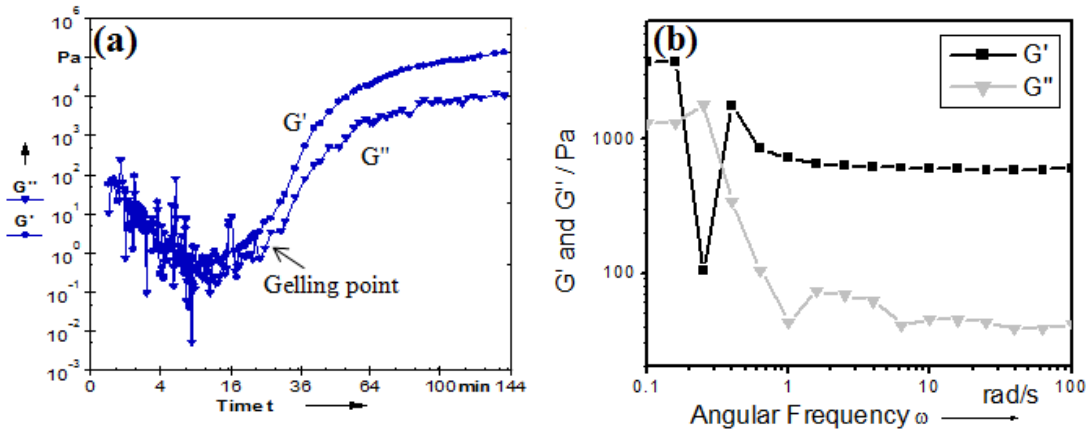

Figure 3.38. *(a) The frequency sweep from oscillatory rheometry shows the gelling point, (b) the frequency sweep of hydrogel **1** at 20 minutes.*

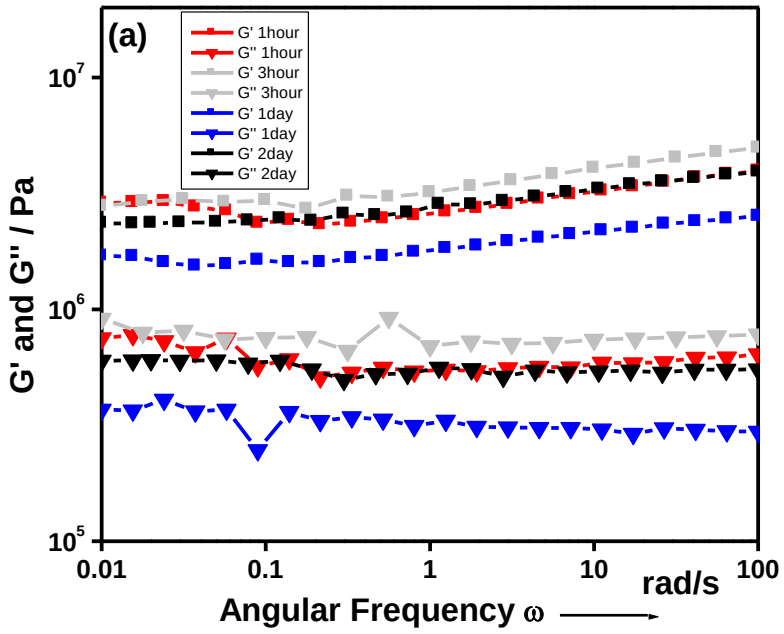

Figure 3.39. *The frequency sweep of hydrogel **1** at various times as 1 hour, 3 hours, 1 day and 2 days.*

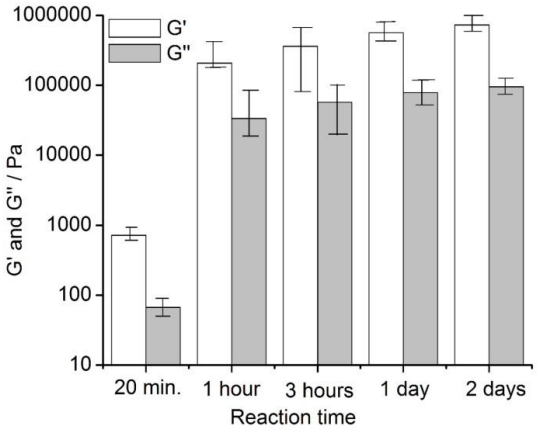

Figure 3.40. *The comparison between the storage modulus (G') and loss modulus (G") at a particular point of angular frequency (10.6 s^{-1}) with the course of reaction time at constant strain as 0.1%.*

3.4.3 FT-IR Analysis

FT-IR data reveal the formation of β-sheet structure[14] in the gel state (Figure 3.41). The FT-IR spectrum was recorded to obtain an insight into the structure of the hydrogel molecules formed via the dynamic reaction after 24 h. The FT-IR spectrum shows a peak centered at 3286 cm^{-1} which indicates the involvement of N-H bonds in hydrogen bonding interactions. In the gel state, a band appeared at 1740 cm^{-1} which supports the formation of a methyl ester from carboxylic acid groups. The amide band appears at 1642 cm^{-1} and a weak band appears at 1660 cm^{-1} which reveals that the hydrogelator molecules self-assemble through hydrogen bonding interactions into a twisted β-sheet structure.[6e]

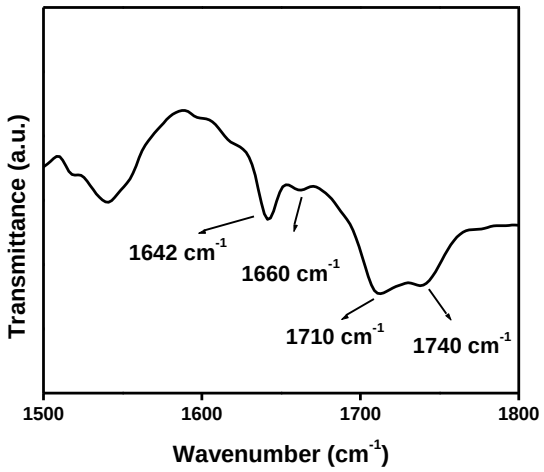

Figure 3.41. *The FT-IR spectrum of peptide bolaamphiphile hydrogel **1** showing the twisted β sheet structure.*

3.4.4 Fluorescence Study

To gain more insight into the molecular arrangement of the gel structures, we monitored the gelation process using fluorescence spectroscopy. The fluorescence emission spectra reveal that π-stacking interactions play an important role towards the formation of higher ordered self-assembled structures in the self-assembly process. The fluorescence emission peak corresponding to the tyrosine moiety is gradually red shifted from 295 nm to 301 nm exhibiting π-π stacking[18] interactions during the self-assembly process. A pronounced excimer peak appears at 467 nm in the higher ordered aggregates of self-assembled molecules (Figure 3.42). The emission band at 467 nm is attributed to the excimer formation between the tyrosyl groups in the β-sheet.[19]

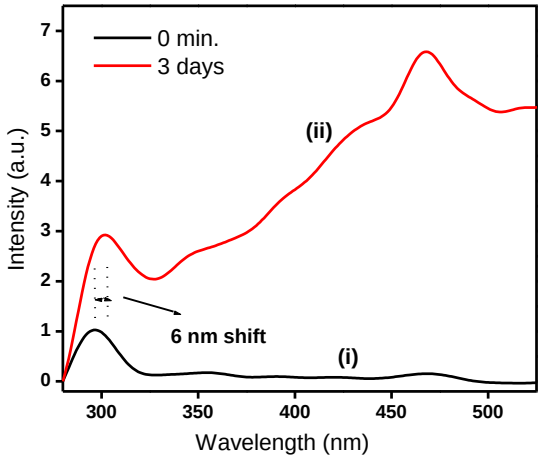

Figure 3.42. *The fluorescence emission spectra of peptide bolaamphiphile **1** (i) prior to DMS addition and (ii) after the addition of DMS at 3 days.*

3.4.5 Morphological Study

The time dependent morphological study of the gel fibers is interesting in helping to understand the kinetics of the self-assembly process. The change in morphology[20] at various time intervals of the dynamic system was studied using scanning electron microscopy (SEM). The SEM images reveal the nucleation and growth of the gel fibers over time (Figure 3.43(a-e)). After 7 min of the reaction in the aqueous state, the SEM image shows the nucleation point from where the fibers start to grow. The diameter of the

straight fibers is ranging from 15 nm to 25 nm at 7 min. These fibers are not capable of entrapping water molecules to form a gel. The nucleation point and the growth of the fibers are more evident after 20 min where the gelation starts. The white portions at the end of the fibers indicate the nucleation point.

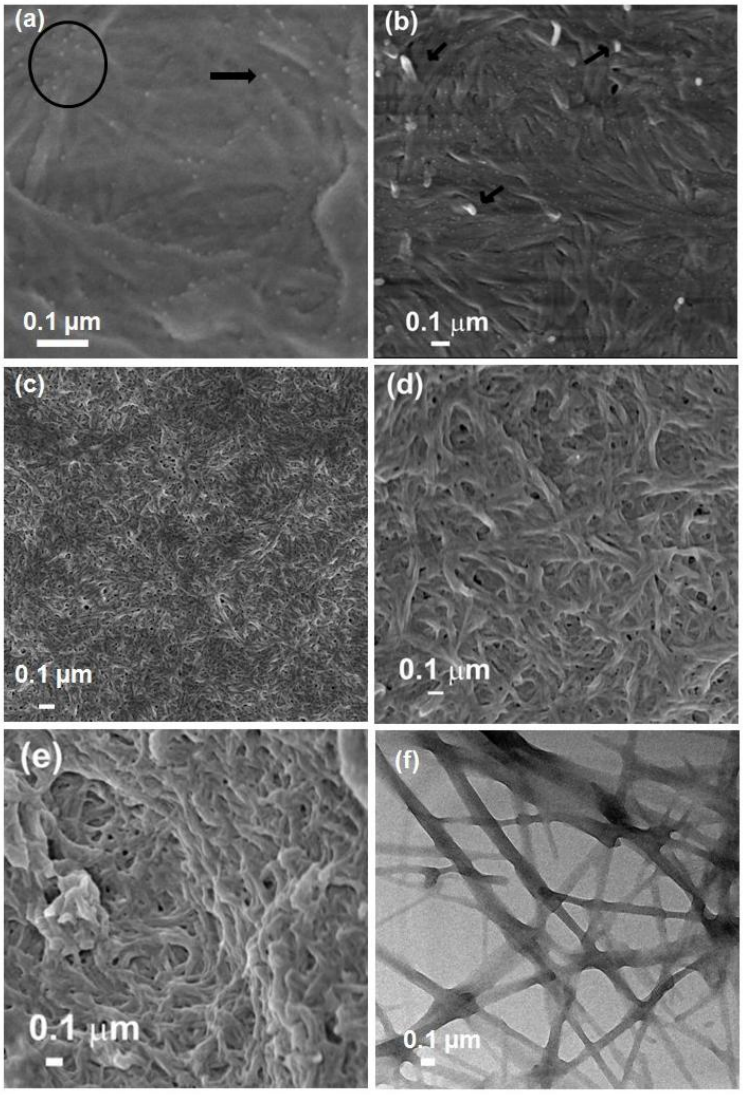

Figure 3.43. *Time dependent scanning electron microscopy (SEM) images (a) after 7 min shows straight fibers with white dot like particles which indicates the nucleation point, (b) after 20 min shows fibers with white edges (indicated by black arrows), (c) after 45 min, (d) after 6 h (twisted fibers) and (e) after 1 day of the dynamic reaction showing a fibrillar morphology. (f) A transmission electron microscopic (TEM) image of hydrogel **1** after 3 days of reaction showing a fibrillar morphology.*

After 45 min of the reaction, the SEM image reveals the network structures with an entangled nanofibrillar morphology which is an indication of gel formation. After 6 h, the SEM image shows the twisted nanofiber morphology with an average fiber diameter of 70 nm. After 1 day, most of the fibers are twisted and form a porous network like structure. The lengths and widths of the fibers increase over time and the average fiber diameter becomes 80 nm, which is responsible for strong gel formation. The SEM experiments show that the morphology changes from non-twisted nanofibers to twisted nanofibers, which is dependent on time. The non-twisted nanofibers turn into twisted nanofibers due to their higher ordered self-assembly at the supramolecular level. After 3 days of reaction, the TEM image reveals the nanofibrillar morphology with a diameter ranging from 70 nm to 90 nm (Figure 3.43(f)).

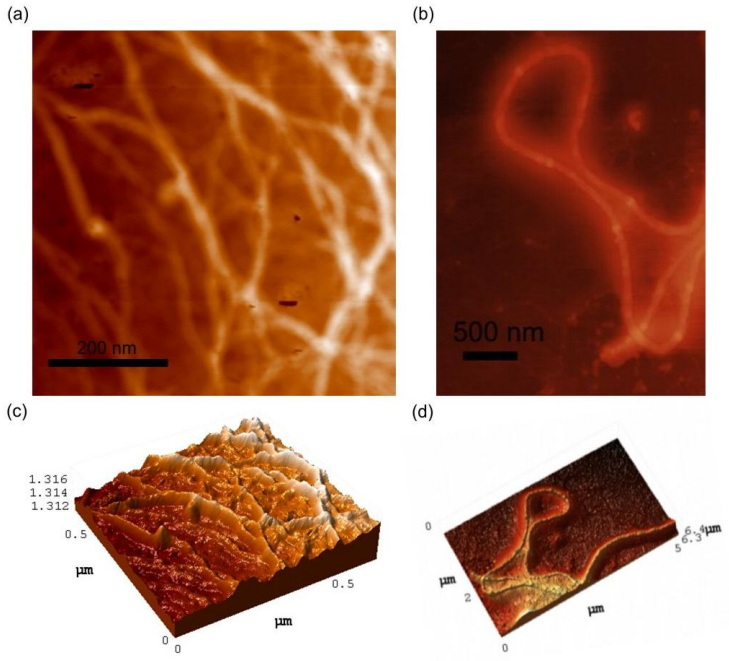

Figure 3.44. *AFM images of nanofibrillar morphology of the dynamic hydrogel (a) after 45 min of reaction time, (b) after 3 days of reaction time. (c) and (d) are three dimensional images of (a) and (b), respectively.*

Atomic force microscopy (AFM) was also used to study the morphology of the hydrogel resulting from the dynamic chemical reaction. The 45 min aged gel sample shows the entangled nanofibrillar morphology with an average fiber height and diameter of 4 nm

and 30 nm, respectively. The 3 days aged gel sample shows a loop of nanofiber with a fiber diameter and height of 80 nm and 10 nm, respectively (Figure 3.44).

3.5 Conclusions

The present study has described a new development of a dynamic peptide based library in a gel phase medium. The dynamic peptide based library was driven by the self-assembly of molecules which lead to an appreciable product distribution in a gel phase medium. We also have described that the system allows the formation of a preferred nanostructured[21] product in a gel phase medium. The time dependent morphology study indicates a mechanism of a directed self-assembly process of small molecules. FT-IR and fluorescence emission spectra show that hydrogen bonding and π-π stacking interactions are responsible, in the self-assembly process, for the evolution of higher ordered supramolecular peptide nanostructures.

3.6 References

1. (a) Shah R. N., Shah N. A., Lim M. M. D. R., Hsieh C., Nuber G., Stupp S. I. (2010), Supramolecular design of self-assembling nanofibers for cartilage regeneration, *Proc. Natl. Acad. Sci. U. S. A.*, 107, 3293-3298 (DOI: 10.1073/pnas.0906501107); (b) Webber M. J., Tongers J., Newcomb C. J., Marquardt K.-T., Bauersachs J., Losordo D. W., Stupp S. I. (2011), Supramolecular nanostructures that mimic VEGF as a strategy for ischemic tissue repair, *Proc. Natl. Acad. Sci. U. S. A.*, 108, 13438-13443 (DOI: 10.1073/pnas.1016546108); (c) Semino C. E., Kasahara J., Hayashi Y., Zhangs S. (2004), Entrapment of migrating hippocampal neural cells in three-dimensional peptide nanofiber scaffold, *Tissue Eng*., 10, 643-655 (DOI:10.1089/107632704323061997); (d) Hudalla G. A., Murphy W. L. (2011), Chemically well-defined self-assembled monolayers for cell culture: toward mimicking the natural ECM, *Soft Matter*, 7, 9561-9571 (DOI: 10.1039/C1SM05596H).

2. (a) Georgieva J. V., Brinkhuis R. P., Stojanov K., Weijers C. A. G. M., Zuilhof H., Rutjes F. P. J. T., Hoekstra D., van Hest J. C. M., Zuhorn I. S. (2012), Peptide-mediated blood–brain barrier transport of polymersomes, *Angew. Chem., Int. Ed*., 51, 8339-8342

(DOI: 10.1002/anie.201202001); (b) Wang H., Yang Z. (2012), Molecular hydrogels of hydrophobic compounds: a novel self-delivery system for anti-cancer drugs, *Soft Matter*, 8, 2344-2347 (DOI: 10.1039/C2SM06923G); (c) Huang Y.-H., Bao Y., Peng W., Goldberg M., Love K., Bumcrot D. A., Cole G., Langer R., Anderson D. G., Sawicki J. A. (2009), Claudin-3 gene silencing with siRNA suppresses ovarian tumor growth and metastasis, *Proc. Natl. Acad. Sci. U. S. A.*, 106, 3426-3430 (DOI: 10.1073/pnas.0813348106); (d) Wang H., Yang Z. (2012), Short-peptide-based molecular hydrogels: Novel gelation strategies and applications for tissue engineering and drug delivery, *Nanoscale*, 4, 5259-5267 (DOI: 10.1039/C2NR31149F); (e) Naskar J., Palui G., Banerjee A. (2009), Tetrapeptide-based hydrogels: For encapsulation and slow release of an anticancer drug at physiological pH, *J. Phys. Chem. B*, 113, 11787-11792 (DOI: 10.1021/jp904251j); (f) Matson J. B., Stupp S. I. (2012), Self-assembling peptide scaffolds for regenerative medicine, *Chem. Commun*., 48, 26-33 (DOI: 10.1039/C1CC15551B); (g) Liang G., Yang Z., Zhang R., Li L., Fan Y., Kuang Y., Gao Y., Wang T., Lu W. W., Xu B. (2009), Supramolecular hydrogel of a D-amino acid dipeptide for controlled drug release in vivo, *Langmuir*, 25, 8419-8422 (DOI: 10.1021/la804271d); (h) Yang Z., Liang G., Guo Z., Guo Z., Xu B. (2007), Intracellular hydrogelation of small molecules inhibits bacterial growth, *Angew. Chem., Int. Ed*., 46, 8216-8219 (DOI: 10.1002/anie.200701697).

3. (a) de. la Rica R., Matsui H. (2010), Applications of peptide and protein-based materials in bionanotechnology, *Chem. Soc. Rev*., 39, 3499-3509 (DOI: 10.1039/b917574c); (b) Basabe-Desmonts L., Reinhoudt D. N., Crego-Calama M. (2007), Design of fluorescent materials for chemical sensing, *Chem. Soc. Rev*., 36, 993-1017 (DOI: 10.1039/B609548H); (c) Kiyonaka S., Sada K., Yoshimura I., Shinkai S., Kato N., Hamachi I. (2004), Semi-wet peptide/protein array using supramolecular hydrogel, *Nat. Mater*., 3, 57-64 (DOI:10.1038/nmat1034).

4. (a) Koutsopoulos S., Unsworth L. D., Nagai Y., Zhang S. (2009), Controlled release of functional proteins through designer self-assembling peptide nanofiber hydrogel scaffold, *Proc. Natl. Acad. Sci. U. S. A.*, 106, 4623-4628 (DOI: 10.1073/pnas.0807506106); (b) Smith K. H., Tejeda-Montes E., Poch M., Mata A. (2011), Integrating top-down and self-assembly in the fabrication of peptide and protein-based biomedical materials, *Chem.*

Soc. Rev., 40, 4563-4577 (DOI: 10.1039/c1cs15064b); (c) Murphy W. L. (2011), Emerging area: Biomaterials that mimic and exploit protein motion, *Soft Matter*, 7, 3679-3688 (DOI: 10.1039/C0SM01351J); (d) Riehemann K., Schneider S. W., Luger T. A., Godin B., Ferrari M., Fuchs H. (2009), Nanomedicine-challenge and perspectives, *Angew. Chem., Int. Ed*., 48, 872-897 (DOI: 10.1002/anie.200802585); (e) Langer R. (2009), Perspectives and challenges in tissue engineering and regenerative medicine, *Adv. Mater*., 21, 3235-3236 (DOI: 10.1002/adma.200902589); (f) Ellis-Behnke R. G., Liang Y.-X., You S.-W., Tay D. K. C., Zhang S., So K.-F., Schneider G. E., (2006), Nano neuro knitting: Peptide nanofiber scaffold for brain repair and axon regeneration with functional return of vision, *Proc. Natl. Acad. Sci. U. S. A*., 103, 5054-5059 (DOI: 10.1073/pnas.0600559103).

5. (a) Kuang Y., Gao Y., Xu B. (2011), Supramolecular hydrogelators of N-terminated dipeptides selectively inhibit cancer cells, *Chem. Commun*., 47, 12625-12627 (DOI: 10.1039/C1CC15577F); (b) Li X., Kuang Y., Lin H-C., Gao Y., Shi J., Xu B. (2011), Supramolecular nanofibers and hydrogels of nucleopeptides, *Angew. Chem., Int. Ed*., 50, 9365-9369 (DOI: 10.1002/anie.201103641).

6. (a) Whitehouse C., Fang J., Aggeli A., Bell M., Brydson R., Fishwick C. W. G., Henderson J. R., Knobler C. M., Owens R. W., Thomson N. H., Smith D. A., Boden N. (2005), Adsorption and self-assembly of peptides on mica substrates, *Angew. Chem., Int. Ed*., 44, 1965-1968 (DOI: 10.1002/anie.200462160); (b) Sahu A., Choi W., Tae G. (2012), A stimuli-sensitive injectable graphene oxide composite hydrogel, *Chem. Commun*., 48, 5820-5822 (DOI: 10.1039/c2cc31862h); (c) Zhou Y., Yi T., Li T., Zhou Z., Li F., Huang W., Huang C. (2006), Morphology and wettability tunable two-dimensional superstructure assembled by hydrogen bonds and hydrophobic interactions, *Chem. Mater*., 18, 2974-2981 (DOI: 10.1021/cm052805h); (d) Park J. S., Jeong S., Chang D. W., Kim J. P., Kim K., Park E.-K., Song K.-W. (2011), Lithium-induced supramolecular hydrogel, *Chem. Commun*., 47, 4736-4738 (DOI: 10.1039/C1CC10532A); (e) Maity I., Rasale D. B., Das A. K. (2012), Sonication induced peptide-appended bolaamphiphile hydrogels for *in situ* generation and catalytic activity of Pt nanoparticles, *Soft Matter*, 8, 5301-5308 (DOI: 10.1039/C2SM25126D); (f) Collier J. H., Hu B.-H., Ruberti J. W., Zhang J., Shum P., Thompson D. H., Messersmith P. B.

(2001), Thermally and photochemically triggered self-assembly of peptide hydrogels, *J. Am. Chem. Soc.*, 123, 9463-9464 (DOI:10.1021/ja011535a); (g) DeForest C. A., Anseth K. S. (2012), Photoreversible patterning of biomolecules within click-based hydrogels, *Angew. Chem., Int. Ed.* 51, 1816-1819 (DOI: 10.1002/anie.201106463).

7. (a) Adams D. J., Butler M. F., Frith W. J., Kirkland M., Mullen L., Sanderson P. (2009), A new method for maintaining homogeneity during liquid–hydrogel transitions using low molecular weight hydrogelators, *Soft Matter*, 5, 1856-1862 (DOI: 10.1039/B901556F); (b) Chen L., Revel S., Morris K., Adams D. J. (2010), Energy transfer in self-assembled dipeptide hydrogels, *Chem. Commun*., 46, 4267-4269 (DOI: 10.1039/C003052J).

8. Nagarkar R. P., Hule R. A., Pochan D. J., Schneider J. P. (2008), De novo design of strand-swapped β-hairpin hydrogels, *J. Am. Chem. Soc.*, 130, 4466-4474 (DOI: 10.1021/ja710295t).

9. Alberts B., Bray D., Lewis J., Raff M., Roberts K., Watson J. D. Molecular biology of the cell, 3rd Ed., Garland Publishing, New York, 1994.

10. (a) Mahler A., Reches M., Rechter M., Cohen S., Gazit E. (2006), Rigid, self-assembled hydrogel composed of a modified aromatic dipeptide, *Adv. Mater*., 18, 1365-1370 (DOI: 10.1002/adma.200501765); (b) Panda J. J., Mishra A., Basu A., Chauhan V. S. (2008), Stimuli responsive self-assembled hydrogel of a low molecular weight free dipeptide with potential for tunable drug delivery, *Biomacromolecules*, 9, 2244-2250 (DOI: 10.1021/bm800404z); (c) Zhang X., Chu X., Wang L., Wang H., Liang G., Zhang J., Long J., Yang Z. (2012), Rational design of a tetrameric protein to enhance interactions between self-assembled fibers gives molecular hydrogels, *Angew. Chem., Int. Ed.*, 51, 4388-4392 (DOI: 10.1002/anie.201108612); (d) Koley P., Pramanik A. (2011), Nanostructures from single amino acid-based molecules: Stability, fibrillation, encapsulation, and fabrication of silver nanoparticles, *Adv. Funct. Mater*., 21, 4126-4136 (DOI: 10.1002/adfm.201101465); (e) Orbach R., Adler-Abramovich L., Zigerson S., Mironi-Harpaz I., Seliktar D., Gazit E. (2009), Self-assembled Fmoc-peptides as a platform for the formation of nanostructures and hydrogels, *Biomacromolecules*, 10, 2646-2651 (DOI: 10.1021/bm900584m); (f) Guilbaud J. B., Saiani A. (2011), Using small angle scattering (SAS) to structurally characterise peptide and protein self-

assembled materials, *Chem. Soc. Rev*., 40, 1200-1210 (DOI: 10.1039/C0CS00105H); (g) Palui G., Nanda J., Ray S., Banerjee A. (2009), Fabrication of luminescent CdS nanoparticles on short-peptide-based hydrogel nanofibers: Tuning of optoelectronic properties, *Chem.-Eur. J.*, 15, 6902-6909 (DOI: 10.1002/chem.200900149).

11. Sreenivasachary N., Lehn J.-M. (2005), Gelation-driven component selection in the generation of constitutional dynamic hydrogels based on guanine-quartet formation, *Proc. Natl. Acad. Sci. U. S. A.*, 102, 5938-5943 (DOI: 10.1073/pnas.0501663102).

12. Carnall J. M. A., Waudby C. A., Belenguer A. M., Stuart M. C. A., Peyralans J. J.-P., Otto S. (2010), Mechanosensitive self-replication driven by self-organization, *Science*, 327, 1502-1506 (DOI: 10.1126/science.1182767).

13. Rasale D. B., Maity I., Das A. K. (2012), Emerging π-stacked dynamic nanostructured library, *RSC Adv*., 2, 9791-9794 (DOI: 10.1039/C2RA21334F).

14. Das A. K., Collins R., Ulijn R. V. (2008), Exploiting enzymatic (reversed) hydrolysis in directed self-assembly of peptide nanostructures, *Small*, 4, 279-287 (DOI: 10.1002/smll.200700889).

15. Boekhoven J., Brizard A. M., Kowlgi K. N. K., Koper G. J. M., Eelkema R., van Esch J. H. (2010), Dissipative self-assembly of a molecular gelator by using a chemical fuel, *Angew. Chem., Int. Ed.*, 49, 4825-4828 (DOI: 10.1002/anie.201001511).

16. (a) Wolfenden R., Yuan Y. (2007), Monoalkyl sulfates as alkylating agents in water, alkylsulfatase rate enhancements, and the "energy-rich" nature of sulfate half-esters, *Proc. Natl. Acad. Sci. U. S. A.*, 104, 83-86 (DOI: 10.1073/pnas.0609644104); (b) Skow C. A. R., Bicking M. K. L. (1986), Direct alkylation of carboxylic in aqueous samples, *Chromatographia*, 21, 157-160 (DOI: 10.1007/BF02311745).

17. (a) Yang Z., Xu K., Guo Z., Guo Z., Xu B. (2007), Intracellular enzymatic formation of nanofibers results in hydrogelation and regulated cell death, *Adv. Mater*., 19, 3152-3156 (DOI: 10.1002/adma.200701971); (b) Zhang J., Tokatlian T., Zhong J., Ng Q. K. T., Patterson M., Lowry W. E., Carmichael S. T., Segura T. (2011), Physically associated synthetic hydrogels with long-term covalent stabilization for cell culture and stem cell transplantation, *Adv. Mater*., 23, 5098-5103 (DOI: 10.1002/adma.201103349); (c) Cheng G., Castelletto V., Jones R. R., Connon C. J., Hamley I. W. (2011), Hydrogelation of self-

assembling RGD-based peptides, *Soft Matter*, 7, 1326-1333 (DOI: 10.1039/C0SM00408A).

18. Das A. K., Hirst A. R., Ulijn R. V. (2009), Evolving nanomaterials using enzyme-driven dynamic peptide libraries (eDPL), *Faraday Discuss*., 143, 293-303 (DOI: 10.1039/B902065A).

19. Lehrer S. S., Fasmen G. D. (1964), Fluorescence studies on poly-α-amino acids. II. Conformation-dependent excimer emission band in poly-L-tyrosine and poly-L-tryptophan, *Biopolymers*, 2, 199-203 (DOI: 10.1002/bip.1964.360020211).

20. (a) Wu D. C., Loh X. J., Wu Y.-L., Lay C. L., Liu Y. (2010), 'Living' controlled in situ gelling systems: Thiol-disulfide exchange method toward tailor-made biodegradable hydrogels, *J. Am. Chem. Soc*., 132, 15140-15143 (DOI: 10.1021/ja106639c); (b) Adler-Abramovich L., Perry R., Sagi A., Gazit E., Shabat D. (2007), Controlled assembly of peptide nanotubes triggered by enzymatic activation of self-immolative dendrimers, *ChemBioChem*, 8, 859-862 (DOI: 10.1002/cbic.200700103).

21. (a) Chatterjee S., Nandi A. K. (2011), Tuning of the morphology of a riboflavin–melamine equimolar supramolecular assembly by in situsilver nanoparticle formation, *Chem. Commun*., 47, 11510-11512 (DOI: 10.1039/C1CC14158A); (b) Gopal A., Varghese R., Ajayaghosh A. (2012), Oligo(p-phenylene-ethynylene)-derived super-π-gelators with tunable emission and self-assembled polymorphic structures, *Chem.-Asian J*., 7, 2061-2067 (DOI: 10.1002/asia.201200410); (c) Sukul P. K., Singh P. K., Maji S. K., Malik S. (2013), Aggregation induced chirality in a self assembled perylene based hydrogel: Application of the intracellular pH measurement, *J. Mater. Chem. B*, 1, 153-156 (DOI: 10.1039/C2TB00007E); (d) Adamcik J., Castelletto V., Bolisetty S., Hamley I. W., Mezzenga R. (2011), Direct observation of time-resolved polymorphic states in the self-assembly of end-capped heptapeptides, *Angew. Chem., Int. Ed.*, 50, 5495-5498 (DOI: 10.1002/anie.201100807); (e) Shao H., Parquette J. R. (2009), Controllable peptide-dendron self-assembly: Interconversion of nanotubes and fibrillar nanostructures, *Angew. Chem., Int. Ed*., 48, 2525-2528 (DOI: 10.1002/anie.200805010).

Chapter 4

Sonication Induced Peptide-Appended Bolaamphiphile Hydrogels for *In Situ* Generation and Catalytic Activity of Pt Nanoparticles

4.1 Introduction

Stimuli responsive supramolecular hydrogels[1] that form nano-network structures through weak non-covalent interactions including hydrogen-bonding, π-stacking and hydrophobic interactions have found various applications in drug delivery,[2] sensors,[3] antibacterial agents,[4] biomedicine[5] and cell culture.[6] Hydrogels derived from peptide self-assembly are attractive materials due to their biodegradability and non-toxic nature.[7] Different types of stimuli such as change in pH, solvent polarity, light, enzymes and metal ions are used to control the peptide self-assembly.[8] Pochan and co-workers have developed a peptide based β-hairpin hydrogel system as the morphology of the gelator molecule changes from random coil to β-hairpin structures induced by heat[9] or light.[10] Very recently, Hamachi *et al.* reported photo and redox responsive hydrogels by N-protected peptide molecules.[11] Enzyme triggered hydrogelation is also attractive in current research in which self-assembly can be achieved and controlled by enzyme catalyzed reactions. Specifically, self-assembly induced by enzyme catalyzed reactions that hydrolyzed the peptide esters or reversed hydrolysis with N-protected amino acids and amino acid methyl esters show significant charge transport.[12] Xu *et al.* demonstrated that an enzyme β-lactamase catalyzed reaction can produce hydrogel materials.[13] Recently, ultrasound has emerged to play an important role in triggering the self-assembly leading to the gelation of liquids. Ultrasound induced gelation is interesting and effective in tuning the self-assembly process.[14] Generally, sonication is used to solubilize and disperse compounds through disruption of weak non-covalent interactions between molecules. Sometimes it can help the small organic molecules to self-assemble into supramolecular structures and tune the gelation properties. Ultrasound breaks the non-covalent weak interactions and provides sufficient energy to achieve self-assembly through reorientation of the assembly process, such as intra-molecular hydrogen bonding to inter-molecular hydrogen bonding, extension of π-π stacking interactions and elongating the fiber to form network structures. Thus, ultrasound modifies the morphology by providing suitable energy. Ultrasound induced organogelation by a dipeptide was described by Ripmeester *et al.*[15] Sonication induced organogels[15] and organogels by a metalated gelator[16] have also been reported. Fu and Yao have shown

ultrasound induced organogels with (R)-N-Fmoc-octylglycine where sonication can tune intramolecular hydrogen bonding to intermolecular hydrogen bonding and intermolecular hydrogen bonding interactions lead to different nanoscale morphologies, from unbranched nanowires to entangled fibrous network structures, which are responsible for gelation.[17] Sonication induced peptide based multi-colour gels, made by up-conversion of rare earth nanoparticles (UCNPs), allow the UCNPs to retain their nanophosphor properties in the gel state.[18] Banerjee *et al.* have reported sonication induced metallo-hydrogels using phenylalanine-based bolaamphiphile as a vitamin B12 carrier.[19] To our knowledge, ultrasound induced hydrogel with peptide molecules, where the gelator molecule can itself form a gel with water, is rare as an example. Moreover, there is a need for the development of ultrasound induced peptide hydrogelators exhibiting a sol-to-gel transition for applications under physiological conditions. Recently, hydrogels composed of peptides and proteins have been unveiled by several groups for tissue engineering[20] and *in situ* synthesis of metal nanoparticles in gel phase networks.[21] Stupp and co-workers have described amphiphilic peptide hydrogels that self-assemble into cylindrical nanofibers depending upon salt concentration at physiological pH levels. These self-assembled peptide-amphiphilic nanofibers are used as effective substrates for nucleation and growth of cadmium sulfide (CdS) nanocrystals.[22] Metal nanoparticles,[23] carbon nanotubes[24] and quantum dots (QDS)[25] can interact with organic molecules to form composite gels. Moreover, in situ synthesis of platinum nanoparticles in the gel phase medium is still unexplored. In this chapter, we report sonication induced hydrogel formation using asymmetric peptide based bolaamphiphile molecules under physiological conditions. Redox active tyrosine containing peptide-based bolaamphiphilic hydrogel can act as a nanoreactor for *in situ* synthesis and stabilization of platinum (Pt) nanoparticles within the gel-phase network. *In situ* synthesized Pt nanoparticles, with a diameter of 1-3 nm, can reduce *p*-nitroaniline to *p*-phenylenediamine, and this catalytic property may be utilized to carry hydrogenation reactions in an aqueous medium.

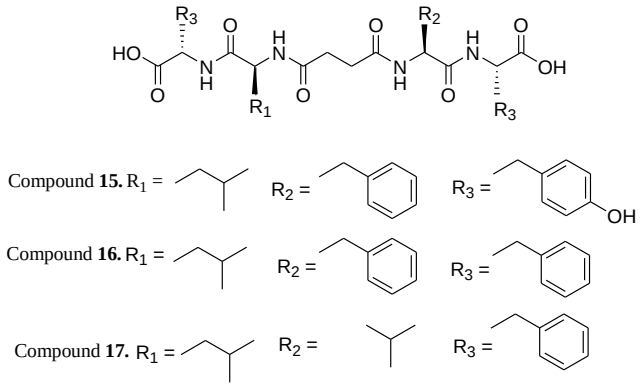

Figure 4.1. *Chemical structures of peptide bolaamphiphiles **15** (HO-Tyr-Leu-Suc-Phe-Tyr-OH), **16** (HO-Phe-Leu-Suc-Phe-Phe-OH) and **17** (HO-Phe-Leu-Suc-Val-Phe-OH).*

4. 2 Experimental

4.2. (1) Synthesis of peptide bolaamphiphiles

Peptide bolaamphiphiles **15**, **16** and **17** employed in this chapter were synthesized by conventional solution phase methodology. The C-terminus of the amino acids was protected as a methyl ester. Couplings were mediated by dicyclohexylcarbodiimide-1-hydroxybenzotriazole (DCC-HOBt). The synthesis of HO-Suc-Phe(1)-OMe **5** and HO-Suc-Leu(1)-OMe **9** are reported in previous chapter. The final compounds were purified and fully characterized by FT-IR, ^{1}H NMR and mass spectral studies.

4.2.1 Synthesis of HO-Tyr(4)-Leu(3)-Suc-Phe(1)-Tyr(2)-OH 15:

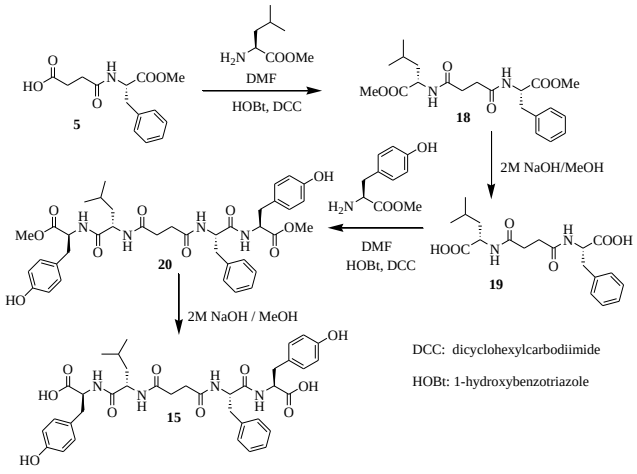

Scheme 4.1. *Synthetic scheme of peptide bolaamphiphile **15.***

*(a) Synthesis of MeO-Leu(2)-Suc-Phe(1)-OMe **18**:* 3.35 g (12 mmol) of HO-Suc-Phe(1)-OMe **5** in 3 mL of DMF was cooled in an ice bath and H-Leu-OMe was isolated from 4.3 g (24 mmol) of the corresponding methyl ester hydrochloride by neutralization and subsequent extraction with ethyl acetate and the ethyl acetate extract was concentrated to 10 mL. It was then added to the reaction mixture, followed immediately by 2.72 g (13.2 mmol) DCC and 1.82 g (13.2 mmol) of HOBt. The reaction mixture was stirred for overnight. The residue was taken up in ethyl acetate (50 mL) and the DCU was filtered off. The organic layer was washed with 1M HCl (3 × 50 mL), brine (2 × 50 mL), 1M sodium carbonate (3 × 50 mL), brine (2 × 50 mL) and dried over anhydrous sodium sulfate and evaporated under vacuum to yield **18** as a white solid. Purification was done by silica gel column (100-200 mesh) using chloroform-methanol (9:1) as eluent.

Yield: 4.24 g (10.4 mmol, 87%); R_f 0.677 ($CHCl_3$:CH_3OH = 9:1); FT-IR (KBr): $\tilde{\upsilon}$ = 3328 (st), 3071 (m), 1736 (ms), 1639 (st), 1546 (st), cm^{-1}; ^1H NMR (400 MHz, $CDCl_3$, δ_{ppm}): 7.22-7.20 (m, 5H, ring protons of Phe(1)), 7.06 (d, J = 6.4 Hz, 2H, NHs of Leu(2) and Phe(1)), 4.75 (m, 1H, $C^{\alpha}H$ of Phe(1)), 4.50 (m, 1H, $C^{\alpha}H$ of Leu(2)), 3.65 (s, 6H, -$COOCH_3$), 3.00 (d, J = 5.6 Hz, 2H, $C^{\beta}Hs$ of Phe(1)), 2.44-2.41(m, 4H, -CH_2- of Suc), 1.54 and 1.47 (m, 3H, $C^{\beta}Hs$ and $C^{\gamma}H$ of Leu(2)), 0.87 (d, J = 5.2 Hz, 6H, $C^{\delta}Hs$ of Leu(2)); $[\alpha]_D^{20}$ = -16.44 (c = 0.5 in CH_3OH); MS (ESI) m/z: 405.0 [M-H]$^-$, $M_{calcd.}$ = 406.0

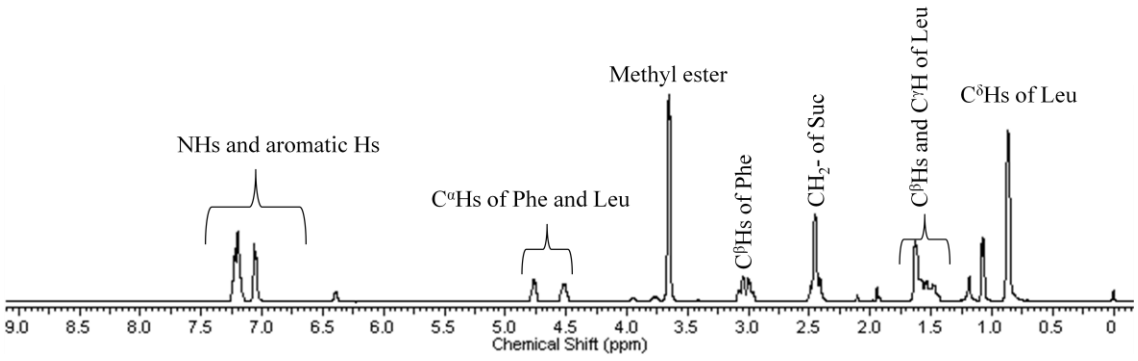

Figure 4.2. *^1H NMR spectrum (400 MHz, $CDCl_3$) of MeO-Leu-Suc-Phe-OMe **18.***

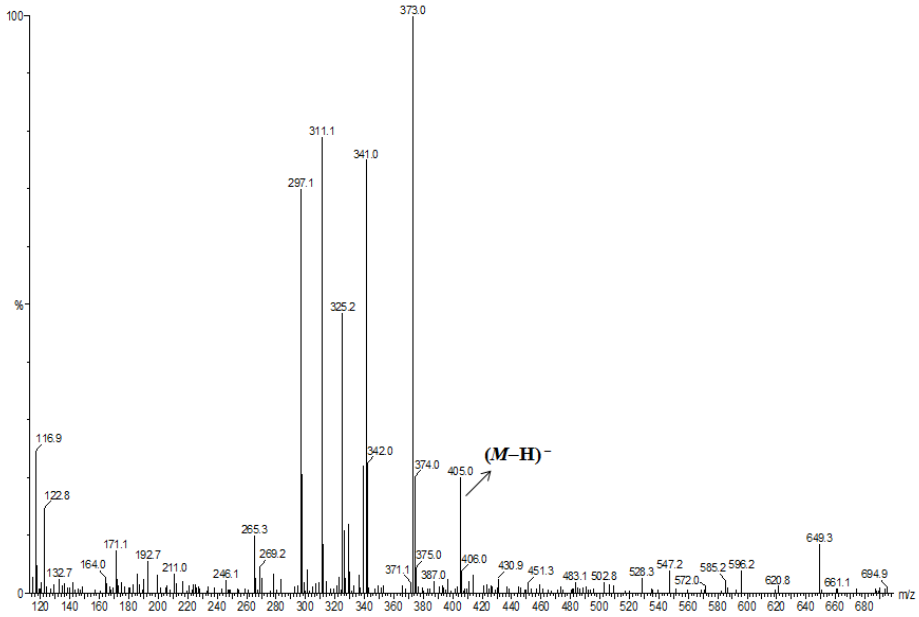

Figure 4.3. *ESI-MS spectrum of MeO-Leu-Suc-Phe-OMe* ***18.***

(b) Synthesis of HO-Leu(2)-Suc-Phe(1)-OH ***19:*** 4.06 g (10 mmol) of MeO-Leu(2)-Suc-Phe(1)-OMe **18** in 6 mL MeOH was taken in a round bottom flask and 15 mL of 2M NaOH was added dropwise. The reaction was monitored by thin layer chromatography (TLC). The reaction mixture was stirred for 6 hours. 15 mL of distilled water was added to the reaction mixture and MeOH was removed under vacuum. The aqueous part was washed with diethyl ether (2 × 30 mL). Then, it was cooled down under ice-bath for 10 minutes and then pH was adjusted to 1 by drop wise addition of 1M HCl. It was extracted with ethyl acetate (3 × 50 mL) and then the ethyl acetate part was dried over anhydrous Na_2SO_4 and evaporated under vacuum to yield **19** as a white solid.

Yield: 3.63 g (9.6 mmol, 96%); R_f 0.54 ($CHCl_3$:CH_3OH:CH_3COOH = 10:2:0.1); FT-IR (KBr): ῡ = 3360 (st), 3031 (m), 1721 (ms), 1614 (st), 1531 (st), 1513 (st) cm^{-1}; ^1H NMR (300 MHz, DMSO-d_6, δ_{ppm}): 12.4 (s, 2H of COOH), 8.15 (d, *J* =7.8 Hz, 1H, NH of Leu(2)), 8.00 (d, *J* = 7.8 Hz, 1H, NH of Phe(1)), 7.25-7.18 (m, 5H, ring protons of Phe(1)), 4.39-4.31 (m, 1H, $C^{\alpha}H$ of Phe(1)), 4.18-4.10 (m, 1H, $C^{\alpha}H$ of Leu(2)), 3.00 (d, *J* = 5.1 Hz, 2H, $C^{\beta}Hs$ of Phe(1)), 2.46-2.36 (m, 4H, -CH_2- of Suc), 1.79 and 1.59-1.50 (m,

3H, C^{β}Hs and C^{γ}H of Leu(2)), 0.84 (d, J = 6.3 Hz, 6H, C^{δ}Hs of Leu(2)); $[\alpha]_D^{20}$ = +6 (c = 0.5 in CH_3OH); MS (ESI) m/z: 377.0 $[M\text{-H}]^-$, $M_{calcd.}$ = 378.1

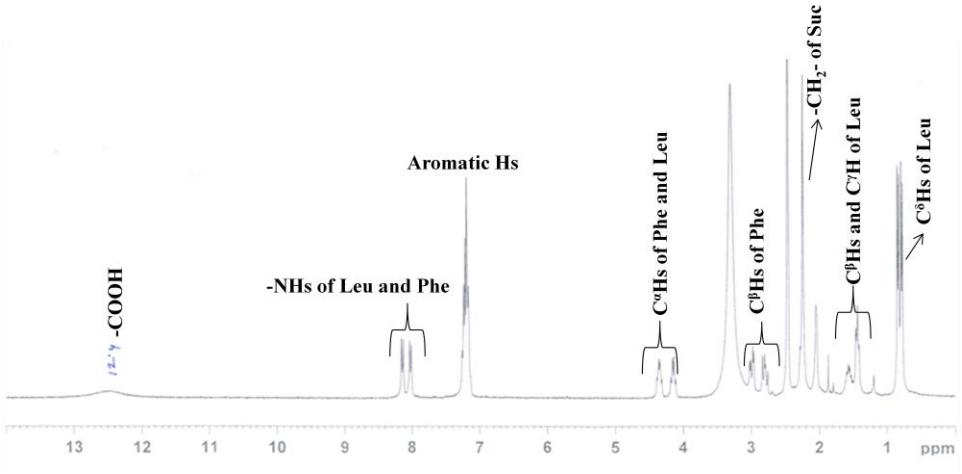

Figure 4.4. *^{1}H NMR spectrum (300 MHz, DMSO-d_6) of HO-Leu-Suc-Phe-OH* ***19.***

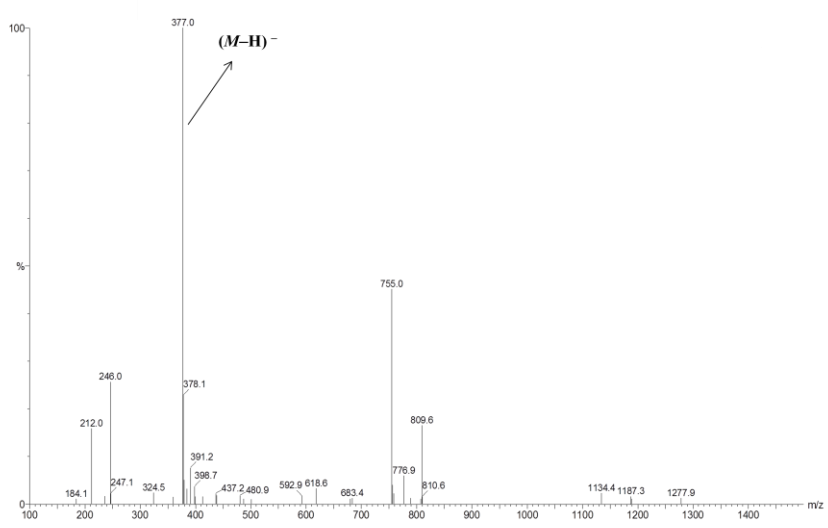

Figure 4.5. *ESI-MS spectrum of HO-Leu-Suc-Phe-OH* ***19.***

(c) Synthesis of MeO-Tyr(4)-Leu(3)-Suc-Phe(1)-Tyr(2)-OMe ***20****:* 1.70 g (4.5 mmol) of HO-Leu-Suc-Phe-OH **19** in 3 mL of DMF was cooled in an ice bath and H-Tyr-OMe was isolated from 4.17 g (18 mmol) of the corresponding methyl ester hydrochloride by neutralization and subsequent extraction with ethyl acetate and the ethyl acetate extract was concentrated to 10 mL. It was then added to the reaction mixture, followed

immediately by 2.04 g (9.9 mmol) DCC and 1.33 g (9.9 mmol) of HOBt. The reaction mixture was stirred for overnight. The residue was taken up in ethyl acetate (50 mL) and the DCU was filtered off. The organic layer was washed with 1M HCl (3 × 50 mL), brine (2 × 50 mL), 1M sodium carbonate (3 × 50 mL), brine (2 × 50 mL) and dried over anhydrous sodium sulfate and evaporated under vacuum to yield **20** as a white solid. Purification was done by silica gel column (100-200 mesh) using chloroform-methanol (9:1) as eluent.

Yield: 2.70 g (3.69 mmol, 82%); R_f 0.63 ($CHCl_3$:CH_3OH = 9:1); FT-IR (KBr): ϑ = 3298 (st), 3066 (ms), 1738 (ms), 1644 (st), 1540 (st), 1516 (st) cm^{-1}; ^1H NMR (400 MHz, $CDCl_3$, δ_{ppm}): 7.45 and 7.10 (m, 5H, ring protons of Phe(1)), 6.94 and 6.89 (d, *J* = 6.4, 4H, ring protons of Tyr(2) and Tyr(4)), 6.89 (d, *J* = 7.6 Hz, 2H, NHs of Tyr(2) and Tyr(4)), 6.57 (d, *J* = 8.4, 4H of Tyr(2) and Tyr(4)), 6.46 (d, *J* = 8.0 Hz, 1H, NH of Phe(1)), 6.35 (d, *J* = 8.0 Hz, 1H, NH of Leu(3)), 4.93 (m, 1H, $C^{\alpha}H$ of Phe(1)), 4.37 (m, 2H, $C^{\alpha}Hs$ of Tyr(2) and Tyr(4)), 4.23 (m, 1H, $C^{\alpha}H$ of Leu(3)), 3.73 (s, 6H, -$COOCH_3$), 3.00 and 2.96 (d, *J* = 8.4 Hz, *J* = 7.2 Hz, 4H, $C^{\beta}Hs$ of Tyr(2) and Tyr(4)), 2.87 (d, *J* = 7.2, 2H, $C^{\beta}Hs$ of Phe(1)), 2.72-2.65 (m, 4H, -CH_2- of Suc), 1.87 and 1.38 (m, 3H, $C^{\beta}Hs$ and $C^{\gamma}H$ of Leu(3)), 0.83 (d, *J* = 4.8 Hz, 6H, $C^{\delta}Hs$ of Leu(3)); $[\alpha]_D^{20}$ = -30.8 (*c* = 0.5 in CH_3OH); MS (ESI) *m/z*: 731.4 $[M\text{-}H]^-$, $M_{calcd.}$ = 732.3

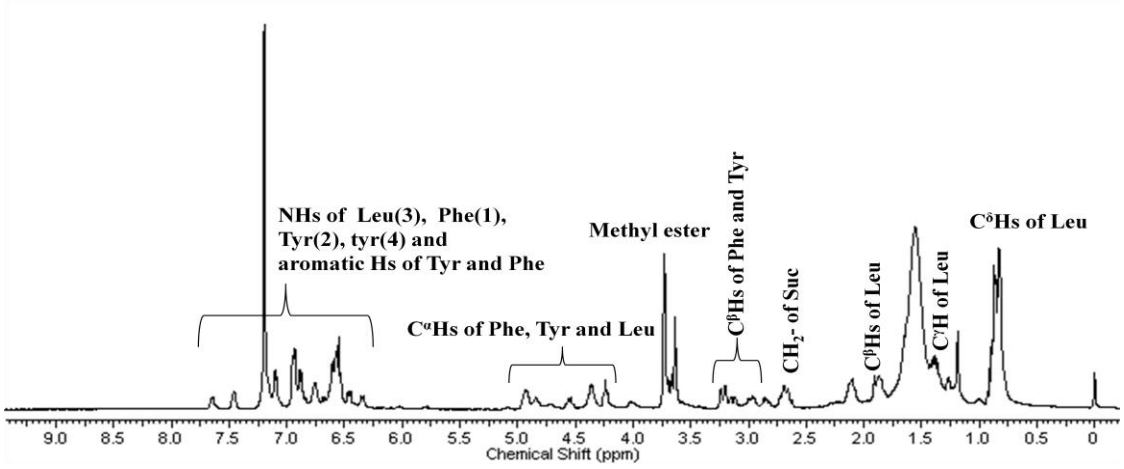

Figure 4.6. *^1H NMR spectrum (400 MHz, $CDCl_3$) of MeO-Tyr-Leu-Suc-Phe-Tyr-OMe* ***20.***

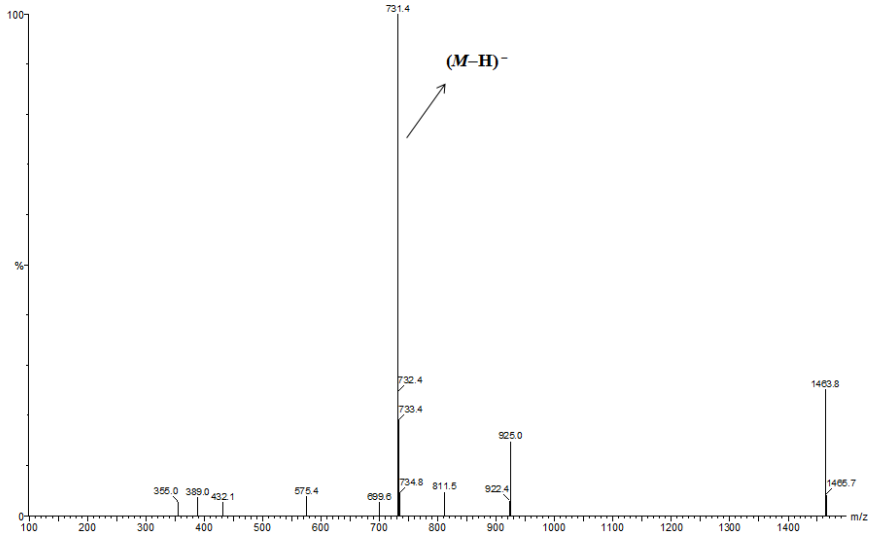

Figure 4.7. *ESI-MS spectrum of MeO-Tyr-Leu-Suc-Phe-Tyr-OMe* ***20.***

(d) Synthesis of HO-Tyr(4)-Leu(3)-Suc-Phe(1)-Tyr(2)-OH ***15****:* 2.56 g (3.5 mmol) of MeO-Tyr(4)-Leu(3)-Suc-Phe(1)-Tyr(2)-OMe **20** in 10 mL MeOH was taken in a round bottom flask and 6 mL of 2M NaOH was added to it dropwise. The reaction was monitored by thin layer chromatography (TLC). The reaction mixture was stirred for 8 hours. 15 mL of distilled water was added to the reaction mixture and MeOH was removed under vacuum. The aqueous part was washed with diethyl ether (2 × 30 mL). Then it was cooled under in ice bath for 10 minutes and then pH was adjusted to 1 by drop wise addition of 1M HCl. It was extracted by ethyl acetate (3 × 50 mL) and then the ethyl acetate part was dried over anhydrous Na_2SO_4 and evaporated under vacuum to yield **15** as a white solid.

Yield: 2.21 g (3.15 mmol, 90%); R_f 0.26 ($CHCl_3$:CH_3OH:CH_3COOH = 10:2:0.1); FT-IR (KBr): ῡ = 3299 (st), 1715 (m), 1645 (st), 1540 (st), 1516 (ms) cm^{-1}; ^1H NMR (400 MHz, DMSO-d_6, δ_{ppm}): 8.39 (d, *J* = 7.2 Hz, 1H, NH of Leu(3)), 8.21 (d, *J* = 6.4 Hz, 1H, NH of Phe(1)), 8.08 (d, *J* = 8.0 Hz, 1H, NH of Tyr(4)), 7.94 (d, *J* = 7.6 Hz, 1H, NH of Tyr(2)), 7.24-7.18 (m, 5H, ring protons of Phe(1)), 6.98 (d, *J* = 6.4 Hz, 4H, ring protons of Tyr(2) and Tyr(4)), 6.65 (d, *J* = 6.8 Hz, 4H, ring protons of Tyr(2) and Tyr(4)), 4.51 (m, 1H, $C^{\alpha}H$ of Leu(3)), 4.38-4.27 (m, 3H, $C^{\alpha}Hs$ of Tyr(2), Tyr(4) and Phe(1)), 2.87 (d, *J* = 6.0, 4H, $C^{\beta}Hs$ of Tyr(2) and Tyr(4)), 2.83 (d, *J* = 8.0 Hz, 2H, $C^{\beta}Hs$ of Phe(1)), 2.25 (m, 4H, -

CH_2- of Suc), 1.53 and 1.37-1.35 (m, 3H, $C^{\beta}Hs$ and $C^{\gamma}H$ of Leu(3)), 0.85 and 0.80 (d, *J* = 5.6 Hz, *J* = 5.2 Hz, 6H, $C^{\delta}Hs$ of Leu(3)), ^{13}C NMR (100 MHz, DMSO-d_6, δ_{ppm}): 172.26 (C=O), 171.92 (C=O), 171.84 (C=O), 171.35 (C=O), 155.93 (C=O), 137.78, 129.97, 129.09, 127.96, 127.04, 126.19, 114.97, 54.03, 53.90, 51.66, 50.59, 35.71, 30.65, 24.03, 22.91,21.54;$[\alpha]_D^{20}$ = -15.35 (*c* = 0.5 in CH_3OH); MS (ESI) *m/z*: 703.2 [*M*-H]$^-$, $M_{calcd.}$ = 704.2

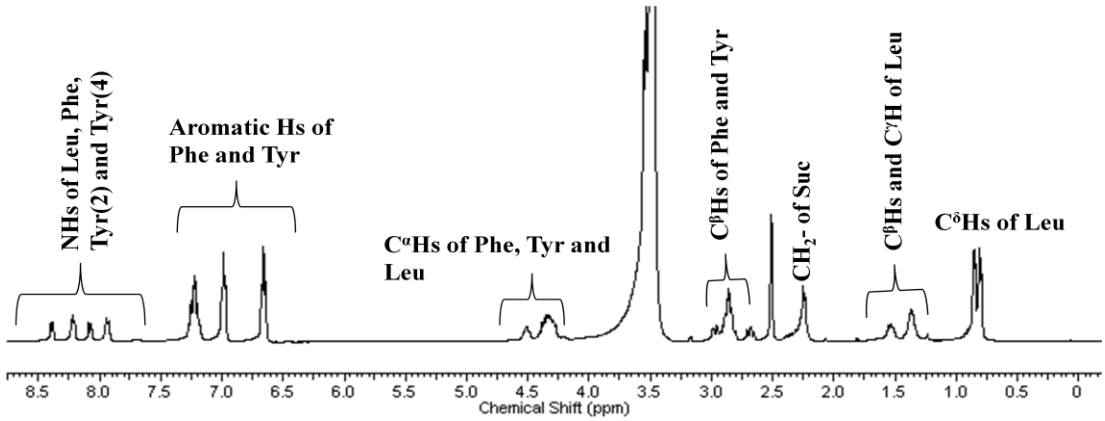

Figure 4.8. *^1H NMR spectrum (400 MHz, DMSO-d_6) of HO-Tyr-Leu-Suc-Phe-Tyr-OH* ***15.***

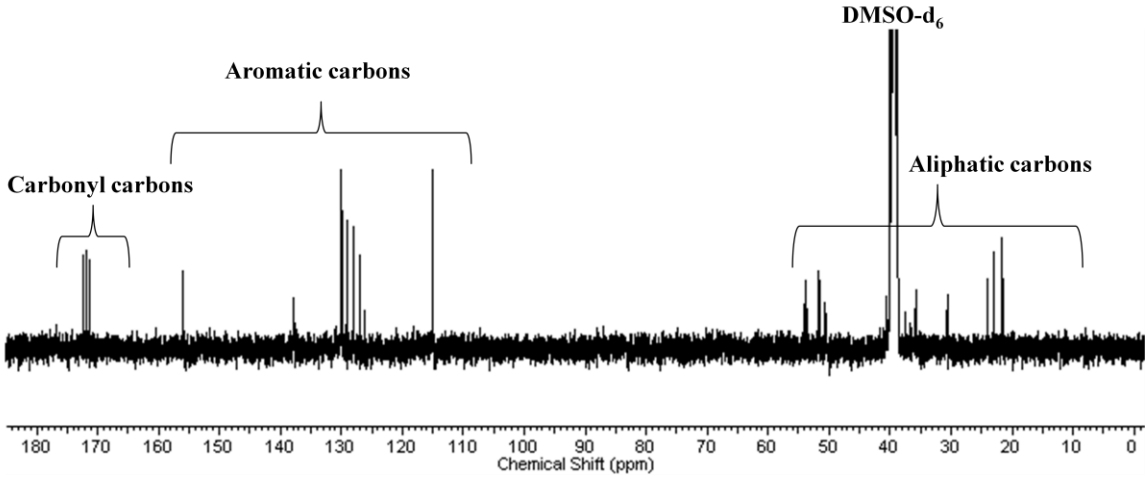

Figure 4.9. *^{13}C NMR spectrum (100 MHz, DMSO-d_6) of HO-Tyr-Leu-Suc-Phe-Tyr-OH* ***15.***

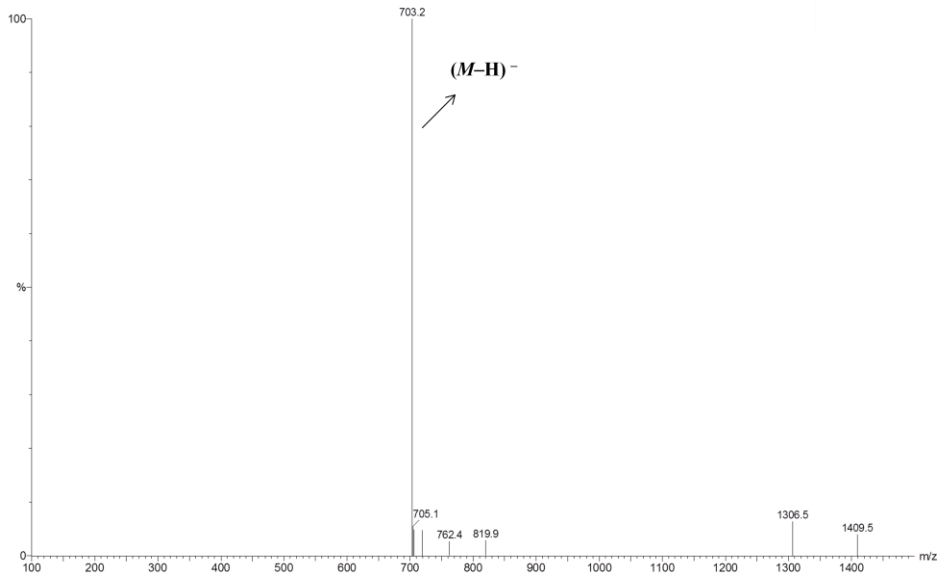

Figure 4.10. *ESI-MS spectrum of HO-Tyr-Leu-Suc-Phe-Tyr-OH* ***15.***

4.2.2 Synthesis of HO-Phe(4)-Leu(3)-Suc-Phe(1)-Phe(2)-OH 16:

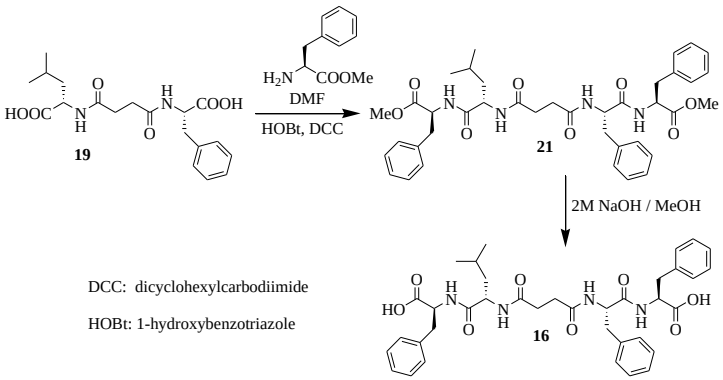

Scheme 4.2. *Synthetic scheme of peptide bolaamphiphile* ***16.***

(a) Synthesis of MeO-Phe(4)-Leu(3)-Suc-Phe(1)-Phe(2)-OMe **21**: 1.70 g (4.5 mmol) of HO-Leu(2)-Suc-Phe(1)-OH **19** in 3 mL of DMF was cooled in an ice bath and H-Phe-OMe was isolated from 3.88 g (18 mmol) of the corresponding methyl ester hydrochloride by neutralization and subsequent extraction with ethyl acetate and the ethyl acetate extract was concentrated to 10 mL. It was then added to the reaction mixture, followed immediately by 2.04 g (9.9 mmol) DCC and 1.33 g (9.9 mmol) of HOBt. The reaction mixture was stirred for overnight. The residue was taken up in ethyl acetate (50

mL) and the DCU was filtered off. The organic layer was washed with 1M HCl (3 × 50 mL), brine (2 × 50 mL), 1M sodium carbonate (3 × 50 mL), brine (2 × 50 mL) and dried over anhydrous sodium sulfate and evaporated under vacuum to yield **21** as a white solid. Purification was done by silica gel column (100-200 mesh) using chloroform-methanol (9:1) as eluent and white solid product was obtained.

Yield: 2.45 g (3.51 mmol, 78%); R_f 0.81 ($CHCl_3$:CH_3OH = 9:1); FT-IR (KBr): ῡ = 3321 (st),1743 (ms), 1634 (st), 1539 (st) cm^{-1}; ^1H NMR (400 MHz, DMSO-d_6, δ_{ppm}): 8.46 (d, *J* = 7.2 Hz, 1H, NH of Leu(3)), 8.29 (d, *J* = 8.1 Hz, 1H, NH of Phe(4)), 8.09 (d, *J* = 8.4 Hz, 1H, NH of Phe(1)), 7.93 (d, *J* = 8 Hz, 1H, NH of Phe(2)), 7.28-7.20 (m, 15H, ring protons of Phe(1), Phe(2) and Phe(4)), 4.51-4.41 (m, 2H, C^{α}Hs of Phe(1), Phe(2) and Phe(4)), 4.28 (m, 1H, C^{α}H of Leu(3), 3.56 and 3.54 (s, 6H of $COOCH_3$), 3.02, 2.98 and 2.95 (d, *J* = 6.8, *J* = 4.4 and *J* = 6.4 Hz, 6H, C^{β}Hs of Phe(1), Phe(2) and Phe(4)), 2.24-2.21 (m, 4H, -CH_2- of Suc), 1.54-1.47 and 1.37-1.33 (m, 3H, C^{β}Hs and C^{γ}H of Leu(3)), 0.85 and 0.80 (d, *J* = 6.8 Hz and *J* = 6.0 Hz, 6H, C^{δ}Hs of Leu(3));$[\alpha]_D^{20}$ = + 8.23 (*c* = 0.5 in $CHCl_3$); MS (ESI) *m/z*: 699.3 $[M\text{-H}]^-$, $M_{calcd.}$ = 700.2

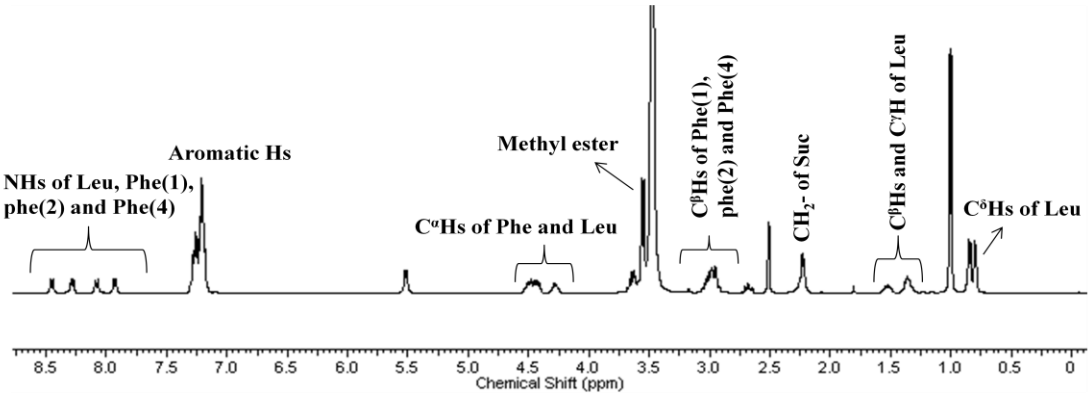

Figure 4.11. *^1H NMR spectrum (400 MHz, DMSO-d_6) of MeO-Phe-Leu-Suc-Phe-Phe-OMe* ***21.***

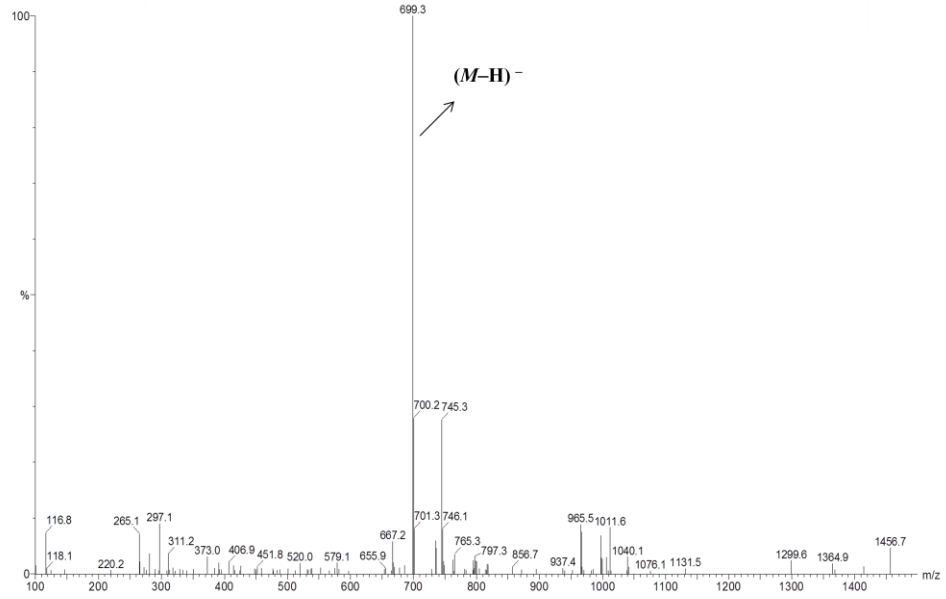

Figure 4.12. *ESI-MS spectrum of MeO-Phe-Leu-Suc-Phe-Phe-OMe* ***21.***

(b) Synthesis of HO-Phe(4)-Leu(3)-Suc-Phe(1)-Phe(2)-OH ***16****:* 2.24 g (3.2 mmol) of MeO-Phe(4)-Leu(3)-Suc-Phe(1)-Phe(2)-OMe **21** in 150 mL MeOH was taken in a round bottom flask and 6 mL of 2M NaOH was added dropwise. The reaction was monitored by thin layer chromatography (TLC). The reaction mixture was stirred for overnight. 15 mL distilled water was added to the reaction mixture and MeOH was removed under vacuum. The aqueous part was washed with diethyl ether (2 × 30 mL). Then it was cooled under ice bath for 10 minutes and then pH was adjusted to 1 by drop wise addition of 1M HCl. It was extracted with ethyl acetate (3 × 50 mL) and then the ethyl acetate part was dried over anhydrous Na_2SO_4 and evaporated under vacuum to yield **16** as a white solid. 2% of racemization was found in this hydrolysis reaction.

Yield: 1.97 g (2.94 mmol, 92%); R_f 0.35 ($CHCl_3$:CH_3OH:CH_3COOH = 10:2:0.1); FT-IR (KBr): ϋ = 3296 (st), 1716 (ms), 1638 (st), 1538 (st) cm^{-1}; ^1H NMR (400 MHz, DMSO-d_6, δ_{ppm}): 8.28 (d, *J* = 7.2 Hz, 1H, NH of Phe(2)), 8.11 (d, *J* = 7.2 Hz, 1H, NH of Phe(4)), 7.99 (d, *J* = 8.0 Hz, 1H, NH of Phe(1)), 7.24-7.30 (m, 15H, ring protons of Phe(1), Phe(2) and Phe(4)), 7.13 (d, *J* = 7.2 Hz, 1H, NH of Leu(3)), 4.53 and 4.46 (m, 3H, $C^{\alpha}Hs$ of Phe(1), Phe(2) and Phe(4)), 4.33 (m, 1H, $C^{\alpha}H$ of Leu(3), 3.10, 3.00 and 2.98 (d, *J* = 4.4, *J* = 8 and *J* = 6.4 Hz, 6H, $C^{\beta}Hs$ of Phe(1), Phe(2) and Phe(4)), 2.28 (m, 4H, -CH_2- of Suc),

1.58 and 1.42 (m, 3H, C^{β}Hs and C^{γ}H of Leu(3)), 0.91 and 0.86 (d, J = 6.4 Hz, J = 6.0 Hz, 6H, C^{δ}Hs of Leu(3)); ^{13}C NMR (100 MHz, DMSO-d_6, δ_{ppm}): 172.28 (C=O), 171.78 (C=O), 171.70 (C=O), 171.39 (C=O), 171.28 (C=O), 156.84 (C=O), 137.78, 137.06, 136.98, 129.08, 129.01, 128.26, 128.19, 127.96, 126.56, 126.50, 126.19, 53.49, 51.80, 51.74, 50.59, 37.36, 36.51, 36.37, 30.61, 30.51, 24.02, 23.23, 22.89, 21.55; $[\alpha]_D^{20}$ = -17.3 (c = 0.5 in CH_3OH); MS (ESI) m/z: 671.2 $[M\text{-H}]^-$, $M_{calcd.}$ = 672.2

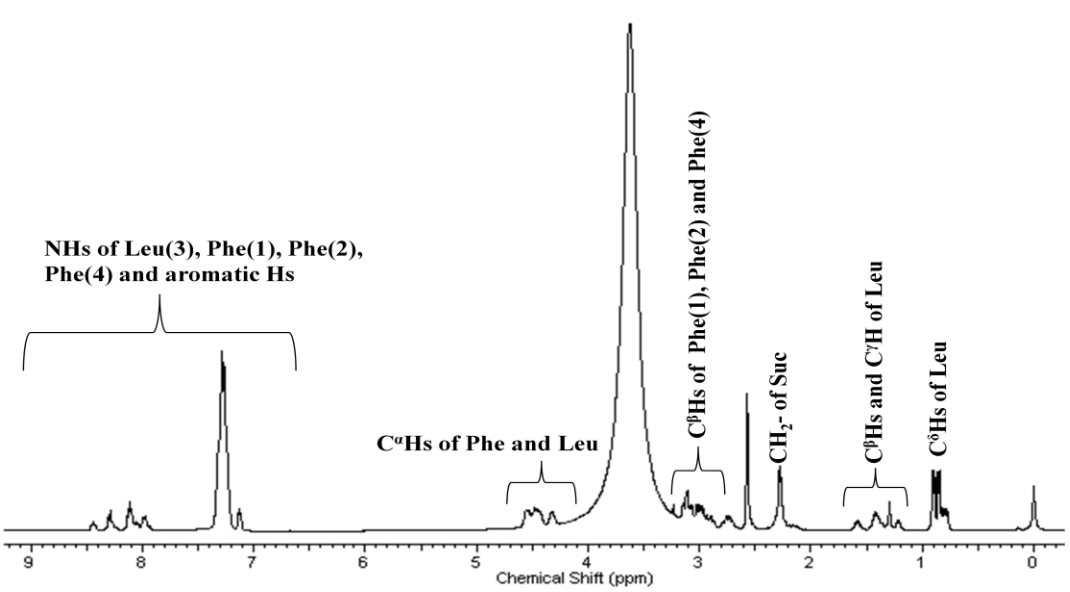

Figure 4.13. *^{1}H NMR spectrum (400 MHz, DMSO-d_6) of HO-Phe-Leu-Suc-Phe-Phe-OH* ***16.***

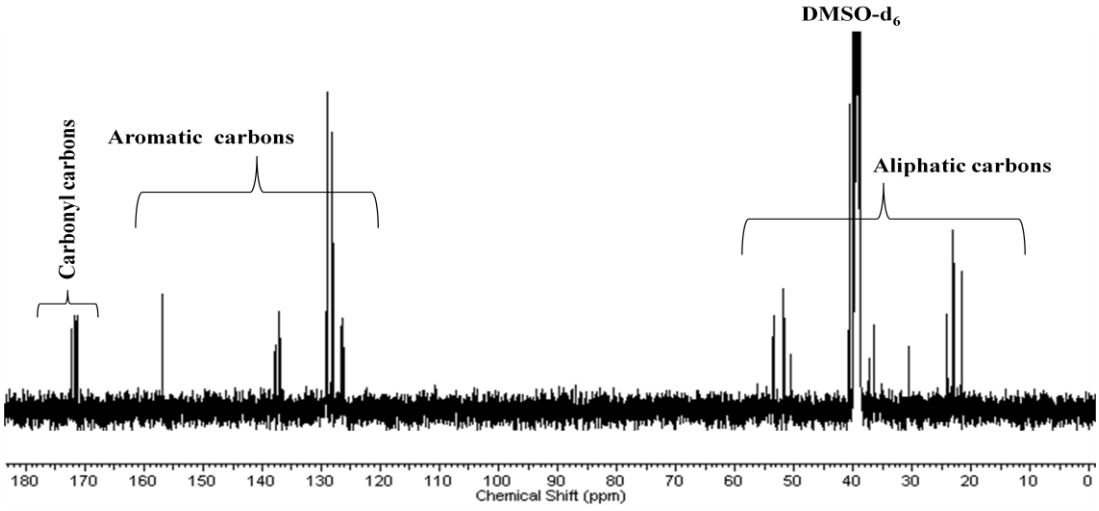

Figure 4.14. *^{13}C NMR spectrum (100 MHz, DMSO-d_6) of HO-Phe-Leu-Suc-Phe-Phe-OH* ***16.***

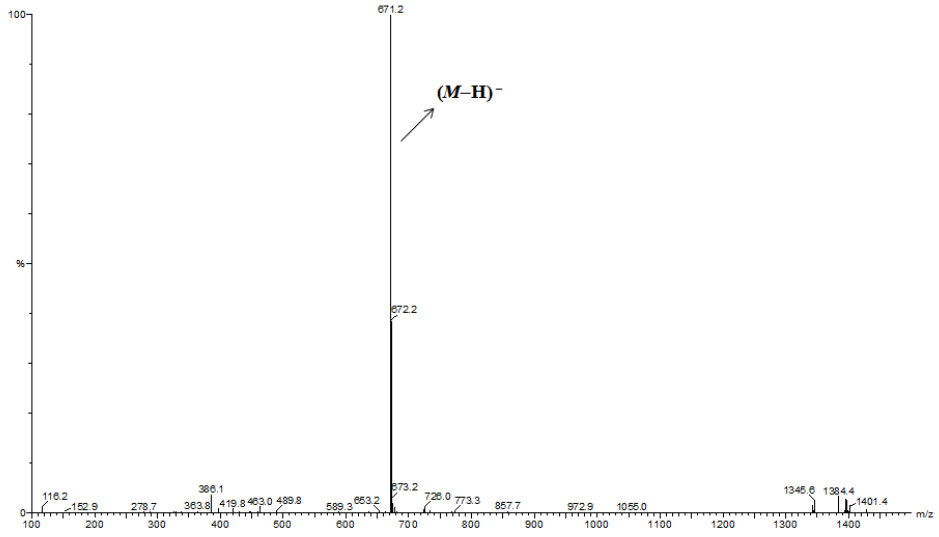

Figure 4.15. *ESI-MS spectrum of HO-Phe-Leu-Suc-Phe-Phe-OH* ***16.***

4.2.3 Synthesis of HO-Phe(4)-Leu(3)-Suc-Val(1)-Phe(2)-OH 17:

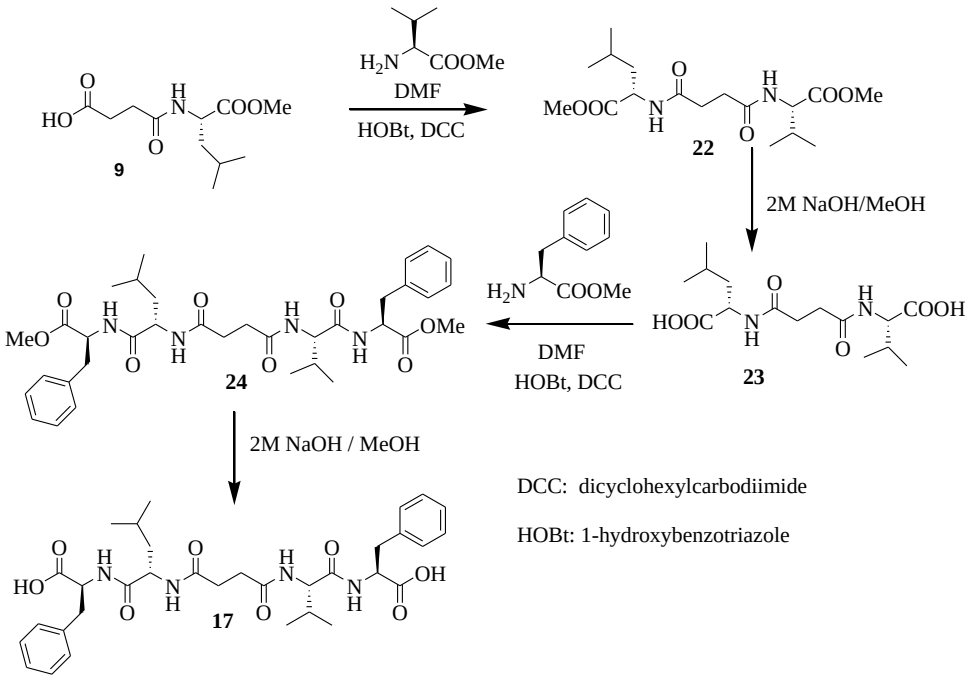

Scheme 4.3. *Synthetic scheme of peptide bolaamphiphile* ***17****.*

*(a) Synthesis of MeO-Val(2)-Suc-Leu(1)-OMe **22**:* 1.71 g (7 mmol) of HO-Suc-Leu(1)-OMe **9** in 3 mL of DMF was cooled in an ice bath and H-Val-OMe was isolated from 2.33 g (14 mmol) of the corresponding methyl ester hydrochloride by neutralization and subsequent extraction with ethyl acetate and the ethyl acetate extract was concentrated to 8 mL. It was then added to the reaction mixture, followed immediately by 1.58 g (7.7 mmol) DCC and 1.04 g (7.7 mmol) of HOBt. The reaction mixture was stirred for overnight. The residue was taken up in ethyl acetate (50 mL) and the DCU was filtered off. The organic layer was washed with 1M HCl (3 × 50 mL), brine (2 × 50 mL), 1M sodium carbonate (3 × 50 mL), brine (2 × 50 mL) and dried over anhydrous sodium sulfate and evaporated under vacuum to yield **22** as a white solid. Purification was done by silica gel column (100-200 mesh) using chloroform-methanol (9:1) as eluent.

Yield: 1.88 g (5.25 mmol, 75%); R_f 0.75 ($CHCl_3$:CH_3OH = 9:1); FT-IR (KBr): ῡ = 3266 (st), 1757 (ms), 1678 (w), 1663 (ms), 1637 (ms), 1560 (st), 1538 (st) cm^{-1}; ^1H NMR (400 MHz, $CDCl_3$, δ_{ppm}): 6.42 (d, *J* = 7.6 Hz, 1H, NH of Val(2)), 6.30 (d, *J* = 7.2 Hz, 1H, NH of Leu(1)), 4.53 (m, 1H, $C^{\alpha}H$ of Leu(1)), 4.45 (m, 1H, $C^{\alpha}H$ of Val(2)), 3.65 (s, 6H, $COOCH_3$), 2.57-2.46 (m, 4H, -CH_2- of Suc), 2.10-2.05 (m, 1H, $C^{\beta}H$ of Val(2)), 1.63-1.56 and 1.46 (m, 3H, $C^{\beta}Hs$ and $C^{\gamma}H$ of Leu(1)), 0.86 (d, *J* = 6.4 Hz, 12H, $C^{\delta}Hs$ of Leu(1) and $C^{\gamma}Hs$ of Val(2)); $[\alpha]_D^{20}$ = - 37.9 (*c* = 0.5 in CH_3OH); MS (ESI) *m/z*: $(M+Na)^+$ Calcd. for $C_{17}H_{30}N_2O_6Na$: 381.1996; found 381.2009.

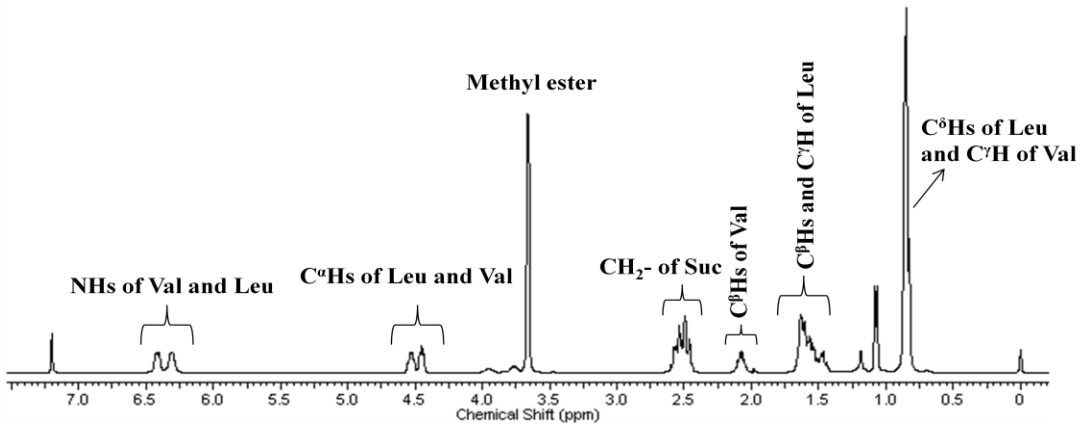

Figure 4.16. *^1H NMR spectrum (400 MHz, $CDCl_3$) of MeO-Val(2)-Suc-Leu(1)-OMe **22**.*

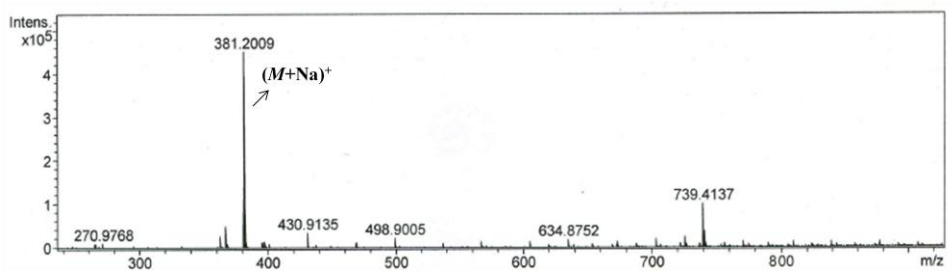

Figure 4.17. *ESI-MS spectrum of MeO-Val(2)-Suc-Leu(1)-OMe* ***22.***

(b) Synthesis of HO-Val(2)-Suc-Leu(1)-OH ***23****:* 1.72 g (4.8 mmol) of MeO-Val(2)-Suc-Leu(1)-OMe **22** in 6 mL MeOH was taken in a round bottom flask and 8 mL of 2M NaOH was added to it dropwise. The reaction was monitored by thin layer chromatography (TLC). The reaction mixture was stirred for 5 hours. 15 mL of distilled water was added to the reaction mixture and MeOH was removed under vacuum. The aqueous part was washed with diethyl ether (2 × 30 mL). Then it was cooled under ice bath for 10 minutes and then pH was adjusted to 1 by drop wise addition of 1M HCl. It was extracted with ethyl acetate (3 × 50 mL) and then the ethyl acetate part was dried over anhydrous Na_2SO_4 and evaporated under vacuum to yield **23** as a white solid.

Yield: 1.50 g (4.56 mmol, 95%); R_f 0.67 ($CHCl_3$:CH_3OH:CH_3COOH = 10:2:0.1); FT-IR (KBr): $\tilde{\upsilon}$ = 3338 (st), 3065 (m), 1715 (ms), 1617 (st), 1534 (st) cm^{-1}; ^1H NMR (400 MHz, DMSO-d_6, δ_{ppm}): 8.14 (d, J = 8.0 Hz, 1H, NH of Val(2)), 8.04 (d, J = 8.8 Hz, 1H, NH of Leu(1)), 4.26-4.23(m, 1H, $C^{\alpha}H$ of Leu(1)), 4.19-4.16 (m, 1H, $C^{\alpha}H$ of Val(2)), 2.48-2.38 (m, 4H, -CH_2 of Suc), 2.07 (m, 1H, $C^{\beta}H$ of Val(2)), 1.66 and 1.54 (m, 3H, $C^{\beta}Hs$ and $C^{\gamma}H$ of Leu(1)), 0.93 (d, J = 7.2 Hz, 12H of $C^{\gamma}Hs$ of Val(2) and $C^{\delta}Hs$ of Leu(1)); $[\alpha]_D^{20}$ = -11.8 (c = 0.5 in CH_3OH); MS (ESI) *m/z*: 329.1 $[M\text{-}H]^-$, $M_{calcd.}$ = 330.1

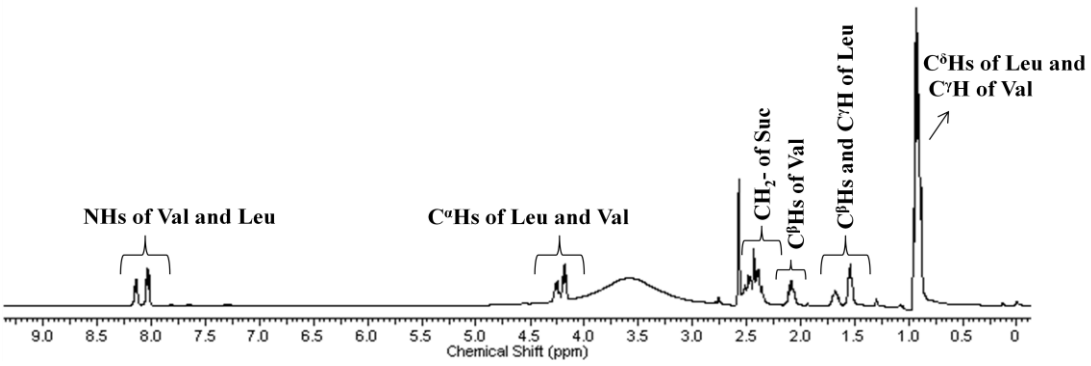

Figure 4.18. *^{1}H NMR spectrum (400 MHz, DMSO-d_6) of HO-Val(2)-Suc-Leu(1)-OH* ***23.***

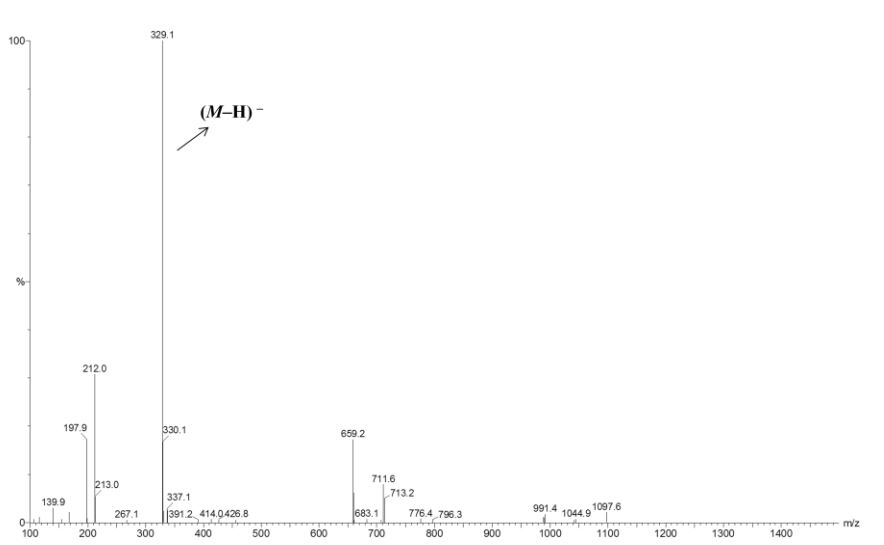

Figure 4.19. *ESI-MS spectrum of HO-Val(2)-Suc-Leu(1)-OH* ***23.***

(c) Synthesis of MeO-Phe(4)-Val(3)-Suc-Leu(1)-Phe(2)-OMe ***24****:* 1.32 g (4 mmol) of HO-Val(2)-Suc-Leu(1)-OH **23** in 4 mL of DMF was cooled in an ice bath and H-Phe-OMe was isolated from 3.45 g (16 mmol) of the corresponding methyl ester hydrochloride by neutralization and subsequent extraction with ethyl acetate and the ethyl acetate extract was concentrated to 8 mL. It was then added to the reaction mixture, followed immediately by 1.81 g (8.8 mmol) DCC and 1.18 g (8.8 mmol) of HOBt. The reaction mixture was stirred for overnight. The residue was taken up in ethyl acetate (50 mL) and the DCU was filtered off. The organic layer was washed with 1M HCl (3 × 50 mL), brine

(2 × 50 mL), 1M sodium carbonate (3 × 50 mL), brine (2 × 50 mL) and dried over anhydrous sodium sulfate and evaporated under vacuum to yield **24** as a white solid. Purification was done by silica gel column (100-200 mesh) using chloroform-methanol (9:1) as eluent to get white solid as product.

Yield: 1.98 g (3.04 mmol, 76%); R_f 0.72 ($CHCl_3$:CH_3OH = 9:1); FT-IR (KBr): $\tilde{\upsilon}$ = 3291 (st), 1747 (ms), 1631 (st), 1541 (st) cm^{-1}; ^1H NMR (400 MHz, $CDCl_3$, δ_{ppm}): 7.23-7.17 and 7.09 (m, 10H, ring protons of Phe(2) and Phe(4)), 7.00 (d, *J* = 8.0 Hz, 1H, NH of Val(3)), 6.89 (d, *J* = 7.6 Hz, 1H, NH of Leu(1)), 6.19 (d, *J* = 8.4 Hz, 1H, NH of Phe(4)), 6.12 (d, *J* = 8.0 Hz, NH of Phe(2)), 4.82-4.78 (m, 2H, C^{α}Hs of Phe(2) and Phe(4)), 4.42 (m, 1H, C^{α}H of Leu(1)), 4.25 (m, 1H, C^{α}H of Val(3)), 3.59 (s, 6H, -$COOCH_3$), 3.06 and 3.02 (d, *J* = 6.4 Hz, *J* = 5.6 Hz, 4H, C^{β}Hs of Phe(2) and Phe(4)), 2.49-2.42 (m, 4H, -CH_2- of Suc), 2.08-2.04 (m, 1H, C^{β}H of Val(3)), 1.34and 1.18 (m, 2H, C^{β}Hs of Leu(1), 1H, C^{γ}H of Leu(1)); 0.81 (d, *J* = 5.4 Hz, 12H, C^{δ}Hs of Leu(1) and C^{γ}Hs of Val(3)); $[\alpha]_D^{20}$ = + 6.17 (*c* = 0.3 in $CHCl_3$); MS (ESI) *m/z*: 651.3 [*M*-H]$^-$, $M_{calcd.}$ = 652.3

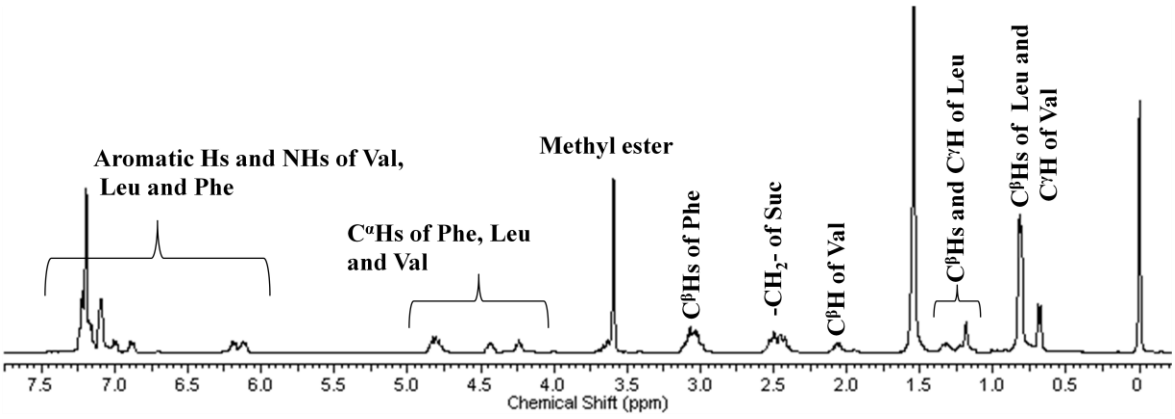

Figure 4.20. *^1H NMR spectrum (400 MHz, $CDCl_3$) of MeO-Phe-Val-Suc-Leu-Phe-OMe* ***24.***

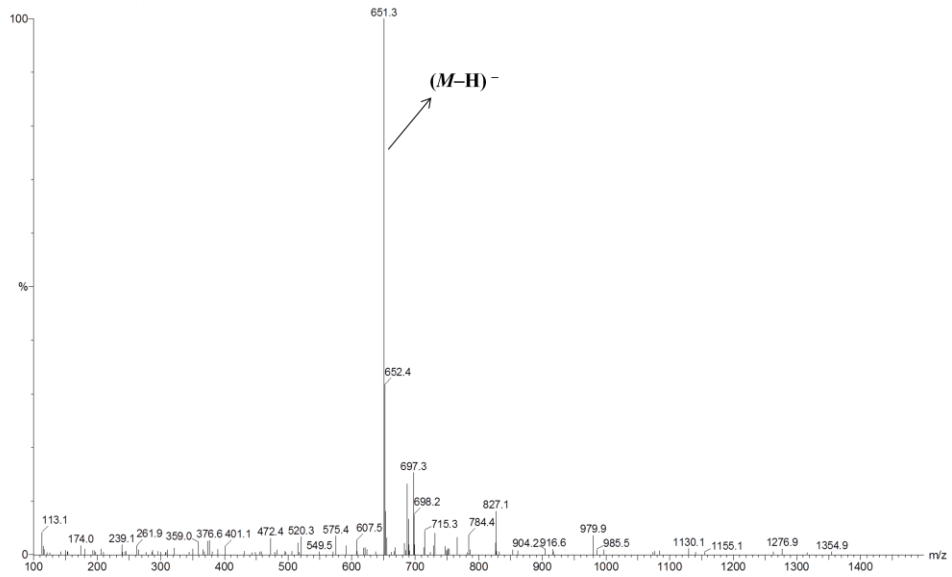

Figure 4.21. *ESI-MS spectrum of MeO-Phe-Val-Suc-Leu-Phe-OMe* ***24.***

(d) Synthesis of HO-Phe(4)-Val(3)-Suc-Leu(1)-Phe(2)-OH ***17:*** 1.63 g (2.5 mmol) of MeO-Phe(4)-Val(3)-Suc-Leu(1)-Phe(2)-OMe **24** in 150 mL MeOH was taken in a round bottom flask and 5 mL of 2M NaOH was added to it dropwise. The reaction was monitored by thin layer chromatography (TLC). The reaction mixture was stirred for 8 hours. 15 mL of distilled water was added to the reaction mixture and MeOH was removed under vacuum. The aqueous part was washed with diethyl ether (2 × 30 mL). Then it was cooled under ice bath for 10 minutes and then pH was adjusted to 1 by drop wise addition of 1M HCl. It was extracted with ethyl acetate (3 × 50 mL) and then the ethyl acetate part was dried over anhydrous Na_2SO_4 and evaporated under vacuum to yield **17** as a white solid.

Yield: 1.43 g (2.3 mmol, 92%); R_f 0.4 ($CHCl_3$:CH_3OH:CH_3COOH = 10:2:0.1); FT-IR (KBr): $\tilde{\upsilon}$ = 3299 (st), 1717 (ms), 1639 (st), 1540 (st) cm^{-1}; ^1H NMR (400 MHz, DMSO-d_6, δ_{ppm}): 8.23 (d, *J* = 7.6 Hz, 1H, NH of Val(3)), 8.10 (d, *J* = 7.2 Hz, 1H, NH of Leu(1)), 8.01 (d, *J* = 8.0 Hz, 1H, NH of Phe(4)), 7.84 (d, *J* = 7.5 Hz, 1H, NH of Phe(2)), 7.31-7.27 (m, 10H, ring protons of Phe(2) and Phe(4)), 4.45-440 (m, 2H, C^{α}Hs of Phe(2) and Phe(4)), 4.34 (m, 1H, C^{α}H of Leu(1)), 4.19 (m, 1H, C^{α}H of Val(3)), 3.09 and 2.98 (d, *J* = 8.8 Hz, 4H, C^{β}Hs of Phe(2) and Phe(4)), 2.45-2.37 (m, 4H, -CH_2- of Suc), 1.99 (m, 1H,

$C^{\beta}H$ of Val(3)), 1.61 and 1.43 (m, 3H, $C^{\beta}Hs$ and $C^{\gamma}H$ of Leu(1)), 0.91 and 0.82 (d, J = 6.0 Hz, J = 6.4 Hz, 12H, $C^{\delta}Hs$ of Leu(1) and $C^{\gamma}Hs$ of Val(3)); ^{13}C NMR (100 MHz, DMSO-d_6, δ_{ppm}): 172.84 (C=O), 172.01 (C=O), 171.44 (C=O), 171.01 (C=O), 137.56, 129.34, 129.14, 129.06, 128.09, 126.32, 53.53, 50.72, 36.51, 30.71, 30.37, 23.99, 22.99, 21.49, 19.12, 17.82; $[\alpha]_D^{20}$ = -28.06 (c = 0.5 in CH_3OH); MS (ESI) *m/z*: 623.1 [*M*-H]$^-$, $M_{calcd.}$ = 624.2

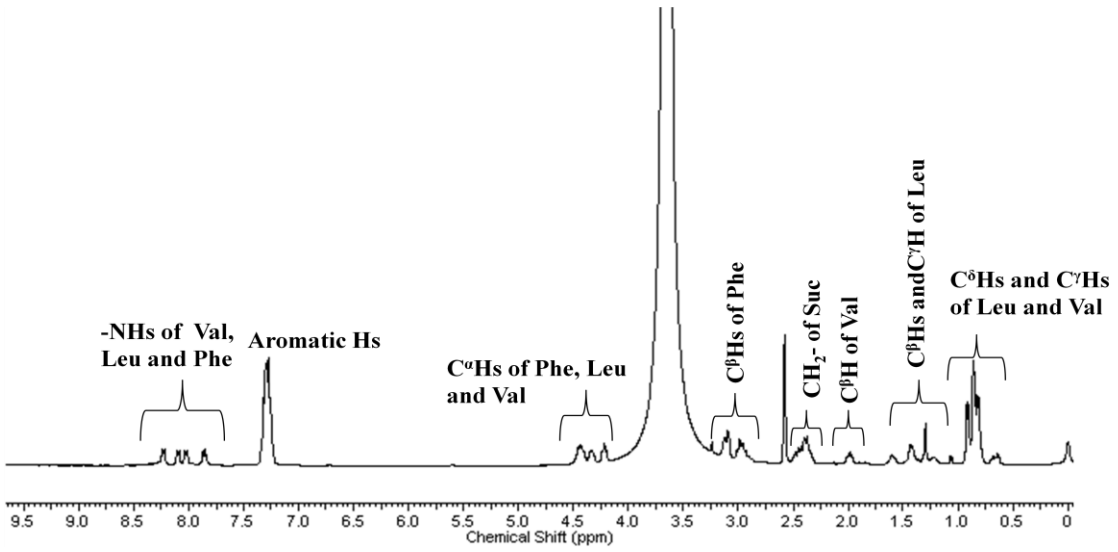

Figure 4.22. *^1H NMR spectrum (400 MHz, DMSO-d_6) of HO-Phe-Val-Suc-Leu-Phe-OH* ***17.***

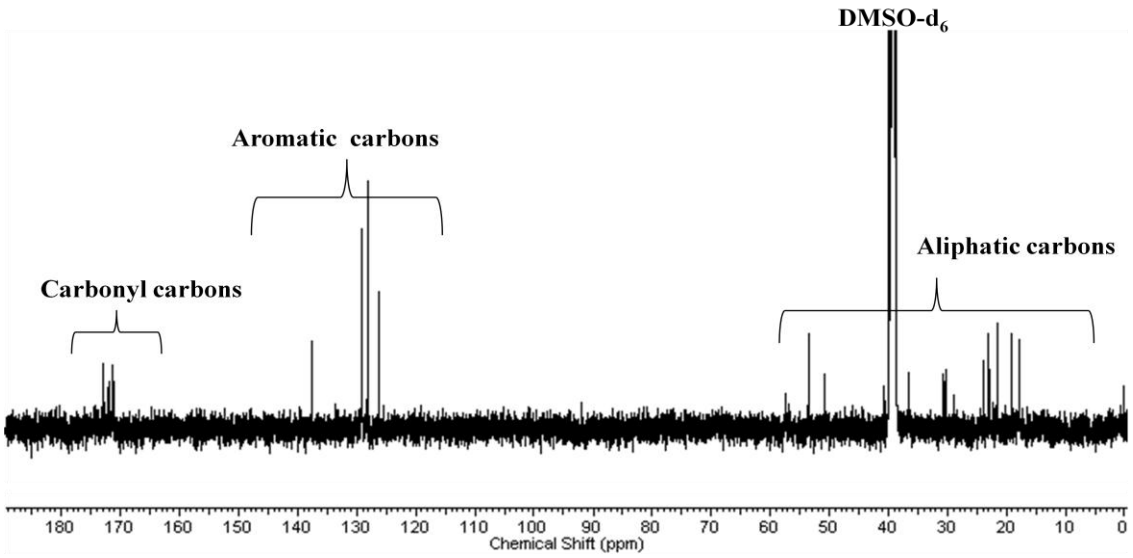

Figure 4.23. *^{13}C NMR spectrum (100 MHz, DMSO-d_6) of HO-Phe-Val-Suc-Leu-Phe-OH* ***17.***

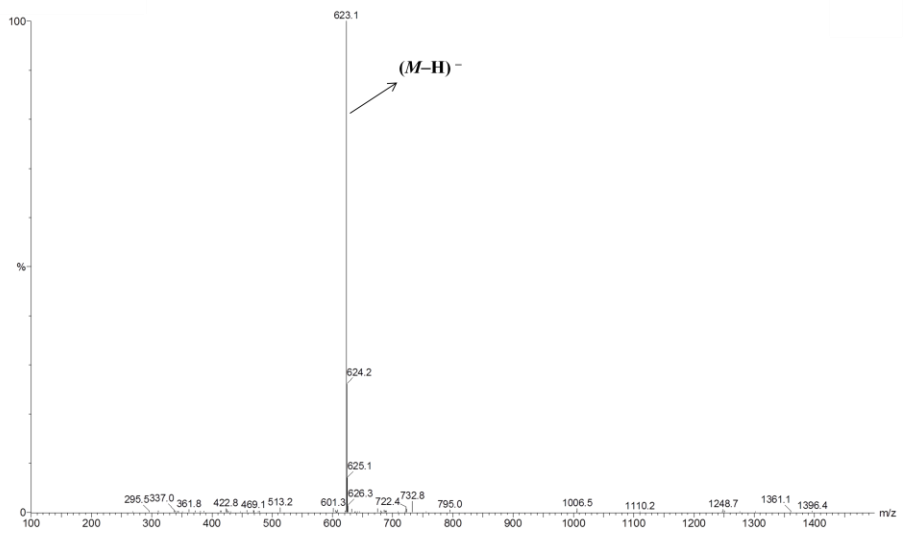

Figure 4.24. *ESI-MS spectrum of HO-Phe-Val-Suc-Leu-Phe-OH* ***17.***

4.3 Preparation of Hydrogel and Characterization Techniques

4.3.1 Gel Melting Temperature

The melting temperatures of the resultant hydrogels (T_{gel}) were determined by the inverted test tube method. The experiment was done with a 15 mL glass vial (diameter = 25 mm). The temperature was increased at a rate of 3 °C min^{-1}.

4.3.2 Rheological Analysis

Oscillating rheology was used to quantify the final mechanical properties of the peptide bolaamphiphile hydrogels. For each case 2 mL of peptide bolaamphiphile hydrogel (20-25 mmol L^{-1}) was prepared. The experiment was done on a Paar Physica Modular Compact Rheometer (MCR 301, Austria). A 50 mm cone plate with a 1° angle configuration was used and the temperature was set constant at 25 °C. Storage (G') and loss (G'') moduli were measured at 0.1% strain with true gap 0.097 mm.

4.3.3 Fluorescence Spectroscopy

Fluorescence emission spectra of the gels (20 mmol L^{-1}) were recorded on a Horiba Scientific Fluoromax-4 spectrophotometer with a 1 cm path length quartz cell at room

temperature. The slit width for the excitation and emission was set at 5 nm and a 1 nm data pitch. Excitations of sample **15** and sample **16** were performed at 276 nm and 264 nm and the data range was between 286 to 530 and 274 nm to 520 nm, respectively.

4.3.4 Catalytic Activity by Platinum Nanoparticles

The *in situ* synthesized Pt nanoparticles were used as a catalyst for the hydrogenation reaction. Pt nanoparticles were synthesized by *in situ* reduction of K_2PtCl_4 with tyrosine containing peptide-appended bolaamphiphile **15** hydrogel in phosphate buffer (10 mmol, pH = 8). 5 mg *p*-nitroaniline was dissolved in 1 mL solution of phosphate buffer (10 mmol, pH = 8) and methanol (1:1). 250 mL Pt nanoparticles in hydrogel was added to it. After cooling the reaction mixture for 5 min in an ice-bath, 6 mg of $NaBH_4$ was added to it and stirred until completion of the reaction. The reaction was completed within 1 h. The success of the catalytic effect of Pt nanoparticles on the hydrogenation reaction was confirmed by UV-Vis and mass spectral studies. After the 1st batch of reduction, the reaction mixture was centrifuged and the Pt nanoparticles were recovered. A similar experiment was set up and the reduction reaction was completed successfully within 1 h. The hydrogenation reaction was confirmed by mass spectrometry, exhibiting the synthesis of *p*-phenylenediamine from *p*-nitroaniline.

4.4 Results and Discussion

4.4.1 Hydrogel Formation

Several examples of peptide based and amphiphilic peptide based hydrogels have been reported, but none of them have exploited bolaamphiphilic peptide based hydrogels upon sonication.[26] In each case, 15 mmol L^{-1} peptide bolaamphiphiles were suspended and dispersed in 10 mmol phosphate buffer at pH 8 using a vortex for 15 min, followed by stirring with a magnetic stirrer for 45 min. But all these compounds were unable to self-assemble to form corresponding self-supporting hydrogels. An effort has been made to investigate the gelation capabilities of bolaamphiphiles upon sonication. We observed that peptide-appended bolaamphiphiles **15** and **16** were capable of forming stable, transparent, self-supporting hydrogels upon sonication at room temperature and a final pH of 5.4, whereas bolaamphiphile **17** was unable to form a gel under similar conditions

(Figure 4.25). After only 15 seconds of sonication, compound **15** forms the hydrogel instantaneously, whereas compound **16**, comprised of an amyloid-like fibril forming dipeptide Phe-Phe,[27] takes 1 h to gel. All these hydrogels are exceptionally stable over a wide range of pH 4-8 for more than 3 months at room temperature. The gelator molecule **15** is able to form a gel with concentration 8 mmol L^{-1} (0.56% w/w), whereas the minimum concentration of gelator molecule **16** is 10 mmol L^{-1} (0.66% w/w). The gelation experiments reveal that molecule **15** is a more efficient gelator relative to molecule **16** upon sonication. Generally ultrasound is frequently used in industries and laboratories to solubilize or disperse molecules with the help of the disruption of weak non-covalent interactions. Here, sonication induces the self-assembly process through non-covalent interactions in three dimensional networks, which are responsible for self-supporting hydrogelation.

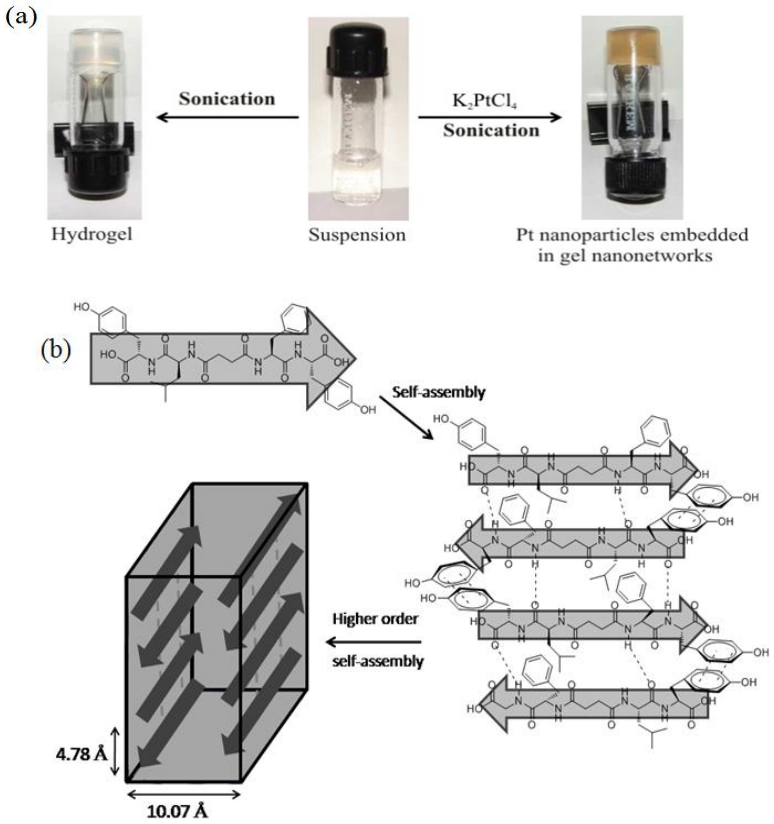

Figure 4.25. *(a) photographs of peptide bolaamphiphile hydrogel **15** and Pt nanoparticles embedded in gel nanonetworks of peptide bolaamphiphile **15** upon sonication. (b) Proposed mechanism of peptide bolaamphiphile **15** self-assembly.*

4.4.2 Thermodynamic Study

Sol-gel transition temperatures (T_{gel}) for hydrogelators **15** and **16** were plotted against different gelator concentrations (Figure 4.26). The gel melting temperature (T_{gel}) increases as the concentration of the gelator molecule increases and finally a plateau region is achieved. From these results it is clear that with higher concentrations of gelator molecules, the supramolecular gel network is stronger. After heating above the boiling point of the solvent (*i.e.* water) it remains in the gel state but T_{gel} depends on the concentration of gelator molecules. These T_{gel} values are related to a hard gel boundary point, which is the temperature at which the solvent molecules come out of the gel state, which is an indication of the strong network morphology. Gelation temperature was measured by the test tube inversion method and the gelation temperature appeared at 85 °C and 120 °C for hydrogels of peptide bolaamphiphiles **15** (15 mmol L^{-1}) and **16** (15 mmol L^{-1}) respectively.

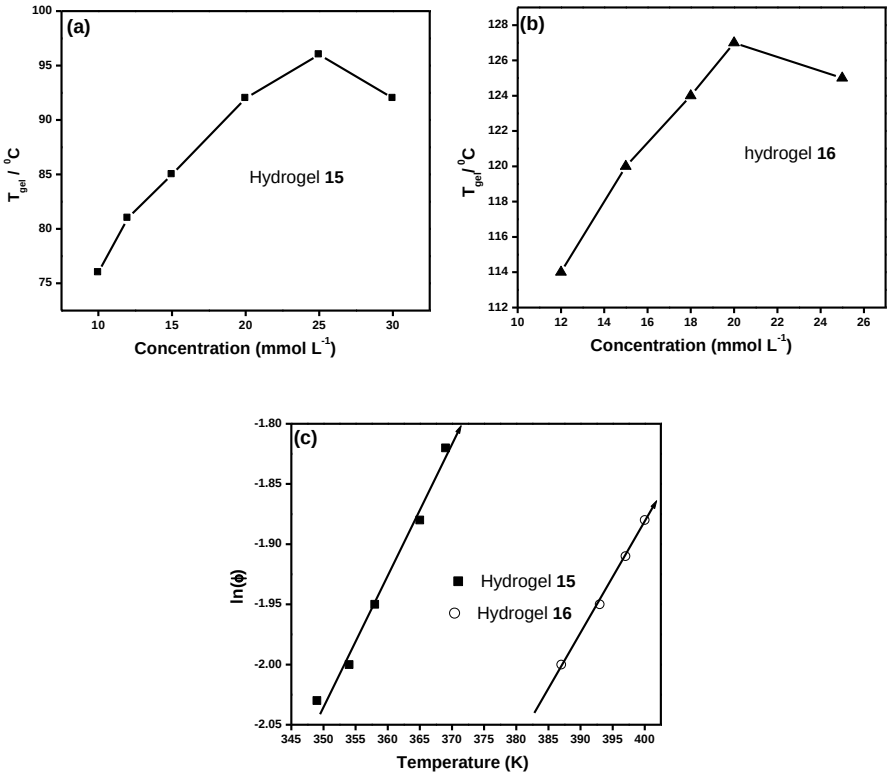

Figure 4.26. *(a) Concentration dependence gelation temperature (T_{gel} / $^{\circ}$C) of (a) the hydrogel of peptide bolaamphiphile **15**, (b) the hydrogel of peptide bolaamphiphiles **16** and (c) concentration-temperature phase diagram ln(φ) vs temp (K) of hydrogels **15** and **16**, where φ is the mole fraction and K is the temperature in Kelvin.*

The thermodynamic parameters of gelation were calculated from the following equations of thermodynamic parameters.[28]

$$\Delta G^0 = RT \ln(\varphi) \quad ...(1)$$

$$\Delta H^0 = -RT^2 [\, \delta \ln(\varphi)/\delta T \,] \quad ...(2)$$

$$\Delta S^0 = -R \ln(\varphi) - RT[\, \delta \ln(\varphi)/\delta T \,] \quad ...(3)$$

Here φ (mole fraction of gelator) = a/(a + b), where a is the number of moles of gelator, b is the number of moles of solvent and T is the corresponding gel-melting temperature. The graph of ln(φ) vs. T (K) is plotted for both gels and the slope [$\delta \ln(\varphi)/\delta T$] of the graph is calculated. Using the value of the slope in these equations, thermodynamic parameters for both gels are calculated (Figure 4.26) and given in Table 4.1.

Table 4.1. *The calculated thermodynamic parameters of hydrogelation*

Compound	$\delta \ln(\varphi)/\delta T$	ΔH [kJmol^{-1}]	ΔG [kJmol^{-1}]	ΔS [Jmol^{-1}K^{-1}]
Hydrogel **15**	0.0118	-12.57	-5.80	-18.90
Hydrogel **16**	0.0092	-11.81	-6.37	-13.85

4.4.3 Rheological Study

The dynamic mechanical properties of hydrogels formed by peptide bolaamphiphiles **15** and **16** were investigated by dynamic rheological study. Figure 4.27 shows the frequency sweep data for both hydrogels, where storage modulus G' is greater than loss modulus G" over the investigated oscillating frequency. The nondestructive frequency sweep, with the storage modulus dominating the loss modulus, exhibits typical solid like rheological behaviour. Both the gels are moderately stiff with G' > 10^5 Pa at low frequency. The value of storage modulus G' exceeds that of loss modulus G" by a factor of 7-14 for both gels, indicating the formation of strong and rigid hydrogels.[29]

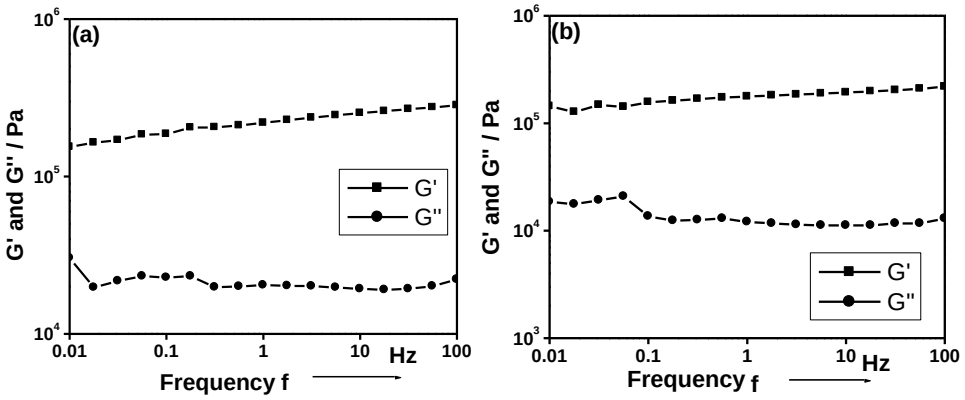

Figure 4.27. *Dynamic rheology (frequency sweep) of (a) peptide bolaamphiphile **15** (c = 20 mmol L^{-1}) and (b) peptide bolaamphiphile **16** (c = 25 mmol L^{-1}). In each case storage modulus G´ is higher than loss modulus G´´. For both cases G´ > 10^5 Pa at low frequency and storage modulus is higher than loss modulus by a factor of 7-14 indicates excellent solid like property of gel materials.*

4.4.4 FT-IR Study

A FT-IR study of solid compounds and their hydrogels was carried out in order to understand the secondary structure of peptide bolaamphiphiles in the gel state. A unique NH-band, centered at around 3300 cm^{-1}, was observed for solid compound **15**, which is typically involved in hydrogen bonding interactions. In the gel state, the peak shifted to 3288 cm^{-1}, which indicates a greater extent of hydrogen bonding interactions. For a solid powder of compound **15**, peaks at 1715 cm^{-1} and 1732 cm^{-1} indicate that some of the carboxylic acid groups are involved in hydrogen bonding interactions (1715 cm^{-1}) and some are about to be free (1732 cm^{-1}). In the gel state, bands appearing at 1710 cm^{-1} and 1723 cm^{-1} support a larger extent of hydrogen bonded carboxylic acid groups. In the gel state, the amide I band split into two peaks at 1626 cm^{-1} and 1616 cm^{-1}. The 19-29 cm^{-1} shift of the amide I band from 1645 cm^{-1} (solid state **15**) to 1626 cm^{-1} and 1616 cm^{-1} (gel state **15**) indicates the formation of a hydrogen bonded supramolecular β-sheet structure (Figure 4.28a) in the respective gel state. The low frequency amide I bands at 1626 cm^{-1}, 1616 cm^{-1} and a weak peak at 1690 cm^{-1} are characteristic of an anti-parallel cross β-sheet structure[8e,30] in the gel state (Figure 4.25b) of compound **15**. For solid compound **16**, the amide I bands at 1667 cm^{-1} and 1639 cm^{-1} shifted to 1666 cm^{-1} and 1635 cm^{-1} in the gel state for the same compound. Other weak intensity bands appeared at 1652 cm^{-1} and 1682

cm^{-1} in the gel state (Figure 4.28b) and are characteristic of an anti-parallel twisted β-sheet structure.

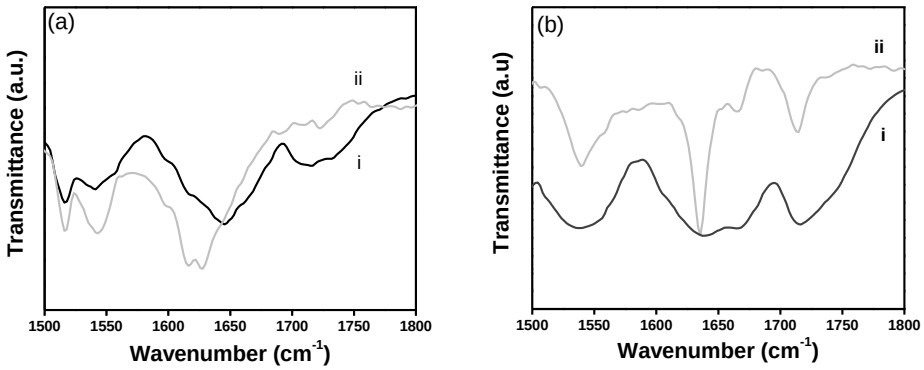

Figure 4.28. *(a) FT-IR spectra of (i) solid powder and (ii) hydrogel of peptide bolaamphiphile **15** indicating antiparallel β sheet structure in gel phase. FT-IR spectra of (i) solid powder and (ii) hydrogel of peptide bolaamphiphile **16.***

4.4.5 Fluorescence Study

Fluorescence spectroscopy was used to investigate the molecular arrangements at the supramolecular level, while π-stacking interactions play a major role in hydrogel formation, besides hydrogen bonding interactions. An emission maximum appearing at 306 nm for hydrogel **15** was slightly red shifted (~3 nm) from the usual emission peak for tyrosine rich peptides (Figure 4.29a). It indicated an ordered arrangement of peptide bolaamphiphiles with aromatic amino acids including phenylalanine and tyrosine. Fluorescence emission spectra for compound **16** were taken just after 30 min of sonication in the viscous state and in the gel state after 2 days. Two emission peaks appeared for both cases, but peaks appeared with a higher intensity for the gel state. One characteristic emission maximum at 294 nm, and pronounced emission at around 370-450 nm, were seen for viscous gel **16** after 30 min of sonication. The pronounced broad emission at around 370-480 nm, along with a red shifted emission maximum at 300 nm, indicate that aromatic phenylalanine groups stack through π-stacking interactions for gel **16** after 2 days of sonication (Figure 4.29b). From this spectroscopic study it is clear that π-π stacking interactions play a vital role in promoting higher order supramolecular structures (Figure 4.25b).[12a,31]

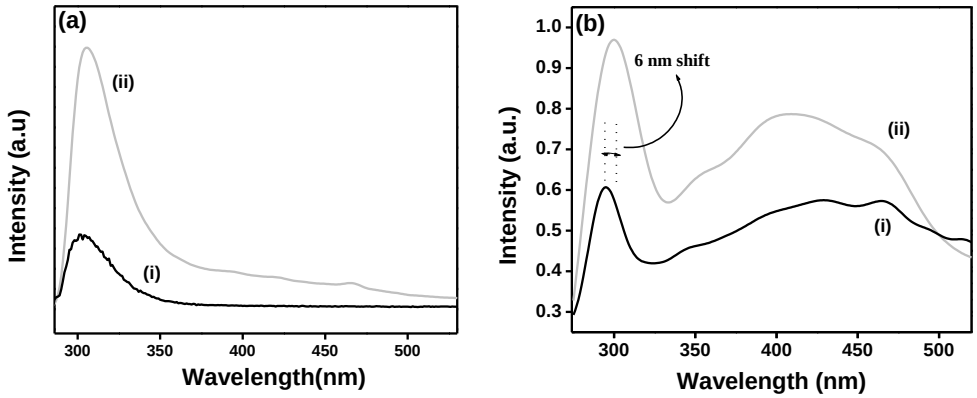

Figure 4.29. *(a) Fluorescence emission spectra of (i) solution (c = 5 mmol L^{-1}, λ_{ex} = 276 nm, λ_{em} = 306 nm) and (ii) the hydrogel of peptide bolaamphiphile **15** (c = 20 mmol L^{-1}, λ_{ex} = 276 nm, λ_{em} = 306 nm). (b) Fluorescence emission spectra of peptide bolaamphiphile **16** (i) after 30 min of sonication and (ii) after 2 days of sonication. Emission maxima at 300 nm and a broad pronounced peak at 370-450 nm correspond to π-π stacking interactions and higher order aggregation in the gel phase.*

4.4.6 Microscopic Study

The nanostructural morphology of gels **15** and **16** at supramolecular level was characterized by using a field-emission scanning electron microscope (FE-SEM) and transmission electron microscope (TEM). The FE-SEM image shows that the hydrogel of compound **15**, assembled into dense entangled helical fibrous aggregates with an average fiber diameter of 35 nm and several millimeters in length, whereas the dried hydrogel of compound **16** shows dense twisted fibrous aggregates with fiber diameter ranging from 32-71 nm (Figure 4.30).

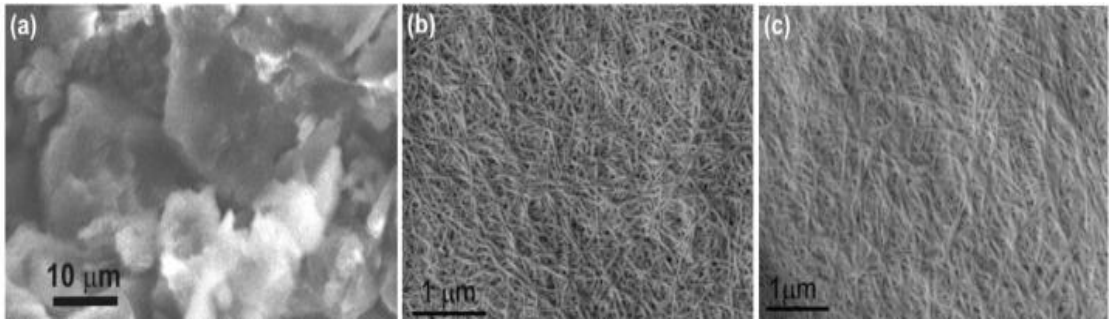

Figure 4.30. *SEM micrographs of (a) suspension of peptide bolaamphiphile **15** prior to sonication, (b) hydrogel of peptide bolaamphiphile **15** made by sonication shows entangled helical fibers and (c) hydrogel of peptide bolaamphiphile **16** indicates the fibrous aggregates.*

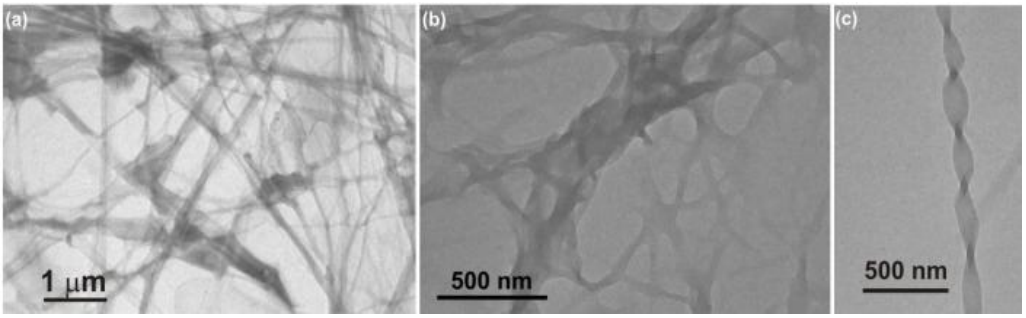

Figure 4.31. *TEM micrographs of (a) the hydrogel of peptide bolaamphiphile **15** shows entangled nanofibers with diameters ranging from 30-39 nm, (b) the hydrogel of peptide bolaamphiphile **16** assembled into nanoribbon and nanofibriller structures and (c) twisted nanoribbon like morphology with diameter 64-70 nm adopted by peptide bolaamphiphile **16** in the gel phase.*

The TEM image of 20 times diluted solution of these peptide hydrogels shows three-dimensional entangled nanofibrillar networks. For the hydrogel of compound **15**, the TEM image shows that the widths of gel nanofibrils are in the range 30-39 nm and each fiber is several micrometers in length. Junctions between these nanofibers are also observed, which are probably responsible for stabilizing the supramolecular hydrogel nanonetworks. The TEM image shows that the hydrogel of compound **16** assembled into twisted nanoribbon structures[32] with a fiber diameter of 64-70 nm and each fiber is several micrometers in length (Figure 4.31). The average distance between two successive twists is around 300 nm in the nanoribbon structure. The SEM results remain the same as in the TEM study for both hydrogels.

4.4.7 X-Ray Diffraction Study

Finally, in order to get further structural information, wide angle X-ray scattering (WAXS) was used to characterize the dried hydrogels of compounds **15** and **16**. The scattering patterns show a series of diffraction peaks from which we are able to correlate different features of the self-assembly model proposed by our system (Figure 4.25b). For the dried hydrogel of compound **15** (Figure 4.32a), a peak at $2\theta = 8.77°$, corresponding to d spacing of 10.07Å, is expected as the distance between two β sheets *i.e.* inter-sheet distance. The characteristic peak at $2\theta = 18.51°$, corresponding to a d spacing of 4.78 Å, indicates the spacing between peptides within the β sheet structure. Another two reflections are observed at 3.57 Å ($2\theta = 24.86°$) and 2.45 Å ($2\theta = 36.55°$). The 3.57 Å

peak is expected from the π-π stacking interaction between two aromatic groups and the peak at 2.45 Å suggests hydrogen bonding interactions between the C=O and N-H of peptide amphiphiles.[11] In the case of the dried hydrogel of compound **16** (Figure 4.32b), a series of characteristic reflection peaks was observed. The characteristic peak observed at 2θ = 10.37° (d spacing of 8.5 Å) is expected from the inter-sheet distance between the two β sheets.[33] Moreover, a peak at 2θ = 18.52° (d spacing of 4.78 Å) represents the distance between two peptide molecules in a sheet. The peak appeared at 2θ =26.23° (d spacing of 3.39 Å), indicating the π-π stacking interaction between two aromatic groups.

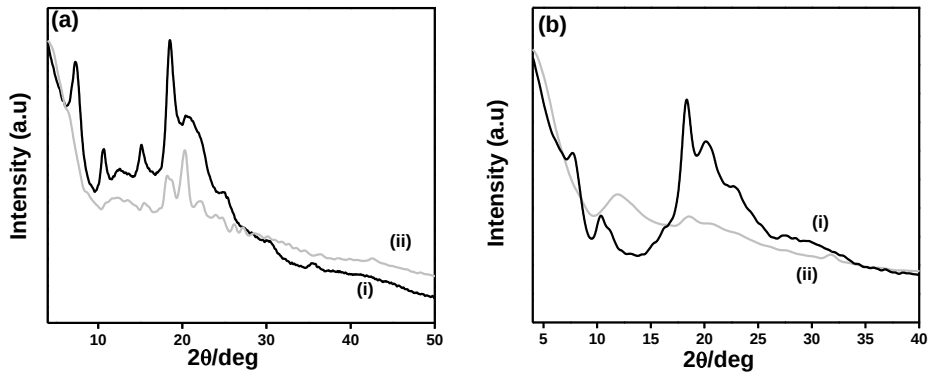

Figure 4.32. *(a) Wide angle powder XRD of (i) solid powder of peptide bolaamphiphile **15** and (ii) it's dried hydrogel.(b) Wide angle powder XRD of (i) solid powder of peptide bolaamphiphile **16** and (ii) it's dried hydrogel.*

4.4.8 Generation of Pt Nanoparticles in Gel Nanofibers

Generation of metal nanoparticles in a gel phase medium is an interesting research area. The three-dimensional cross-linked nanofibrillar networks in the gel phase medium act as a nanoreactor for the nucleation and growth of nanoparticles. Stabilization and size of nanoparticles can be easily controlled in the gel phase nano-networks. There are several examples of the formation of metal nanoparticles in the gel phase medium.[34] However, *in situ* synthesis of metal nanoparticles embedded in gel nanofibers, using the gel as the reaction medium, is interesting. The three-dimensional network, consisting of nanofibers of hydrogel, is an important template for the growth of nanoparticles because peptide based soft biomaterials are nontoxic and biodegradable in nature.[35] In this chapter, we report the *in situ* generation of Pt nanoparticles in a supramolecular hydrogel of short

peptide based bolaamphiphile hydrogelator molecules. In our experiment, 1.5 mg K_2PtCl_4 was dissolved in 2 mL phosphate buffer (pH = 8, 10 mmol) and then 16.9 mg (12 mmol L^{-1}) solid peptide bolaamphiphile molecule **15** followed by 1M NaOH were immediately added to it to adjust the pH to 9. It turned to a transparent hydrogel after a few seconds of sonication.

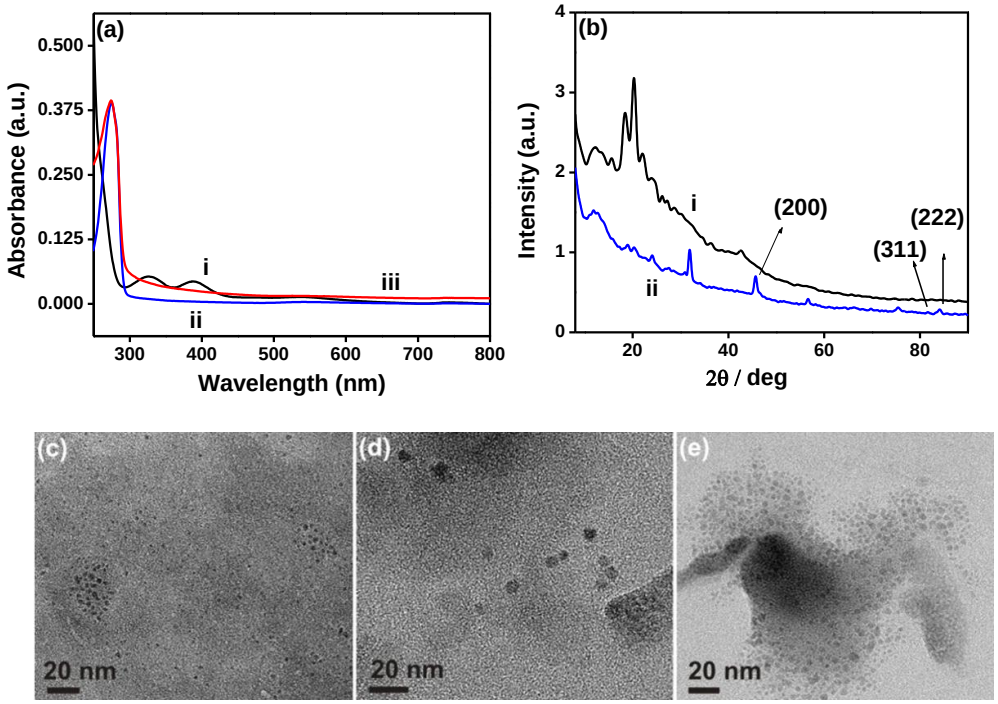

Figure 4.33. *(a) UV-Vis spectroscopy to monitor the synthesis of Pt nanoparticles in gel nanofiber (i) K_2PtCl_4 in phosphate buffer, (ii) diluted hydrogel of peptide bolaamphiphile **15** and (iii) Pt nanoparticles embedded in hydrogel **15**. (b) Wide angle powder XRD of (i) dried hydrogel of peptide bolaamphiphile **15** and (ii) Pt nanoparticles embedded in hydrogel **15**. (c) and (d) are the TEM images of Pt nanoparticles after 2.5 h reaction time and (e) Pt nanoparticles after 1 day of reaction ranging in size from 3-6 nm.*

After 5 h the transparent hydrogel changed to light yellowish in color, which turned to intense yellow after 1 day and dark brown after a long time. Thus, the formation of PtNPs can be visibly monitored by color change from light yellow to dark brown. The nanoparticles were studied by UV-Vis spectroscopy, transmission electron microscopy and powder XRD. In here, the redox active tyrosine moiety is responsible for the reduction of Pt^{2+} to Pt nanoparticles.[23b] We have characterized the Pt nanoparticles by

UV-Vis spectroscopy with respect to several control experiments. In 2 mL phosphate buffer (pH = 8, 10 mmol), 1.5 mg K_2PtCl_4 was dissolved and immediately characterized through UV-Vis spectroscopy.[36] Two characteristic peaks appeared at around 327 nm and 386 nm, which are the characteristic absorption peaks for K_2PtCl_4. The Pt nanoparticles in the gel system were characterized through UV-Vis spectroscopy. For this case, peaks at 327 nm and 386 nm disappeared, suggesting the generation of Pt nanoparticles (Figure 4.33a).

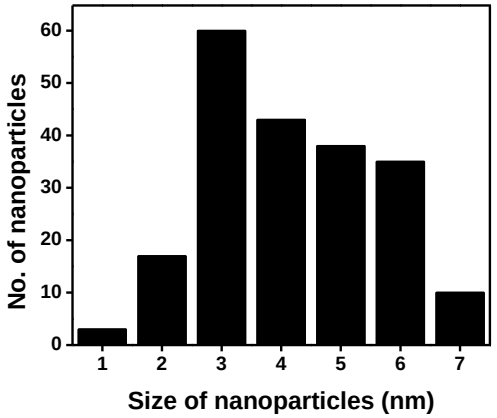

Figure 4.34. *The size distribution of Pt nanoparticles after 1 day of reaction time.*

The size of the nanoparticles was investigated through transmission electron microscopy. The TEM images of nanoparticles in hydrogel showed that Pt nanoparticles had been synthesized. The particle size distribution from TEM images showed that the diameter of the nanoparticles increased with reaction time. TEM images revealed that the nanoparticles had diameters of 1 nm to 3 nm after 2.5 h reaction time. After 1 day of reaction growth of the nanoparticles was observed (Figure 4.33(c–e)). The particle distribution showed that most of the nanoparticles had diameters ranging from 3 nm to 6 nm (Figure 4.34). The Pt nanoparticles embedded in the hydrogel were dried and studied by wide angle powder X-ray diffraction. The XRD patterns (Figure 4.33b) show the characteristic peaks at $2\theta = 31.8°$, 45.5°, 84.3° for Pt nanoparticles. The peak at 31.8° (d = 2.81 Å) corresponds to the average size of nanoparticles, which was confirmed by TEM study, and the peak at around 45.84° (d = 1.977 Å) corresponds to Pt nanoparticles from

the (200) plane. Peaks at 81.63° (d = 1.178 Å) and 84.24° (d = 1.14 Å) are the characteristic peaks of (311) and (222) planes for Pt nanoparticles.[37]

4.4.9 Catalytic Activity of Pt Nanoparticles

The Pt nanoparticles generated in the hydrogel medium of peptide bolaamphiphiles have many potential applications such as catalysis in many chemical reactions. The *in situ* synthesized Pt nanoparticles (PtNPs) having a size of 1-3 nm in diameter were used as a catalyst for the hydrogenation reaction. The catalytic activity of PtNPs was done using *p*-nitroaniline as a substrate for the hydrogenation reaction. Pt nanoparticles embedded in hydrogel were added to *p*-nitroaniline dissolved in a solution of phosphate buffer and methanol.

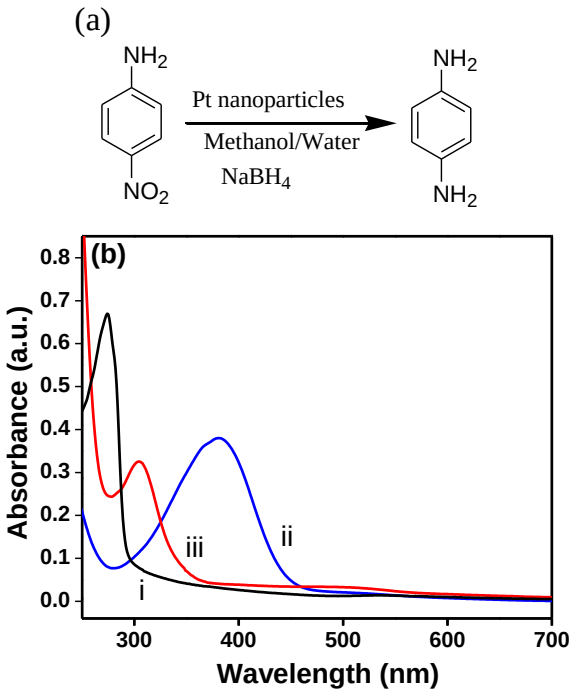

Figure 4.35. *(a) Schematic representation of Pt nanoparticle catalyzed hydrogenation reaction. (b) UV-Vis spectroscopy to monitor the reduction of p-nitroaniline catalyzed by Pt nanoparticles where (i) Pt nanoparticles are embedded in gel nanofibers, (ii) p-nitroaniline solution shows a characteristic absorption peak at 380 nm and (iii) Pt nanoparticle catalyzed reduction of p-nitroaniline to p-phenylenediamine resulted in the disappearance of the absorption peak at 380 nm and the appearance of a new peak at 305 nm.*

The reaction mixture was cooled for 5 min in an ice-water bath. Sodium borohydrate as a source of hydrogen was added to it and stirred until the reaction was complete. The reaction was completed within 1 h. The success of the catalytic effect of Pt nanoparticles on the hydrogenation reaction was confirmed by UV-Vis (Figure 4.35) and mass spectral studies (Figure 4.36). The diluted solution of *p*-nitroaniline gave the characteristic absorption peak at 380 nm which had completely disappeared after 1 h of reaction time. A new absorption peak at 305 nm confirmed the hydrogenation reaction of *p*-nitroaniline to *p*-phenylenediamine.[36a] These Pt nanoparticles were successfully reused further for hydrogenation reactions.

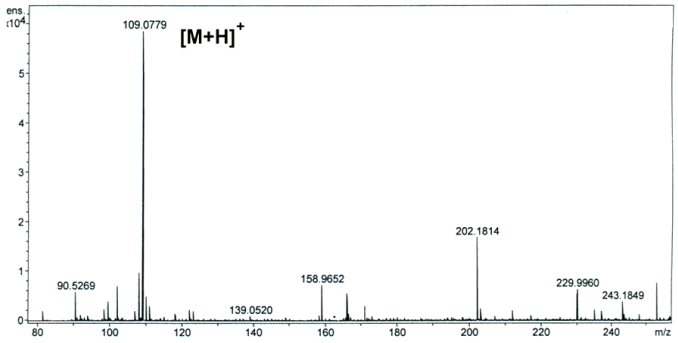

Figure 4.36. *Mass spectrum of Pt catalyzed hydrogenation of p-nitroaniline to p-phenylenediamine. The peak m/z* $(M+H)^+$ *= 109.0779 corresponds to synthesis of p-phenylenediamine.*

4.5 Conclusions

Two peptide appended bolaamphiphiles **15** and **16** form strong and rigid self-supporting hydrogels under physiological conditions upon sonication. The self-assembly process occurs mainly through hydrogen bonding interactions and π-stacking interactions. In the gel phase, these peptide bolaamphiphiles molecules adopt long, twisted nanofibrillar network structures. Finally, the hydrogel of the tyrosine rich peptide bolaamphiphile molecule is used as a nanoreactor for *in situ* synthesis of Pt nanoparticles and stabilization of these particles which is used as a catalyst in the hydrogenation reaction of *p*-nitroaniline to *p*-phenylenediamine.

4.6 References

1. (a) Hirst A. R., Escuder B., Miravet J. F., Smith D. K. (2008), High-tech applications of self-assembling supramolecular nanostructured gel-phase materials: From regenerative medicine to electronic devices, *Angew. Chem., Int. Ed.*, 47, 8002-8018 (DOI: 10.1002/anie.200800022); (b) Peppas N. A., Hilt J. Z., Khademhosseini A., Langer R. (2006), Hydrogels in biology and medicine: From molecular principles to bionanotechnology, *Adv. Mater*., 18, 1345-1360 (DOI: 10.1002/adma.200501612); (c) Jung J. P., Gasiorowski J. Z., Collier J. H. (2010), Fibrillar peptide gels in biotechnology and biomedicine, *Peptide Sci*., 94, 49-59 (DOI: 10.1002/bip.21326); (d) Banerjee S., Das R. K., Maitra U. (2009), Supramolecular gels 'in action', *J. Mater. Chem*., 19, 6649-6687 (DOI: 10.1039/B819218A).

2. (a) Koutsopoulos S., Unswortha L. D., Nagaia Y., Zhang S. (2009), Controlled release of functional proteins through designer self-assembling peptide nanofiber hydrogel scaffold, *Proc. Natl. Acad. Sci. U. S. A.*, 106, 4623-4628 (DOI: 10.1073/pnas.0807506106); (b) Komatsu H., Matsumoto S., Tamaru I. S., Kaneko K., Ikeda M., Hamachi I. (2009), Supramolecular hydrogel exhibiting four basic logic gate functions to fine-tune substance release, *J. Am. Chem. Soc*., 131, 5580-5585 (DOI: 10.1021/ja8098239); (c) Matson J. B., Stupp S. I. (2011), Drug release from hydrazone-containing peptide amphiphiles, *Chem. Commun*., 47, 7962-7964 (DOI: 10.1039/C1CC12570B).

3. Ikeda M., Yoshii T., Matsui T., Tanida T., Komatsu H., Hamachi I. (2011), Montmorillonite-supramolecular hydrogel hybrid for fluorocolorimetric sensing of polyamines, *J. Am. Chem. Soc*., 133, 1670-1673 (DOI: 10.1021/ja109692z).

4. Salick D. A., Kretsinger J. K., Pochan D. J., Schneider J. P. (2007), Inherent antibacterial activity of a peptide-based β-hairpin hydrogel, *J. Am. Chem. Soc*., 129, 14793-14799 (DOI: 10.1021/ja076300z).

5. (a) Silva G. A., Czeisler C., Niece K. L., Beniash S., Harrington D. A., Kessler J. A., Stupp S. I. (2004), Selective differentiation of neural progenitor cells by high-epitope density nanofibers, *Science*, 303, 1352-1355 (DOI:10.1126/science.1093783); (b) Butterick L. H., Rajogopal K., Branco M., Salick D., Rughani R., Pilarz M., Lamm M. S., Pochan D. J., Schneider J. P. (2007), Controlling hydrogelation kinetics by peptide design

for three-dimensional encapsulation and injectable delivery of cells, *Proc. Natl. Acad. Sci. U. S. A.*, 104, 7791-7796 (DOI: 10.1073/pnas.0701980104).

6. (a) Zhou M., Smith A. M., Das A. K., Hodson N. W., Collins R. F., Ulijn R. V., Gough J. E. (2009), Self-assembled peptide-based hydrogels as scaffolds for anchorage-dependent cells, *Biomaterials*, 30, 2523-2530 (DOI: 10.1016/j.biomaterials.2009.01.010); (b) Lee K. Y., Moony D. J. (2001), Hydrogels for tissue engineering, *Chem. Rev*., 101, 1869-1880 (DOI: 10.1021/cr000108x); (c) Langer R., Tirrell D. A. (2004), Designing materials for biology and medicine, *Nature*, 428, 487-492 (DOI:10.1038/nature02388).

7. Adhikari B., Banerjee A. (2010), Short-peptide-based hydrogel: A template for the *in situ* synthesis of fluorescent silver nanoclusters by using sunlight, *Chem.-Eur. J.*, 16, 13698-13705 (DOI: 10.1002/chem.201001240).

8. (a) Aggeli A., Bell M., Boden N., Keen J. N., Knowles P. F., McLeish T. C. B., Pitkeathly M., Radford S. E. (1997), Responsive gels formed by the spontaneous self-assembly of peptides into polymeric β-sheet tapes, *Nature*, 386, 259-262 (DOI:10.1038/386259a0); (b) Saiani A., Mohammed A., Frielinghaus H., Collins R., Hodson N., Kielty C. M., Sherratt M. J., Miller A. F. (2009), Self-assembly and gelation properties of α-helix versus β-sheet forming peptides, *Soft Matter*, 5, 193-202 (DOI: 10.1039/B811288F); (c) de Jong J. J. D., Lucas L. N., Kellogg R. M., van Esch J. H., Feringa B. L. (2004), Reversible optical transcription of supramolecular chirality into molecular chirality, *Science*, 304, 278-281 (DOI: 10.1126/science.1095353); (d) Das A. K., Collins R., Ulijn R. V. (2008), Exploiting enzymatic (reversed) hydrolysis in directed self-assembly of peptide nanostructures, *Small*, 4, 279-287 (DOI: 10.1002/smll.200700889).

9. Nagarkar R. P., Hule R. A., Pochan D. J., Schneider J. P. (2008), De novo design of strand-swapped beta-hairpin hydrogels, *J. Am. Chem. Soc*., 130, 4466-4474 (DOI: 10.1021/ja710295t).

10. Haines L. A., Rajagopal K., Ozbas B., Salick D. A., Pochan D. J., Schneider J. P. (2005), Light-activated hydrogel formation via the triggered folding and self-assembly of a designed peptide, *J. Am. Chem. Soc*., 127, 17025-17029 (DOI: 10.1021/ja054719o).

11. Ikeda M., Tanida T., Yoshii T., Hamachi I. (2011), Rational molecular design of stimulus-responsive supramolecular hydrogels based on dipeptides, *Adv. Mater*., 23, 2819-2822 (DOI: 10.1002/adma.201004658).

12. (a) Hirst A. R., Roy S., Arora M., Das A. K., Hodson N., Murray P., Marshall S., Javid N., Sefcik J., Boekhoven J., van Esch J. H., Santabarbara S., Hunt N. T., Ulijn R. V. (2010), Biocatalytic induction of supramolecular order, *Nat. Chem*., 2, 1089-1094 (DOI:10.1038/nchem.861); (b) Das A. K., Hirst A. R., Ulijn R. V. (2009), Evolving nanomaterials using enzyme-driven dynamic peptide libraries (eDPL), *Faraday Discuss.*, 143, 293-303 (DOI: 10.1039/B902065A); (c) Xu H., Das A. K., Horie M., Shaik M. S., Smith A. M., Luo Y., Lu X., Collins R., Liem S. Y., Song A., Popelier P. L. A., Turner M. L., Xiao P., Kinloch I. A., Ulijn R. V. (2010), An investigation of the conductivity of peptide nanotube networks prepared by enzyme-triggered self-assembly, *Nanoscale*, 2, 960-966 (DOI: 10.1039/B9NR00233B).

13. Yang Z., Ho P. L., Liang G., Chow K. H., Wang Q., Cao Y., Guo Z., Xu B. (2007), Using β-lactamase to trigger supramolecular hydrogelation, *J. Am. Chem. Soc*., 129, 266-267 (DOI: 10.1021/ja0675604).

14. Cravotto G., Cintas P. (2009), Molecular self-assembly and patterning induced by sound waves. The case of gelation, *Chem. Soc. Rev*., 38, 2684-2697 (DOI: 10.1039/B901840A).

15. Bardelang D., Camerel F., Margeson J. C., Leek D. M., Schmutz M., Zaman M. B., Yu K., Soldatov D. V., Ziessel R., Ratcliffe C. I., Ripmeester J. A. (2008), Unusual sculpting of dipeptide particles by ultrasound induces gelation, *J. Am. Chem. Soc*., 130, 3313-3315 (DOI: 10.1021/ja711342y).

16. Naota T., Koori H. (2005), Molecules that assemble by sound: An application to the instant gelation of stable organic fluids, *J. Am. Chem. Soc*., 127, 9324-9325 (DOI: 10.1021/ja050809h).

17. Wang Y., Zhan C., Fu H., Li X., Sheng X., Zhao Y., Xiao D., Ma Y., Ma J. S.,Yao J. (2008), Switch from intra- to intermolecular H-bonds by ultrasound: Induced gelation and distinct nanoscale morphologies, *Langmuir*, 24, 7635-7638 (DOI: 10.1021/la801499y).

18. Wu J., Tian Q., Hu H., Xia Q., Zou Y., Li F., Yi T., Huang C. (2009), Self-assembly of peptide-based multi-colour gels triggered by up-conversion rare earth nanoparticles, *Chem. Commun.*, 4100-4102 (DOI: 10.1039/B907517H).

19. Ray S., Das A. K., Banerjee A. (2007), pH-Responsive, bolaamphiphile-based smart metallo-hydrogels as potential dye-adsorbing agents, water purifier, and vitamin B12 carrier, *Chem. Mater*., 19, 1633-1639 (DOI: 10.1021/cm062672f).

20. Banwell E. F., Abelardo E. S., Adams D. J., Birchall M. A., Corrigan A., Donald A. M., Kirkland M., Serpell L. C., Butler M. F., Woolfson D. N. (2009), Rational design and application of responsive alpha-helical peptide hydrogels, *Nat. Mater*., 8, 596-600 (DOI:10.1038/nmat2479).

21. (a) Piepenbrock M. O. M., Clarke N., Steed J. W. (2011), Rheology and silver nanoparticle templating in a bis(urea) silver metallogel, *Soft Matter*, 7, 2412-2418 (DOI: 10.1039/C0SM00647E) ; (b) Das D., Maiti S., Brahmachari S. Das P. K. (2011), Refining hydrogelator design: Soft materials with improved gelation ability, biocompatibility and matrix for in situ synthesis of specific shaped GNP, *Soft Matter*, 7, 7291-7303 (DOI: 10.1039/C1SM05608E).

22. Sone E. D., Stupp S. I. (2004), Semiconductor-encapsulated peptide-amphiphile nanofibers, *J. Am. Chem. Soc*., 126, 12756-12757 (DOI: 10.1021/ja0499344).

23. (a) Li L. S., Stupp S. I. (2005), One-dimensional assembly of lipophilic inorganic nanoparticles templated by peptide-based nanofibers with binding functionalities, *Angew. Chem., Int. Ed*., 44, 1833-1836 (DOI: 10.1002/anie.200462142); (b) Ray S., Das A. K., Banerjee A. (2006), Smart oligopeptide gels: *In situ* formation and stabilization of gold and silver nanoparticles within supramolecular organogel networks, *Chem. Commun.*, 2816-2818 (DOI: 10.1039/B605498F).

24. (a) Nobusawa K., Ikeda A., Kikuchi J., Kawano S., Fujita N., Shinkai S. (2008), Reversible solubilization and precipitation of carbon nanotubes through oxidation–reduction reactions of a solubilizing agent, *Angew. Chem., Int. Ed.*, 47, 4577-4580 (DOI: 10.1002/anie.200800095); (b) Srinivasan S., Babu S. S., Praveen V. K., Ajayaghosh A. (2008), Carbon nanotube triggered self-assembly of oligo(p-phenylene vinylene)s to stable hybrid π-gels, *Angew. Chem., Int. Ed.*, 47, 5746-5749 (DOI: 10.1002/anie.200801000).

25. Bardelang D., Zaman M. Z., Moudrakovski I. L., Pawsey S., Margeson J. C., Wang D., Wu X., Ripmeester J. A., Ratcliffe C. I., Yu K. (2008), Interfacing supramolecular gels and quantum dots with ultrasound: Smart photoluminescent dipeptide gels, *Adv. Mater*., 20, 4517-4520 (DOI: 10.1002/adma.200801812).

26. (a) Mahler A., Reches M., Rechter M., Cohen S., Gazit E. (2006), Rigid, self-assembled hydrogel composed of a modified aromatic dipeptide, *Adv. Mater*., 18, 1365-1370 (DOI: 10.1002/adma.200501765); (b) Orbach R., Adler-Abramovich L., Zigerson S., Mironi-Harpaz I., Seliktar D., Gazit E. (2009), Self-assembled Fmoc-peptides as a platform for the formation of nanostructures and hydrogels, *Biomacromolecules*, 10, 2646-2651 (DOI: 10.1021/bm900584m); (c) Nanda J., Banerjee A. β-Amino acid containing proteolitically stable dipeptide based hydrogels: Encapsulation and sustained release of some important biomolecules at physiological pH and temperature, *Soft Matter*, 2012, 8, 3380-3386 (DOI: 10.1039/C2SM07168A); (d) Chen L., Pont G., Morris K., Lotze G., Squires A., Serpell L. C., Adams D. J. (2011), Salt-induced hydrogelation of functionalised-dipeptides at high pH, *Chem. Commun*., 47, 12071-12073 (DOI: 10.1039/C1CC15474E); (e) Yan H., Saiani A., Gough J. E., Miller A. F. (2006), Thermoreversible protein hydrogel as cell scaffold, *Biomacromolecules*, 7, 2776-2782 (DOI: 10.1021/bm0605560); (f) Mata A., Hsu L., Capito R., Aparicio C., Henrikson K., Stupp S. I. (2009), Micropatterning of bioactive self-assembling gels, *Soft Matter*, 5, 1228-1236 (DOI: 10.1039/B819002J).

27. Reches M., Gazit E. (2003), Casting metal nanowires within discrete self-assembled peptide nanotubes, *Science*, 300, 625-627 (DOI: 10.1126/science.1082387).

28. Naskar J., Palui G., Banerjee A. (2009), Tetrapeptide-based hydrogels: For encapsulation and slow release of an anticancer drug at physiological pH, *J. Phys. Chem. B*, 113, 11787-11792 (DOI: 10.1021/jp904251j).

29. (a) Cheng G., Castelletto V., Jones R. R., Connon C. J., Hamley I. W. (2011), Hydrogelation of self-assembling RGD-based peptides, *Soft Matter*, 7, 1326-1333 (DOI: 10.1039/C0SM00408A); (b) Helen W., de Leonardis P., Ulijn R. V., Gough J., Tirelli N. (2011), Mechanosensitive peptide gelation: Mode of agitation controls mechanical properties and nano-scale morphology, *Soft Matter*, 7, 1732-1740 (DOI: 10.1039/C0SM00649A); (c) Chen D. T. N., Chen K., Hough L. A., Islam M. F., Yodh A.

G. (2010), Rheology of carbon nanotube networks during gelation, *Macromolecules*, 43, 2048-2053 (DOI: 10.1021/ma902230a).

30. Pelton J. T., McLean L. R. (2000), Spectroscopic methods for analysis of protein secondary structure, *Anal. Biochem.*, 277, 167-176 (DOI: 10.1006/abio.1999.4320).

31. (a) Smith A. M., Williams R. J., Tang C., Coppo P., Collins R. F., Turner M. L., Saiani A., Ulijn R. V. (2008), Fmoc-diphenylalanine self assembles to a hydrogel via a novel architecture based on π-π interlocked β-sheets, *Adv. Mater.*, 20, 37-41 (DOI: 10.1002/adma.200701221); (b) Jayawarna V., Ali M., Jowitt T. A., Miller A. F., Saiani A., Gough J. E., Ulijn R. V. (2006), Nanostructured hydrogels for three-dimensional cell culture through self-assembly of fluorenylmethoxycarbonyl-dipeptides, *Adv. Mater.*, 18, 611-614 (DOI: 10.1002/adma.200501522).

32. Fishwick C. W. G., Beevers A. J., Carrick L. M., Whitehouse C. D., Aggeli A., Boden N. (2003), Structures of helical β-tapes and twisted ribbons: The role of side-chain interactions on twist and bend behavior, *Nano Lett.*, 3, 1475-1479 (DOI: 10.1021/nl034095p).

33. (a) Jahn T. R., Makin O. S., Morris K. L., Marshall K. E., Tian P., Sikorski P., Serpell L. C. (2010), The common architecture of cross-β amyloid, *J. Mol. Biol.*, 395, 717-727 (DOI: 10.1016/j.jmb.2009.09.039); (b) Squires A. M., Devlin G. L., Gras S. L., Tickler A. K., MacPhee C. E., Dobson C. M. (2006), X-ray scattering study of the effect of hydration on the cross-β structure of amyloid fibrils, *J. Am. Chem. Soc.*, 128, 11738-11739 (DOI: 10.1021/ja063751v).

34. (a) Love C. S., Chechik V., Smith D. K., Wilson K., Ashworth I., Brennan C. (2005), Synthesis of gold nanoparticles within a supramolecular gel-phase network, *Chem. Commun.*, 1971-1973 (DOI: 10.1039/B418190E); (b) Li Y., Liu M. (2008), Fabrication of chiral silver nanoparticles and chiral nanoparticulate film via organogel, *Chem. Commun.*, 5571-5573 (DOI: 10.1039/B812567H); (c) Zhang J., Xu S., Kumacheva E. (2004), Polymer microgels: Reactors for semiconductor, metal, and magnetic nanoparticles, *J. Am. Chem. Soc.*, 126, 7908-7914 (DOI: 10.1021/ja031523k); (d) Roy S., Banerjee A. (2011), Amino acid based smart hydrogel: Formation, characterization and fluorescence properties of silver nanoclusters within the hydrogel matrix, *Soft Matter*, 7, 5300-5308 (DOI: 10.1039/C1SM05034F).

35. (a) Carny O., Shalev D. E., Gazit E. (2006), Fabrication of coaxial metal nanocables using a self-assembled peptide nanotube scaffold, *Nano Lett*., 6, 1594-1597 (DOI: 10.1021/nl060468l); (b) Yu L., Banerjee I. A., Shima M., Rajan K., Matsui H. (2004), Size-controlled Ni nanocrystal growth on peptide nanotubes and their magnetic properties, *Adv. Mater*., 16, 709-712 (DOI: 10.1002/adma.200306373); (c) Gao X., Djalali R., Haboosheh A., Samson J., Nuraje N., Matsui H. (2005), Self-assembly and properties of main-chain reversible polymer brushes, *Adv. Mater*., 17, 1753-1753 (DOI: 10.1002/adma.200401355); (d) Yang Z., Liang G., Xu B. (2006), Supramolecular hydrogels based on β-amino acid derivatives, *Chem.Commun*., 738-740 (DOI: 10.1039/B516133A).

36. (a) San B. H., Kim S., Moh S. H., Lee H., Jung D. Y., Kim K. K. (2011), Platinum nanoparticles encapsulated by aminopeptidase: A multifunctional bioinorganic nanohybrid catalyst, *Angew. Chem., Int. Ed*., 50, 11924-11929 (DOI: 10.1002/anie.201101833); (b) Song Y., Challa S. R., Medforth C. J., Qiu Y., Watt R. K., Pena D., Miller J. E., Swol F. V., Shelnutt J. A. (2004), Synthesis of peptide-nanotube platinum-nanoparticle composites, *Chem. Commun*., 1044-1045 (DOI: 10.1039/B402126F).

37. (a) Kundu P., Nethravathi C., Deshpande P. A., Rajamathi M., Madras G., Ravishankar N. (2011), Ultrafast microwave-assisted route to surfactant-free ultrafine Pt nanoparticles on graphene: Synergistic Co-reduction mechanism and high catalytic activity, *Chem. Mater*., 23, 2772-2780 (DOI: 10.1021/cm200329a); (b) Yin J., Wang J., Zhang Y., Li H., Song Y., Jin C., Lu T., Zhang T. (2011), Monomorphic platinum octapod and tripod nanocrystals synthesized by an iron nitrate modified polyol process, *Chem. Commun*., 47, 11966-11968 (DOI: 10.1039/c1cc14747a).

Chapter 5

Peptide Nanofibers Decorated with Pd Nanoparticles to Enhance the Catalytic Activity for C–C Coupling Reactions in Aerobic Conditions

5.1 Introduction

Bioinspired peptide nanofibers[1] have a wide range of applications in the fields of tissue engineering[2] and nanotechnology.[3] Peptides and peptide bolaamphiphiles can adopt various types of well defined nanostructures[4] in their self-assembled hydrogel state. Several challenges have been achieved in the formation of well-defined nanomaterials for use as catalysts, however, the interactions at the biotic/abiotic interface remain poorly understood. Recently, we reported a peptide bolaamphiphile nanofiber templated synthesis of Pt nanoparticles in a hydrogel matrix and the efficient catalytic activity for the hydrogenation reaction of *p*-nitroaniline to *p*-phenylenediamine.[5] A gel-based trihybrid system containing Au nanoparticles has been used as a catalyst for the reduction of 4-nitrophenol to 4-aminophenol.[6] Recently, Knecht *et al.* reported the fabrication of peptide capped Pd nanoparticles, which enhanced the catalytic activity of C–C coupling reactions under non-traditional conditions of a water-based solvent at room temperature.[7] The catalytic activity of metal nanoparticles can be enhanced by using a nanostructured templated synthesis of metal nanoparticles and providing a high surface area.[8] Therefore, bioinspired peptide or peptide bolaamphiphile nanostructures are the best choice to use as a template for the synthesis and stabilization of metal nanoparticles. Several groups have used palladium nanoparticles (PdNPs) as a catalyst for a wide range of organic reactions[9] including Suzuki coupling reactions,[10] Stille coupling reactions,[11] Heck reactions[12] and Sonogashira coupling reactions.[13] Generally, various ligands and quaternary ammonium salts such as tetrabutylammonium bromide (TBAB) or cetyltrimethylammonium bromide (CTAB) have been used for effective Suzuki coupling reactions in aqueous media.[14] Suzuki coupling reactions catalysed by peptide nanofibers decorated with Pd nanoparticles with improved yields under mild reaction conditions still remains unexplored. In this chapter, we demonstrate the self-assembly of a peptide bolaamphiphile molecule for the fabrication of Pd nanoparticles on peptide nanofibers to enhance the catalytic ability for C-C coupling reactions under mild and aerobic conditions (Scheme 5.2). The peptide nanofibers were anticipated to anchor the aromatic reactants and metal nanoparticles, which would result in an enhanced catalytic activity for C-C coupling reactions.

5.2 Experimental

5.2.(1) Synthesis of Bolaamphiphiles

Peptide bolaamphiphile **25** employed in this report was synthesized by conventional solution phase methodology. The C-terminus of amino acid was protected as methyl ester. Couplings were mediated by diisopropylcarbodiimide-1-hydroxybenzotriazole (DIPC-HOBt). The final compounds were purified and fully characterized by ^{1}H NMR and mass spectral studies.

5.2.1 Synthesis of Bolaamphiphile (HO-Phe(4)-Tyr(3)-Suc-Tyr(1)-Phe(2)-OH) 25:

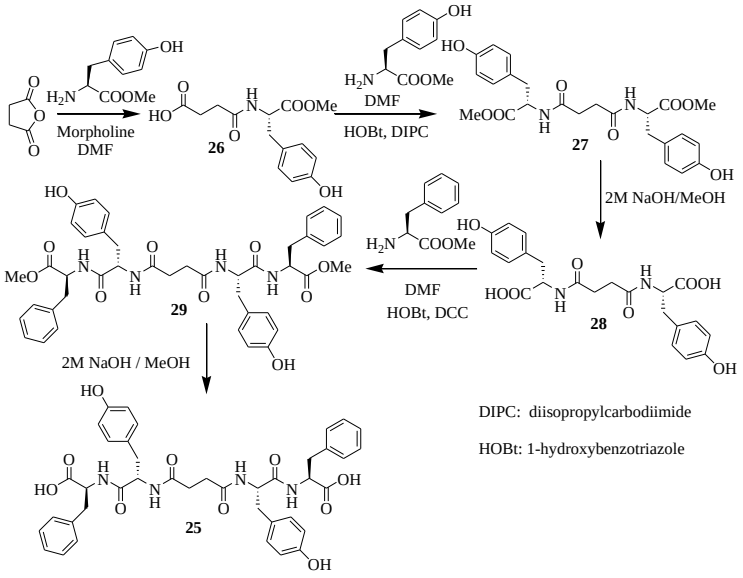

Scheme 5.1. *Synthetic scheme of peptide bolaamphiphile **25** .*

*(a) Synthesis of HO-Tyr(1)-Suc-OMe **26**:* 0.5 g (5 mmol) succinic anhydride in 3 mL of DMF was cooled in an ice bath and H-Tyr-OMe was isolated from 1.16 g (5 mmol) of the corresponding methyl ester hydrochloride by neutralization and subsequent extraction by ethyl acetate. The ethyl acetate extract was concentrated to 8 mL. It was then added to the reaction mixture, followed immediately by 0.5 g (5 mmol, 550 μL) N-methyl morpholine. The reaction mixture was stirred for overnight. 50 mL ethyl acetate was added to the reaction mixture and the organic layer was washed with 1M HCl (3 x 50 mL). The ethyl acetate part was dried over anhydrous Na_2SO_4 and filtered. It was evaporated under

vacuum to yield **26** as sticky compound. Purification was done by silica gel column (100-200 mesh) using chloroform-methanol (9:1) as eluent.

Yield: 1.32 g (4.5 mmol, 90%); ῡ = 3294 (st), 1721 (st), 1646 (st), 1543 (st) cm^{-1}; ^1H NMR (400 MHz, DMSO-d_6, δ_{ppm}): 12.06 (s, 1H, -COOH), 8.29 (d, *J* = 7.6 Hz, 1H, NH of Tyr(1)), 7.00 (d, *J* = 8 Hz, 2H, ring protons of Tyr(1)), 6.67 (d, *J* = 8 Hz, 2H, ring protons of Tyr(1)), 4.36 (m, 1H, $C^{\alpha}H$ of Tyr(1)), 3.57 (s, 3H, $COOCH_3$), 2.86 (d, *J* = 6 Hz, 1H, $C^{\beta}Hs$ of Tyr(1)), 2.80 (d, *J* = 8.8 Hz, 1H, $C^{\beta}Hs$ of Tyr(1)), 2.35 (m, 4H, $-CH_2-$ of Suc); $[\alpha]_D^{20}$ = +15.53 (*c* = 1.03 in CH_3OH); MS (ESI) *m/z*: $(M+Na)^+$ Calcd. for $C_{14}H_{17}NNaO_6$: 318.0948; found 318.0934.

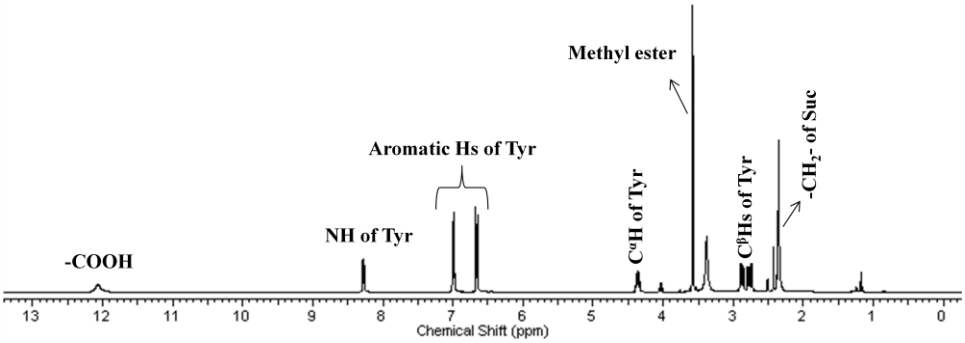

Figure 5.1. *^1H NMR spectrum (400 MHz, DMSO-d_6) of HO-Suc-Y-OMe* ***26.***

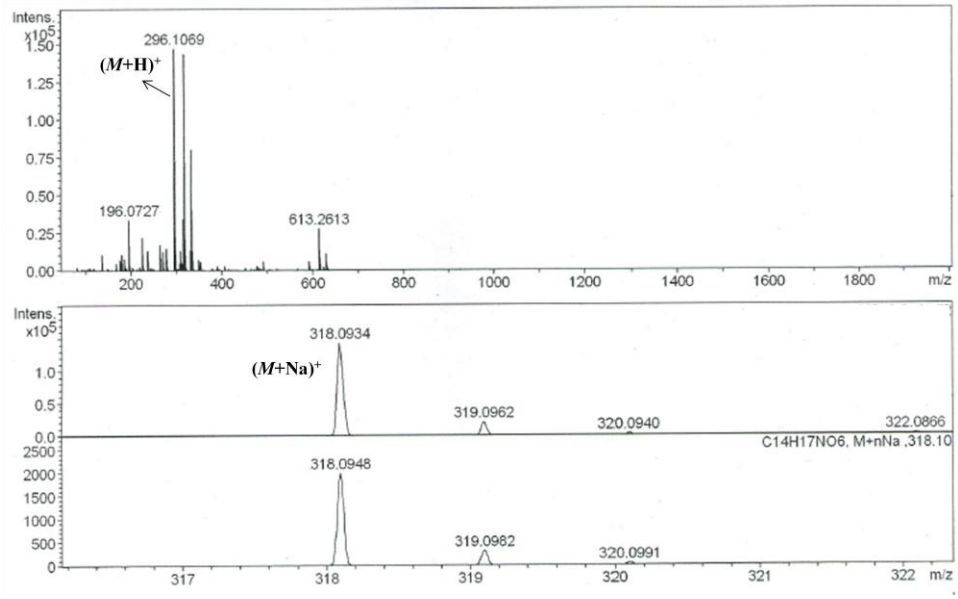

Figure 5.2. *ESI-MS spectra of HO-Suc-Y-OMe* ***26.***

*(b) Synthesis of MeO-Tyr(2)-Suc-Tyr(1)-OMe **27**:* 1.03 g (3.5 mmol) of HO-Suc-Tyr(1)-OMe **26** in 3 mL of DMF was cooled in an ice bath and H-Tyr-OMe was isolated from 1.62 g (7 mmol) of the corresponding methyl ester hydrochloride by neutralization and subsequent extraction with ethyl acetate and the ethyl acetate extract was concentrated to 8 mL. It was then added to the reaction mixture, followed immediately by 0.48 g (3.85 mmol, 592 μL) DIPC and 0.520 g (3.85 mmol) of HOBt. The reaction mixture was stirred for overnight. The residue was taken up in ethyl acetate (50 mL) and the diisopropyl urea was filtered off. The organic layer was washed with 1M HCl (3 × 50 mL), brine (2 × 50 mL), 1M sodium carbonate (3 × 50 mL), brine (2 × 50 mL) and dried over anhydrous sodium sulfate and evaporated under vacuum to yield **27** as a white solid. Purification was done by silica gel column (100-200 mesh) using chloroform-methanol (9:1) as eluent.

Yield: 1.37 g (2.9 mmol, 82.8%); ῡ = 3322 (w), 3264(w), 1725 (st), 1639 (st), 1617 (st), 1568 (st) cm^{-1} ; ^{1}H NMR (400 MHz, $CDCl_3$, δ_{ppm}): 6.89 (d, *J* = 8.8 Hz, 4H, ring protons of Tyr(1) and Tyr(2)), 6.68 (d, *J* = 8.4 Hz, 4H, ring protons of Tyr(1) and Tyr(2)), 6.25 (d, *J* = 8.0 Hz, 2H, NHs of Tyr(1) and Tyr(2)), 4.73 (m, 2H, C^{α}Hs of Tyr(1) and Tyr(2)), 3.66 (s, 6H, -$COOCH_3$), 2.99 and 2.91 (d, *J* = 5.2 Hz, *J* = 6.8 Hz, 4H, C^{β}Hs of Tyr(1) and Tyr(2)), 2.44 (m, 4H, -CH_2- of Suc); $[\alpha]_D^{20}$ = + 12.67 (*c* = 0.31 in $CHCl_3$); MS (ESI, *m/z*): $(M+H)^+$ Calcd. for $C_{24}H_{29}N_2O_8$: 473.1924; found 473.2321.

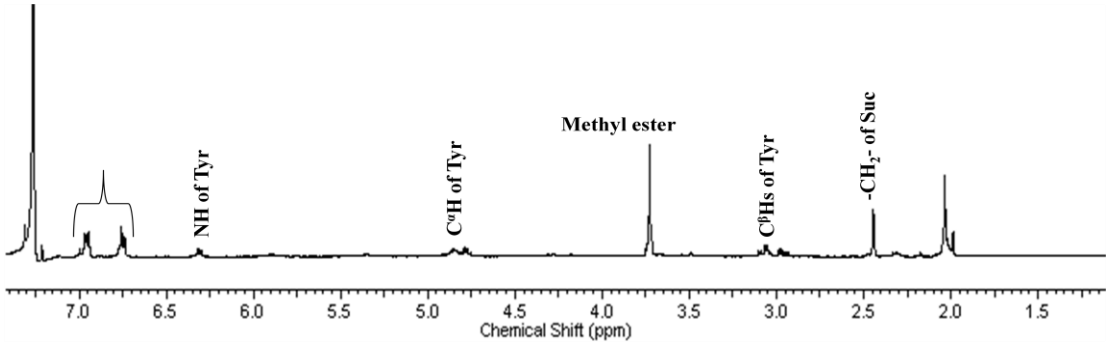

Figure 5.3. *^{1}H NMR spectrum (400 MHz, $CDCl_3$) of MeO-Y-Suc-Y-OMe **27**.*

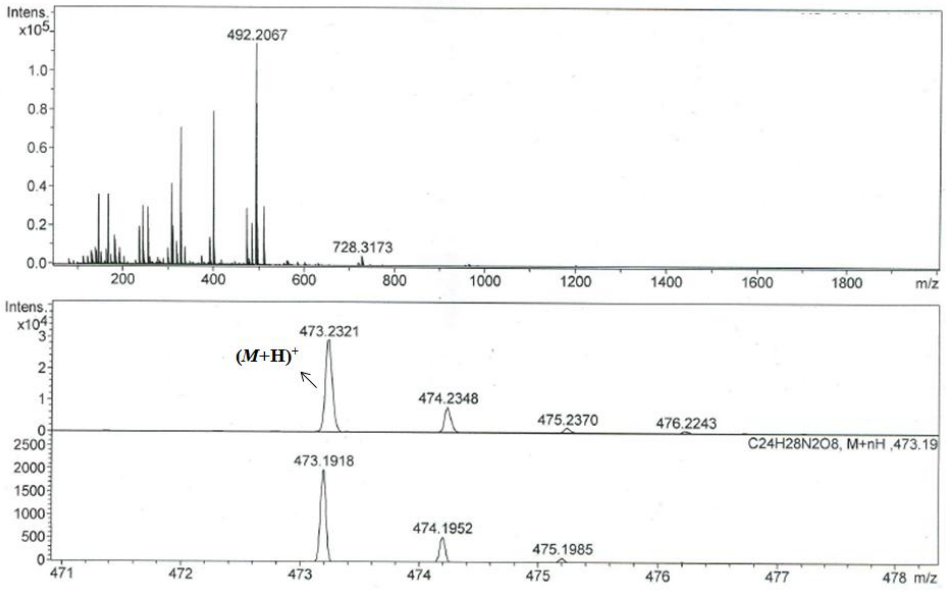

Figure 5.4. *ESI-MS spectra of MeO-Y-Suc-Y-OMe* ***27.***

(c) Synthesis of HO-Tyr-(2)-Suc-Tyr(1)-OH ***28****:* 1.27 g (2.7 mmol) of MeO-Tyr(2)-Suc-Tyr(1)-OMe **27** in 6 mL MeOH was taken in a round bottom flask and 4.5 mL of 2M NaOH was added dropwise. The reaction was monitored by thin layer chromatography (TLC). The reaction mixture was stirred for overnight. 15 mL of distilled water was added to the reaction mixture and MeOH was removed under vacuum. The aqueous part was washed with diethyl ether (2 × 30 mL). Then it was cooled down under ice bath for 10 minutes and then pH was adjusted to 1 by drop wise addition of 1M HCl. It was extracted with ethyl acetate (3 × 50 mL) and then the ethyl acetate part was dried over anhydrous Na_2SO_4 and evaporated in vacuum to yield **28** as a white solid.

Yield: 1.15 g (2.6 mmol, 96.29%); ῡ = 3297 (m), 1711 (st), 1649 (st), 1614 (st), 1537 (st) cm^{-1}; ^1H NMR (400 MHz, DMSO-d_6, δ_{ppm}): 12.57 (s, 1H, -COOH), 8.16 (d, *J* = 8 Hz, 2H, NHs of Tyr(1) and Tyr(2)), 7.06 (d, *J* = 8 Hz, 4H, ring protons of Tyr(1) and Tyr(2)), 6.71 (d, *J* = 8 Hz, 4H, ring protons of Tyr(1) and Tyr(2)), 4.34 (m, 2H, C^{α}Hs of Tyr(1) and Tyr(2)), 2.97 and 2.93 (d, *J* = 4.8 Hz, 2H, C^{β}Hs of Tyr(1) and Tyr(2)), 2.80 and 2.76 (d, *J* = 9.2 Hz, 2H, C^{β}Hs of Tyr(1) and Tyr(2)), 2.29 (m, 4H, -CH_2- of Suc); $[\alpha]_D^{20}$ = +35.34 (*c* = 0.43 in CH_3OH); MS (ESI) *m/z*: $(M+H)^+$ Calcd. for $C_{22}H_{25}N_2O_6$: 445.1611; found 445.1639.

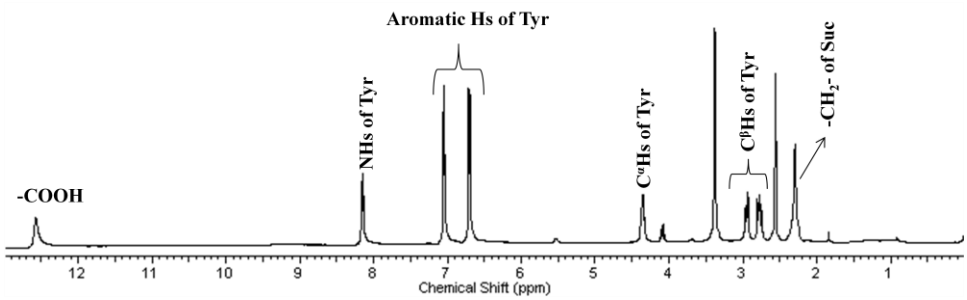

Figure 5.5. *^{1}H NMR spectrum (400 MHz, DMSO-d_6) of HO-Y-Suc-Y-OH* ***28.***

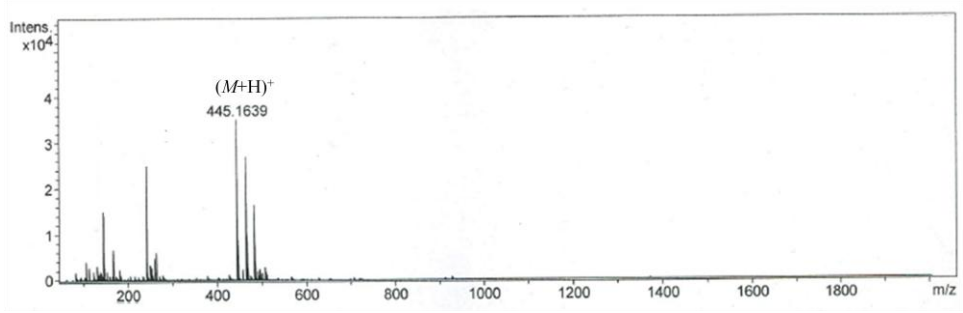

Figure 5.6. *ESI-MS spectrum of HO-Y-Suc-Y-OH* ***28.***

(d) Synthesis of MeO-Phe(4)-Tyr(3)-Suc-Tyr(1)-Phe(2)-OMe ***29****:* 1.07 g (2.42 mmol) of HO-Tyr(2)-Suc-Tyr(1)-OH **28** in 3 mL of DMF was cooled in an ice bath and H-Phe-OMe was isolated from 2.09 g (9.7 mmol) of the corresponding methyl ester hydrochloride by neutralization and subsequent extraction with ethyl acetate and the ethyl acetate extract was concentrated to 8 mL. It was then added to the reaction mixture, followed immediately by 0.67 g (5.32 mmol, 830 μL) DIPC and 0.718 g (5.32 mmol) of HOBt. The reaction mixture was stirred for overnight. The residue was taken up in ethyl acetate (50 mL) and the diisopropyl urea was filtered off. The organic layer was washed with 1M HCl (3 × 50 mL), brine (2 × 50 mL), 1M sodium carbonate (3 × 50 mL), brine (2 × 50 mL) and dried over anhydrous sodium sulfate and evaporated in vacuum to yield **29** as a white solid. Purification was done by silica gel column (100-200 mesh) using chloroform-methanol (9:2) as eluent.

Yield: 1.53 g (2.0 mmol, 82.64%); ^{1}H NMR (400 MHz, DMSO-$d_{6,}$ δ_{ppm}): 8.36 (d, J = 7.6 Hz, 2H, NHs of Phe(2) and Phe(4)), 7.98 (d, J = 8.8 Hz, 2H, NHs of Tyr(1) and Tyr(3)), 7.25(d, J = 6.8 Hz, 4H, ring protons of Phe(2) and Phe(4)), 7.21 (t, J = 7.6 Hz, 6H, ring protons of Phe(2) and Phe(4)), 6.99 (d, J = 8.4, Hz, 4H, ring protons of Tyr(1) and

Tyr(3)), 6.63 (d, *J* = 8.8, Hz, 4H of Tyr(1) and Tyr(3)), 4.46 (m, 2H, C^{α}Hs of Phe(2) and Phe(4)), 4.40 (m, 2H, C^{α}Hs of Tyr(1) and Tyr(3)), 3.56 (s, 6H, -$COOCH_3$), 2.99 and 2.97 (d, *J* = 6 Hz and *J* = 4.8 Hz, 4H, C^{β}Hs of Phe(2) and Phe(4)), 2.86 and 2.82 (d, *J* = 4.8 Hz and *J* = 4.0 Hz, 4H, C^{β}Hs of Tyr(1) and Tyr(3)), 2.25-2.15 (m, 4H, -CH_2- of Suc); $[\alpha]_D^{20}$ = -23.18 (*c* = 0.2 in CH_3OH); MS (ESI) *m/z*: $(M+Na)^+$ Calcd. for $C_{42}H_{46}N_4O_{10}Na$: 789.3112; found 789.3184.

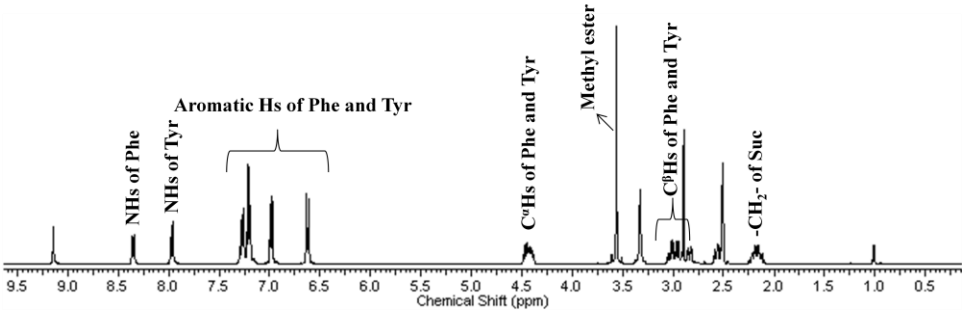

Figure 5.7. *^{1}H NMR spectrum (400 MHz, DMSO-d_6) of MeO-F-Y-Suc-Y-F-OMe* ***29.***

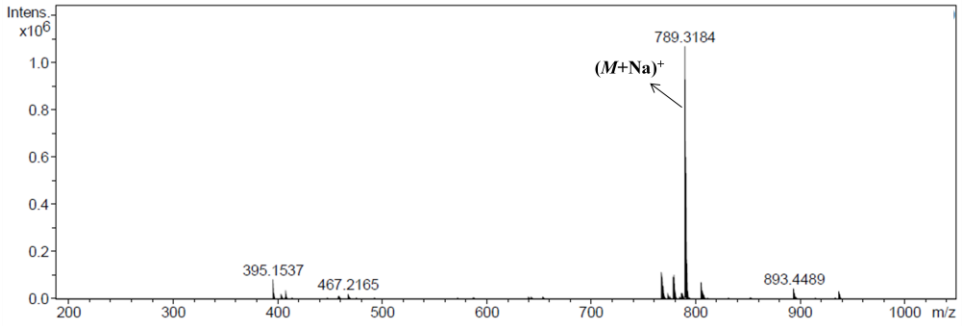

Figure 5.8. *ESI-MS spectrum of MeO-F-Y-Suc-Y-F-OMe* ***29.***

(e) Synthesis of HO-Phe(4)-Tyr(3)-Suc-Tyr(1)-Phe(2)-OH ***25****:* 1.38 g (1.8 mmol) of MeO-Phe(4)-Tyr(3)-Suc-Tyr(1)-Phe(2)-OMe **29** in 10 mL MeOH was taken in a round bottom flask and 4 mL of 2M NaOH was added to it dropwise. The reaction was monitored by thin layer chromatography (TLC). The reaction mixture was stirred for overnight. 15 mL of distilled water was added to the reaction mixture and MeOH was removed under vacuum. The aqueous part was washed with diethyl ether (2 × 30 mL).

Then it was cooled under ice water bath for 10 minutes and then pH was adjusted to 1 by drop wise addition of 1M HCl. It was extracted by ethyl acetate (3 × 50 mL) and then the ethyl acetate part was dried over anhydrous Na_2SO_4 and evaporated in vacuum to yield **25** as a white solid. 5% of racemization was found in this hydrolysis.

Yield: 1.25 g (1.7 mmol, 94.4%); ῡ = 3391 (st), 1708 (m), 1636 (st), 1559 (st), 1513 (m) cm^{-1}; ^1H NMR (400 MHz, DMSO-d_6, δ_{ppm}): 12.72 (s, 2H, -COOH), 8.23 (d, *J* = 7.6 Hz, 2H, NHs of Phe(2) and Phe(4)), 8.00 (d, *J* = 8.4 Hz, 2H, NHs of Tyr(1) and Tyr(3)), 7.32-7.27 (m, 10H, ring protons of Phe(2) and Phe(4)), 7.05 (d, *J* = 8.0, Hz, 4H, ring protons of Tyr(1) and Tyr(3)), 6.68 (d, *J* = 8.4, Hz, 4H of Tyr(1) and Tyr(3)), 4.46 (m, 4H, $C^{\alpha}Hs$ of Tyr(1), Phe(2), Tyr(3) and Phe(4)), 3.10 and 2.98 (d, *J* = 5.2 Hz and *J* = 8.8 Hz, 4H, $C^{\beta}Hs$ of Phe(2) and Phe(4)), 2.89 and 2.61 (d, *J* = 10.8 Hz and *J* = 10.0 Hz, 4H, $C^{\beta}Hs$ of Tyr(1) and Tyr(3)), 2.25 (m, 4H, -CH_2- of Suc); ^{13}C NMR (100 MHz, DMSO-d_6, δ_{ppm}): 173.13, 172.82, 172.69, 171.38, 171.08, 169.19, 155.63, 137.68, 137.41, 130.02, 129.10, 129.00, 128.15, 127.97, 126.40, 114.75, 53.93, 53.44, 36.73, 36.58, 30.73, 23.26, 22.29; $[\alpha]_D^{20}$ = -23.75 (*c* = 0.12 in CH_3OH); MS (ESI) *m/z*: $(M+Na)^+$ Calcd. for $C_{40}H_{42}N_4O_{10}Na$: 761.2793; found 761.2622.

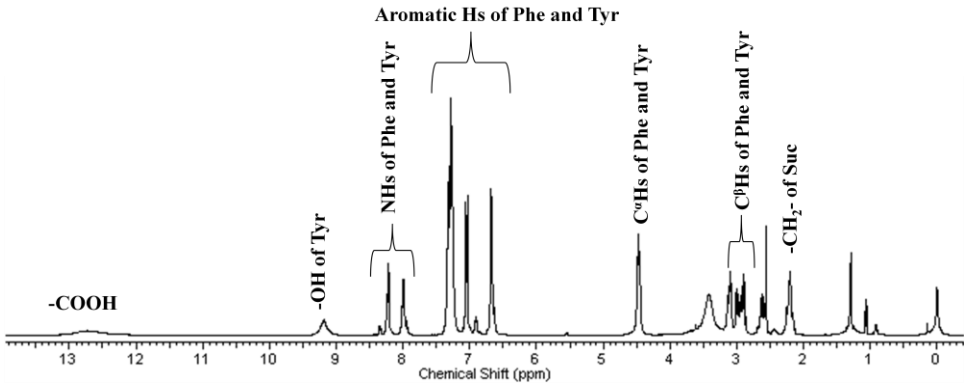

Figure 5.9. *^1H NMR spectrum (400 MHz, DMSO-d_6) of HO-F-Y-Suc-Y-F-OH* ***25.***

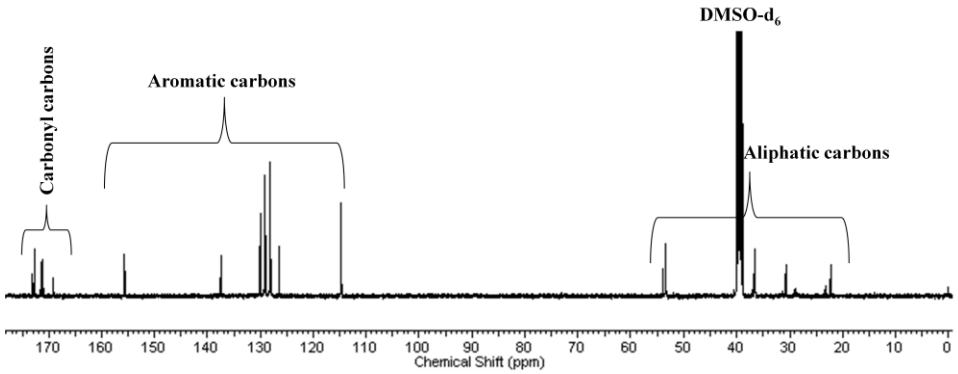

Figure 5.10. *^{13}C NMR spectrum (100 MHz, DMSO-d_6) of HO-F-Y-Suc-Y-F-OH* ***25.***

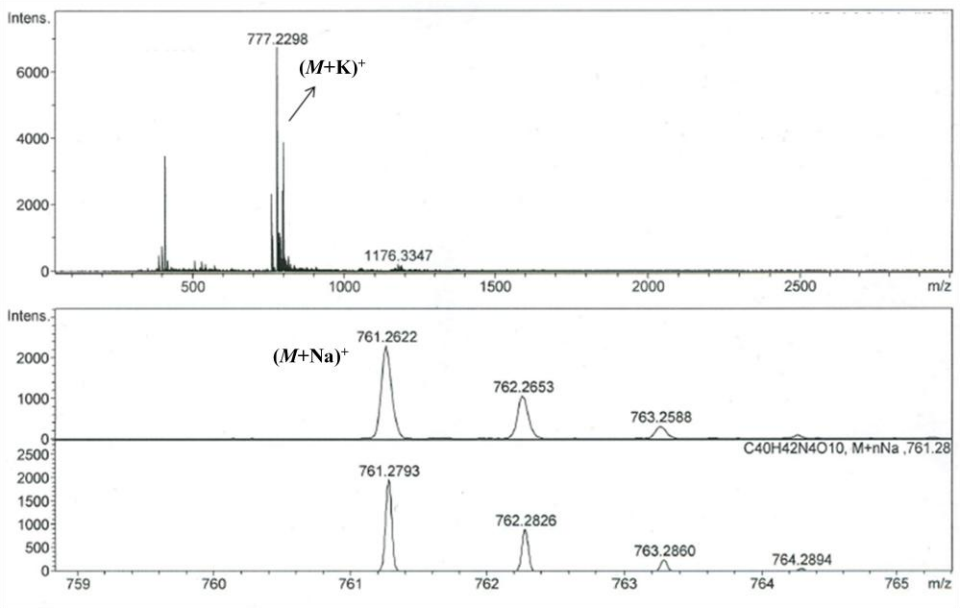

Figure 5.11. *ESI-MS spectrum of HO-F-Y-Suc-Y-F-OH* ***25.***

5.3 Method and Characterization Techniques

5.3.1 Preparation of the Hydrogel

29.53 mg (20 mmol L^{-1}) of the peptide bolaamphiphile (HO-F-Y-Suc-Y-F-OH) **25** was dispersed in 2 mL of doubly distilled water. The peptide bolaamphiphile was completely dissolved by the addition of 0.3 mL of 1M NaOH and the final pH of the solution was found to be 11.2. Eight equivalents (32 mg, 160 mmol L^{-1}) of succinic anhydride were added to the peptide bolaamphiphile solution. The hydrolysis of succinic anhydride to succinic acid is slow and the pH continued to drop over time. The final pH of the solution was found to be 3.3 after 30 minutes. A self-supporting hydrogel was formed upon vortexing the resulting solution for 10 seconds.

5.3.2 Synthesis of Pd Nanoparticles

Pd nanoparticles were synthesized in the hydrogel matrix without the addition of any external reducing agent. The peptide bolaamphiphile **25** (20 mmol L^{-1}) was dispersed in 2 mL of doubly distilled water and the peptide bolaamphiphile was completely dissolved by the addition of 0.3 mL of 1M NaOH. Then, $PdCl_2$ (2 mg, 5.6 mmol L^{-1}) was dispersed in the solution and the solution was sonicated for a few minutes to completely dissolve the dispersion. Eight equivalents (32 mg, 160 mmol L^{-1}) of succinic anhydride were added to decrease the pH in a controlled manner through its hydrolysis to succinic acid. The hydrogel formed after 30 minutes when the pH was found to be 3.3. The formation of the PdNPs was monitored by the change in color. The color changed to dark brown within 12 hours, which indicated the formation of Pd nanoparticles in the hydrogel matrix.

5.3.3 Catalytic Studies

In a Suzuki coupling reaction, a mixture of 0.08 mmol of the aryl halide and 0.12 mmol of the aryl boronic acid were dissolved in 2 mL of water-methanol (1:1) solvent. The Pd nanoparticles (0.0024 mmol, 500 mL of the hydrogel containing Pd nanoparticles decorated on the nanofibers) were added to the reaction mixture. Potassium carbonate (6 equiv., 0.48 mmol) was used as a base for all the coupling reactions. The reactions were carried out at 40-50 °C depending on the substrates used.

5.3.4 Circular Dichroism (CD) Spectroscopy

Secondary structure of peptide bolaamphiphile was analyzed with Jasco J-815 circular dischroism spectrometer. For all the case, peptide hydrogel (20 mmol L^{-1}) and the Pd nanoparticles embedded in hydrogel, were diluted to final concentration of 10 μM in ddH_2O and measured from 260 nm to 190 nm with 0.1 data pitch, 20 nm/min scanning speed, 1 nm band width and 4 s D.I.T. The percentage of β-sheet structure was measured by using a free online program as http://perry.freeshell.org.

5.3.5 Fluorescence Spectroscopy

Fluorescence emission spectra of gel (20 mmol L^{-1}) were recorded on a Horiba Scientific Fluoromax-4 spectrophotometer with 1 cm path length quartz cell at room temperature. The slit width for the excitation and emission was set at 5 nm and a 1 nm data pitch. Excitation of gel sample **25** was performed at 270 nm and data range was in between 280 to 525 nm.

5.4 Results and Discussion

5.4.1 Preparation of Hydrogel

A synthesized peptide bolaamphiphile **25** (HO-F-Y-Suc-Y-F-OH) was able to self-assemble in an aqueous medium and formed a self-supporting hydrogel. We utilized the hydrolysis of succinic anhydride in an aqueous medium to form succinic acid and lower the pH in a controlled manner. In our experiment, 29.53 mg (20 mmol L^{-1}) of peptide bolaamphiphile **25** was dispersed in 2 mL of doubly distilled water. The peptide bolaamphiphile was completely dissolved by the addition of 300 μL of 1M NaOH and the final pH of the solution was found to be 11.2. Eight equivalents (32 mg, 160 mmol L^{-1}) of succinic anhydride were added to the peptide bolaamphiphile solution. The hydrolysis of succinic anhydride to succinic acid is slow and the pH continued to drop over time (Figure 5.12). The final pH of the solution was found to be 3.3 after 30 minutes and a self-supporting hydrogel was formed.

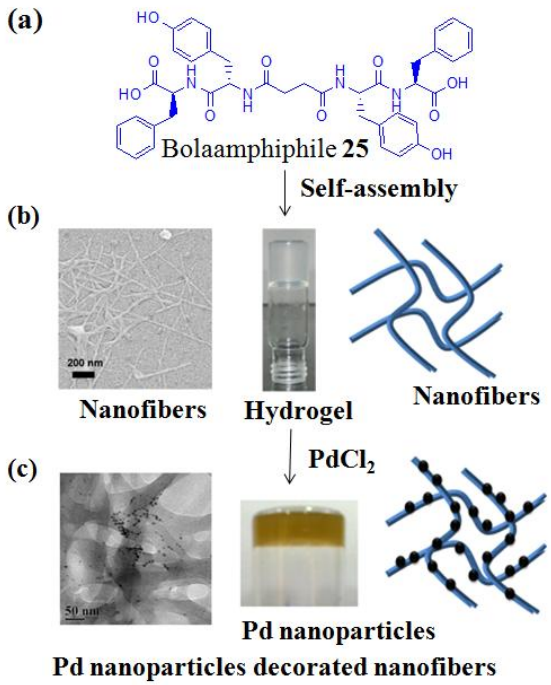

Scheme 5.2. *(a) Molecular structure of peptide bolaamphiphile* ***25*** *used in the self-assembly study, (b) a photograph of a self-supporting hydrogel which forms nanofibrillar structures, and (c) the in situ synthesized Pd nanoparticles decorated on peptide nanofibers.*

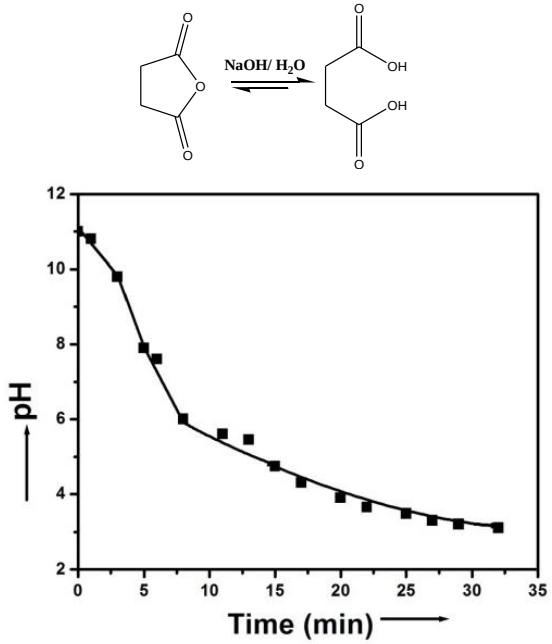

Figure 5.12. *The pH of solution of peptide bolaamphiphile decreases over time during the hydrolysis of succinic anhydride to succnic acid.*

5.4.2 Self-assembly Study

The self-assembly study of the peptide bolaamphiphile **25** was carried out using various spectroscopic and microscopic techniques. FT-IR spectroscopy was used to study the secondary structure of the hydrogel **25**. The FT-IR spectrum of the hydrogel exhibited an amide I band at 1629 cm^{-1}, which signifies a β sheet structure (Figure 5.13a(i)) of self-assembled gelator molecules.[5,15] A circular dichroism (CD) spectrum was recorded to understand the secondary structural information of the self-assembled peptide bolaamphiphile **25** in the gel phase. The CD spectrum of peptide bolaamphiphile **25** (Figure 5.13(b)i) exhibited a strong positive band at 198 nm for the π-π* transition and a weak shoulder around 217 nm for the n-π* transition in -CONH-.[16] The CD signature showed a mixture of β-sheet (42.8%) and random coil (39.6%) structures of the hydrogel.

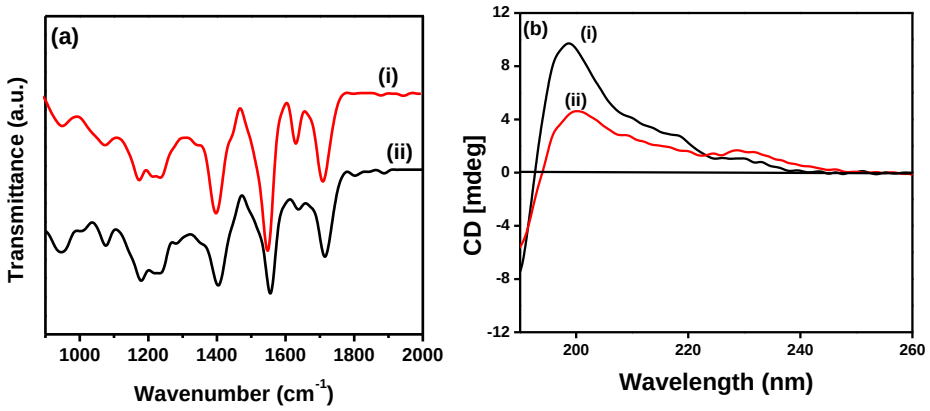

Figure 5.13. *(a) FT-IR spectra of hydrogel show (i) an amide **I** band at 1629 cm^{-1} and amide **II** band at 1554 cm^{-1}. (ii) The amide **I** band appeared at 1635 cm^{-1} and amide **II** band at 1556 cm^{-1} for peptide nanofibers decorated with Pd nanoparticles. (b) The CD spectra of (i) hydrogel **25** and (ii) peptide nanofibers decorated with Pd nanoparticles.*

To acquire more insight into the structural information at the supramolecular level, the hydrogel was characterized by fluorescence spectroscopy. The emission spectrum of the hydrogel (Figure 5.14a) showed two characteristic peaks centered at 297 nm and 320 nm. These two peaks are attributed to the extensive π-π stacking interactions between the aromatic groups present in the backbone of the peptide bolaamphiphile **25**.[17]

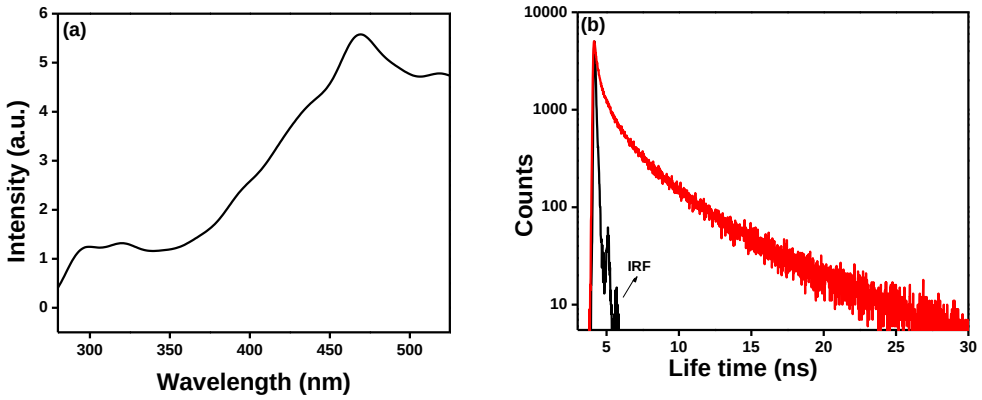

Figure 5.14. *(a) Emission spectroscopy of hydrogel* ***25*** *reveals the π-π stacking interaction and self-assembly towards higher ordered aggregated structures. Concentration of the sample is 20 mmol* L^{-1} *and* λ_{ex} *= 270 nm. (b) TCSPC spectroscopy for the hydrogel.*

Table 5.1. *Decay parameters for hydrogel* ***25*** *at different concentration.*

Hydrogel at different concentration	α_1	α_2	α_3	τ_1 (ns)	τ_2(ns)	τ_3(ns)	τ_a (ns)	χ^2
20 mmol L^{-1}	0.26	0.09	0.65	0.96	3.81	0.18	0.69	1.09

Another pronounced peak appeared at 468 nm, which is assigned to a higher order supramolecular structure of the peptide bolaamphiphile hydrogel **25**.[18] These results reveal that the self-assembly of peptide bolaamphiphile **25** is governed by hydrogen bonding and π-π stacking interactions between the aromatic residues. The time correlated single photon counting (TCSPC) experiment showed that the average lifetime for the hydrogel (10 mmol L^{-1}) was 0.69 ns (Figure 5.14b and Table 5.1).

The FE-SEM image (Figure 5.15(a)) shows that the peptide bolaamphiphile molecules self-assembled into entangled and helical nanofibrillar structures.[5,19] Each fiber diameter was 20 ± 5 nm and several micrometers in length. The TEM image of a diluted solution of the peptide hydrogel shows three-dimensional nanofibrillar networks (Figure 5.15(b)). The average diameter of the nanofibers was 22 nm and each fiber was several

micrometers in length. The nanofibrillar network structures are responsible for the formation of the self-supporting hydrogel.

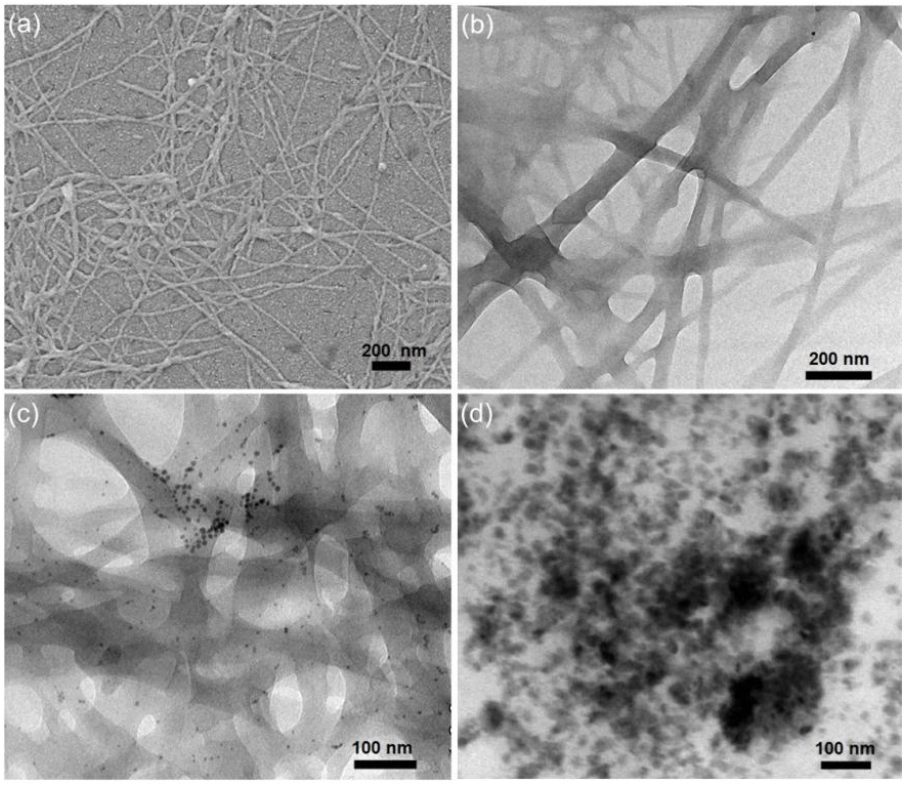

Figure 5.15. *(a) FE-SEM image showing entangled nanofibrillar structures, (b) TEM image showing nanofibrillar network structure of the hydrogel. TEM images show that: (c) Pd nanoparticles were decorated on the surface of the peptide nanofibers and (d) Pd nanoparticles were completely aggregated without peptide nanofibers.*

5.4.3 Synthesis of Nanofibers Supported Pd Nanoparticles

The nanofibrillar hydrogel **25** matrix was used to synthesis Pd nanoparticles without any external reducing agent. The redox active tyrosine molecules[5,20] reduced the Pd^{2+} to Pd^{0}. In our experiment, the peptide bolaamphiphile **25** (20 mmol L^{-1}) and $PdCl_2$ (2 mg, 5.6 mmol L^{-1}) was dispersed in doubly distilled water and the self-supporting hydrogel was prepared as per the above-mentioned method. The hydrogel formed as a light brown color. The formation of the PdNPs was monitored by the change in color. The color changed to dark brown within 12 hours, which indicated the formation of the Pd

nanoparticles in the hydrogel matrix. The effect in the secondary structure of the peptide bolaamphiphile from the interaction between the metal nanoparticles and the peptide bolaamphiphile was recorded by FT-IR and CD analysis. The amide I band appeared as a weak intensity band at 1635 cm^{-1} for the peptide nano-fibers decorated with Pd nanoparticles whereas a more intense band at 1629 cm^{-1} appeared for the peptide hydrogel without Pd nanoparticles (Figure 5.13(a)ii). This indicates that the secondary structure was slightly affected by the decoration of Pd nanoparticles on the peptide nanofibers. The secondary structure of the Pd nanoparticles bound to the peptide bolaamphiphile nanofibers was also studied by CD measurements. The CD spectrum of the Pd-bound peptide bolaamphiphile nanofibers showed the presence of a shoulder between 225 nm and 240 nm and a wavelength shift from 198 to 200.5 nm at the positive side of spectrum (Figure 5.13(b)ii). This indicates a compact peptide structure with the Pd nanoparticles.[7] The decrease in ellipticity at the wavelength of 200.5 nm reveals that the Pd-bound peptide hydrogel composite appeared to be of a less ordered structure than the peptide bolaamphiphile hydrogel itself. The CD spectrum of the Pd-bound peptide bolaamphiphile hydrogel showed a mixture of β-sheet (36.8%) and random coil (37.3%) structures. The nanoparticles were characterized by transmission electron microscopy. The TEM images show that the Pd nanoparticles were synthesized and stabilized by the peptide nanofibers (Figure 5.16). The Pd nanoparticles were decorated and monodispersed on the surface of the peptide nanofibers (Figure 5.15(c)).[21]

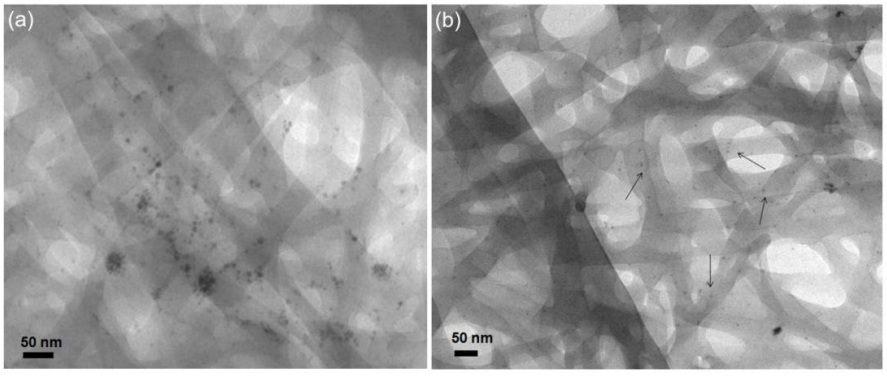

Figure 5.16. *TEM images of Pd nanoparticles decorated peptide nanofibers.*

The size of the nanoparticles ranged from 4 to 7 nm. To understand the role of the peptide nanofibers in stabilizing and dispersing the Pd nanoparticles, we prepared Pd nanoparticles without nanofibers for TEM characterization. $NaBH_4$ (1 mmol) was added to a 2 mL solution of $PdCl_2$ (5.6 mmol L^{-1}) to reduce Pd^{2+} to Pd. Pd nanoparticles were collected by several washings and centrifugation. The TEM image shows that the Pd nanoparticles were completely aggregated in this case (Figure 5.15(d)). This clearly suggests that the peptide nanofibers have a crucial role in the stabilization and dispersion of Pd nanoparticles.

5.4.4 Catalytic Activity

Pd nanoparticles are used as a catalyst in an extensive range of reactions in organic synthesis. They are used in Suzuki coupling reactions, where the ligands and temperature play crucial roles. Here, we have efficiently used Pd nanoparticles for Suzuki coupling reactions under mild conditions and at a relatively low temperature in an aerobic environment (Scheme 5.3).

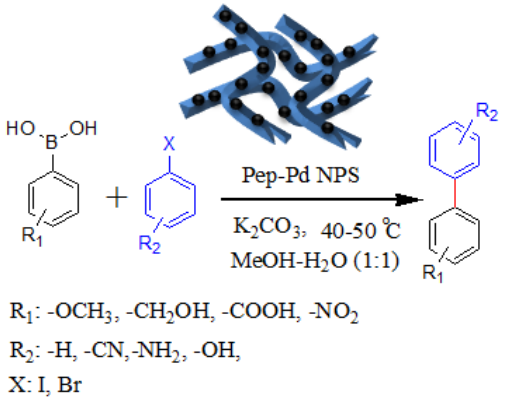

Aryl halides (0.08 mmol), phenylboronic acid (0.12 mmol), Pd catalyst (0.0024 mmol), K_2CO_3 (0.48 mmol), MeOH-H_2O (1 : 1), 40-50 ˚C. The products were isolated by column chromatography.

Scheme 5.3. *Suzuki-coupling reaction using Pd nanoparticles decorated on peptide nanofibers.*

The *in situ* synthesized well dispersed and decorated Pd nanoparticles with sizes ranging from 4 to 7 nm were used efficiently for Suzuki coupling reactions. All the coupling reactions were carried out in water-methanol (1:1) solvent. All the aryl halides and

boronic acids used were completely soluble in the water-methanol (1:1) solvent. In the Suzuki coupling reactions, a mixture of 0.08 mmol of the aryl halide and 0.12 mmol of the aryl boronic acid were dissolved in 2 mL of the water-methanol (1:1) solvent. The Pd nanoparticles (0.0024 mmol, 500 mL of the hydrogel containing Pd nanoparticles decorated on the nanofibers) were added to the reaction mixture. Potassium carbonate (6 equiv., 0.48 mmol) was used as a base for all the coupling reactions. The C-C coupling reaction was very fast and completed within 2 hours at 40 °C for the aryl iodides. The Suzuki coupling reaction is less feasible under mild conditions for the comparatively less reactive aryl bromides. We observed that all the C-C coupling reactions took 4 hours to complete at 50 °C for the aryl bromides. The products were obtained in high yields for all the C-C coupling reactions, even in the cases of the electron-rich (R_2 = 4-OH, 4-NH_2) substrates (Table 5.2). After each reaction, the methanol was evaporated and 1M Na_2CO_3 was added to the reaction mixture to remove the peptide nanofibers and the Pd nanoparticles. The reaction mixture was extracted with chloroform (3 × 20 mL). The organic layer was evaporated to isolate the coupling products. The products were purified by column chromatography. The isolated yield for all these coupling reactions was around 90%. After the first batch of reactions, the Pd nanoparticles were recovered and reused for further reactions. The coupling products were well characterized by mass spectrometry, and ^{1}H and ^{13}C NMR spectroscopy. We anticipated that the coupling reactions happened on the surface of the peptide nanofibers. The TEM image showed that the nanoparticles were decorated on the peptide nanofibers. The peptide nanofibers have hydrogen bonding sites along with aromatic cores. We anticipate that the hydrophobic aryl halides are stacked on the fiber surface through hydrophobic and π-π stacking interactions of the aromatic residues of the nanofibers, and the boronic acid groups interact with the nanofiber surface through hydrogen bonding interactions. This surface phenomenon could be related to the enhanced catalytic activity of Pd nanoparticles for C-C coupling reactions (Figure 5.17). The yields were significantly less when Pd nanoparticles catalyzed the C-C coupling reactions without being decorated on peptide nanofibers.

Table 5.2. *Table for Suzuki coupling reactions between aryl halides and phenyl boronic acids*

Entry	Boronic acids	Aryl halides	Products	Time (h)	Yield [b] (%)
1	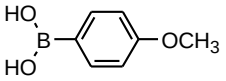	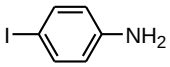	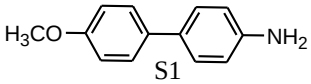 S1	1.5	92
2	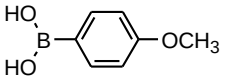	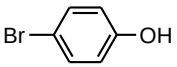	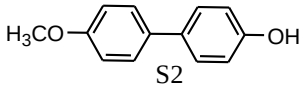 S2	4	90
3	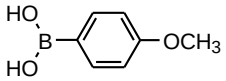	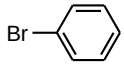	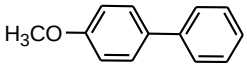 S3	4	87
4	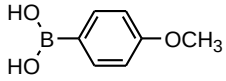	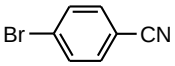	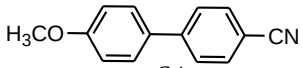 S4	3	90
5	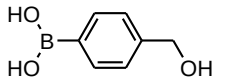	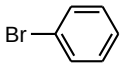	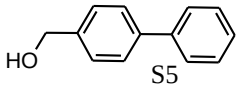 S5	4	88
6	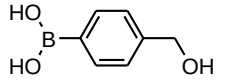	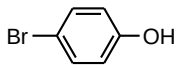	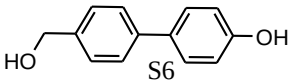 S6	4	90
7	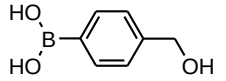	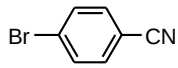	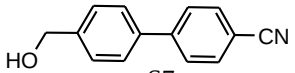 S7	3	87
8	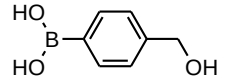	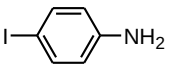	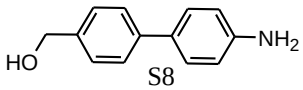 S8	1.5	91
9	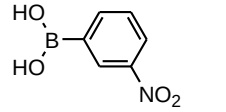	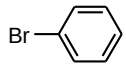	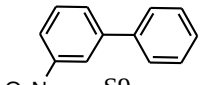 S9	4	90
10	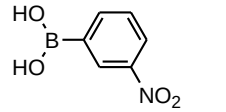	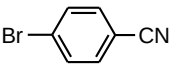	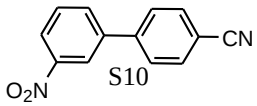 S10	3	90
11	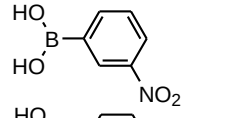	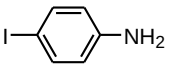	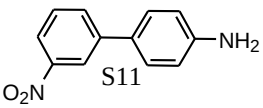 S11	1.5	89
12	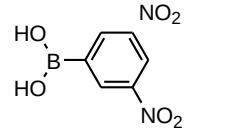	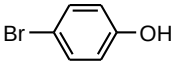	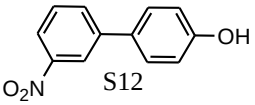 S12	4	87
13	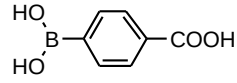	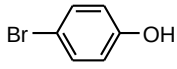	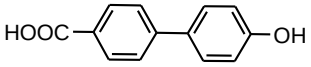 S13	4	90

[b] Isolated yield (S1, S2, S3.....are the Suzuki Coupling products)

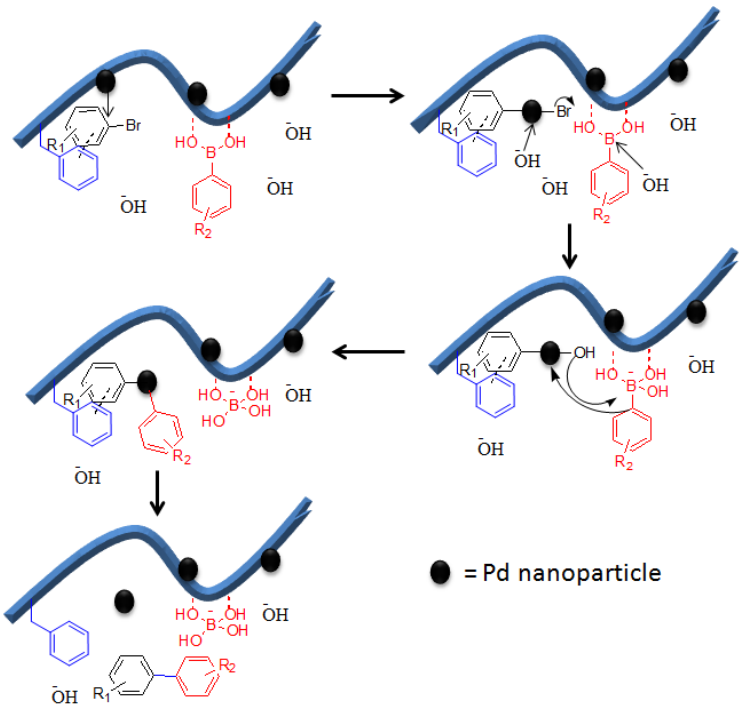

Figure 5.17. *The possible reaction mechanism for the C–C coupling (Suzuki) reaction on the surface of Pd nanoparticles decorated on peptide nanofibers.*

5.4.5 Recovery and Recyclability of the Catalyst

After the 1st batch of reaction, methanol was evaporated and 1M Na_2CO_3 was added to the reaction mixture for the removal of peptide nanofibers decorated Pd nanoparticles. The reaction mixture was extracted with chloroform (3 × 20 mL). The organic layer was evaporated to isolate the coupling products and the aqueous layer was centrifuged for five times by using a high-speed centrifuge (10000 rpm). After centrifugation, the Pd nanoparticles were precipitated out at the bottom of centrifuge tube. The Pd nanoparticles decorated on peptide nanofibers (~ 60%) were recovered after the 1st batch of reaction. To test the recyclability, several experiments were set up. The recovered Pd nanoparticles were used further for Suzuki coupling reactions (Table 5.3). In the 2nd batch, the mixture of 0.08 mmol aryl halide and 0.12 mmol of aryl boronic acid were dissolved in 2 mL of water-methanol (1:1) solvent. The recovered Pd nanoparticles (0.0024 mmol) were added to the reaction mixture. Potassium carbonate (6 equiv., 0.48 mmol) was used as a base for

the coupling reactions. We observed that 87-90% C-C coupling products were synthesized after 4 hours of reaction at 50 °C without loss in catalytic activity during 2nd batch of reaction.

Table 5.3. *Suzuki coupling reactions by using the recovered Pd nanoparticles after the 1st batch of reaction.*

Entry	Boronic acids	Aryl halides	Products	Time (h)	Yield [b] (%)
1	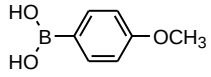	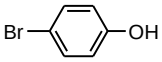	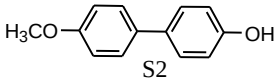 S2	4	89
2	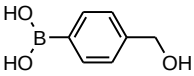	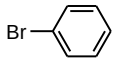	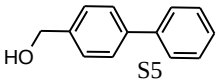 S5	4	87
3	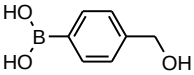	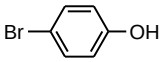	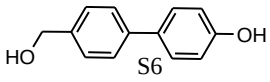 S6	4	90
4	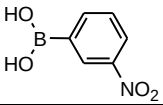	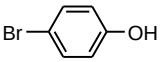	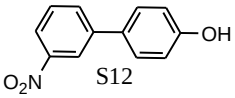 S12	4	87

[b] Isolated yield

5.5 Conclusions

We have reported the development of a peptide bolaamphiphile hydrogel. The self-assembly of the peptide nanostructures could be controlled by the hydrolysis of succinic anhydride. The self-assembly process was driven by hydrogen bonding and π-π stacking interactions, which led to the formation of nanofibrillar structures. This succinic anhydride hydrolysis method to trigger the formation of a biocompatible nanofibrous hydrogel matrix was used to synthesis Pd nanoparticles. The Pd nanoparticles were stabilized and decorated on the surface of peptide bolaamphiphile nanofibers. The Pd nanoparticles decorated on the peptide nanofibers enhanced the catalytic activity for C-C coupling reactions. This indicates that self-assembled peptide bolaamphiphiles could be used to switch and control the activity of a material's functionality. We believe that this study will lead to the development of bio-inspired functional smart materials.

5.6 Characterisation of Suzuki Coupling Products

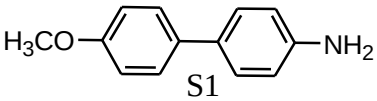

S1

^{1}H NMR (400 MHz, $CDCl_3$, δ_{ppm}): 7.46 (d, 2H), 7.37 (d, *J* = 8.4 Hz, 2H), 6.95 (d, 2H), 6.75 (d, *J* = 8 Hz, 2H), 3.84 (s, 3H), 3.68 (s, 2H); ^{13}C NMR (100 MHz, $CDCl_3$, δ_{ppm}): 157.39, 144.26, 132.87, 130.37, 126.71, 126.58, 126.38, 114.41, 113.14, 113.08, 54.31; MS (ESI) *m/z*: $(M+H)^+$ Calcd. for $C_{13}H_{14}NO$: 200.1070; found 200.1069.

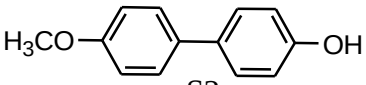

S2

^{1}H NMR (400 MHz, $CDCl_3$, δ_{ppm}): 7.47 (d, *J* = 8 Hz, 2H), 7.43 (d, *J* = 8.4 Hz, 2H), 6.96 (d, *J* = 6.4 Hz, 2H), 6.89 (d, *J* = 6.8 Hz, 2H), 3.84 (s, 3H).

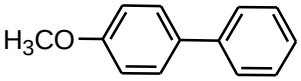

S3

^{1}H NMR (400 MHz, $CDCl_3$, δ_{ppm}): 7.54 (d, *J* = 8.4 Hz, 4H), 7.42 (t, *J* = 7.6 Hz, 2H), 7.32 (t, *J* = 7.6 Hz, 1H), 6.99 (d, *J* = 8.8 Hz, 2H), 3.85 (s, 3H); ^{13}C NMR (100 MHz, $CDCl_3$, δ_{ppm}): 158.12, 139.80, 132.76, 127.68, 127.12, 126.71, 125.71, 113.12, 54.31.

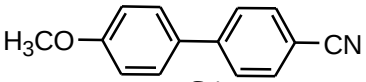

S4

^{1}H NMR (400 MHz, $CDCl_3$, δ_{ppm}): 7.68 (d, *J* = 8 Hz, 2H), 7.65 (d, *J* = 8.4 Hz, 2H), 7.55 (d, *J* = 8.8 Hz, 2H), 6.99 (d, *J* = 8.8 Hz, 2H), 3.86 (s, 3H); ^{13}C NMR (100 MHz, $CDCl_3$, δ_{ppm}): 159.19, 144.21, 131.56, 130.51, 127.34, 126.71, 126.10, 118.07, 113.53, 113.14, 109.11, 54.38; MS (ESI) *m/z*: $(M+Na)^+$ Calcd. for $C_{14}H_{11}NONa$: 232.0738; found 232.1586

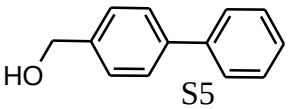

S5

^{1}H NMR (400 MHz, $CDCl_3$, δ_{ppm}): 7.99 (d, *J* = 8.4 Hz, 1H), 7.95 (d, *J* = 8.4 Hz, 1H), 7.79 (d, *J* = 8 Hz, 1H), 7.75 (d, *J* = 8.4 Hz, 1H), 7.65 (d, *J* = 7.6 Hz, 2H), 7.48 (t, *J* = 7.2 Hz, 2H), 7.43 (t, *J* = 7.2 Hz, 1H), 4.72 (s, 2H), 3.35 (s, 1H); ^{13}C NMR (100 MHz, $CDCl_3$, δ_{ppm}): 129.35, 129.25, 127.99, 127.02, 126.68, 126.35, 126.17, 125.48, 28.67.

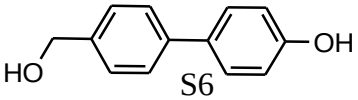

S6

^{1}H NMR (400 MHz, $CDCl_3$, δ_{ppm}): 7.60 (d, *J* = 7.6 Hz, 1H), 7.54 (d, *J* = 7.6 Hz, 1H), 7.45 (d, *J* = 8 Hz, 2H), 7.34 (d, *J* = 8.4 Hz, 2H), 6.73 (d, *J* = 8 Hz, 2H), 4.75 (s, 2H), 3.35 (s, 1H); MS (ESI) *m/z*: $(M\text{-H})^-$ Calcd. for $C_{13}H_{11}O_2$: 199.0754; found 199.0769.

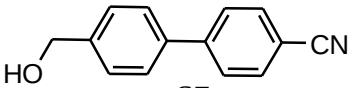

S7

MS (ESI) *m/z*: $(M+K)^+$ Calcd. for $C_{14}H_{11}NOK$: 248.0478; found 248.0158.

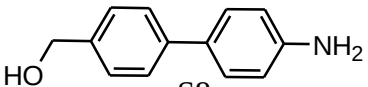

S8

HRMS (ESI) *m/z*: $(M+H)^+$ Calcd. for $C_{13}H_{14}NO$: 200.1075; found 200.1051.

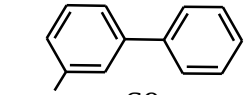

S9

^{1}H NMR (400 MHz, $CDCl_3$, δ_{ppm}): 8.43 (s, 1H), 8.25 (d, *J* = 8.4 Hz, 1H), 8.14 (d, *J* = 9.2 Hz, 1H), 7.91 (d, *J* = 7.6 Hz, 2H), 7.63 (t, *J* = 8 Hz, 3H), 7.43 (t, *J* = 6.8 Hz, 1H); MS (ESI) *m/z*: $(M+H)^+$ Calcd. for $C_{12}H_{10}NO_2$: 200.0712; found 200.0624.

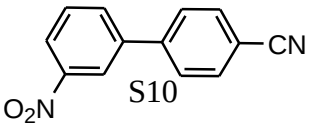

S10

^{1}H NMR (400 MHz, $CDCl_3$, δ_{ppm}): 8.43 (s, 1H), 8.24 (d, *J* = 6.8 Hz, 1H), 7.91 (d, *J* = 8.4 Hz, 1H), 7.86 (d, *J* = 8 Hz, 1H), 7.74 (d, *J* = 8.4 Hz, 1H), 7.68 (d, *J* = 8.4 Hz, 1H), 7.63 (m, 1H), 7.53 (d, *J* = 8 Hz, 1H); ^{13}C NMR (100 MHz, $CDCl_3$, δ_{ppm}): 132.16, 132.03, 131.95, 129.27, 129.19, 126.87, 126.40, 122.29, 121.11, 120.63, 109.94.

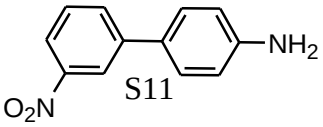

S11

^{1}H NMR (400 MHz, $CDCl_3$, δ_{ppm}): 8.38 (s, 1H), 8.10 (d, *J* = 6.8 Hz, 1H), 7.85 (d, *J* = 6.4 Hz, 1H), 7.54 (t, *J* = 6.8 Hz, 1H), 7.45 (d, *J* = 6 Hz, 2H), 6.79 (d, *J* = 6 Hz, 2H), 3.83 (s, 2H); MS (ESI) *m/z*: $(M+H)^+$ Calcd. for $C_{12}H_{11}N_2O_2$: 215.0815; found 215.0819.

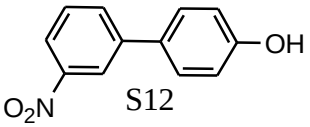

S12

MS (ESI) *m/z*: $(M+H)^+$ Calcd. for $C_{12}H_{10}NO_3$: 216.06; found 215.94.

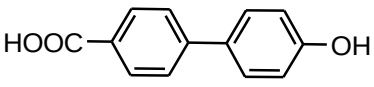

S13

MS (ESI) *m/z*: $(M+Na)^+$ Calcd. for $C_{13}H_{10}NaO_3$: 237.0528; found 237.0996.

5.7 References

1. (a) Tomasini C., Castellucci N. (2013), Peptides and peptidomimetics that behave as low molecular weight gelators, *Chem. Soc. Rev*., 42, 156-172 (DOI: 10.1039/C2CS35284B); (b) Nagy K. J., Giano M. C., Jin A., Pochan D. J., Schneider J. P. (2011), Enhanced mechanical rigidity of hydrogels formed from enantiomeric peptide assemblies, *J. Am. Chem. Soc*., 133, 14975-14977 (DOI: 10.1021/ja206742m); (c) Stone D. A., Hsu L., Stupp S. I. (2009), Self-assembling quinquethiophene-oligopeptide hydrogelators, *Soft Matter*, 5, 1990-199 (DOI: 10.1039/B904326H); (d) Zhang X., Chu X., Wang L., Wang H., Liang G., Zhang J., Long J., Yang Z. (2012), Rational design of a tetrameric protein to enhance interactions between self-assembled fibers gives molecular hydrogels, *Angew. Chem., Int. Ed.*, 51, 4388-4392 (DOI: 10.1002/anie.201108612); (e) Raeburn J., McDonald T. O., Adams D. J. (2012), Dipeptide hydrogelation triggered via ultraviolet light, *Chem. Commun*., 48, 9355-9357 (DOI: 10.1039/C2CC34677J).

2. (a) Frandsen J. L., Ghandehari H. (2012), Recombinant protein-based polymers for advanced drug delivery, *Chem. Soc. Rev*., 41, 2696-2706 (DOI: 10.1039/C2CS15303C); (b) Nicolas J., Mura S., Brambilla D., Mackiewicz N., Couvreur P. (2013), Design, functionalization strategies and biomedical applications of targeted biodegradable/biocompatible polymer-based nanocarriers for drug delivery, *Chem. Soc. Rev.*, 42, 1147-1235 (DOI: 10.1039/C2CS35265F).

3. Hirst A. R., Escuder B., Miravet J. F., Smith D. K. (2008), High-tech applications of self-assembling supramolecular nanostructured gel-phase materials: From regenerative medicine to electronic devices, *Angew. Chem., Int. Ed.*, 47, 8002-8018 (DOI: 10.1002/anie.200800022).

4. (a) Versluis F., Marsden H. R., Kros A. (2010), Power struggles in peptide-amphiphile nanostructures, *Chem. Soc. Rev*., 39, 34343444 (DOI: 10.1039/B919446K);

(b) Kameta N., Masuda M., Shimizu T. (2012), Soft nanotube hydrogels functioning as artificial chaperones, *ACS Nano*, 6, 5249-5258 (DOI: 10.1021/nn301041y); (c) Reches M., Gazit E. (2006), Molecular self-assembly of peptide nanostructures: Mechanism of association and potential uses, *Curr. Nanosci*., 2, 105-111 (DOI: 10.2174/157341306776875802).

5. Maity I., Rasale D. B., Das A. K. (2012), Sonication induced peptide-appended bolaamphiphile hydrogels for *in situ* generation and catalytic activity of Pt nanoparticles, *Soft Matter*, 8, 5301-5308 (DOI: 10.1039/C2SM25126D).

6. Nanda J., Biswas A., Adhikari B., Banerjee A. (2013), A gel-based trihybrid system containing nanofibers, nanosheets, and nanoparticles: Modulation of the rheological property and catalysis, *Angew. Chem., Int. Ed.*, 52, 5041-5045 (DOI: 10.1002/anie.201301128).

7. Coppage R., Slocik J. M., Ramezani-Dakhel H., Bedford N. M., Heinz H., Naik R. R., Knecht M. R. (2013), Exploiting localized surface binding effects to enhance the catalytic reactivity of peptide-capped nanoparticles, *J. Am. Chem. Soc*., 135, 11048-11054 (DOI: 10.1021/ja402215t).

8. (a) Lang H. F., May R. A., Iversen B. L., Chandler B. D. (2003), Dendrimer-encapsulated nanoparticle precursors to supported platinum catalysts, *J. Am. Chem. Soc.*, 125, 14832-14836 (DOI: 10.1021/ja0364120); (b) Patra S., Viswanath B., Barai K., Ravishankar N., Munichandraiah N. (2010), High-surface step density on dendritic Pd leads to exceptional catalytic activity for formic acid oxidation, *ACS Appl. Mater. Interfaces*, 2, 2965-2969 (DOI: 10.1021/am100647u).

9. (a) Huang X., Li Y., Chen Y., Zhou E., Xu Y., Zhou H., Duan X., Huang Y. (2013), Palladium- based nanostructures with highly porous features and perpendicular pore channels as enhanced organic catalysts, *Angew. Chem., Int. Ed*., 52, 2520-2524 (DOI: 10.1002/anie.201208901); (b) Verho O., Nagendiran A., Johnston E. V., Tai C.-w., Backvall J.-E. (2013), Nanopalladium on amino-functionalized mesocellular foam: An efficient catalyst for Suzuki reactions and transfer hydrogenations, *ChemCatChem*, 5, 612-618 (DOI: 10.1002/cctc.201200247).

10. (a) Saha D., Chattopadhyay K., Ranu B. C. (2009), Aerobic ligand-free Suzuki coupling catalyzed by in situ-generated palladium nanoparticles in water, *Tetrahedron Lett.*, 50, 1003-1006 (DOI: 10.1016/j.tetlet.2008.12.063); (b) Ohtaka A., Teratani T., Fujii R., Ikeshita K., Kawashima T., Tatsumi K., Shimomura O., Nomura R. (2011), Linear polystyrene-stabilized palladium nanoparticles-catalyzed C-C coupling reaction in water, *J. Org. Chem*., 76, 4052-4060 (DOI: 10.1021/jo200485q); (c) Bej A., Srimani D., Sarkar A. (2012), Palladium nanoparticle catalysis: Borylation of aryl and benzyl halides

and one-pot biaryl synthesis via sequential borylation-Suzuki–Miyaura coupling, *Green Chem*., 14, 661-667 (DOI: 10.1039/c2gc16111g).

11. Garcia-Martinez J. C., Lezutekong R., Crooks R. M. (2005), Dendrimer-encapsulated Pd nanoparticles as aqueous, room-temperature catalysts for the Stille reaction, *J. Am. Chem. Soc.*, 127, 5097-5103 (DOI: 10.1021/ja042479r).

12. (a) Bhattacharya S., Srivastava A., Sengupta S. (2005), Remarkably facile Heck and Suzuki reactions in water using a simple cationic surfactant and ligand-free palladium catalysts, *Tetrahedron Lett*., 46, 3557-3560 (DOI: 10.1016/j.tetlet.2005.03.118); (b) Ranu B. C., Chattopadhyay K. (2007), A new route to the synthesis of (*E*)- and (*Z*)-2-alkene-4-ynoates and nitriles from vic-diiodo-(*E*)-alkenes catalyzed by Pd(0) nanoparticles in water, *Org. Lett*., 9, 2409-2412 (DOI: 10.1021/ol0708121).

13. (a) Bhattacharya S., Sengupta S. (2004), Palladium catalyzed alkynylation of aryl halides (Sonogashira reaction) in water, *Tetrahedron Lett.*, 45, 8733-8736 (DOI: 10.1016/j.tetlet.2004.09.131); (b) Saha D., Dey R., Ranu B. C. (2010), A simple and efficient one-pot synthesis of substituted benzo[*b*]furans by Sonogashira coupling-5-endo-dig cyclization catalyzed by palladium nanoparticles in water under ligand- and copper-free aerobic conditions, *Eur. J. Org.Chem*., 6067-6071 (DOI: 10.1002/ejoc.201000980).

14. (a) Yuan B., Pan Y., Li Y., Yin B., Jiang H. (2010), A highly active heterogeneous palladium catalyst for the Suzuki-Miyaura and Ullmann coupling reactions of aryl chlorides in aqueous media, *Angew. Chem., Int. Ed*., 49, 4054-4058 (DOI: 10.1002/anie.201000576); (b) Keller M., Colliere V., Reiser O., Caminade A.-M., Majoral J.-P., Ouali A. (2013), Pyrene-tagged dendritic catalysts noncovalently grafted onto magnetic Co/C nanoparticles: An efficient and recyclable system for drug synthesis, *Angew. Chem., Int. Ed.*, 52, 3626-3629 (DOI: 10.1002/anie.201209969).

15. Pelton J. T., McLean L. R. (2000), Spectroscopic methods for analysis of protein secondary structure, *Anal. Biochem*., 277, 167-176 (DOI: 10.1006/abio.1999.4320).

16. (a) Yan X., Cui Y., He Q., Wang K., Li J., (2008), Organogels based on self-assembly of diphenylalanine peptide and their application to immobilize quantum dots, *Chem. Mater*., 20, 1522-1526 (DOI: 10.1021/cm702931b); (b) Kelly S. M., Jess T. J., Price N.

C. (2005), How to study proteins by circular dichroism, *Biochim. Biophys. Acta, Proteins Proteomics*, 1751, 119-139 (DOI: 10.1016/j.bbapap.2005.06.005).

17. Maity I., Rasale D. B., Das A. K. (2013), Exploiting a self-assembly driven dynamic nanostructured library, *RSC Adv*., 3, 6395-6400 (DOI: 10.1039/C3RA22401E).

18. Das A. K., Hirst A. R., Ulijn R. V. (2009), Evolving nanomaterials using enzyme-driven dynamic peptide libraries (eDPL), *Faraday Discuss*., 143, 293-303 (DOI: 10.1039/B902065A).

19. (a) Afrasiabi R., Kraatz H.-B. (2013), Sonication-induced coiled fibrous architectures of Boc-L-Phe-L-Lys(*Z*)-OMe, *Chem.–Eur. J.*, 19, 1769-1777 (DOI: 10.1002/chem.201202268); (b) Divya K. P., Sreejith S., Suresh C. H., Ajayaghosh A. (2010), Conformational control in a bipyridine linked π-conjugated oligomer: Cation mediated helix unfolding and refolding, *Chem. Commun*., 46, 8392-8394 (DOI: 10.1039/c0cc03287e); (c) Rasale D. B., Maity I., Konda M., Das A. K. (2013), Peptide self-assembly driven by oxo-ester mediated native chemical ligation, *Chem. Commun*., 49, 4815-4817 (DOI: 10.1039/C3CC41475B).

20. Ray S., Das A. K., Banerjee A. (2006), Smart oligopeptide gels: in situ formation and stabilization of gold and silver nanoparticles within supramolecular organogel networks, *Chem. Commun*., 2816-2818 (DOI: 10.1039/B605498F).

21. (a) Koley P., Pramanik A. (2011), Nanostructures from single amino acid-based molecules: Stability, fibrillation, encapsulation, and fabrication of silver nanoparticles, *Adv. Funct. Mater*., 21, 4126-4136 (DOI: 10.1002/adfm.201101465); (b) Guha S., Banerjee A. (2009), Self-assembled robust dipeptide nanotubes and fabrication of dipeptide-capped gold nanoparticles on the surface of these nanotubes, *Adv. Funct. Mater*., 19, 1949-1961 (DOI: 10.1002/adfm.200800955); (c) Yang Z., Gu H., Du J., Gao J., Zhang B., Zhang X., Xu B. (2007), Self-assembled hybrid nanofibers confer a magnetorheological supramolecular hydrogel, *Tetrahedron*, 63, 7349-7357 (DOI: 10.1016/j.tet.2007.02.009).

Chapter 6

Peptide-Nanofiber-Supported Palladium Nanoparticles as an Efficient Catalyst for the Removal of N-Terminus Protecting Group

6.1 Introduction

Self-assembly-driven peptide hydrogels[1-3] have a wide range of biological applications.[4,5] Self-assembly plays a crucial role in constructing various nanostructures that have potential applications in nanoscience and nanotechnology.[6-9] Several stimuli have been used to tune the self-assembly process.[10] Hydrogel and organogel matrices have been extensively used as a nanoreactor for the synthesis and stabilization of metal nanoparticles.[11-19] Metal nanoparticles have higher catalytic activities[20,21] than their bulk materials because of their ultra-small size and large surface-to-volume ratio. One major disadvantage is that the metal nanoparticles readily aggregate and thus lose their catalytic activity. Therefore, a stabilizing agent is required for the synthesis of metal nanoparticles. Various toxic organic solvents and reagents have been used to stabilize metal nanoparticles.[22-25] Therefore, a simple and eco-friendly method to synthesize stable metal nanoparticles needs to be developed. For this, peptides or peptide amphiphiles can serve satisfactorily for both the synthesis and stabilization of metal nanoparticles in aqueous medium. Recently, a nanostructured peptide hydrogel matrix was used as a template for *in situ* synthesis and stabilization of Pt nanoparticles.[26] The catalytic activity of peptide-nanofiber-supported Pt nanoparticles was also reported. Recently, Pd nanoparticles have attracted considerable attention for their crucial applications in temperature reduction of pollutant gases and most particularly in many organic reactions as catalyst.[27-37] Pd nanoparticles have been frequently used for C-C coupling reactions including Suzuki, Heck, and Sonogasira.[38-40] Very recently, the synthesis of Pd nanoparticles supported on mesoporous N-doped carbon and its catalytic ability for the upgrading of biofuels has also been reported.[41] In peptide chemistry, the number of N-protecting groups are well known but some of them are base sensitive (9-fluorenylmethoxycarbonyl (Fmoc)) or acid sensitive (tert-butoxycarbonyl (Boc), naphthalene-2-methoxycarbonyl (Nmoc)), and others (carbobenzyloxy (Cbz)) are stable towards both acid and base. The protection and deprotection of N-terminus amino acids and peptides are frequently used in synthesis. The Cbz group was deprotected by using Pd metal on activated charcoal in the presence of hydrogen gas.[42,43] The Fmoc group can be deprotected from the N-terminus site by using a base.[44] The Boc group can be

removed from N-terminus sites of amino acids and peptides by using a strong acid[45] including trifluoroacetic acid (TFA) and HF, but these acids are corrosive in nature. However, there is no report of a general method to deprotect the N terminus of protected amino acids and peptides. Therefore, there is a need for the development of a general method to deprotect a wide range of N-protecting groups from the N-terminus site of amino acids and peptides that is quite easy and mild in nature. Our objective is to develop such a method to deprotect the N-terminus protecting groups under mild conditions. Bolaamphiphiles are an interesting class of amphiphilic molecules, which can self-assemble into well-defined nanostructures under aqueous conditions. Recently, several groups have reported the self-assembly of bolaamphiphiles.[46,47] We have designed a peptide bolaamphiphile with two dipeptide sites, which are covalently connected with a succinic acid moiety, a hydrophobic spacer. Two dipeptides along with two carboxylic acid groups can provide hydrogen-bonding interactions in the self-assembly process. The hydrophobic aromatic side chains can also play an important role in the self-assembly process by providing π-π stacking interactions. These molecules are ideal for the design of self-assembling soft materials through extensive hydrogen bonding and π-π stacking interactions. The peptide bolaamphiphile-based hydrogel matrix can be used as a nanoreactor to synthesize metal nanoparticles.[48] In this chapter, we report the sonication-induced formation of a tyrosine and tryptophan based peptide bolaamphiphile hydrogel. The peptide nanofibers were used as a template to synthesize Pd nanoparticles. The Pd nanoparticles were decorated on the surface of peptide bolaamphiphile nanofibers, which provide extra stability to the Pd nanoparticles (Scheme 6.2). We report a general method in which peptide-nanofiber-supported Pd nanoparticles can efficiently deprotect various types of N-protecting groups from the N-terminus of amino acids and peptides in the presence of $NaBH_4$ in aqueous medium at room temperature.

6.2 Experimental

6.2.(1) Synthesis of Bolaamphiphile

Peptide bolaamphiphile **30** employed in this report was synthesized by conventional solution phase methodology. The C-terminus of amino acid was protected as methyl ester. Couplings were mediated by diisopropylcarbodiimide-1-hydroxybenzotriazole (DIPC-HOBt). The final compounds were purified and fully characterized by ^{1}H NMR and mass spectral studies.

6.2.1 Synthesis of Bolaamphiphile (HO-Tyr(4)-Trp(3)-Suc-Trp(1)-Tyr(2)-OH) 30:

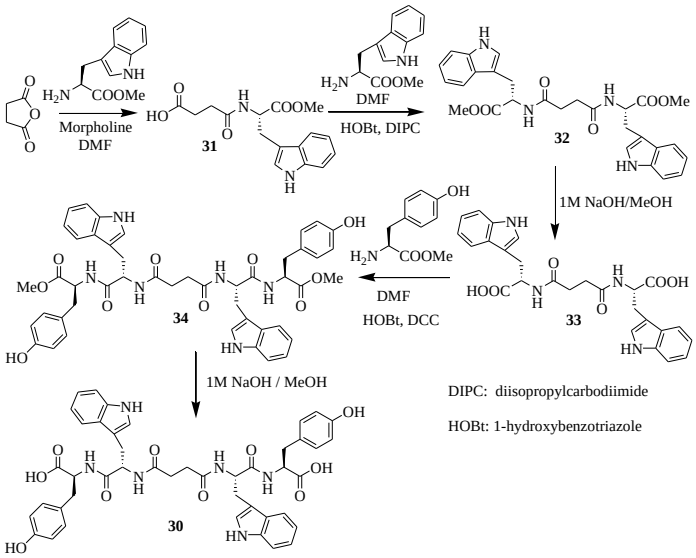

Scheme 6.1. *Synthetic scheme of peptide bolaamphiphile **30**.*

*(a) Synthesis of HO-Suc-Trp(1)-OMe **31**:* 1.17 g (11.7 mmol) succinic anhydride in 3 mL of DMF was cooled in an ice bath and H-Trp-OMe was isolated from 2.96 g (11.7 mmol) of the corresponding methyl ester hydrochloride by neutralization and subsequent extraction by ethyl acetate and the ethyl acetate extract was concentrated to 10 mL. It was then added to the reaction mixture, followed immediately by 1.82 g (11.7 mmol, 1 mL 287 μL) N-methyl morpholine. The reaction mixture was stirred for overnight. 50 mL ethyl acetate was added to the reaction mixture and the organic layer was washed with 1M HCl (3 × 50 mL). The ethyl acetate part was dried over anhydrous Na_2SO_4 and

filtered. It was evaporated under vacuum to yield **31** as sticky compound. Purification was done by silica gel column (100-200 mesh) using chloroform-methanol (9:1) as eluent.

Yield: 2.85 g (8.97 mmol, 78 %); FT-IR (KBr): ῡ = 3334 (w), 3297 (w), 1728 (ms), 1663 (st), 1528 (st) cm^{-1}; ^{1}H NMR (400 MHz, DMSO-$d_{6,}$ δ_{ppm}): 12.11 (s, 1H, -COOH), 10.81 (1H, ring -NH- of Trp), 8.33 (d, *J* = 7.6 Hz, 1H, -NH- of Trp), 7.49 (d, *J* = 8 Hz, 1H, ring proton of Trp), 7.35 (d, *J* = 8 Hz, 1H, ring proton of Trp), 7.08 (t, *J* = 7.4 Hz, 1H, ring proton of Trp), 7.00 (t, *J* = 7.4 Hz, 1H, ring proton of Trp), 4.50 (m, 1H, $C^{\alpha}H$ of Trp), 3.56 (s, 3H, $COOCH_3$), 3.12 (d, *J* = 5.6 Hz, 2H, $C^{\beta}Hs$ of Trp), 2.42 and 2.36 (m, 4H, -CH_2- of Suc); $[\alpha]_D^{20}$ = + 9.67 (*c* = 0.31 in CH_3OH); MS (ESI) *m/z*: $(M+Na)^+$ Calcd. for $C_{16}H_{18}N_2O_5Na$: 341.1113; found: 341.1124.

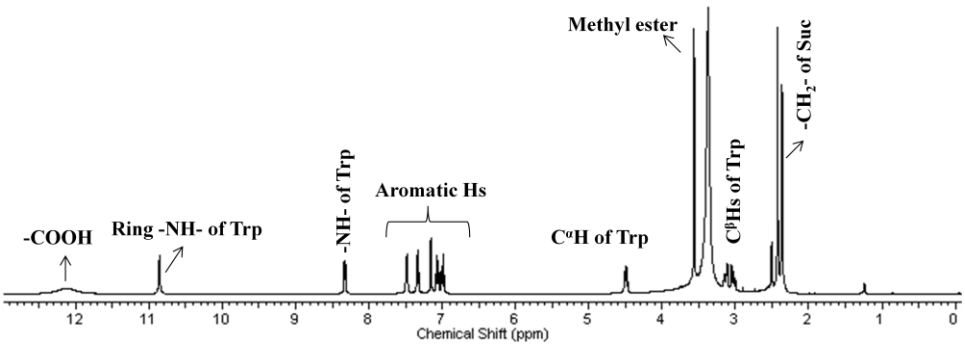

Figure 6.1. *^{1}H NMR spectrum (400 MHz, DMSO-d_6) of HO-Suc-W-OMe* ***31.***

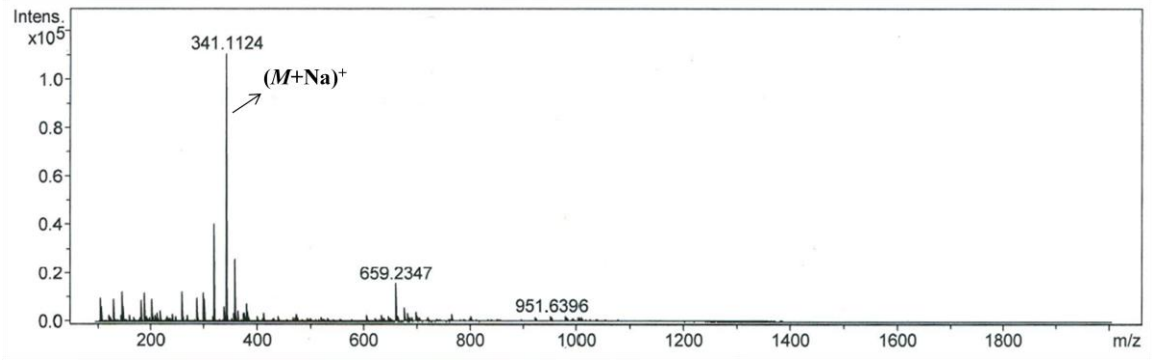

Figure 6.2. *ESI-MS spectrum of HO-Suc-W-OMe* ***31***.

*(b) Synthesis of MeO-Trp(2)-Suc-Trp(1)-OMe **32**:* 2.54 (8 mmol) of HO-Suc-Trp(1)-OMe **31** in 3 mL of DMF was cooled in an ice bath and H-Trp-OMe was isolated from 4.06 g (16 mmol) of the corresponding methyl ester hydrochloride by neutralization and subsequent extraction with ethyl acetate and the ethyl acetate extract was concentrated to 8 mL. It was then added to the reaction mixture, followed immediately by 1.11 g (8.8 mmol, 1 mL 372 μL) DIPC and 1.18 g (8.8 mmol) of HOBt. The reaction mixture was stirred for overnight. The residue was taken up in ethyl acetate (50 mL) and the DCU was filtered off. The organic layer was washed with 1M HCl (3 × 50 mL), brine (2 × 50 mL), 1M sodium carbonate (3 × 50 mL), brine (2 × 50 mL) and dried over anhydrous sodium sulfate and evaporated under vacuum to yield **32** as a white solid. Purification was done by silica gel column (100-200 mesh) using chloroform-methanol (9:2) as eluent.

Yield: 3.10 g (6 mmol, 75%); FT-IR (KBr): ῡ = 3312 (b), 1740 (st), 1647 (st), 1535 (st), 1437 (st), 1458 (ms) cm^{-1}; ^1H NMR (400 MHz, $CDCl_3$, δ_{ppm}): 8.81 (2H, ring -NHs of Trp(1) and Trp(2)), 7.51 (d, *J* = 8 Hz, 2H, ring protons of Trp(1) and Trp(2)), 7.32 (d, *J* = 8 Hz, 2H, ring protons of Trp(1) and Trp(2)), 7.16 (t, *J* = 7.6 Hz, 2H, ring protons of Trp(1) and Trp(2)), 7.08 (t, *J* = 7.4 Hz, 2H, ring protons of Trp(1) and Trp(2)), 6.97 (s, 2H, ring protons of Trp(1) and Trp(2)), 6.81 (d, *J* = 8 Hz, 2H, -NHs of Trp(1) and Trp(2)), 4.80 (m, 2H, $C^{\alpha}Hs$ of Trp(1) and Trp(2)), 3.65 (s, 6H, $COOCH_3$), 3.25 and 3.21 (d, *J* = 5.6 Hz, and *J* = 6.8 Hz, 4H, $C^{\beta}Hs$ of Trp(1) and Trp(2)), 2.39 (m, 4H, $-CH_2-$ of Suc); $[\alpha]_D^{20}$ = + 5.16 (*c* = 0.31 in CH_3OH); MS (ESI) *m/z*: $(M+Na)^+$ Calcd. for $C_{28}H_{30}N_4O_6Na$: 541.2063; found: 541.2088.

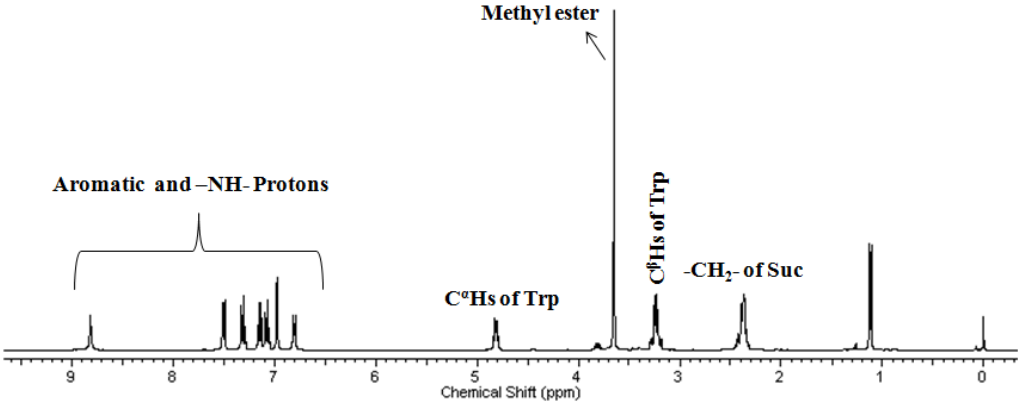

Figure 6.3. *^1H NMR spectrum (400 MHz, $CDCl_3$) of MeO-W-Suc-W-OMe **32**.*

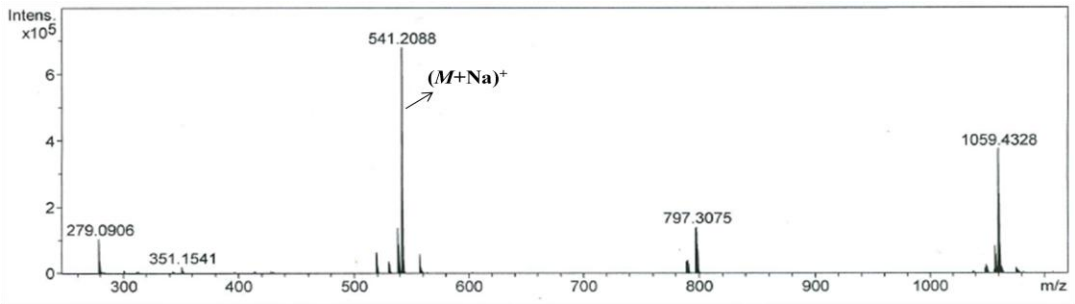

Figure 6.4. *ESI-MS spectrum of MeO-W-Suc-W-OMe* ***32****.*

(c) Synthesis of HO-Trp(2)-Suc-Trp(1)-OH ***33*** *:* 2.59 g (5 mmol) of MeO-Trp(2)-Suc-Trp(1)-OMe **32** in 10 mL MeOH was taken in a round bottom flask and 10 mL of 1M NaOH was added dropwise. The reaction was monitored by thin layer chromatography (TLC). The reaction mixture was stirred for overnight. 15 mL of distilled water was added to the reaction mixture and MeOH was removed under vacuum. The aqueous part was washed with diethyl ether (2 × 30 mL). Then it was cooled down under ice bath for 10 minutes and then pH was adjusted to 1 by drop wise addition of 1M HCl. It was extracted with ethyl acetate (3 × 50 mL) and then the ethyl acetate part was dried over anhydrous Na_2SO_4 and evaporated under vacuum to yield **33** as a white solid.

Yield: 2.30 g (4.7mmol, 94%); FT-IR (KBr): $\tilde{\upsilon}$ = 3419 (w), 3355 (w), 1720 (ms), 1613 (st), 1536 (st), 1454 (ms) cm^{-1}; ^1H NMR (400 MHz, DMSO-d_6, δ_{ppm}): 12.60 (s, 2H, -COOH), 10.89 (2H, ring -NHs of Trp(1) and Trp(2)), 8.22 (d, *J* = 7.6 Hz, 2H, -NHs of Trp(1) and Trp(2)), 7.59 (d, *J* = 8 Hz, 2H, ring protons of Trp(1) and Trp(2)), 7.39 (d, *J* = 8 Hz, 2H, ring protons of Trp(1) and Trp(2)), 7.19 (d, *J* = 2 Hz, 2H, ring protons of Trp(1) and Trp(2)), 7.13 (t, *J* = 7.2 Hz, 2H, ring protons of Trp(1) and Trp(2)), 7.05 (t, *J* = 7.2 Hz, 2H, ring protons of Trp(1) and Trp(2)), 4.51 (m, 2H, C^{α}Hs of Trp(1) and Trp(2)), 3.17 and 3.05 (d, *J* = 5.2 Hz, and *J* = 8 Hz, 4H, C^{β}Hs of Trp(1) and Trp(2)), 2.33 (m, 4H, -CH_2- of Suc); $[\alpha]_D^{20}$ = +15.77 (*c* = 0.3 in CH_3OH); MS (ESI) *m/z*: $(M+Na)^+$ Calcd. For $C_{26}H_{26}N_4O_6Na$: 513.1750; found: 513.1659.

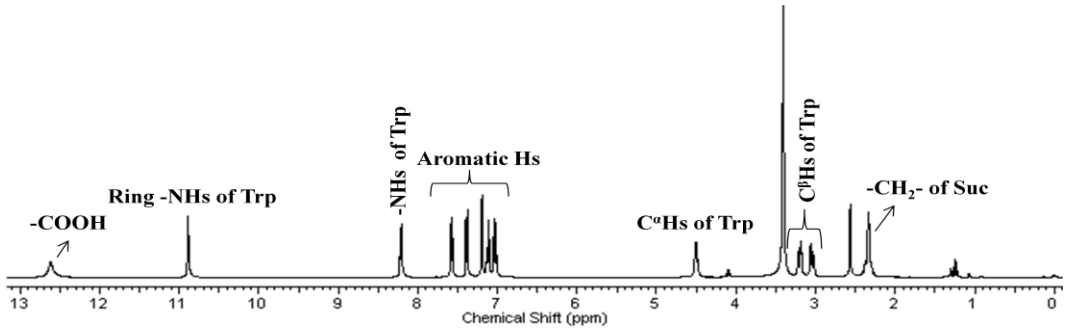

Figure 6.5. *^{1}H NMR spectrum (400 MHz, DMSO-d_6) of HO-W-Suc-W-OH **33**.*

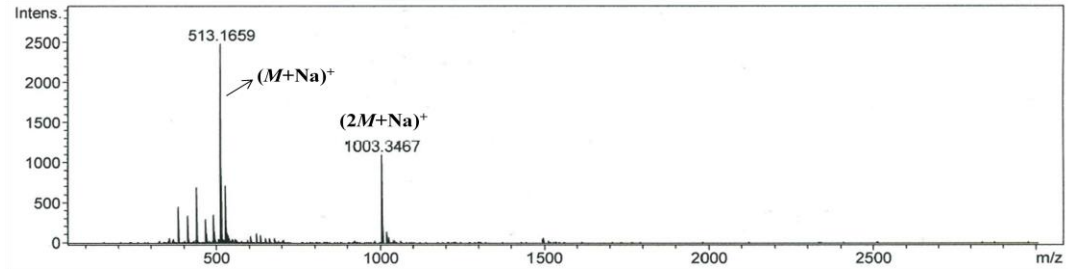

Figure 6.6. *ESI-MS spectrum of HO-W-Suc-W-OH **33**.*

*(d) Synthesis of MeO-Tyr(4)-Trp(3)-Suc-Trp(1)-Tyr(2)-OMe **34**:* 1.96 g (4 mmol) of HO-Trp(2)-Suc-Trp(1)-OH **33** in 5 mL of DMF was cooled in an ice bath and H-Tyr-OMe was isolated from 3.70 g (16 mmol) of the corresponding methyl ester hydrochloride by neutralization and subsequent extraction with ethyl acetate and the ethyl acetate extract was concentrated to 8 mL. It was then added to the reaction mixture, followed immediately by 1.11 g (8.8 mmol, 1 mL 372 μL) DIPC and 1.18 g (8.8 mmol) of HOBt. The reaction mixture was stirred for overnight. The residue was taken up in ethyl acetate (50 mL) and the DIU was filtered off. The organic layer was washed with 1M HCl (3 × 50 mL), brine (2 × 50 mL), 1M sodium carbonate (3 × 50 mL), brine (2 × 50 mL) and dried over anhydrous sodium sulfate and evaporated in vacuum to yield **34** as a white solid. Purification was done by silica gel column (100-200 mesh) using chloroform-methanol (9:1) as eluent.

Yield: 2.70 g (3.2 mmol, 80%); FT-IR (KBr): ϑ = 3292 (st), 1737 (ms), 1640 (st), 1516 (st), 1440 (ms) cm^{-1}; ^{1}H NMR (400 MHz, $CDCl_3$, δ_{ppm}): 9.25 (2H, ring -NHs of Trp(1)

and Trp(3)), 7.50 (d, *J* = 7.2 Hz, 4H, ring protons of Trp(1) and Trp(3)), 7.29 (t, *J* = 7.4 Hz, 4H, ring protons of Trp(1) and Trp(3)), 7.06 (d, *J* = 7.6 Hz, 2H, ring protons of Tyr(2) and Tyr(4)), 6.97 (d, *J* = 7.6 Hz, 2H, -NHs of Tyr(2) and Tyr(4)), 6.88 (d, *J* = 6 Hz, 2H, ring protons of Trp(1) and Trp(3)), 6.77 (d, *J* = 7.6 Hz, 2H, -NHs of Trp(1) and Trp(3)), 6.58 (d, *J* = 8 Hz, 4H, ring protons of Tyr(2) and Tyr(4)), 4.60 (m, 2H, C^{α}Hs of Trp(1) and Trp(3)), 4.58 (m, 2H, C^{α}Hs of Tyr(2) and Tyr(4)), 3.53 (s, 6H, -$COOCH_3$), 3.06 (d, *J* = 6.4 Hz, 4H, C^{β}Hs of Trp(1) and Trp(3)), 2.93 and 2.77 (d, *J* = 8 Hz, and *J* = 7.6 Hz, 4H, C^{β}Hs of Tyr(2) and Tyr(4)), 2.17 (m, 4H, -CH_2- of Suc); $[\alpha]_D^{20}$ = -27.41 (*c* = 0.31 in CH_3OH); MS (ESI) *m/z*: $(M+Na)^+$ Calcd. for $C_{46}H_{48}N_6O_{10}Na$: 867.3330; found: 867.3505

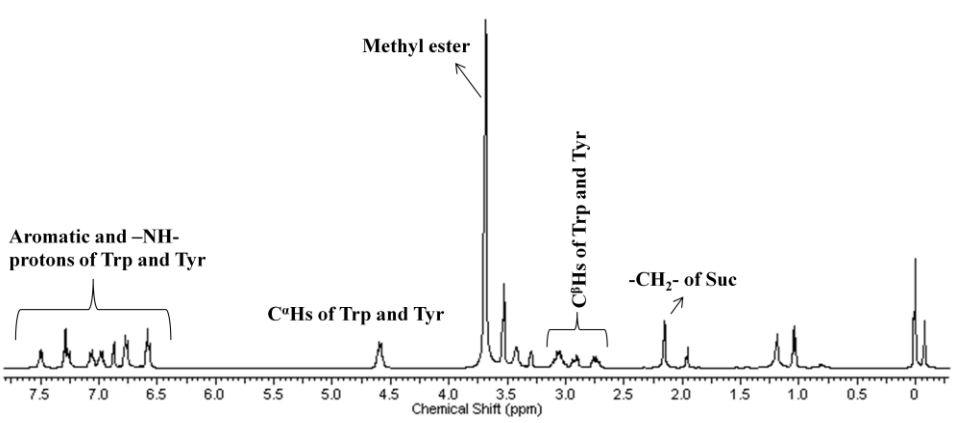

Figure 6.7. *^{1}H NMR spectrum (400 MHz, $CDCl_3$) of MeO-Y-W-Suc-W-Y-OMe* ***34****.*

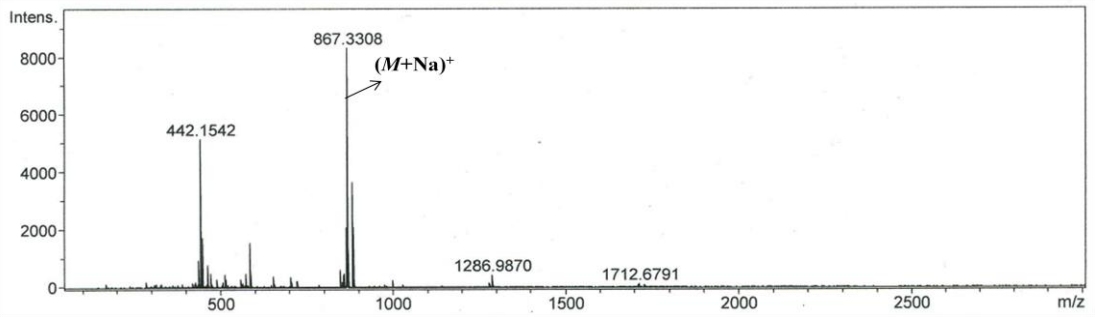

Figure 6.8. *ESI-MS spectrum of MeO-Y-W-Suc-W-Y-OMe* ***34****.*

*(e) Synthesis of HO-Tyr(4)-Trp(3)-Suc-Trp(1)-Tyr(2)-OH **30**:* 1.68 g (2 mmol) of MeO-Tyr(4)-Trp(3)-Suc-Trp(2)-Tyr(1)-OMe **34** in 10 mL MeOH was taken in a round bottom flask and 6 mL of 1M NaOH was added to it dropwise. The reaction was monitored by thin layer chromatography (TLC). The reaction mixture was stirred for 8 hours. 15 mL of distilled water was added to the reaction mixture and MeOH was removed under vacuum. The aqueous part was washed with diethyl ether (2 × 30 mL). Then it was cooled under ice water bath for 10 minutes and then pH was adjusted to 1 by drop wise addition of 1M HCl. It was extracted by ethyl acetate (3 × 50 mL) and then the ethyl acetate part was dried over anhydrous Na_2SO_4 and evaporated under vacuum to yield **30** as a white solid. Yield: 1.55 g (1.9 mmol, 95%); FT-IR (KBr): ῡ = 3394 (st), 3060 (ms), 1725 (m), 1649 (st), 1515 (ms), 1456 (st) cm^{-1}; ^1H NMR (400 MHz, DMSO-d_6, δ_{ppm}): 12.70 (s, 2H, -COOH), 10.80 (2H, ring -NHs of Trp(1) and Trp(3)), 8.15 (d, *J* = 7.2 Hz, 2H, -NHs of Tyr(2) and Tyr(4)), 8.03 (d, *J* = 8 Hz, 2H, -NHs of Trp(1) and Trp(3)), 7.62 (d, *J* = 7.6 Hz, 2H, ring protons of Trp(1) and Trp(3)), 7.37 (d, *J* = 8 Hz, 2H, ring protons of Trp(1) and Trp(3)), 7.14 (2H, ring protons of Trp(1) and Trp(3)), 7.11 (t, *J* = 7.4 Hz, 2H, ring protons of Trp(1) and Trp(2)), 7.06 (d, *J* = 8.4 Hz, 2H, ring protons of Tyr(2) and Tyr(4)), 7.02 (t, *J* = 7.6 Hz, 2H, ring protons of Trp(1) and Trp(3)), 6.71 (d, *J* = 8.4 Hz, 2H, ring protons of Tyr(2) and Tyr(4)), 4.58 (m, 2H, C^{α}Hs of Trp(1) and Trp(3)), 4.38 (m, 2H, C^{α}Hs of Tyr(2) and Tyr(4)), 3.16 and 3.01 (d, *J* = 4 Hz, and *J* = 5.2 Hz, 4H, C^{β}Hs of Trp(1) and Trp(3)), 2.91 and 2.88 (d, *J* = 5.6 Hz, and *J* = 6.8 Hz, 4H, C^{β}Hs of Tyr(2) and Tyr(4)), 2.30 (m, 4H, -CH_2- of Suc); ^{13}C NMR (100 MHz, DMSO-d_6, δ_{ppm}): 172.82, 171.49, 171.19, 155.88, 135.95, 130.06, 127.42, 127.30, 123.45, 120.76, 118.13, 114.94, 111.20, 110.19, 53.88, 53.18, 35.92, 30.73, 27.53, 23.26; $[\alpha]_D^{20}$ = -15.29 (*c* = 0.33 in CH_3OH); MS (ESI) *m/z*: $(M+Na)^+$ Calcd. for $C_{44}H_{44}N_6O_{10}Na$: 839.3017; found: 839.3036.

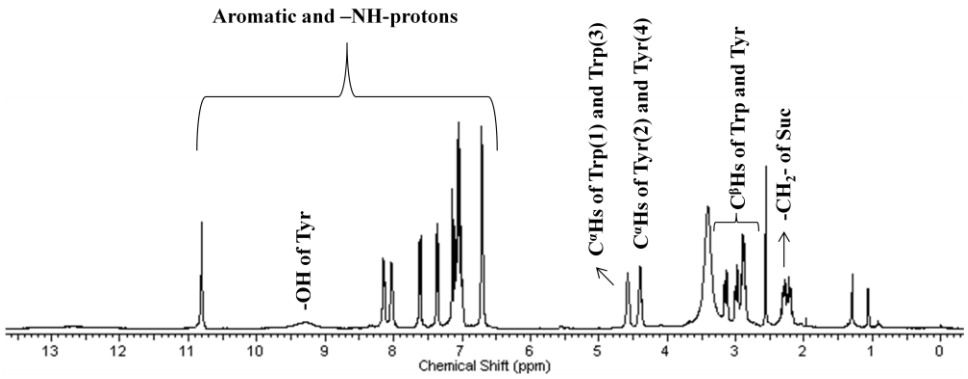

Figure 6.9. *^{1}H NMR spectrum (400 MHz, DMSO-d_6) of HO-Y-W-Suc-W-Y-OH* ***30.***

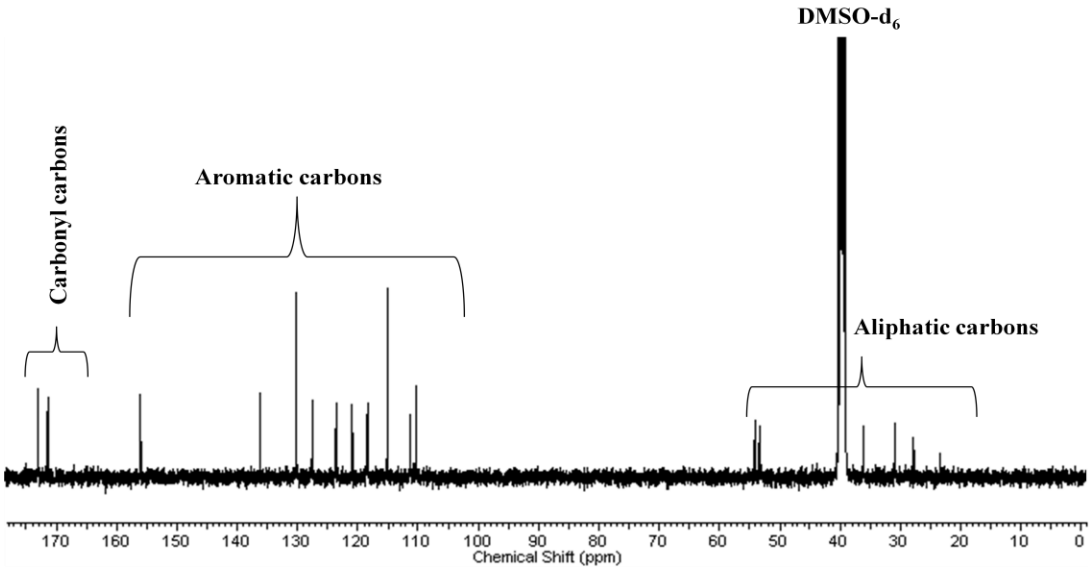

Figure 6.10. *^{13}C NMR spectrum (100 MHz, DMSO-d_6) of HO-Y-W-Suc-W-Y-OH* ***30.***

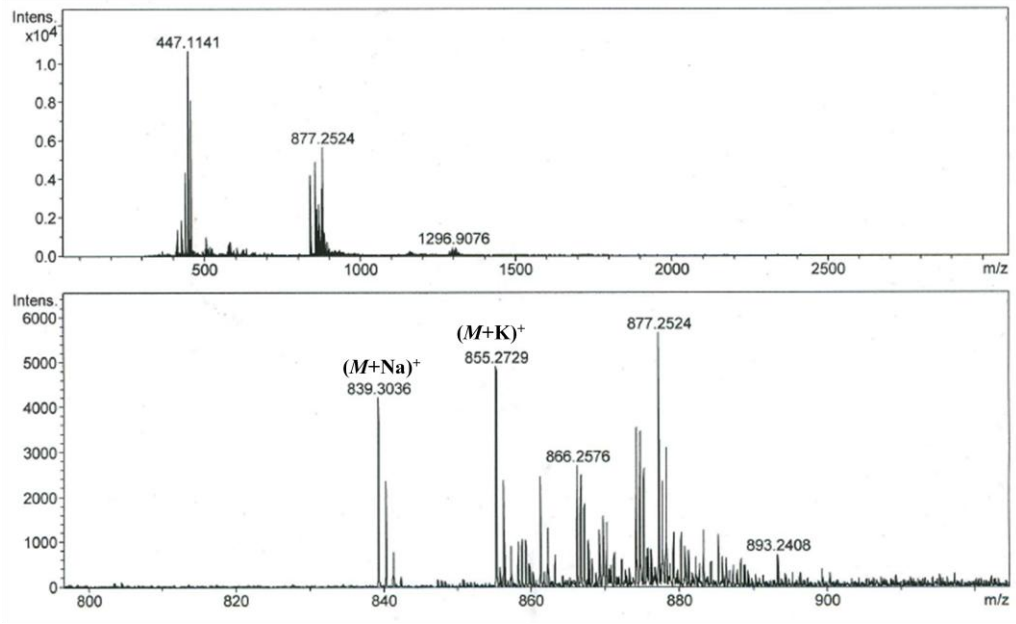

Figure 6.11. *ESI-MS spectra of HO-Y-W-Suc-W-Y-OH* ***30.***

6.2.2 Synthesis of Compounds for Deprotection Reaction

(a) Synthesis of Boc-Tyr-C_{hex}-OH ***D3****:*

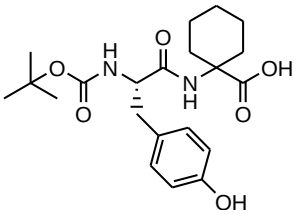

^{1}H NMR (400 MHz, DMSO-d_6, δ_{ppm}): 12.09 (s, 2H, -COOH), 7.68 (s, 1H, -NH- of C_{hex}), 7.04 (d, J = 8 Hz, 2H, ring protons of Tyr), 6.73 (d, J = 8.8 Hz, 1H, -NH- of Tyr), 6.65 (d, J = 8 Hz, 2H, ring protons of Tyr), 4.13 (m, 1H, $C^{\alpha}H$ of Tyr), 2.81 (d, J = 3.2 Hz, 2H, $C^{\beta}Hs$ of Tyr), 1.62 and 1.49 (m, 10H, ring protons of C_{hex}), 1.31 (s, 9H, -CH_3 of Boc-); MS (ESI) *m/z*: $(M+Na)^+$ Calcd. for $C_{21}H_{30}N_2O_6Na$: 429.2002; found 429.2003.

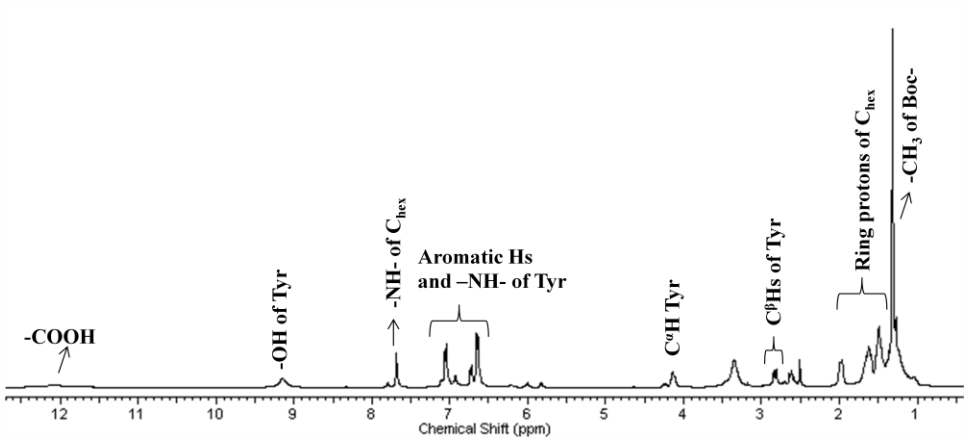

Figure 6.12. *^{1}H NMR spectrum (400 MHz, DMSO-d_6) of Boc-Tyr-C_{hex}-OH* ***D3.***

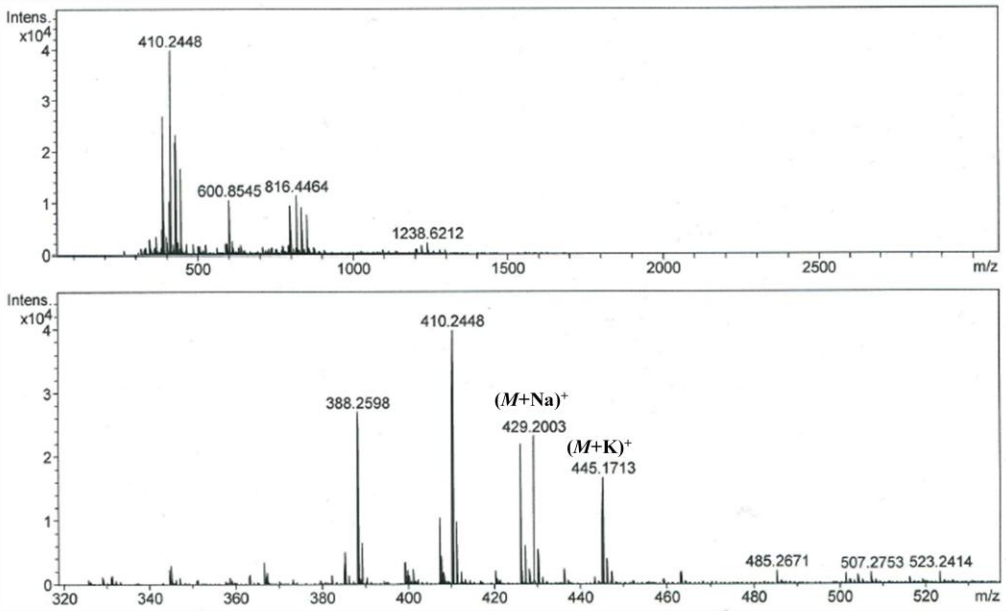

Figure 6.13. *ESI-MS spectra of Boc-Tyr-C_{hex}-OH* ***D3.***

(b) Synthesis of Boc-Tyr-C_{hex}-Aib-OH ***D4****:*

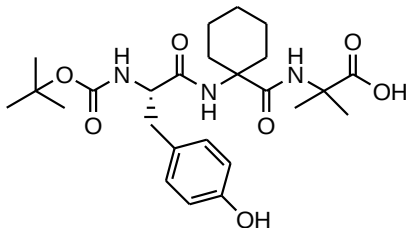

^{1}H NMR (400 MHz, DMSO-d_6, δ_{ppm}): 12.05 (s, 2H, -COOH), 7.66 (s, 1H, -NH- of C_{hex}), 7.27 (s, 1H, -NH- of Aib), 7.11 (d, *J* = 7.6 Hz, 2H, ring protons of Tyr), 7.00 (d, *J* = 6.4 Hz, 1H, -NH- of Tyr), 6.65 (d, *J* = 7.6 Hz, 2H, ring protons of Tyr), 4.15 (m, 1H, $C^{\alpha}H$ of Tyr), 2.82 (d, *J* = 4.8 Hz, 2H, $C^{\beta}Hs$ of Tyr), 1.55 and 1.43 (s, 6H of Aib), 1.35 (m, 10H, ring protons of C_{hex}), 1.30 (s, 9H, -CH_3 of Boc-); MS (ESI) *m/z*: $(M+Na)^+$ Calcd. for $C_{25}H_{37}N_3O_7Na$: 514.2529; found 514.2473.

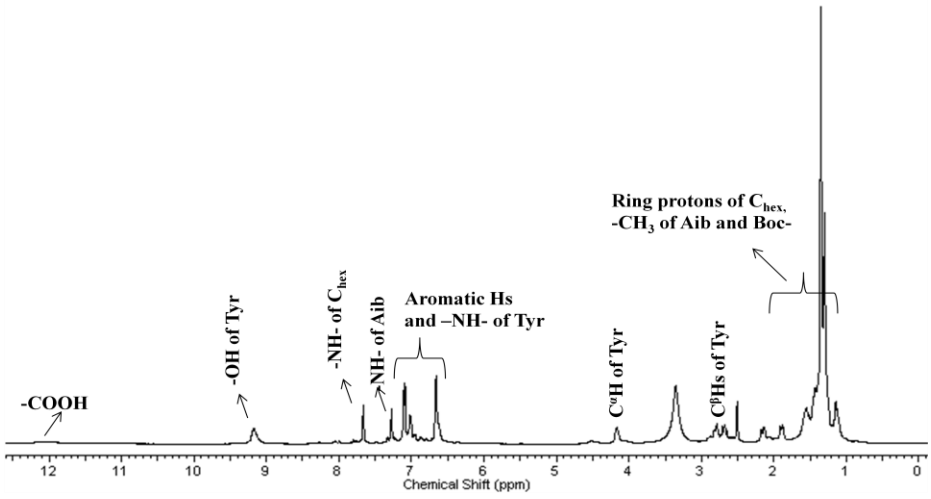

Figure 6.14. *^{1}H NMR spectrum (400 MHz, DMSO-d_6) of Boc-Tyr-C_{hex}-Aib-OH* ***D4.***

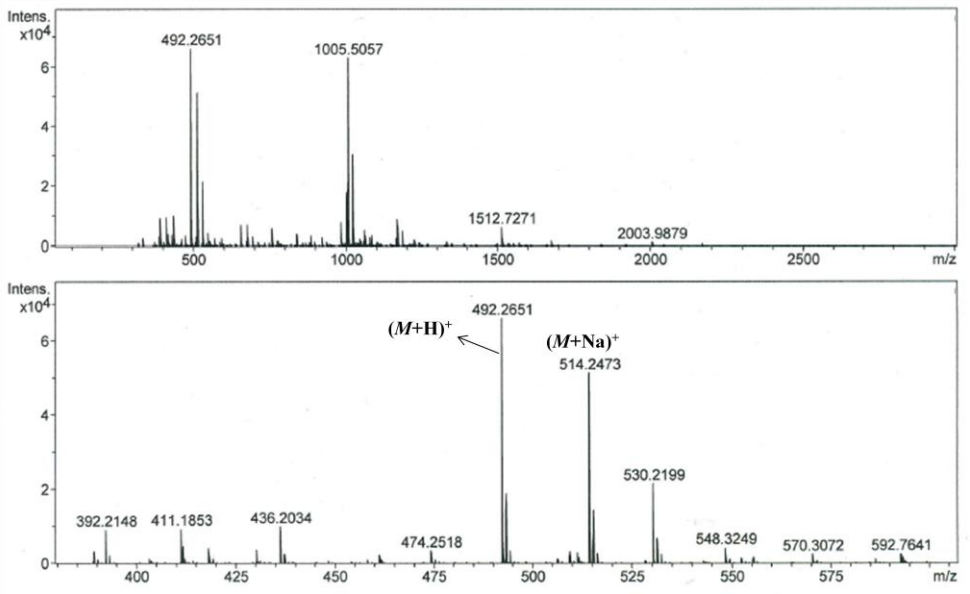

Figure 6.15. *ESI-MS spectra of Boc-Tyr-C_{hex}-Aib-OH* ***D4.***

(c) Synthesis of Nmoc-Phe(1)-Phe(2)-OH ***D8:***

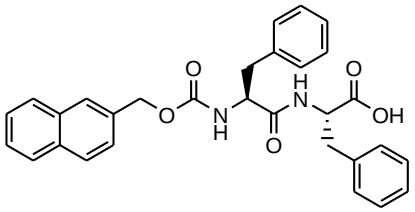

^{1}H NMR (400 MHz, DMSO-d_6, δ_{ppm}): 8.29 (d, *J* = 8 Hz, -NH- of Phe(2)), 7.88 (d, *J* = 9.6 Hz, 3H, ring protons of Nmoc-), 7.76 (s, 1H, ring protons of Nmoc-), 7.50 (m, 2H, ring protons of Nmoc-), 7.36 (d, *J* = 8 Hz, -NH- of Phe(1)), 7.23-7.20 (m, 10H, aromatic protons of Phe(1) and Phe(2)), 7.18 (d, *J* = 6.4 Hz, 1H, ring protons of Nmoc-), 5.08 (s, 2H, -CH_2-of Nmoc), 4.46 and 4.29 (m, 2H, C^{α}Hs of Phe(1) and Phe(2)), 3.06 and 2.95 (d, *J* = 8.4 Hz and *J* = 9.6 4H, C^{β}Hs of Phe(1) and Phe(2)); MS (ESI) *m/z*: $(M+Na)^+$ Calcd. for $C_{30}H_{28}N_2O_5Na$: 519.5435; found 519.3244.

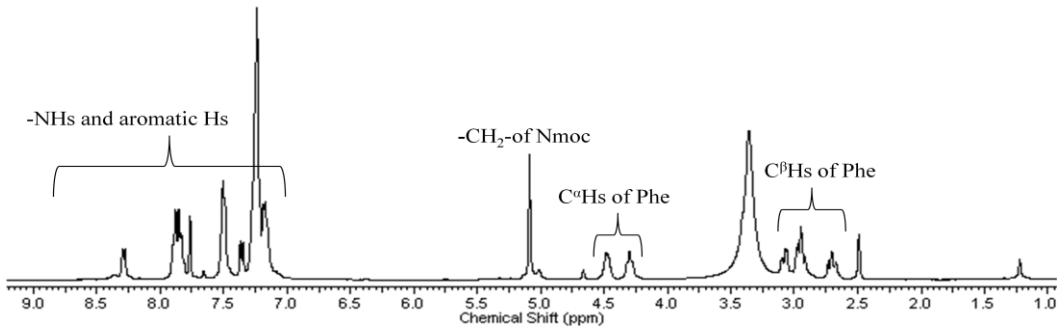

Figure 6.16. *^{1}H NMR spectrum (400 MHz, DMSO-d_6) of Nmoc-Phe(1)-Phe(2)-OH* ***D8.***

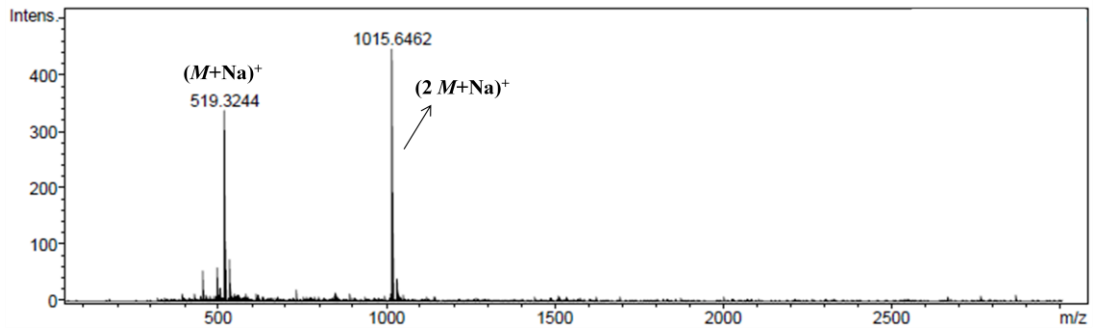

Figure 6.17. *ESI-MS spectrum of Nmoc-Phe(1)-Phe(2)-OH* ***D8.***

6.3 Method and Characterization Techniques

6.3.1 Preparation of the Hydrogel

Peptide bolaamphiphile **30** (HO-Y-W-Suc-W-Y-OH; 16.8 mg, 10 mmol L^{-1}) was dispersed in sodium phosphate buffer solution (2 mL, pH 8, 10 mmol L^{-1}) and sonicated for 5 min. A self-supporting hydrogel formed after 10 min.

6.3.2 Synthesis of Pd Nanoparticles

Pd nanoparticles were synthesized in a hydrogel matrix without the addition of any external reducing agent. In our experiment, peptide bolaamphiphile molecules with tyrosine and tryptophan residues (10 mmol L^{-1}) were sonicated to enable dissolution in phosphate buffer (2 mL) and then $PdCl_2$ (2.8 mmol L^{-1}) was mixed followed by sonication for 5 min. It was seen that the gel became brown after 2 h, which is an indication of the formation of Pd nanoparticles inside the hydrogel matrix.

6.3.3 Catalytic Studies

The peptide bolaamphiphile hydrogel (2 mL, 10 mmol) containing Pd nanoparticles (0.006 to 0.01 mmol) was used for catalytic studies. In a typical experiment, the N-terminus amino acid or peptide substrate (0.1 mmol; Table 1, entries 1 to 8) was dissolved in water/methanol (1:1) solution (1 mL). The peptide hydrogel (1 mL, 10 mmol) containing Pd nanoparticles (0.006 to 0.01 mmol) was added to the substrate (compounds D2 to D 9) and cooled in an ice bath for 5 min. After cooling, $NaBH_4$ (0.264 mmol) was added and sealed in the reaction tube. The reaction mixture was stirred and the reaction was completed within 2 h at room temperature. $NaBH_4$ plays an important role in the reductive cleavage of N-protected groups. $NaBH_4$ provides H^- for reductive cleavage of N-terminus protecting groups. The success of the catalytic effect of Pd nanoparticles on the deprotection reaction was confirmed by mass spectral studies. For a control experiment, Pd nanoparticles were synthesized by reduction of Pd^{2+} with $NaBH_4$. $PdCl_2$ (1 mg, 0.0056 mmol, 2.8 mmol L^{-1}) was dissolved in methanol/water (1:1; 2 mL) and cooled in an ice bath for 5 min. $NaBH_4$ (0.529 mmol) was added to the above reaction mixture to reduce Pd^{2+} to Pd. The Pd nanoparticles were isolated by centrifugation followed by washing with methanol/water (1:1) solution. The protected amino acid (0.1 mmol) was dissolved in methanol/water (1:1; 1 mL) and Pd nanoparticles (0.01 mmol) were added to it. After cooling for 5 min, $NaBH_4$ (0.264 mmol) was added to the reaction mixture and the reaction tube was sealed. The reaction mixture was kept stirring for 2 h at room temperature to allow the deprotection reactions to occur. After 2 h, the reaction was monitored by mass analysis.

6.3.4 HRTEM Study

High-resolution transmission electron microscopic images were recorded using a PHILIPS electron microscope (model: CM 200) operated at an accelerating voltage of 200 kV. Dilute solution of the Pd nanoparticles embedded in the hydrogel was dried on carbon coated copper grids (300 mesh) by slow evaporation in air, then allowed to dry separately under vacuum at room temperature. The average size of the nanoparticles was determined from the TEM images.

6.4 Results and Discussion

6.4.1 Preparation of the Hydrogel

The synthesized peptide bolaamphiphile molecule **30** (HO-Y-W-Suc-W-Y-OH, Y = tyrosine and W = tryptophan) is capable of forming a self-supporting hydrogel in phosphate buffer (pH 8, 10 mmol) upon sonication. Peptide bolaamphiphile **30** (HO-Y-W-Suc-W-Y-OH; 16.8 mg, 10 mmol L^{-1}) was dispersed in sodium phosphate buffer solution (2 mL; pH 8, 10 mmol L^{-1}) and sonicated for 5 min. A self-supporting hydrogel was formed after only 10 min. The amino acid sequence including tryptophan and tyrosine was chosen for its delicate balance of hydrophobic/hydrophilic character, which helps the hydrogelation process.

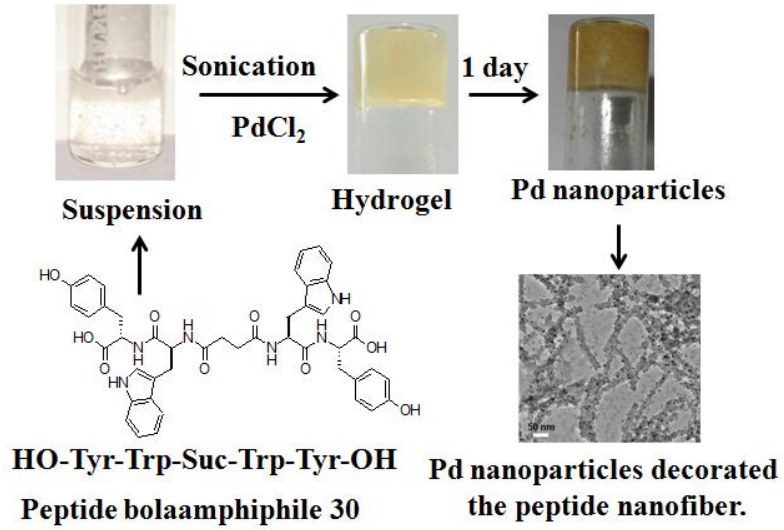

Scheme 6.2. *A self-supporting hydrogel was formed by the self-assembly of peptide bolaamphiphile **30** upon sonication. The hydrogel matrix was used for in situ generation of Pd nanoparticles, which were stabilized and decorated on the surface of peptide bolaamphiphile nanofibers.*

6.4.2 Rheological Study

The mechanical property of the hydrogel was characterized by using an oscillating rheometer. Rheological analysis showed that the storage modulus (G') is greater than the loss modulus (G") for peptide hydrogel **30**. In the frequency sweep mode, the values of the storage modulus (G') exceed that of the loss modulus (G") by a factor of 5-10 times

that of hydrogel **30**, which indicates the formation of a strong and rigid hydrogel (Figure 6.18).[49]

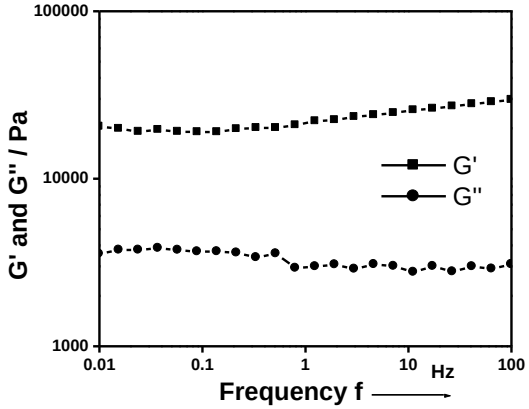

Figure 6.18. *Frequency sweep of peptide bolaamphiphile hydrogel **30** (c = 10 mmol L^{-1}). Storage modulus G' is higher than the loss modulus G''. G'>10^4 Pa at low frequency, and the storage modulus is higher than the loss modulus by a factor of 5-10, which indicates excellent solid-like behavior of the gel materials.*

6.4.3 FT-IR and CD Studies

An FTIR study was carried out to obtain the secondary structure of peptide bolaamphiphile **30** in the gel state (Figure 6.19a). In the gel state, two peaks appeared at 1714 and 1736 cm^{-1}, which suggests that some of the carboxylic acid groups are involved in hydrogen-bonding interactions (1714 cm^{-1}), whereas some of them are free (1736 cm^{-1}). The characteristic amide I band appeared at 1635 and 1615 cm^{-1} along with an amide II band at 1516 cm^{-1}, which indicate that the peptide bolaamphiphiles self-assemble into a supramolecular β-sheet structure through hydrogen-bonding interactions.[50] The self-assembly of the peptide bolaamphiphiles was also examined by circular dichroism (CD) spectroscopy to realize the role of the chirality of the individual molecules owing to the presence of the chiral amino acid moieties (Figure 6.19b). The hydrogel was diluted to a 100 μm concentration in phosphate buffer to investigate the nature of the secondary structure of the self-assembled peptide bolaamphiphile molecules. The CD spectrum showed a characteristic positive peak at around 198 nm and a negative peak at 211 nm, which is attributed to the n-π* transition of the CO-NH groups of the peptide

bolaamphiphile molecule. This signature is analogous to the reported CD signature of peptides adopting the β-sheet secondary structure.[51]

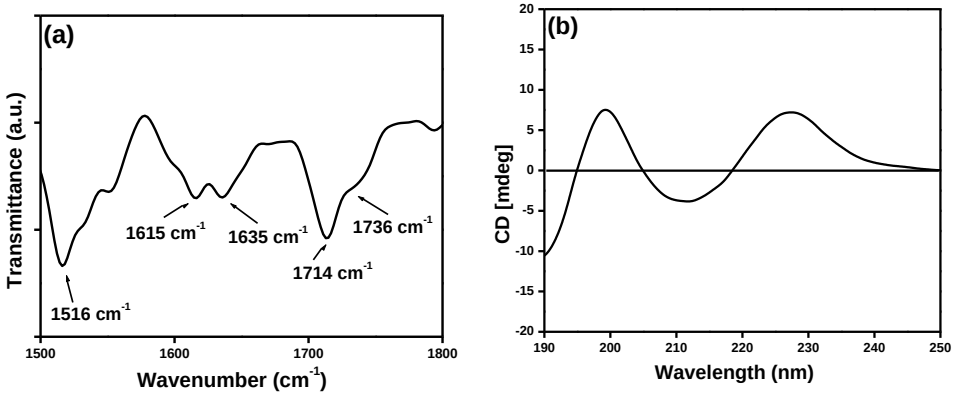

Figure 6.19. *(a) FTIR spectrum of peptide bolaamphiphile hydrogel **30** (c = 10 mmol L^{-1}), which indicates the formation of a supramolecular β-sheet structure in the gel phase and (b) the CD spectrum of hydrogel **30** (c = 100 μm) reveals the formation of a β-sheet structure through extensive hydrogen-bonding interactions.*

This observation indicates that the gelator molecules self-assemble into a β-sheet structure through extensive hydrogen-bonding interactions. Another strong positive band appeared at 230 nm, which is attributed to the electron-transfer transition involving excitation of the nonbonding electron of the oxygen atom into the π* orbital system of the aromatic ring of the tyrosine moiety.[52]

6.4.4 Fluorescence Study

Fluorescence spectroscopy results suggest that the π-stacking interaction also plays a key role in the self-assembly process towards hydrogel formation (Figure 6.20). The emission peak of the aromatic phenolic groups of tyrosine residues and indole groups of tryptophan residues at 380 nm after 10 min shifts to 388 nm after 1 day for hydrogel **30**, which suggests that the aromatic groups are overlapped. The redshift of the emission maxima occurs as a result of the extensive self-assembly of gelator molecules through π-π stacking interactions and the decrease in intensity results from the quenching of the aromatic core present in gelator molecules during the self-assembly process.[53] Another

important emission maxima at 468 nm supports the formation of a higher ordered supramolecular nanostructure.[26]

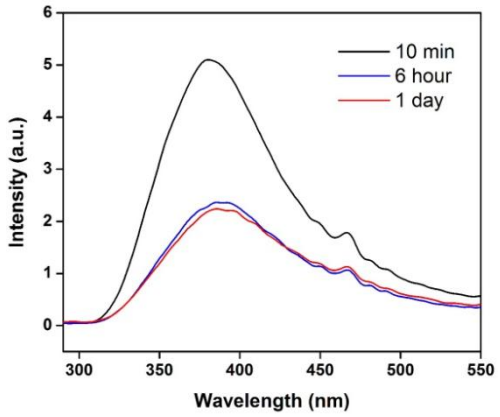

Figure 6.20. *The fluorescence spectra of the peptide bolaamphiphile hydrogel* ***30*** *(c = 10 mmol* L^{-1}*), the results of which suggest extensive* π-π *stacking interactions between the aromatic residues of peptide bolaamphiphile* ***30*** *during the self-assembly process.*

6.4.5 Morphological Study

The nanostructural morphology [54-59] of hydrogel **30** was characterized by field-emission scanning electron microscopy (FESEM) and atomic force microscopy (AFM) (Figure 6.21).

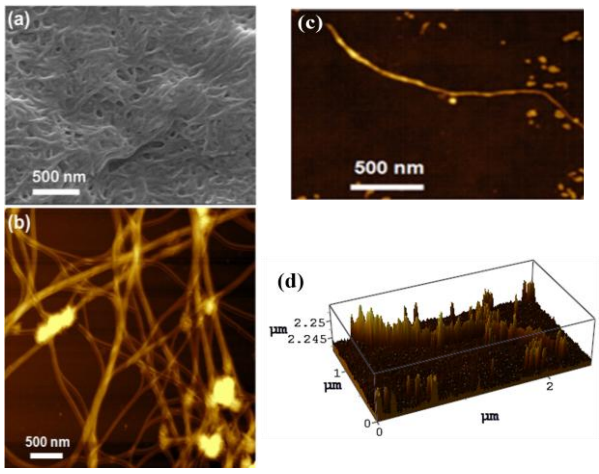

Figure 6.21. *(a) A SEM image showing the entangled nanofibrous aggregates and (b) an AFM image showing the nanofiber morphology of hydrogel* ***30****. (c) AFM image of peptide bolaamphiphile hydrogel* ***30*** *and it's (d) three dimensional image.*

The FESEM image of the hydrogel shows that compound **30** assembled into dense entangled fibrous networks with fiber diameters of (25±5) nm and lengths of several millimeters. The AFM image also shows that the peptide bolaamphiphile molecules self-assembled into nanofibrillar structures. The average diameter of the fibers was found to be 30 nm and the average height of an individual fiber was 4 nm (Figure 6.21d).

6.4.6 Powder Wide-Angle X-Ray Scattering (WAXS) Study

To obtain further structural information, powder wide-angle X-ray scattering (WAXS) was used to characterize peptide bolaamphiphile **30** and its dried hydrogel (Figure 6.22). We correlated the different features of self-assembled **30** from the series of characteristic reflection patterns obtained from the wide-angle powder X-ray diffraction. Two reflection peaks at 2θ = 13.14 and 20.05° were observed for powdered compound **30**, whereas the dried hydrogel **30** showed several characteristic reflection peaks. The characteristic peak at 2θ = 7.82°, corresponding to a d spacing of 11.29Å, is a signature of a β-sheet structure, which is adopted by self-assembled peptide molecules. This reflection pattern indicates the distance between two successive β sheets, that is, the intersheet distance.

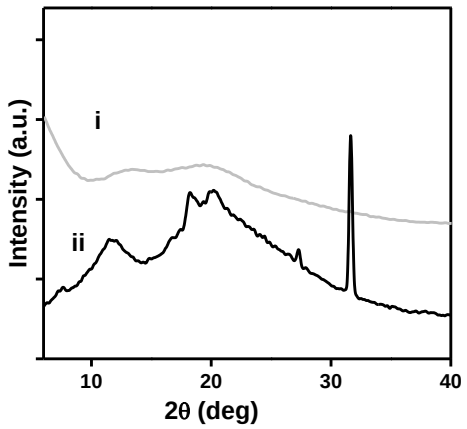

Figure 6.22. *Wide-angle powder XRD pattern of (i) peptide bolaamphiphile **30** powder and (ii) its dried hydrogel **30**. The powder X-ray diffraction pattern exhibits the characteristic pattern of a β-sheet structure of peptide bolaamphiphile **30**, which is adopted through π–π stacking interactions between the aromatic moieties through the self-assembly process.*

The characteristic peak at 2θ = 18.15°, corresponding to a d spacing of 4.88 Å, reveals the spacing between two peptide molecules within the same β-sheet structure.[60] Another reflection peak at 2θ = 27.35° (d spacing of 3.26 Å) is expected from the π-π stacking interaction[61] between two aromatic groups, which also plays a vital role during the self-assembly process along with hydrogen-bonding interactions.

6.4.7 Generation and Characterization of Pd Nanoparticles

The redox-active tyrosine and tryptophan-based peptide bolaamphiphile **30** was used to synthesize Pd nanoparticles in its hydrogel matrix. Pd nanoparticles were synthesized in the hydrogel matrix without addition of any external reducing agent. Redox-active tyrosine and tryptophan molecules in peptide bolaamphiphile molecules reduced Pd^{2+} to Pd^0.[12,62] The synthesized Pd nanoparticles were stabilized by the peptide bolaamphiphile nanofibers. In our experiment, peptide bolaamphiphiles were sonicated to dissolve them in phosphate buffer and then $PdCl_2$ was mixed and sonicated for 5 min. The colour of the solution changed to brown within 2 hours, which is an indication of the formation of Pd nanoparticles. The nanoparticles were characterized by UV/Vis spectroscopy and transmission electron microscopy. The $PdCl_2$ salt was dissolved in phosphate buffer and analyzed by UV/Vis spectroscopy.

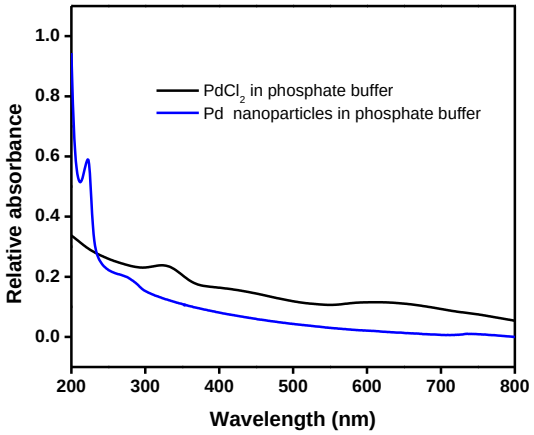

Figure 6.23. *UV/Vis spectra used to monitor the synthesis of Pd nanoparticles in gel nanofibers. The black line indicates $PdCl_2$ in phosphate buffer whereas the blue line indicates the generation of Pd nanoparticles.*

The UV/Vis spectra showed one characteristic peak at around 332 nm and another weak intensity peak at 430 nm for the $PdCl_2$ salt. After the generation of Pd nanoparticles, the solution was centrifuged three times and washed with methanol. The black mass was dispersed in phosphate buffer and characterized by UV/Vis spectroscopy. The UV/Vis spectrum showed that the peaks at 332 and 430 nm completely disappeared and a new peak appeared at 274 nm. The absorption band at 274 nm is attributed to Pd^0 nanoparticles (Figure 6.23).[27,63] After the synthesis of Pd nanoparticles in the hydrogel matrix, the size of the nanoparticles was investigated by transmission electron microscopy. The TEM images of the in situ synthesized nanoparticles in the hydrogel showed that the diameter of the nanoparticles increased with reaction time. TEM images revealed that the diameter of the Pd nanoparticles is 3 to 5 nm after 3 hours of reaction time (Figure 6.24a) and the Pd nanoparticles were decorated on the peptide nanofibers. Peptide bolaamphiphile **30** consists of tyrosine and tryptophan residues along with two carboxylic acid groups. The Pd nanoparticles are stabilized by carboxylic acid groups. The attachment of Pd nanoparticles on the surface of peptide bolaamphiphile nanofibers is due to the charges on $-COO^-$ in peptide bolaamphiphile **30**.[7] Another possibility is that the CO and NH of amide bonds, which do not participate in backbone hydrogen bonding, may play a crucial role in decoration.[8]

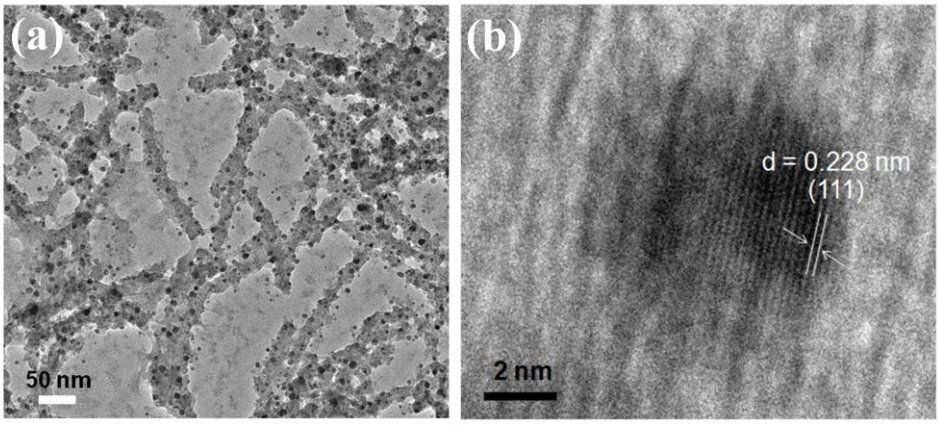

Figure 6.24. *(a) A TEM image of the Pd nanoparticles after 3 h of reaction time. The Pd nanoparticles were decorated and stabilized on the surface of the peptide nanofibers. The scale bar is 50 nm. (b) The HRTEM image of a Pd nanoparticle showing the lattice fringes.*

We characterized the Pd nanoparticles by HRTEM. The HRTEM image shows clear lattice fringes with a d spacing of 0.228 nm, which is attributed to the (111) lattice planes [64] of face-centered cubic (fcc) Pd (Figure 6.24b). The HRTEM image confirms the formation of crystalline Pd nanoparticles.

6.4.8 Catalytic Activity of Pd Nanoparticles

Pd nanoparticles have many potential applications. One of the most important applications is to act as a nanocatalyst in many chemical reactions.[65,66] The in situ synthesized Pd nanoparticles with a diameter of 3-9 nm were used as a potential catalyst for the deprotection of various types of N-protected amino acids and peptides (Scheme 6.3).

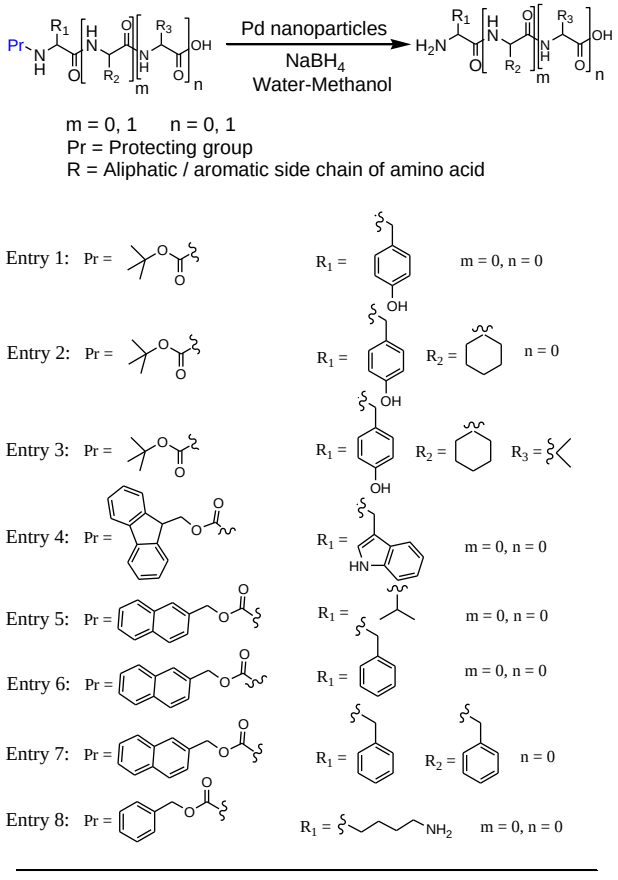

Scheme 6.3. *The palladium-nanoparticle-catalyzed deprotection reaction of N-terminus amino acids and peptides.*

Table 6.1. *Summary of the deprotection reactions.*

Entry	Substrate (N-terminus protected amino acids or peptides)[a]	Product (deprotected amino acid or peptide)[b]	Time (min.)	Isolated yield (%)
1	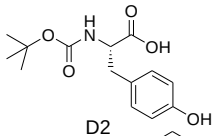 D2	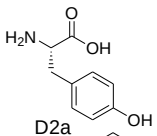 D2a	60	87
2	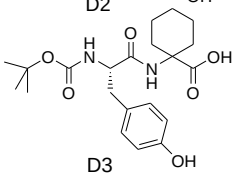 D3	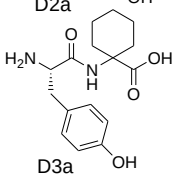 D3a	60	80
3	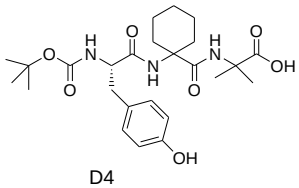 D4	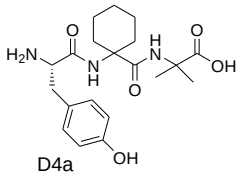 D4a	60	82
4	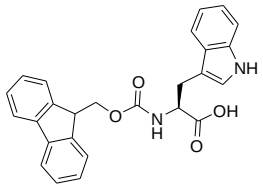 D5	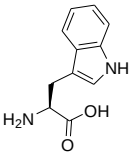 D5a	60	90
5	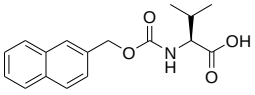 D6	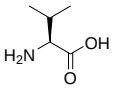 D6a	80	88
6	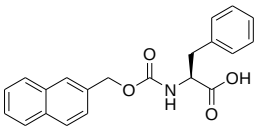 D7	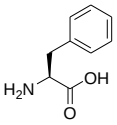 D7a	80	85
7	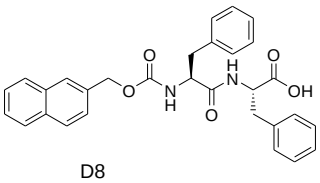 D8	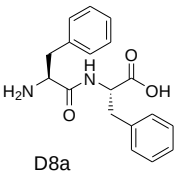 D8a	90	78
8	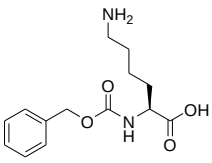 D9	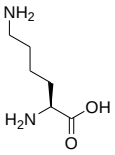 D9a	120	90

[a] The number as D2, D3, D4...refers the specific substrate, which is used for deprotection reaction, [b] The products D2a, D3a, D4a.....obtained from the corressponding substrates after peptide nanofibers decorated Pd catalyzed deprotection reactions.

Pd nanoparticles in the presence of $NaBH_4$ were effectively used for deprotection reactions. The catalytic activity was examined with different types of N-terminus (Boc-, Cbz-, Fmoc-, and Nmoc) amino acids and peptides (Table 6.1). All of these palladium-catalyzed deprotection reactions were carried out in a water/methanol (1:1) solution at room temperature. Peptide-nanofiber-supported Pd nanoparticles completed the reaction within 2 hours and all the reactions were monitored by mass spectrometry. Boc and Nmoc groups were deprotected by acid whereas Fmoc group was deprotected by base. This novel method can effectively deprotect Boc, Nmoc and Fmoc groups from the N-protected amino acids or peptides. N-terminus protected Cbz group is stable towards acid or base. In this case, palladium-nanoparticle-catalyzed deprotection reactions are very effective. For the Nmoc-protected amino acid or peptide, the reactions give unprotected amino acid or peptide and the corresponding naphthalene methanol. The isolated yield was about 80-90% for all the reactions. After the first batch of reactions, the Pd nanoparticles were recovered by using centrifugation and washing of the reaction mixture. The recovered Pd nanoparticles were also used for deprotection reactions, which were completed successfully within 2 hours. Here, peptide-nanofiber-supported Pd nanoparticles act as an efficient catalyst for deprotection reactions. Pd nanoparticles were also synthesized without a peptide support to determine the catalytic effect of the deprotection reactions. The Boc-protected tyrosine remained unaffected by the catalysis reaction. No significant yield was observed for the palladium-catalyzed deprotection reactions with Nmoc-Phe-OH and Cbz-protected lysine (Table 6.2). In a control experiment, the Pd nanoparticles were synthesized by reduction of Pd^{2+} with $NaBH_4$ without peptide nanofibers. These Pd nanoparticles are not stable in methanol/water solvent and the Pd nanoparticles aggregate. The Pd nanoparticles lose their catalytic activity owing to aggregation, whereas the peptide-bolaamphiphile-supported Pd nanoparticles are stable and show efficient catalytic activity in deprotection reactions. Several control experiments were performed without the Pd nanoparticle catalyst. The N-protected amino acids and peptides were treated with only $NaBH_4$ for 5 hours. The Fmoc group of Fmoc-Trp-OH (substrate 5) was deprotected with 48% yield. Boc-, Nmoc, and Cbz-protected substrates remained silent (Table 6.3) under the same conditions. So,

peptide nanofiber-supported Pd nanoparticles play a vital role in the deprotection reactions.

Table 6.2. *Deprotection reactions with Pd nanoparticles without peptide nanofibers*

Entry	Substrate (N-terminus protected amino acids or peptides)[a]	Product (deprotected amino acid or peptide)[b]	Time (min.)	Isolated yield (%)
1	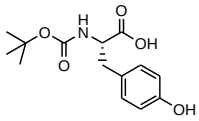	No reaction	120	0
2	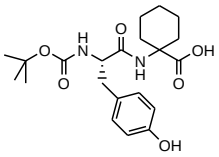	No reaction	120	0
3	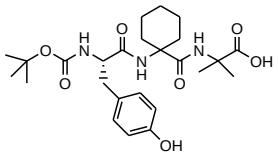	No reaction	120	0
4	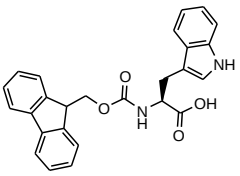	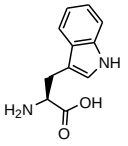	120	65
5	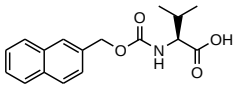	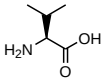	120	45
6	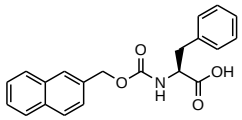	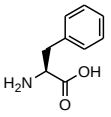	120	42
7	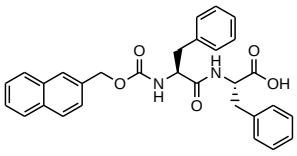	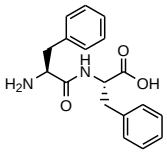	120	38
8	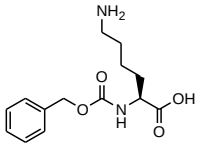	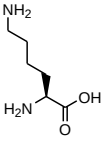	120	10

[a] substrates, which are used for deprotection reaction, [b] The products obtained from the corressponding substrates after Pd catalyzed deprotection reactions without peptide nanofibers.

Table 6.3. *Deprotection reactions with NaBH4 without Pd nanoparticles catalyst*

Entry	Substrate (N-terminus protected amino acids or peptides)[a]	Product (deprotected amino acid or peptide)[b]	Time (min.)	Isolated yield (%)
1	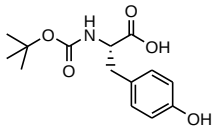	No reaction	120	0
2	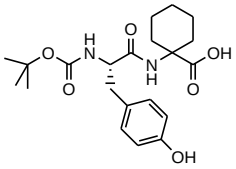	No reaction	120	0
3	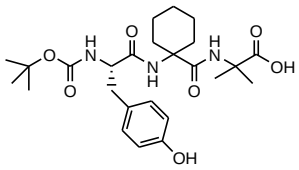	No reaction	120	0
4	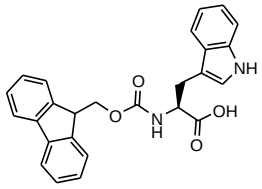	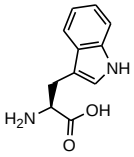	120	48
5	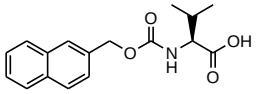	No reaction	120	0
6	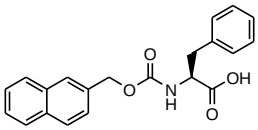	No reaction	120	0
7	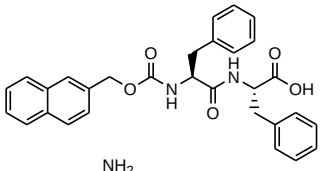	No reaction	120	0
8	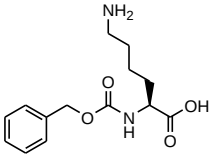	No reaction	120	0

[a] substrates, which are used for deprotection reaction, [b] The products obtained from the corressponding substrates after the treatment of $NaBH_4$ without Pd nanoparticles.

6.5 Conclusion

The tyrosine and tryptophan-containing bolaamphiphile peptide forms a self-supporting hydrogel upon sonication under physiological conditions. The self-assembly process was studied through CD, fluorescence spectroscopy, and rheological experiments. Hydrogen bonding and π-stacking interactions are the driving force for the formation of the self-assembled peptide hydrogel. The SEM and AFM images reveal that the bolaamphiphile peptide molecules self-assembled into nanofibrillar structures. Furthermore, peptide nanofibers were used as a template for in situ generation of Pd nanoparticles. Peptidenanofiber-supported Pd nanoparticles show efficient catalytic activity towards the deprotection of the N terminus of amino acids and peptides.

6.6 References

1. Micklitsch C. M., Knerr P. J., Branco M. C., Nagarkar R., Pochan D. J., Schneider J. P. (2011), Zinc-triggered hydrogelation of a self-assembling β-hairpin peptide, *Angew. Chem. Int. Ed*., 50, 1577-1579 (DOI: 10.1002/anie.201006652).

2. Ma M., Kuang Y., Gao Y., Zhang Y., Gao P., Xu B. (2010), Aromatic-aromatic interactions induce the self-assembly of pentapeptidic derivatives in water to form nanofibers and supramolecular hydrogels, *J. Am. Chem. Soc.*, 132, 2719-2728 (DOI: 10.1021/ja9088764).

3. Johnson E. K., Adams D. J., Cameron P. J. (2010), Directed self-assembly of dipeptides to form ultrathin hydrogel membranes, *J. Am. Chem. Soc.*, 132, 5130 -5136 (DOI: 10.1021/ja909579p).

4. Matson J. B., Stupp S. I. (2012), Self-assembling peptide scaffolds for regenerative medicine, *Chem. Commun.* 48, 26-33 (DOI: 10.1039/C1CC15551B).

5. Yang Z., Liang G., Guo Z., Guo Z., Xu B. (2007), Intracellular hydrogelation of small molecules inhibits bacterial growth, *Angew. Chem. Int. Ed.*, 46, 8216-8219 (DOI: 10.1002/anie.200701697).

6. Reches M., Gazit E. (2003), Casting metal nanowires within discrete self-assembled peptide nanotubes, *Science,* 300, 625-627 (DOI: 10.1126/science.1082387).

7. Guha S., Banerjee A. (19), Self-assembled robust dipeptide nanotubes and fabrication of dipeptide-capped gold nanoparticles on the surface of these nanotubes. *Adv. Funct. Mater.*, 2009, 1949-1961 (DOI: 10.1002/adfm.200800955).

8. Koley P., Pramanik A. (2011), Nanostructures from single amino acid-based molecules: Stability, fibrillation, encapsulation, and fabrication of silver nanoparticles, *Adv. Funct. Mater*., 21, 4126-4136 (DOI: 10.1002/adfm.201101465).

9. Lakshmanan A., Zhang S., Hauser C. A. E. (2012), Short self-assembling peptides as building blocks for modern nanodevices, *Trends Biotechnol.*, 30, 155-165 (DOI: 10.1016/j.tibtech.2011.11.001).

10. Lçwik D. W. P. M., Leunissen E. H. P., van den Heuvel M., Hansen M. B., van Hest J. C. M. (2010), Stimulus responsive peptide based materials, *Chem. Soc. Rev*,. 39, 3394-3412 (DOI: 10.1039/B914342B).

11. Adhikari B., Banerjee A. (2010), Short-peptide-based hydrogel: A template for the *in situ* synthesis of fluorescent silver nanoclusters by using sunlight, *Chem. Eur. J.*, 16, 13698-13705 (DOI: 10.1002/chem.201001240).

12 Ray S., Das A. K., Banerjee A. (2006), Smart oligopeptide gels: *In situ* formation and stabilization of gold and silver nanoparticles within supramolecular organogel networks, *Chem. Commun*., 2816-2818 (DOI: 10.1039/B605498F).

13. Palui G., Nanda J., Ray S., Banerjee A. (2009), Fabrication of luminescent CdS nanoparticles on short-peptide-based hydrogel nanofibers: Tuning of optoelectronic properties, *Chem. Eur. J.*, 15, 6902-6909 (DOI: 10.1002/chem.200900149).

14. Vemula P. K., John G. (2006), Smart amphiphiles: hydro/organogelators for in situ reduction of gold, *Chem. Commun.*, 2218-2220 (DOI: 10.1039/B518289A).

15. Chakrabarty A., Maitra U., Das A. D. (2012), Metal cholate hydrogels: Versatile supramolecular systems for nanoparticle embedded soft hybrid materials, *J. Mater. Chem.*, 22, 18268-18274 (DOI:10.1039/C2JM34016J).

16. Bhattacharya S., Srivastava A., Pal A. (2006), Modulation of viscoelastic properties of physical Gels by nanoparticle doping: Influence of the nanoparticle capping agent, *Angew. Chem. Int. Ed*., 45, 2934-2937 (DOI: 10.1002/anie.200504461).

17. Basit H., Pal A., Sen S., Bhattacharya S. (2008), Two-component hydrogels comprising fatty acids and amines: Structure, properties, and application as a template for

the synthesis of metal nanoparticles, *Chem. Eur. J.*, 14, 6534-6545 (DOI: 10.1002/chem.200800374).

18. Pal A., Basit H., Sen S., Aswal V. K., Bhattacharya S. (2009), Structure and properties of two component hydrogels comprising lithocholic acid and organic amines, *J. Mater. Chem.* 19, 4325-4334 (DOI: 10.1039/B903407B).

19. Pal A., Srivastava A., Bhattacharya S. (2009), Role of capping ligands on the nanoparticles in the modulation of properties of a hybrid matrix of nanoparticles in a 2D film and in a supramolecular organogel, *Chem. Eur. J.*, 15, 9169-9182 (DOI: 10.1002/chem.200900304).

20. Fukuzumi S., Yamada Y. (2012), Catalytic activity of metal-based nanoparticles for photocatalytic water oxidation and reduction, *J. Mater. Chem.*, 22, 24284-24296 (DOI: 10.1039/C2JM32926C).

21. Villa A., Schiavoni M., Prati L. (2012), Material science for the support design: A powerful challenge for catalysis, *Catal. Sci. Technol.*, 2, 673-682 (DOI: 10.1039/c2cy00355d).

22. Chen L. J., Wan C. C., Wang Y. Y. (2006), Chemical preparation of Pd nanoparticles in room temperature ethylene glycol system and its application to electroless copper deposition, *J. Colloid Interface Sci.*, 297, 143-150 (DOI: 10.1016/j.jcis.2005.10.029).

23. Niu Y., Crooks R. M. (2003), Preparation of dendrimer-encapsulated metal nanoparticles using organic solvents, *Chem. Mater*., 15, 3463-3467 (DOI: 10.1021/cm034172h).

24. Puranik S. S., Joshi M. H., Ogale B. S., Paknikar M. K. (2008), Hydrazine based facile synthesis and ordered assembly of metal nanoparticles (Au, Ag) on a bacterial surface layer protein template, *J. Nanosci. Nanotechnol*., 8, 3565-3569 (DOI:10.1166/jnn.2008.135).

25. Wu Z. G., Munoz M., Montero O. (2010), The synthesis of nickel nanoparticles by hydrazine reduction, *Adv. Powder Technol*., 21, 165-168 (DOI: 10.1016/j.apt.2009.10.012).

26. Maity I., Rasale D. B., Das A. K. (2012), Sonication induced peptide-appended bolaamphiphile hydrogels for *in situ* generation and catalytic activity of Pt nanoparticles, *Soft Matter*, 8, 5301-5308 (DOI: 10.1039/C2SM25126D).

27. Xu L., Wu X.-C., Zhu J.-J. (2008), Green preparation and catalytic application of Pd nanoparticles, *Nanotechnology,* 19, 305603 (DOI:10.1088/0957-4484/19/30/305603).

28. Ogasawara S., Kato S. (2010), Palladium nanoparticles captured in microporous polymers: A tailor-made catalyst for heterogeneous carbon cross-coupling reactions, *J. Am. Chem. Soc.,* 132, 4608-4613 (DOI: 10.1021/ja9062053).

29. Jones S., Qu J., Tedsree K., Gong X.-Q., Tsang S. C. E. (2012), Prominent electronic and geometric modifications of palladium nanoparticles by polymer stabilizers for hydrogen production under ambient conditions, *Angew. Chem. Int. Ed.,* 51, 11275-11278 (DOI: 10.1002/anie.201206035).

30. Sawai K., Tatumi R., Nakahodo T., Fujihara H. (2008), Asymmetric Suzuki–Miyaura coupling reactions catalyzed by chiral palladium nanoparticles at room temperature, *Angew. Chem. Int. Ed.,* 47, 6917- 6917 (DOI: 10.1002/anie.200802174).

31. Ranu B. C., Chattopadhyay K., Adak L. (2007), Solvent-controlled highly selective bis- and monoallylation of active methylene compounds by allyl acetate with palladium(0) nanoparticle, *Org. Lett.* 9, 4595-4598 (DOI: 10.1021/ol702099v).

32. Marrodan C. M., Berti D., Liguori F., Barbaro P. (2012), *In situ* generation of resin-supported Pd nanoparticles under mild catalytic conditions: a green route to highly efficient, reusable hydrogenation catalysts, *Catal. Sci. Technol.,* 2, 2279-2290 (DOI: 10.1039/C2CY20205K).

33. Layek K., Kantam M. L., Shirai M., Nishio-Hamane D., Sasaki T., Maheswaran H. (2012), Gold nanoparticles stabilized on nanocrystalline magnesium oxide as an active catalyst for reduction of nitroarenes in aqueous medium at room temperature, *Green Chem.,* 14, 3164 (DOI: 10.1039/C2GC35917K).

34. Kharisov B. I., Dias H. V. R., Kharissova O. V., Jime'nez-Pe'rez V. M., O.Pe'rez B., Flores B. M. (2012), Iron-containing nanomaterials: Synthesis, properties and environmental applications, *RSC Adv.,* 2, 9325-9358 (DOI: 10.1039/C2RA20812A).

35. Maity I., Rasale D. B., Das A. K. (2014), Peptide nanofibers decorated with Pd nanoparticles to enhance the catalytic activity for C–C coupling reactions in aerobic conditions, *RSC Adv.,* 4, 2984-2988 (DOI: 10.1039/C3RA44787A).

36. Bej A., Srimani D., Sarkar A. (2012), Palladium nanoparticle catalysis: Borylation of aryl and benzyl halides and one-pot biaryl synthesis via sequential borylation-Suzuki–Miyaura coupling, *Green Chem.* 14, 661- 667 (DOI: 10.1039/C2GC16111G).

37. Liu C., Tang S., Lei A. (2013), Oxidant controlled Pd-catalysed selective oxidation of primary alcohols, *Chem. Commun.*, 49, 1324-1326 (DOI: 10.1039/C2CC38086B).

38. Ohtaka A., Teratani T., Fujii R., Ikeshita K., Kawashima T., Tatsumi K., Shimomura O., Nomura R. (2011), Linear polystyrene-stabilized palladium nanoparticles-catalyzed C–C coupling reaction in water, *J. Org. Chem.*, 76, 4052-4060 (DOI: 10.1021/jo200485q).

39. Thielbeer F., Chankeshwara S. V., Johansson E. M. V., Norouzi N., Bradley M. (2013), Palladium-mediated bioorthogonal conjugation of dual-functionalised nanoparticles and their cellular delivery, *Chem. Sci.*, 4, 425-431 (DOI: 10.1039/C2SC20706K).

40. Declerck V., Colacino E., Bantreil X., Martinez J., Lamaty F. (2012), Poly(ethylene glycol) as reaction medium for mild Mizoroki–Heck reaction in a ball-mill, *Chem. Commun.*, 48, 11778-11780 (DOI: 10.1039/C2CC36286D).

41. Xu X., Li Y., Gong Y., Zhang P., Li H., Wang Y. (2012), Synthesis of palladium nanoparticles supported on mesoporous N-doped carbon and their catalytic ability for biofuel upgrade, *J. Am. Chem. Soc.*, 134, 16987-16990 (DOI: 10.1021/ja308139s).

42. Anderson J. T., Toogood P. L., Marsh E. N. G. (2002), A short and efficient synthesis of l-5,5,5,5',5',5'-hexafluoroleucine from N-Cbz-l-serine, *Org. Lett.*, 4, 4281-4283 (DOI: 10.1021/ol026922j).

43. Johnson II D. C., Widlanski T. S. (2004), Facile deprotection of O-Cbz-protected nucleosides by hydrogenolysis: An alternative to O-benzyl ether-protected nucleosides, *Org. Lett.*, 6, 4643-4646 (DOI: 10.1021/ol048426w).

44. Fujita Y., Fujita S., Okada Y., Chiba K. (2013), Soluble tag-assisted peptide head-to-tail cyclization: Total synthesis of mahafacyclin B, *Org. Lett.*, 15, 1155-1157 (DOI: 10.1021/ol4003477).

45. Pellois J. P., Wang W., Gao X. (2000), Peptide synthesis based on t-Boc chemistry and solution photogenerated acids, *J. Comb. Chem.*, 2, 355-360 (DOI: 10.1021/cc0000139).

46. Ray S., Das A. K., Banerjee A. (2007), pH-Responsive, bolaamphiphile-based smart metallo-hydrogels as potential dye-adsorbing agents, water purifier, and vitamin B12 carrier, *Chem. Mater*., 19, 1633-1639 (DOI: 10.1021/cm062672f).

47. Kameta N., Yoshida K., Masuda M., Shimizu T. (2009), Supramolecular nanotube hydrogels: Remarkable resistance effect of confined proteins to denaturants, *Chem. Mater*., 21, 5892-5898 (DOI: 10.1021/cm903108h).

48. Yang Z., Gu H., Du J., Gao J., Zhang B., Zhang X., Xu B. (2007), Self-assembled hybrid nanofibers confer a magnetorheological supramolecular hydrogel, *Tetrahedron*, 63, 7349-7357 (DOI:10.1016/j.tet.2007.02.009).

49. Cheng G., Castelletto V., Jones R. R., Connon C. J., Hamley I. W. (2011), Hydrogelation of self-assembling RGD-based peptides, *Soft Matter*, 7, 1326-1336 (DOI: 10.1039/C0SM00408A).

50. Pelton J. T., McLean L. R. (2000), Spectroscopic methods for analysis of protein secondary structure, *Anal. Biochem*., 277, 167-176 (DOI:10.1006/abio.1999.4320).

51. Datta S., Samanta S. K., Bhattacharya S. (2013), Induction of supramolecular chirality in the self-assemblies of lipophilic pyrimidine derivatives by choice of the amino acid-based chiral spacer, *Chem. Eur. J.*, 19, 11364-11373 (DOI: 10.1002/chem.201300605).

52. Brown R. A., Marcelli T., De Poli M., Sol J., Clayden J. (2012), Induction of unexpected left-handed helicity by an N-terminal L-amino acid in an otherwise achiral peptide chain, *Angew. Chem. Int. Ed*., 51, 1395-1399 (DOI: 10.1002/anie.201107583).

53. Mandal S. K., Kar T., Das D., Das P. K. (2012), The striking influence of SWNT–COOH on self-assembled gelation, *Chem. Commun.*, 48, 1814-1816 (DOI: 10.1039/C2CC165.67H).

54. Chatterjee S., Nandi A. K. (2011), Tuning of the morphology of a riboflavin–melamine equimolar supramolecular assembly by in situsilver nanoparticle formation, *Chem. Commun.*, 47, 11510-11512 (DOI: 10.1039/C1CC14158A).

55. Sukul P. K., Singh P. K., Maji S. K., Malik S. (2013), Aggregation induced chirality in a self assembled perylene based hydrogel: Application of the intracellular pH measurement, *J. Mater. Chem. B*, 1, 153- 156 (DOI: 10.1039/C2TB00007E).

56. Adamcik J., Castelletto V., Bolisetty S., Hamley I. W., Mezzenga R. (2011), Direct observation of time-resolved polymorphic states in the self-assembly of end-capped heptapeptides, *Angew. Chem. Int. Ed.*, 50, 5495-5498 (DOI: 10.1002/anie.201100807).

57. Wu D. C., Loh X. J., Wu Y.-L., Lay C. L., Liu Y. (2010), Living' controlled *in situ* gelling systems: Thiol-disulfide exchange method toward tailor-made biodegradable hydrogels, *J. Am. Chem. Soc.*, 132, 15140 -15143 (DOI: 10.1021/ja106639c).

58. Adler-Abramovich L., Perry R., Sagi A., Gazit E., Shabat D. (2007), Controlled assembly of peptide nanotubes triggered by enzymatic activation of self-immolative dendrimers, *ChemBioChem*, 8, 859-862 (DOI: 10.1002/cbic.200700103).

59. Gopal A., Varghese R., Ajayaghosh A. (2012), Oligo(*p*-phenylene-ethynylene)-derived super-π-gelators with tunable emission and self-assembled polymorphic structures, *Chem. Asian J.*, 7, 2061-2067 (DOI: 10.1002/asia.201200410).

60. Jahn T. R., Makin O. S., Morris K. L., Marshall K. E., Tian P., Sikorski P., Serpell L. C. (2010), The common architecture of cross-β amyloid, *J. Mol. Biol.*, 395, 717-727 (DOI: 10.1016/j.jmb.2009.09.039).

61. Ikeda M., Tanida T., Yoshii T., Hamachi I. (2011), Rational molecular design of stimulus-responsive supramolecular hydrogels based on dipeptides, *Adv. Mater.*, 23, 2819-2822 (DOI: 10.1002/adma.201004658).

62. Mitra R. N., Das P. K. (2008), *In situ* preparation of gold nanoparticles of varying shape in molecular hydrogel of peptide amphiphiles, *J. Phys. Chem. C*, 112, 8159-8166 (DOI: 10.1021/jp712106d).

63. Yu Y., Zhao Y., Huang T., Liu H. (2009), Shape-controlled synthesis of palladium nanocrystals by microwave irradiation, *Pure Appl. Chem.*, 81, 2377-2385 (DOI:10.1351/PAC-CON-08-11-22).

64. Chen L.-M., Liu Y.-N. (2011), Palladium crystals of various morphologies for SERS enhancement, *CrystEngComm.*, 13, 6481-6487 (DOI: 10.1039/C1CE05557G).

65. Bhattacharya S., Srivastava A., Sengupta S. (2005), Remarkably facile Heck and Suzuki reactions in water using asimple cationic surfactant and ligand-free palladium catalysts, *Tetrahedron Lett.*, 46, 3557 -3560 (DOI:10.1016/j.tetlet.2005.03.118).

66. Bhattacharya S., Sengupta S. (2004), Palladium catalyzed alkynylation of aryl halides (Sonogashira reaction) in water, *Tetrahedron Lett.,* 45, 8733-8736 (DOI:10.1016/j.tetlet.2004.09.131).

Chapter 7

Self-Programmed Nanovesicle to Nanofiber Transformation of a Dipeptide Appended Bolaamphiphile and Its Dose Dependent Cytotoxic Behaviour

7.1 Introduction

Precise control in the nanostructural transition of small peptide-based bolaamphiphile molecules via molecular self-assembly is a challenging task. Peptide-based nanostructures[1-10] are envisaged through a bottom-up self-assembly approach,[11-15] and they possess a wide range of applications in drug delivery,[16-19] tissue engineering[20-25] and supramolecular electronics.[26-28] However, peptide self-assembly processes are highly sensitive towards changes in stimuli such as pH,[29-31] temperature,[32,33] light,[34] metal ions[35,36] and enzymes.[37-40] The delicate hydrophobic/hydrophilic balance and non-covalent interactions of a molecule are the driving forces for the self-assembly process in a particular solvent, which results in the formation of peptide nanostructures. Stimuli-responsive peptide self-assembly proceeds through an alteration of molecular conformations, which leads to the adoption of different secondary structures. The self-assembly process is dynamic in nature. The dynamic behaviour acts in between the more and relatively less ordered conformational arrangements at the molecular level. Nanostructural transition occurs because of the need to achieve a more stable and ordered molecular arrangement from the loosely ordered arrangement in a particular system. In most of the cases, a change in stimuli directs the morphological transformation from one nanostructure to another. Stimuli-responsive peptide nano-fibers have attracted attention because of their potential applications in drug delivery and waste water treatment.[41] The nanostructural transition of peptide into tapes, ribbons, nano-fibrils and nanofibers depends on the change in pH.[42] Parquette *et al.* reported peptide-based dendron self-assembly in a controlled manner and the inter-conversion of nanotubes and fibrillar nanostructures.[43] Direct morphological transformation from twisted ribbons to helical ribbons was reported by Stupp *et al.*[44] The Ulijn group reported a morphological transformation from a micellar solution to a fibrous hydrogel *via* the enzymatic dephosphorylation of a peptide amphiphile.[45] The same group again demonstrated direct enzymatic amide condensation and light induced controlled gelation, which is associated with the morphological transition from a micellar structure to entangled nanofibers.[46] Yang *et al.* tuned the hydrogelation process by the enzymatic dephosphorylation of a small molecule and reported the occurrence of a morphological transformation.[47]

Peptide bolaamphiphiles are an interesting class of organic molecules. In a bolaamphiphile molecule, two terminal hydrophilic groups are attached with a hydrophobic backbone. Shimizu *et al.* demonstrated various types of nanostructure forming peptide bolaamphiphiles.[48] Nano-doughnut-forming self-assembled peptide bolaamphiphile was also used as a nanoreactor to synthesis Au nanocrystals.[49] The nanostructural transformation requires a stimulus, which can break weak non-covalent interactions and induce another supramolecular arrangement. The change in pH can tune the evolution of different nanostructures of bolaamphiphiles.[50] In this chapter, we report the self-programmed morphological transition from nanovesicles to nanofibers *via* a third polymorphic state of nanocapsules. The cytotoxicity study of small molecules has emerged as a promising tool for the development of drugs.[51] Understanding the dose dependent behavior of a small molecule is a crucial and important aspect in the field of biomedicine.[52,53] Hydrogels of small peptide-based molecules are interesting because of their applications in cell-biology.[54] The objectives of this chapter are: (a) to incorporate a flexible alkane chain which can give different structures due to conformational heterogeneity, (b) to study the nanostructural transition driven by molecular self-assembly, (c) to understand the mechanism of nanostructural transition with respect to time and (d) to investigate the cytotoxicity and cell proliferation using the self-assembled hydrogel scaffold.

7.2 Experimental

7.2.(1) Synthesis of Bolaamphiphile

Peptide bolaamphiphile **35** employed in this chapter was synthesized by conventional solution phase methodology. The C-terminus of amino acid was protected as methyl ester. Couplings were mediated by diisopropylcarbodiimide-1-hydroxybenzotriazole (DIPC-HOBt).The final compounds were purified and fully characterized by FT-IR, ^{1}H NMR and mass spectral studies. The synthesis of HO-Suc-Phe-OMe **5**, MeO-Leu-Suc-Phe-OMe **18** and HO-Leu-Suc-Phe-OH **19** are described in chapter 3 and 4.

7.2.1 Synthesis of Bolaamphiphile (HO-Trp(4)-Phe(3)-Suc-Leu(1)-Trp(2)-OH) 35:

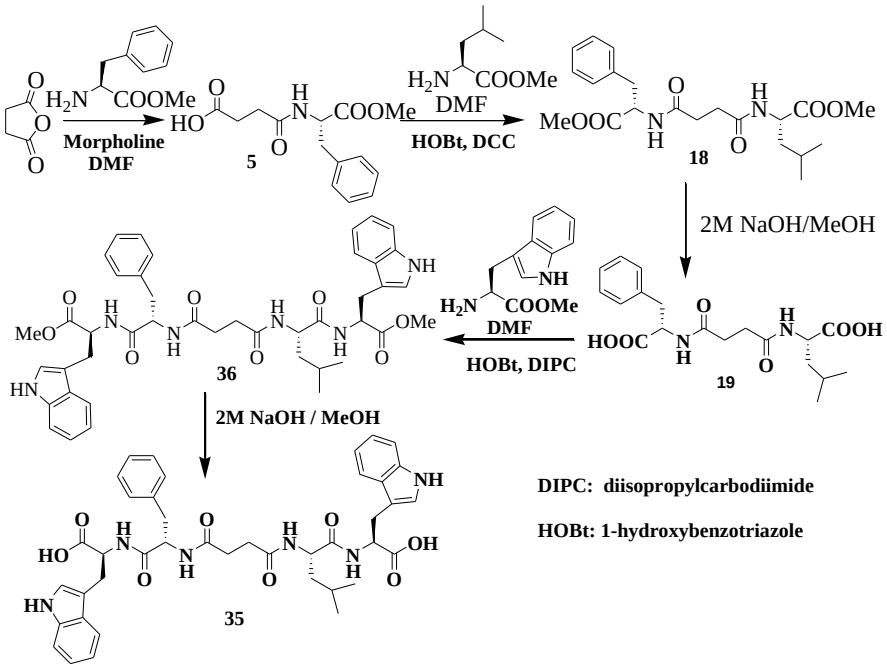

Scheme 7.1. *Synthetic scheme of peptide bolaamphiphile **35**.*

*(a) Synthesis of MeO-Trp(4)-Phe(3)-Suc-Leu(1)-Trp(2)-OMe **36**:* 1.51 g (4 mmol) of HO-Phe(2)-Suc-Leu(1)-OH **19** in 3 mL of DMF was cooled in an ice bath and H-Trp-OMe was isolated from 4.06 g (16 mmol) of the corresponding methyl ester hydrochloride by neutralization and subsequent extraction with ethyl acetate and the ethyl acetate extract was concentrated to 8 mL. It was then added to the reaction mixture, followed immediately by 1.11 g (8.8 mmol, 1 mL 372 μL) DIPC and 1.18 g (8.8 mmol) of HOBt. The reaction mixture was stirred for overnight. The residue was taken up in ethyl acetate (50 mL) and the DIU was filtered off. The organic layer was washed with 1M HCl (3 × 50 mL), brine (2 × 50 mL), 1M sodium carbonate (3 × 50 mL), brine (2 × 50 mL), dried over anhydrous sodium sulfate and evaporated under vacuum to yield **36** as a white solid. Purification was done by silica gel column (100-200 mesh) using chloroform-methanol (9:1) as eluent.

Yield: 2.64 g (3.4 mmol, 85%); FT-IR (KBr): ῡ = 3330 (st), 1740 (st), 1649 (st), 1537 (st), 1438 (ms) cm^{-1}; ^1H NMR (400 MHz, $CDCl_3$, δ_{ppm}): 8.77 (d, *J* = 12.8 Hz, 2H, ring -NHs of Trp(2) and Trp(4)), 7.53 (d, *J* = 8 Hz, 2H, ring protons of Trp(2) and Trp(4)), 7.45 (d, *J* = 6.0 Hz, 2H, ring protons of Phe(3)), 7.30 (d, *J* = 8 Hz, 1H, -NH- of Phe(3)),

7.26 (d, *J* = 8 Hz, 1H, -NH- of Leu(1)), 7.15 (t, *J* = 7.6 Hz, 4H, ring protons of Phe(3)), 7.10 and 7.06 (d, *J* = 6.8 Hz, 2H, ring protons of Trp(2) and Trp(4)), 7.03 (t, *J* = 7.6 Hz, 4H, ring protons of Trp(2) and Trp(4)), 6.92 (d, *J* = 4.8 Hz, 2H, ring protons of Trp(2) and Trp(4)), 5.83 (d, *J* = 9.6 Hz, 1H, -NH- of Trp(2)), 5.69 (d, *J* = 9.2 Hz, 1H, -NH- of Trp(4)), 4.87 (m, 2H, $C^{\alpha}Hs$ of Trp(2) and Trp(4)), 4.67 (m, 1H, $C^{\alpha}H$ of Phe(3)), 4.50 (m, 1H, $C^{\alpha}H$ of Leu(1)), 3.59 and 3.57 (s, 6H, $-COOCH_3$), 3.34 and 3.12 (d, *J* = 4.4 Hz and *J* = 5.6 Hz, 4H, $C^{\beta}Hs$ of Trp(2) and Trp(4)), 3.08 and 2.97 (d, *J* = 7.6 Hz, and *J* = 6 Hz, 2H, $C^{\beta}Hs$ of Phe(3)), 2.43 and 2.31 (m, 4H, $-CH_2-$ of Suc), 1.49 (m, 2H, $C^{\beta}Hs$ of Leu(1)), 1.38 (m, 1H, $C^{\gamma}H$ of Leu(1)), 0.75 (d, *J* = 6.4 Hz, 6H, $C^{\delta}Hs$ of Leu(1)); $[\alpha]_D^{20}$ = -30.96 (*c* = 0.31 in CH_3OH); MS (ESI) *m/z*: $(M+Na)^+$ Calcd. for $C_{43}H_{50}N_6O_8Na$: 801.3588; found 801.3512.

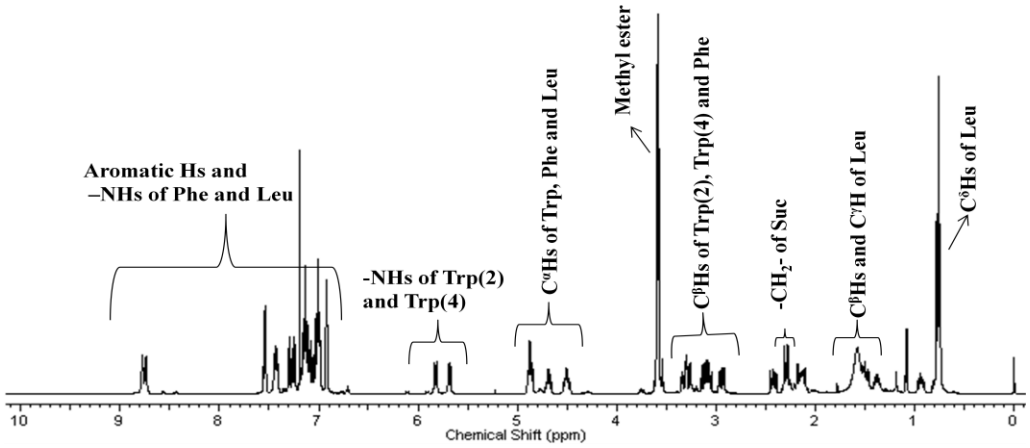

Figure 7.1. *^{1}H NMR spectrum (400 MHz, $CDCl_3$) of MeO-W-F-Suc-L-W-OMe* ***36***.

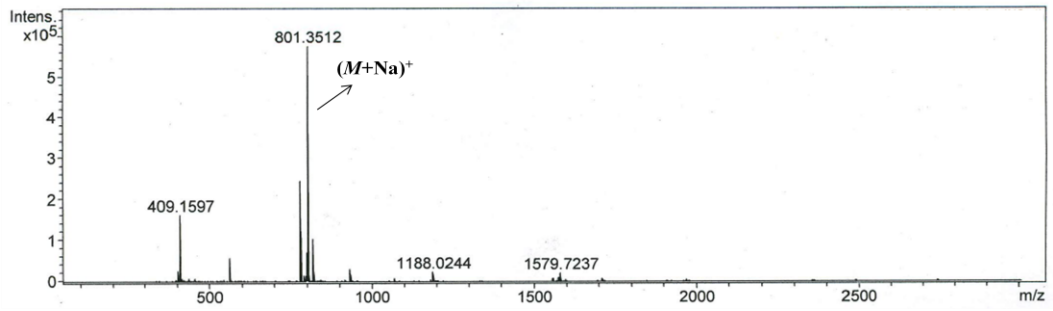

Figure 7.2. *ESI-MS spectrum of MeO-W-F-Suc-L-W-OMe* ***36***.

*(b) Synthesis of HO-Trp(4)-Phe(3)-Suc-Leu(1)-Trp(2)-OH **35**:* 1.94 g (2.5 mmol) of MeO-Trp(4)-Phe(3)-Suc-Leu(1)-Trp(2)-OMe **36** in 10 mL MeOH was taken in a round bottom flask and 2M NaOH was added to it dropwise. The reaction was monitored by thin layer chromatography (TLC). The reaction mixture was stirred for overnight. 15 mL of distilled water was added to the reaction mixture and MeOH was removed under vacuum. The aqueous part was washed with diethyl ether (2 × 30 mL). Then it was cooled under ice bath for 10 minutes and then pH was adjusted to 1 by drop wise addition of 1M HCl. It was extracted by ethyl acetate (3 × 50 mL) and then the ethyl acetate part was dried over anhydrous Na_2SO_4 and evaporated under vacuum to yield **35** as a white solid.

Yield: 1.72 g (2.3 mmol, 92%); FT-IR (KBr): ῡ = 3394 (st), 3305 (ms), 1717 (m), 1637 (st), 1526 (ms), 1455 (s) cm^{-1}; ^{1}H NMR (400 MHz, DMSO-d_6, δ_{ppm}): 12.59 (s, 2H, -COOH), 10.90 (d, *J* = 6.4 Hz, 2H, ring -NHs- of Trp(2) and Trp(4)), 8.31 (d, *J* = 7.6 Hz, 1H, -NH- of Phe(3)), 8.12 and 8.08 (d, *J* = 7.6 Hz, 2H, -NHs of Trp(2) and Trp(4)), 7.98 (d, *J* = 8 Hz, 1H, -NH- of Leu(1)), 7.60 (t, *J* = 8.4 Hz, 2H, ring protons of Phe(3)), 7.40 (d, *J* = 4 Hz, 2H, ring protons of Trp(2) and Trp(4)), 7.28 (d, *J* = 3.6 Hz, 2H, ring protons of Trp(2) and Trp(4)),7.22 (d, *J* = 2.0 Hz, 3H, ring protons of Phe(3)), 7.12 and 7.04 (m, 4H, ring protons of Trp(2) and Trp(4)), 4.61 (m, 1H, $C^{\alpha}H$ of Phe(3)), 4.54-4.49 (m, 2H, $C^{\alpha}Hs$ of Trp(2) and Trp(4)), 4.38 (m, 1H, $C^{\alpha}H$ of Leu(1)), 3.24 and 3.14 (d, *J* = 4.8 Hz and *J* = 7.2 Hz, 4H, $C^{\beta}Hs$ of Trp(2) and Trp(4)), 3.05 and 2.76 (d, *J* = 4 Hz, 2H, $C^{\beta}Hs$ of Phe(3)), 2.39 (m, 4H, -CH_2- of Suc), 1.61 (m, 1H, $C^{\gamma}H$ of Leu(1)), 1.45 (m, 2H, $C^{\beta}Hs$ of Leu(1)), 0.91 and 0.87 (d, *J* = 6.4 Hz and *J* = 6.8 Hz, 6H, $C^{\delta}Hs$ of Leu(1)); ^{13}C NMR (100 MHz, DMSO-d_6, δ_{ppm}): 173.13, 172.11, 171.97, 171.25, 137.91, 136.02, 129.14, 127.90, 127.16, 126.12, 123.63, 120.57, 118.31, 118.10, 111.32, 109.65, 59.71, 53.59, 52.80, 50.70, 37.44, 30.75, 26.92, 24.06, 23.01, 21.57; $[\alpha]_D^{20}$ = -27.55 (*c* = 0.5 in CH_3OH); MS (ESI) *m/z*: $(M+Na)^+$ Calcd. for $C_{41}H_{46}N_6O_8Na$: 773.3275; found 773.3226.

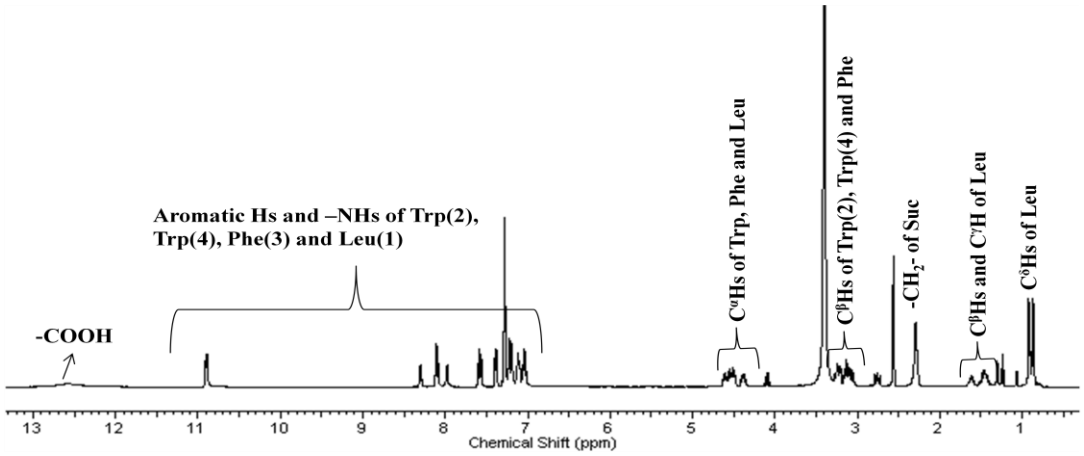

Figure 7.3. *^{1}H NMR spectrum (400 MHz, DMSO-d_6) of HO-W-F-Suc-L-W-OH **35**.*

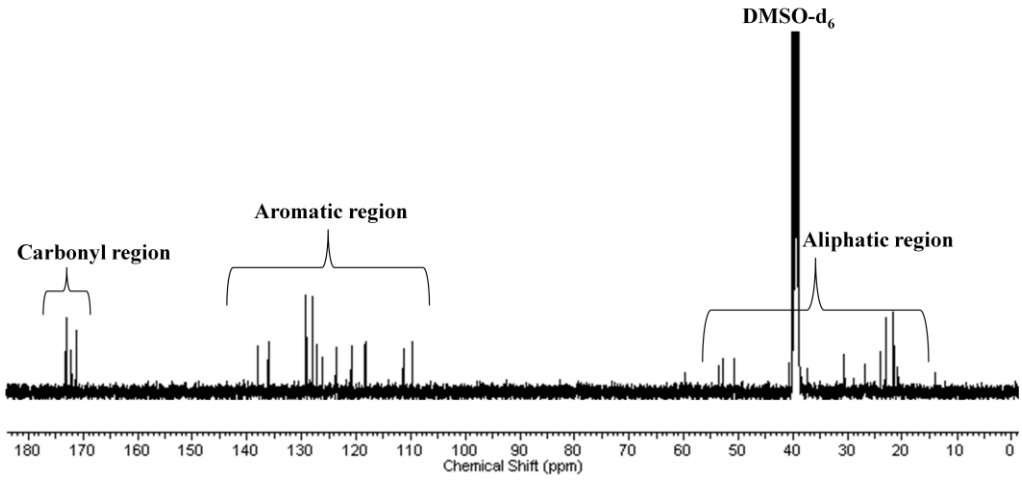

Figure 7.4. *^{13}C NMR spectrum (100 MHz, DMSO-d_6) of HO-W-F-Suc-L-W-OH **35**.*

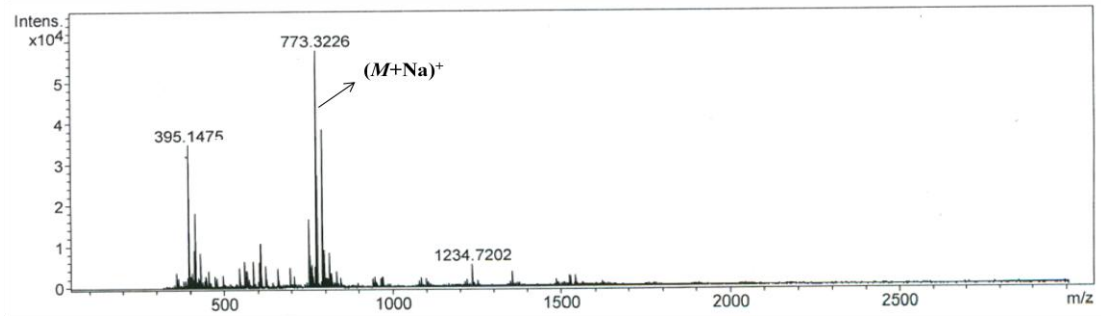

Figure 7.5. *ESI-MS spectrum of HO-W-F-Suc-L-W-OH **35**.*

7.3 Method and Characterization Techniques

7.3.1 Preparation of Hydrogel

15 mg (10 mmol L^{-1}) of peptide bolaamphiphile (HO-W-F-Suc-L-W-OH) was dispersed in 2 mL of sodium phosphate buffer solution (pH 8, 10 mmol L^{-1}) and sonicated for 10 minutes. The self-supporting hydrogel was formed after 3 hours.

7.3.2 AFM Study

For the AFM study, the gel samples were diluted in Milli Q water to a final concentration of 0.5 mmol L^{-1}, placed on a mica slip, and then dried by slow evaporation. Images were obtained with an AIST-NT instrument (model no. smartSPM 1000) using the soft tapping-mode.

7.3.3 Fluorescence Microscopy Study

Fluorescence microscopy experiments were performed on a home-built epifluorescence microscopy set-up. An air-cooled argon ion laser (Melles Griot, model 400-A03) with an excitation wavelength of 500 nm was used to excite the vesicle sample placed on an inverted microscope (Nikon, model Eclipse Ti-U). The laser beam was expanded and subsequently focused on the back-focal plane of an oil immersion objective (100 × 1.49 NA Nikon) to illuminate a 60 x 60 μm^2 area of the sample. The PL from the sample was recorded by a B2A filter cube (Nikon) with a 505 nm dichroic mirror and a 520 nm long-pass filter and finally imaged with a back-illuminated EMCCD camera (Andor, model iXon X3 897) at an exposure time of 300 ms. The images were analyzed with an ImageJ (Version 1.46r) NIH.

7.3.4 Optical Microscopy Study

Optical microscopy images were taken with a Zeiss AxioCam ERc5s microscope using 40 × magnification. The peptide bolaamphiphile vesicles and Congo red loaded vesicles were diluted in double distilled water and the samples were prepared by depositing a few drops on a cover slip.

7.3.5 CD (Circular Dichroism) Spectrometer

The secondary structure of peptide bolaamphiphile was analyzed with a Jasco J-815 circular dichroism spectrometer. The peptide hydrogel (10 mmol L^{-1}) was diluted to a final concentration of 500 μM in ddH_2O for both the vesicles and nanofibers and measured from 280 nm to 190 nm with a 0.1 data pitch, 20 nm min^{-1} scanning speed, 1 nm band width and 4 s D.I.T.

7.3.6 Cell Culture (MTT Assay)

Total WBCs were isolated from chicken blood. The 1×10^6 mL^{-1} concentration of cells was taken from 100 μL in each well. A 20 mmol L^{-1} concentration of hydrogel stock solution was used to prepare the final concentrations of 10-100% in different wells (each in triplicate) at a pH of 7.4. Commercially available kit from Hi-Media Pvt. Ltd., Mumbai was used to conduct the MTT assay. Cells were mixed with the hydrogel and incubated for 48 hours with the hydrogel or in media (control). The minimum essential media without phenol red was used to culture the cells. After culturing the cells, the MTT reagent was added to each well. After 4 hours, the MTT solution was carefully removed and the purple crystals were solubilized in DMSO. The optical density of the reagent was then measured at a wavelength of 570 nm with a reference wavelength of 650 nm. The effect on cell viability or number was calculated in percentages, considering the average absorbance value from the control samples to be 100%.

7.3.7 Statistical Analysis

Data are expressed as mean ± SEM (standard error of the mean) and were analyzed by the analysis of variance (ANOVA) followed by a post hoc Newman-Keuls multiple comparison test using a trial version of Prism 5 software for Windows (GraphPad Software, Inc., La Jolla, CA, USA).

7.4 Results and Discussion

7.4.1 Hydrogel and Morphological Transformation

We synthesized a peptide bolaamphiphile HO-W-F-Suc-L-W-OH (W: tryptophan, L: leucine, F: phenylalanine and Suc: succinic acid) with a centrally located flexible succinic acid moiety. 15 mg of peptide bolaamphiphile (10 mmol L^{-1}) was dispersed in 2 mL of phosphate buffer (pH = 8, 10 mM). A self-supporting hydrogel was achieved by successive sonication, and was used to investigate the morphological transformation (Scheme 7.2).

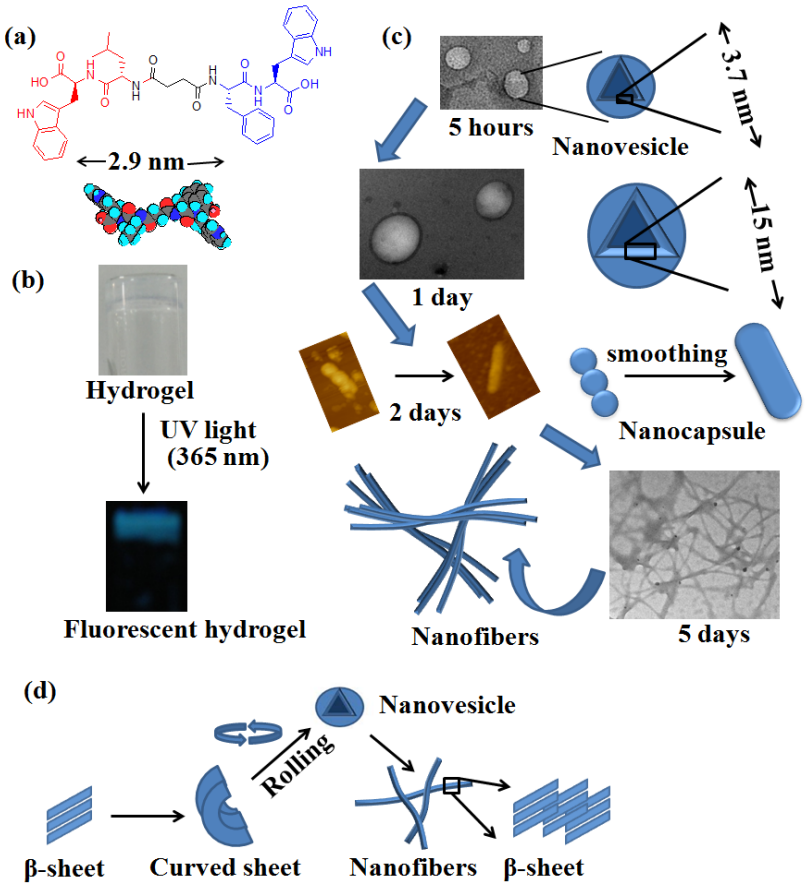

Scheme 7.2. *(a) Molecular structure of peptide bolaamphiphile* ***35****, (b) the self-supporting peptide bolaamphiphile hydrogel under daylight which emits blue light upon irradiation at 365 nm UV light, (c) self-programmed morphological transformation from nanovesicles to nanofibers through a third polymorphic capsular nanostructure, and (d) the scheme representing the formation of β-sheets, which form vesicles via a rolling up of the sheet, and then nanofibers are formed via a reorientation of the β-sheets.*

The critical gelation concentration of the precursor was found to be 8 mmol L^{-1}. The self-programmed nanostructural transition from nanovesicle to nanofiber of hydrogel **35** (10 mmol L^{-1}) with a self-assembly mechanism with respect to time was investigated by transmission electron microscopy (TEM) and atomic force microscopy (AFM).

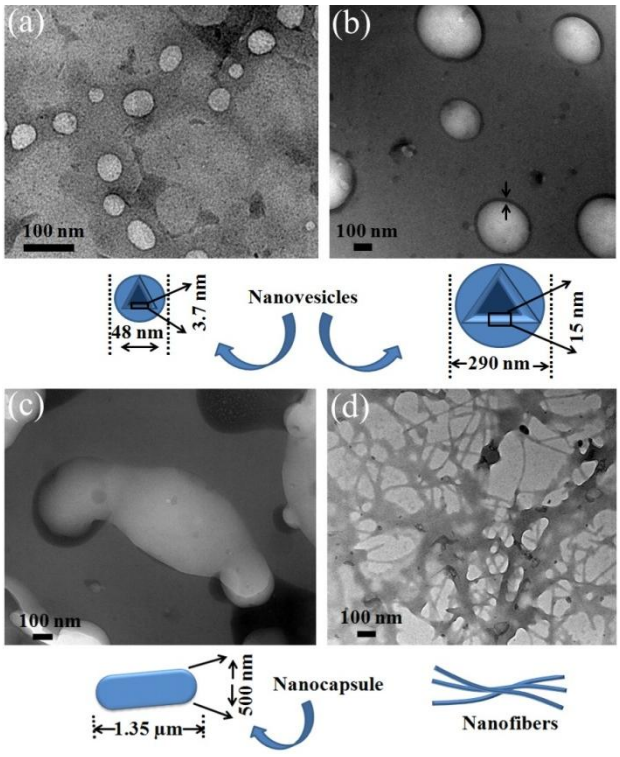

Figure 7.6. *TEM images showing the nanostructural evolution of (a) nanovesicles at 5 hours, (b) multilayered nanovesicles at 1 day, (c) nanocapsules at 2 days and (d) nanofibrillar structures at 5 days of hydrogelation.*

The transmission electron microscopy image (Figure 7.6) showed that the peptide bolaamphiphile self-assembled to form nanovesicles within 5 hours of hydrogelation. At this early stage, the evolution of nanovesicles[55] occurred through a loose molecular arrangement of the self-assembled molecules (Figure 7.7). The TEM image revealed the average diameter of the nanovesicles to be 48 nm. The average wall thickness of these nanovesicles is 3.7 nm. At day 1, the TEM image showed that the early evolved nanovesicles became larger in size and the average diameter was found to be 290 nm. The average wall thickness was estimated from the TEM image, and was observed to be

15 nm. The vesicle-wall was formed by a multi-lamellar arrangement of self-assembled molecules, which adopted a loose β-sheet-like structure. At day 2, a nanocapsule like nanostructure was observed with an increased dimension. The length of the capsule was about 1.35 μm and the diameter was around 500 nm at the middle of the nanostructure.

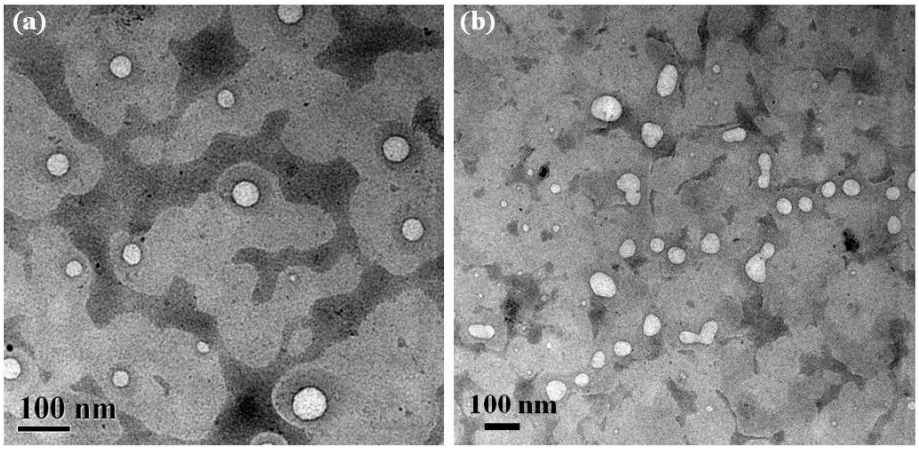

Figure 7.7. *TEM images (a) and (b) show that peptide bolaamphiphiles are self-assembled into vesicle structure within 5 hours of sonication.*

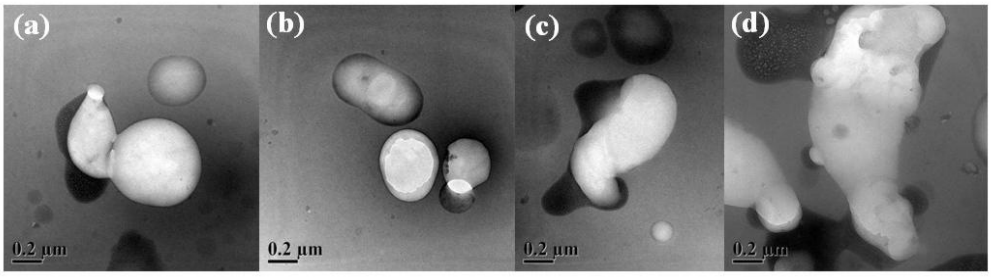

Figure 7.8. *TEM images showing the formation of nanocapsules from the association of nanovesicles. TEM images showing the (a) association of two vesicles towards the formation of a nanocapsule, (b)-(d) show the self-assembled peptide bolaamphiphile nanocapsules at 2 days.*

At this stage, the association of two or more nanovesicles was also observed. It is evident that the nanocapsule-like nanostructure evolved from the association of the nanovesicles (Figure 7.8). Nanofibrillar structures [31] were observed after 4 days of hydro-gelation. The TEM image showed that the nanofibrillar network structures were formed from

previously collapsed nanostructures, and the nucleation point was clearly observed in the TEM image. The nanofibers were several micrometers in length and the average diameter of the nanofiber was 12 nm. At this stage, no nanovesicle was found, which indicates the complete conversion of nanovesicles to nanofibers (Figure 7.9).

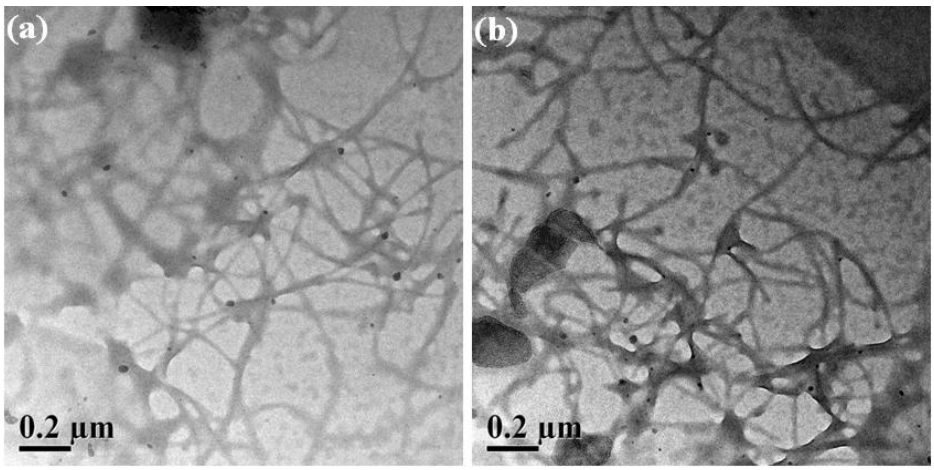

Figure 7.9. *TEM images show that peptide bolaamphiphiles self-assembled into well-defined nanofibrillar structures at 5 day.*

The atomic force microscopy (AFM) images[56,57] (Figure 7.10) were also showed a similar trend as the TEM images. The peptide bolaamphiphile molecules self-assembled into nanovesicles at an early stage. The size of the nanovesicles after 1 day of hydrogelation was in the range of 45 to 250 nm. The line scan shows the average height of nanovesicles is 30 nm (Figure 7.10d). After that, the nanovesicles fused with each other to form cocoon-like nanostructures. The average diameter of these nanostructures was 300 nm. At 2 days of self-assembly, the cocoon-like nanostructures transformed into nanocapsule-like structures, which were 0.6 to 1.3 µm in length. The average diameter of these nanocapsules was 500 nm and the height was in the range of 5 to 10 nm (Figure 7.11). At 5 days of sonication, nanofibers were formed. The diameter of the nanofiber was 20 nm. The self-assembly process was initiated by sonication but the morphological transition from nanovesicles to nanofibers occurred by a self-programmed process of smart bolaamphiphile.

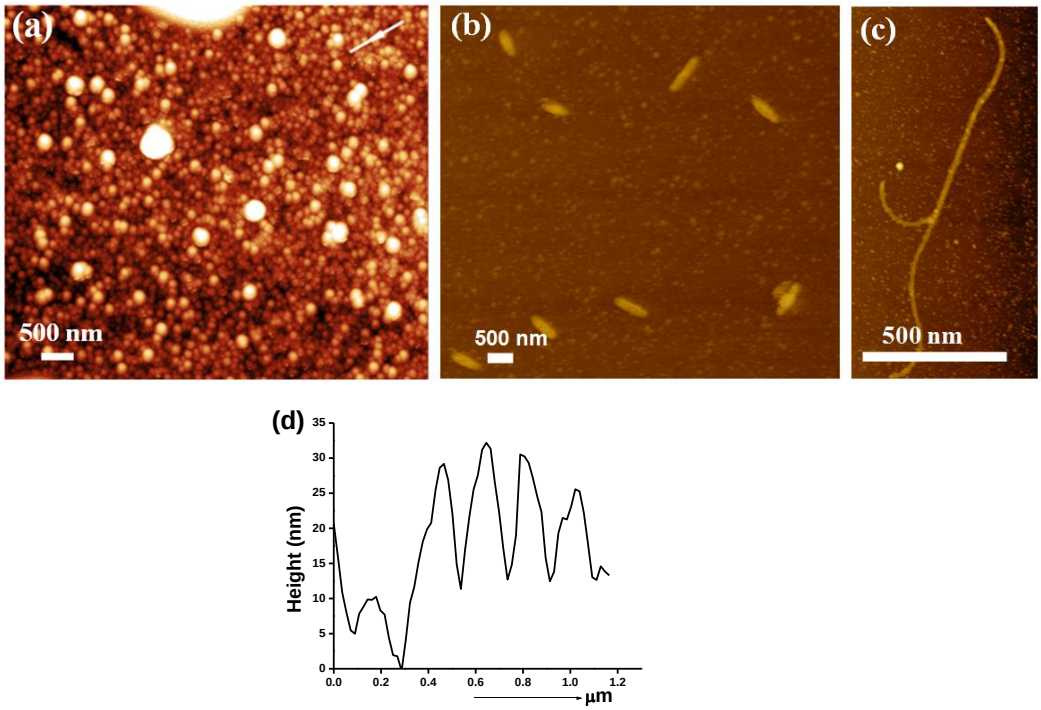

Figure 7.10. *AFM images showing the nanostructural evolution of (a) nanovesicles at 1 day, (b) nanocapsules at 2 days and (c) nanofibrillar structures at 5 days of hydrogelation. (d) The line scan of nanovesicles indicated by white arrow in (a) shows the average height of nanovesicles is 30 nm which is twice of the wall thickness estimated from TEM images.*

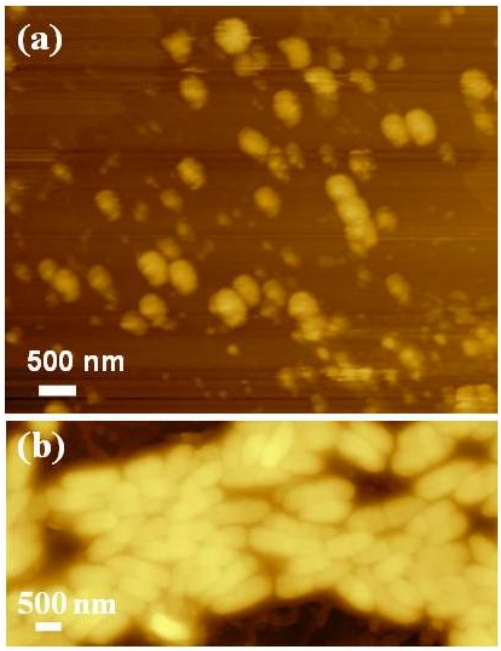

Figure 7.11. *AFM images show the (a) association of two vesicles towards formation of a nanocapsule and (b) the matured nanocapsules.*

The hollow nature of the nanovesicles was proven by the Congo red dye encapsulation experiment.[58] An aqueous solution (2 mg mL^{-1}) of the Congo red dye was prepared and added to the vesicles. These vesicles entrapped the Congo red dye within a period of 4 and 5 hours. After 5 hours, the fluorescence microscopy images (Figure 7.12) clearly demonstrated that the physiological dye, Congo red, was successfully encapsulated inside the vesicles. In addition to the fluorescence microscopy images, the optical microscopy images [59] also showed the vesicle structure of the peptide bolaamphiphile hydrogel at 1 day of self-assembly (Figure 7.13).

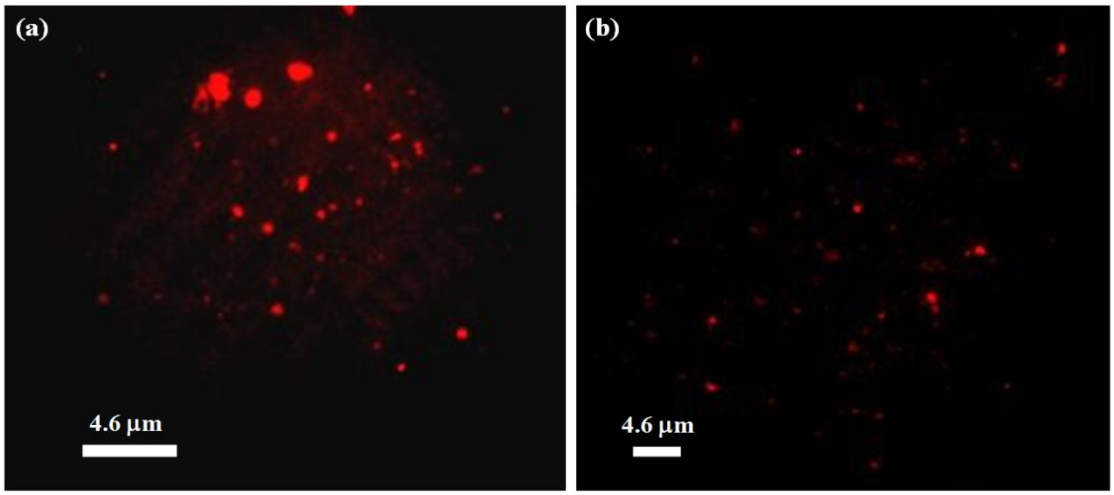

Figure 7.12. *Fluorescence microscopic images showing the encapsulation of a physiological dye, Congo red, by nanovesicles.*

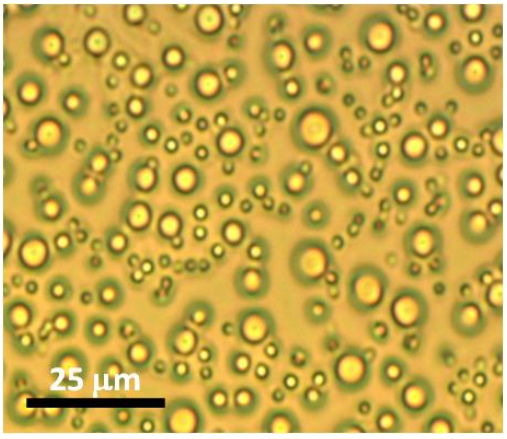

Figure 7.13. *Optical microscopic image clearly shows the formation of vesicles where distribution of nano to micro vesicles are observed.*

7.4.2 FT-IR Study

From the abovementioned observations, we were interested in elucidating the differences in molecular arrangement at the supramolecular level inside these two different nanostructures. To gain more insight into the molecular conformations of the two different nanostructures, several spectroscopic analyses were performed. FT-IR studies were carried out at day 1 and 5 of the hydrogelation to understand the secondary structures adopted by the self-assembled peptide bolaamphiphiles inside the two different nanostructures. At day 1, two peaks appeared at 1646 cm^{-1} and 1714 cm^{-1} for the hydrogel enriched with nanovesicles. The peak at 1714 cm^{-1} suggested that the carboxylic acid groups are involved in hydrogen bonding interactions, whereas the appearance of a characteristic amide I peak at 1646 cm^{-1} revealed a turn type of β-sheet arrangement.[60] At day 5, several characteristic peaks appeared for the hydrogel consisting of nanofibrillar morphology. The C=O stretching band at 1702 cm^{-1} indicated a hydrogen bonded carboxylic acid functionality in the peptide nanofibers. The amide I band at 1635 cm^{-1}, along with a weak shoulder at 1608 cm^{-1}, revealed that the peptide bolaamphiphile molecules are self-assembled into hydrogen bonded β-sheet arrangement [9] in the nanofibers (Figure 7.14). From the FT-IR spectra, it is clear that the molecular packing is more ordered and more compact in the β-sheet arrangement for the nanofibers rather than for the nanovesicles.

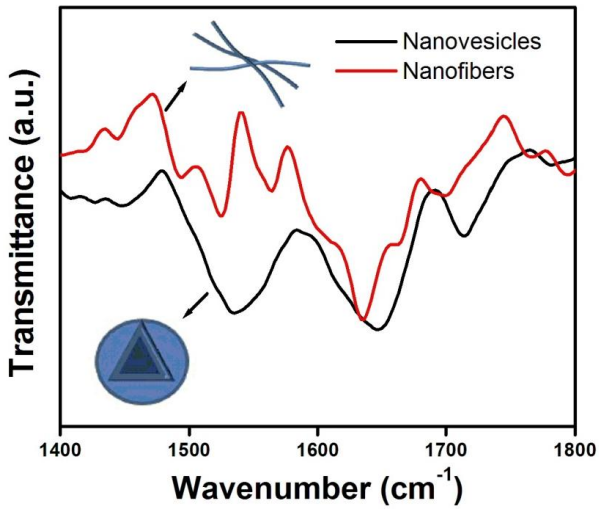

Figure 7.14. *FT-IR spectra for both the nanostructures of nanovesicles and nanofibers. FT-IR spectra show more ordered β-sheet arrangement inside the nanofibers rather than nanovesicles.*

7.4.3 Circular Dichroism (CD) Analysis

The difference in the molecular conformations inside the two different nanostructures at two different stages of self-assembly was examined by circular dichroism (CD) spectroscopy (Figure 7.15).[61,62] For both the cases, the hydrogels were diluted to 500 μM concentration in ddH_2O to investigate the secondary structures of the two different nanostructures. The CD spectrum of the nanovesicles showed a characteristic negative peak around 201 nm with a weak shoulder at 211 nm, which resulted from the n-π* transition of the CO-NH groups of the peptide bolaamphiphile molecule. This CD signature represented a coil type β-sheet arrangement of peptide bolaamphiphiles in the nanovesicle. Another strong positive band appeared at 226 nm, which is responsible for the electron-transfer of the nonbonding electron of the nitrogen atom into the π* orbital system of the indole ring of the tryptophan moiety.[63] The CD spectrum for the nanofibers showed a characteristic negative band at 216 nm with a weak negative band at 201 nm for the n-π* transition of the CO-NH groups. This CD signature confirmed the hydrogen bonded β-sheet arrangement, which is more ordered for nanofibers than nanovesicles.

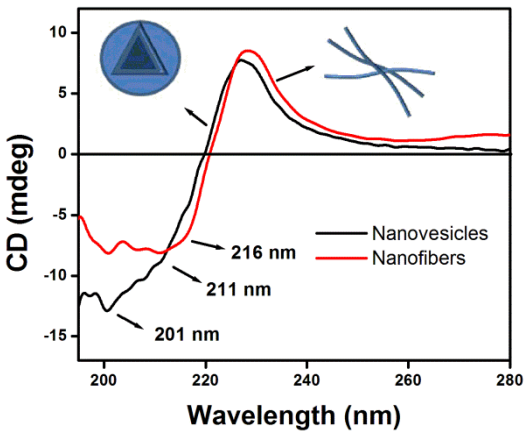

Figure 7.15. *CD spectra for both the nanostructures of nanovesicles and nanofibers. The spectroscopic studies confirm a more compact β-sheet arrangement inside the nanofibers rather than nanovesicles through the synergistic effect of hydrogen bonding and π-π stacking interactions.*

Another positive band at 229 nm appeared because of the tryptophan moiety, which was slightly red shifted with an increase in ellipticity from the corresponding peak for the

nanovesicles. This occurred from the extended π-π stacking interactions of the tryptophan aromatic rings during the self-assembly process to form nanofibers.

7.4.4 Fluorescence Spectroscopy Study

The fluorescence spectroscopy technique was also exploited to explore π-π stacking interactions during the self-assembly process of peptide bolaamphiphile and to understand the role of the aromatic moieties of peptide bolaamphiphile during structural transition from nanovesicles to nanofibers (Figure 7.16). The fluorescence spectra showed that the nanovesicles emitted at 353 nm, whereas the nanofibers showed an emission maxima at 357 nm upon excitation at 280 nm. The emission peak for both the cases resulted from the tryptophan moiety of the self-assembled bolaamphiphile molecules. The 4 nm red shift of the emission maxima occurred from the nanostructural transition of nanovesicles to nanofibers, which suggests that the peptide bolaamphiphiles are arranged into more ordered and compact β-sheet structures through the synergic effects of hydrogen bonding and extended π-π stacking interactions of the tryptophan residues inside the nanofibers.[9]

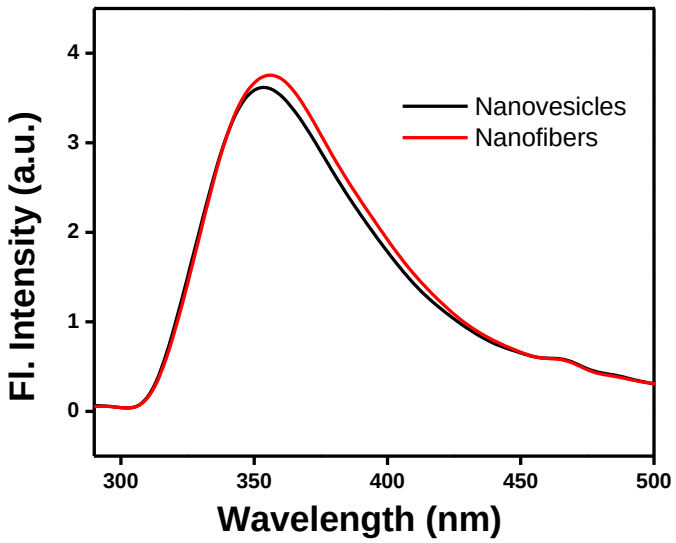

Figure 7.16. *Fluorescence spectra (concentration: 10 mmol L^{-1}, λ_{ex} = 280 nm) for both the nanostructures of nanovesicles and nanofibers.*

7.4.5 Powder X-Ray Diffraction (PXRD) Study

The powder X-ray diffraction (PXRD) data (Figure 7.17) clearly revealed the conformational differences between the two morphological states of nanovesicles and nanofibers. For the nanovesicles, the reflection peak at 2θ = 10.22°, corresponding to a d spacing of 8.64 Å, was observed which was assigned for spacing between two successive β-sheets. Another characteristic peak at 2θ = 18.32°, corresponding to a d spacing of 4.76 Å, was observed. The peak at 4.83 Å is related to the spacing between the two peptide bolaamphiphiles in a β-sheet arrangement.[64]

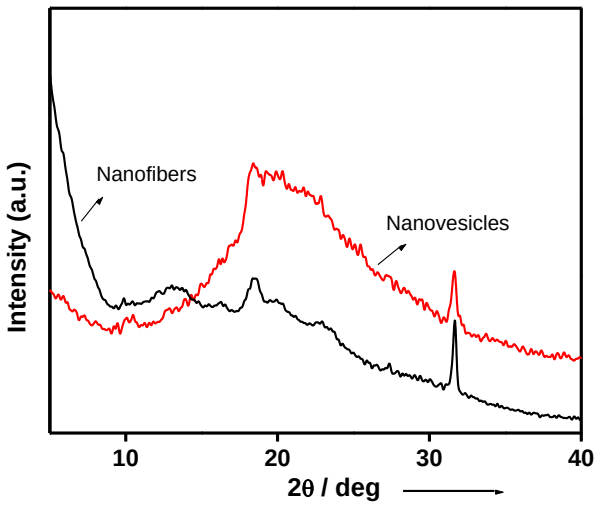

Figure 7.17. *PXRD for both nanovesicles and nanofibers confirm loose molecular arrangement inside the nanovesicles and a more compact molecular arrangement inside the nanofibers.*

For the nanofibers, a signal at 2θ = 18.57°, corresponding to a d spacing of 4.77 Å, was observed, which is related to the spacing between two successive peptide backbones in a β-sheet arrangement. In addition, the characteristic reflection at 2θ = 10.20°, corresponding to a d spacing of 8.67 Å, was observed which is clearly demonstrated the distance between two β-sheets in the self-assembled nanofibers.[55] A typical peak at 2θ = 23.00°, corresponding to a d spacing of 3.86 Å, revealed the π-π stacking interactions. The powder X-ray diffraction data clearly demonstrated that the peptide bolaamphiphiles are self-assembled into a more ordered β-sheet arrangement inside the nanofibers rather than the nanovesicles.

7.4.6 NMR Study

To obtain more structural information, the hydrogel at two different states was characterized by ^{1}H and 2D NMR spectroscopy. Nanovesicles and nanofibers enriched hydrogels were lyophilized and characterized by NMR in DMSO-d_6 (Figure 7. 18-7. 21). All the ^{1}H NMR, ^{1}H-^{1}H COSY and ROESY spectra showed similar patterns for both the nanovesicle and nanofiber states. The ROESY spectra (Figure 7. 22-7. 23) for both the states showed that the tryptophan amide -CONH- protons are interacting with the -CH_2- protons of the succinic moiety. The NMR results demonstrated the twisting conformation of the selfassembled peptide bolaamphiphile in the hydrogel phase for both the nanostructures.

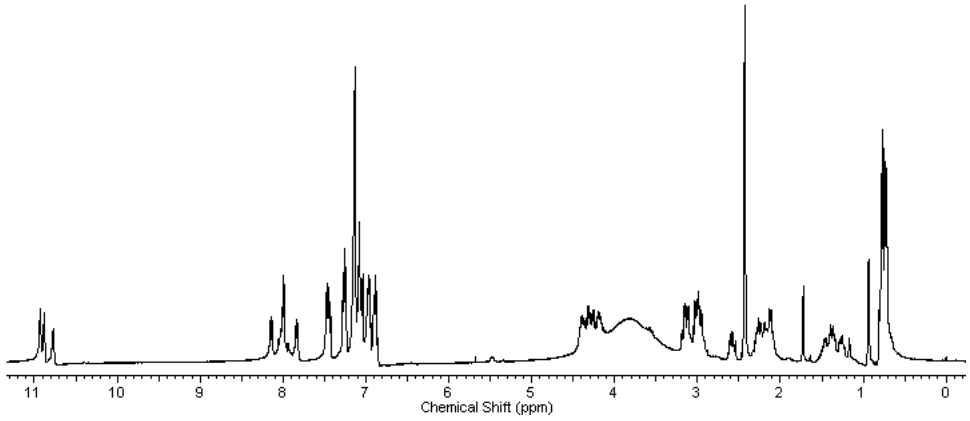

Figure 7.18. *^{1}H NMR (400 MHz) spectrum of dried hydrogel at 1 day (nanovesicle state) in DMSO-d_6.*

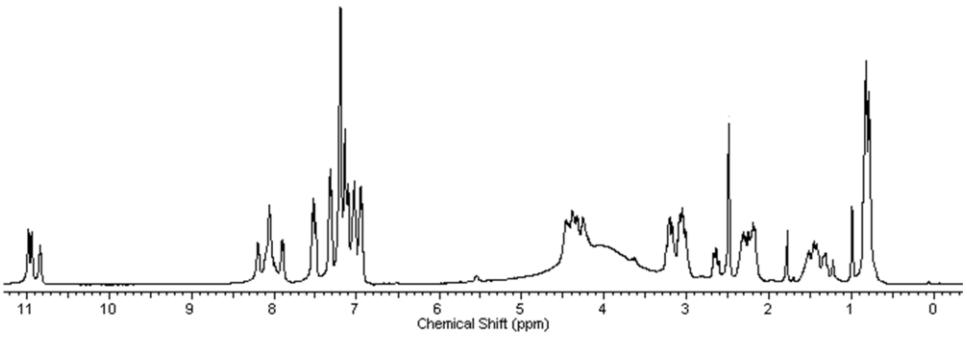

Figure 7.19. *^{1}H NMR (400 MHz) spectrum of dried hydrogel at 5 day (nanofiber state) in DMSO-d_6.*

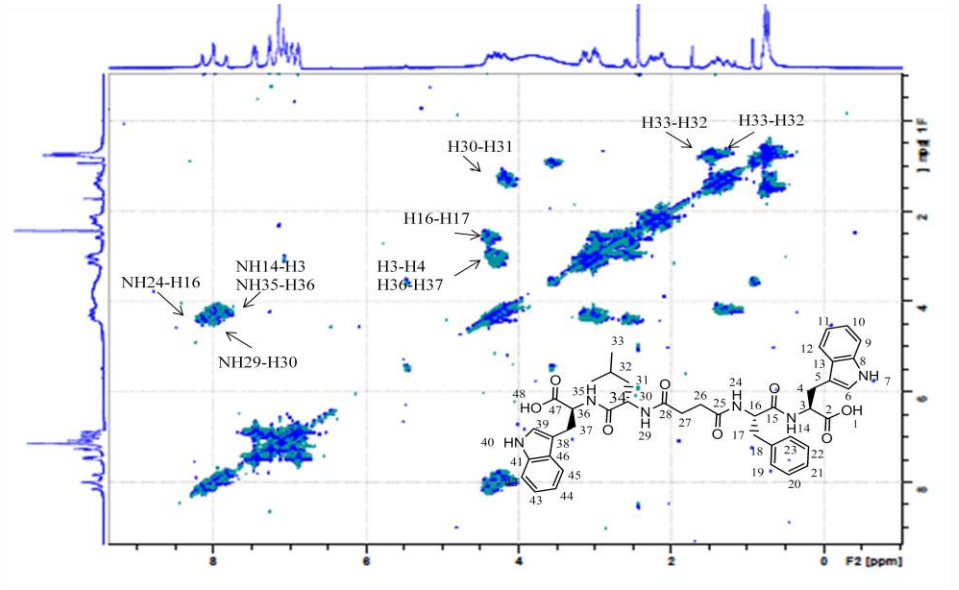

Figure 7.20. *^{1}H-^{1}H COSY spectrum of dried hydrogel at 1 day (nanovesicle state) in DMSO-d_6.*

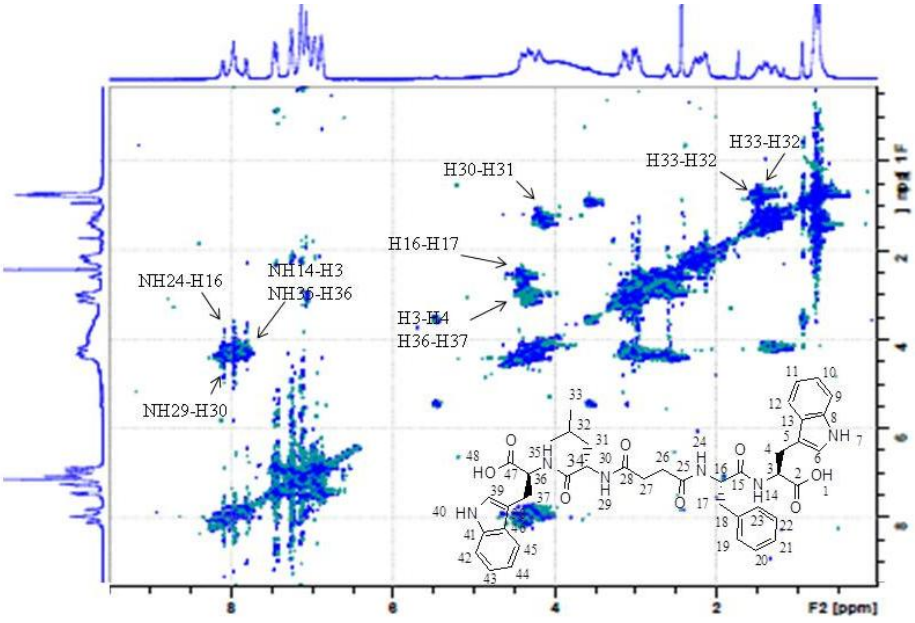

Figure 7.21. *^{1}H-^{1}H COSY spectrum of dried hydrogel at 5 day (nanofiber state) in DMSO-d_6.*

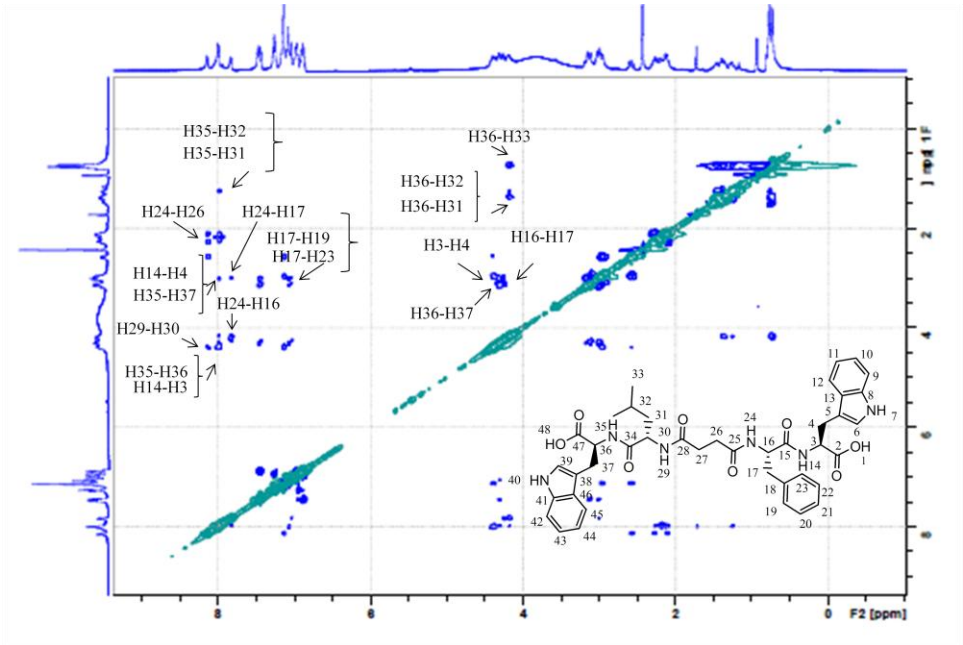

Figure 7.22. *ROESY spectrum of dried hydrogel at 1 day (nanovesicle state) in DMSO-d_6.*

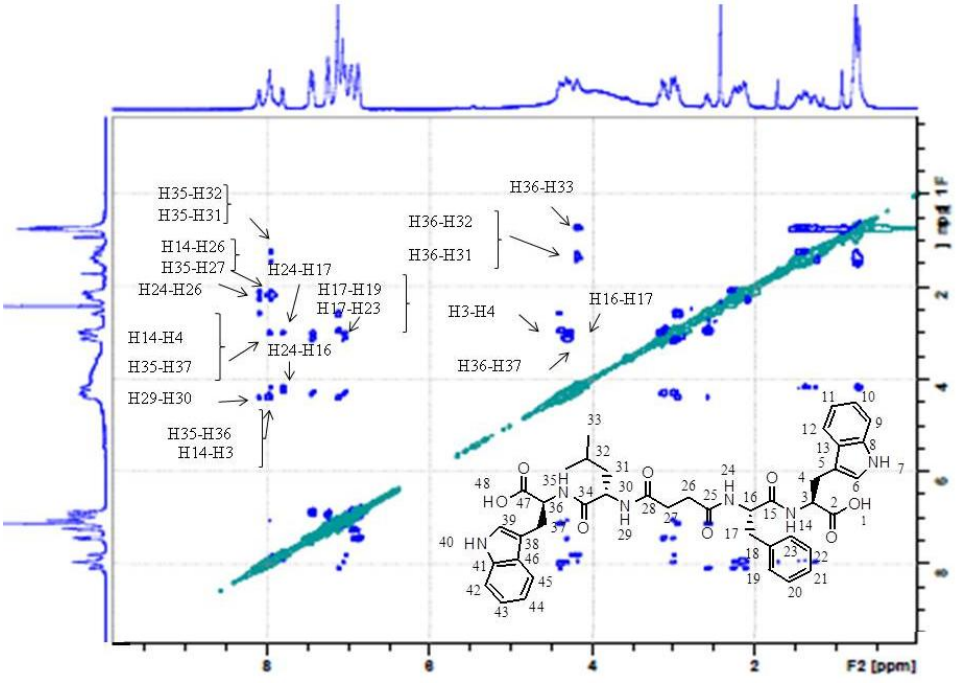

Figure 7.23. *ROESY spectrum of dried hydrogel at 5 day (nanofiber state) in DMSO-d_6.*

Here, we proposed a mechanism for the self-assembly process, which formulates the nanostructural transition from nanovesicles to nanofibers. Scheme 7.2.(d) gives a schematic representation of the morphological transformation. At an early stage, self-assembly leads to the formation of β-sheets, which form a curved sheet by a higher ordered self-assembly. Two-dimensional curved sheets result in the formation of nanovesicle structures.[65] After 4 days, nanofibrous morphology is formed *via* a reorientation of the stable β-sheet structures.

7.4.7 Dose Dependent Cytotoxicity

Cellular toxicity and proliferation studies with peptide-based materials have attracted increased research interest in the field of biomedicine and biotechnology.[66,67] We investigated the cytotoxic and biocompatible behaviour with the cell proliferation of this peptide bolaamphiphile. For this investigation, we cultured WBC (white blood corpuscle) cells with different concentrations of hydrogel. Total WBCs were isolated from chicken blood. A 20 mmol L^{-1} concentration of hydrogel stock solution was used to prepare the final concentrations of 10-100% in different wells (each in triplicate). Cells were incubated for 48 hours with the hydrogel solution and in media for the control experiment. The minimum essential media without phenol red was used to culture the cells. The effects on cell viability were calculated in percentages, considering the average absorbance value from the control samples to be 100%. The data from Table 7.1 shows that the cell viability and cell proliferation occurred at 40% and 50% hydrogel concentrations but the maximum increase in cell viability was found at a 50% concentration of hydrogel solution. The 30% concentration of hydrogel solution appeared to be safe but the rest of the concentrations were found to be either too suboptimal to exert any substantial effects or toxic (at higher doses). Data from the MTT assay consistently revealed the dose dependency of the used hydrogel as the best effect, which was observed at 50% media supplementation by hydrogel. Lower concentrations proved to be less effective and higher concentrations were found to be toxic in nature. The replacement of 50% of the culture media by hydrogel was most effective for cell proliferation. Cell viability suggested that the use of hydrogel along with media may be suitable to prevent toxicity and to increase viability and cell growth. Similar effects on

cellular viability and membrane fluidity were also observed earlier for drug compounds and herbal extracts.[68-70]

Table 7.1. *Evaluation of hydrogel preparation on cell viability and proliferation using MTT (3-[4,5-dimethylthiazol-2-yl]-2,5-diphenyl tetrazolium bromide) cell assay*

Percentage viability as compare to control	% of hydrogel
77.983 ± 2.608^{aa}	10
91.126 ± 2.310^{bb}	20
99.69 ± 1.862^{bb}	30
126.293 ± 1.184^{cc}	40
197.126 ± 4.063^{dd}	50
95.82 ± 2.263^{be}	60
93.26 ± 1.330^{be}	70
92.656 ± 2.343^{be}	80
49.843 ± 1.222^{ff}	90
35.47 ± 1.102^{gg}	100

Values are the mean ± SE of three measurements. Means in columns without letters in common differ significantly ($P \leq 0.05$).

7.5 Conclusions

In summary, we describe a sonication-induced phenylalanine and tryptophan-rich peptide bolaamphiphile **35** self-assembly through the synergistic effects of H-bonding and π-π stacking interactions. The self-assembling peptide bolaamphiphiles form self-supporting nanostructured fluorescent hydrogel. The self-programmed nanostructural transition from nanovesicles to nanofibers of peptide bolaamphiphiles occurs through the structural continuity of stable β-sheets. The real time nanostructural transition was examined by TEM and AFM. The molecular conformations and arrangements for both the cases were investigated thoroughly by various spectroscopic techniques. Spectroscopic studies

suggest loose β-sheet arrangements of peptide bolaamphiphiles inside the vesicles. Moreover, peptide bolaamphiphiles are self-assembled into more ordered and compact β-sheet arrangements inside the nanofibers. Furthermore, the peptide bolaamphiphile shows dose-dependent cytotoxic and cell-proliferation behaviour.

7.6 References

1. Ni R., Childers W. S., Hardcastle K. I., Mehta A. K., Lynn D. G. (2012), Remodeling cross-β nanotube surfaces with peptide/lipid chimeras, *Angew. Chem., Int. Ed*., 51, 6635-6638 (DOI: 10.1002/anie.201201173).

2. Yuran S., Razvag Y., Reches M. (2012), Coassembly of aromatic dipeptides into biomolecular necklaces, *Acs Nano*, 6, 9559-9566 (DOI: 10.1021/nn302983e).

3. Reiriz C., Brea R. J., Arranz R., Carrascosa J. L., Garibotti A., Manning B., Valpuesta J. M., Eritja R., Castedo L., Granja J. R. (2009), α,γ-Peptide nanotube templating of one-dimensional parallel fullerene arrangements, *J. Am. Chem. Soc.*, 131, 11335-11337 (DOI: 10.1021/ja904548q).

4. Montero A., Beierle J. M., Olsen C. A., Ghadiri M. R. (2009), Design, synthesis, biological evaluation, and structural characterization of potent histone deacetylase inhibitors based on cyclic α/β-tetrapeptide architectures, *J. Am. Chem. Soc.*, 131, 3033-3041 (DOI: 10.1021/ja809508f).

5. Scanlon S., Aggeli A. (2008), Self-assembling peptide nanotubes, *Nano Today*, 3, 22-30 (DOI: 10.1016/S1748-0132(08)70041-0).

6. Santoso S., Hwang W., Hartman H., Zhang S. (2002), Self-assembly of surfactant-like peptides with variable glycine tails to form nanotubes and nanovesicles, *Nano Lett.*, 2, 687-691 (DOI: 10.1021/nl025563i).

7. Marsden H. R., Handgraaf J.-W., Nudelman F., Sommerdijk N. A. J. M., Kros A. (2010), Uniting polypeptides with sequence-designed peptides: Synthesis and assembly of poly(γ-benzyl L-glutamate)-*β*-coiled-coil peptide copolymers, *J. Am. Chem. Soc.*, 132, 2370-2377 (DOI: 10.1021/ja909540a).

8. Matson J. B., Newcomb C. J., Bitton R., Stupp S. I. (2012), Nanostructure-templated control of drug release from peptide amphiphile nanofiber gels, *Soft Matter*, 8, 3586-3595 (DOI: 10.1039/C2SM07420F).

9. Maity I., Rasale D. B., Das A. K. (2012), Sonication induced peptide-appended bolaamphiphile hydrogels for *in situ* generation and catalytic activity of Pt nanoparticles, *Soft Matter*, 8, 5301-5308 (DOI: 10.1039/C2SM25126D).

10. Lee E., Kim J.-K., Lee M. (2008), Lateral association of cylindrical nanofibers into flLateral association of cylindrical nanofibers into flat ribbons triggered by molecular glue, *Angew. Chem., Int. Ed.*, 47, 6375-6378 (DOI: 10.1002/anie.200801496).

11. de Jong J. J. D., Lucas L. N., Kellogg R. M., van Esch J. H., Feringa B. L. (2004), Reversible optical transcription of supramolecular chirality into molecular chirality, *Science*, 304, 278-281 (DOI: 10.1126/science.1095353).

12. Segarra-Maset M. D., Nebot V. J., Miravet J. F., Escuder B. (2013), Control of molecular gelation by chemical stimuli, *Chem. Soc. Rev*., 42, 7086-7098 (DOI: 10.1039/C2CS35436E).

13. Ulijn R. V., Smith A. M. (2008), Designing peptide based nanomaterials, *Chem. Soc. Rev*., 37, 664-675 (DOI: 10.1039/B609047H).

14. Rehm T., Schmuck C. (2008), How to achieve self-assembly in polar solvents based on specific interactions? Some general guidelines, *Chem. Commun*., 801-813 (DOI: 10.1039/B710951M).

15. Smith K. H., Tejeda-Montes E., Poch M., Mata A. (2011), Integrating top-down and self-assembly in the fabrication of peptide and protein-based biomedical materials, *Chem. Soc. Rev.*, 40, 4563-4577 (DOI: 10.1039/C1CS15064B).

16. Kopecek J., Yang J. (2012), Smart self-assembled hybrid hydrogel biomaterials, *Angew. Chem., Int. Ed.*, 51, 7396-7417 (DOI: 10.1002/anie.201201040).

17. Georgieva J. V., Brinkhuis R. P., Stojanov K., Weijers C. A. G. M., Zuilhof H., Rutjes F. P. J. T., Hoekstra D., van Hest J. C. M., Zuhorn I. S. (2012), Peptide-mediated blood-brain barrier transport of polymersomes, *Angew. Chem., Int. Ed.*, 51, 8339-8342 (DOI: 10.1002/anie.201202001).

18. Naskar J., Palui G., Banerjee A. (2009), Tetrapeptide-based hydrogels: For encapsulation and slow release of an anticancer drug at physiological pH, *J. Phys. Chem. B*, 113, 11787-11792 (DOI: 10.1021/jp904251j).

19. Lim Y.-B., Lee E., Yoon Y.-R., Lee M. S., Lee M. (2008), Filamentous artificial virus from a self-assembled discrete nanoribbon, *Angew. Chem., Int. Ed.*, 47, 4525-4528 (DOI: 10.1002/anie.200800266).

20. Kehr N. S., Prasetyanto E. A., Benson K., Ergun B., Galstyan A., Galla H.-J. (2013), Periodic mesoporous organosilica-based nanocomposite hydrogels as three-dimensional scaffolds, *Angew. Chem., Int. Ed.*, 52, 1156-1160 (DOI: 10.1002/anie.201206951).

21. DeForest C. A., Anseth K. S. (2012), Photoreversible patterning of biomolecules within click-based hydrogels, *Angew. Chem., Int. Ed*., 51, 1816-1819 (DOI: 10.1002/anie.201106463).

22. Webber M. J., Tongers J., Newcomb C. J., Marquardt K.-T., Bauersachs J., Losordo D. W., Stupp S. I. (2011), Supramolecular nanostructures that mimic VEGF as a strategy for ischemic tissue repair, *Proc. Natl. Acad. Sci. U. S. A.*, 108, 13438-13443 (DOI: 10.1073/pnas.1016546108).

23. Tian B., Liu J., Dvir T., Jin L., Tsui J. H., Qing Q., Suo Z., Langer R., Kohane D. S., Lieber C. M. (2012), Macroporous nanowire nanoelectronic scaffolds for synthetic tissues, *Nat. Mater*., 11, 986-994 (DOI:10.1038/nmat3404).

24. Seliktar D. (2012), Designing cell-compatible hydrogels for biomedical applications, *Science*, 336, 1124-1128 (DOI: 10.1126/science.1214804).

25. Omenetto F. G., Kaplan D. L. (2010), New opportunities for an ancient material, *Science*, 329, 528-531 (DOI: 10.1126/science.1188936).

26. Hirst A. R., Escuder B., Miravet J. F., Smith D. K. (2008), High-tech applications of self-assembling supramolecular nanostructured gel-phase materials: From regenerative medicine to electronic devices, *Angew. Chem., Int. Ed.*, 47, 8002-8018 (DOI: 10.1002/anie.200800022).

27 Roy S., Maiti D. K., Panigrahi S., Basak D., Banerjee A. (2012), A new hydrogel from an amino acid-based perylene bisimide and its semiconducting, photo-switching behaviour, *RSC Adv*., 2, 11053-11060 (DOI: 10.1039/C2RA21319B).

28. Xu H., Das A. K., Horie M., Shaik M. S., Smith A. M., Luo Y., Lu X., Collins R., Liem S. Y., Song A., Popelier P. L. A., Turner M. L., Xiao P., Kinloch I. A., Ulijn R. V. (2010), An investigation of the conductivity of peptide nanotube networks prepared by enzyme-triggered self-assembly, *Nanoscale*, 2, 960-966 (DOI: 10.1039/B9NR00233B).

29. Whitehouse C., Fang J., Aggeli A., Bell M., Brydson R., Fishwick C. W. G., Henderson J. R., Knobler C. M., Owens R. W., Thomson N. H., Smith D. A., Boden N. (2005), Adsorption and self-assembly of peptides on mica substrates, *Angew. Chem., Int. Ed.*, 44, 1965-1968 (DOI: 10.1002/anie.200462160).

30. Larsen T. H., Branco M. C., Rajagopal K., Schneider J. P., Furst E. M. (2009), Sequence-dependent gelation kinetics of β-hairpin peptide hydrogels, *Macromolecules*, 42, 8443-8450 (DOI: 10.1021/ma901423n).

31. Maity I., Rasale D. B., Das A. K. (2013), Exploiting a self-assembly driven dynamic nanostructured library, *RSC Adv*., 3, 6395-6400 (DOI: 10.1039/C3RA22401E).

32. Pochan D. J., Schneider J. P., Kretsinger J., Ozbas B., Rajagopal K., Haines L. (2003), Thermally reversible hydrogels via intramolecular folding and consequent self-assembly of a de novo designed peptide, *J. Am. Chem. Soc*., 125, 11802-11803 (DOI: 10.1021/ja0353154).

33. Sanchez-Ferrer A., Kotharangannagari V. K., Ruokolainen J., Mezzenga R. (2013), Thermo-responsive peptide-based triblock copolymer hydrogels, *Soft Matter*, 9, 4304-4311 (DOI: 10.1039/C3SM27690B).

34. Haines L. A., Rajagopal K., Ozbas B., Salick D. A., Pochan D. J., Schneider J. P. (2005), Light-activated hydrogel formation via the triggered folding and self-assembly of a designed peptide, *J. Am. Chem. Soc*.,127, 17025-17029 (DOI: 10.1021/ja054719o).

35. Lowik D. W. P. M., Leunissen E. H. P., van den Heuvel M., Hansen M. B., van Hest J. C. M. (2010), Stimulus responsive peptide based materials, *Chem. Soc. Rev.*, 39, 3394-3412 (DOI: 10.1039/B914342B).

36. Yucel T., Micklitsch C. M., Schneider J. P., Pochan D. J. (2008), Direct observation of early-time hydrogelation in β-hairpin peptide self-assembly, *Macromolecules*, 41, 5763-5772 (DOI: 10.1021/ma702840q).

37. Yang Z., Liang G., Xu B. (2008), Enzymatic hydrogelation of small molecules, *Acc. Chem. Res*., 41, 315-326 (DOI: 10.1021/ar7001914).

38. Hu J., Zhang G., Liu S. (2012), Enzyme-responsive polymeric assemblies, nanoparticles and hydrogels, *Chem. Soc. Rev*., 41, 5933-5949 (DOI: 10.1039/C2CS35103J).

39. Rasale D. B., Maity I., Das A. K. (2012), Emerging π-stacked dynamic nanostructured library, *RSC. Adv*., 2, 9791-9794 (DOI: 10.1039/C2RA21334F).

40. Das A. K., Collins R., Ulijn R. V. (2008), Exploiting enzymatic (reversed) hydrolysis in directed self-Assembly of peptide nanostructures, *Small*, 4, 279-287 (DOI: 10.1002/smll.200700889).

41. Ray S., Das A. K., Banerjee A. (2007), pH-responsive, bolaamphiphile-based smart metallo-hydrogels as potential dye-adsorbing agents, water purifier, and vitamin B12 carrier, *Chem. Mater*., 19, 1633-1639 (DOI: 10.1021/cm062672f).

42. Aggeli A., Bell M., Carrick L. M., Fishwick C. W. G., Harding R., Mawer P. J., Radford S. E., Strong A. E., Boden N. (2003), pH as a trigger of peptide β-sheet self-assembly and reversible switching between nematic and isotropic phases, *J. Am. Chem. Soc*., 125, 9619-9628 (DOI: 10.1021/ja021047i).

43. Shao H., Parquette J. R. (2009), Controllable peptide-dendron self-assembly: Interconversion of nanotubes and fibrillar nanostructures, *Angew. Chem., Int. Ed*., 48, 2525-2528 (DOI: 10.1002/anie.200805010).

44. Pashuck E. T., Stupp S. I. (2010), Direct observation of morphological tranformation from twisted ribbons into helical ribbons, *J. Am. Chem. Soc*., 132, 8819-8821 (DOI: 10.1021/ja100613w).

45. Sadownik J. W., Leckie J., Ulijn R. V. (2011), Micelle to fibre biocatalytic supramolecular transformation of an aromatic peptide amphiphile, *Chem. Commun*., 47, 728-730 (DOI: 10.1039/C0CC03796F).

46. Sahoo J. K., Nalluri S. K. M., Javid N., Webb H., Ulijn R. V. (2014), Biocatalytic amide condensation and gelation controlled by light, *Chem. Commun.*, 50, 5462-5464 (DOI: 10.1039/C4CC01431F).

47. Gao J., Wang H., Wang L., Wang J., Kong D., Yang Z. (2009), Enzyme promotes the hydrogelation from a hydrophobic small molecule, *J. Am. Chem. Soc*., 131, 11286-11287 (DOI: 10.1021/ja9042142).

48. Shimizu T., Masuda M., Minamikawa H. (2005), Supramolecular nanotube architectures based on amphiphilic molecules, *Chem. Rev*., 105, 1401-1443 (DOI: 10.1021/cr030072j).

49. Djalali R., Samson J., Matsui H. (2004), Doughnut-shaped peptide nano-assemblies and their applications as nanoreactors, *J. Am. Chem. Soc.*, 126, 7935-7939 (DOI: 10.1021/ja0319691).

50. Wang T., Jiang J., Liu Y., Li Z., Liu M. (2010), Hierarchical self-assembly of bolaamphiphiles with a hybrid spacer and L-glutamic acid headgroup: pH- and surface-triggered hydrogels, vesicles, nanofibers, and nanotubes, *Langmuir*, 26, 18694-18700 (DOI: 10.1021/la103435t).

51. Krall N., Scheuermann J., Neri D. (2013), Small targeted cytotoxics: Current state and promises from DNA-encoded chemical libraries, *Angew. Chem., Int. Ed*, 52, 1384-1402 (DOI: 10.1002/anie.201204631).

52. von Nussbaum F., Brands M., Hinzen B., Weigand S., Habich D. (2006), Antibacterial natural products in medicinal chemistry-exodus or revival?, *Angew. Chem., Int. Ed*., 45, 5072-5129 (DOI: 10.1002/anie.200600350).

53. Kwiatkowska A., Couture F., Levesque C., Ly K., Desjardins R., Beauchemin S., Prahl A., Lammek B., Neugebauer W., Dory Y. L., Day R. (2014), Design, synthesis, and structure-activity relationship studies of a potent PACE4 inhibitor, *J. Med. Chem*., 57, 98-109 (DOI: 10.1021/jm401457n).

54. Baral A., Roy S., Dehsorkhi A., Hamley I. W., Mohapatra S., Ghosh S., Banerjee A. (2014), Assembly of an injectable noncytotoxic peptide-based hydrogelator for sustained release of drugs, *Langmuir*, 30, 929-936 (DOI: 10.1021/la4043638).

55. Ke D., Zhan C., Li A. D. Q., Yao J. (2011), Morphological transformation between nanofibers and vesicles in a controllable bipyridine-tripeptide self-assembly, *Angew. Chem., Int. Ed*., 50, 3715-3719 (DOI: 10.1002/anie.201006897).

56. Ghosh S., Reches M., Gazit E., Verma S. (2007), Bioinspired design of nanocages by self-assembling triskelion peptide elements, *Angew. Chem., Int. Ed.*, 46, 2002-2004 (DOI: 10.1002/anie.200604383).

57. Rasale D. B., Maity I., Konda M., Das A. K. (2013), Peptide self-assembly driven by oxo-ester mediated native chemical ligation, *Chem. Commun.*, 49, 4815-4817 (DOI: 10.1039/C3CC41475B).

58. Bose P. P., Das A. K., Hegde R. P., Shamala N., Banerjee A. (2007), pH-Sensitive nanostructural transformation of a synthetic self-assembling water-soluble tripeptide: Nanotube to nanovesicle, *Chem. Mater.*, 19, 6150-6157 (DOI: 10.1021/cm0716147).

59. Sun K., Chen K., Xue G., Cai J., Zou G., Li Y., Zhang Q. (2013), Near-infrared light induced fusion and fission of azobenzene-containing polymer vesicles, *RSC Adv.*, 3, 23997-24000 (DOI: 10.1039/c3ra44055a).

60. Pelton J. T., McLean L. R. (2000), Spectroscopic methods for analysis of protein secondary structure, *Anal. Biochem.*, 277, 167-176 (DOI: 10.1006/abio.1999.4320).

61. Datta S., Samanta S. K., Bhattacharya S. (2013), Induction of supramolecular chirality in the self-assemblies of lipophilic pyrimidine derivatives by choice of the amino acid-based chiral spacer, *Chem.-Eur. J.*, 19, 11364-11373 (DOI: 10.1002/chem.201300605).

62. Yan X., Cui Y., He Q., Wang K., Li J. (2008), Organogels based on self-assembly of diphenylalanine peptide and their application to immobilize quantum dots, *Chem. Mater.*, 20, 1522-1526 (DOI: 10.1021/cm702931b).

63. Maity I., Manna M. K., Rasale D. B., Das A. K. (2014), Peptide-nanofiber-supported palladium nanoparticles as an efficient catalyst for the removal of N-terminus protecting groups, *ChemPlusChem.*, 79, 413-420 (DOI: 10.1002/cplu.201300348).

64. Morris K. L., Zibaee S., Chen L., Goedert M., Sikorski P., Serpell L. C. (2013), The structure of cross-β tapes and tubes formed by an octapeptide, αSβ1, *Angew. Chem., Int. Ed.*, 52, 2279-2283 (DOI: 10.1002/anie.201207699).

65. Naskar J., Banerjee A. (2009), Concentration dependent transformation of oligopeptide based nanovesicles to nanotubes and an application of nanovesicles, *Chem.-Asian J.*, 4, 1817-1823 (DOI: 10.1002/asia.200900274).

66. Jayawarna V., Ali M., Jowitt T. A., Miller A. F., Saiani A., Gough J. E., Ulijn R. V. (2006), Nanostructured hydrogels for three-dimensional cell culture through self-assembly of fluorenylmethoxycarbonyl-dipeptides, *Adv. Mater.*, 18, 611-614 (DOI: 10.1002/adma.200501522).

67. Kuang Y., Xu B. (2013), Disruption of the dynamics of microtubules and selective inhibition of glioblastoma cells by nanofibers of small hydrophobic molecules, *Angew. Chem., Int. Ed.*, 52, 6944-6948 (DOI: 10.1002/anie.201302658).

68. Parmar H. S., Kar A. (2008), Medicinal values of fruit peels from citrus sinensis, punica granatum, and musa paradisiaca with respect to alterations in tissue lipid peroxidation and serum concentration of glucose, insulin, and thyroid hormones, *J. Med. Food*., 11, 376-381 (DOI:10.1089/jmf.2006.010.).

69. Parmar H. S., Kar A. (2009), Comparative analysis of free radical scavenging potential of several fruit peel extracts by in vitro methods, *Drug Discov. Ther*., 3, 49-55.

70. Sethi A., Parmar H. S., Kumar A. (2011), The effect of aspirin on atherogenic diet-induced diabetes mellitus, *Basic Clin. Pharmacol*. *Toxicol.*, 108, 371-377 (DOI: 10.1111/j.1742-7843.2010.00663.x).

Chapter 8

Lipase Catalyzed Dissipative Self-Assembly of a Thixotropic Peptide Bolaamphiphile Hydrogel for Human Umbilical Cord Stem Cells Proliferation.

8.1 Introduction

Dissipative self-assembly is observed when non-assembling building blocks get activated towards assembling building blocks through constant influx of chemical energy.[1] In nature, self-assembled structures are evolved transiently. Self-assembled systems are guided by dissipative self-assembly (DSA) process[2,3] which are far from equilibrium. In this process, non-assembling building blocks are activated by a constant influx of energy which further on self-assembly process organized into ordered structures. However, the ordered structures can collapse by dissipation of energy, which is associated with reproduction of initial non-assembling building blocks. On the way of natural evolution, self-assembled bio-architectures such as cytoskeleton[4] and phospholipid membranes[5] are formed by dissipative self-assembly process. An abiotic example of dissipative self-assembly was described by van Esch *et al.*. An unactivated dibenzoyl-(L)-cystine (DBC) turned to activated self-assembling unit of diesters by a constant energy source of methyl iodide.[6] The subsequent hydrolysis again resulted in the formation of non-assembling dibenzoyl-(L)-cystine (DBC). Dissipative self-assembly[7,8] and reversible chemical reactions directed self-assembly[9] are indispensable for natural evolution and critical cellular functions. Otto *et al.* reported the evolution of several peptide networks based on dynamic combinatorial libraries where self-assembly process played a pioneer role to direct the molecules for their own formation.[10,11] They reported an interesting example of hydrogel formation upon photoinduced covalent capture of macrocycle stacks from dynamic combinatorial libraries.[12] Giuseppone *et al.* presented the dynamic combinatorial evolution within self-replicating supramolecular assemblies.[13] Our group has also dedicated to design hydrogels through dynamic combinatorial libraries of peptide networks.[14] Ulijn *et al.* reported enzyme-assisted self-assembly of Fmoc-capped peptides under thermodynamic control.[15]

To deal with biological system, enzymes are the best choice for effective biocatalyst. Generally, an esterase lipase shows its hydrolysis ability towards esters in aqueous medium with substrate specificity. The ester hydrolysis is preferred process rather than ester formation in aqueous medium. Enzymatically sugar-containing self-assembled

organogels with nanostructured morphologies were reported where numbers of sugar based diesters were synthesized by lipase B from *candida Antarctica* (CALB) in acetonitrile medium.[16] Another interesting example of dynamic combinatorial library was reported in which first step was thermodynamically controlled nitroaldol reaction and the second step was kinetically controlled lipase mediated acylation reaction.[17] There are several examples of enzymatic ester formation in organic medium[18,19] but the esterase mediated esterification in aqueous medium is extremely difficult.[20] Inspite of these challenging issues, our effort establish to design soft thixotropic hydrogel material *via* lipase catalysed dynamic esterification reaction. Here, we report enzyme catalyzed dissipative self-assembly under the influx of a chemical fuel. Thixotropic materials[21,22] are less viscous under stress and capable to go back in their original state when stress is removed. These materials are used in tissue engineering applications.[23] Thixotropic materials are also used as therapeutic agents as well as to make gel-cell constructs.[24] Here, our objectives are (a) lipase catalyzed regiospecific inclusion of *p*-hydroxybenzyl alcohol in aqueous medium, (b) to extend the scope of biocatalytic evolution of dynamic combinatorial library, (c) to mimic the natural dissipative self-assembly systems[25] and (d) to design the thixotropic hydrogel material for stem cell proliferation.

8.2 Experimental

8.2.(1) Synthesis of Bolaamphiphile

Peptide bolaamphiphiles **37, 38, 25, 39, 40** and **3** employed in this chapter were synthesized by conventional solution phase methodology. The C-terminus of amino acid was protected as methyl ester. Couplings were mediated by diisopropylcarbodiimide-1-hydroxybenzotriazole (DIPC-HOBt). The final compounds were purified and fully characterized by FT-IR, ^{1}H NMR and mass spectral studies. The synthesis of HO-Tyr-Suc-Tyr-OH **28**, HO-Phe-Tyr-Suc-Tyr-Phe-OH **25,** HO-Leu-Suc-Leu-OH **11** and HO-Leu-Leu-Suc-Leu-Leu-OH **3** are described in chapters 5 and 3.

8.2.1 Synthesis of Bolaamphiphile (HO-Trp(4)-Tyr(3)-Suc-Tyr(1)-Trp(2)-OH) 37:

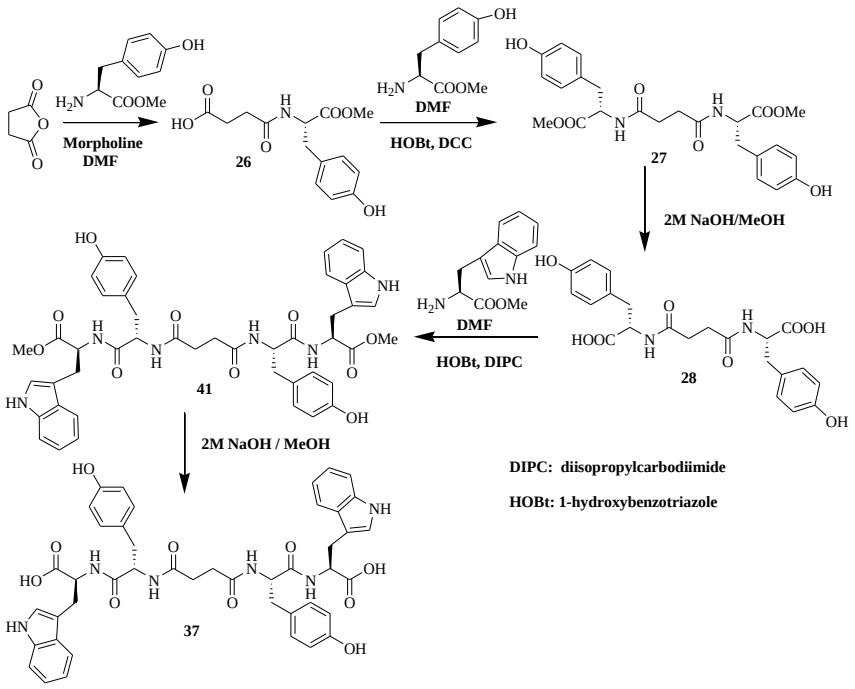

Scheme 8.1. *Synthetic scheme of peptide bolaamphiphile **37**.*

*(a) Synthesis of MeO-Trp(4)-Tyr(3)-Suc-Tyr(1)-Trp(2)-OMe **41**:* 1.77 g (4 mmol) of HO-Tyr(2)-Suc-Tyr(1)-OH **28** in 3 mL of DMF was cooled in an ice bath and H-Trp-OMe was isolated from 4.06 g (16 mmol) of the corresponding methyl ester hydrochloride by neutralization and subsequent extraction with ethyl acetate and the ethyl acetate extract was concentrated to 8 mL. It was then added to the reaction mixture, followed immediately by 1.11 g (8.8 mmol, 1 mL 372 μL) DIPC and 1.18 g (8.8 mmol) of HOBt. The reaction mixture was stirred for overnight. The residue was taken up in ethyl acetate (50 mL) and the DIU was filtered off. The organic layer was washed with 1M HCl (3 × 50 mL), brine (2 × 50 mL), 1M sodium carbonate (3 × 50 mL), brine (2 × 50 mL) and dried over anhydrous sodium sulfate and evaporated under vacuum to yield **41** as a white solid. Purification was done by silica gel column (100-200 mesh) using chloroform-methanol (9:1) as eluent.

Yield: 2.87 g (3.4 mmol, 85%); FT-IR (KBr): ῡ = 3390 (st), 3310 (broad), 1733 (ms), 1647 (st), 1616 (st), 1541 (ms), 1515 (ms) cm^{-1}; ^{1}H NMR (400 MHz, DMSO-d_6, δ_{ppm}):

10.84 (2H, ring -NHs of Trp(2) and Trp(4)), 8.40 (d, *J* = 7.6 Hz, 2H, -NHs of Tyr(1) and Tyr(3)), 8.07 (d, *J* = 8.4 Hz, 2H, -NHs of Trp(2) and Trp(4)), 7.63 (d, *J* = 8 Hz, 2H, ring protons of Trp(2) and Trp(4)), 7.38 (d, *J* = 8 Hz, 2H, ring protons of Trp(2) and Trp(4)), 7.10 (t, *J* = 7.2 Hz, 4H, ring protons of Trp(2) and Trp(4)), 7.04 (d, *J* = 8.4 Hz, 6H, ring protons of Tyr(1), Tyr(3) and Trp(2) and Trp(4)), 6.72 (d, *J* = 8 Hz, 4H, ring protons of Tyr(1) and Tyr(3)), 4.60 (m, 2H, $C^{\alpha}Hs$ of Trp(2) and Trp(4)), 4.42 (m, 2H, $C^{\alpha}Hs$ of Tyr(1) and Tyr(3)), 3.59 (s, 6H, $-COOCH_3$), 3.11 and 2.97 (d, *J* = 4.8 Hz and *J* = 6.8 Hz, 4H, $C^{\beta}Hs$ of Trp(2) and Trp(4)), 2.92 and 2.88 (d, *J* = 6 Hz, and *J* = 8.4 Hz, 4H, $C^{\beta}Hs$ of Tyr(1) and Tyr(3)), 2.33-2.21 (m, 4H, $-CH_2-$ of Suc); $[\alpha]_D^{20}$ = -28.33 (*c* = 0.3 in CH_3OH); MS (ESI) m/z: $(M+Na)^+$ Calcd. for $C_{46}H_{48}N_6O_{10}Na$: 867.3330; found: 867.3338.

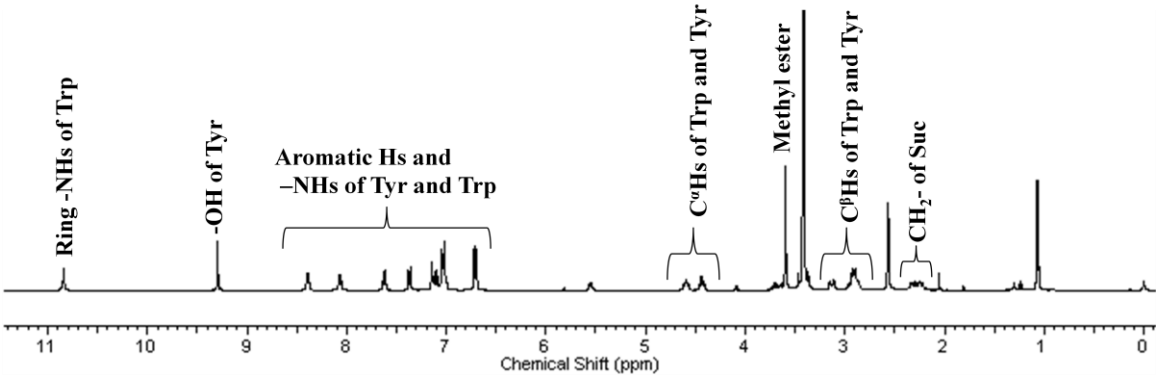

Figure 8.1. *^{1}H NMR spectrum (400 MHz, DMSO-d_6) of MeO-W-Y-Suc-Y-W-OMe* ***41***.

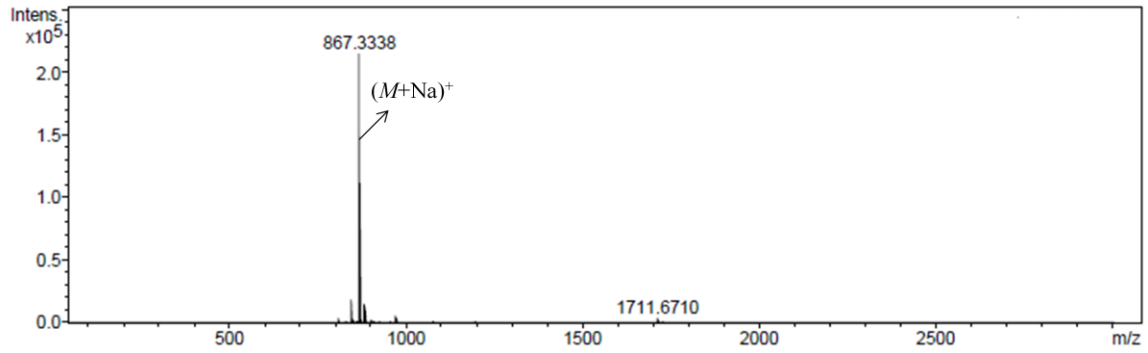

Figure 8.2. *ESI-MS spectrum of MeO-W-Y-Suc-Y-W-OMe* ***41***.

*(b) Synthesis of HO-Trp(4)-Tyr(3)-Suc-Tyr(1)-Trp(2)-OH **37**:* 2.53 g (3 mmol) of MeO-Trp(4)-Tyr(3)-Suc-Tyr(1)-Trp(2)-OMe **41** in 15 mL MeOH was taken in a round bottom flask and 2M NaOH was added to it dropwise. The reaction was monitored by thin layer chromatography (TLC). The reaction mixture was stirred for overnight. 15 mL of distilled water was added to the reaction mixture and MeOH was removed under vacuum. The aqueous part was washed with diethyl ether (2 × 30 mL). Then it was cooled under ice bath for 10 minutes and then pH was adjusted to 1 by drop wise addition of 1M HCl. It was extracted by ethyl acetate (3 × 50 mL) and then the ethyl acetate part was dried over anhydrous Na_2SO_4 and evaporated under vacuum to yield **37** as a white solid.

Yield: 2.32 g (2.85 mmol, 95%); FT-IR (KBr): ῡ = 3311 (broad), 1717 (ms), 1647 (st), 1637 (st), 1616 (st), 1541 (ms), 1514 (ms) cm^{-1}; ^1H NMR (400 MHz, DMSO-d_6, δ_{ppm}): 12.71 (2H, -COOH), 10.90 (2H, ring -NHs of Trp(2) and Trp(4)), 8.27 (d, *J* = 7.2 Hz, 2H, -NHs of Tyr(1) and Tyr(3)), 8.03 (d, *J* = 8.4 Hz, 2H, -NHs of Trp(2) and Trp(4)), 7.59 (d, *J* = 8 Hz, 2H, ring protons of Trp(2) and Trp(4)), 7.39 (d, *J* = 8 Hz, 2H, ring protons of Trp(2) and Trp(4)), 7.21 (d, *J* = 2 Hz, 2H, ring protons of Trp(2) and Trp(4)), 7.11 (t, *J* = 7.2 Hz, 2H, ring protons of Trp(2) and Trp(4)), 7.06 (d, *J* = 8.4 Hz, 4H, ring protons of Tyr(1) and Tyr(3)), 7.02 (t, *J* = 8.4 Hz, 2H, ring protons of Trp(2) and Trp(4)), 6.67 (d, *J* = 8.4 Hz, 4H, ring protons of Tyr(1) and Tyr(3)), 4.55-4.46 (m, 4H, C^{α}Hs of Tyr(1), Tyr(3), Trp(2) and Trp(4)), 3.22 and 3.12 (d, *J* = 5.6 Hz and *J* = 8 Hz, 4H, C^{β}Hs of Trp(2) and Trp(4)), 2.94 and 2.62 (d, *J* = 3.6 Hz, and *J* = 3.6 Hz, 4H, C^{β}Hs of Tyr(1) and Tyr(3)), 2.26-2.16 (m, 4H, -CH_2- of Suc); ^{13}C NMR (100 MHz, DMSO-d_6, δ_{ppm}): 173.16, 171.45, 171.18, 155.61, 136.00, 130.04, 127.97, 127.13, 123.62, 120.88, 118.35, 118.10, 114.74, 111.32, 109.59, 53.97, 52.85, 36.64, 30.73, 26.91; $[\alpha]_D^{20}$ = -10.75 (*c* = 0.3 in CH_3OH); MS (ESI) *m/z*: $(M+K)^+$ Calcd. for $C_{44}H_{44}N_6O_{10}K$, 855.2756; found 855.2753.

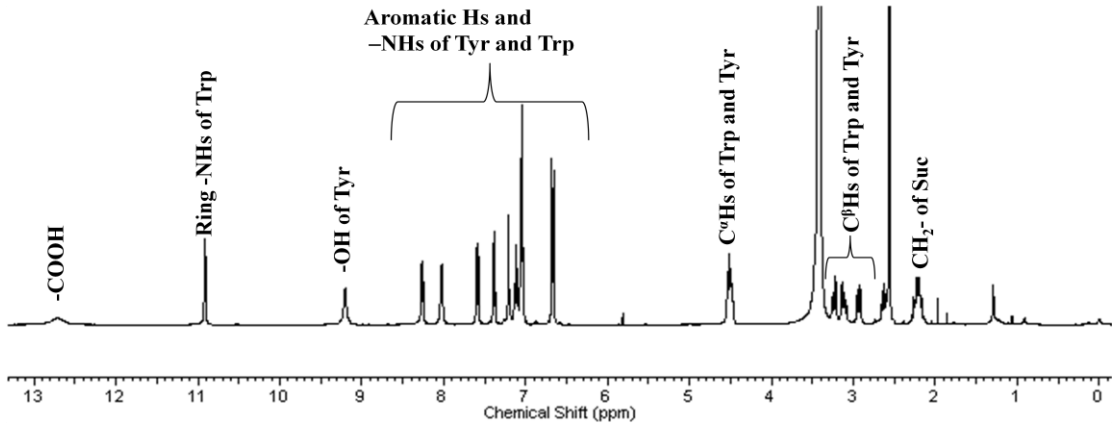

Figure 8.3. *^{1}H NMR spectrum (400 MHz, DMSO-d_6) of HO-W-Y-Suc-Y-W-OH **37**.*

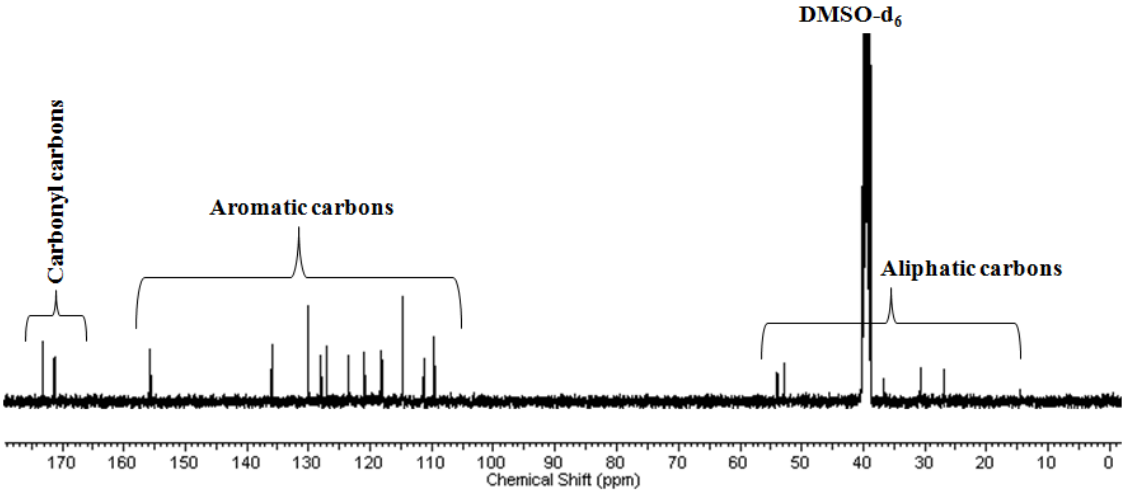

Figure 8.4. *^{13}C NMR spectrum (100 MHz, DMSO-d_6) of HO-W-Y-Suc-Y-W-OH **37**.*

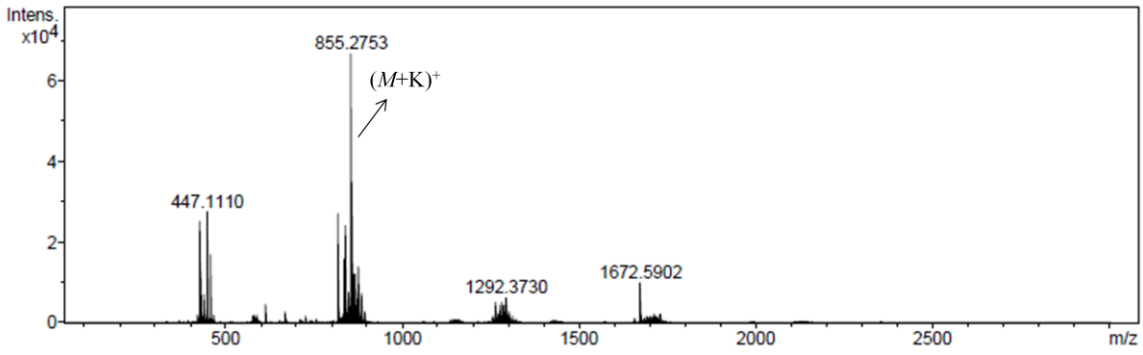

Figure 8.5. *ESI-MS spectrum of HO-W-Y-Suc-Y-W-OH **37**.*

8.2.2 Synthesis of Bolaamphiphile (HO-Trp(4)-Leu(3)-Suc-Leu(1)-Trp(2)-OH) 38:

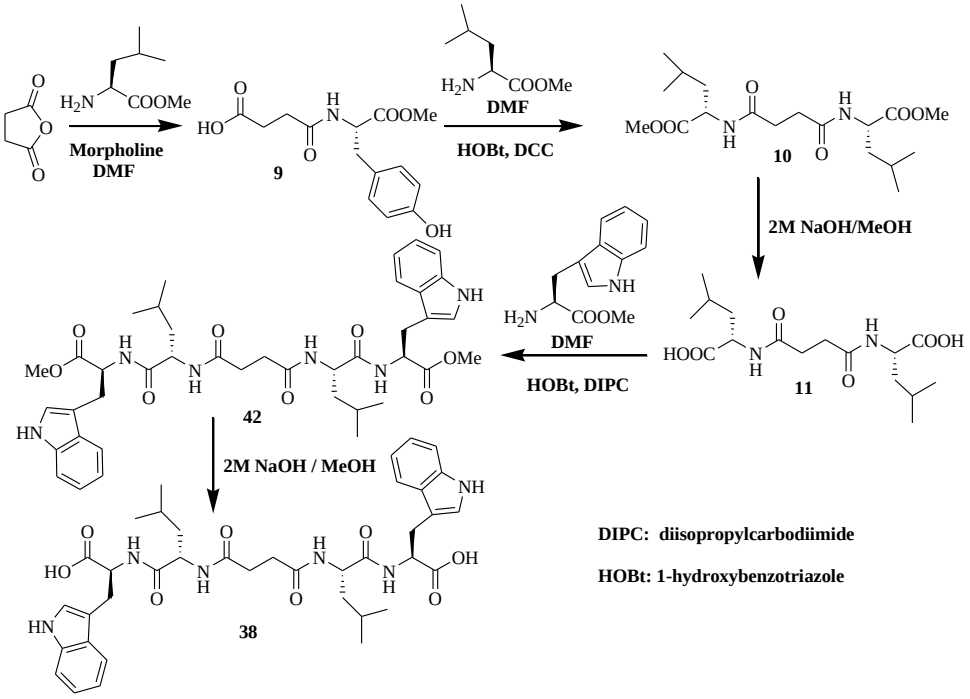

Scheme 8.2. *Synthetic scheme of peptide bolaamphiphile **38**.*

*(a) Synthesis of MeO-Trp(4)-Leu(3)-Suc-Leu(1)-Trp(2)-OMe **42**:* 1.72 g (5 mmol) of HO-Leu(2)-Suc-Leu(1)-OH **11** in 5 mL of DMF was cooled in an ice bath and H-Trp-OMe was isolated from 5.07 g (20 mmol) of the corresponding methyl ester hydrochloride by neutralization and subsequent extraction with ethyl acetate and the ethyl acetate extract was concentrated to 10 mL. It was then added to the reaction mixture, followed immediately by 1.38 g (11 mmol, 1 mL 715 μL) DIPC and 1.47 g (11 mmol) of HOBt. The reaction mixture was stirred for overnight. The residue was taken up in ethyl acetate (50 mL) and the DIU was filtered off. The organic layer was washed with 1M HCl (3 × 50 mL), brine (2 × 50 mL), 1M sodium carbonate (3 × 50 mL), brine (2 × 50 mL) and dried over anhydrous sodium sulfate and evaporated under vacuum to yield **42** as a white solid. Purification was done by silica gel column (100-200 mesh) using chloroform-methanol (9:1) as eluent.

Yield: 3.05 g (4.1 mmol, 82%); FT-IR (KBr): ῡ = 3389 (w), 3296 (broad), 1735 (ms), 1638 (st), 1618 (ms), 1541 (ms), 1523 (ms) cm^{-1}; ^1H NMR (400 MHz, $CDCl_3$, δ_{ppm}): 8.86

(2H, ring -NHs of Trp(2) and Trp(4)), 7.62 (d, *J* = 7.6 Hz, 2H, ring protons of Trp(2) and Trp(4)), 7.50 (d, *J* = 8.8 Hz, 2H, ring protons of Trp(2) and Trp(4)), 7.30 (d, *J* = 7.6 Hz, 2H, -NHs of Leu(1) and Leu(3)), 7.11 and 7.04 (t, *J* = 6.4 Hz and *J* = 7.6 Hz, 4H, ring protons of Trp(2) and Trp(4)), 6.98 (s, 2H, ring protons of Trp(2) and Trp(4)), 5.83 (d, *J* = 8.8 Hz, 2H, -NHs of Trp(2) and Trp(4)), 4.89 (m, 2H, C^{α}Hs of Trp(2) and Trp(4)), 4.52 (m, 2H, C^{α}Hs of Leu(1) and Leu(3)), 3.62 (s, 6H, $-COOCH_3$), 3.30 and 3.12 (d, *J* = 4.4 Hz and *J* = 5.2 Hz, 4H, C^{β}Hs of Trp(2) and Trp(4)), 2.44 and 2.29 (m, 4H, $-CH_2-$ of Suc), 1.44 and 1.38 (m, 6H, C^{β}Hs and C^{γ}Hs of Leu(1) and Leu(3)), 0.78 and 0.75 (d, *J* = 6.0 Hz and *J* = 6.4 Hz, 12H, C^{δ}Hs of Leu(1) and Leu(3)); $[\alpha]_D^{20}$ = -34.33 (*c* = 0.3 in CH_3OH); MS (ESI) m/z: $(M+Na)^+$ Calcd. for $C_{40}H_{52}N_6O_8Na$: 767.3744; found: 767.3758.

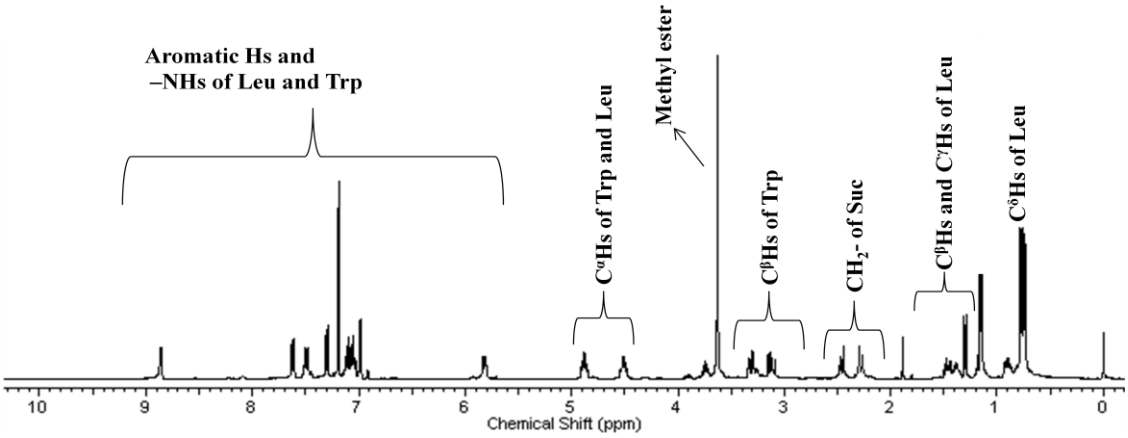

Figure 8.6. *^{1}H NMR spectrum (400 MHz, $CDCl_3$) of MeO-W-L-Suc-L-W-OMe* ***42***.

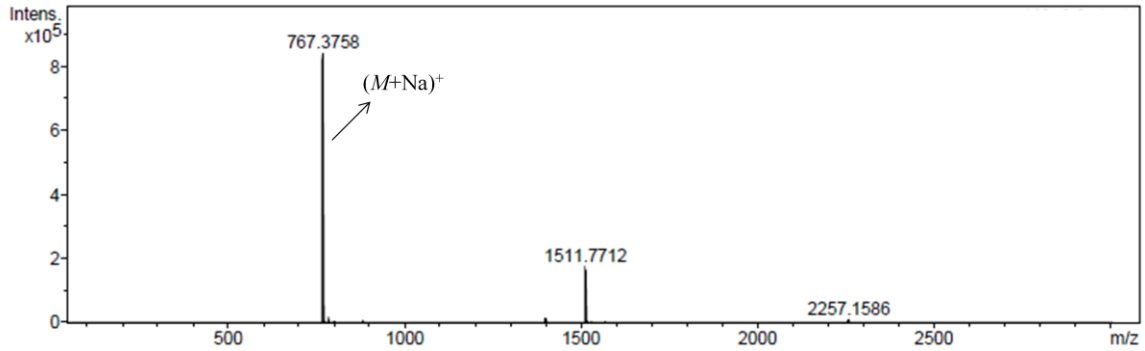

Figure 8.7. *ESI-MS spectrum of MeO-W-L-Suc-L-W-OMe* ***42***.

*(b) Synthesis of HO-Trp(4)-Leu(3)-Suc-Leu(1)-Trp(2)-OH **38**:* 2.60 g (3.5 mmol) of MeO-Trp(4)-Leu(3)-Suc-Leu(1)-Trp(2)-OMe **42** in 10 mL MeOH was taken in a round bottom flask and 2M NaOH was added to it dropwise. The reaction was monitored by thin layer chromatography (TLC). The reaction mixture was stirred for overnight. 15 mL of distilled water was added to the reaction mixture and MeOH was removed under vacuum. The aqueous part was washed with diethyl ether (2 × 30 mL). Then, it was cooled under ice bath for 10 minutes and then pH was adjusted to 1 by drop wise addition of 1M HCl. It was extracted by ethyl acetate (3 × 50 mL) and then the ethyl acetate part was dried over anhydrous Na_2SO_4 and evaporated under vacuum to yield **38** as a white solid.

Yield: 2.25 g (3.15 mmol, 90%); FT-IR (KBr): ῡ = 3301 (broad), 1718 (ms), 1645 (st), 1619 (ms), 1540 (ms), 1520 (ms) cm^{-1}; ^1H NMR (400 MHz, DMSO-d_6, δ_{ppm}): 10.94 (2H, ring -NHs of Trp(2) and Trp(4)), 8.13 (d, *J* = 7.6 Hz, 2H, -NHs of Leu(1) and Leu(3)), 8.05 (d, *J* = 8.8 Hz, 2H, -NHs of Trp(2) and Trp(4)), 7.58 (d, *J* = 8 Hz, 2H, ring protons of Trp(2) and Trp(4)), 7.40 (d, *J* = 8 Hz, 2H, ring protons of Trp(2) and Trp(4)), 7.20 (d, *J* = 1.6 Hz, 2H, ring protons of Trp(2) and Trp(4)), 7.11 and 7.03 (t, *J* = 7.2 Hz and *J* = 7.2 Hz, 4H, ring protons of Trp(2) and Trp(4)), 4.48 (m, 2H, C^{α}Hs of Trp(2) and Trp(4)), 4.38 (m, 2H, C^{α}Hs of Leu(1) and Leu(3)), 3.22 and 3.15 (d, *J* = 7.6 Hz and *J* = 8 Hz, 4H, C^{β}Hs of Trp(2) and Trp(4)), 2.40 (m, 4H, -CH_2- of Suc), 1.61 and 1.48 (m, 6H, C^{β}Hs and C^{γ}Hs of Leu(1) and Leu(3)), 0.92 and 0.88 (d, *J* = 6.4 Hz and *J* = 6.8 Hz, 12H, C^{δ}Hs of Leu(1) and Leu(3)); ^{13}C NMR (100 MHz, DMSO-d_6, δ_{ppm}): 173.20, 172.04, 171.32, 135.98, 127.21, 123.56, 120.80, 118.26, 118.10, 111.30, 109.73, 52.96, 50.70, 30.76, 26.81, 24.04, 23.04, 21.52; $[\alpha]_D^{20}$ = -28.60 (*c* = 0.5 in CH_3OH); MS (ESI) m/z: $(M+H)^+$ Calcd. for $C_{38}H_{49}N_6O_8$: 717.3612; found: 717.3609.

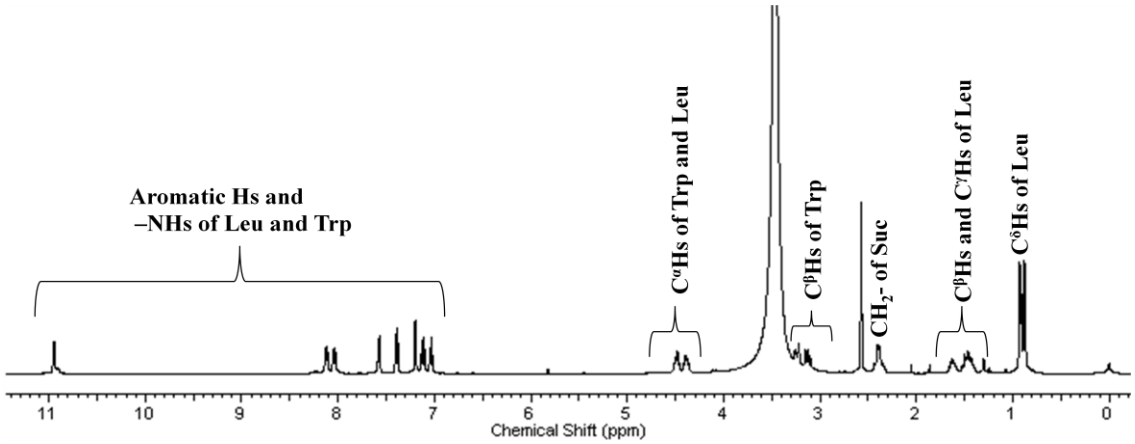

Figure 8.8. *^{1}H NMR spectrum (400 MHz, DMSO-d_6) of HO-W-L-Suc-L-W-OH **38**.*

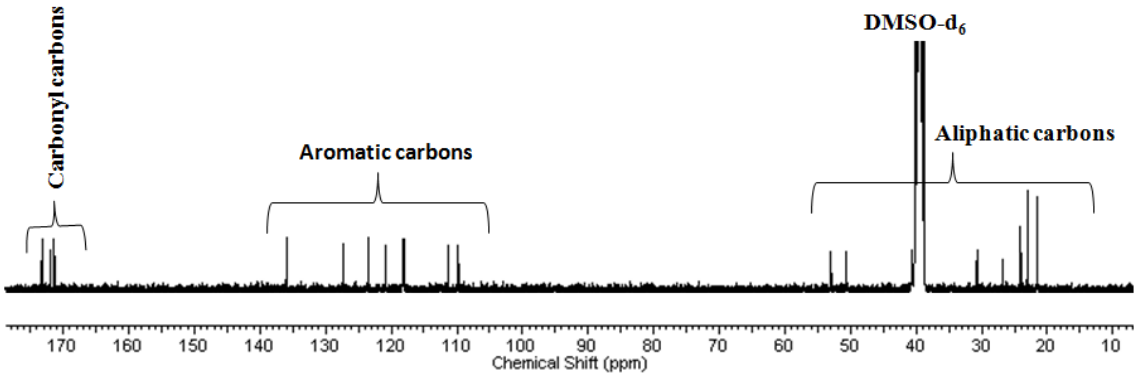

Figure 8.9. *^{13}C NMR spectrum (100 MHz, DMSO-d_6) of HO-W-L-Suc-L-W-OH **38**.*

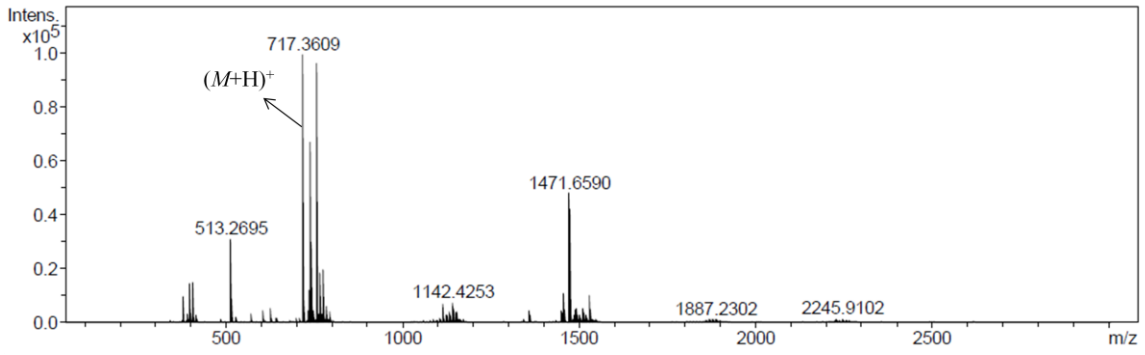

Figure 8.10. *ESI-MS spectrum of HO-W-L-Suc-L-W-OH **38**.*

8.2.3 Synthesis of Bolaamphiphile (HO-Ala(4)-Tyr(3)-Suc-Tyr(1)-Ala(2)-OH) 39:

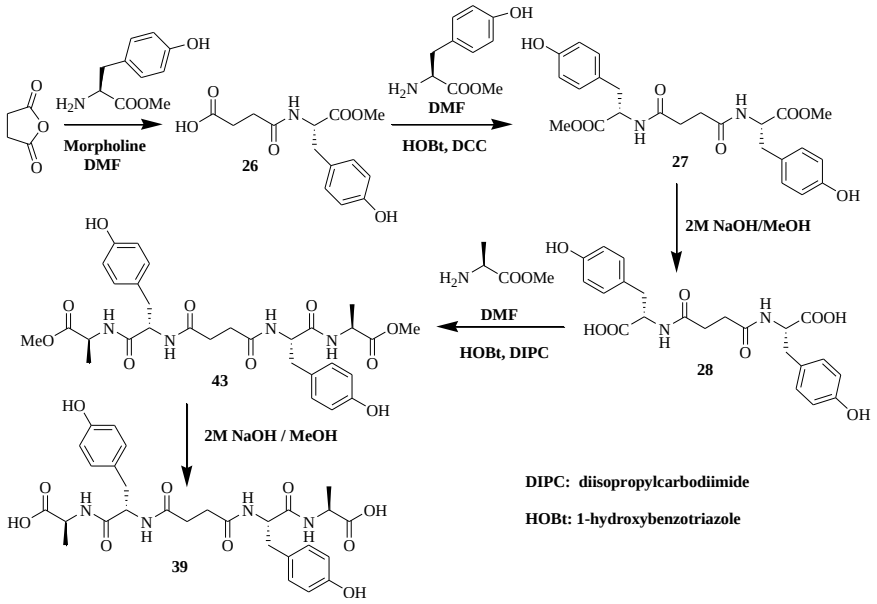

Scheme 8.3. *Synthetic scheme of peptide bolaamphiphile **39**.*

*(a) Synthesis of MeO-Ala(4)-Tyr(3)-Suc-Tyr(1)-Ala(2)-OMe **43**:* 0.89 g (2 mmol) of HO-Tyr(2)-Suc-Tyr(1)-OH **28** in 3 mL of DMF was cooled in an ice bath and H-Ala-OMe was isolated from 1.12 g (8 mmol) of the corresponding methyl ester hydrochloride by neutralization and subsequent extraction with ethyl acetate and the ethyl acetate extract was concentrated to 8 mL. It was then added to the reaction mixture, followed immediately by 0.55 g (4.4 mmol, 686 μL) DIPC and 0.59 g (4.4 mmol) of HOBt. The reaction mixture was stirred for overnight. The residue was taken up in ethyl acetate (50 mL) and the DIU was filtered off. The organic layer was washed with 1M HCl (3 × 50 mL), brine (2 × 50 mL), 1M sodium carbonate (3 × 50 mL), brine (2 × 50 mL) and dried over anhydrous sodium sulfate and evaporated under vacuum to yield **43** as a white solid. Purification was done by silica gel column (100-200 mesh) using chloroform-methanol (9:1) as eluent.

Yield: 1.10 g (1.8 mmol, 90%); FT-IR (KBr): ῡ = 3337 (bw), 3280 (bw), 1748 (ms), 1616 (st), 1558 (st), 1517 cm^{-1}; ^1H NMR (400 MHz, DMSO-d_6, δ_{ppm}): 8.46 (d, *J* = 6.8 Hz, 2H, -NHs of Ala(2) and Ala(4)), 8.12 (d, *J* = 8.8 Hz, 2H, -NHs of Tyr(1) and Tyr(3)), 7.09 (d, *J* = 8.4 Hz, 4H, ring protons of Tyr(1) and Tyr(3)), 6.70 (d, *J* = 8.8 Hz, 4H, ring protons of Tyr(1) and Tyr(3)), 4.44 (m, 2H, C^{α}Hs of Tyr(1) and Tyr(3)), 4.29 (m, 2H, C^{α}Hs of

Ala(2) and Ala(4)), 3.66 (s, 6H, -$COOCH_3$), 2.97 and 2.94 (d, J = 4 Hz, 4H, $C^{\beta}Hs$ of Tyr(1) and Tyr(3)), 2.31 and 2.18 (m, 4H, -CH_2- of Suc), 1.35 (d, J = 7.6 Hz, 6H, $C^{\beta}Hs$ of Ala(2) and Ala(4)); $[\alpha]_D^{20}$ = - 6.2 (c = 0.5 in CH_3OH); MS (ESI) m/z: $(M+H)^+$ Calcd. for $C_{30}H_{39}N_4O_{10}$, 615.2666; found 615.2666.

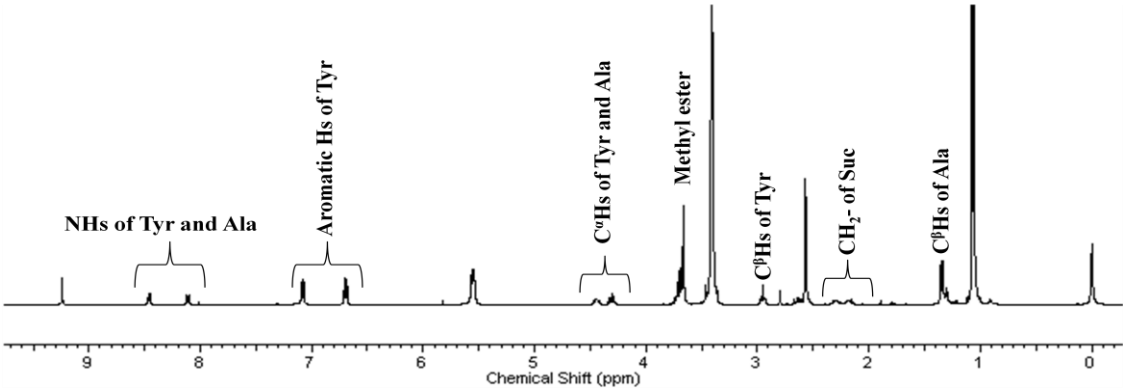

Figure 8.11. *^{1}H NMR spectrum (400 MHz, DMSO-d_6) of MeO-A-Y-Suc-Y-A-OMe* ***43****.*

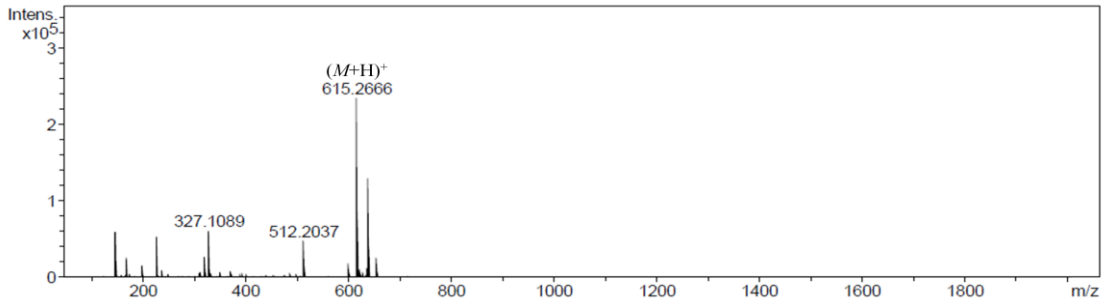

Figure 8.12. *ESI-MS spectrum of MeO-A-Y-Suc-Y-A-OMe* ***43****.*

(b)Synthesis of HO-Ala(4)-Tyr(3)-Suc-Tyr(1)-Ala(2)-OH ***39****:* 0.74 g (1.2 mmol) of MeO-Ala(4)-Tyr(3)-Suc-Tyr(1)-Ala(2)-OMe **43** in 8 mL MeOH was taken in a round bottom flask and 2M NaOH was added to it dropwise. The reaction was monitored by thin layer chromatography (TLC). The reaction mixture was stirred for overnight. 10 mL of distilled water was added to the reaction mixture and MeOH was removed under vacuum. The aqueous part was washed with diethyl ether (2 × 30 mL). Then it was cooled under ice bath for 10 minutes and then pH was adjusted to 1 by drop wise addition of 1M HCl. It was extracted by ethyl acetate (3 × 50 mL) and then the ethyl acetate part was dried over anhydrous Na_2SO_4 and evaporated under vacuum to yield **39** as a white solid.

Yield: 0.668 g (1.14 mmol, 95%); FT-IR (KBr): ῡ = 3305 (bw), 3285 (bw), 1708 (ms), 1624 (s), 1545 (s), 1515 cm^{-1}; ^{1}H NMR (400 MHz, DMSO-d_6, δ_{ppm}): 8.30 (d, *J* = 7.2 Hz, 2H, -NHs of Ala(2) and Ala(4)), 8.05 (d, *J* = 8.4 Hz, 2H, -NHs of Tyr(1) and Tyr(3)), 7.09 (d, *J* = 8.4 Hz, 4H, ring protons of Tyr(1) and Tyr(3)), 6.69 (d, *J* = 8.4 Hz, 4H, ring protons of Tyr(1) and Tyr(3)), 4.45 (m, 2H, C^{α}Hs of Tyr(1) and Tyr(3)), 4.23 (m, 2H, C^{α}Hs of Ala(2) and Ala(4)), 2.98 and 2.94 (d, *J* = 4 Hz, 4H, C^{β}Hs of Tyr(1) and Tyr(3)), 2.27 and 2.19 (m, 4H, -CH_2- of Suc), 1.35 (d, *J* = 7.2 Hz, 6H, C^{β}Hs of Ala(2) and Ala(4)); ^{13}C NMR (100 MHz, DMSO-d_6, δ_{ppm}): 173.97, 171.30, 171.27, 156.74, 155.62, 130.03, 128.11, 114.74, 53.91, 47.49, 36.58, 30.61, 23.26, 16.96; $[\alpha]_D^{20}$ = 12.5 (*c* = 0.11 in CH_3OH); MS (ESI) *m/z*: $(M+Na)^+$ Calcd. for $C_{28}H_{34}N_4O_{10}Na$, 609.2167; found 609.2163.

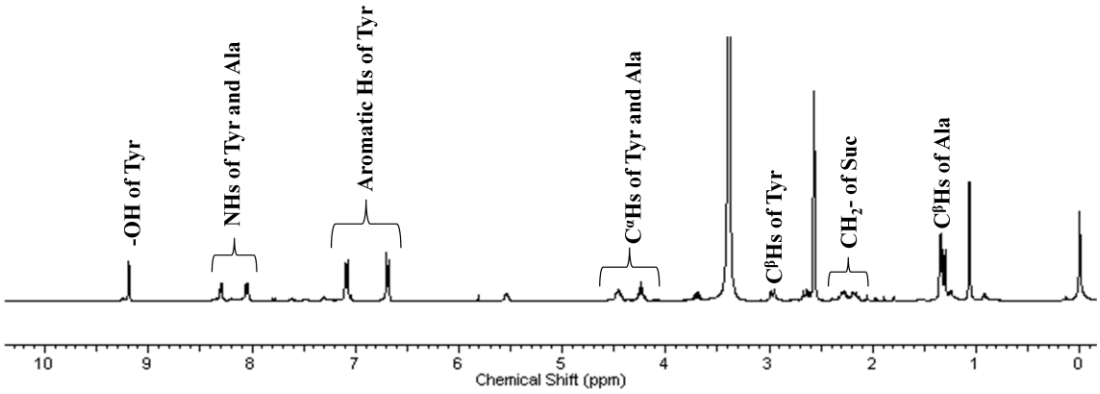

Figure 8.13. *^{1}H NMR spectrum (400 MHz, DMSO-d_6) of HO-A-Y-Suc-Y-A-OH **39**.*

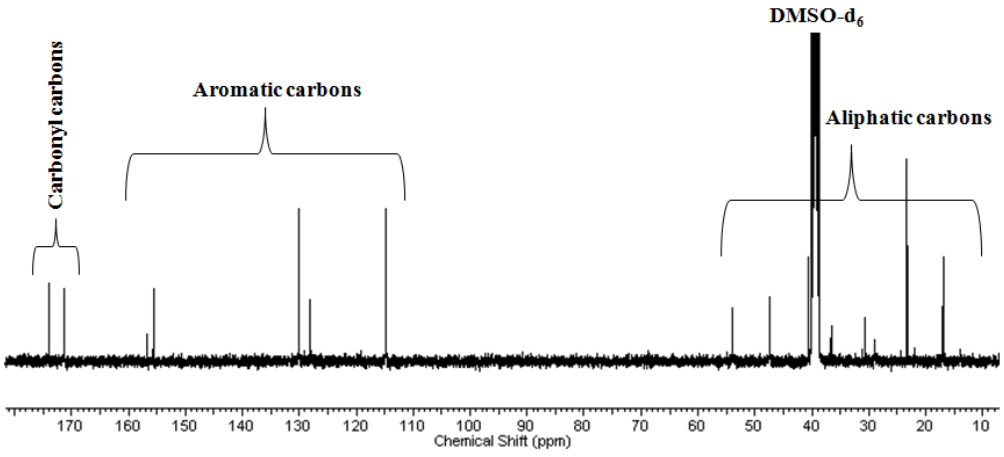

Figure 8.14. *^{13}C NMR spectrum (100 MHz, DMSO-d_6) of HO-A-Y-Suc-Y-A-OH **39**.*

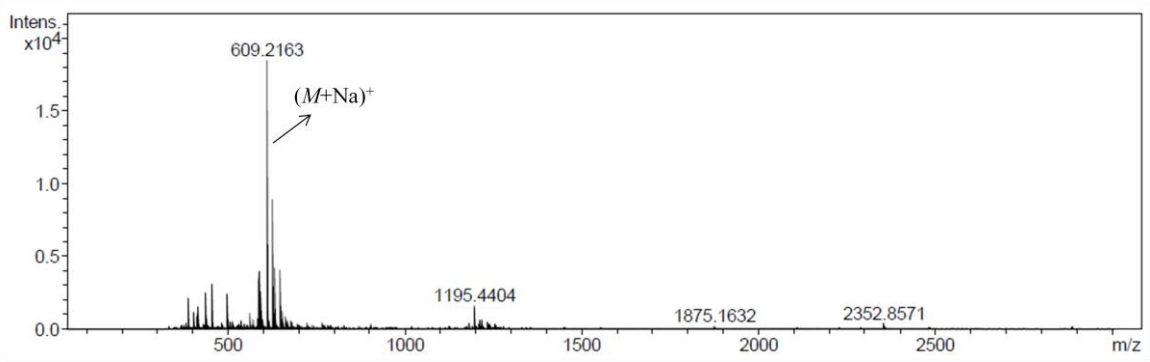

Figure 8.15. *ESI-MS spectrum of HO-A-Y-Suc-Y-A-OH **39**.*

8.2.4 Synthesis of Bolaamphiphile (HO-Val(4)-Tyr(3)-Suc-Tyr(1)-Val(2)-OH) 40:

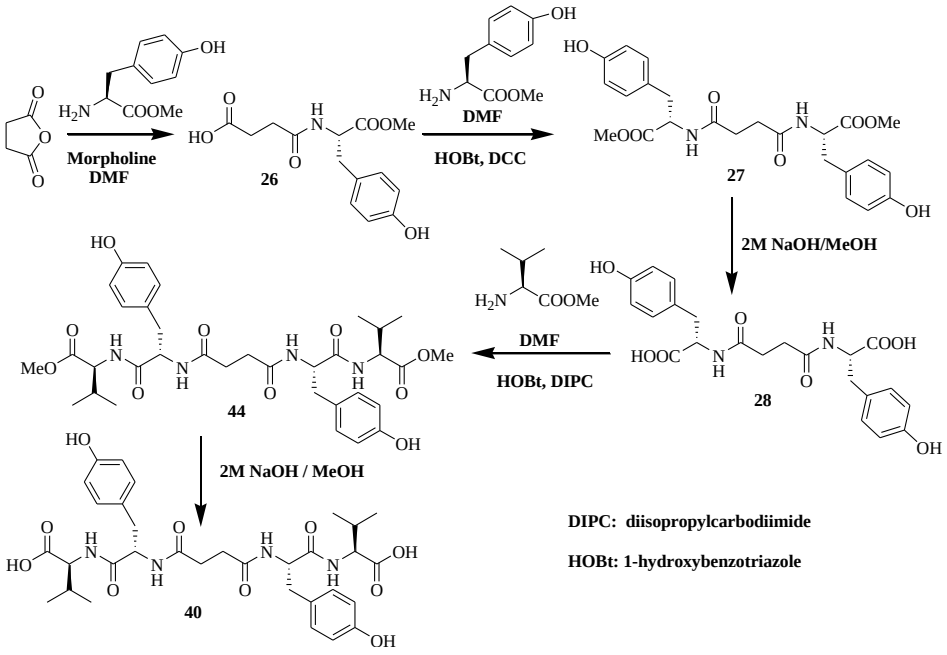

Scheme 8.4. *Synthetic scheme of peptide bolaamphiphile **40**.*

*(a) Synthesis of MeO-Val(4)-Tyr(3)-Suc-Tyr(1)-Val(2)-OMe **44**:* 0.89 g (2 mmol) of HO-Tyr(2)-Suc-Tyr(1)-OH **28** in 3 mL of DMF was cooled in an ice bath and H-Val-OMe was isolated from 1.167 g (8 mmol) of the corresponding methyl ester hydrochloride by neutralization and subsequent extraction with ethyl acetate and the ethyl acetate extract was concentrated to 8 mL. It was then added to the reaction mixture, followed immediately by 0.55 g (4.4 mmol, 686 μL) DIPC and 0.59 g (4.4 mmol) of HOBt. The reaction mixture was stirred for overnight. The residue was taken up in ethyl acetate (50

mL) and the DCU was filtered off. The organic layer was washed with 1M HCl (3 × 50 mL), brine (2 × 50 mL), 1M sodium carbonate (3 × 50 mL) and brine (2 × 50 mL). The organic layer was dried over anhydrous sodium sulfate and evaporated under vacuum to yield **44** as a white solid. Purification was done by silica gel column (100-200 mesh) using chloroform-methanol (9:1) as eluent.

Yield: 1.13 g (1.68 mmol, 84%); FT-IR (KBr): ῡ = 3333 (bw), 3292 (bw), 1735 (ms), 1638 (st), 1610 (st), 1541 (st), 1515 cm^{-1}; ^{1}H NMR (400 MHz, DMSO-d_6, δ_{ppm}): 8.21 (d, *J* = 8 Hz, 2H, -NHs of Val(2) and Val(4)), 8.08 (d, *J* = 8.4 Hz, 2H, -NHs of Tyr(1) and Tyr(3)), 7.09 (d, *J* = 8.4 Hz, 4H, ring protons of Tyr(1) and Tyr(3)), 6.70 (d, *J* = 8 Hz, 4H, ring protons of Tyr(1) and Tyr(3)), 4.45 (m, 2H, C^{α}Hs of Tyr(1) and Tyr(3)), 4.19 (m, 2H, C^{α}Hs of Val(2) and Val(4)), 3.67 (s, 6H, -$COOCH_3$), 2.93 and 2.90 (d, *J* = 4.4 Hz, 4H, C^{β}Hs of Tyr(1) and Tyr(3)), 2.29-2.18 (m, 4H, -CH_2 of Suc), 2.06 (m, 2H, C^{β}Hs of Val(2) and Val(4)), 0.95 and 0.93 (d, *J* = 6.8 Hz and *J* = 7.2 Hz, 12H, C^{γ}Hs of Val(2) and Val(4)); $[\alpha]_D^{20}$ = - 22.66 (*c* = 0.3 in CH_3OH); MS (ESI) *m/z*: $(M+H)^+$ Calcd. for $C_{34}H_{47}N_4O_{10}$, 671.3292; found 671.3287.

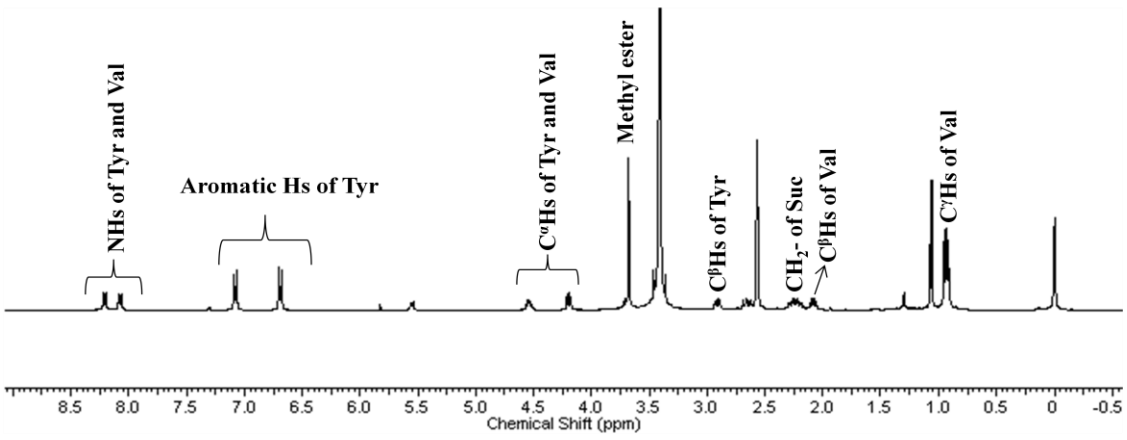

Figure 8.16. *^{1}H NMR spectrum (400 MHz, DMSO-d_6) of MeO-V-Y-Suc-Y-V-OMe **44**.*

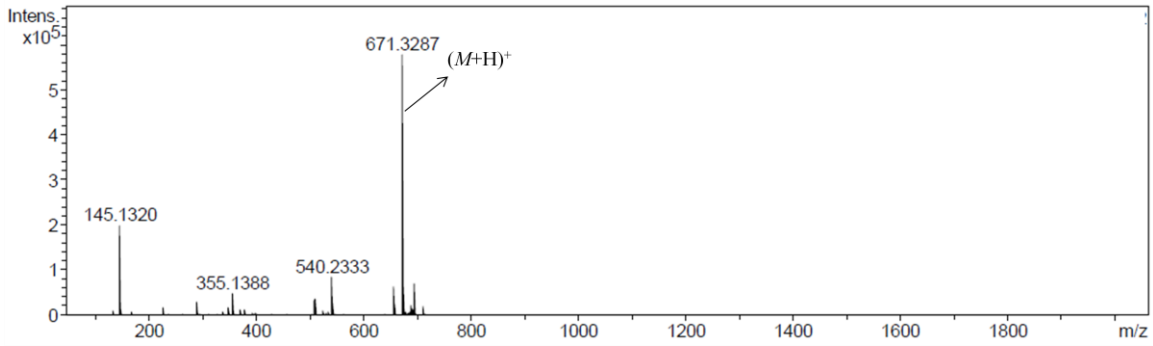

Figure 8.17. *ESI-MS spectrum of MeO-V-Y-Suc-Y-V-OMe* ***44****.*

(b) Synthesis of HO-Val(4)-Tyr(3)-Suc-Tyr(1)-Val(2)-OH ***40****:* 0.87 g (1.3 mmol) of MeO-Val(4)-Tyr(3)-Suc-Tyr(1)-Val(2)-OMe **44** in 6 mL MeOH was taken in a round bottom flask and 2M NaOH was added to it dropwise. The reaction was monitored by thin layer chromatography (TLC). The reaction mixture was stirred for overnight. 10 mL of distilled water was added to the reaction mixture and MeOH was removed under vacuum. The aqueous part was washed with diethyl ether (2 × 30 mL). Then, it was cooled under ice bath for 10 minutes and then pH was adjusted to 1 by drop wise addition of 1M HCl. It was extracted by ethyl acetate (3 × 50 mL) and then the ethyl acetate part was dried over anhydrous Na_2SO_4 and evaporated under vacuum to yield **40** as a white solid.

Yield: 0.784 g (1.22 mmol, 94%); FT-IR (KBr): ῡ = 3287 (bw), 1703 (ms), 1626 (st), 1543 (st), 1515 cm^{-1}; ^1H NMR (400 MHz, DMSO-d_6, δ_{ppm}): 8.05 (d, *J* = 8 Hz, 2H, -NHs of Val(2) and Val(4)), 8.01 (d, *J* = 8.4 Hz, 2H, -NHs of Tyr(1) and Tyr(3)), 7.10 (d, *J* = 8.4 Hz, 4H, ring protons of Tyr(1) and Tyr(3)), 6.69 (d, *J* = 8.8 Hz, 4H, ring protons of Tyr(1) and Tyr(3)), 4.55 (m, 2H, $C^{\alpha}Hs$ of Tyr(1) and Tyr(3)), 4.19 (m, 2H, $C^{\alpha}Hs$ of Val(2) and Val(4)), 2.96 and 2.92 (d, *J* = 4.0 Hz, 4H, $C^{\beta}Hs$ of Tyr(1) and Tyr(3)), 2.29-2.18 (m, 4H, -CH_2 of Suc), 2.12 (m, 2H, $C^{\beta}Hs$ of Val(2) and Val(4)), 0.95 and 0.93 (d, *J* = 2 Hz, 12H, $C^{\gamma}Hs$ of Val(2) and Val(4)); ^{13}C NMR (100 MHz, DMSO-d_6, δ_{ppm}): 172.83, 171.66, 171.18, 155.62, 130.08, 127.95, 114.72, 57.16, 53.89, 36.51, 30.71, 29.79, 19.05, 18.00; $[\alpha]_D^{20}$ = - 1.33 (*c* = 0.1 in CH_3OH); MS (ESI) *m/z*: $(M+Na)^+$ Calcd. for $C_{32}H_{42}N_4O_{10}Na$, 665.2799; found 665.2794.

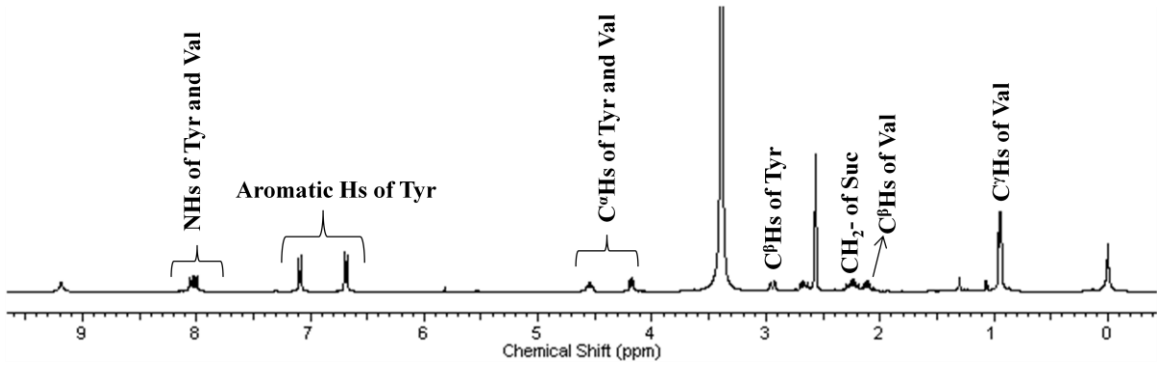

Figure 8.18. *^{1}H NMR spectrum (400 MHz, DMSO-d_6) of HO-V-Y-Suc-Y-V-OH* ***40***.

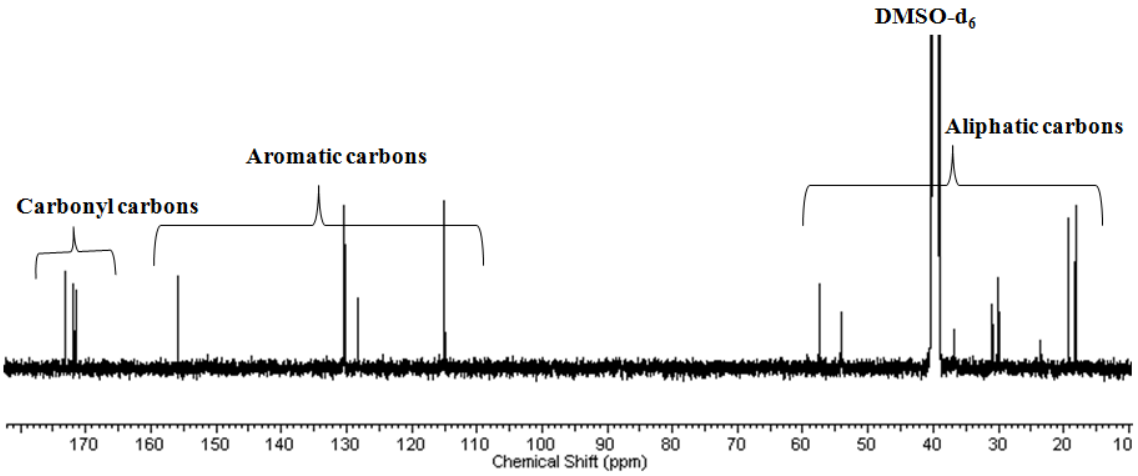

Figure 8.19. *^{13}C NMR spectrum (100 MHz, DMSO-d_6) of HO-V-Y-Suc-Y-V-OH* ***40***.

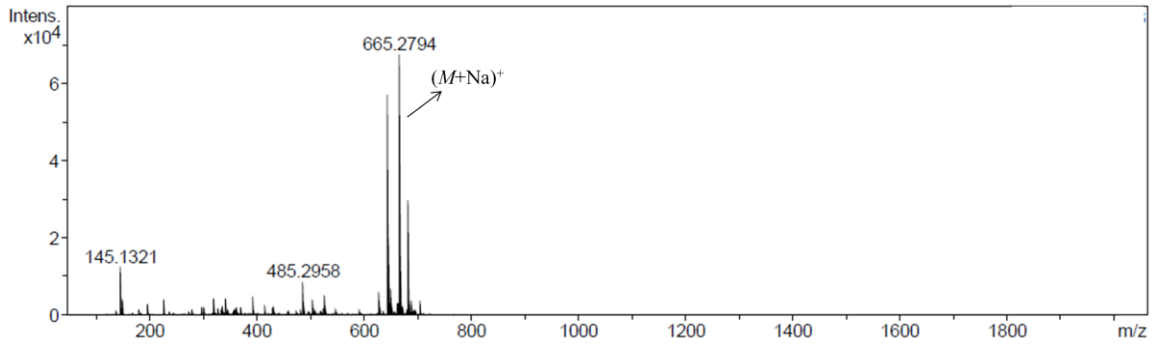

Figure 8.20. *ESI-MS spectrum of HO-V-Y-Suc-Y-V-OH* ***40***.

8.3 Method and Characterization Techniques

8.3.1 Preparation of Peptide Bolaamphiphile Based Dynamic Libraries: 20 mmol L^{-1} peptide bolaamphiphile with 4 equivalents of *p*-hydroxy benzyl alcohol (80 mmol L^{-1}) was sonicated to make a suspension in double distilled water and then 80 μL of 1M NaOH was added dropwise to maintain the pH of 8 for complete dissolution. After the addition of 1 mg of lipase, the reaction mixture was made homogeneous by vortex and incubated at 37 °C for dynamic reaction. After 10 days, the peptide bolaamphiphile **37** (HO-Trp(4)-Tyr(3)-Suc-Tyr(1)-Trp(2)-OH) based dynamic reaction turned to hydrogel but other bolaamphiphiles based DCLs remained in solution.

8.3.2 HPLC Analysis: HPLC grade acetonitrile and water were used for HPLC analysis. The dynamic reaction mixture was characterized by reverse phase symmetry C18 column (250 × 4.6 cm, 5 μm particle size). UV-Vis absorbance was monitored at 280 nm. Separations were achieved by running the column with acetonitrile-water as eluent at a flow rate of 1 mL min^{-1} at 25 °C. The sample preparation involved mixing 100 μL of gel with acetonitrile-water (900 μL, 50:50 mixture). The samples were then filtered through a 0.45 μm syringe filter (Whatman, 150 units, 13 mm diameter, 2.7 mm pore size) prior to injection. A 20 μL of sample was injected into a Dionex Acclaim ® 120 C18 column of 250 mm length with an internal diameter of 4.6 mm and 5 μm fused silica particles at a flow rate of 1 mL $min.^{-1}$ Bolaamphiphiles **37-40, 25** were analyzed at 280 nm of wavelength of detectors and bolaamphiphile **3** was analyzed at 225 nm of wavelength of detectors.

Solvent gradiant used in HPLC analysis is given below.

Time/min.	**% of H_2O (0.1% TFA)**	**% of Acetonitrile (0.1% TFA)**
0	80	20
4	80	20
35	20	80
40	20	80
42	80	20

8.3.3 Circular Dischroism (CD) Spectrometer: Secondary structures of peptide bolaamphiphiles in both the DCLs (**37** and **38**) were analyzed with Jasco J-815 circular dischroism spectrometer with the course of dynamic reactions. Peptide DCLs (20 mmol L^{-1}) were diluted to final concentration of 200 μM in ddH_2O for experiment and measured from 280 nm to 195 nm with 0.1 data pitch, 20 nm/min scanning speed, 1 nm band width and 4 s D.I.T.

8.3.4 UV-Vis Spectroscopy: UV-Vis absorption spectra of the DCLs were recorded using a Varian Cary100 Bio UV-Vis spectrophotometer. DCL samples were diluted to 50 μM as concentration and then the experiments were performed.

8.3.5 Fluorescence Spectroscopy: Real time fluorescence emission spectra for both the DCLs (20 mmol L^{-1}) were recorded on a Horiba Scientific Fluoromax-4 spectrophotometer with 1 cm path length quartz cell at room temperature. The slit width for the excitation and emission was set at 2 nm and a 1 nm data pitch. Excitation of gel sample was performed at 280 nm and data range was in between 300 to 540 nm. The excitation spectra of DCLs were also taken at different time period of the reactions. DCL **37** was excited at 341 nm prior to enzyme addition, 416 nm at 6 day and 420 nm at 10 and 15 day to record the fluorescence spectra. DCL **38** was excited at 365 nm prior to enzyme addition, 418 nm at 6 day, 10 day and 420 nm at 15 day to record the fluorescence spectra.

8.3.6 Wide Angle X-ray Diffraction: Data were collected for both the DCLs on a Rigaku Smart Lab X-ray diffractometer with a wavelength of 1.5406 Å. The X-rays were produced using a sealed tube and the X-rays were detected using a linear counting detector based on silicon strip technology (Scintillator NaI photomultiplier detector).

8.3.7 Microscopic Study: For SEM study, the DCL samples were dried on a glass slide and coated with gold. Then the micrographs were recorded in a SEM apparatus (Jeol Scanning Microscope-JSM-7600F). High-resolution transmission electron

microscopic images were taken using a JEOL electron microscope (model: JEM 2100) operated at an accelerating voltage of 200kV. Transmission electron microscopy (TEM) studies of the DCL samples were carried out using uranyl acetate negative staining method. The DCL hydrogel (20 mmol L^{-1}) and solutions were diluted to 1 mmol L^{-1} in double distilled water and a drop of diluted DCL sample was adsorbed on a 400 mesh copper grid with carbon coated formvar support, and stained with 1% uranyl acetate. The carbon-coated copper grids (400 mesh) were dried by slow evaporation in air and then allowed to dry separately in a vacuum at room temperature.

8.3.8 Rheology: Oscillating rheology was used to quantify the final mechanical properties and thixotropic nature of the peptide bolaamphiphile based DCL hydrogel. 2 mL of peptide bolaamphiphile DCL hydrogel (20 mmol L^{-1}) was prepared. The experiment was done on a Paar Physica Modular Compact Rheometer (MCR 301, Austria). A 25 mm cone plate with 1° angle configuration was used and the temperature was set to be constant at 25 °C. Storage (G') and loss (G") moduli were measured at 0.1% strain with a true gap of 0.05 mm. To determine the exact strain for the frequency sweep experiment, the linear visco-elastic (LVE) regime was performed at a constant frequency of 10 rad s^{-1}.

8.3.9 Cell Culture Experiment: Human umbilical cord stem cells were supplied by Hi-media Pvt., Ltd. India. DMEM+ cell culture media was used to culture Human umbilical cord stem cells, XTT and MTT kits were also purchased from Hi-media Pvt., Ltd., India. Cells were seeded and grown upto 60% confluence in DMEM+ media. Then cells were counted by haemocytometer and 3×10^8 cells were seeded in each well. Three different plated were seeded with cells and marked with 01, 03 and 05 days. In these plated media and cell controls were used. In control only media was added into the wells (devoid of hydrogel). Three different concentrations of hydrogel were used to culture cells in wells *i.e.* 20 mM (only hydrogel), 10 mM hydrogel (50% media + 50% hydrogel) and 8 mM hydrogel (60% media + 40% hydrogel). In all the plates above mentioned scheme was used, but the duration of study were different *viz.* 1, 3 and 5 days. After the

incubation each plate was used to conduct MTT, XTT and DNA concentration determination in the medium they were grown.

8.3.9(1) **XTT/ MTT Assay:** XTT or MTT assays are mainly used for the detection of cell survival and proliferation, but do not detect dead cells thus also applicable to detect cytotoxicity by any of the agent under study. In both of these assays, tetrazolium salts have been used to develop a quantitative colorimetric assay. These assays are based on the extracellular reduction of XTT or MTT by mitochondrial dehydrogenase enzymes. This reduction results into the formation of crystals soluble in DMSO or in solubilisation buffer provided in the kits. The intensity of the color formed is directly proportional to the number of surviving cells. Briefly, in XTT assay, 0.1 mL of electron coupling reagent was added into 5 mL of XTT to form activated XTT reagent solution. Then 50 µL of this reagent was added to each well after the completion of the experimental durations of incubation time (1, 3 and 5 days). Plates were again kept inside the incubator for 4 hours at 37 $^{\circ}$C with 5% CO_2 atmosphere. Then after, plates were stir gently on shaker and absorbance was taken at 450 and 630 nm. Data showed as $\Delta A_{450\text{-}630}$. Similarly, in case of MTT assay, MTT reagent to a final concentration 10% total volume was added to the wells and incubated for 4 hours at 37 $^{\circ}$C with 5% CO_2 atmosphere. Then after, 100 µL of solubilization solution was added to each well followed by stirring on gyratory shaker. Absorbance was taken at 570 and 670 nm wavelengths. Data showed as $\Delta A_{570\text{-}670}$.

8.3.9(2) **DNA Concentration Measurements:** DNA concentration in medium in which cells were grown is a marker of the cell population present in later stages of apoptosis of necrosis. Therefore, this parameter was used to detect the influence of hydrogel on the growth and survival of stem cells. Briefly, 10 µL of media sample from each well was taken out after the completion of required incubation period. This was diluted with 990 µL of respective media and absorbance was taken at 260, 280 and 320 nm against the respective blanks. It is to be noted that the composition of respective diluents or blank was the same as present in the respective wells. The concentration of the purified DNA present in the media was calculated by the formula:

DNA concentration (µg/ml) = $[(\Delta A_{260}\text{-}A_{320}/ A_{280}) / 1.6] \times$ dilution factor $\times$ 50

8.3.10 Statistical Analysis: Non parametric ANOVA was followed by Neuman Keuls multiple comparison test using trial version of Graph pad Prism 5.

8.4 Results and Discussion

In order to achieve lipase catalysed dissipative self-assembly, six peptide bolaamphiphiles **37, 38, 25, 39, 40** and **3** with a centrally located succinic acid moiety were synthesized and characterized (Figure 8.21a). The esterification reactions of the peptide bolaamphiphiles with *p*-hydroxy benzylalcohol were carried out in aqueous medium at room temperature by using lipase from *candida cyllendarisa*. Among these peptide bolaamphiphiles, bolaamphiphiles **37** and **38** with terminal tryptophan residues formed DCL with sufficient conversion of monoesters and di-esters in aqueous medium at 37 °C, which exclusively turns to di-esters after several days. The DCL of bolaamphiphile **37** produced a hydrogel. The DCL of bolaamphiphile **38** remained in solution because the lacks of optimum hydrophobic/hydrophilic balance (Figure 8.22). On the other hand, peptide bolaamphiphiles **25, 39, 40** and **3** with terminal phenylalanine, alanine, valine and leucine residues formed products with conversion < 15% (Figure 8.23). In here, lipase from *candida cyllendarisa* catalyzed the esterification reactions specifically with the tryptophan ends of peptide bolaamphiphile precursors. In the experiment, the peptide bolaamphiphiles (20 mmol L^{-1}) with 4 equivalents of *p*-hydroxy benzyl alcohol were sonicated to make a suspension in double distilled water. Then, 1M NaOH was added dropwise to maintain the pH of 8 till complete dissolution. After the addition of 1 mg of lipase, the reaction mixture was made homogeneous by vortex. The product conversions (Figure 8.24) were studied by HPLC with the course of reaction time. It was found that the conversion at the early stage of the reactions was slow. After 9 days, the DCL **37** resulted in the formation of a hydrogel with total conversion of 68% including the monoester (46%) and diester (22%) while peptide bolaamphiphile **38** formed 33.5% as monoester and 5% as diester. After 19 days, the hydrogel of DCL **37** became stiffer with complete conversion of di-esters but the solution of DCL **38** produced a mixture of monoester as 40.5% and di-ester as 45% conversion. At the day of 30, DCL **38** was formed by 100% conversion with monoester as 9% and di-ester as 91%.

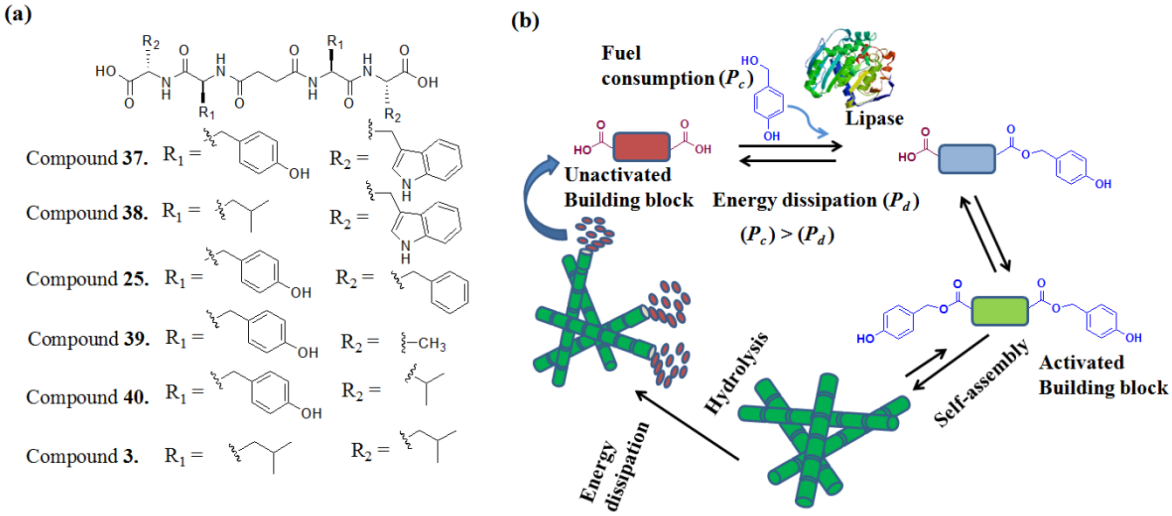

Figure 8.21. *(a) Structures of peptide bolaamphiphiles (**37-40, 25 and 3**). (b) Dissipative reaction cycle of the system. Unactivated peptide bolaamphiphile **37** incorporates energy in the form of p-hydroxy benzylalcohol to give monoester and then di-ester. The diester self-assembles into nanofibers and forms hydrogel. The subsequent hydrolysis leads to dissipate the energy of di-ester which results in collapse the hydrogel. The rate of enzymatic energy dissipation (Pd) (ester hydrolysis) is lower than the consumption of the energy (Pc) (esterification) to allow the formation of self-assembled architecture.*

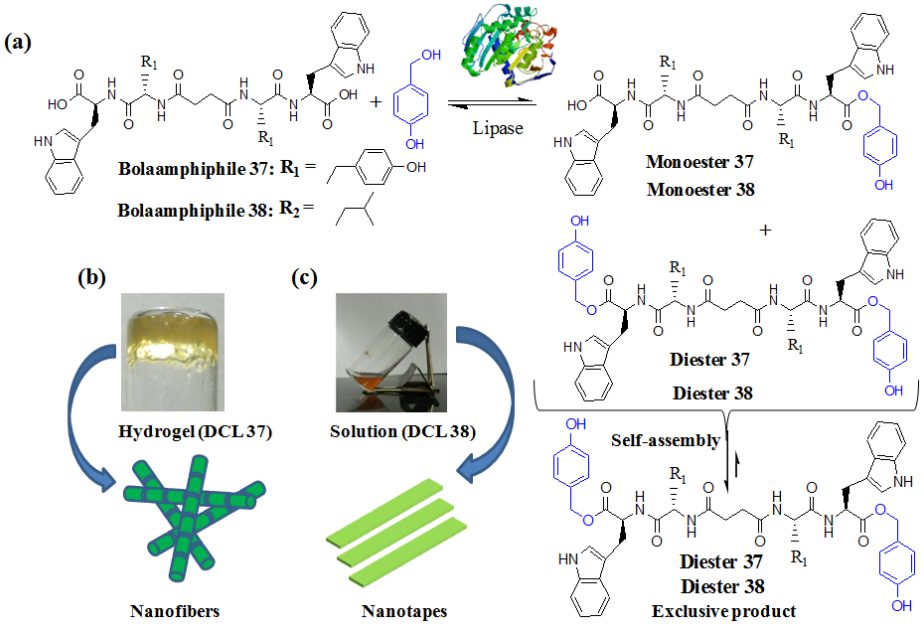

Figure 8.22. *(a) The lipase catalyzed esterification reaction initially leads to form the mixture of monoester and di-ester. After the lag phase, the self-assembly process solely drives to form the di-ester. (b) The DCL **37** forms the nanofibrillar hydrogel whereas (c) the solution of DCL **38** forms nanotape structures in supramolecular level.*

From the kinetics data, it is evident that the rate of ester formation was higher at the early stage of chemical reactions than the rate of ester hydrolysis under reversible condition. Afterward, di-esters were formed exponentially by consuming all the parent peptide bolaamphiphiles and their mono-esters after several days of lag period.

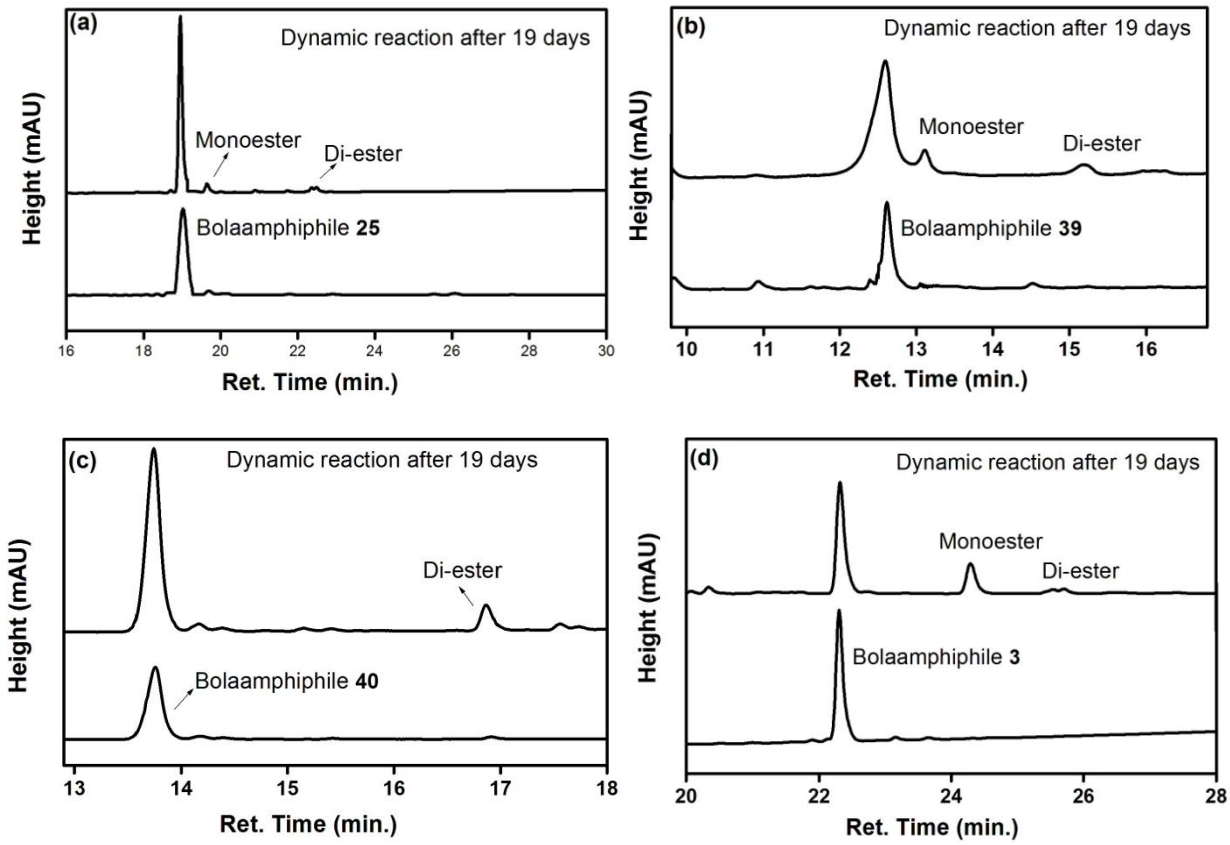

Figure 8.23. *HPLC chromatograms (a) peptide bolaamphiphile **25** (HO-Phe(4)-Tyr(3)-Suc-Tyr(1)-Phe(2)-OH) and DCL, (b) peptide bolaamphiphile **39** (HO-Ala(4)-Tyr(3)-Suc-Tyr(1)-Ala(2)-OH) and DCL, (c) peptide bolaamphiphile **40** (HO-Val(4)-Tyr(3)-Suc-Tyr(1)-Val(2)-OH) and DCL and (d) peptide bolaamphiphile **3**(HO-Leu(4)-Leu(3)-Suc-Leu(1)-Leu(2)-OH) and DCL.*

The self-assembly process favoured the formation of di-esters to attain the reaction out of equilibrium. The products resulting from lipase catalyzed DCL reactions were also confirmed from mass spectrometry (Figure 8.25a and Figure 8.26a). Two hydroxyl groups (-OH) of *p*-hydroxy benzyl alcohol can take part in DCL reactions. To confirm this, we characterized biocatalytic dynamic esterification reactions by ^{1}H NMR

spectroscopy. For peptide bolaamphiphile **37** based DCL, ^{1}H NMR spectrum showed a significant chemical shift (δ value) at 5.26 ppm. The chemical shift value (δ value) at 5.26 ppm confirmed two benzylic protons of *p*–hydroxy benzyl alcohol. The aliphatic –OH functionality was involved in ester bond formation (Figure 8.25b). For peptide bolaamphiphile **38** based DCL, the characteristic chemical shift appeared at 5.24 ppm which supported the involvement of aliphatic –OH functionality in ester bond formation (Figure 8.26b).

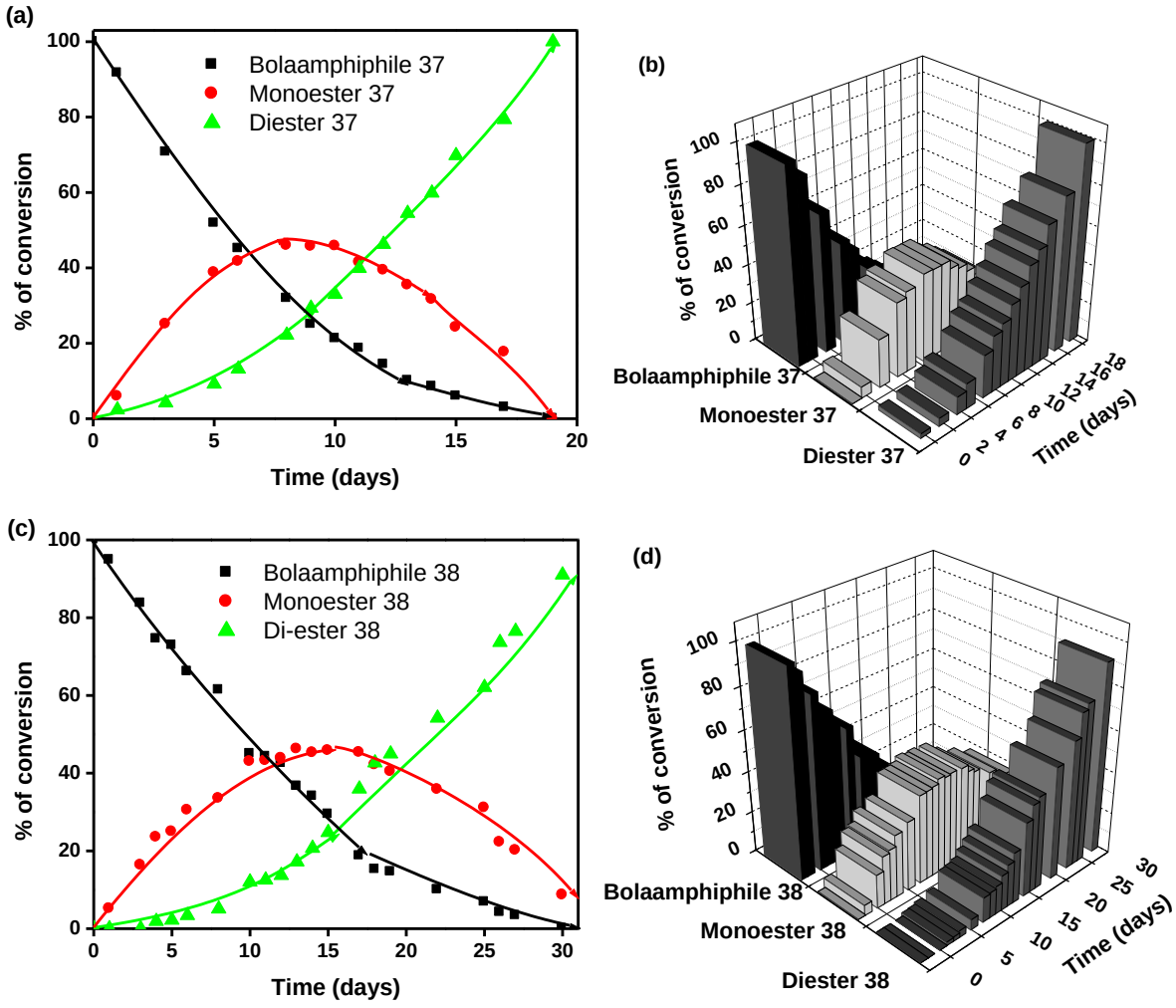

Figure 8.24. *The product distribution of a dynamic system from the lipase catalyzed reaction of (a) peptide bolaamphiphile **37**, (b) it's 3D presentation and (c) peptide bolaamphiphile **38**, (d) it's 3D presentation with a chemical energy in the form of p-hydroxy benzylalcohol as determined by HPLC over time at 37 °C.*

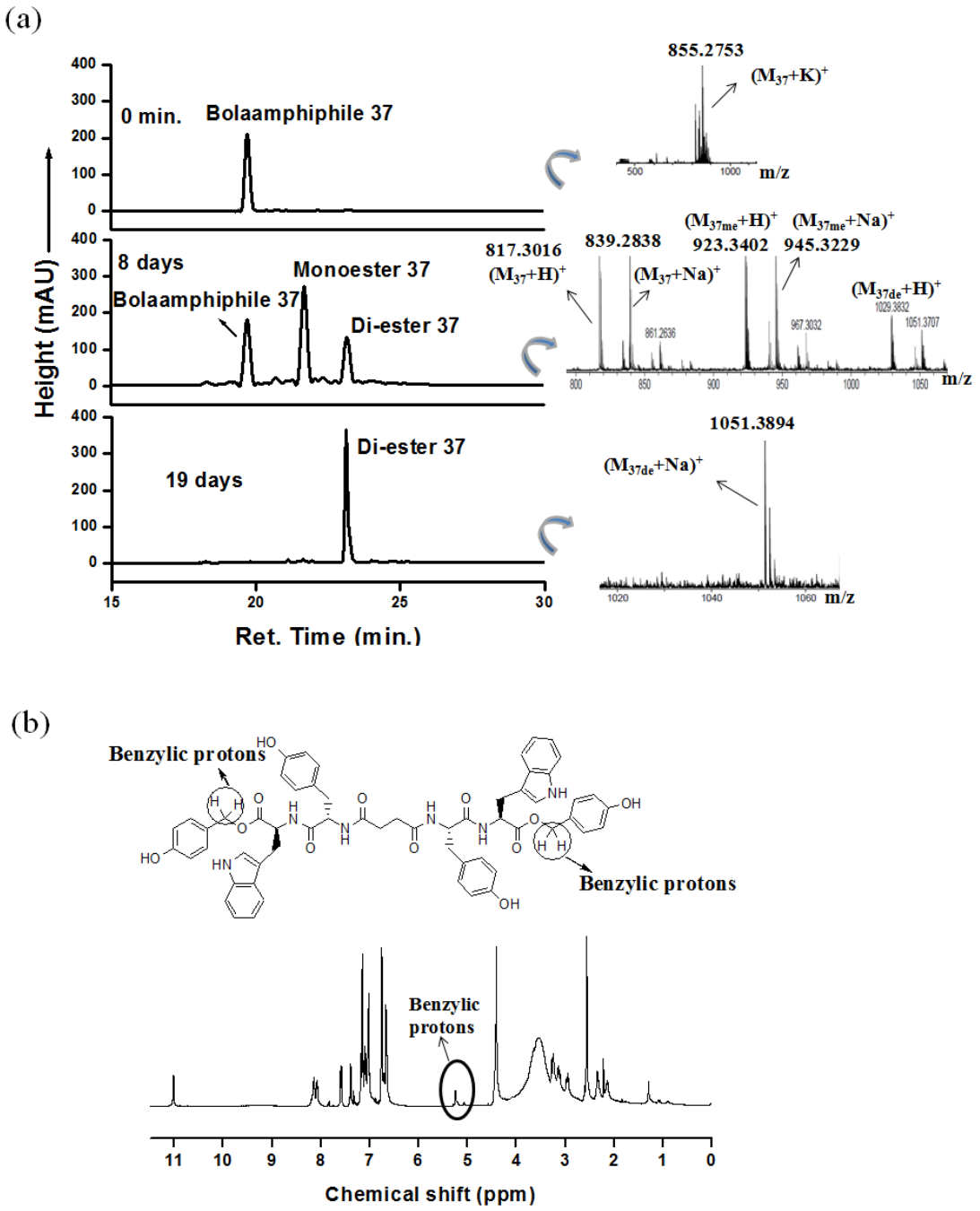

Figure 8.25. *(a) Real time HPLC and mass analysis for the generation of DCL **37** via the enzymatic reaction of peptide bolaamphiphile **37** with p-hydroxy benzylalcohol (M_{37me} and M_{37de} are the mass of monoester and di-ester of bolaamphiphile **37**). (b) The ^{1}H NMR spectrum of di-ester **37** in DMSO-d_6 confirms the involvement of aliphatic hydroxyl group of p-hydroxy benzylalcohol in esterification reaction.*

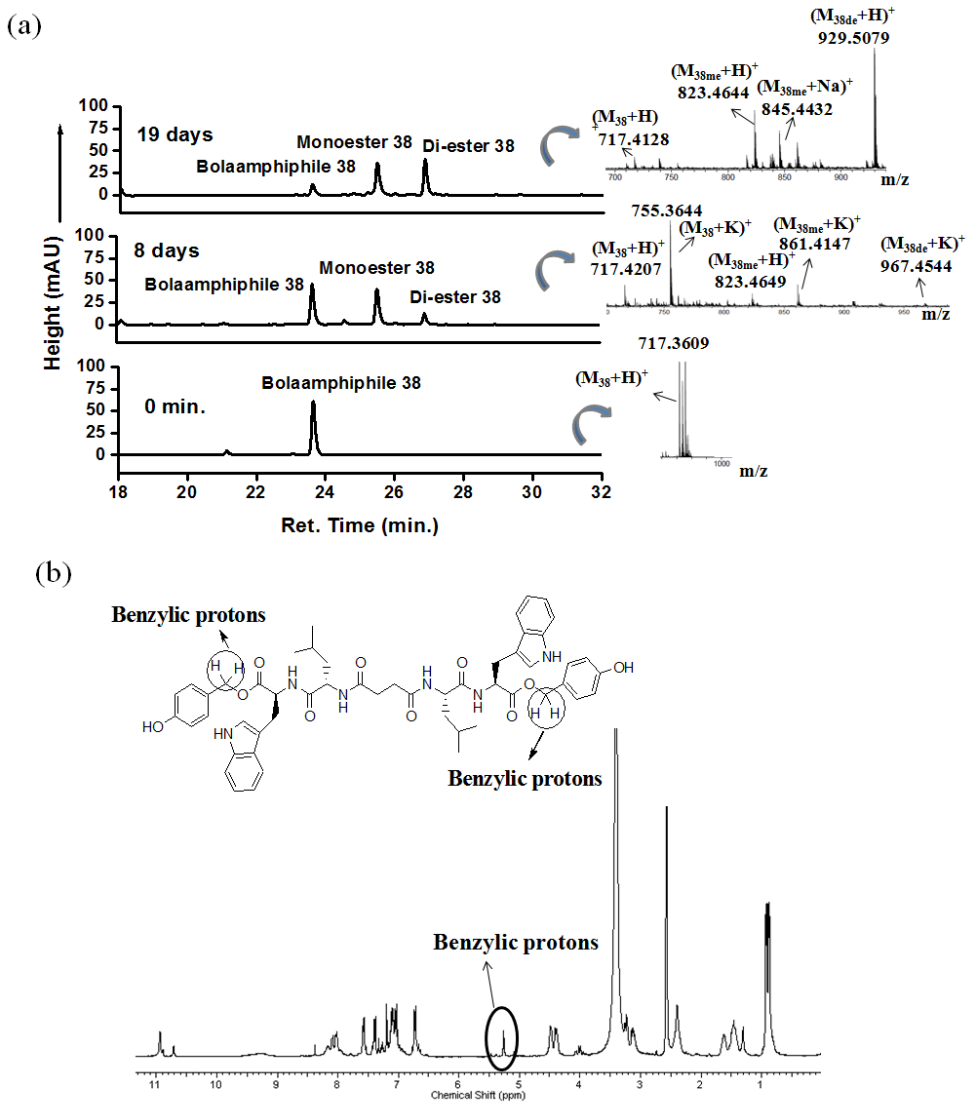

Figure 8.26. *(a) Real time HPLC and mass analysis for the generation of DCL **38** via the enzymatic reaction of peptide bolaamphiphile **38** with p-hydroxy benzylalcohol (M_{38me} and M_{38de} are the mass of monoester and di-ester of bolaamphiphile **38**). (b) The ^{1}H NMR spectrum of di-ester **38** in DMSO-d_6 confirms the involvement of aliphatic hydroxyl group of p-hydroxy benzylalcohol in esterification reaction.*

Here, lipase acts as a chemical engine where the unactivated building block of peptide bolaamphiphile **37** consumes the chemical energy in the form of *p*-hydroxy benzylalcohol to form an activated building block of di-ester. The activated diester of peptide bolaamphiphile **37** produces a self-assembled nanostructured hydrogel.

Upon hydrolysis, the activated building block of di-esters is forced to dissipate its energy as *p*-hydroxy benzylalcohol, which results in the formation of initial unactivated building block of parent bolaamphiphile **37**. The energy dissipation causes the dis-assembly and destruction of the nanostructural hydrogel. The ester hydrolysis and subsequent dis-assembly processes are irreversible in here. This system meets all the criteria of a dissipative self-assembly (DSA) process (Figure 8.21b).[6] The system follows the key requirement of DSA as the rate of enzymatic energy dissipation (*P*d) (ester hydrolysis) is lower than the consumption of energy (*P*c) (esterification) which allows to form the self-assembled architecture. Self-assembly process favours the formation of di-esters by consuming the parent bolaamphiphile and its monoesters after the lag phase of this biocatalytic reaction. After reaching a certain concentration of monoester, the di-ester facilitates its own growth exponentially via formation of supramolecular structure through hydrogen bonding and π-π stacking interactions.

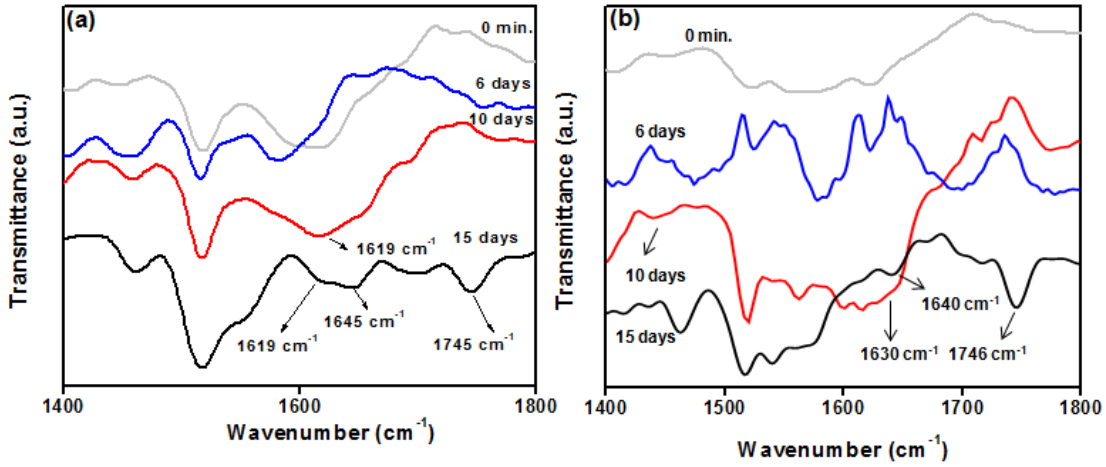

Figure 8.27. *Real time FT-IR spectra of dynamic reactions of (a) peptide bolaamphiphile **37** and (b) peptide bolaamphiphile **38**, show the formation of β-sheet structures with progression of the enzymatic reactions.*

Self-assembly driven hydrogel resulting from the biocatalytic esterification reaction was well characterized by various spectroscopic and microscopic techniques. To realize the secondary structures of DCL hydrogel **37** and solution of DCL **38** resulting in

biocatalytic dynamic reaction, FT-IR study was performed at different reaction times (Figure 8.27). At 10 day, DCL hydrogel **37** showed amide I band at 1616 cm^{-1} indicating the formation of β-sheet structure while at 15 day, amide I band appeared at 1616 cm^{-1} along with a peak at 1645 cm^{-1} indicating the hydrogen bonded turn type supramolecular β-sheet arrangement in gel state.[26] Another characteristic band at 1745 cm^{-1} suggested the formation of ester functionality.[27] For DCL **38**, at day 10, amide I band appeared at 1630 cm^{-1} where at 15 day, it was centered at 1640 cm^{-1}. These results signified the structural transition from β-sheet to β-turn type structures. A characteristic peak at 1746 cm^{-1} confirms the existence of ester functionality in the dynamic library.

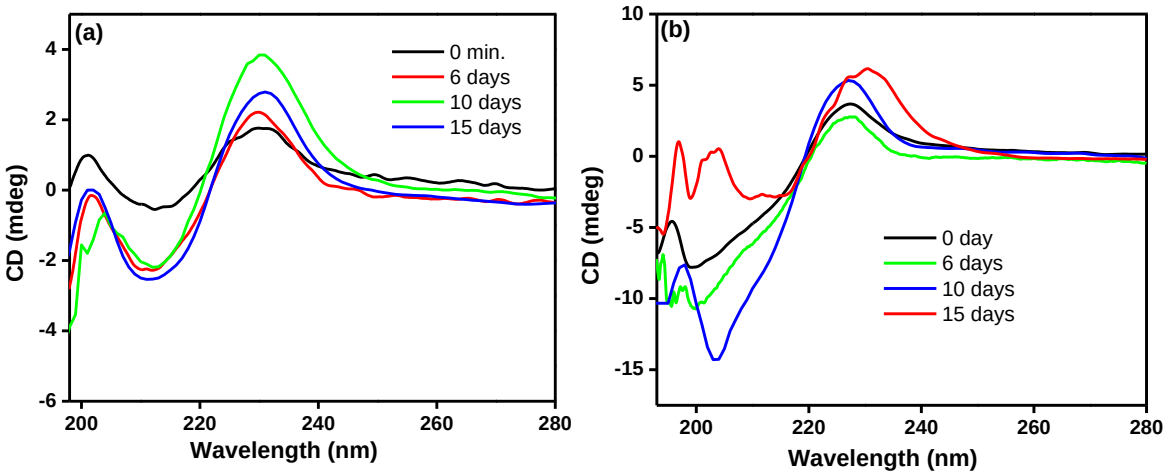

Figure 8.28. *Real time CD spectra of dynamic reactions of (a) peptide bolaamphiphile **37** and (b) peptide bolaamphiphile **38**, show the formation of ordered β-sheet structures with progression of the enzymatic reactions.*

The overall chirality of the chiral peptide based bolaamphiphile molecules has direct influences on its orientation during the self-assembly process. Circular dichroism (CD) spectra offers clear insight about the self-assembly of peptide based molecules within their chiral environments.[28] Peptide bolaamphiphile based DCLs were designed through enzyme mediated biocatalytic process. Therefore, CD spectra were recorded to investigate the structural conformations of DCLs at various time points during the course of the dynamic reactions (Figure 8.28). The CD signal appeared at negative region at

around 213 nm along with a weak shoulder at positive region at 201 nm prior to enzyme addition (at 0 min) which was ascribed from n-π* and π-π* transitions of the CO-NH groups of peptide bolaamphiphile **37** molecule. This characteristic CD signature confirmed β-sheet structure.[29] Another positive band appeared at 229 nm resulting from the excitation of the non-bonding electron of the oxygen atom into the π* orbital system of the aromatic ring of the tyrosine moiety.[30] The CD spectra showed similar trends of CD signature but the ellipticity at the negative band was increased during the course of the reaction. The CD spectra revealed that self-assembling di-esters progressively arranged into more ordered β-sheet structures. For peptide bolaamphiphile **38** based dynamic library, the CD spectra showed a progressive change at a negative band, which was gradually shifted from 200 nm to 215 nm during the course of the reaction. At initial stage of the reaction, the negative band at 200 nm signified random coil structure. After 15 days of reaction, the characteristic negative CD band at 215 nm along with a positive band at 196 nm revealed the ordered β-sheet structures of self-assembling molecules.[31] Another positive band corresponding to n-π* transition of tyrosine moiety was also observed which was shifted from 227 nm to 232 nm during the progression of the dynamic reaction.

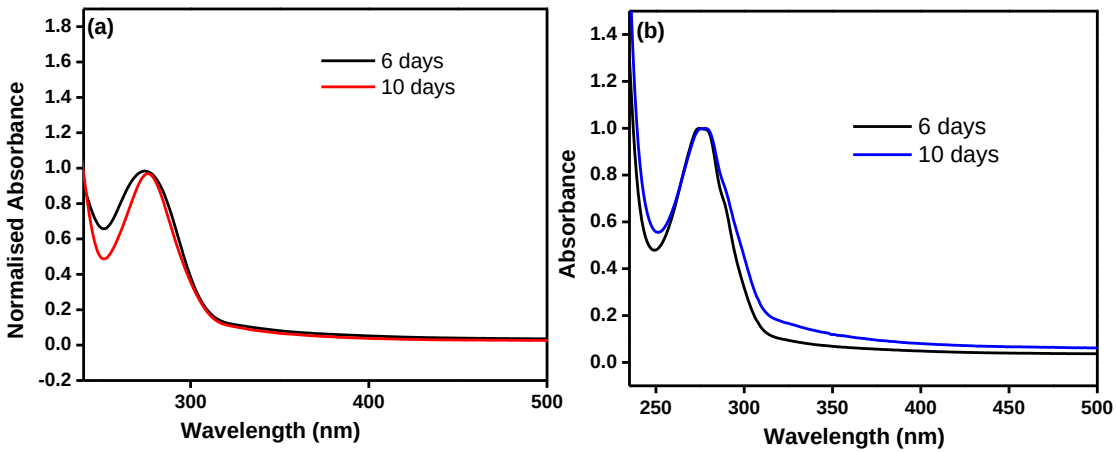

Figure 8.29. *Real time UV-Vis spectra of (a) DCL **37** and (b) DCL **38**.*

Real time UV-Vis spectra were taken to understand the variation in absorption spectra of molecules during the progress of dynamic reactions (Figure 8.29**)**. DCL **37** absorbed at

274 nm at 6 day of reaction which was shifted to 277 nm at 10 day of reaction. DCL **38** also showed a characteristic absorbance at 277 nm.

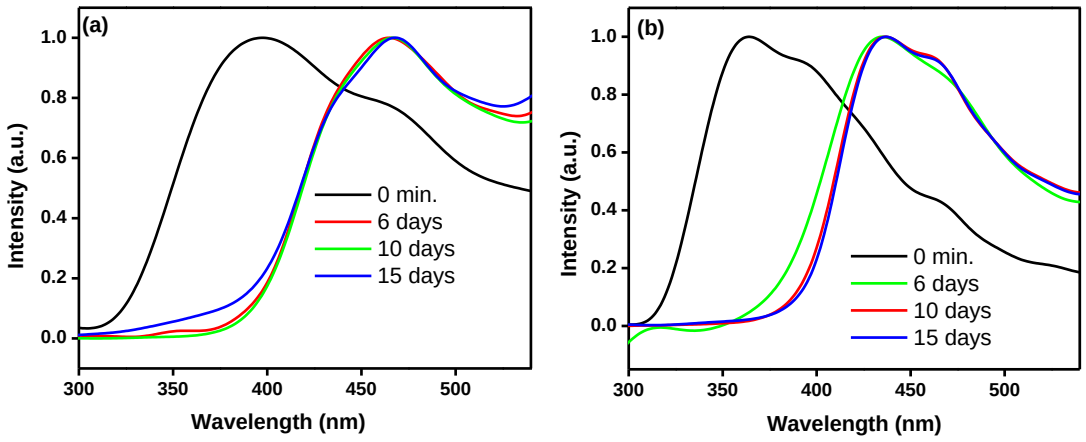

Figure 8.30. *Real time fluorescence spectra of dynamic reactions of (a) peptide bolaamphiphile **37** and (b) peptide bolaamphiphile **38**, show significant red shift with progression of both the reactions from 0 minute (mixture of peptide bolaamphiphile and p-hydroxybenzyl alcohol before enzyme addition) to 15 days. This revealed that π-π stacking interactions facilitate the product formation in enzymatic dynamic reactions.*

Excitation at 280 nm resulted in a broad emission band centered at 396 nm for dynamic reaction **37** in initial time which was gradually red-shifted during the reaction. A fluorescence band was observed at 463 nm at 6 day of reaction. The enormous red-shift indicated the progressive stable molecular arrangement via π-π stacking interactions[32] which was associated with biocatalytic esterification of peptide bolaamphiphile to enrich aromatic chromophores (Figure 8.30a). The DCL **37** showed an emission peak centred at 470 nm at 15 day of reaction. The 6 nm red-shift from solution (at 6 day) to hydrogel (at 15 day) indicated more compact molecular arrangement in gel state. The fluorescence nature of DCL **38** also showed the similar trends during the course of the reaction. A fluorescence band appeared at 363 nm prior to enzyme addition while it appeared at 437 nm with huge red-shift of 77 nm at 15 day of dynamic reaction (Figure 8.30b). The significant red-shift suggested the progressive ordered molecular arrangement via π-π stacking interactions during the course of reaction. Such fluorescent enhancement of

organic compound has potential applications in biology. Recently, red-shifted fluorescent proteins are widely used for *in vivo* tomographic imaging.[33]

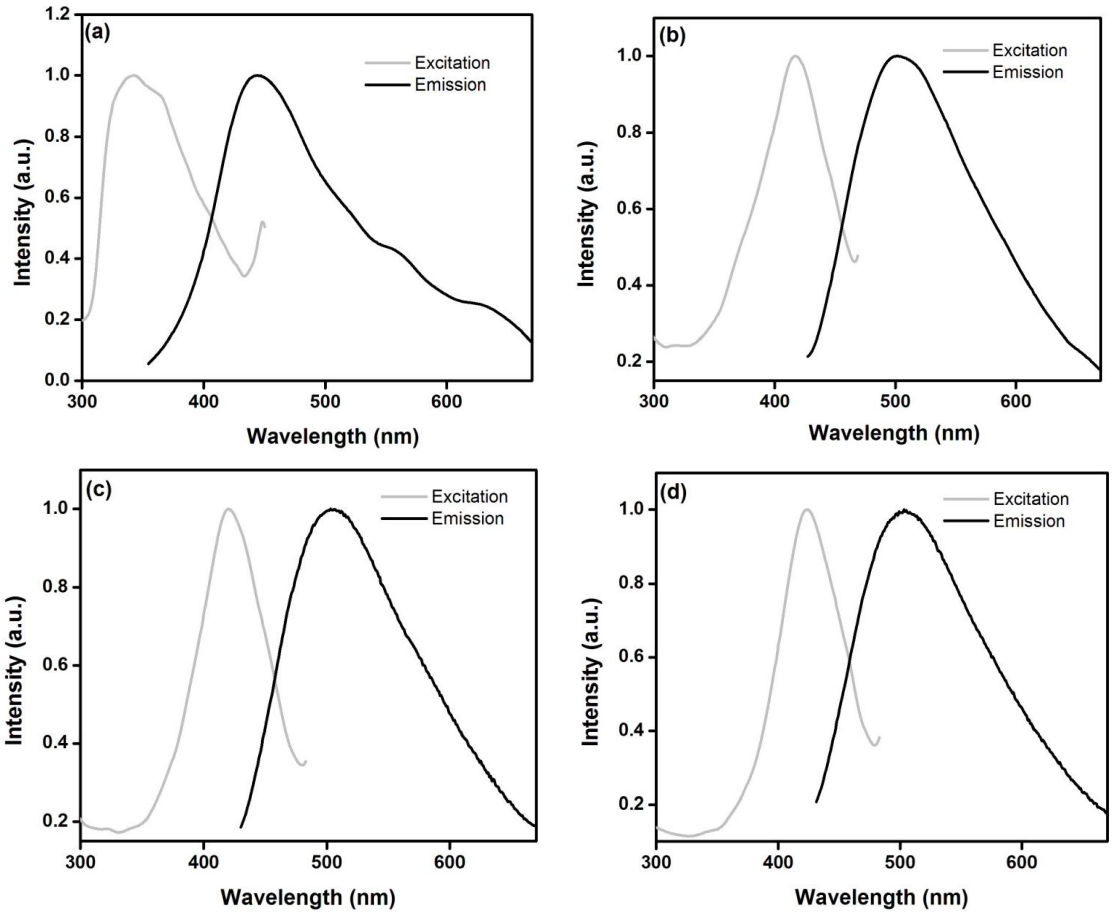

Figure 8.31. *Excitation (grey line) and emission spectra (black line) of DCL **37** at (a) 0 day (prior to enzyme addition, λ_{ex}= 341 nm), (b) at 6 day (λ_{ex}= 416 nm), (c) at 10 day (λ_{ex}= 420 nm) and (d) at 15 day (λ_{ex}= 420 nm).*

To capture higher ordered aggregation via spectroscopic technique, excitation spectroscopy is more relevant than UV-Vis spectroscopy because the dilution effect sometimes perturbs higher ordered aggregation for small molecules. We observed that time dependent UV-Vis spectroscopic analyses of DCL **37** and DCL **38** did not signify any higher ordered aggregation with progression of dynamic reactions. To avoid the dilution effect, we characterized the DCLs using by excitation spectroscopy[34] at different reaction times (Figure 8.31 and Figure 8.32). A pronounced peak at 341 nm

appeared before the enzyme addition and upon excitation at 341 nm resulted in the emission maxima at 444 nm for DCL **37**. This result clearly stated that higher ordered aggregated complex was generated prior to enzyme addition.[35] At 6 day of DCL **37**, the excitation spectroscopy showed the characteristic higher ordered aggregated peak at 416 nm and the corresponding emission peak appeared at 502 nm upon excitation on 416 nm. This observation signified that the origin of higher ordered aggregation was completely different from the initial aggregation.

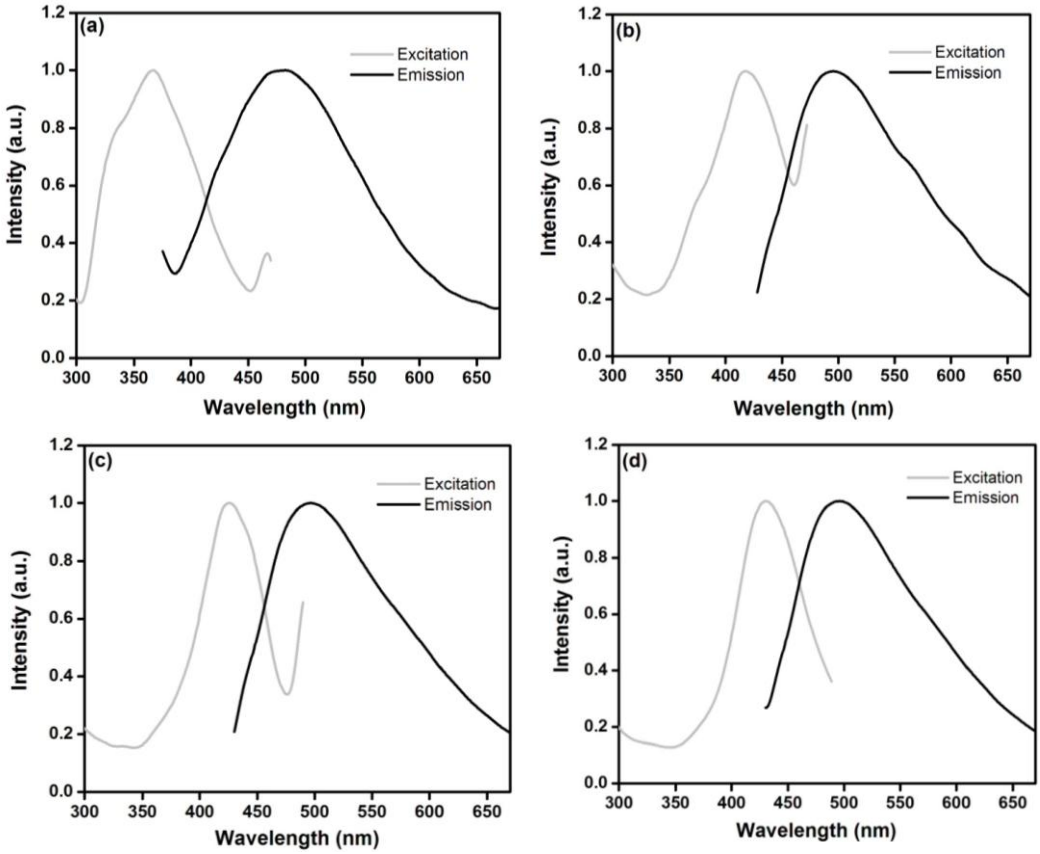

Figure 8.32. *Excitation (grey line) and emission spectra (black line) of DCL **38** at (a) 0 day (prior to enzyme addition, λ_{ex}= 365 nm), (b) at 6 day (λ_{ex}= 418 nm), (c) at 10 day (λ_{ex}= 418 nm) and (d) at 15 day (λ_{ex}= 420 nm).*

The excitation spectra showed the distinctive peaks at 420 and 422 nm at 10 day and 15 day of DCL **37**, and their corresponding emissions exhibited the fluorescence maxima at 504 nm. The observation clearly demonstrated that the higher ordered aggregation became more pronounced with increase in population of esters in DCL **37** with the

progression of reaction time. We also observed the similar results from DCL **38.** The increase population of ester moieties with the progression of reaction time favoured the formation of higher ordered aggregation at supramolecular level which formed well defined nanostructures.

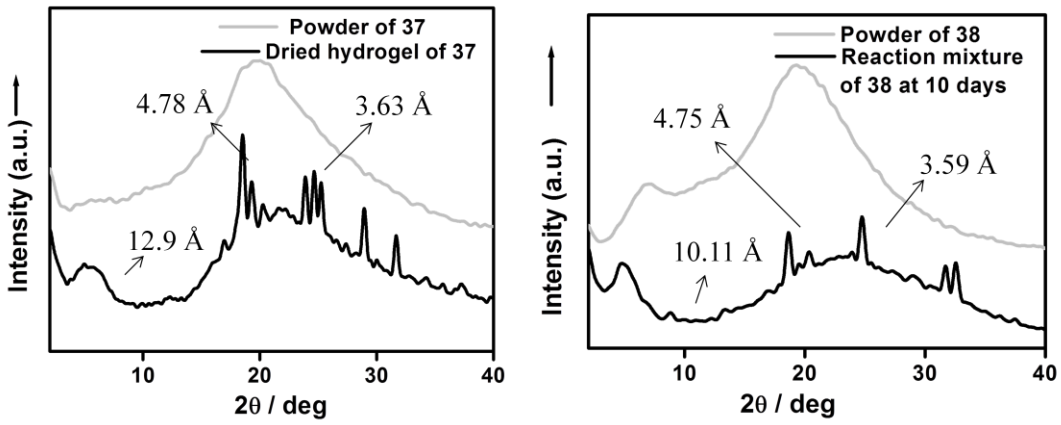

Figure 8.33. *PXRD spectra for both the DCL **37** and DCL **38** confirm that self-assembling molecules arranged into β-sheet structures in their respective nanoarchitectures.*

Wide angle X-ray scattering (WAXS) was used to investigate further structural information of dried DCLs. A series of diffraction patterns for both the dried DCLs correlated different features of the self-assembly (Figure 8.33). The dried hydrogel produced from DCL **37** at 10 day of dynamic reaction, showed several characteristic scattering patterns at 2θ = 6.8°, 18.54° and 24.56°. The characteristic peak at 2θ = 6.8° corresponding to a d spacing of 12.9 Å signified the spacing between two successive β-sheets while the diffraction peak at 2θ = 18.54° corresponding to a d spacing of 4.78 Å indicated the distance between two molecules in a β-sheet arrangement.[36] The π-π stacking interactions between the aromatic moieties played a leading role during the self-assembly process which was revealed from the diffraction peak at 2θ = 24.56° corresponding to a d spacing of 3.63 Å. For DCL **38**, the distinctive diffraction peak at 2θ = 8.73° corresponding to a d spacing of 10.11 Å revealed the inter-sheet distance inside the self-assembled nanostructure. Another significant peak at 2θ = 18.65° corresponding to a d spacing of 4.75 Å suggested the spacing between two successive self-assembling molecules within the β sheet structures. The characteristic peak at 2θ = 24.78°

corresponding to a d spacing of 3.59 Å was attributed from π-π stacking interactions.[37] The powder X-ray diffraction data evidently demonstrated that the peptide DCLs were self-assembled into a ordered β-sheet arrangement to form well defined nanostructures.

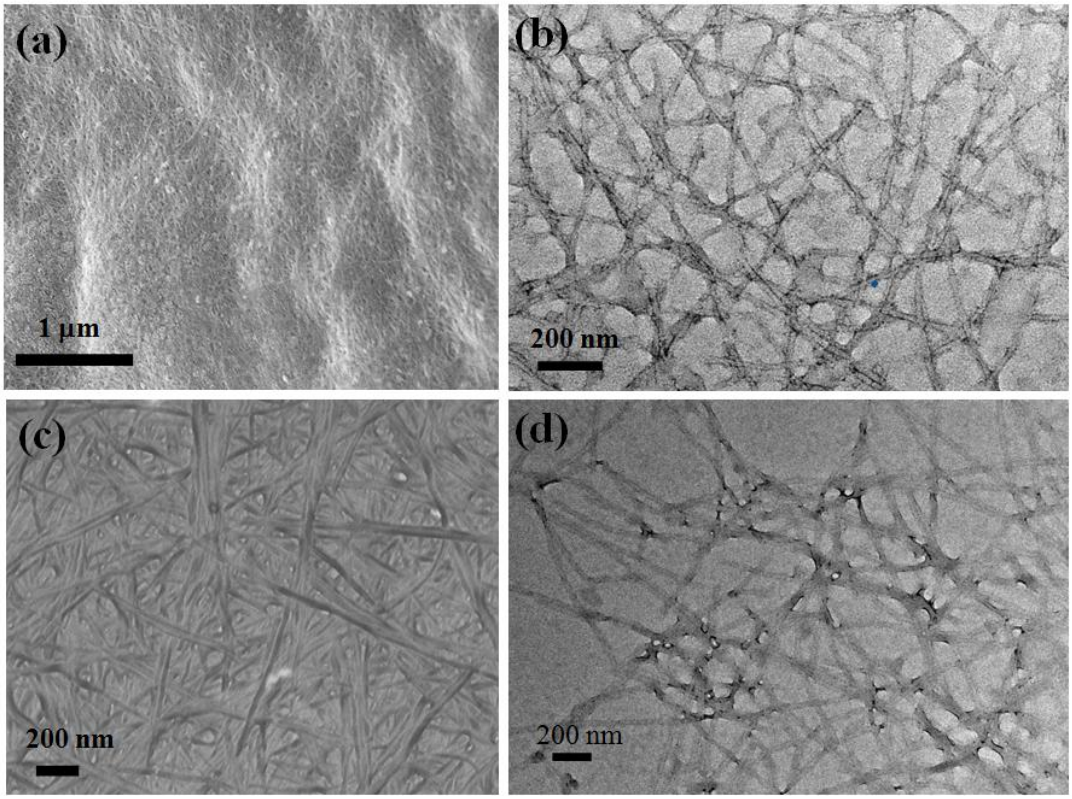

Figure 8.34. *(a) Scanning electron microscopy and (b) Transmission electron microscopy images of DCL **37** hydrogel at 10 day of dynamic reaction reveal entangled nanofibrillar morphology. (c) Scanning electron microscopy and (d) Transmission electron microscopy images of DCL **38** at 10 day of dynamic reaction show nanotapes morphology.*

Several microscopic studies demonstrated the self-assembly in supramolecular level accompanied by formation of nanofibrillar networks[38] in the dynamic reactions. The DCLs were not able to generate any well-defined nanostructures for initial 10 days. After that, the DCL **37** turned to become gel at day 10 which was associated with the formation of nanofibrillar structures (Figure 8.34a-b). The SEM image showed dense nanofibrils in the hydrogel. The average width of the nanofiber was 16 nm and each fiber was several micrometers in length. The TEM image revealed the entangled nanofibrillar structures in hydrogel.[39,40] The average diameter of the nanofibers was 14 nm which was in good agreement with the SEM study. The DCL **38** did not form gel over 30 days time period.

However, the self-assembled nanostructures were observed after 10 days of dynamic reaction for DCL **38**. The SEM image demonstrated the formation of well-defined nanotapes (Figure 8.34c-d).[41,42] The average width of the nanotapes was 42 nm and each of them was several micrometers in length. However, the TEM image exhibited the existence of nanotapes with average diameter of 32 nm. The other dynamic reaction mixtures were also found to adopt distinct nanostructures but they failed to form hydrogel with noticeable conversion. The SEM image of the dynamic reaction mixture of **25** showed the evolution of nanodisk which formed a distinct nanoarchitecture by their successive stacking (Figure 8.35a**)**.[43] The reaction mixture of **39** showed spherical morphology (Figure 8.35b).[44] The reaction mixture of **40** produced nanosheets while the reaction mixture of **3** exhibited the crystalline nanofibers (Figure 8.35c-d).[45]

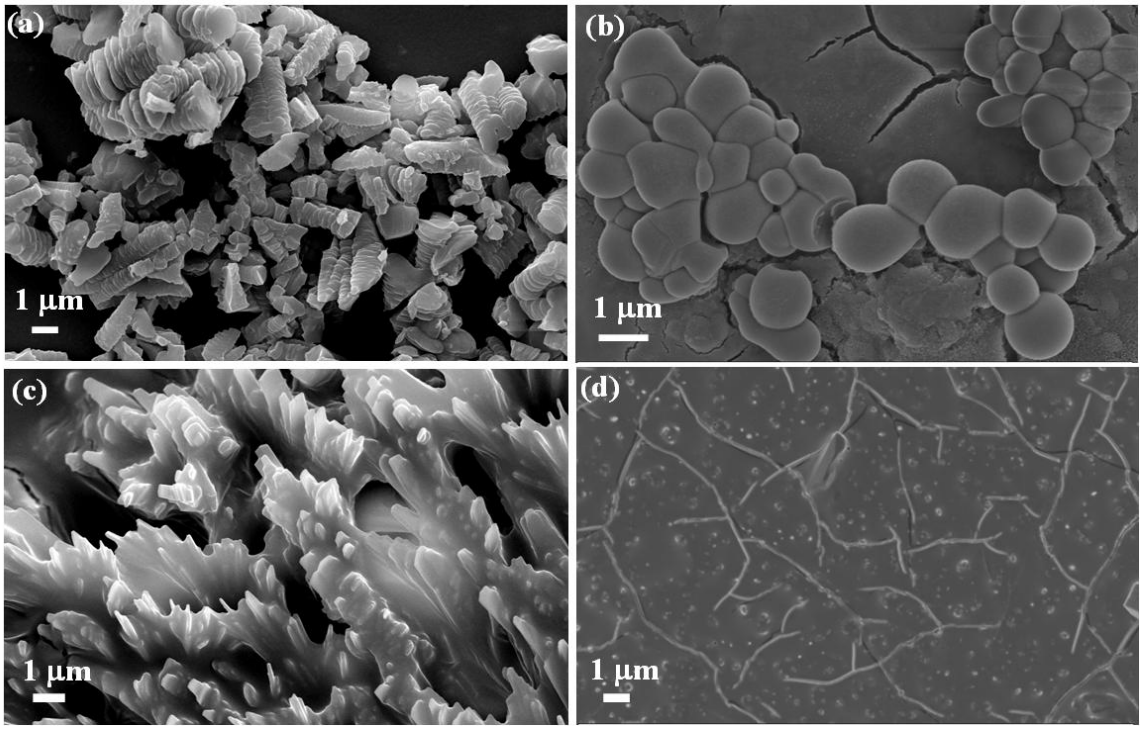

Figure 8.35. *Scanning electron microscopic images of (a) DCL **25** (HO-Phe(4)-Tyr(3)-Suc-Tyr(1)-Phe(2)-OH based DCL) shows nanodisk like structure and (b) DCL **39** (HO-Ala(4)-Tyr(3)-Suc-Tyr(1)-Ala(2)-OH based DCL) reveals spherical morphology after 10 days of enzymatic reaction. (c) DCL **40** (HO-Val(4)-Tyr(3)-Suc-Tyr(1)-Val(2)-OH based DCL) shows nanosheets like structures whereas (d) DCL **3** (HO-Leu(4)-Leu(3)-Suc-Leu(1)-Leu(2)-OH based DCL) demonstrates crystalline nanofibers after 10 days of enzymatic reaction.*

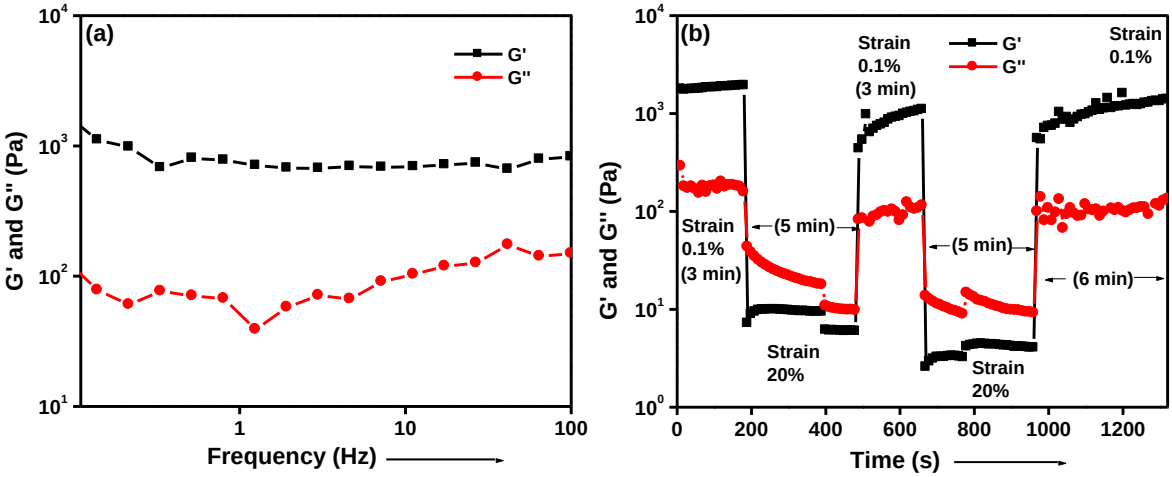

Figure 8.36. *(a) Frequency sweep of DCL **37** hydrogel (c = 20 mmol L^{-1}). Storage modulus G' is higher than the loss modulus G''. G' >10^3 Pa at low frequency, and the storage modulus is higher than the loss modulus by a factor of 5-10, which indicates excellent solid-like behavior of the gel materials. (b)The step strain experiment shows the thixotropic nature of DCL **37** hydrogel. Concentration was maintained at 20 mmol L^{-1}.*

The dynamic mechanical deed of hydrogel **37** was elucidated by rheological study.[46] Figure 8.36a illustrated that storage modulus (G') exceeded that of loss modulus (G") over the oscillating frequency. The gel was moderately stiff, with G' > 10^3 Pa at low frequency. The value of storage modulus G' exceeded that of loss modulus G" by a factor of 5 in the higher frequency region, which signified the formation of a strong and rigid hydrogel.[47] The thixotropic nature[48,49] of the DCL hydrogel **37** was investigated using a hysteresis loop test (Figure 8.36b). A loop test was performed by applying successive low/high strains, to assure the complete gel-to-sol (G" > G') and sol-to-gel (G' > G") conversion. These results showed that the mechanical property of the gel was recovered within 4 ± 1 min after reduction of the large strain. Initially, gel was subjected to a constant strain of 0.1% (step 1). Then the strain was increased from 0.1% to 20% and kept for 5 minutes at 20% strain to break the gel completely (step 2). Again the strain was reduced to 0.1% and allowed it for 3 minutes at a 0.1% to view the gel restoration kinetics (step 3). Again the strain was increased from 0.1% to 20% for 5 minutes (step 4) to destroy the gel and at last (step 5) the strain was reduced to its initial value of 0.1% and kept for 6 minutes for restoring its mechanical strength. The angular frequency was set

constant at 10 rad/sec throughout the entire experiment. It was observed that loss modulus values (G″) exceeded over the storage modulus (G′) when the constant strain was 20% indicating the breakage of gel (sol-like nature) during the second interval of the experiment. At step 3, after removing 20% strain, the gel recovered 70% of its original stiffness within 3 minutes. At step 4, the gel was destroyed by application of 20% strain while after removal of 20% strain, the gel regained 80% of its original mechanical property within 6 minutes. This type of thixotropic gel would be very useful in realizing shape memory performance.

The study on cellular toxicity and proliferation are very essential in the area of biomedicine and cell-biology. Previously, Stupp *et al.* demonstrated bioactive nanofibrous hybrid peptide scaffolds that supported selective differentiation of neural progenitor cells.[50,51] Recently, we investigated dose dependent cytotoxicity and cell proliferation behavior of WBC by using peptide bolaamphiphile hydrogel material.[52] Ulijn *et al.* used peptide hydrogels as scaffold materials in 3D cell culture.[53,54] Here, we reported a novel enzymatic dissipative hydrogel as a supreme scaffold for human umbilical cord stem cells proliferation. The cells were mixed with the hydrogel and then the number of metabolically active cells within the hydrogel was investigated by MTT, XTT and DNA leaching experiments (Table 8.1). Cell proliferation was studied at three different concentration of hydrogel at three different time points within a period of five days. At day 1, 3 and 5, increased absorbance of MTT and XTT consistently revealed that gel exerted positive influence on the cell survival and also facilitated proliferation which can be consolidated by increase in DNA and MTT/XTT both. As DNA in media is representation of dead cells, thus increase in MTT and XTT along with DNA suggest increased number of total cells population due to proliferation/survival and because of this increase in total number of cells, dead cells were also higher than the media control. From the results, it is evident that gel at 20 mM concentration significantly supports the cells survival and proliferation of human umbilical cord mesenchymal stem cells.

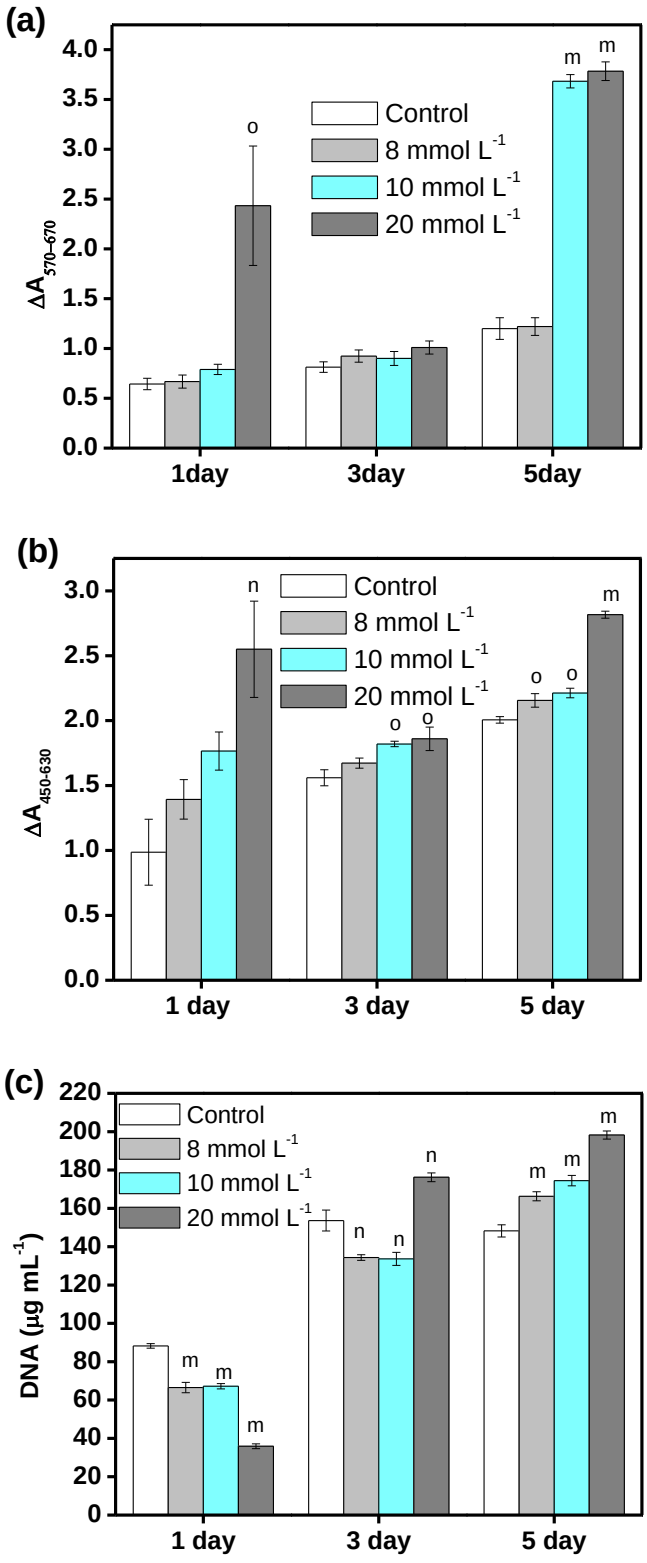

Figure 8.37. *Stem cell viability based on (a) MTT , (b) XTT and (c) DNA leaching assay within the peptide hydrogels. Data are means ± S.E.M. (n=3);* ^{m}*, P<0.001;* ^{n}*, P<0.01 and* ^{o}*, P<0.05 as compared to the respective media control values. (S.E.M represents* standard error *of* measurement*)*

8.5 Conclusions

Here, we demonstrate lipase catalysed generation of dipeptide appended bolaamphiphilic DCLs. Lipase is used for regioselective inclusion of a chemical fuel *p*-hydroxy benzylalcohol to a series of peptide bolaamphiphiles. Biocatalytic self-assembly of a peptide bolaamphiphilic hydrogel mimics the natural dissipative self-assembly system by using a chemical fuel *p*-hydroxy benzylalcohol. A nongelating unactivated acid functionalized peptide bolaamphiphile is activated to self-assemble through a double esterification by a chemical fuel of *p*-hydroxy benzylalcohol. After a certain period of lag phase, when the monoester reaches at a sufficient concentration, the self-assembly of di-ester accelerates its formation exponentially by consuming the monoester. The self-assembly of diesters leads to the formation of nanofibrillar hydrogel. The subsequent hydrolysis of the di-ester gelators dissipate its energy, which results in dis-assembly of the system. This system follows all requirements for dissipative self-assembly where the activation occurs at higher rate than deactivation. The activation results to form self-assembled nanoarchitecture. Furthermore, we use the thixotropic nanofibrillar hydrogel as a scaffold for human umbilical cord stem cells proliferation.

8.6 References

1. Whitesides G. M., Ismagilov R. F. (1999), Complexity in chemistry, *Science*, 284, 89-92 (DOI: 10.1126/science.284.5411.89).

2. Grzybowski B. A., Wilmer C. E., Kim J., Browne K. P., Bishop K. J. M. (2009), Self-assembly: From crystals to cells, *Soft Matter*, 5, 1110-1128 (DOI: 10.1039/B819321P).

3. Desai A., Mitchison T. J. (1997), Microtubule polymerization dynamics, *Annu. Rev. Cell Dev. Biol.*, 13, 83-117 (DOI: 10.1146/annurev.cellbio.13.1.83).

4. Fletcher D. A., Mullins R. D. (2010), Cell mechanics and the cytoskeleton, *Nature*, 463, 485-492 (DOI: 10.1038/nature08908).

5. Alberts B., Bray D., Lewis J., Raff M., Roberts K., Watson J. D. (1994), Molecular biology of the cell, 3rd ed., Garland publishing, New York,

6. Boekhoven J., Brizard A. M., Kowlgi K. N. K., Koper G. J. M., Eelkema R., van Esch J. H. (2010), Dissipative self-assembly of a molecular gelator by using a chemical fuel, *Angew. Chem. Int. Ed.*, 49, 4825-4828 (DOI: 10.1002/anie.201001511).

7. Dinu C. Z., Opitz J., Pompe W., Howard J., Mertig M., Diez S. (2006), Parallel manipulation of bifunctional DNA molecules on structured surfaces using kinesin-driven microtubules, *Small*, 2, 1090-1098 (DOI: 10.1002/smll.200600112).

8. Liu H., Spoerke E. D., Bachand M., Koch S. J., Bunker B. C., Bachand G. D. (2008), Biomolecular motor-powered self-assembly of dissipative nanocomposite rings, *Adv. Mater*., 20, 4476-4481 (DOI: 10.1002/adma.200801291).

9. Sadownik J. W., Philp D. (2008), A simple synthetic replicator amplifies itself from a dynamic reagent pool, *Angew. Chem. Int. Ed*., 47, 9965-9970 (DOI: 10.1002/anie.200804223).

10. Malakoutikhah M., Peyralans J. J.-P., Colomb-Delsuc M., Fanlo-Virgós H., Stuart M. C. A., Otto S. (2013), Uncovering the selection criteria for the emergence of multi-building-block replicators from dynamic combinatorial libraries, *J. Am. Chem. Soc.*, 135, 18406-18417 (DOI: 10.1021/ja4067805).

11. Carnall J. M. A., Waudby C. A., Belenguer A. M., Stuart M. C. A., Peyralans J. J.-P., Otto S. (2010), Mechanosensitive self-replication driven by self-organization, *Science*, 327, 1502-1506 (DOI: 10.1126/science.1182767).

12. Li J., Carnall J. M. A., Stuart M. C. A., Otto S. (2011), Hydrogel formation upon photoinduced covalent capture of macrocycle stacks from dynamic combinatorial libraries, *Angew. Chem. Int. Ed.*, 50, 8384 -8386 (DOI: 10.1002/anie.201103297).

13. Nguyen R., Allouche L., Buhler E., Giuseppone N. (2009), Dynamic combinatorial evolution within self-replicating supramolecular assemblies, *Angew. Chem. Int. Ed*. 48, 1093-1096 (DOI: 10.1002/anie.200804602).

14. Rasale D. B., Maity I., Das A. K. (2012), Emerging π-stacked dynamic nanostructured library, *RSC Adv.*, 2, 9791-9794 (DOI: 10.1039/C2RA21334F).

15. Williams R. J., Smith A. M., Collins R., Hodson N., Das A. K., Ulijn R. V. (2009), Enzyme-assisted self-assembly under thermodynamic control, *Nature Nanotechnol*., 4, 19-24 (DOI: 10.1038/NNANO.2008.378).

16. John G., Zhu G., Li J., Dordick J. S. (2006), Enzymatically derived sugar-containing self-assembled organogels with nanostructured morphologies, *Angew. Chem. Int. Ed*., 45, 4772 -4775 (DOI: 10.1002/anie.200600989).

17. Vongvilai P., Angelin M., Larsson R., Ramstrom O. (2007), Dynamic combinatorial resolution: Direct asymmetric lipase-mediated screening of a dynamic nitroaldol library, *Angew. Chem. Int. Ed.*, 46, 948-950 (DOI: 10.1002/anie.200603740).

18. Yang Z., Huang Z.-L. (2012), Enzymatic synthesis of sugar fatty acid esters in ionic liquids, *Catal. Sci. Technol*., 2, 1767-1775 (DOI: 10.1039/c2cy20109g)

19. Brun N., Garcia A. B., Deleuze H., Achard M.-F., Sanchez C., Durand F., Oestreicher V., Backov R. (2010), Enzyme-based hybrid macroporous foams as highly efficient biocatalysts obtained through integrative chemistry, *Chem. Mater*., 22, 4555-4562 (DOI:10.1021/cm100823d).

20. Paravidino M., Hanefeld U. (2011), Enzymatic acylation: Assessing the greenness of different acyl donors, *Green Chem*., 13, 2651-2657 (DOI: 10.1039/c1gc15576h).

21. Barnes H. A. (1997), Thixotropy a review, *J. Non-Newtonian Fluid Mech*., 70, 1-33 (DOI: 10.1016/S0377-0257(97)00004-9).

22. Bhattacharjee S., Bhattacharya S. (2014), Pyridylenevinylene based Cu^{2+}-specific, injectable metallo(hydro)gel: thixotropy and nanoscale metal–organic particles, *Chem. Commun.*, 50, 11690-11693 (DOI: 10.1039/c4cc04712e).

23. Nanda J., Biswas A., Banerjee A. (2013), Single amino acid based thixotropic hydrogel formation and pH-dependent morphological change of gel nanofibers, *Soft Matter*, 9, 4198-4208 (DOI: 10.1039/c3sm27050e).

24. Chen C., Gu Y., Deng L., Han S., Sun X., Chen Y., Lu J. R., Xu H. (2014), Tuning gelation kinetics and mechanical rigidity of β-hairpin peptide hydrogels via hydrophobic amino acid substitutions *ACS Appl. Mater. Interfaces*, 6, 14360-14368 (DOI: 10.1021/am5036303).

25. Dambenieks A. K., Vu P. H. Q., Fyles T. M. (2014), Dissipative assembly of a membrane transport system, *Chem. Sci*., 5, 3396-3403 (DOI: 10.1039/c4sc01258e).

26. Pelton J. T., McLean L. R. (2000), Spectroscopic methods for analysis of protein secondary structure, *Anal Biochem*., 277, 167-176 (DOI:10.1006/abio.1999.4320).

27. Maity I., Rasale D. B., Das A. K. (2013), Exploiting a self-assembly driven dynamic nanostructured library, *RSC Adv*., 3, 6395-6400 (DOI: 10.1039/c3ra22401e).

28. Datta S., Samanta S. K., Bhattacharya S. (2013), Induction of supramolecular chirality in the self-assemblies of lipophilic pyrimidine derivatives by choice of the amino acid-based chiral spacer, *Chem. Eur. J*., 19, 11364 -11373 (DOI: 10.1002/chem.201300605).

29. Yan X., Cui Y., He Q., Wang K., Li J. (2008), Organogels based on self-assembly of diphenylalanine peptide and their application to immobilize quantum dots, *Chem. Mater*., 20, 1522-1526 (DOI: 10.1021/cm702931b).

30. Maity I., Manna M. K., Rasale D. B., Das A. K. (2014), Peptide-nanofiber-supported palladium nanoparticles as an efficient catalyst for the removal of N-terminus protecting groups, *ChemPlusChem*, 79, 413- 420 (DOI: 10.1002/cplu.201300348).

31. Haines L. A., Rajagopal K., Ozbas B., Salick D. A., Pochan D. J., Schneider J. P. (2005), Light-activated hydrogel formation via the triggered folding and self-assembly of a designed peptide, *J. Am. Chem. Soc.*, 127, 17025-17029 (DOI: 10.1021/ja054719o).

32. Maity I., Mukherjee T. K., Das A. K. (2014), Photophysical study of a π-stacked β-sheet nanofibril forming peptide bolaamphiphile hydrogel, *New J. Chem*., 38, 376-385 (DOI: 10.1039/c3nj00814b).

33. Deliolanis N. C., Wurdinger T., Pike L., Tannous B. A., Breakefield X. O., Weissleder R., Ntziachristos V. (2011), In vivo tomographic imaging of red-shifted fluorescent proteins, *Biomedical Optics Express*, 2, 887-900.

34. Leon A. R., Olatunde A. O., Morrow J. R., Achim C. (2012), Binding of EuIII to 1,2-hydroxypyridinone-modified peptide nucleic acids, *Inorg. Chem*., 51, 12597-12599 (DOI: 10.1021/ic301790v).

35. Das A. K., Hirst A. R., Ulijn R. V. (2009), Evolving nanomaterials using enzyme-driven dynamic peptide libraries (eDPL), *Faraday Discuss*., 143, 293-303 (DOI: 10.1039/B902065A).

36. Maity I., Rasale D. B., Das A. K. (2012), Sonication induced peptide-appended bolaamphiphile hydrogels for in situ generation and catalytic activity of Pt nanoparticles, *Soft Matter*, 8, 5301-5308 (DOI: 10.1039/c2sm25126d).

37. Koley P., Pramanik A. (2012), Multilayer vesicles, tubes, various porous structures and organo gels through the solvent-assisted self-assembly of two modified tripeptides and their different applications, *Soft Matter*, 8, 5364-5374 (DOI: 10.1039/c2sm25205h).

38. Muraoka T., Cui H., Stupp S. I. (2008), Quadruple helix formation of a photoresponsive peptide amphiphile and its light-triggered dissociation into single fibers, *J. Am. Chem. Soc*., 130, 2946-2947 (DOI: 10.1021/ja711213s).

39. Ray S., Das A. K., Banerjee A. (2007), pH-responsive, bolaamphiphile-based smart metallo-hydrogels as potential dye-adsorbing agents, water purifier, and vitamin B12 carrier, *Chem. Mater*., 19, 1633-1639 (DOI: 10.1021/cm062672f).

40. Song B., Wei H., Wang Z., Zhang X., Smet M., Dehaen W. (2007), Supramolecular nanofibers by self-organization of bola-amphiphiles through a combination of hydrogen bonding and π-π stacking interactions, *Adv. Mater*., 19, 416-420 (DOI: 10.1002/adma.200600779).

41. Cui H., Cheetham A. G., Pashuck E. T., Stupp S. I. (2014), Amino acid sequence in constitutionally isomeric tetrapeptide amphiphiles dictates architecture of one-dimensional nanostructures, *J. Am. Chem. Soc*., 136, 12461-12468 (DOI: 10.1021/ja507051w).

42. Castelletto V., Hamley I. W., Adamcik J., Mezzenga R., Gummel J. (2012), Modulating self-assembly of a nanotape-forming peptide amphiphile with an oppositely charged surfactant, *Soft Matter*, 8, 217-226 (DOI: 10.1039/c1sm06677c).

43. Xie J., Wu Q., Zhang D., Ding Y. (2009), Biomolecular-induced synthesis of self-assembled hierarchical $La(OH)CO_3$ one-dimensional nanostructures and its morphology-held conversion toward La_2O_3 and $La(OH)_3$, *Crystal Growth & Design*, 9, 3889-3897 (DOI: 10.1021/cg801053p).

44. Zhu X., Liu M. (2011), Self-assembly and morphology control of new L-glutamic acid-based amphiphilic random copolymers: Giant vesicles, vesicles, spheres, and honeycomb Film, *Langmuir*, 27, 12844-12850 (DOI: 10.1021/la202680j).

45. Zhang D., Wang J., Chen S., Cheng X., Li T., Zhang J., Zhang A. (2012), Surface hybrid self-assembly, mechanism, and crystalline behavior of a carboxyl-ended hyperbranched polyester/platinum complex, *Langmuir*, 28, 16772-16781 (DOI: 10.1021/la3040209).

46. Nair G. G., Prasad S. K., Bhargavi R., Jayalakshmi V., Shanker G., Yelamaggad C. V. (2010), Soft glass rheology in liquid crystalline gels formed by a monodisperse dipeptide, *J. Phys. Chem. B*, 114, 697-704 (DOI: 10.1021/jp9071394).

47. Liao S. W., Yu T.-B., Guan Z. (2009), De novo design of saccharide-peptide hydrogels as synthetic scaffolds for tailored cell responses, *J Am Chem Soc*., 131,17638-17646 (DOI: 10.1021/ja907097t).

48. Basak S., Nanda J., Banerjee A. (2014), Multi-stimuli responsive self-healing metallo-hydrogels: Tuning of the gel recovery property, *Chem. Commun*., 50, 2356-2359 (DOI: 10.1039/b000000x).

49. Ramirez M., Guan D., Ugaz V., Chen Z. (2013), Intein-triggered artificial protein hydrogels that support the immobilization of bioactive proteins, *J. Am. Chem. Soc*., 135, 5290-5293 (DOI: 10.1021/ja401075s).

50. Silva G. A., Czeisler C., Niece K. L., Beniash E., Harrington D. A., Kessler J. A., Stupp S. I. (2004), Selective differentiation of neural progenitor cells by high-epitope density nanofibers, *Science*, 303, 1352-1355 (DOI: 10.1126/science.1093783).

51. Sur S., Pashuck E. T., Guler M. O., Ito M., Stupp S. I., Launey T. (2012), A hybrid nanofiber matrix to control the survival and maturation of brain neurons, *Biomaterials*, 33, 545-555 (DOI: 10.1016/j.biomaterials.2011.09.093).

52. Maity I., Parmar H. S., Rasale D. B., Das A. K. (2014), Self-programmed nanovesicle to nanofiber transformation of a dipeptide appended bolaamphiphile and its dose dependent cytotoxic behaviour, *J. Mater. Chem. B*, 2, 5272-5279 (DOI: 10.1039/C4TB00365A).

53. Zhou M., Smith A. M., Das A. K., Hodson N. W., Collins R. F., Ulijn R. V., Gough J. E. (2009), Self-assembled peptide-based hydrogels as scaffolds for anchoragedependent cells, *Biomaterials*, 30, 2523-2530 (DOI:10.1016/j.biomaterials.2009.01.010).

54. Jayawarna V., Ali M., Jowitt T. A., Miller A. F., Saiani A., Gough J. E., Ulijn R. V. (2006), Nanostructured hydrogels for three-dimensional cell culture through self-assembly of fluorenylmethoxycarbonyl–dipeptides, *Adv. Mater*., 18, 611-614 (DOI: 10.1002/adma.200501522).

Chapter 9

Conclusion and Scopes For Future Work

9.1 Conclusion

Self-assembly driven peptide and peptide bolaamphiphiles based soft materials have great potential to generate powerful scaffolds for tissue engineering[1] and nanocatalysis.[2] Molecular gels are formed by the self-assembly of short peptide derivatives by weak non-covalent interactions which can be tuned by external stimuli. Functional molecular gels are found very sensitive to pH, metal ions, light, heat, sonication and enzymes.[3-8] Such stimuli responsive small peptide and peptide bolaamphiphilic gels are capable to create a platform to mediate the growth of tissues and organs for regenerative medicine. In addition, gel nanostructures support the synthesis and stabilization of metal nanoparticles in mild conditions. *In situ* synthesized metal nanoparticles can be used as nanocatalysts in several organic reactions. Therefore, the self-assembly of peptide and peptide derivatives still need to explore for material sciences, nanobiotechnology. We are engaged to synthesis several peptide appended bolaamphiphilic molecules[9] which are covalently connected by centrally located succinic acid moiety. These molecules are ideal for designing self-assembling soft materials through extensive hydrogen bonding and π-π stacking interactions which can be tuned by various stimuli. In this thesis, we have reported the stimuli responsive peptide bolaamphiphilic hydrogels monitoring by sonication, chemical fuel, pH and enzymes. We have also described the potential applications of such soft materials for tissue engineering and nanocatalysis.

Chapter 2 revealed the materials which were used to carry out these research works. This chapter also clearly described various spectroscopic and experimental techniques which were used in these studies.

Chapter 3 described a chemical fuel catalyzed esterification and etherification of peptide bolaamphiphiles in aqueous medium at room temperature (25 °C). In this chapter, we have designed a self-assembly driven hydrogel based on dynamic combinatorial library (DCL) of peptide bolaamphiphiles which is made using a reversible chemical fuel-catalyzed reaction. The reaction between tyrosine rich peptide based bolaamphiphiles and dimethyl sulphate (chemical fuel) facilitates the formation of a dynamic library containing mono-ester, mono-ether, di-ester, di-ether of peptide bolaamphiphiles but self-

assembly process selects the mono-ester of peptide bolaamphiphile as a predominant nanostructured product in gel phase medium. The microscopic studies confirmed the nanofibrillar structures which are responsible for the formation of self-supporting hydrogel.

Chapter 4 reports the synthesis of several peptide bolaamphiphles to exploit stimulus responsive self-assembly. We have tuned the peptide bolaamphiphiles self-assembly by using sonication as a stimulus which provides sufficient energy to reorient the peptide bolaamphiphiles into ordered structures to form hydrogel materials. The self-assembly process leads to the formation of interesting nanostructures including nanofibers and twisted nanoribbons. We have utilized the gel material of tyrosine rich bolaamphiphile as a nanoreactor to synthesis Pt nanoparticles inside the gel matrix. The nanoparticles showed enhanced catalytic activity in the hydrogenation reaction of *p*-nitroaniline to *p*-phenylenediamine.

Chapter 5 accounted peptide bolaamphiphilic self-assembly by monitoring the stimulus pH which was tuned by hydrolysis of an internal additive such as succinic anhydride. In this chapter, we have demonstrated the self-assembly of a peptide bolaamphiphile molecule for the fabrication of Pd nanoparticles on peptide nanofibers to enhance the catalytic ability for C-C coupling reactions under mild and aerobic conditions. The peptide bolaamphiphile nanofibers were anticipated to anchor the aromatic reactants and metal nanoparticles, which would result in an enhanced catalytic activity for C–C coupling reactions.

Chapter 6 described the sonication-induced formation of a tyrosine and tryptophan based peptide bolaamphiphile hydrogel. The Pd nanoparticles were decorated on the surface of peptide bolaamphiphile nanofibers, which provide extra stability to the Pd nanoparticles. In this chapter, we have reported a general method in which peptide-nanofiber-supported Pd nanoparticles can efficiently deprotect various types of N-protecting groups from the N terminus of amino acids and peptides in the presence of $NaBH_4$ in aqueous medium at room temperature.

Chapter 7 revealed the morphological transformation of a small fluorescent peptide bolaamphiphile via molecular self-assembly process. We have observed the self-programmed morphological transformation from nanovesicles to nanofibers of a smart peptide bolaamphiphile in its self-assembling hydrogel state via a third polymorphic state of nanocapsule. The nanostructural transition occurred based on the structural continuity of stable β-sheet structures. Spectroscopic studies confirmed different molecular arrangements of two different nanostructures. Furthermore, the smart bolaamphiphile shows a dose-dependent cytotoxicity and cell-proliferation behaviour.

Chapter 8 described lipase catalyzed generation of dynamic combinatorial libraries (DCL) of peptide bolaamphiphiles where gastrodigenin (*p*-hydroxy benzylalcohol) was used as a chemical fuel. At early stage of dynamic reactions, the mono-ester becomes major product but the self-assembly process selects the di-ester as predominant product which forms a hydrogel. After 19 days, all the library members (parent bolaamphiphiles and mono-ester) consume *p*-hydroxy benzylalcohol to form entirely di-ester. The gel/sol transition is associated with the dissipative self-assembly process, where peptide bolaamphiphile consumes energy in the form of *p*-hydroxy benzylalcohol to form activated building block of di-ester to self-assemble into nanofibrous hydrogel. Again, the subsequent hydrolysis results in dissipation of energy to form non-assembling parent bolaamphiphile with collapsed nanofibers. Furthermore, 3D cell culture experiments with the thixotropic DCL hydrogel matrix at different time periods significantly support the cells survival and proliferation of human umbilical cord mesenchymal stem cells.

9.2 Scopes For Future Works

Bolaamphiphiles are an interesting class of amphiphilic molecules, which can self-assemble to form well-defined nanostructures. The balance between the hydrophobic and hydrophilic groups can lead the peptide bolaamphiphile to self-assemble in aqueous media. There are hydrogen-bonding sites in the peptide stations, along with two carboxylic acid groups. The hydrophobic aromatic side chains can also take part in the self-assembly process through π–π stacking interactions. These molecules are ideal for designing self-assembling soft materials through extensive hydrogen bonding and π–π

stacking interactions. There are great scopes with such types of synthesized self-assembling molecules to explore the soft biomaterials. The chemical functionality of the head groups and spacer can be varied to tune the self-assembling behavior of bolaamphiphiles. The peptide bolaamphiphile nanostructures can be used as template to design several metal nanoarchitectures, which can be used in nanomedicine and nanotechnology including nanocatalysis. The peptide bolaamphiphiles with highly conjugated spacer can meet the essential requirements of material sciences with potential applications in opto-electronic, photovoltaic solar cell and highly conducting materials. Besides such organo-electronic applications,[10] these types of conjugated bolaamphiphiles will have interesting fluorescence properties. As the peptide bolaamphiphiles are easily water soluble, there are scopes for potential applications for cell imaging and tissue engineering in near future.

9.3 References

1. Bera M. K., Chakraborty C., Singh P. K., Sahu C., Sen K., Maji S., Das A. K., Malik S. (2014), Fluorene-based chemodosimeter for "turn-on" sensing of cyanide by hampering ESIPT and live cell imaging, *J. Mater. Chem. B*, 2, 4733-4739 (DOI: 10.1039/c4tb00388h).

2. Djalali R., Samson J., Matsui H. (2004), Doughnut-shaped peptide nano-assemblies and their applications as nanoreactors, *J. Am. Chem. Soc*., 126, 7935-7939 (DOI:10.1021/ja0319691).

3. Miravet J. F., Escuder B. (2005), Pyridine-functionalised ambidextrous gelators: towards catalytic gels, *Chem. Commun*., 5796-5798 (DOI: 10.1039/b510874h).

4. Sobczuk A. A., Tamarua S.-i., Shinkai S. (2011), New strategy for controlling the oligothiophene aggregation mode utilizing the gel-to-sol phase transition induced by crown-alkali metal interactions, *Chem. Commun*., 47, 3093-3095 (DOI: 10.1039/c1cc00026h).

5. Aoki K., Nakagawa M., Ichimura K. (2000), Self-assembly of amphoteric azopyridine carboxylic acids: Organized structures and macroscopic organized morphology influenced by heat, pH change, and light, *J. Am. Chem. Soc.*, 122, 10997-11004 (DOI: 10.1021/ja001790f)

6. Qiao Y., Lin Y., Yang Z., Chen H., Zhang S., Yan Y., Huang J. (2010), Unique temperature-dependent supramolecular self-assembly: From hierarchical 1D nanostructures to super hydrogel, *J. Phys. Chem. B*, 114, 11725-11730 (DOI:10.1021/jp1047369).

7. Yu X., Chen L., Zhang M., Yi T. (2014), Low-molecular-mass gels responding to ultrasound and mechanical stress: towards self-healing materials, *Chem. Soc. Rev*., 43, 5346-5371 (DOI: 10.1039/c4cs00066h).

8. Vemula P. K., Cruikshank G. A., Karp J. M., John G. (2009), Self-assembled prodrugs: An enzymatically triggered drug-delivery platform, *Biomaterials*, 30 383-393 (DOI:10.1016/j.biomaterials.2008.09.045).

9. Maity I., Mukherjee T. K., Das A. K. (2014), Photophysical study of a π-stacked β-sheet nanofibril forming peptide bolaamphiphile hydrogel, *New J. Chem*., 38, 376-385 (DOI: 10.1039/c3nj00814b).

10. Wall B. D., Diegelmann S. R., Zhang S., Dawidczyk T. J., Wilson W. L., Katz H. E., Mao H.-Q., Tovar J. D. (2011), Aligned macroscopic domains of optoelectronic nanostructures prepared via shear-flow assembly of peptide hydrogels, *Adv. Mater.*, 23, 5009-5014 (DOI: 10.1002/adma.201102963).

11. Brizard A. M., van Esch J. H. (2009), Self-assembly approaches for the construction of cell architecture mimics, *Soft Matter*, 5, 1320-1327 (DOI: 10.1039/b812388h).

12. Ruiz-Mirazo K., Briones C., de la Escosura A. (2014), Prebiotic systems chemistry: New perspectives for the Origins of Life, *Chem. Rev*., 114, 285-366 (DOI: org/10.1021/cr2004844).

Annexure 1

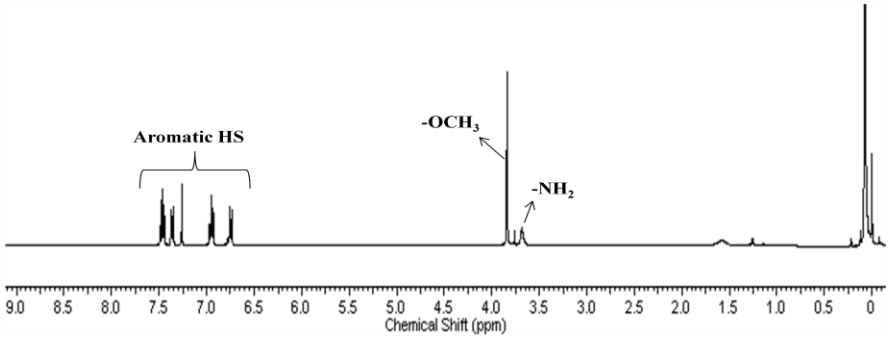

Figure A1.1. *^{1}H NMR spectrum (400 MHz, $CDCl_3$) of product **S1.***

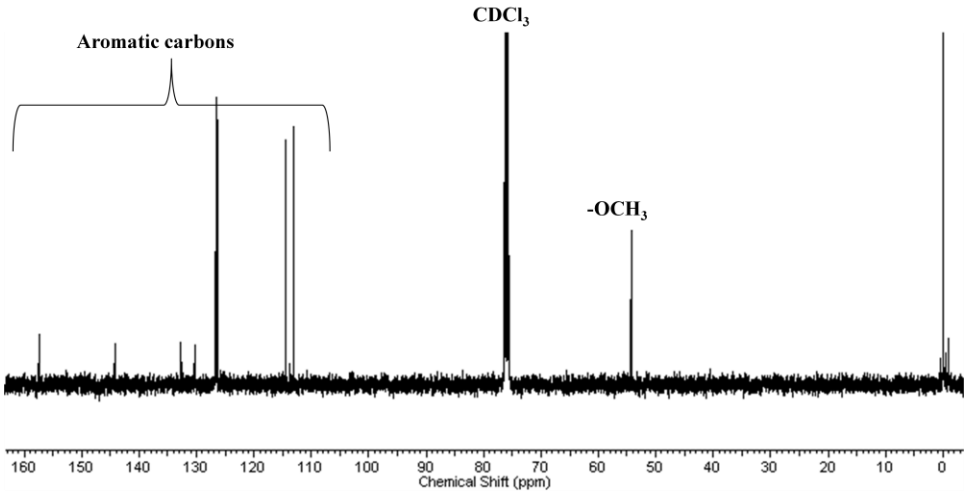

Figure A1.2. *^{13}C NMR spectrum (100 MHz, $CDCl_3$) of product **S1.***

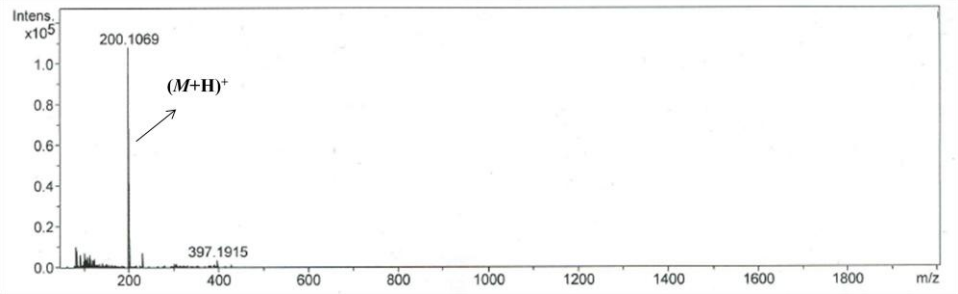

Figure A1.3. *ESI-MS spectrum of product **S1.***

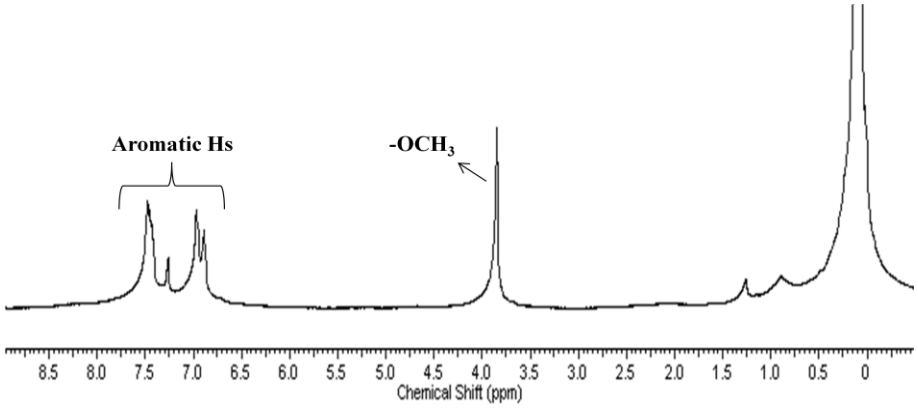

Figure A1.4. *^{1}H NMR spectrum (400 MHz, $CDCl_3$) of product* ***S2.***

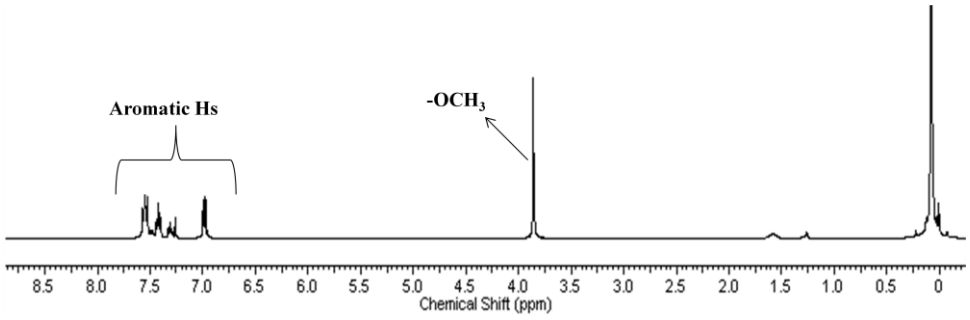

Figure A1.5. *^{1}H NMR spectrum (400 MHz, $CDCl_3$) of product* ***S3.***

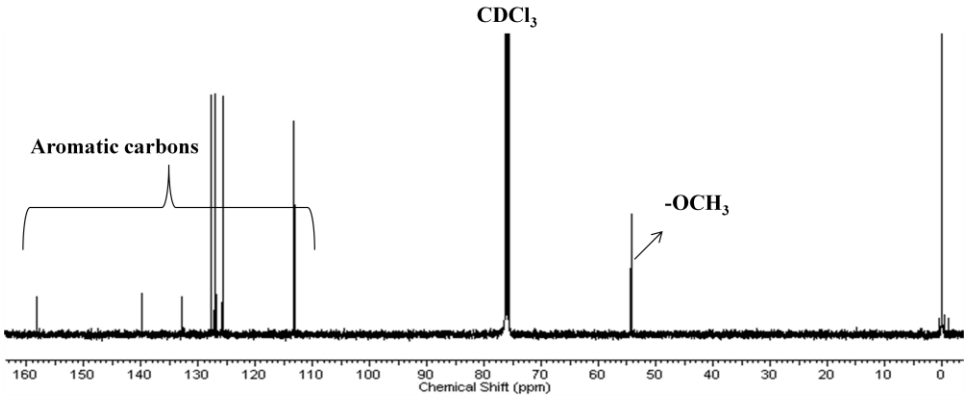

Figure A1.6. *^{13}C NMR spectrum (100 MHz, $CDCl_3$) of product* ***S3.***

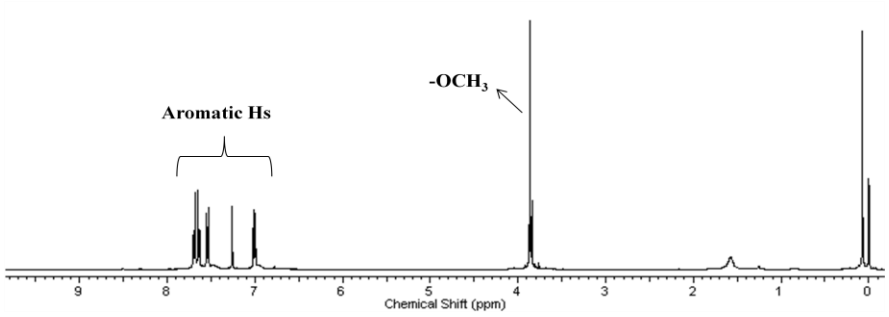

Figure A1.7. *^{1}H NMR spectrum (400 MHz, $CDCl_3$) of product **S4.***

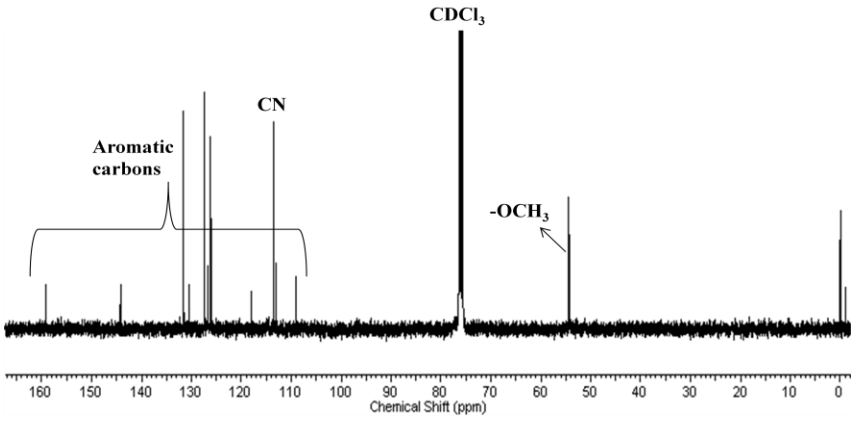

Figure A1.8. *^{13}C NMR spectrum (100 MHz, $CDCl_3$) of product **S4.***

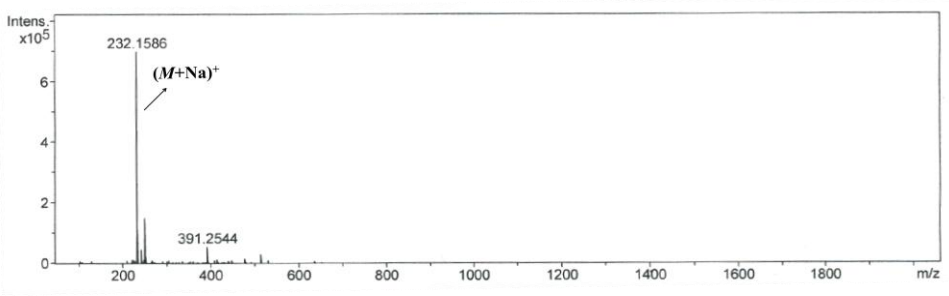

Figure A1.9. *ESI-MS spectrum of product **S4.***

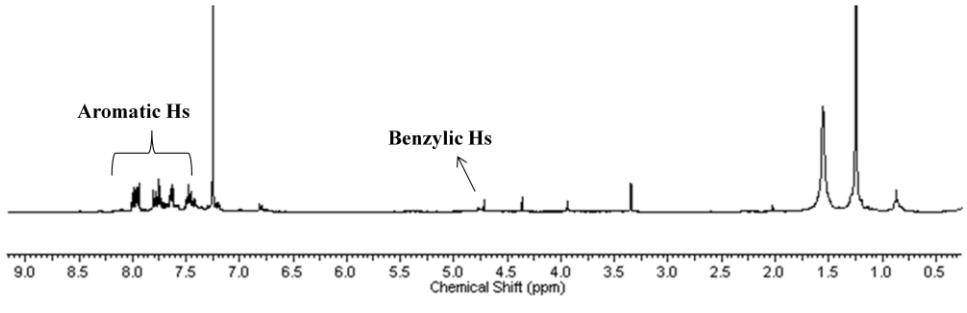

Figure A1.10. *^{1}H NMR spectrum (400 MHz, $CDCl_3$) of product **S5.***

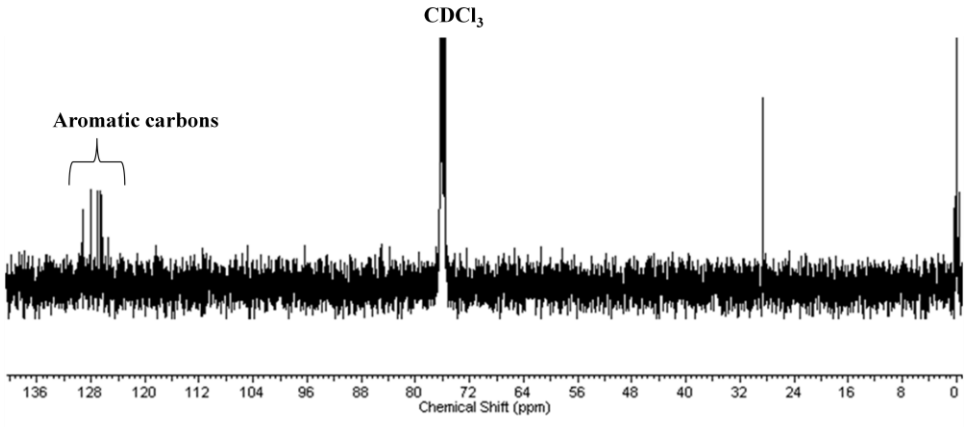

Figure A1.11. *^{13}C NMR spectrum (100 MHz, $CDCl_3$) of product **S5.***

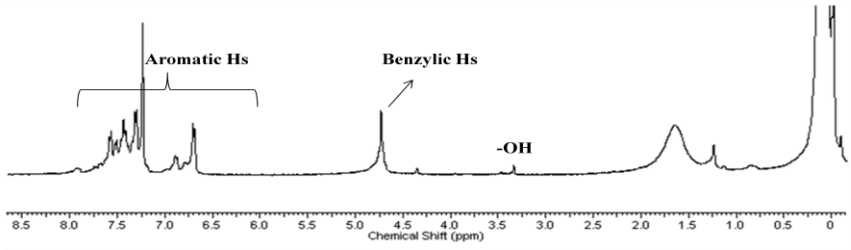

Figure A1.12. *^{1}H NMR spectrum (400 MHz, $CDCl_3$) of product **S6.***

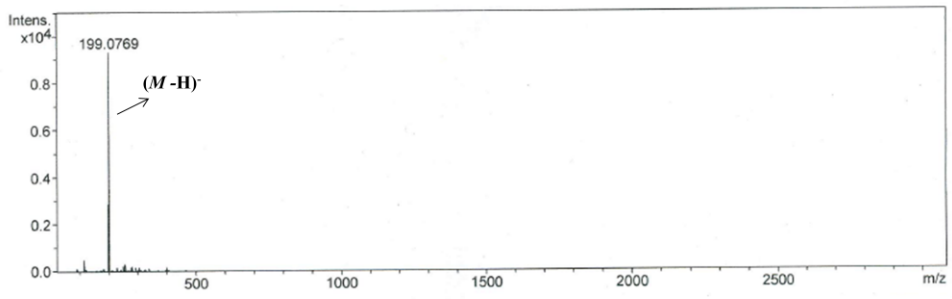

Figure A1.13. *ESI-MS spectrum of product* ***S6.***

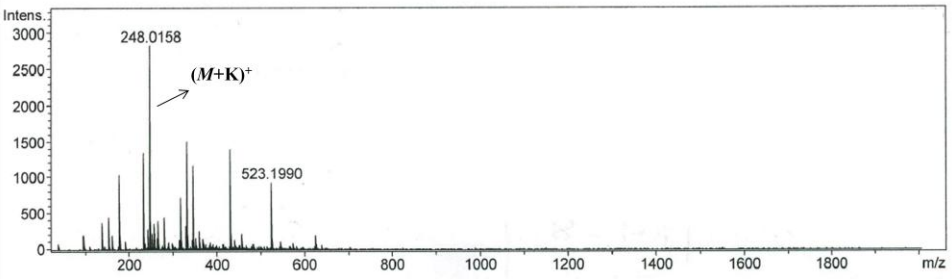

Figure A1.14. *ESI-MS spectrum of product* ***S7.***

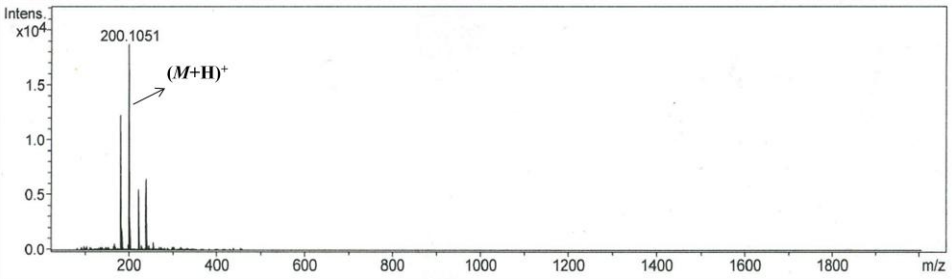

Figure A1.15. *ESI-MS spectrum of product* ***S8.***

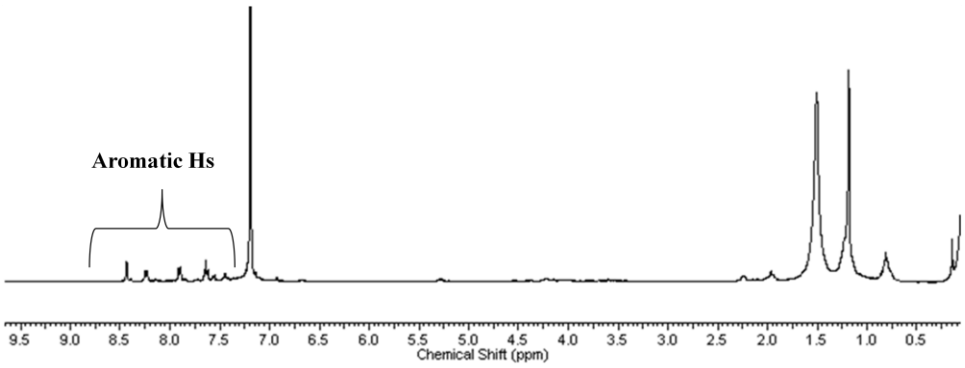

Figure A1.16. *^{1}H NMR spectrum (400 MHz, $CDCl_3$) of product* ***S9.***

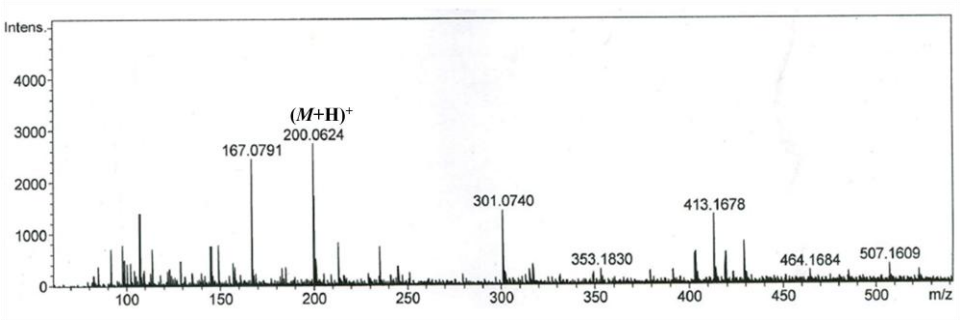

Figure A1.17. *ESI-MS spectrum of product* ***S9.***

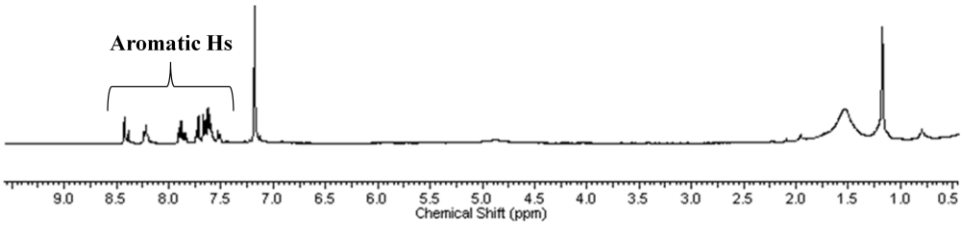

Figure A1.18. *^{1}H NMR spectrum (400 MHz, $CDCl_3$) of product* ***S10.***

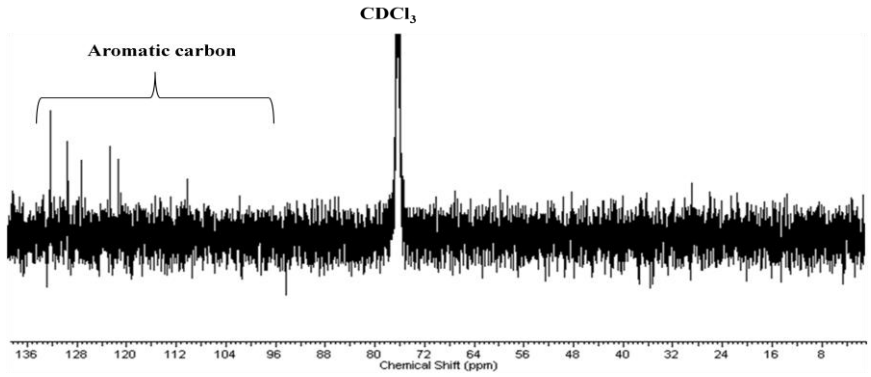

Figure A1.19. *^{13}C NMR spectrum (100 MHz, $CDCl_3$) of product* ***S10.***

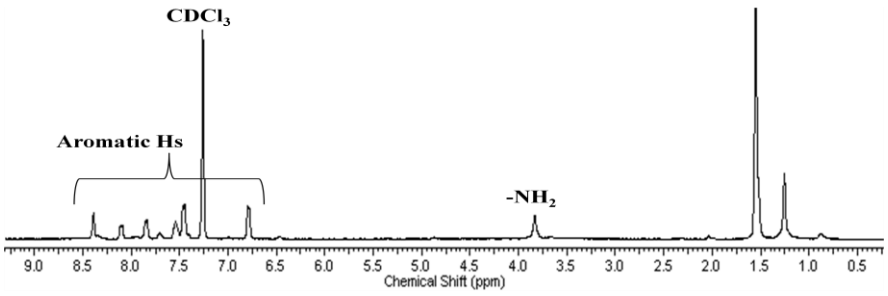

Figure A1.20. *^{1}H NMR spectrum (400 MHz, $CDCl_3$) of product* ***S11.***

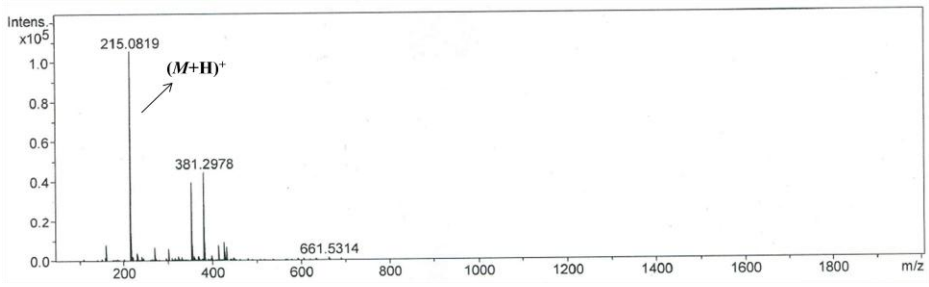

Figure A1.21. *ESI-MS spectrum of product* ***S11.***

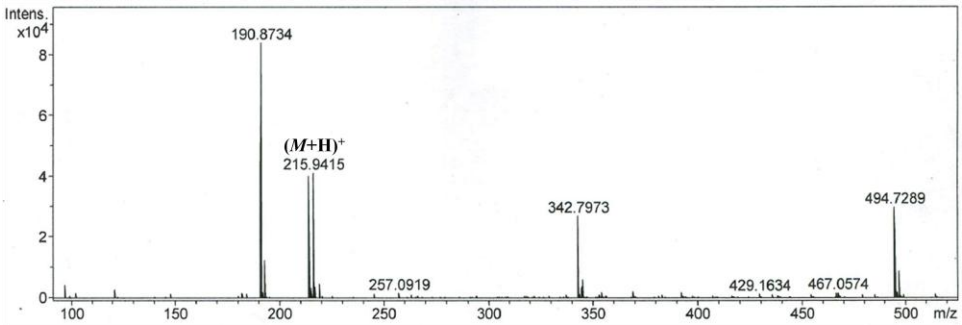

Figure A1.22. *ESI-MS spectrum of product* ***S12.***

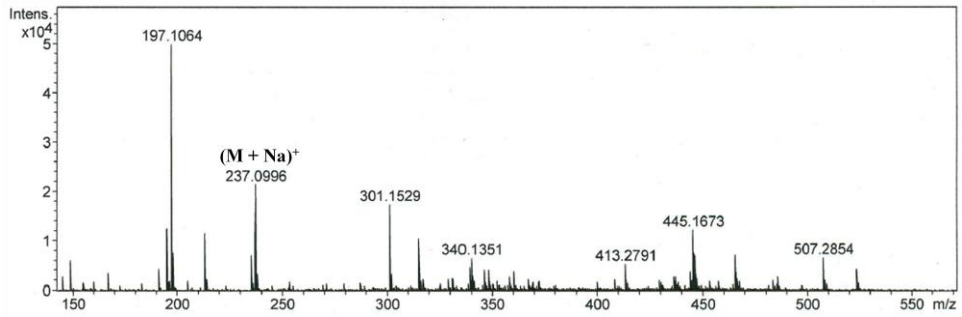

Figure A1.23. *ESI-MS spectrum of product* ***S13.***

Annexure 2

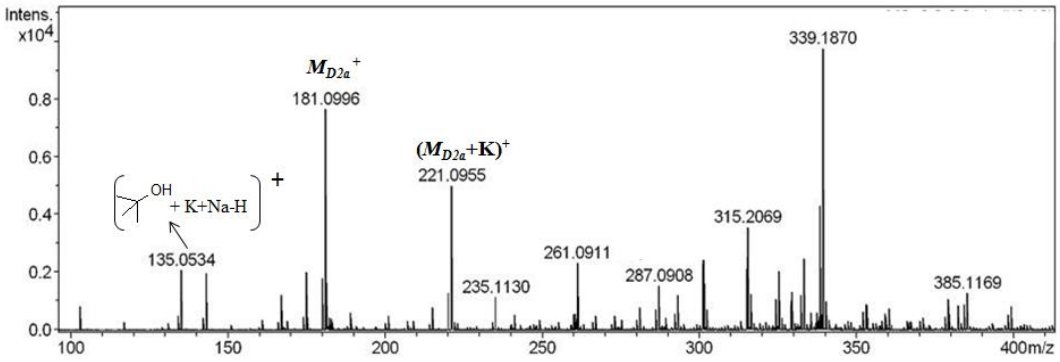

Figure A2.1. *Mass spectrum of Pd catalyzed deprotection reaction of D**2** to form D**2a**.*

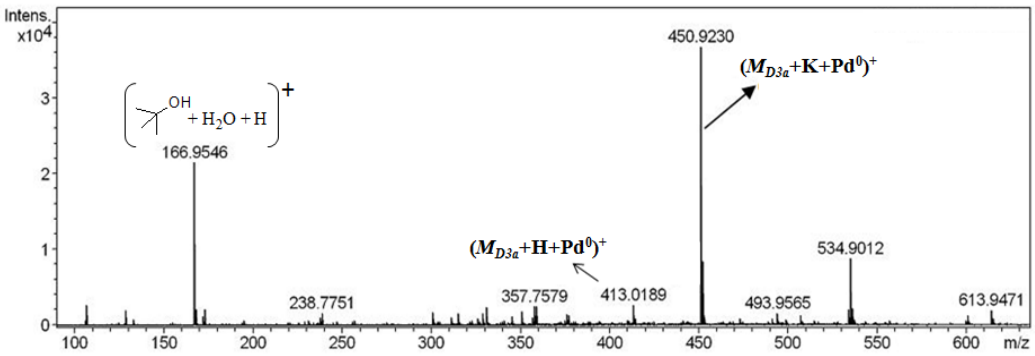

Figure A2.2. *Mass spectrum of Pd catalyzed deprotection reaction of D**3** to form D**3a**.*

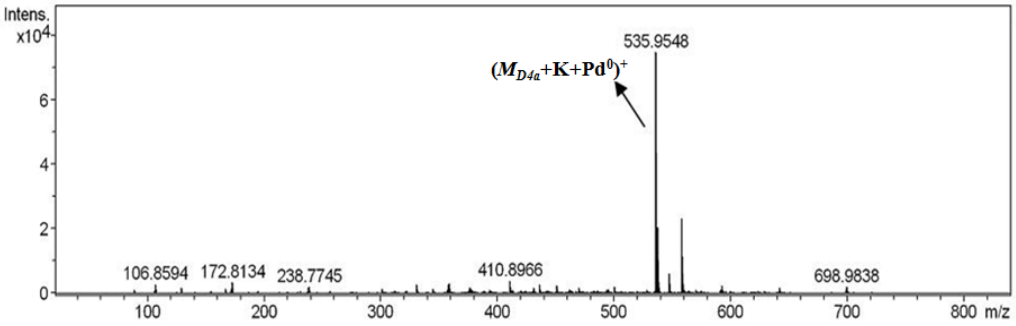

Figure A2.3. *Mass spectrum of Pd catalyzed deprotection reaction of D**4** to form D**4a**.*

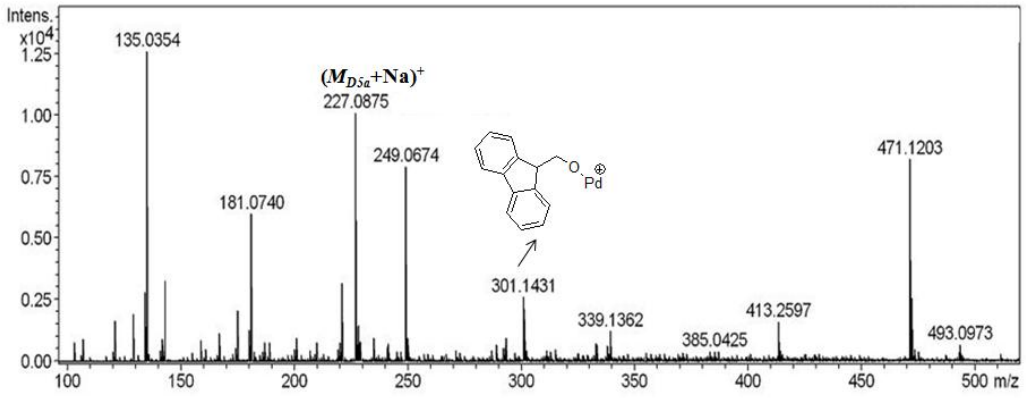

Figure A2.4. *Mass spectrum of Pd catalyzed deprotection reaction of D**5** to form D**5a**.*

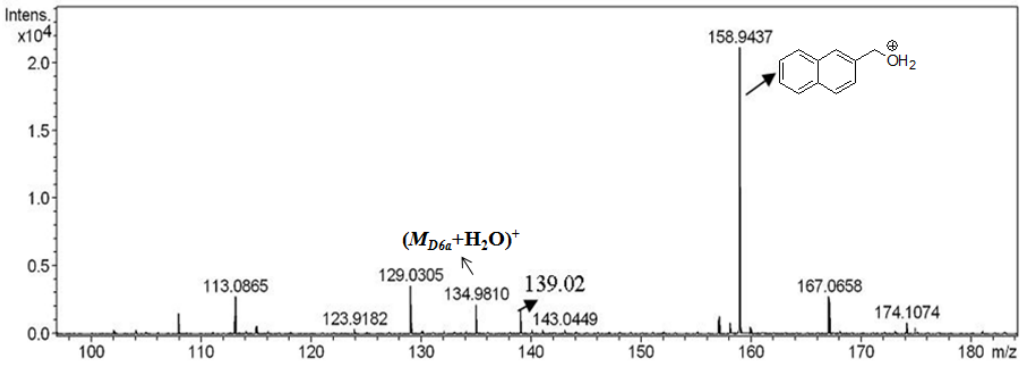

Figure A2.5. *Mass spectrum of Pd catalyzed deprotection reaction of D**6** to form D**6a**.*

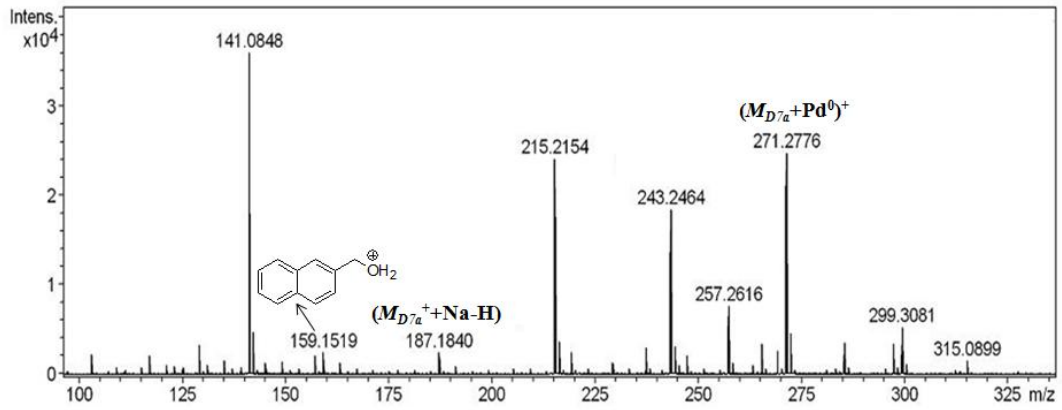

Figure A2.6. *Mass spectrum of Pd catalyzed deprotection reaction of D7 to form D**7a**.*

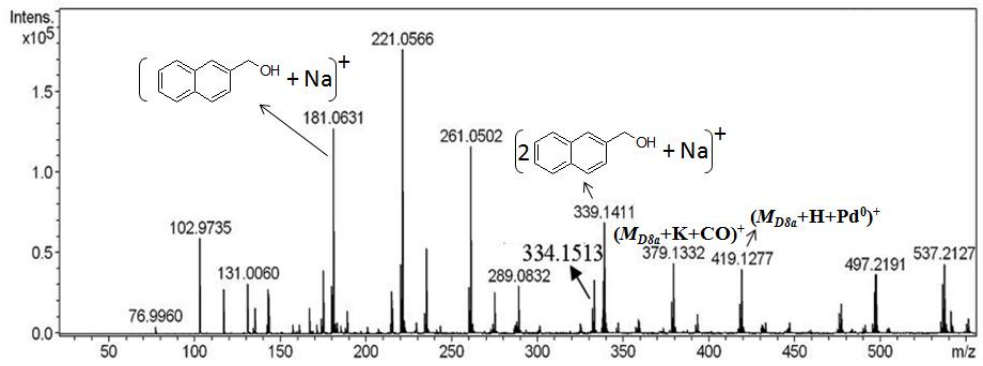

Figure A2.7. *Mass spectrum of Pd catalyzed deprotection reaction of D**8** to form D**8a**.*

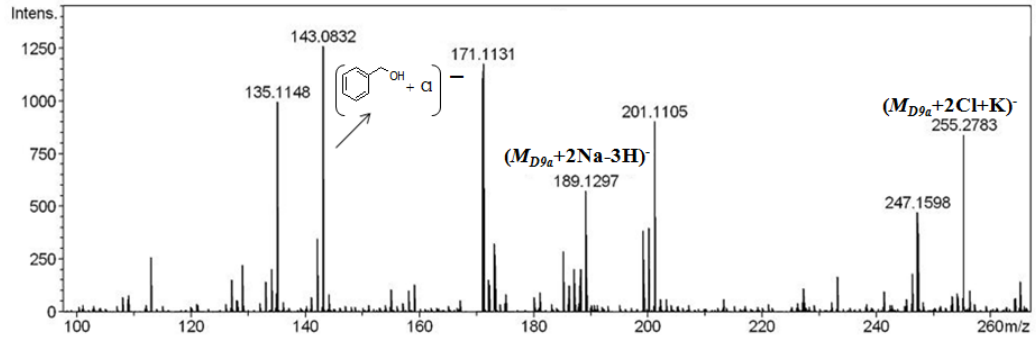

Figure A2.8. *Mass spectrum (Negative mode) of Pd catalyzed deprotection reaction of D**9** to form D**9a**.*